

The copyright of this thesis vests in the author. No quotation from it or information derived from it is to be published without full acknowledgement of the source. The thesis is to be used for private study or non-commercial research purposes only.

Published by the University of Cape Town (UCT) in terms of the non-exclusive license granted to UCT by the author.

SOLUTION METHODS FOR DYNAMIC AND NONLINEAR
FINITE ELEMENT ANALYSIS

by

Klaus-Jürgen Bathe

A work submitted in fulfillment of the requirements for the
degree of Doctor of Science in the Faculty of Engineering
at the University of Cape Town

Department of Mechanical Engineering
Massachusetts Institute of Technology

May 1981

Table of Contents

	<u>page</u>
Acknowledgements-----	1
Introduction and Overview-----	3
References-----	7
PART I Solution Methods for Large Generalized Eigenvalue Problems	
PART II Formulation and Implementation of Finite Elements and Material Models for Nonlinear Analysis	
PART III Solution of Finite Element Equations in Nonlinear Dynamic Analysis	

Acknowledgements

I am thankful to many people for their interest, support and help in my work over the last decade - some of the names are given in this document, but to name them all and thank them appropriately would fill too many pages. All I can do here is to express to all my former and current collaborators, students and colleagues collectively my deep appreciation for their very valuable help and support.

However, there are a few persons who greatly influenced my professional development, and those I would like to acknowledge specifically. I would like to thank Prof. E. L. Wilson of the University of California, Berkeley, for his support and collaboration in the early 1970's. During these years I also enjoyed a most valuable association with Fred Peterson of Engineering Analysis Corporation, Berkeley. Further, I would like to thank Prof. J. T. Oden of the University of Texas, Austin, for his collaboration and important influence to my professional thinking in recent years.

My work in the development of finite element procedures is largely based on the excellent engineering education that I received in the Civil Engineering Department of the University of Cape Town. It was particularly during my final year undergraduate studies in 1967 that I was able to recognize the valuable and exciting contributions to be made in automated structural analysis. My thoughts which I summarized in the paper "The Use of the Electronic Computer in Structural Analysis" (by K.J. Bathe, Journal of the UCT Engineering Society, 1967, pp. 57-61) clearly show what importance I correctly was able to attribute to this new field, and what I wanted to pursue in my research for the years to come. I am very thankful that - as a foreigner - I was received so warmly at the University of

Cape Town and obtained such excellent undergraduate education. Because of this special thankfulness I am very pleased to submit this document to the Faculty of Engineering at the University of Cape Town.

To pursue research effectively it is also most important to work in an appropriate environment. In this regard, I am very fortunate that I am now working in the Department of Mechanical Engineering at M.I.T., where excellent conditions are provided for my research and teaching endeavors.

Finally, I would like to thank my wife Zorka who with her constant love and understanding has provided immeasurably valuable support for the work that is documented herein.

K. J. Bathe
M.I.T.

Introduction and Overview

The computer analysis of structures and solids using finite element methods has now taken on very significant proportions [1-4]. In many cases the safety of a structure may be significantly increased and its cost reduced if an appropriate finite element analysis can be and is performed.

In the development and use of finite element methods, we recognize that, considering static linear analysis, already towards the end of the nineteen sixties the methods were highly developed -- thus it had taken only about one decade from the inception to the extensive practical use of finite element methods. Although difficulties were still encountered in the linear static analysis of some structures, e.g. complex shells, most of the structures could already be analysed in a routine manner.

This situation in engineering analysis was, however, quite different when dynamic or nonlinear conditions had to be considered. Whereas the finite element methods could be developed relatively quickly for linear static analysis, methods for practical dynamic and nonlinear analyses are much more difficult to establish. Although much emphasis has been placed on research in nonlinear analysis, the progress in the development of valuable techniques has been quite slow [5-7].

The practical objectives in the development of finite element methods for dynamic and nonlinear analysis are, in essence, that we want to be able to analyze increasingly more complex structures which are subjected to loads that vary rapidly -- causing dynamic response -- and loads of high intensity -- causing the structure to respond beyond its linear range. In nonlinear conditions, geometric and/or material nonlinearities may have to be taken into consideration.

These analysis conditions are encountered already in many industries (e.g. design of nuclear power plants) and, with the current needs towards usage of new materials and more efficient structures, nonlinear analysis will undoubtedly be required to an increasing extent.

Considering research in finite element analysis procedures, emphasis must be placed on the development of *reliable, general and cost-effective* techniques. The reliability of the analysis techniques is of utmost concern in order that the analyst can employ the methods with confidence. The results of an analysis can only be interpreted with confidence if reliable methods have been employed. The generality and cost-effectiveness of the methods are important in order to produce analysis tools that, in a design office, are applicable to a relatively large number of problems.

With the above aims in mind, the development of finite element procedures for dynamic and nonlinear analysis becomes a very formidable task. Not only is it necessary to propose -- guided by knowledge and intuition -- improved analysis techniques and then to implement and test these methods, but it is of major importance and difficulty to "fully" verify and qualify these theories and their computer program implementations. Whereas the verification and qualification of a finite element method is usually quite straight-forward in linear static analysis, this process may represent the major task in the development of a method for nonlinear analysis.

During the last decade I have endeavored to advance the state-of-the-art of general and reliable finite element analysis procedures for dynamic and nonlinear response calculations. The areas in which I have worked primarily are

- the development of eigensolution methods for large eigenproblems that arise in dynamic and buckling analysis of structures;
- the development of finite element procedures for nonlinear analysis with emphasis on
 - the formulation of finite elements and material models,
 - the methods of solution for the nonlinear equations.

The finite element procedures proposed in this research have been implemented in computer programs that are now in very wide use [8-12].

In accordance with the above areas of my research activities, I am presenting in this document relevant papers in three different Parts. The contents of each Part are briefly described below.

Part I Solution Methods for Large Generalized Eigenproblems

The eigenproblems considered in this research are the one arising in dynamic analysis,

$$\underline{K} \underline{\phi}_i = \lambda_i \underline{M} \underline{\phi}_i \quad (1)$$

and the one arising in linearized buckling analysis,

$$\underline{K} \underline{\phi}_i = \lambda_i \underline{K}_G \underline{\phi}_i \quad (2)$$

where \underline{K} , \underline{K}_G and \underline{M} are the linear stiffness, geometric stiffness and mass matrices of the finite element assemblage, and $(\lambda_i, \underline{\phi}_i)$, $i=1, 2, 3 \dots$ are the eigenpairs to be evaluated.

Part II Formulation and Implementation of Finite Elements and Material Models for Nonlinear Analysis

In these papers effective finite elements for nonlinear analysis and various nonlinear material models with their implementations are developed. Emphasis in this work was placed on continuum-mechanics-based consistent and effective finite elements and on general, practical and effective material descriptions.

Part III Solution of Finite Element Equations in Nonlinear Dynamic Analysis

The efficient and accurate solution of the finite element equations in nonlinear analysis is a very important aspect of the complete solution process. In these papers the stability and accuracy of time integration schemes, the selection of appropriate time step sizes and the development and use of effective iterative schemes for the nonlinear equations are discussed. The analyses and experiences given in these papers result into recommendations on the actual usage of the techniques available at present.

This document really represents a progress report on some of my work in finite element analysis, or more generally, in the area of computational mechanics. I am indeed very fortunate to work in this field: to me the area of computational mechanics represents a most exciting research area and promises to provide a very rich research environment for many years to come.

References

1. Zienkiewicz, O.C., The Finite Element Method, McGraw-Hill Book Co., 1977.
2. Oden, J.T., Finite Elements of Nonlinear Continua, McGraw-Hill Book Co., 1972.
3. Gallagher, R.H., Finite Element Analysis - Fundamentals, Prentice-Hall, Inc., 1975.
4. Bathe, K.J., and Wilson, E.L., Numerical Methods in Finite Element Analysis, Prentice-Hall, Inc., 1976.
Bathe, K.J., Finite Element Procedures in Engineering Analysis, Prentice-Hall, Inc., in press.
5. Oden, J.T., and Bathe, K.J., "A Commentary on Computational Mechanics," *Appl. Mech. Reviews*, Sept. 1978.
6. Bathe, K.J., "On the Current State of Finite Element Methods and Our ADINA Endeavours," *J. Adv. Eng. Software*, Vol. 2, 1980, pp. 59-65.
7. Bathe, K.J., "The Current State of Finite Element Methods in Structural Mechanics," *Proceedings of the Symposium of Design Applications of the Finite Element Method*, Jan. 1981, Univ. of Cape Town.
8. Bathe, K.J., Wilson, E.L. and Peterson, F.E., "SAP IV - A Structural Analysis Program for Static and Dynamic Response of Linear Systems," Report EERC 73-11, Department of Civil Engineering, Univ. of California, Berkeley, June 1973, rev. April 1974.
9. Bathe, K.J., Wilson, E.L. and Iding, R., "NONSAP - A Structural Analysis Program for Static and Dynamic Response of Nonlinear Systems," Report UCSESM 74-3, Department of Civil Engineering, Univ. of California, Berkeley, Feb. 1974.
10. Bathe, K.J., "ADINA - A Finite Element Program for Automatic Dynamic Incremental Nonlinear Analysis," Report AVL 82448-1, Department of Mechanical Engineering, M.I.T., September 1975, rev. Dec. 1978.
11. Bathe, K.J., "ADINAT - A Finite Element Program for Automatic Dynamic Incremental Nonlinear Analysis of Temperatures," Report AVL 82448-5, Department of Mechanical Engineering, M.I.T., May 1976, rev. Dec. 1978.
12. Bathe, K.J., (ed.), *Proceedings of the ADINA Conferences* Aug. 1977, Aug. 1979, and June 1981 at the Massachusetts Institute of Technology.

Part I Solution Methods for Large Generalized Eigenproblems

Large Eigenvalue Problems in Dynamic Analysis

Eigensolution of Large Structural Systems with Small Bandwidth

Solution Methods for Eigenvalue Problems in Structural Mechanics

An Accelerated Subspace Iteration Method

Journal of the
ENGINEERING MECHANICS DIVISION
Proceedings of the American Society of Civil Engineers

LARGE EIGENVALUE PROBLEMS IN DYNAMIC ANALYSIS

By Klaus-Jürgen Bathe¹ and Edward L. Wilson,² M. ASCE

INTRODUCTION

Problem Definition.—The equations of motion for a system of structural elements can be written as

$$M\ddot{u} + C\dot{u} + Ku = P \dots\dots\dots (1)$$

in which M = the mass, C = the damping, and K = the stiffness matrix of the system; vectors u , \dot{u} , \ddot{u} , and P are the displacements, velocities, accelerations and loads, respectively (4). The matrices M , C , and K are obtained in the analysis of building structures idealized as an assemblage of beam elements and in the analysis of continuums using a discretization technique such as the finite element method (13).

Assume that the elements in the stiffness, mass, and damping matrix are constant and that a mode superposition analysis is considered to be most economical. The first step in this analysis is to consider free vibration conditions

$$M\ddot{u} + Ku = 0 \dots\dots\dots (2)$$

$$\text{Substituting } u = \phi \sin \omega(t - t_0) \dots\dots\dots (3)$$

the generalized eigenvalue problem

$$K\phi = \omega^2 M\phi \dots\dots\dots (4)$$

is obtained. The n eigenvalues give the natural frequencies of the system and the eigenvectors are the corresponding vibration modes. The complete solu-

Note.—Discussion open until May 1, 1973. To extend the closing date one month, a written request must be filed with the Editor of Technical Publications, ASCE. This paper is part of the copyrighted Journal of the Engineering Mechanics Division, Proceedings of the American Society of Civil Engineers, Vol. 98, No. EM6, December, 1972. Manuscript was submitted for review for possible publication on April 5, 1972.

¹Asst. Research Engr., Civ. Engrg. Dept., Univ. of California, Berkeley, Calif.

²Prof., Civ. Engrg. Dept., Univ. of California, Berkeley, Calif.

tion to Eq. 4 can be written as

$$K\Phi = M\Phi\Omega^2 \dots\dots\dots (5)$$

in which the columns in Φ are the eigenvectors ϕ_i and $\Omega^2 = \text{diag}(\omega_i^2)$.

The basis is now changed from the physical coordinate basis which was used to establish Eq. 1 to the M-orthonormal basis of eigenvectors. Using $u = \Phi X$ with the vector, X , listing the coordinates in the new basis, the equilibrium Eqs., Eq. 1, become

$$\ddot{X} + \Delta\dot{X} + \Omega^2 X = \Phi^T P \dots\dots\dots (6)$$

in which $\Delta = \Phi^T C \Phi$ and is assumed to be diagonal. This requires that the damping matrix is of a restricted form as described in Ref. 12; Eq. 6 then consists of n uncoupled equations, which can readily be solved (4).

The most time consuming step in the analysis can be the solution of the eigenvalue problem. If the order of the matrices is large, the computer time required to solve for all eigenvalues and vectors can be enormous. However, the structure may respond primarily in a few modes and the contribution of the other modes may be negligible. In particular, in earthquake response analysis it is often sufficiently accurate to consider only the lowest frequencies and corresponding vibration modes. In this case a solution routine is needed which calculates only the required frequencies and vectors with optimum efficiency.

For the eigenvalue solution it is of particular importance that for most structural systems both matrices K and M are banded, i.e., $k_{ij} = 0$ for $j > i + m_K$ and $m_{ij} = 0$ for $j > i + m_M$ in which $(2m_K + 1)$ and $(2m_M + 1)$ are the bandwidths of the matrices. If all rigid body modes have been removed from the system, K is positive definite. If a consistent mass formulation is used, M is also positive definite and $m_M = m_K$. But experience has shown that accurate results may often be obtained using a lumped mass formulation in which M is diagonal with m_{ii} positive or zero.

Rayleigh-Ritz Method.—For large structural systems the order of the matrices can be several thousand; therefore, approximate techniques have been developed to calculate the lowest eigenvalues and vectors. A very general technique is the Rayleigh-Ritz analysis (5). Let V_n denote the n -dimensional space in which the operators K and M are defined. The Rayleigh minimum principle states that

$$\omega_1^2 = \min \rho(v) \dots\dots\dots (7)$$

in which the minimum is taken over all vectors v in V_n and $\rho(v)$ is the Rayleigh quotient defined as

$$\rho(v) = \frac{v^T K v}{v^T M v} > 0 \dots\dots\dots (8)$$

In the Ritz analysis all vectors \bar{v} in a q -dimensional subspace of V_n are considered. A typical element in the subspace is given by

$$\bar{v} = \sum_{i=1}^q a_i x_i \dots\dots\dots (9)$$

in which the x_i = the Ritz basis vectors and the a_i = the Ritz coordinates. Substituting Eq. 9 into Eq. 8,

$$\rho(\bar{v}) = \frac{\sum_{j=1}^q \sum_{i=1}^q a_j a_i \tilde{k}_{ij}}{\sum_{j=1}^q \sum_{i=1}^q a_j a_i \tilde{m}_{ij}} \dots \dots \dots (10)$$

is obtained with $\tilde{k}_{ij} = \mathbf{x}_i^T \mathbf{K} \mathbf{x}_j \dots \dots \dots (11)$

$$\tilde{m}_{ij} = \mathbf{x}_i^T \mathbf{M} \mathbf{x}_j \dots \dots \dots (12)$$

The necessary condition for a minimum of $\rho(\bar{v})$ is $\partial \rho(\bar{v}) / \partial a_i = 0, i = 1, \dots, q$. This gives

$$\tilde{\mathbf{K}} \mathbf{a} = \rho \tilde{\mathbf{M}} \mathbf{a} \dots \dots \dots (13)$$

in which \mathbf{a} = a vector listing the Ritz coordinates; $\tilde{\mathbf{K}}$ and $\tilde{\mathbf{M}}$ = the generalized stiffness and the generalized mass matrix with typical elements given in Eqs. 11 and 12.

The solution of Eq. 13 yields q values ρ_1, \dots, ρ_q and corresponding vectors $\bar{v}_1, \dots, \bar{v}_q$, which are obtained using Eq. 9. The values $\rho_i, i = 1, \dots, q$ are upper bound approximations to the exact eigenvalues of Eq. 4, (5), i.e.:

$$\omega_1^2 \leq \rho_1; \omega_2^2 \leq \rho_2; \dots; \omega_q^2 \leq \rho_q \dots \dots \dots (14)$$

The actual error in the solution is, in general, not estimated. It depends on the Ritz basis vectors chosen because the approximate eigenvectors $\bar{v}_1, \dots, \bar{v}_q$ are elements of the subspace.

The Ritz analysis has been implemented in various ways (9). Ritz basis vectors can be obtained from a static analysis in which q load patterns are specified in $\mathbf{P}_D(4)$; then

$$\mathbf{K} \mathbf{X}_D = \mathbf{P}_D \dots \dots \dots (15)$$

and $\tilde{\mathbf{K}} = \mathbf{X}_D^T \mathbf{P}_D; \tilde{\mathbf{M}} = \mathbf{X}_D^T \mathbf{M} \mathbf{X}_D \dots \dots \dots (16)$

The obvious difficulty is in selecting good load patterns.

Static Condensation Method.—In another scheme which is known as static condensation of the massless degrees-of-freedom, it is assumed that all mass can be lumped at q degrees-of-freedom. Therefore, as an approximation to Eq. 4

$$\begin{bmatrix} \mathbf{K}_{aa} & \mathbf{K}_{ac} \\ \mathbf{K}_{ca} & \mathbf{K}_{cc} \end{bmatrix} \begin{bmatrix} \psi_a \\ \psi_c \end{bmatrix} = \omega^2 \begin{bmatrix} \mathbf{M}_a & 0 \\ 0 & 0 \end{bmatrix} \begin{bmatrix} \psi_a \\ \psi_c \end{bmatrix} \dots \dots \dots (17)$$

is obtained with q finite and $(n - q)$ infinite eigenvalues. A reduced eigenvalue problem for the finite eigenvalues is obtained by using static condensation on the ψ_c degrees-of-freedom, then

$$\mathbf{K}_a \psi_a = \omega^2 \mathbf{M}_a \psi_a \dots \dots \dots (18)$$

in which $\mathbf{K}_a = \mathbf{K}_{aa} - \mathbf{Z}^T \mathbf{Z}; \mathbf{K}_{cc} = \tilde{\mathbf{L}} \tilde{\mathbf{L}}^T; \tilde{\mathbf{L}} \mathbf{Z} = \mathbf{K}_{ca} \dots \dots \dots (19)$

This solution is actually a Ritz analysis of the lumped mass model considered

in Eq. 17. The Ritz basis vectors are the displacement patterns associated with the ψ_a degrees-of-freedom when the ψ_c degrees-of-freedom are released. Solving

$$\begin{bmatrix} K_{aa} & K_{ac} \\ K_{ca} & K_{cc} \end{bmatrix} \begin{bmatrix} f_a \\ f_c \end{bmatrix} = \begin{bmatrix} I \\ 0 \end{bmatrix} \dots \dots \dots (20)$$

in which $f_a = K_a^{-1}$,

$$X_D = \begin{bmatrix} I \\ f_c & K_a \end{bmatrix} \dots \dots \dots (21)$$

and in Eq. 16 $\tilde{K} = K_a$ and $\tilde{M} = M_a$. In this analysis the lowest q eigenvalues of the lumped mass model in Eq. 17 are calculated exactly, because the Ritz basis vectors span the q -dimensional subspace corresponding to the finite eigenvalues. The accuracy with which the eigenvalues of the lumped mass model approximate the q lowest eigenvalues of the original model in Eq. 4 depends on how well mass was lumped.

In both analyses, the Rayleigh-Ritz and the static condensation method, the smallest eigenvalues are usually approximated best; however, nothing can be said about the accuracy of the eigenvalue approximations obtained. In fact, an approximation to an important eigenvalue may be missed completely.

Accurate Calculation of Required Eigensystem.—Various solution routines have been established to calculate the lowest eigenvalues and corresponding vectors in the generalized eigenvalue problem, Eq. 4, exactly (10). The problem may be transformed into a standard eigenvalue problem and then a Rayleigh quotient iteration with matrix deflation can be used (6). This has the disadvantage that M must be diagonal and positive definite. It is more efficient to solve Eq. 4 directly without a transformation. This is done in Ref. 7. However, the algorithm uses only the Sturm sequence property and is therefore costly unless the bandwidth of the system is very small. A very efficient solution routine has been developed for systems with small to medium bandwidth by combining a determinant search technique with the information obtained from the Sturm sequence property and vector inverse iteration (1). But for systems with large bandwidth and which cannot be taken into high speed storage of the computer, this solution becomes also expensive, mainly because many triangular factorizations are required. The most promising approach for the solution of systems of large order and large bandwidth is the simultaneous iteration with a number of vectors (2,3,8).

The aim of this paper is to present the simultaneous iteration with p vectors in Eq. 4 as a subspace iteration which then leads to a very effective implementation. The algorithm was developed as part of an automatic package for the calculation of eigenvalues and eigenvectors in a general structural analysis program (1,11). The mass matrix can be diagonal with zero elements or may be banded as in a consistent mass formulation. Operation counts are given for both cases in order to enable solution cost estimates. The algorithm is particularly suited for the solution of systems which are too large for the high speed storage of the computer. A program which was written for systems of practically any order and bandwidth is described herein. Two example solutions, namely, the eigensolution of a plane frame and of a complex three-

dimensional building frame, are given in order to show typical convergence characteristics and iteration times needed.

SUBSPACE ITERATION ALGORITHM

Basic Theory.—The objective is to solve for the p lowest eigenvalues and associated eigenvectors satisfying

$$K \Phi = M \Phi \Omega^2 \dots\dots\dots (22)$$

in which Φ stores the p eigenvectors and Ω^2 the corresponding eigenvalues. The eigenvectors are an M -orthonormal basis of the p -dimensional, least dominant subspace of the operators, which will now be called E_∞ .

Before developing the algorithm, it may be pointed out that the essential idea is to iterate simultaneously with p linearly independent vectors which initially span the starting subspace E_0 , until E_∞ is spanned. The required eigenvectors are then computed without further iteration. The total number of required iterations depends, of course, on how close E_0 is to E_∞ . But the effectiveness of the algorithm lies in that it is much easier to establish a p -dimensional starting subspace which is close to E_∞ than to find p vectors which each are close to a required eigenvector. Also, convergence of the subspace is all that is required and not of individual iteration vectors to eigenvectors.

To present the algorithm let X_0 store the p starting vectors which span E_0 . Consider simultaneous inverse iteration with the vectors, expressed as

$$K X_k = M X_{k-1} \quad k = 1, 2, \dots \dots\dots (23)$$

The iteration vectors in X_k span a p -dimensional subspace E_k and the sequence of subspaces generated converges to E_∞ . This seems to contradict the fact that in this iteration each column in X_k is known to converge to the least dominant eigenvector unless the column is deficient in ϕ_1 . Actually, there is no contradiction. Although in exact arithmetic the vectors in X_k span E_k , they do become more and more parallel and therefore a poorer and poorer basis. One way to preserve numerical stability is to generate orthogonal bases in the subspaces E_k using the Gram-Schmidt process. In this case the iteration is

$$K X_k = M X_{k-1} R_k^{-1} \quad k = 1, 2, \dots \dots\dots (24)$$

in which R_k = an upper triangular matrix; provided the starting vectors in X_0 are not deficient in the eigenvectors corresponding to $\omega_1^2, \omega_2^2, \dots, \omega_p^2$ in which $\omega_1^2 \leq \omega_2^2 \leq \omega_3^2 \dots \leq \omega_p^2 < \omega_{p+1}^2$ it holds $X_k \rightarrow \Phi$; $R_k^{-1} \rightarrow \Omega^2$ as $k \rightarrow \infty$. Apart from round-off, this iteration generates the same sequence of subspaces as Eq. 23, but in this case the i 'th column in X_k converges to ϕ_i with a rate of $\max \{ \omega_{i-1}^2 / \omega_i^2, \omega_i^2 / \omega_{i+1}^2 \}$. Essentially, this poor convergence rate results from the orthogonalization of the iteration vectors from the left to the right. For example, no advantage is taken if the third column in X_k is much closer to ϕ_1 than the first column. In particular, assume that the vectors in X_k span E_∞ but are not eigenvectors; then, although the subspace already converged, many more iterations may be needed in order to turn the orthogonal basis of iteration vectors into the basis of eigenvectors.

The following algorithm finds an orthogonal basis of vectors in E_k , thus preserving numerical stability in the iteration of Eq. 23, and also calculates

in one step the required eigenvectors when E_k converged to E_∞ .
 For $k = 1, 2, \dots$ iterate from E_{k-1} to E_k

$$K \bar{X}_k = M X_{k-1} \dots \dots \dots (25)$$

Find the projections of the operators K and M onto E_k

$$K_k = \bar{X}_k^T K \bar{X}_k \dots \dots \dots (26)$$

$$M_k = \bar{X}_k^T M \bar{X}_k \dots \dots \dots (27)$$

Solve for the eigensystem of the projected operators

$$K_k Q_k = M_k Q_k \Omega_k^2 \dots \dots \dots (28)$$

Find an improved approximation to the eigenvectors

$$X_k = \bar{X}_k Q_k \dots \dots \dots (29)$$

Then provided E_0 is not orthogonal to one of the required eigenvectors,

$$\Omega_k^2 \rightarrow \Omega^2; X_k \rightarrow \Phi \text{ as } k \rightarrow \infty$$

is obtained.

Assuming that E_k is close to E_∞ the convergence rate of the i 'th column in X_k to ϕ_i is $\omega_i^2/\omega_{p+1}^2$. Although this is an asymptotic convergence rate, it indicates that the lowest eigenvalues converge fastest. Also, faster convergence can be obtained by using q iteration vectors, with $q > p$. In the implementation $q = \min \{2p, p + 8\}$ has been used. Note that then multiple eigenvalues do not decrease the convergence rate provided $\omega_{q+1}^2 > \omega_p^2$.

In practice, it is of interest to know what happens in the first few iterations when E_k is not yet close to E_∞ . Eqs. 26 to 29 are identified as a Ritz analysis with the vectors in \bar{X}_k as the Ritz basis vectors. Therefore, the eigenvalues in Ω_k^2 are stationary points in conformity with the Rayleigh minimum principle, Eq. 7, and they are upper bound approximations on the eigenvalues sought, Eq. 14.

Starting Subspace.—The number of subspace iterations required for convergence depends on how close the starting subspace is to E_∞ . Whenever starting vectors approximate quite well the eigenvectors sought, these vectors should be used in X_0 . In this case, the algorithm is ideally suited for solution. For instance, in dynamic optimization, as the structure is modified in small steps, the eigensystem of the previous structure would be a good approximation to the eigensystem of the new structure. Sometimes it may be difficult to judge if the transformation vectors at hand can be considered to be good. In particular, it is important to note that in exact arithmetic, convergence to an eigenvector is not possible, if the starting vectors in X_0 are all orthogonal to the eigenvector. But the conventional Ritz analysis, if excellent load patterns are known, the component mode synthesis and related methods summarized by Uhrig can all be good first subspace iterations (9).

Assume that good transformation vectors are not present and that it is desirable to establish X_0 from the elements in K and M only. It is not necessary to use vectors in X_0 which are close to the required eigenvectors, but only vectors which span a subspace close to E_∞ .

The following scheme has been found very effective. The first column in MX_0 is simply the diagonal of M. This assures that all mass degrees-of-freedom are excited in order not to miss a mode. The other columns in MX_0

are unit vectors with + 1 at the coordinates with largest ratios m_{ii}/k_{ii} . This scheme is used because for the special case when K and M are diagonal, these vectors span E_∞ . In actual analysis, the same or nearly the same ratio m_{ii}/k_{ii} may occur at many coordinates and it is equally important that the unit entries in the vectors are well spaced for better convergence.

Convergence.—It is apparent that the closeness of E_k to E_∞ and thus convergence, can be measured by the eigenvalue (or eigenvector) approximations calculated using Eqs. 26 to 29. Assuming that in the iterations $(k - 1)$ and k eigenvalue approximations $\omega_i^{2(k-1)}$ and $\omega_i^{2(k)}$ are calculated, then the ratio $|\omega_i^{2(k)} - \omega_i^{2(k-1)}|/\omega_i^{2(k)}$ may be used as a measure of convergence. For example, for the eigenvalues to be accurate to about 5 digits, it is necessary to iterate until this tolerance is less than 10^{-6} .

Verification of Results.—The starting subspace previously described has proven to be very satisfactory. However, the resulting eigenvalues and eigenvectors may be checked by using the Sturm sequence property (10). This states that in Gauss elimination to evaluate $LDL^T = K - \mu M$, in which μ = the shift, the number of negative elements in D = the number of eigenvalues smaller than μ . In order to use a meaningful μ , it is necessary to find bounds for the exact eigenvalues ω_i^2 using the calculated values $\omega_i^{2(k)}$. A conservative estimate for a region in which the exact eigenvalues lie is given by

$$0.99 \omega_i^{2(k)} < \omega_i^2 < 1.01 \omega_i^{2(k)} \dots \dots \dots (30)$$

TABLE 1.—OPERATION COUNT FOR SUBSPACE ITERATIONS

Method (1)	Calculation (2)	Number of Operations	
		$m = m_K = m_M$ (3)	$m = m_K ; m_M = 0$ (4)
Simple inverse iteration Total	$K \bar{X}_k = Y_{k-1}$	$nq(2m + 1)$	$nq(2m + 1)$
	$Y_k = M \bar{X}_k$	$nq(2m + 1)$	nq
	Total	$2nq(2m + 1)$	$2nq(m + 1)$
Inverse iteration with Gram-Schmidt orthogonalization Total	$K \bar{X}_k = Y_{k-1}$	$nq(2m + 1)$	$nq(2m + 1)$
	$\bar{Y}_k = M \bar{X}_k$	$nq(2m + 1)$	nq
	$Y_k = \bar{Y}_k R_k^{-1}$	$nq/2(3q + 3)$	$nq/2(3q + 3)$
	Total	$2nq(2m + 3/4q + 7/4)$	$2nq(m + 3/4q + 7/4)$
Inverse iteration with calculation of operator projections Total	$K \bar{X}_k = Y_{k-1}$	$nq(2m + 1)$	$nq(2m + 1)$
	$K_k = \bar{X}_k^T Y_{k-1}$	$nq/2(q + 1)$	$nq/2(q + 1)$
	$\bar{Y}_k = M \bar{X}_k$	$nq(2m + 1)$	nq
	$M_k = \bar{X}_k^T \bar{Y}_k$	$nq/2(q + 1)$	$nq/2(q + 1)$
	$K_k Q_k = M_k Q_k \Omega_k^2$	$0(q^3)$ neglected . . .	
	$Y_k = \bar{Y}_k Q_k$	nq^2	nq^2
Total		$2nq(2m + q + 3/2)$	$2nq(m + q + 3/2)$

Table 1 shows that for $m \gg q$ about the same number of operations are needed in all three iteration schemes. Note that about twice as many operations are needed when M is banded.

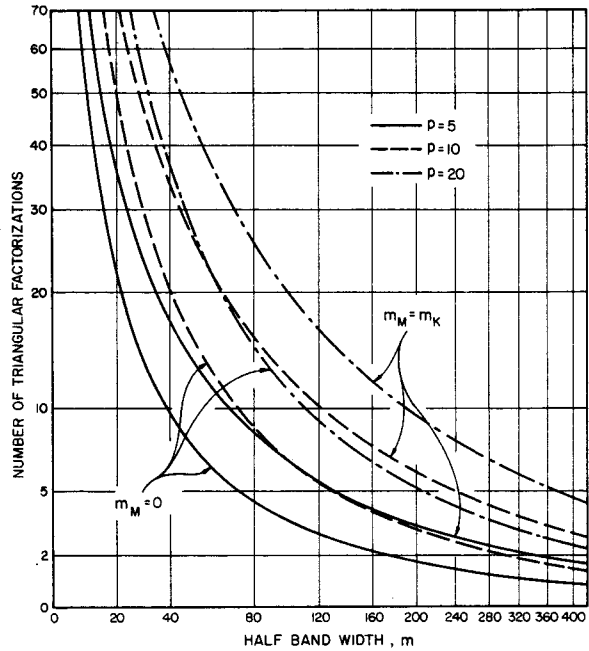


FIG. 1.—NUMBER OF TRIANGULAR FACTORIZATIONS EQUIVALENT TO SUBSPACE ITERATIONS

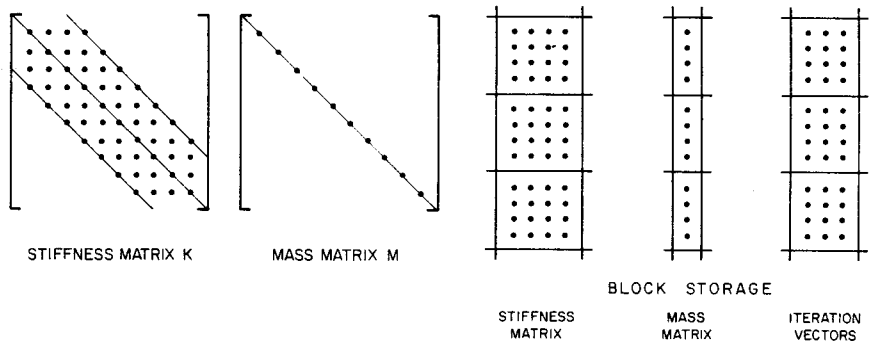


FIG. 2.—BLOCK STORAGE OF STIFFNESS MATRIX, MASS MATRIX, AND ITERATION VECTORS

Let the eigenvalues be required to about five digit precision and let $q = \min \{2p, p + 8\}$, then, with the starting subspace described, by experience about eight subspace iterations are needed. Assume that the projections of K and M

are calculated in each iteration, then the number of triangular factorizations equivalent in operations to the subspace iterations are

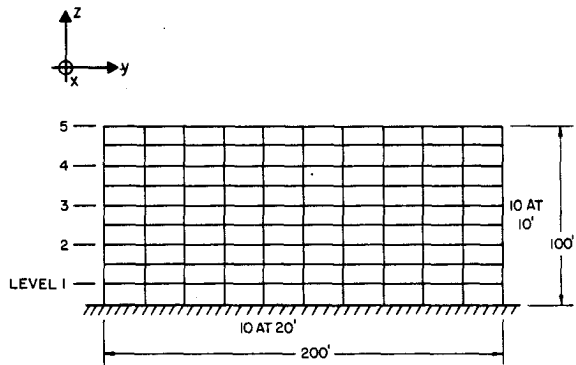
$$\frac{32qm + 32q^2 + 48q}{m^2 + 3m} \text{ for } m_M = 0 \dots\dots\dots (34)$$

and $\frac{64qm + 32q^2 + 48q}{m^2 + 3m}$ for $m_M = m_K \dots\dots\dots (35)$

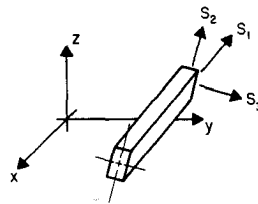
Fig. 1 shows these relations for various values of p . It is seen that with m large the operations required in the subspace iterations are of the order of a triangular factorization. But when m is small, the iterations are equivalent to many factorizations. In this case a determinant search solution algorithm is more efficient (1). Note that at convergence in the iteration a Sturm sequence check is carried out which requires one more triangular factorization.

LARGE CAPACITY SOLVER

A large capacity solver was written for the solution of systems which have practically any order and bandwidth (1). The program stores the stiffness



(a) ELEVATION OF FRAME
 DATA: YOUNG'S MODULUS = 432000, MASS DENSITY = 1.0
 FOR ALL BEAMS AND COLUMNS $A_1=3.0, I_1=I_2=I_3=1.0$
 UNITS : FT, KIPS



(b) BEAM ELEMENT DEFINITION
 S_1, S_2 AND S_3 = BEAM LOCAL AXES
 I_1, I_2 AND I_3 = FLEXURAL INERTIA ABOUT $S_1, S_2,$ AND S_3
 A_1 = AREA ASSOCIATED WITH S_1

FIG. 3.—PLANE FRAME OF EXAMPLE 1

matrix, the mass matrix, and the iteration vectors in blocks on tape (Fig. 2).

In the solution, the same number of Central Processor operations as in an in-core solution are performed. But in all operations it is now necessary to have at any one time the required matrix elements in high speed storage. In the stiffness factorization, Eq. 31, always only two blocks of K are in high speed core. To perform the reduction and back-substitution of the iteration vectors in Eq. 33, sequentially one block of the factored stiffness matrix and as many vector blocks as are necessary to reduce one block of vectors—or,

TABLE 2.—CALCULATED EIGENVALUES AND SOLUTION TIMES TAKEN IN EXAMPLE ANALYSES

Example (1)	Calculated Eigenvalues ω_i^2				Solution time, central processor sec on CDC 6400 (6)
	$i = 1$ (2)	$i = 2$ (3)	$i = 3$ (4)	$i = 4$ (5)	
Plane frame	0.589541..	5.52695..	16.5878..		24.48
Building frame	0.41537..	0.54930..	0.78606..	1.0325..	159.59

TABLE 3.—CONVERGENCE CHARACTERISTICS OF SUBSPACE ITERATIONS

Analysis (1)	Number of iteration (2)	Eigenvalue approximations (3)							
		Plane frame	1	0.5971	6.937	27.30	80.59	101.1	142.3
	2	0.5895	5.530	16.73	38.44	46.91	75.81		
	3	0.5895	5.527	16.59	35.75	42.85	67.93		
	4	0.5895	5.527	16.59	35.48	41.74	65.41		
	5	0.5895	5.527	16.59	35.43	41.38	64.44		
	6	0.5895	5.527	16.59	35.42	41.26	64.02		
Building frame	1	0.5206	0.9007	1.329	1.869	4.320	7.550	23.67	296.7
	2	0.4177	0.5529	0.7992	1.075	1.676	3.002	4.666	194.9
	3	0.4154	0.5493	0.7864	1.035	1.498	2.210	2.395	3.656
	4	0.4154	0.5493	0.7861	1.033	1.488	2.008	2.293	3.463
	5	0.4154	0.5493	0.7861	1.033	1.487	1.971	2.272	3.432
	6	0.4154	0.5493	0.7861	1.033	1.487	1.962	2.268	3.415
	7	0.4154	0.5493	0.7861	1.033	1.487	1.959	2.266	3.403
	8	0.4154	0.5493	0.7861	1.033	1.487	1.958	2.266	3.391

in the back-substitution, to obtain the new iteration vectors in one block—are taken into high speed storage. In the stiffness factorization and in the vector reductions and back-substitutions, due account is taken of the varying bandwidth of the system and of zero elements within the band.

The starting subspace is established as previously described. In each subspace iteration the projections of K and M are calculated. When m is large, relatively little more operations are required for the vector orthogonalization, and the advantage is that eigenvalue estimates are obtained in each iteration. Also, in some eigenvalue solutions, as in the analysis of frames, even good

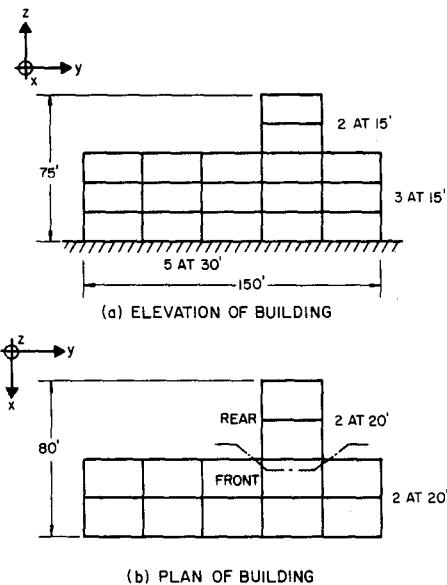
starting vectors may be nearly parallel and should be orthogonalized in the first subspace iteration. With the storage scheme adopted, a Gram-Schmidt orthogonalization would require much tape handling and is not preferable.

For the solution of the eigenvalue problem in Eq. 28, a generalized Jacobi iteration is used. In this iteration K_k and M_k are reduced simultaneously to diagonal form, without a transformation to the standard eigenvalue problem. This avoids numerical difficulties when M_k is ill-conditioned and takes advantage of the fact that K_k and M_k tend towards diagonal form as the number of subspace iterations increases.

EXAMPLE SOLUTIONS

The program described in the previous section was used for the example analyses. The solution times always include the initial factorization of the stiffness matrix, the subspace iterations and the Sturm sequence check.

Eigensolution of Plane Frame.—The three lowest eigenvalues and corresponding eigenvectors of the 9-story high and 10-bay long frame shown in Fig. 3 were calculated. The stiffness matrix was of order 297, the maximum half



DATA:

YOUNG'S MODULUS = 432000 , MASS DENSITY = 1.0
 COLUMNS IN FRONT BUILDING : $A_1 = 3.0$, $I_1 = I_2 = I_3 = 1.0$
 COLUMNS IN REAR BUILDING : $A_1 = 4.0$, $I_1 = I_2 = I_3 = 1.25$
 ALL BEAMS INTO X-DIRECTION : $A_1 = 2.0$, $I_1 = I_2 = I_3 = 0.75$
 ALL BEAMS INTO Y-DIRECTION : $A_1 = 3.0$, $I_1 = I_2 = I_3 = 1.0$
 UNITS : FT, KIP

FIG. 4.—THREE-DIMENSIONAL BUILDING FRAME OF EXAMPLE 2

bandwidth was 29, and three blocks were used. A lumped mass formulation was employed with zero masses at all rotational degrees-of-freedom. Table 2 gives the final eigenvalues calculated at convergence to a tolerance of 10^{-6} together with the solution time taken. The convergence characteristics of the subspace iteration can be observed in Table 3. Note that the calculated eigenvalues are already accurate to four digits after only three iterations. It is of interest that a Ritz analysis with five transformation vectors obtained by applying unit loads into the y -direction at levels 1, 2, 3, 4, and 5 in Fig. 3 gave as eigenvalue approximations $\omega_1^2 = 0.6113$, $\omega_2^2 = 7.320$ and $\omega_3^2 = 30.08$.

Eigensolution of Three-Dimensional Building Frame.—Fig. 4 shows the building which was analyzed for the four lowest eigenvalues and corresponding vectors. The building was idealized as an assemblage of beam elements only with six degrees-of-freedom at each joint. A lumped mass matrix was used with no mass at all rotational degrees-of-freedom. The order of the system was 468, the maximum half bandwidth was 155, and 13 blocks were used in the solution. Tables 2 and 3 give the eigenvalue approximations calculated in each iteration, the final eigenvalues at convergence to a tolerance of 10^{-6} and the solution time taken. The good convergence of the starting subspace can again be observed.

Note that in both solutions the lowest eigenvalues converge fastest and, that, in each iteration there are upper bounds to the eigenvalues of the discrete element assemblage.

CONCLUSIONS

A very efficient solution technique for large eigenvalue problems in dynamic analysis has been presented. The subspace iteration algorithm solves the eigenvalue problem directly without a transformation to the standard form. The mass matrix may be diagonal with zero elements or banded. The operation counts and the example analyses show the cost effectiveness of the solution technique. A program has been described which solves the eigenvalue problem for any system size and bandwidth. Very large systems, which generally have been analyzed using approximate techniques such as the Rayleigh-Ritz and static condensation method, can economically be solved with this solution routine.

APPENDIX I.—REFERENCES

1. Bathe, K. J., "Solution Methods for Large Generalized Eigenvalue Problems in Structural Engineering," *SESM Report 71-20*, Dept. of Civ. Engrg., Univ. of California, Berkeley, Calif., Nov., 1971.
2. Bauer, F. L., "Das Verfahren der Treppen-Iteration und Verwandte Verfahren zur Lösung Algebraischer Eigenwertprobleme," *Zeitschrift Für Angewandte Mathematik und Physik*, 1957, pp. 214-235.
3. Brönlund, O. E., "Eigenvalues of Large Matrices," Symposium on Finite Element Techniques, Institut für Statik and Dynamik der Luft und Raumfahrtskonstruktionen, University of Stuttgart, Stuttgart, Germany, June, 1969.

4. Clough, R. W., "Analysis of Structural Vibrations and Dynamic Response," *Proceedings, U.S.-Japan Symposium on Recent Advances in Matrix Methods of Structural Analysis and Design*, Tokyo, Japan, 1969.
5. Collatz, L., *The Numerical Treatment of Differential Equations*, Springer, New York, N.Y., 1966.
6. Felippa, C. A., "BANEIG—Eigenvalue Routine for Symmetric Band Matrices," Computer Programming Series, Division of Structural Engineering and Structural Mechanics, Univ. of California, Berkeley, Calif., July, 1966.
7. Gupta, K. K., "Vibration of Frames and other Structures with Banded Stiffness Matrix," *International Journal for Numerical Methods in Engineering*, Vol. 2, 1970, pp. 221-228.
8. Jennings, A., "A Direct Iteration Method of Obtaining Latent Roots and Vectors of a Symmetric Matrix," *Proceedings, Cambridge Philosophical Society*, Vol. 63, 1967, pp. 755-765.
9. Uhrig, R., "Reduction of the Number of Unknowns in the Displacement Method Applied to Kinetic Problems," *Journal of Sound and Vibration*, Vol. 4, 1966, pp. 149-155.
10. Wilkinson, J. H., *The Algebraic Eigenvalue Problem*, Clarendon Press, Oxford, England, 1965.
11. Wilson, E. L., "SAP-A General Structural Analysis Program," *Structural Engineering Laboratory Report No. 70-20*, University of California, Berkeley, Calif., Sept., 1970.
12. Wilson, E. L., and Penzien, J., "Evaluation of Orthogonal Damping Matrices," *International Journal for Numerical Methods in Engineering*, Vol. 4, 1972, pp. 5-10.
13. Zienkiewicz, O. C., *The Finite Element Method in Engineering Science*, McGraw-Hill Book Comp., London, England, 1971.

APPENDIX II.—NOTATION

The following symbols are used in this paper:

- a = vector of Ritz coordinates;
- a_i = Ritz coordinates;
- C = damping matrix;
- D = diagonal matrix;
- E_k = subspace spanned by vectors in X_k ;
- f_a, f_c = flexibility matrices defined in Eq. 20;
- i, j = indices of matrix elements;
- K = stiffness matrix;
- \tilde{K} = generalized stiffness matrix;
- K_k = projection of stiffness matrix, see Eq. 26;
- $K_{aa}, K_{cc}, K_{ac}, K_{ca}$ = submatrices of K, see Eq. 17;
- K_a = stiffness matrix obtained from K by static condensation of massless degrees-of-freedom, see Eq. 19;
- k = subscript indicating number of iteration;
- k_{ij} = element of K;
- \tilde{k}_{ij} = element of \tilde{K} , see Eq. 11;
- \tilde{L} = lower unit triangular matrix;
- \tilde{L} = Cholesky factor of K_{cc} , see Eq. 19;
- l_{ij} = element of L;
- M = mass matrix;
- \tilde{M} = generalized mass matrix;
- M_a = submatrix of M, see Eq. 17;

- m = maximum of m_K and m_M ;
 m_{ij} = element of M ;
 \tilde{m}_{ij} = element of \tilde{M} , see Eq. 12;
 m_K = half bandwidth of K ;
 m_M = half bandwidth of M ;
 n = order of stiffness and mass matrix;
 P = load vector;
 P_D = load matrix used in Ritz analysis, see Eq. 15;
 p = number of required eigenvalues and eigenvectors;
 Q_k = eigenvectors of stiffness and mass matrix projections, see Eq. 28;
 q = number of iteration vectors used;
 R_k = upper triangular matrix, see Eq. 24;
 U = upper triangular matrix;
 u, \dot{u}, \ddot{u} = displacement, velocity, and acceleration vectors;
 u_{ij} = element of U ;
 V_n = n -dimensional space in which K and M are defined;
 v = element of V_n ;
 \bar{v} = element of q -dimensional subspace of V_n , see Eq. 9;
 \bar{v}_i = eigenvector approximations calculated in Ritz analysis;
 X, \dot{X}, \ddot{X} = modal displacement, velocity, and acceleration vectors;
 X_D = displacement matrix calculated in Ritz analysis, see Eq. 15;
 X_k = iteration vectors;
 x_i = Ritz basis vector;
 Y_k = iteration vectors weighted with M ;
 Z = matrix used in the static condensation, see Eq. 19;
 Δ = damping matrix;
 ρ = Rayleigh quotient, see Eq. 8;
 ρ_i = eigenvalue approximations calculated in Ritz analysis;
 Φ = matrix of M -orthonormal eigenvectors;
 ϕ_i = M -orthonormal eigenvector;
 ψ_a, ψ_c = displacements associated with mass and massless degrees-of-freedom, see Eq. 17;
 Ω^2 = diagonal matrix storing the eigenvalues;
 Ω_k^2 = diagonal matrix storing eigenvalue approximations;
 ω_i^2 = eigenvalue and circular frequency squared; and
 $\omega_i^{(k)2}$ = approximation to ω_i^2 calculated in iteration k .

9433 LARGE EIGENVALUE PROBLEMS IN DYNAMIC ANALYSIS

KEY WORDS: Analysis; Computation; Computers; Dynamics; Eigenvalues; Eigenvectors; Engineering mechanics; Matrices (mathematics)

ABSTRACT: An effective solution technique is presented to calculate the p lowest eigenvalues and corresponding vectors in the problem $K\phi = \omega^2 M\phi$, when the order and bandwidth of the matrices is large. The eigenvalue problem is solved directly without a transformation to the standard form. The mass matrix, M , may be diagonal with zero elements as in a lumped mass analysis or may be banded as in a consistent mass formulation. The algorithm establishes q starting vectors, $q > p$, from the elements in M and K and iterates with all vectors simultaneously. This iteration is described as a subspace iteration, where best eigenvalue and eigenvector approximations can be calculated in each iteration. Operation counts are given which show the cost effectiveness of the algorithm when the bandwidth of the system is large. A program is described to solve the eigenvalue problem when the system has practically any order and bandwidth. Two example analyses are presented.

REFERENCE: Bathe, Klaus-Jurgen, and Wilson, Edward L., "Large Eigenvalue Problems in Dynamic Analysis," *Journal of the Engineering Mechanics Division*, ASCE, Vol. 98, No. EM6, Proc. Paper 9433, December, 1972, pp. 1471-1485

JOURNAL OF THE ENGINEERING MECHANICS DIVISION

EIGENSOLUTION OF LARGE STRUCTURAL SYSTEMS WITH SMALL BANDWIDTH

By Klaus-Jürgen Bathe¹ and Edward L. Wilson,² M. ASCE

INTRODUCTION

The solution of large generalized eigenvalue problems arising in dynamic and in buckling analysis of discrete parameter structural systems has attracted much attention during the last few years (1,3,4,14).

The most important eigenvalue problem arising in dynamic analysis is the calculation of the lowest eigenvalues and corresponding eigenvectors in the equation

$$\mathbf{K} \phi = \omega^2 \mathbf{M} \phi \quad (1)$$

in which \mathbf{K} = the stiffness matrix; and \mathbf{M} = the mass matrix of the system. The eigenvalues are the free vibration frequencies squared, and the eigenvectors represent the corresponding vibration mode shapes (4).

In bifurcation buckling analysis the eigenvalue problem to be solved is

$$\mathbf{K}_G \psi = \kappa \mathbf{K} \psi \quad (2)$$

in which \mathbf{K}_G = the geometric stiffness matrix of the system. The eigenvalues give the buckling loads, with the largest eigenvalue giving the lowest critical load, and the eigenvectors are the corresponding buckling modes (10).

Both generalized eigenvalue problems can be written in the form

$$\mathbf{A} \mathbf{v} = \lambda \mathbf{B} \mathbf{v} \quad (3)$$

in which \mathbf{A} and \mathbf{B} = symmetric and banded matrices. Corresponding to Eq.

Note.—Discussion open until November 1, 1973. To extend the closing date one month, a written request must be filed with the Editor of Technical Publications, ASCE. This paper is part of the copyrighted Journal of the Engineering Mechanics Division, Proceedings of the American Society of Civil Engineers, Vol. 99, No. EM3, June, 1973. Manuscript was submitted for review for possible publication on October 2, 1972.

¹Asst. Research Engr., Civ. Engrg. Dept., Univ. of California, Berkeley, Calif.

²Prof., Civ. Engrg. Dept., Univ. of California, Berkeley, Calif.

1, the matrix, A , is positive definite, the matrix, B , is either also positive definite and has the same bandwidth as A (in a consistent mass formulation) or is diagonal with possibly some zero diagonal elements (in a lumped mass formulation). Therefore, all eigenvalues are positive. Corresponding to Eq. 2, the matrix, A , is in general indefinite, the matrix, B , is positive definite and both matrices have, in general, the same bandwidth. There are in this case negative and positive eigenvalues, but it can be assumed that only the largest eigenvalue (and possibly the next smaller one) is required.

As is well known, the cost of finding the required eigensystem of Eq. 3 can be high when the order of the matrices is large. For this reason variations approximate solution techniques, such as the Ritz analysis and the static condensation method, are in use (4,11). However, recognizing the various shortcomings of these approximate techniques currently much research is being devoted towards the development of accurate and economical solution algorithms (1,3,7). As the order of the matrices is large and only the smallest or largest eigenvalues are required, solution methods which calculate all eigenvalues, such as the Householder-QR method (12) are inefficient regarding computer storage and number of operations. Instead, one of the following techniques need be considered.

One solution method is based on the fact that the leading principal minors of the matrix $A - \mu B$, in which μ is a shift, form a Sturm sequence. Specific eigenvalues can, therefore, be found by bisection exactly as first proposed by Givens for tridiagonal matrices (6). When an eigenvalue has been isolated by bisection, it can be calculated accurately using linear interpolation (7,9).

In an alternative technique the eigenvalues are calculated using the fact that they are the zeros of the polynomial $p(\mu) = \det(A - \mu B)$. To locate the zeroes of p , the Newton iteration, Muller's method, the secant method, and other techniques can be used (12). Once the required eigenvalue has been obtained accurately by some technique, two steps of inverse iteration gives the corresponding eigenvector (12).

In both these solution methods first the eigenvalue and then the eigenvector is calculated. A different strategy is adopted in inverse iteration. In this case the eigenvector is calculated first and the eigenvalue is then obtained using the Rayleigh quotient. Alternatively, if a Rayleigh quotient iteration is carried out convergence is achieved simultaneously to both an eigenvalue and the corresponding eigenvector. After calculation of an eigenpair it is necessary to deflate (in some sense) in order to insure convergence to the next required eigenvalue and eigenvector (12).

A very effective technique is the subspace iteration method, which was presented in an earlier paper (2). In this case inverse iteration is used with an orthogonalization procedure to calculate all required eigenvalues and vectors simultaneously. As was demonstrated, the technique is most efficiently used in the analysis of systems with large bandwidth. It is the aim now to present an algorithm which is very efficient in the analysis of small banded systems.

Polynomial iterations, algorithms based on the Sturm sequence property, and vector iteration techniques have been implemented on various occasions. (A list of references is found in Ref. 12). The purpose of this paper is to consider the methods in terms of their solution efficiencies and to present a combination of them as a very effective practical solution procedure.

In the design of the algorithm the question is whether to iterate first for the eigenvalue and then calculate the corresponding eigenvector, or vice versa, or whether to iterate for both of them simultaneously. Basically, the cost of a triangular factorization to the cost of a vector inverse iteration plus the total number of iterations needed to obtain convergence with the particular acceleration techniques used determine the choice. The algorithm thus arrived at combines an accelerated secant iteration, in which the Sturm sequence information is used with stationary vector inverse iteration. Example analyses using the algorithm are given in order to show typical convergence characteristics and solution times.

GENERAL CONSIDERATIONS ON FINDING EIGENPAIRS OF $A\mathbf{v} = \lambda\mathbf{B}\mathbf{v}$

Assume that an eigenvalue, λ_i , and the corresponding eigenvector, \mathbf{v}_i , satisfying Eq. 3 are required. Let the eigenvalues be ordered so that $\lambda_1 \leq \lambda_2 \leq \lambda_3 \dots \leq \lambda_n$, in which n is the order of the matrices.

A first observation is that if either member of the eigenpair λ_i, \mathbf{v}_i is given, then theoretically the other member can be obtained immediately, i.e.:

1. Given λ_i the eigenvector, \mathbf{v}_i , is obtained solving the equation $(A - \lambda_i B)\mathbf{v}_i = 0$.
2. Given \mathbf{v}_i the eigenvalue, λ_i , is $\mathbf{v}_i^T A \mathbf{v}_i / (\mathbf{v}_i^T B \mathbf{v}_i)$, in which the superscript, T , denotes transpose.

If only an acceptable approximation to either λ_i or \mathbf{v}_i is given, then a member of the eigenpair can be obtained as follows.

3. Given μ with $|\lambda_j - \mu| / |\lambda_i - \mu|$ small for all $j, j \neq i$, inverse iteration is used to calculate \mathbf{v}_i

$$(A - \mu B)\mathbf{x}_k = B\mathbf{x}_{k-1} \xi_k; \quad k = 1, 2, \dots \text{ and } \mathbf{x}_0 = \mathbf{e}^T = (1, \dots, 1) \dots \dots \dots (4)$$

in which ξ_k is selected so that $\|\mathbf{x}_k\|_2 = 1$ ($\|\mathbf{v}\|_2 = (\mathbf{v}^T B \mathbf{v})^{1/2}$). Unless $\mathbf{x}_0^T B \mathbf{v}_i = 0$ the iteration gives $\mathbf{x}_k \rightarrow \mathbf{v}_i$ as $k \rightarrow \infty$.

4. Given \mathbf{x}_k making a much smaller angle with \mathbf{v}_i than with any other eigenvector the Rayleigh quotient

$$\rho(\mathbf{x}_k) = \frac{\mathbf{x}_k^T A \mathbf{x}_k}{\mathbf{x}_k^T B \mathbf{x}_k} \dots \dots \dots (5)$$

can be computed as an approximation to λ_i . If this approximation is not satisfactory, the Rayleigh quotient iteration can be used

$$\left. \begin{aligned} [A - \rho(\mathbf{x}_{k-1}) B] \mathbf{x}_k &= B\mathbf{x}_{k-1} \xi_k \\ \text{in which } \mathbf{x}_k &\rightarrow \mathbf{v}_i, \rho(\mathbf{x}_k) \rightarrow \lambda_i \text{ as } k \rightarrow \infty \end{aligned} \right\} \dots \dots \dots (6)$$

Basically, therefore, the problem reduces to finding an approximation to either the next required eigenvalue or the corresponding eigenvector. Once an acceptable approximation has been obtained, convergence by the iteration in 3 or 4 herein is assured. Naturally, the choice of finding an approximation to the eigenvalue or the eigenvector or to both of them simultaneously depends on the relative cost of the corresponding solution procedures.

Triangular Factorization.—The basic technique to obtain an approximation

to an eigenvalue is to work with the characteristic polynomial $p(\mu) = \det(A - \mu B)$. A typical polynomial is shown in Fig. 1. The polynomial can be evaluated at μ using Gauss elimination; i.e., factorizing

$$(A - \mu B) = LDL^T \dots \dots \dots (7)$$

in which L = a lower unit triangular matrix; and D = a diagonal matrix, $p(\mu)$

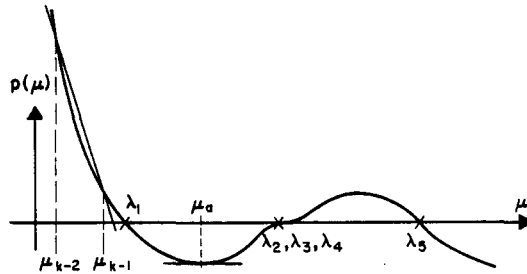


FIG. 1.—Characteristic Polynomial $p(\mu)$

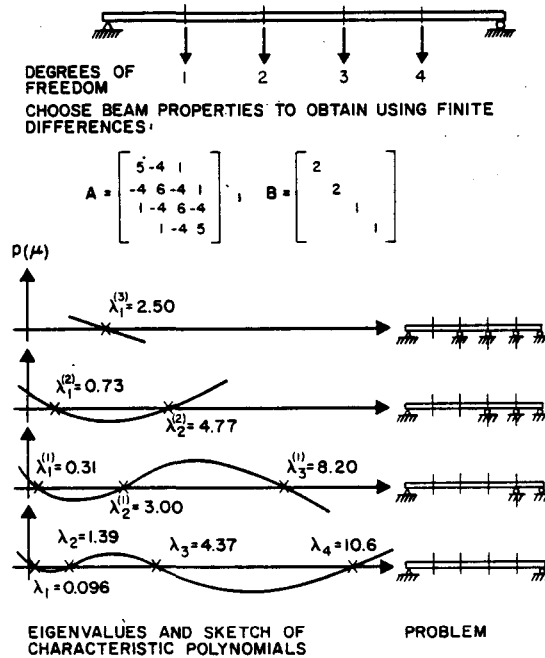


FIG. 2.—Eigenvalues of Simply Supported Beam and of Associated Constraint Problems

is the product of the diagonal elements in D, i.e.:

$$p(\mu) = \prod_{i=1}^n d_{ii} \dots \dots \dots (8)$$

As an estimate of the work involved in the evaluation of Eqs. 7 and 8 consider the number of operations. One operation is equal to one multiplication which nearly always is followed by an addition. Assume that the half bandwidths m_A and m_B of A and B, respectively, are full and constant; i.e., the bandwidth of A is $(2m_A + 1)$ and the bandwidth of B is $(2m_B + 1)$. Taking account of symmetry, i.e., working on the upper band of $A - \mu B$ (1), and neglecting terms involving the bandwidth only the number of operations required are

$$\left. \begin{aligned} \frac{1}{2} nm^2 + \frac{5}{2} nm + 2n, \quad \text{when } m = m_A = m_B \\ \frac{1}{2} nm^2 + \frac{3}{2} nm + 2n, \quad \text{when } m = m_A, m_B = 0 \end{aligned} \right\} \dots \dots \dots (9)$$

in which it must be pointed out that Gauss elimination without interchanges is used. Therefore, the stability of the decomposition is theoretically not guaranteed when $\mu > \lambda_1$, i.e., multiplier growth could occur (12) but will always be detected. As will be examined later, it is most economical to calculate in the iteration only modest approximations to the eigenvalues. Therefore, if in the algorithm to be presented unacceptable multiplier growth occurs, μ is slightly changed and another factorization is carried out. This condition has not been observed so far in extensive applications.

There are a number of different iterative methods available for calculating the eigenvalues from the knowledge of $p(\mu)$ (12). Best known are the secant method (successive linear interpolation) and the Newton method. Also much used is Muller's method (successive quadratic interpolation). The Newton iteration requiring the derivative $p'(\mu)$ has efficiently been used when A and B are tridiagonal, but for systems with larger bandwidth the method does not seem competitive (1).

In addition to the polynomial values at each triangular factorization, a very important information obtained from the Sturm sequence property of the leading principal minors of $A - \mu B$ can be used. Let $A^{(r)}$ be the matrix of order $n - r$ obtained by deleting from A the last r rows and columns; similarly define $B^{(r)}$. Then $A^{(r)} v^{(r)} = \lambda^{(r)} B^{(r)} v^{(r)}$, in which $v^{(r)}$ is a vector of order $n - r$, is the eigenvalue problem of the r th associated constraint problem (Fig. 2). It can be shown that the eigenvalues of the $r + 1$ st constraint problem separate those of the r th constraint problem (1,12), i.e., the characteristic polynomials of the eigenvalue problem $Av = \lambda Bv$ and the associated constraint problems form a Sturm sequence, as shown for the example in Fig. 2. It follows that in Eq. 7 the number of negative elements in D is equal to the number of eigenvalues smaller than μ . As will be described later, it is largely this property that made possible the design of an accelerated secant iteration as part of the solution algorithm to be presented.

Vector Iteration.—The basic technique for calculating an eigenvector is inverse iteration. Assume that the first t eigenpairs have been found and that inverse iteration with Gram-Schmidt orthogonalization is used at the shift μ to calculate the eigenvector v_i . Then one step of inverse iteration can efficiently be formulated as

$$(A - \mu B) \bar{x}_k = y_{k-1} \dots \dots \dots (10)$$

in which the triangular factorization of Eq. 7 is used to solve for \bar{x}_k ; furthermore

$$\bar{y}_k = \mathbf{B}\bar{x}_k \dots\dots\dots (11)$$

$$y_k = \frac{\bar{y}_k - \sum_{j=1}^t \alpha_j w_j}{(\bar{x}_k^T \bar{y}_k)^{1/2}} \dots\dots\dots (12)$$

in which $\alpha_j = \bar{x}_k^T w_j \dots\dots\dots (13)$

and $w_j = \mathbf{B} v_j \dots\dots\dots (14)$

The k th approximation, $\lambda_i^{(k)}$, to the required eigenvalue, λ_i , is obtained as

$$\lambda_i^{(k)} = \mu + \frac{\bar{x}_k^T y_{k-1}}{\bar{x}_k^T \bar{y}_k} \dots\dots\dots (15)$$

Convergence in the iteration is obtained when

$$\frac{|\lambda_i^{(k)} - \lambda_i^{(k-1)}|}{\lambda_i^{(k)}} \leq \text{tol} \dots\dots\dots (16)$$

in which tol should be 10^{-s} or smaller when the eigenvalues are required to s digit accuracy. In these convergence calculations no account is taken of round-off errors. The calculation of accurate error bounds is possible as given in (1,12) but in practice, accurate error bounds are probably not needed; instead s is chosen conservatively (say by two larger than the required accuracy).

Let l be the last iteration, then

$$\left. \begin{aligned} \lambda_i &\approx \lambda_i^{(l)} \\ \text{and } v_i &= \frac{\bar{x}_l}{(\bar{x}_l^T \bar{y}_l)^{1/2}} \end{aligned} \right\} \dots\dots\dots (17)$$

Noting that the w_j , $j = 1, 2, \dots, t$, are kept in high speed storage and are therefore not calculated, the total number of operations performed in Eqs. 10 to 15 are

$$\left. \begin{aligned} 4nm + 2nt + 5n, & \text{ for } m = m_A = m_B \\ 2nm + 2nt + 5n, & \text{ for } m = m_A, m_B = 0 \end{aligned} \right\} \dots\dots\dots (18)$$

Recalling that λ_i is the eigenvalue nearest to μ , (excluding the eigenvalues already calculated) the ultimate convergence rate in this iteration is $\max \{ |\lambda_j - \mu| / |\lambda_i - \mu| \}$ for all $j > t$ and $j \neq i$. The simplest scheme would use $\mu = 0.0$; however, in this case convergence is slow if eigenvalues are of nearly equal magnitude.

Very fast convergence is obtained using the Rayleigh quotient iteration in which case a new μ is evaluated in each iteration, i.e.

$$\mu_k = \mu_{k-1} + \frac{\bar{x}_k^T y_{k-1}}{\bar{x}_k^T \bar{y}_k} \dots\dots\dots (19)$$

Therefore, each iteration requires a triangular factorization plus a vector inverse iteration. Parlett and Kahan have shown that, except for a very rare theoretical

possibility, in this iteration μ_k, x_k converge cubically to an eigenpair as $k \rightarrow \infty$ (7). However, it is not easy to control to which eigenpair the iteration converges. For the objective of finding only the lower eigenvalues, it would be necessary to wait until the iteration vector has settled down and then make use of a shift strategy (1).

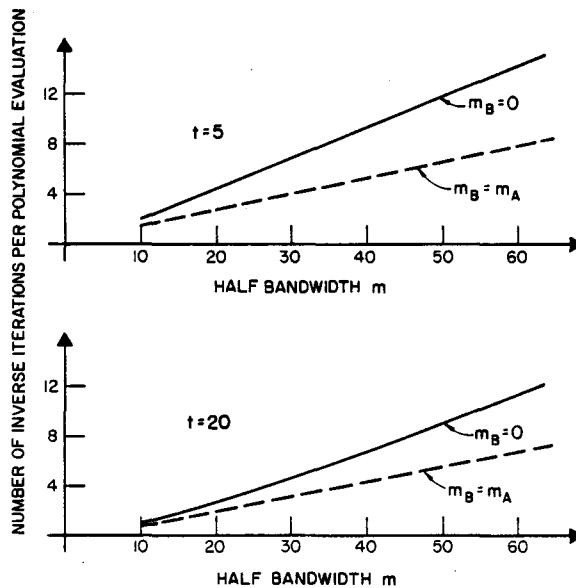


FIG. 3.—Number of Inverse Iterations per Polynomial Evaluation (t = number of vectors already calculated)

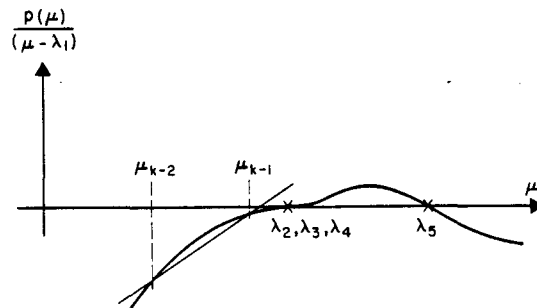


FIG. 4.— $p(\mu)$ with μ_1 Suppressed

Triangular Factorization Versus Vector Iteration.—In the choice for a polynomial or a vector iteration scheme it is important to consider the relative cost of a triangular factorization to a vector inverse iteration. Fig. 3 shows the number of inverse iterations equivalent in operations to a polynomial evaluation. For systems with small bandwidth the cost of calculating the determinant is comparable to the cost of a vector iteration, but as the bandwidth increases

vector iteration is much cheaper. In order not to limit the efficiency of the algorithm to be presented to systems with very small bandwidths it is concluded that the algorithm should use a minimum number of triangular factorizations but at the same time have a high overall solution efficiency. For this reason the solution technique developed uses a secant iteration merely to shift into the vicinity of the next required eigenvalue. The convergence rate in the vector inverse iteration is then sufficiently high to calculate the corresponding eigenpair with only a few vector iterations.

SOLUTION ALGORITHM

The algorithm solves for the smallest (or largest) eigenvalues and associated eigenvectors.

Consider the iteration for the eigenpair λ_1, v_1 which, as is pointed out later, is typical. Let μ_{k-2} and μ_{k-1} be two approximations to λ_1 , where $\mu_{k-2} < \mu_{k-1} \leq \lambda_1$ (Fig. 1). The algorithm uses an accelerated secant iteration expressed as

$$\mu_k = \mu_{k-1} - \eta \frac{p(\mu_{k-1})}{p(\mu_{k-1}) - p(\mu_{k-2})} (\mu_{k-1} - \mu_{k-2}) \dots \dots \dots (20)$$

in which η is a constant. When $\eta = 1$ this is the standard secant iteration, in which $\mu_k \rightarrow \lambda_1$ as $k \rightarrow \infty$. Convergence in this iteration can be slow. However, for the objective of obtaining only a shift near λ_1 the algorithm uses $\eta \geq 2$. For $\eta = 2$ it is known that $\mu_k \leq \mu_a$ in which μ_a is the smallest stationary point of p (12). Thus the iteration with $\eta = 2$ can only jump over one root, which would be detected by a sign change in p ; but it must be observed that in case λ_1 is a multiple root the iteration can still be slow.

If the only information available is the value of p then it is vitally important that the iteration not be able to jump over more than one root. It would be impossible to detect when a number of roots had been passed. Fortunately, the triangular factorization at μ_k also yields the number of eigenvalues smaller than μ_k . Therefore, there is no restriction to $\eta = 2$ and the iteration can be accelerated further. In the algorithm η is doubled after each iteration in which the iterates did not change in their two most significant digits, i.e., when the correction to the current shift is already relatively small. The iteration may thus jump over a single root, a multiple root or into a cluster of roots, but this is always detected by counting the number of negative diagonal elements in the triangular factorization. Also, with the strategy adopted the algorithm cannot jump far beyond the unknown roots.

Once it has been established that the secant iteration jumped over one or more unknown eigenvalues, vector inverse iteration is used to calculate the eigenvalues and eigenvectors accurately as described in Eqs. 10-16. Except in rare cases, no Rayleigh quotient shift is carried out, because once the iteration vector is an approximation to the eigenvector sought convergence is rapid, and another factorization would be inefficient. Note that in this iteration eigenvectors corresponding to eigenvalues larger than μ_k may be calculated if μ_k lies in an eigenvalue cluster. This is hardly a disadvantage because these eigenvalues and eigenvectors are probably required anyway.

As the aim is to merely obtain a shift near the next unknown eigenvalue, it may happen that before any jump occurs two successive iterates in Eq. 20 do not differ any more in their six most significant digits. The last iterate is then accepted as the place at which to switch to inverse iteration.

This iteration for λ_1 and v_1 is typical because the advantage of the one-sided approach to the root is also obtained for any other eigenpair, say λ_{j+1} , v_{j+1} , by using instead of $p(\mu)$ in Eq. 20 the deflated polynomial $p_j(\mu)$ (Fig. 4) in which

$$p_j(\mu) = \frac{p(\mu)}{\prod_{i=1}^j (\mu - \lambda_i^{(j)})} \dots \dots \dots (21)$$

Therefore, to iterate towards the next unknown eigenvalue, Eq. 21 is used to suppress all calculated eigenvalues from two previously obtained polynomial values which are the starting points in Eq. 20. Note that in order not to divide in Eq. 21 by values close to zero, two μ - values need be selected which are far enough from the calculated roots.

A few practical details are worth mentioning:

1. A principal advantage of this solution procedure is that each eigenpair is essentially obtained independently from all those previously calculated. Eigenvalues and eigenvectors, therefore, need not be calculated to very high precision as is the case when an explicit matrix deflation procedure is used (12). If a not very high accuracy is required the errors in earlier computed eigenpairs will not prevent attaining the required accuracy in the remaining eigenvalues and eigenvectors.

2. At a shift near the next required eigenvalue Gram-Schmidt orthogonalization to all previously calculated eigenvectors is not necessary. Allowing for multiple eigenvalues in the program developed the iteration vector is only orthogonalized to the last six calculated eigenvectors.

3. Note that in practical examples $p(\mu)$ can be much larger than the overflow of the computer; therefore a scale factor need be introduced in the evaluation of Eq. 8.

4. To start the secant iteration two lower bounds on λ_1 are needed. The first bound is $\mu_1 = 0.0$; the other bound is obtained from an approximation to v_1 calculated by vector inverse iteration at μ equal to zero. Assume that x_k is the iteration vector after k inverse iterations, then the following μ_2 can be used

$$\mu_2 = (1 - 0.01) \frac{x_k^T A x_k}{x_k^T B x_k} \dots \dots \dots (22)$$

It may happen that μ_2 is larger than λ_1 . However, this is detected by the Sturm sequence count in the factorization at μ_2 . Let γ be the number of negative pivots in the triangular factorization then μ_2 is divided by $(\gamma + 1)$ until γ equals zero.

5. The algorithm is most efficiently used in an in-core solution routine. Because a few triangular factorizations are required in the calculation of each

eigenpair, a relatively great deal of Peripheral Processor (tape and disc reading and writing) time would be required in an out-of-core solution (1,2). Since the algorithm has been designed for the analysis of small banded systems, on reasonable size computers relatively large order systems can be solved in high speed storage.

Calculation of Largest Eigenvalues and Corresponding Eigenvectors.—The procedure for the calculation of the largest eigenvalues and associated eigenvectors in a buckling analysis using Eq. 3 should be mentioned. In this case the solution scheme is modified to iterate from the right towards λ_n . As the starting value μ_1 , the quantity $\|A\|/\lambda_{1B}$ is used, in which λ_{1B} is the smallest eigenvalue of **B** and $\|A\|$ is any convenient norm of **A**. Only an approximation for λ_{1B} is required which is obtained from an approximation to the least dominant eigenvec-

TABLE 1.—Analysis of Plane Frame— $n = 297$; $m_A = 29$; $m_B = 0$

Eigenvalues (1)	Number of polynomial evaluations (2)	Number of vector iterations (3)	Central processor seconds (4)	Computer used (5)
0.589541280301	3	8	9.1	CDC 6400
5.52695591012	5	5	12.3	
16.5878695983	8	4	18.2	

TABLE 2.—Analysis of Piping System— $n = 566$; $m_A = 11$; $m_B = 0$

Eigenvalues (1)	Number of polynomial evaluations (2)	Number of vector iterations (3)	Central processor seconds (4)	Computer used (5)
19.2365110867	4	13	2.2	CDC 6600
40.6501461634	1	8	1.0	
97.5359717709	3	5	1.3	
188.081456300	1	7	1.0	
480.676129205	5	4	1.8	
593.988388279	1	7	1.1	

TABLE 3.—Sturm-Liouville Problem— $n = 200$; $m_A = 3$; $m_B = 3$

Eigenvalues (1)	Number of polynomial evaluations (2)	Number of vector iterations (3)	Central processor seconds (4)	Computer used (5)
79.7492188875	4	11	1.8	CDC 6400
238.742921619	8	4	1.3	
396.722312473	8	4	1.3	
553.677579972	8	4	1.3	

tor of \mathbf{B} . If $\mu_1 < \lambda_n$ the shift is increased until in the factorization, Eq. 7, all elements d_{ii} are negative.

EXAMPLE ANALYSES

An in-core solution routine for the calculation of the smallest eigenvalues and corresponding eigenvectors has been incorporated into a dynamic analysis program (1,13). To obtain relatively high precision in the eigenvalues and vectors $\text{tol} = 10^{-12}$ is used in the convergence calculations (see Eq. 16). From many different analyses the results of two typical cases are summarized in Tables 1 and 2, where also the necessary informations about the system sizes and the bandwidths are given. Table 1 refers to a nine-story 10-bay frame, which was already analyzed in Ref. 2. The solution of a piping system is described in Table 2. In both analyses a lumped mass formulation was used. Experience shows that in general about six secant steps and six inverse iterations are required for the solution of an eigenpair.

Table 3 refers to a less practical but instructive finite element solution for the smallest eigenvalues and corresponding eigenvectors of a Sturm Liouville problem (5). Both matrices have in this case the same bandwidth.

CONCLUSIONS

For the solution of the eigenvalue problems in mode superposition and bifurcation buckling analysis, accurate and more economical algorithms are required. In the analysis of small banded systems the evaluation of the characteristic polynomial is not much more costly than a vector iteration. For the design of an optimum algorithm the choice lies, therefore, between polynomial iteration schemes, vector iteration methods, and in particular, combinations of these techniques. In this paper, a very effective solution technique which uses an accelerated secant iteration with Sturm sequence information and vector inverse iteration has been presented.

ACKNOWLEDGMENTS

The writers would like to thank B. N. Parlett, Department of Computer Science, University of California, Berkeley, Calif. for many helpful suggestions during this research work.

APPENDIX I.—REFERENCES

1. Bathe, K. J., "Solution Methods for Large Generalized Eigenvalue Problems in Structural Engineering," *SESM Report No. 71-20*, University of California, Berkeley, Calif., 1971.
2. Bathe, K. J., and Wilson, E. L., "Large Eigenvalue Problems in Dynamic Analysis," *Journal of the Engineering Mechanics Division*, ASCE, Vol. 98, No. EM6, Proc. Paper 9433, Dec., 1972, pp. 1471-1485.
3. Brönlund, O. E., "Eigenvalues of Large Matrices," Symposium on Finite Element Techniques, Institut für Statik und Dynamik der Luft-und Raumfahrtkonstruktionen, University of Stuttgart, Stuttgart, Germany, 1969.
4. Clough, R. W., "Analysis of Structural Vibrations and Dynamic Response," *Proceedings*, U.S.-Japan Symposium, Recent Advances in Matrix Methods of Structural Analy-

- sis and Design, University of Alabama Press, University of Alabama, Huntsville, Ala., 1971.
5. Courant, R., and Hilbert, D., *Methods of Mathematical Physics*, Vol. 1, Interscience Publishers, New York, N.Y., 1953.
 6. Givens, J. W., "A Method of Computing Eigenvalues and Eigenvectors Suggested by Classical Results on Symmetric Matrices," National Bureau of Standards Applied Mathematics Series No. 29, U.S. Government Printing Office, Washington, D.C., 1953.
 7. Gupta, K. K., "Vibration of Frames and Other Structures with Banded Stiffness Matrix," *International Journal for Numerical Methods in Engineering*, Vol. 2, 1970, pp. 221-228.
 8. Parlett, B. N., and Kahan, W., "On the Convergence of a Practical QR Algorithm," *Proceedings of the International Federation for Information Processing Congress*, 1968.
 9. Peters, G., and Wilkinson, J. H., " $Ax = \lambda Bx$ and the Generalized Eigenvalue Problem," *Society for Industrial and Applied Mathematics Journal of Numerical Analysis*, Vol. 7, 1970, pp. 479-492.
 10. Rubinstein, M. F., *Structural Systems—Statics, Dynamics and Stability*, Prentice Hall, Inc., Englewood Cliffs, N.J., 1970.
 11. Uhrig, R., "Reduction of the Number of Unknowns in the displacement Method applied to Kinetic Problems," *Journal of Sound and Vibration*, Vol. 4, 1966, pp. 149-155.
 12. Wilkinson, J. H., *The Algebraic Eigenvalue Problem*, Clarendon Press, Oxford, England, 1965.
 13. Wilson, E. L., "SAP-A General Structural Analysis Program," *SESM Report No. 70-20*, University of California, Berkeley, Calif., 1970.
 14. Zienkiewicz, O. C., *The Finite Element Method in Engineering Science*, McGraw-Hill Book Co., London, England, 1971.

APPENDIX II.—NOTATION

The following symbols are used in this paper:

- A = matrix of order n in generalized eigenvalue problem considered;
- B = matrix of order n in generalized eigenvalue problem considered;
- D = diagonal matrix;
- d_{ii} = i th diagonal element of D;
- K = stiffness matrix;
- K_G = geometrix stiffness matrix;
- k = subscript indicating number of iteration (superscript in brackets when quantity has already subscript);
- i, j = subscripts indicating number of eigenvalue or eigenvector;
- L = lower unit triangular matrix, see Eq. 7;
- l = subscript indicating last iteration;
- M = mass matrix;
- m = maximum of m_A and m_B ;
- m_A = half bandwidth of A;
- m_B = half bandwidth of B;
- n = order of matrices;
- $p(\mu) = \det(A - \mu B)$ = characteristic polynomial;

- $p_j(\mu)$ = characteristic polynomial with λ_1 to λ_j suppressed see Eq. 21;
 t = number of eigenvectors already calculated;
 tol = convergence tolerance, see Eq. 16;
 \mathbf{v}_i = i th **B**-orthonormalized eigenvector;
 \mathbf{w}_i = i th **B**-orthonormalized eigenvector weighted with **B**, see Eq. 14;
 $\mathbf{x}_k, \bar{\mathbf{x}}_k$ = iteration vectors obtained in k th iteration;
 $\mathbf{y}_k, \bar{\mathbf{y}}_k$ = iteration vectors $\mathbf{x}_k, \bar{\mathbf{x}}_k$ weighted with **B**, see Eq. 11;
 α = constant defined in Eq. 13;
 η = constant used in accelerated secant iteration, see Eq. 20;
 κ = eigenvalue calculated in buckling analysis, see Eq. 2;
 λ_i = i th eigenvalue of generalized eigenvalue problem;
 μ_k = shift calculated in k th iteration;
 ξ_k = normalizing factor in k th inverse iteration, see Eq. 4;
 ρ = Rayleigh quotient defined in Eq. 5;
 ϕ = eigenvector calculated in dynamic analysis, see Eq. 1;
 ψ = eigenvector calculated in buckling analysis, see Eq. 2;
 and
 ω^2 = eigenvalue calculated in dynamic analysis, see Eq. 1.

9782 EIGENSOLUTION OF SYSTEMS WITH SMALL BANDWIDTH

KEY WORDS: Buckling; Computation; Computers; Dynamics; Eigenvalues; Eigenvectors; Engineering mechanics; Matrices (mathematics); Structural analysis

ABSTRACT: The basic techniques for the accurate calculation of the smallest (largest) eigenvalues and coresponding eigenvectors in large generalized eigenvalue problems arising in dynamic and buckling analysis are considered. This leads to the design of a very efficient practical algorithm when the system has small bandwidth. The solution technique combines an accelerated secant iteration in which the Sturm sequence of the leading principal minors is used with vector inverse iteration. Example analyses are presented to show typical convergence characteristics and solution times.

REFERENCE: Bathe, Klaus-Jurgen, and Wilson, Edward L., "Eigensolution of Large Structural Systems with Small Bandwidth," *Journal of the Engineering Mechanics Division*, ASCE, Vol. 99, No. EM3, Proc. Paper 9782, June, 1973, pp. 467-479

SOLUTION METHODS FOR EIGENVALUE PROBLEMS IN STRUCTURAL MECHANICS

KLAUS-JÜRGEN BATHE* AND EDWARD L. WILSON†
University of California, Berkeley, California, U.S.A.

SUMMARY

A survey of probably the most efficient solution methods currently in use for the problems $\mathbf{K}\phi = \omega^2\mathbf{M}\phi$ and $\mathbf{K}\psi = \lambda\mathbf{K}_G\psi$ is presented. In the eigenvalue problems the stiffness matrices \mathbf{K} and \mathbf{K}_G and the mass matrix \mathbf{M} can be full or banded; the mass matrix can be diagonal with zero diagonal elements. The choice is between the well-known QR method, a generalized Jacobi iteration, a new determinant search technique and an automated subspace iteration. The system size, the bandwidth and the number of required eigenvalues and eigenvectors determine which method should be used on a particular problem. The numerical advantages of each solution technique, operation counts and storage requirements are given to establish guidelines for the selection of the appropriate algorithm. A large number of typical solution times are presented.

INTRODUCTION

In the dynamic response analysis of an assemblage of structural elements using conventional mode superposition the generalized eigenvalue problem

$$\mathbf{K}\phi = \omega^2\mathbf{M}\phi \quad (1)$$

is considered. In this equation \mathbf{K} is the stiffness matrix and \mathbf{M} is the mass matrix of the element assemblage, both are of order n .^{7,20} The n solutions to equation (1) can be written as

$$\mathbf{K}\Phi = \mathbf{M}\Phi\Omega^2 \quad (2)$$

where the columns in Φ are the \mathbf{M} -orthonormalized eigenvectors (free vibration modes) ϕ_1, \dots, ϕ_n and Ω^2 is a diagonal matrix listing the eigenvalues $\omega_1^2, \dots, \omega_n^2$ (free vibration frequencies squared).

Considering the complete dynamic analysis the most time consuming phase is usually the solution of the eigenvalue problem. For a most efficient solution it is necessary to take maximum advantage of the special properties of the matrices \mathbf{K} and \mathbf{M} and the specific solution requirements.

It is of particular importance that in structural analysis both matrices \mathbf{K} and \mathbf{M} are banded, i.e.

$$\left. \begin{aligned} k_{ij} &= 0 & \text{for } j > i + m_{\mathbf{K}} \\ m_{ij} &= 0 & \text{for } j > i + m_{\mathbf{M}} \end{aligned} \right\} \quad (3)$$

where $(2m_{\mathbf{K}} + 1)$ and $(2m_{\mathbf{M}} + 1)$ are the bandwidths of the matrices \mathbf{K} and \mathbf{M} , respectively. Assuming that all rigid body modes have been removed from the system, \mathbf{K} is positive definite. If in a finite element formulation a consistent mass matrix is used, \mathbf{M} is also positive definite and $m_{\mathbf{M}} = m_{\mathbf{K}}$. In a lumped mass analysis \mathbf{M} is diagonal with m_{ii} positive or zero.^{7,20}

With regard to solution requirements it is usually not necessary to include in the mode superposition analysis the response in all modes. Many structures respond to particular types of dynamic loading primarily in a few modes, and the contribution of the other modes can be neglected. Also, the element assemblage must have been selected such that its lower frequencies and vibration mode shapes can accurately represent the structural response.¹ Therefore, in the solution of the eigenvalue problem we may reduce the numerical effort by only solving for the required lowest eigenvalues and corresponding eigenvectors.

* Assistant Research Engineer.

† Professor of Civil Engineering.

*Received 24 June 1972
Revised 4 September 1972*

Another generalized eigenvalue problem arises in buckling analysis. The equations governing buckling of an assemblage of structural elements are

$$\mathbf{K}\psi = \lambda\mathbf{K}_G\psi \quad (4)$$

where \mathbf{K} is the small deflection stiffness matrix used in equation (1) and \mathbf{K}_G , which is always banded, is the geometric stiffness matrix of the element system. The eigenvalues give the buckling loads and the eigenvectors represent the corresponding buckling modes.¹⁷ Because \mathbf{K}_G is in general indefinite, equation (4) is re-written as

$$\mathbf{K}_G\psi = \kappa\mathbf{K}\psi \quad (5)$$

where $\kappa = 1/\lambda$ and can be negative or positive. In this equation the maximum value of κ is required (and possibly the next lowest values) which gives the lowest buckling load. Using a shift which is an upper bound on the maximum eigenvalue in equation (5), the problem is to determine the eigenvalue nearest to the shift.³

Many different solution procedures have been developed for eigenvalue problems in general, see Reference 19 for a list of references. More specifically of interest are the solution methods surveyed by Peters and Wilkinson¹⁶ and Brönlund.⁶ Reference should also be made to the work by Bauer,⁵ Dong and others,⁸ Jennings,¹² Jennings and Orr,¹³ Gupta,¹¹ Felippa¹⁰ and Rutishauser.¹⁸ With a large number of different solution techniques available it need be noted that for the specific eigenvalue problems considered here, there is no single algorithm which always provides an efficient solution; however, it is only necessary to choose between a few most effective techniques.

The purpose of this paper is to summarize the probably most efficient solution techniques currently in use and to establish guidelines for the selection of the appropriate solution method for a given problem. The methods under consideration are the Householder-QR-inverse iteration technique,¹⁹ a generalized Jacobi iteration,^{2,9} a determinant search method^{2,3} and an automated subspace iteration.^{2,4} Only the basic steps of these solution methods are presented, where it is hoped that a structural analyst with relatively little experience in eigenvalue solution techniques can follow the exposition. The development of the individual techniques and their detailed relationships to other methods are given in the references.

The proper choice of solution method is most important in the analysis of large systems; however, the guidelines given are general and apply to the solution of any order eigenvalue problem. The numerical advantages of each of the solution methods are discussed. The high speed storage requirements and the number of operations needed for solution largely determine which of the methods is most efficient in specific practical problems. Typical solution times using the algorithms in a wide spectrum of practical analyses are presented in order to emphasize the recommendations given for their use.

As will be apparent later, there is little difficulty in choosing the appropriate algorithm in buckling analysis. For this reason, in the next sections specifically the solution of the problem $\mathbf{K}\phi = \omega^2\mathbf{M}\phi$ is discussed; however, guidelines for the choice of algorithm in the solution of buckling problems also follow.

TRANSFORMATION OF GENERALIZED EIGENVALUE PROBLEM TO STANDARD EIGENVALUE PROBLEM

Much attention has been given to the solution of the standard eigenvalue problem.¹⁹ The solution procedures developed can be used if the more general form of the eigenvalue problem

$$\mathbf{K}\phi = \omega^2\mathbf{M}\phi \quad (6)$$

is first transformed to the standard form.

Assume that \mathbf{M} is positive definite, then if $\mathbf{M} = \mathbf{S}\mathbf{S}^T$ for any non-singular matrix \mathbf{S} , the problem in equation (6) is equivalent to the solution of the standard eigenvalue problem

$$\tilde{\mathbf{K}}\tilde{\phi} = \omega^2\tilde{\phi} \quad (7)$$

where

$$\tilde{\mathbf{K}} = \mathbf{S}^{-1}\mathbf{K}\mathbf{S}^{-T}, \quad \tilde{\phi} = \mathbf{S}^T\phi \quad (8)$$

It is computationally efficient to use as \mathbf{S} the Cholesky factor $\bar{\mathbf{L}}_{\mathbf{M}}$ of \mathbf{M} , i.e. $\mathbf{M} = \bar{\mathbf{L}}_{\mathbf{M}} \bar{\mathbf{L}}_{\mathbf{M}}^T$. The transformation is then a stable process provided \mathbf{M} is well-conditioned with respect to inversion. However, if \mathbf{M} is ill-conditioned the transformation process is also ill-conditioned; namely, as \mathbf{M} becomes semi-definite, the system has very large eigenvalues and as $\omega_n^2 \ll \|\bar{\mathbf{L}}_{\mathbf{M}}^{-1} \mathbf{K} \bar{\mathbf{L}}_{\mathbf{M}}^{-T}\|$ † the elements in $\bar{\mathbf{K}}$ are large and the eigenvalues of normal size are determined inaccurately.

Another transformation matrix \mathbf{S} is obtained using the spectral decomposition of \mathbf{M} , i.e. $\mathbf{M} = \mathbf{R} \mathbf{D}^2 \mathbf{R}^T$, in which case $\mathbf{S} = \mathbf{R} \mathbf{D}$, where the columns in \mathbf{R} are the eigenvectors and \mathbf{D}^2 is a diagonal matrix with the eigenvalues of \mathbf{M} . The use of this transformation matrix has an advantage because an ill-conditioning of \mathbf{M} may now be concentrated in only a few small elements of \mathbf{D} . Then in $\bar{\mathbf{K}}$ only those rows and columns corresponding to the small elements in \mathbf{D} will have large elements and the eigenvalues of normal size are more likely to be preserved.

It is important to note that $\bar{\mathbf{K}}$ has the same bandwidth as \mathbf{K} when \mathbf{M} is diagonal. In this case both transformation procedures give $\bar{\mathbf{K}} = \mathbf{M}^{-1} \mathbf{K} \mathbf{M}^{-1}$, and the transformation is very cheap. However, consider that \mathbf{M} is not a diagonal matrix; then the Cholesky transformation is still quite economical, but $\bar{\mathbf{K}}$ is full, and if the order of the matrices is large, the solution of the standard eigenvalue problem in equation (7) can be very expensive.

It should also be pointed out that if \mathbf{M} is ill-conditioned we may consider the problem $\mathbf{M} \phi = (1/\omega^2) \mathbf{K} \phi$ and use a decomposition of \mathbf{K} instead. However, \mathbf{K} is banded and therefore the transformation always leads to a full matrix.

STATIC CONDENSATION

The transformation of the generalized eigenvalue problem $\mathbf{K} \phi = \omega^2 \mathbf{M} \phi$ to the standard eigenvalue problem $\bar{\mathbf{K}} \bar{\phi} = \omega^2 \bar{\phi}$ can only be carried out when \mathbf{M} is positive definite. In lumped mass analysis \mathbf{M} can have in general zero elements on the diagonal. In this case it is necessary to use first static condensation on the massless degrees of freedom.

Re-writing equation (6) as

$$\begin{bmatrix} \mathbf{K}_{aa} & \mathbf{K}_{ac} \\ \mathbf{K}_{ca} & \mathbf{K}_{cc} \end{bmatrix} \begin{bmatrix} \phi_a \\ \phi_c \end{bmatrix} = \omega^2 \begin{bmatrix} \mathbf{M}_a & \mathbf{0} \\ \mathbf{0} & \mathbf{0} \end{bmatrix} \begin{bmatrix} \phi_a \\ \phi_c \end{bmatrix} \quad (9)$$

where \mathbf{M}_a is positive definite, we obtain the reduced generalized eigenvalue problem

$$\mathbf{K}_a \phi_a = \omega^2 \mathbf{M}_a \phi_a \quad (10)$$

where

$$\mathbf{K}_a = \mathbf{K}_{aa} - \mathbf{K}_{ac} \mathbf{K}_{cc}^{-1} \mathbf{K}_{ca} \quad (11)$$

and

$$\phi_c = -\mathbf{K}_{cc}^{-1} \mathbf{K}_{ca} \phi_a \quad (12)$$

In practice \mathbf{K}_a can be obtained as follows

$$\mathbf{K}_{cc} = \bar{\mathbf{L}}_c \bar{\mathbf{L}}_c^T, \quad \bar{\mathbf{L}}_c \mathbf{Y} = \mathbf{K}_{ca}, \quad \mathbf{K}_a = \mathbf{K}_{aa} - \mathbf{Y}^T \mathbf{Y} \quad (13)$$

where $\bar{\mathbf{L}}_c$ is the Cholesky factor of \mathbf{K}_{cc} .

Instead of using equation (10), alternatively, a flexibility matrix \mathbf{F}_a corresponding to the mass degrees of freedom, i.e. $\mathbf{F}_a = \mathbf{K}_a^{-1}$, could be calculated.² The eigenvalue problem then to be considered is $(1/\omega^2) \phi_a = \mathbf{F}_a \mathbf{M}_a \phi_a$, which using a factorization of \mathbf{M}_a can obviously also be transformed to the standard form.

Although the order of the matrices in the eigenvalue problem has been reduced, matrix \mathbf{K}_a (and certainly \mathbf{F}_a) is in general full. To decrease computational requirements in the solution of equation (10) the mass of

† ||| denotes any norm.

the structure may have been lumped at only a few degrees of freedom. This can be appropriate in the analysis of some structures, such as high-rise buildings. However, depending on the engineer's experience, in the analysis of complex structures the calculated eigensystem may then only be a very crude approximation to the required eigensystem of the actual structure.

HOUSEHOLDER-QR-INVERSE ITERATION SOLUTION

A very efficient procedure, which is probably regarded as the best method for finding the complete eigensystem of $\bar{\mathbf{K}}$ in equation (7), is the Householder-QR-inverse iteration solution.¹⁹ The name suggests the following three solution steps:

1. Householder transformations are used to reduce the matrix to tridiagonal form.
2. QR iteration yields the eigenvalues.
3. Using inverse iteration the eigenvectors of the tridiagonal matrix are calculated and transformed to the eigenvectors of $\bar{\mathbf{K}}$.

The Householder reduction

The Householder reduction to tridiagonal form involves $(n-2)$ orthogonal similarity transformations

$$\bar{\mathbf{K}}_{k+1} = \mathbf{P}_k^T \bar{\mathbf{K}}_k \mathbf{P}_k, \quad k = 1, 2, \dots, n-2, \quad \bar{\mathbf{K}}_1 = \bar{\mathbf{K}} \quad (14)$$

where

$$\mathbf{P}_k = \mathbf{I} - \theta \mathbf{w}_k \mathbf{w}_k^T \quad (15)$$

$$\theta = \frac{2}{\mathbf{w}_k^T \mathbf{w}_k} \quad (16)$$

Consider the case $k = 1$, which is typical. Let

$$\mathbf{P}_1 = \left[\begin{array}{c|c} 1 & \mathbf{0} \\ \hline \mathbf{0} & \bar{\mathbf{P}}_1 \end{array} \right], \quad \mathbf{w}_1 = \left[\begin{array}{c} 0 \\ \bar{\mathbf{w}}_1 \end{array} \right]$$

and

$$\bar{\mathbf{K}}_1 = \left[\begin{array}{c|c} \bar{k}_{11} & \bar{\mathbf{k}}_1^T \\ \hline \bar{\mathbf{k}}_1 & \bar{\mathbf{K}}_{11} \end{array} \right]$$

Then

$$\bar{\mathbf{K}}_2 = \left[\begin{array}{c|c} \bar{k}_{11} & \bar{\mathbf{k}}_1^T \bar{\mathbf{P}}_1 \\ \hline \bar{\mathbf{P}}_1^T \bar{\mathbf{k}}_1 & \bar{\mathbf{P}}_1^T \bar{\mathbf{K}}_{11} \bar{\mathbf{P}}_1 \end{array} \right] \quad (17)$$

The vector $\bar{\mathbf{w}}_1$ is determined from the condition

$$(\mathbf{I} - \theta \bar{\mathbf{w}}_1 \bar{\mathbf{w}}_1^T) \bar{\mathbf{k}}_1 = \pm \|\bar{\mathbf{k}}_1\|_2 \mathbf{e}_1 \dagger \quad (18)$$

where \mathbf{e}_1 is the $(n-1)$ dimensional unit vector, i.e., $\mathbf{e}_1^T = [1 \ 0 \ 0 \ \dots \ 0]$. It is only necessary to solve from equation (18) for a multiple of $\bar{\mathbf{w}}_1$, and we can use

$$\bar{\mathbf{w}}_1 = \bar{\mathbf{k}}_1 + \text{sign}(\bar{k}_{21}) \|\bar{\mathbf{k}}_1\|_2 \mathbf{e}_1 \quad (19)$$

The equivalent steps for $k = 2, 3, \dots, n-2$ are obvious.

In the calculations we can use the symmetry property of $\bar{\mathbf{K}}$ and store only the lower triangular part of the matrix. Also, we can use the storage locations of the elements which are zeroed in the reduction in order to store the \mathbf{w}_k for the calculation of the eigenvectors.

† $\|\cdot\|_2$ denotes Euclidean norm.

The QR iteration

Consider now the QR iteration with shifts on the tridiagonal matrix $\tilde{\mathbf{K}}_{n-1}$, which we call \mathbf{T}_1 . The iteration is as follows

$$\mathbf{T}_k - \mu_k \mathbf{I} = \mathbf{Q}_k \mathbf{R}_k \quad (20)$$

$$\mathbf{T}_{k+1} = \mathbf{R}_k \mathbf{Q}_k + \mu_k \mathbf{I}, \quad k = 1, 2, \dots \quad (21)$$

where \mathbf{Q}_k is an orthogonal matrix, \mathbf{R}_k is an upper triangular matrix and μ_k is the shift. In each iteration we perform an orthogonal similarity transformation

$$\mathbf{T}_{k+1} = \mathbf{Q}_k^T \mathbf{T}_k \mathbf{Q}_k \quad (22)$$

and then

$$\mathbf{T}_{k+1} \rightarrow \Omega^2 \quad \text{as } k \rightarrow \infty$$

Regarding the convergence of the iteration it can be shown that the QR iteration is intimately related to the probably more familiar inverse iteration.¹⁹ In particular, the QR iteration with μ_k properly chosen corresponds to the Rayleigh quotient iteration, which converges cubically in the neighbourhood of an eigenvalue.¹⁵ In the iteration the eigenvalues are not found in order of their magnitudes and it is usual practice to calculate them all. Ortega and Kaiser¹⁴ have developed explicit formulae which relate the elements in \mathbf{T}_{k+1} to the elements in \mathbf{T}_k .

Solution of eigenvectors

Once the eigenvalues have been obtained to full machine precision we calculate only the required eigenvectors of \mathbf{T}_1 by simple inverse iteration with shifts equal to the corresponding eigenvalues. Two steps of inverse iteration are usually sufficient. These vectors need be transformed with the Householder transformations used to obtain the eigenvectors of $\tilde{\mathbf{K}}$.

Table I summarizes the Householder-QR-inverse iteration algorithm and gives the high speed storage and number of operations required for solution. In the operation counts one operation is assumed to consist of one multiplication which nearly always is followed by an addition.

Table I. Summary of Householder-QR-inverse iteration solution

Operation	Calculation	Number of operations	Required storage
Householder transformations	$\tilde{\mathbf{K}}_{k+1} = \mathbf{P}_k^T \tilde{\mathbf{K}}_k \mathbf{P}_k, \quad k = 1, 2, \dots, n-2$ $\tilde{\mathbf{K}}_1 = \tilde{\mathbf{K}}$	$\frac{3}{2}n^3 + \frac{3}{2}n^2$	
QR iterations	$\mathbf{T}_{k+1} = \mathbf{Q}_k^T \mathbf{T}_k \mathbf{Q}_k, \quad k = 1, 2, \dots$ $\mathbf{T}_1 = \tilde{\mathbf{K}}_{n-1}$	$9n^2$	Using symmetry of matrix
Calculation of p eigenvectors	$(\tilde{\mathbf{K}}_{n-1} - \omega_i^2 \mathbf{I}) \mathbf{x}_i^{(k+1)} = \mathbf{x}_i^{(k)}, \quad k = 1, 2$ $i = 1, 2, \dots, p$	$10pn$	$\frac{1}{2}[n(n+1)] + 6n$
Transformation of eigenvectors	$\tilde{\phi}_i = \mathbf{P}_1 \dots \mathbf{P}_{n-2} \mathbf{x}_i^{(3)}, \quad i = 1, 2, \dots, p$	$pn(n-1)$	
Total for all eigenvalues and p eigenvectors		$\frac{3}{2}n^3 + \frac{3}{2}n^2 + pn^2 + 9pn$	

As was noted above, the complete solution of the generalized eigenvalue problem requires static condensation of the massless degrees of freedom and the transformation to the standard eigenvalue problem. The storage requirements and operations for these calculations are not included in the table.

It should be noted that this operation count as well as those given in the next sections represents an estimate of the actual number of operations performed by a solution routine. Only the significant terms are included in the operation counts and the actual number of operations will vary slightly depending on programming details.

Table II. Summary of generalized Jacobi solution

Operation	Calculation	Number of operations	Required storage
Calculation of coupling factors	$\frac{k_{ij}^{(k)s}}{k_{ii}^{(k)} k_{jj}^{(k)}}, \frac{m_{ij}^{(k)s}}{m_{ii}^{(k)} m_{jj}^{(k)}}$	6	
Transformation to zero elements (i, j)	$\bar{k}_{ii}^{(k)} = k_{ii}^{(k)} m_{jj}^{(k)} - m_{ii}^{(k)} k_{jj}^{(k)}$ $\bar{k}_{jj}^{(k)} = k_{jj}^{(k)} m_{ii}^{(k)} - m_{jj}^{(k)} k_{ii}^{(k)}$ $\bar{k}^{(k)} = k_{ij}^{(k)} m_{jj}^{(k)} - k_{jj}^{(k)} m_{ii}^{(k)}$ $x = \frac{\bar{k}^{(k)}}{2} + (\text{sign } \bar{k}^{(k)}) \sqrt{\left[\left(\frac{\bar{k}^{(k)}}{2}\right)^2 + \bar{k}_{ii}^{(k)} \bar{k}_{jj}^{(k)}\right]}$ $\gamma = -\frac{\bar{k}_{ii}^{(k)}}{x}, \quad \alpha = \frac{\bar{k}_{jj}^{(k)}}{x}$ $\mathbf{K}_{k+1} = \mathbf{P}_k^T \mathbf{K}_k \mathbf{P}_k, \quad \mathbf{M}_{k+1} = \mathbf{P}_k^T \mathbf{M}_k \mathbf{P}_k$	4n + 12	Using symmetry of matrices n(n + 2)
Calculation of eigenvectors	$(\mathbf{P}_1 \dots \mathbf{P}_{k-1}) \mathbf{P}_k$	2n	n ²
Total for one sweep		3n ² + 6n ²	2n ² + 2n

For matrices with small bandwidth a determinant search algorithm provides a very efficient solution.^{2,3} The algorithm uses triangular factorization and vector inverse iteration directly on the general problem $\mathbf{K}\phi = \omega^2 \mathbf{M}\phi$ and solves for the required eigenvalues and vectors in succession from the leastdom inant eigenpair upwards. In the eigenvalue problem M can be diagonal, with zero diagonal elements, or may be banded positive definite.

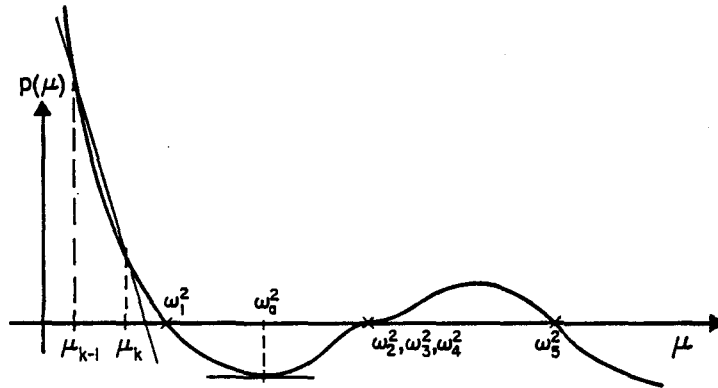


Figure 1. Characteristic polynomial p(μ)

Consider the solution for the eigenpair (ω_1^2, ϕ_1) , where ω_1^2 may be a multiple root.

The first objective in the iteration is to obtain a shift near ω_1^2 . Here we use the fact that the eigenvalues are the roots of the characteristic polynomial $p(\mu) = \det(\mathbf{K} - \mu \mathbf{M})$. To evaluate $p(\mu)$ the matrix $\mathbf{K} - \mu \mathbf{M}$ is factored into \mathbf{LDL}^T using Gauss elimination, where L is a unit lower triangular matrix and D is a diagonal matrix. We then have $p(\mu) = \prod_{i=1}^n d_{ii}$.

Let $\mu_{k-1} < \mu_k < \omega_1^2$ as shown in Figure 1. The next shift μ_{k+1} is calculated using an accelerated secant iteration in which

$$\mu_{k+1} = \mu_k + \eta \frac{p(\mu_k)}{p(\mu_k) - p(\mu_{k-1})} (\mu_{k-1} - \mu_k) \tag{28}$$

where η is a constant. When $\eta = 1.0$ we have the well-known secant iteration in which case $\mu_{k+1} \leq \omega_1^2$ and $\mu_{k+1} \rightarrow \omega_1^2$ as $k \rightarrow \infty$. However, convergence in this iteration can be slow. Because the aim is to obtain merely

a shift near ω_1^2 the program uses an efficient acceleration scheme in which $\eta \geq 2.0$. Starting the iteration η equals 2.0 because in this case $\mu_{k+1} \leq \omega_a^2$, where ω_a^2 is the smallest stationary point of p . A jump over a simple root would be detected by a sign change in p . However, when we iterate towards a multiple root or a cluster of roots, convergence with $\eta = 2.0$ is still slow. Fortunately, in this case the eigenvalue separation theorem (Sturm sequence property) allows us to accelerate the iteration further by increasing η still more.

Once a shift near ω_1^2 has been obtained by either jumping over it or by approaching it sufficiently close from below, inverse iteration is used to calculate the eigenvector ϕ_1 and the Rayleigh correction ρ^c , which added to the shift gives the eigenvalue to the required precision (see Table III).

Table III. Summary of determinant search solution

Operation	Calculation	Number of operations	
		$m = m_K = m_M$	$m = m_K, m_M = 0$
Secant iteration	$\bar{K} = K - \mu_k M$	$n(m+1)$	n
	$\bar{K} = LDL^T$	$\frac{1}{2}nm^2 + \frac{3}{2}nm$	$\frac{1}{2}nm^2 + \frac{3}{2}nm$
	$p(\mu_k) = \prod_{i=1}^n d_{ii}$	n	n
Inverse iteration	$\bar{K}\bar{x}_{k+1} = y_k$	$n(2m+1)$	$n(2m+1)$
	$\bar{y}_{k+1} = M\bar{x}_{k+1}$	$n(2m+1)$	n
	$\rho^c(\bar{x}_{k+1}) = \frac{\bar{x}_{k+1}^T y_k}{\bar{x}_{k+1}^T \bar{y}_{k+1}}$	$2n$	$2n$
	$y_{k+1} = \left(\bar{y}_{k+1} - \sum_{j=1}^6 \alpha_{i-j} \bar{\phi}_{i-j} \right) / (\bar{x}_{k+1}^T \bar{y}_{k+1})^\dagger$ where $\bar{\phi}_j = M\phi_j, \alpha_j = \frac{T}{k+1} \bar{x} \bar{\phi}_j$	$13n$	$13n$
Total for p lowest eigenvalues and associated eigenvectors assuming six secant and six inverse iterations per eigenpair		$(3nm^2 + 39nm + 114n)p$	$(3nm^2 + 21nm + 114n)p$

Required storage
 $m = m_K = m_M \quad m = m_K, m_M = 0$

Using symmetry of matrices

$2n(m+1) + 9n \quad n(m+1) + 10n$

This iteration for ω_1^2 and ϕ_1 is typical because the advantage of the one-sided approach to ω_1^2 is also obtained for any other root, say ω_{j+1}^2 by using instead of $p(\mu)$ in equation (28) the deflated polynomial $p_j(\mu)$, Figure 2, where

$$p_j(\mu) = p(\mu) \prod_{i=1}^j (\mu - \omega_i^2) \quad (29)$$

The calculations in a secant iteration and in a vector inverse iteration are summarized in Table III, where also the required number of operations and the storage requirements are given. Note that the factorization of $K - \mu M$ is performed without interchanges which has proven to be numerically adequate.² Also, the iteration vector is orthogonalized in each iteration to the last found six eigenvectors. In this operation count the half bandwidths m_M and m_K are assumed to be full, and terms involving the bandwidths only have been neglected. In most actual systems the bandwidths vary and many zeros occur within the band. The solution routine should take due account of both. The number of iterations required for the solution of an eigenpair depends on the system under consideration; experience shows that about six secant steps and six inverse iterations are required.

The determinant search technique is most efficient and has been implemented as an in-core solution routine. Because relatively many triangular factorizations are required, much tape handling would be necessary in an out-of-core solution.² Also, the technique is most efficient in the analysis of small-banded systems, and in this case relatively large order systems can be solved on reasonable size computers.

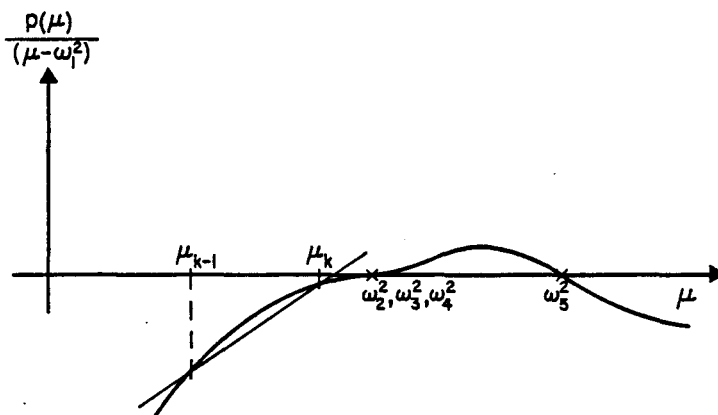


Figure 2. $p(\mu)$ with ω_1^2 suppressed

SUBSPACE ITERATION SOLUTION

In the subspace iteration solution the required eigenvalues and vectors are also calculated directly without a transformation to the standard form.^{2,4}

The aim is to solve for the p lowest eigenvalues and associated eigenvectors satisfying

$$\mathbf{K}\Phi = \mathbf{M}\Phi\Omega^2 \quad (30)$$

where the columns in Φ are the p eigenvectors and Ω^2 is a diagonal matrix with the corresponding eigenvalues. The specific idea used in the solution is that the eigenvectors form an \mathbf{M} -orthonormal basis of the p -dimensional least dominant subspace of the operators \mathbf{K} and \mathbf{M} .

In the solution we iterate simultaneously with q linearly independent vectors, where $q > p$. In the k th iteration the vectors span the q -dimensional subspace \mathcal{E}_{k+1} and 'best' eigenvalue and eigenvector approximations are calculated, i.e. when the vectors span the p -dimensional least dominant subspace the required eigenvalues and eigenvectors are obtained.

Let \mathbf{X}_1 store the starting vectors, then the algorithm is defined as follows:

For $k = 1, 2, \dots$ iterate from \mathcal{E}_k to \mathcal{E}_{k+1}

$$\mathbf{K}\bar{\mathbf{X}}_{k+1} = \mathbf{M}\mathbf{X}_k \quad (31)$$

Find the projections of the operators \mathbf{K} and \mathbf{M} onto \mathcal{E}_{k+1}

$$\mathbf{K}_{k+1} = \bar{\mathbf{X}}_{k+1}^T \mathbf{K} \bar{\mathbf{X}}_{k+1} \quad (32)$$

$$\mathbf{M}_{k+1} = \bar{\mathbf{X}}_{k+1}^T \mathbf{M} \bar{\mathbf{X}}_{k+1} \quad (33)$$

Solve for the eigensystem of the projected operators

$$\mathbf{K}_{k+1} \mathbf{Q}_{k+1} = \mathbf{M}_{k+1} \mathbf{Q}_{k+1} \Omega_{k+1}^2 \quad (34)$$

Find an improved approximation to the eigenvectors

$$\mathbf{X}_{k+1} = \bar{\mathbf{X}}_{k+1} \mathbf{Q}_{k+1} \quad (35)$$

Then provided the starting subspace is not orthogonal to one of the required eigenvectors, we have

$$\Omega_{k+1}^2 \rightarrow \Omega^2, \quad \mathbf{X}_{k+1} \rightarrow \Phi \quad \text{as } k \rightarrow \infty$$

The iteration is performed with q vectors because the asymptotic convergence rate of the i th column in X_{k+1} to ϕ_i is given by $\omega_i^2/\omega_{q+1}^2$; therefore, the larger q the higher the convergence rate for the p vectors of interest, but also more operations need be carried out in each iteration. In the implementation of the algorithm $q = \min\{2p, p+8\}$ has been found to be effective.

Table IV. Summary of subspace iteration solution

Operation	Calculation	Number of operations		Required storage
		$m = m_K = m_M$	$m = m_K, m_M = 0$	
Factorization of K	$K = LDL^T$	$\frac{1}{2}nm^2 + \frac{3}{2}nm$	$\frac{1}{2}nm^2 + \frac{3}{2}nm$	
Subspace iteration	$K\bar{X}_{k+1} = Y_k$	$nq(2m+1)$	$nq(2m+1)$	Algorithm is implemented as out-of-core solver
	$K_{k+1} = \bar{X}_{k+1}^T Y_k$	$\frac{1}{2}nq(q+1)$	$\frac{1}{2}nq(q+1)$	
	$\bar{Y}_{k+1} = M\bar{X}_{k+1}$	$nq(2m+1)$	nq	
	$M_{k+1} = \bar{X}_{k+1}^T \bar{Y}_{k+1}$	$\frac{1}{2}nq(q+1)$	$\frac{1}{2}nq(q+1)$	
	$K_{k+1} Q_{k+1} = M_{k+1} Q_{k+1} \Omega_{k+1}^2$	$O(q^3)$ neglected		
	$Y_{k+1} = \bar{Y}_{k+1} Q_{k+1}$	nq^2	nq^2	
Sturm sequence check	$\bar{K} = K - \mu M$	$n(m+1)$	n	
	$\bar{K} = LDL^T$	$\frac{1}{2}nm^2 + \frac{3}{2}nm$	$\frac{1}{2}nm^2 + \frac{3}{2}nm$	
Total for solution of p lowest eigenvalues and associated eigenvectors assuming that eight iterations are required and $q = \min\{2p, p+8\}$		$nm^2 + 4nm$ $+ 16nq(2m+q+\frac{3}{2})$	$nm^2 + 3nm$ $+ 16nq(m+q+\frac{3}{2})$	

The total number of iterations required depends on how 'close' the starting subspace is to the p -dimensional least dominant subspace of the operators and, of course, on the required accuracy of the eigenvalues and associated eigenvectors. Also, it should be noted that in exact arithmetic convergence to an eigenvector is not possible if the starting vectors are all orthogonal to the eigenvector. It is therefore most important to establish a 'good' starting subspace. But there is no need to find for the columns in X_1 vectors each of which is 'close' to a required eigenvector. In the implementation a scheme has proven very effective which, for the special case when K and M are diagonal, establishes a starting subspace, which is the least dominant one of the operators. At convergence error bounds on the eigenvalues can be evaluated and a Sturm sequence check can be applied to verify the results. As the solution accuracy for the lowest eigenvalues and corresponding vectors is highest, in general, a four to five digit accuracy in the p th eigenvalue can be sufficient.

Table IV summarizes the algorithm and gives the number of operations required for solution. Based on the experience with the algorithm it is assumed that eight iterations are required. Also, it is assumed that the number of required eigenvalues and vectors is much smaller than the order of the matrices. In this case the solution for the eigensystem of the subspace operators requires a negligible amount of operations.

The subspace iteration solution is most efficient in the analysis of systems with large bandwidth and in out-of-core solutions because relatively little tape handling is necessary. For the routine developed the high speed storage requirements are small, and the lowest eigenvalues and corresponding vectors of very large systems can be calculated. However, it should be noted that the actual cost of an out-of-core solution also includes the cost of the Peripheral Processor (tape and disc reading) time. This time is very system and programming dependent and is not mentioned in Table IV.

SELECTION OF SOLUTION TECHNIQUE

The appropriate solution technique for a given problem should be selected by considering the information given in Tables I-IV. The choice for a solution routine is governed by the number of operations needed for solution and the required high speed storage. The Householder-QR-inverse iteration solution, the generalized Jacobi iteration and the determinant search method have been presented as in-core solution routines because they are likely to be used on systems which can be solved in the high speed storage of the computer. If the

techniques are implemented in out-of-core solution routines, relatively much tape handling is necessary, but the high speed storage requirements would be small.

The generalized Jacobi iteration is most efficient when the complete eigensystem is required and either not many off-diagonal elements are present or they are already small, i.e. the eigenproblem is already 'nearly' solved. For this reason the technique is efficiently used for the solution of the eigensystem of \mathbf{K}_{k+1} and \mathbf{M}_{k+1} in the subspace iteration, equation (34). When the order of the matrices is relatively small, the solution of the eigenvalue problem is not very expensive and the Jacobi iteration may also be attractive because of its simplicity and elegance of solution.

The Householder-QR-inverse iteration solution is most efficient when all eigenvalues and eigenvectors of a matrix are required which has a large bandwidth or is full. As was pointed out, this solution requirement can arise after static condensation of the massless degrees of freedom. A full matrix is also obtained if the generalized eigenvalue problem with a banded mass matrix is transformed to the standard form.

Whether the procedure of static condensation and solution of the reduced eigenvalue problem is efficient depends on the original bandwidth of the stiffness matrix, the increase in bandwidth due to static condensation, the number of original and final degrees of freedom and the number of required eigenvalues and vectors. In most analyses mass is associated with about one half or more of the degrees of freedom; therefore, if the order of the system is large, the static condensation still leads to a large order system which may have lost the bandform. In this case a direct solution of the eigenvalue problem which takes full advantage of the banding characteristics and solves only for the required eigenvalues and associated vectors is more efficient.

When the mass matrix is banded and the system is large the transformation to the standard eigenvalue problem is practically always very inefficient.

The determinant search technique is very effectively used to calculate the lowest eigenvalues and corresponding vectors of systems with small bandwidth. In the solution the eigenvalues and vectors are calculated to high precision. If compacted storage is used also relatively large order systems can be solved in core. The use of a banded mass matrix increases the cost of solution relatively little. Note also that depending on the bandwidth to find the complete eigensystem the determinant search method can be more efficient than the Householder-QR-inverse iteration solution.

The subspace iteration solution is very efficient in the calculation of the lowest eigenvalues and corresponding eigenvectors of systems with large bandwidth and which are too large for the high speed storage of the computer. Note, however, that the eigensystem of the projected operators in equation (34) is calculated in high speed storage, and that, in case many vectors are calculated, this high speed storage requirement may solution govern the problem size.

The most important eigenvalue problem in dynamic analysis is the solution of the lowest eigenvalues and corresponding eigenvectors. However, in some dynamic analyses eigenvalues within a specified intermediate range only are of interest.¹⁷ If the order of the matrices is not large, a solution using the Householder-QR-inverse iteration technique or the determinant search method is efficient, unless only a few eigenvalues and corresponding eigenvectors are needed. In that case a bisection technique such as described in References 11 and 16 can be economical. When the order and bandwidth of the matrices is large, a subspace iteration solution with a shift should be carried out.²

The above considerations for the choice of the appropriate algorithm are also applicable to buckling analysis, equation (4). As only one eigenvalue is required, for large order systems the Householder-QR inverse iteration solution and the Jacobi method are obviously inefficient. Depending on the order and bandwidth of the system either the determinant search or the subspace iteration method provides the more efficient solution.

SAMPLE SOLUTIONS

The sample solutions summarized in Table V are actual practical analyses. They have been selected to show typical solution times. In the Jacobi, Householder-QR-inverse iteration and the determinant search solution the eigenvalues have been obtained to near full word precision (12 digits). The subspace iteration

Table V. Sample solutions

Sample number	System	System order n	Maximum half bandwidth m	Mass matrix	Number of required vectors	Solution technique	Computer used	Central processor seconds
1	Plate-beam system	50	Full	Full	50	Jacobi	CDC 7600	2
2	General system	100	Full	Banded positive definite	100	Householder-QR-inverse iteration	CDC 6400	46
3	Plane frame	297	29	Diagonal semi-definite	3	Determinant search	CDC 6400	40
4	Plane frame	297	29	Diagonal semi-definite	3	Subspace iteration	CDC 6400	25
5	Three-dimensional building frame	468	155	Diagonal semi-definite	4	Subspace iteration	CDC 6400	160
6	Three-dimensional box	403	114	Diagonal semi-definite	8	Subspace iteration	CDC 7600	12
7	Dam	724	113	Banded	20	Subspace iteration	CDC 6600	518
8	Dam	226	68	Banded	7	Determinant search	CDC 6600	71
9	Piping system	566	11	Diagonal semi-definite	28	Subspace iteration	CDC 6600	142
10	Piping system	566	11	Diagonal semi-definite	7	Determinant search	CDC 6600	11
11	Building with foundation	1174	137	Diagonal semi-definite	45	Subspace iteration	CDC 6600	890
12	Building	340	31	Diagonal semi-definite	7	Determinant search	CDC 6600	20
13	Bridge	342	35	Diagonal semi-definite	10	Subspace iteration	CDC 6600	31

solved in each case for the largest required eigenvalue to about 5 digit precision with the lower eigenvalues being more accurate. Note that the central processor speeds of the CDC 6400, CDC 6600 and CDC 7600 computers are approximately as 1 : 3 : 8.

The Jacobi iteration was only used on rather small order systems such as indicated in the table. The size of the systems which have been solved by the Householder–QR–inverse iteration and the determinant search technique was restricted by the maximum high speed storage available. As indicated in Tables I and III the determinant search method can solve larger order systems. The subspace iteration solution has been used in most cases because the algorithm has been programmed to allow practically unlimited system size and bandwidth.

The solution times in Table V can only be used as a guide to estimate the computer effort involved in using the appropriate algorithm in a required analysis. The table does not demonstrate the relative efficiencies of the different solution techniques when used on the same problems. Tables I–IV do this and it would be too expensive to run comparative example analyses merely to arrive at the same conclusions. However, the solution times do emphasize the points made in the previous section about the selection of the appropriate algorithm for a given problem.

CONCLUSIONS

A single algorithm which always gives a very efficient solution of the generalized eigenvalue problems does not exist. In this paper the probably most efficient solution methods currently in use have been summarized. An efficient solution of a specific eigenvalue problem is obtained if the appropriate one of these methods is used.

The Householder–QR–inverse iteration technique is a general method for the solution of standard eigenvalue problems and requires a transformation into this form.

The generalized Jacobi iteration, the determinant search method and the subspace iteration algorithm have been developed specifically for direct solution of the generalized eigenvalue problems. The methods are very efficient because advantage is taken of the specific solution requirements and the specific properties of the stiffness and mass matrices, e.g. the banding characteristics, the relative magnitude and the relative positioning of the elements in the matrices. Using the specific properties of the matrices it appears that much potential lies in the subspace iteration solution. The starting subspace generated by the algorithm has proven to be very effective, i.e. only about eight iterations are required for convergence. However, the potential of the method lies in that a 'better' starting subspace would further reduce the number of required iterations, and it is felt that future research should be directed towards this aim.

REFERENCES

1. J. S. Archer, 'Consistent mass matrix for distributed mass systems', *Proc. ASCE*, **89**, *J. Str. Div.* **4**, 161–178 (1963).
2. K. J. Bathe, 'Solution methods for large generalized eigenvalue problems in structural engineering', *SESM Rep.*, 71–20, Civ. Engng Dept., Univ. of Calif., Berkeley, U.S.A. (1971).
3. K. J. Bathe and E. L. Wilson, 'Eigensolution of large structural systems with small bandwidth', *ASCE, J. Engng. Mech. Div.* (to appear).
4. K. J. Bathe and E. L. Wilson, 'Large eigenvalue problems in dynamic analysis', *ASCE, J. Engng. Mech. Div.* **98**, 1471–1485 (1972).
5. F. L. Bauer, 'Das Verfahren der Treppen-Iteration und Verwandte Verfahren zur Lösung Algebraischer Eigenwertprobleme', *ZAMP* **8**, 214–235 (1957).
6. O. E. Brönlund, 'Eigenvalues of large matrices', *Symp. Finite Element Techniques* at Inst. für Statik und Dynamik der Luft und Raumfahrtkonstruktionen, Univ. of Stuttgart, Germany (1969).
7. R. W. Clough, 'Analysis of structural vibrations and dynamic response', *Proc. U.S.–Japan Symp. Recent Advances in Matrix Methods of Structural Analysis and Design*, Tokyo, Japan (1969).
8. S. B. Dong, J. A. Wolf and F. E. Peterson, 'On a direct-iterative eigensolution technique', *Int. J. num. Meth. Engng.* **4**, 155–162 (1972).
9. S. Falk and P. Langemeyer, 'Das Jacobische Rotationsverfahren für Reell-symmetrische Matrizenpaare', *Elektron. Datenverarb.* 30–34 (1960).
10. C. A. Felippa, 'BANEIG-eigenvalue routine for symmetric band matrices', *Comp. Prog. Ser., SESM*, Civ. Engng Dept., Univ. of Calif., Berkeley, U.S.A. (1966).
11. K. K. Gupta, 'Vibration of frames and other structures with banded stiffness matrix', *Int. J. num. Meth. Engng.* **2**, 221–228 (1970).

12. A. Jennings, 'A direct iteration method of obtaining latent roots and vectors of a symmetric matrix', *Proc. Camb. Phil. Soc.* 63, 755-765 (1967).
13. A. Jennings and D. R. L. Orr, 'Application of the simultaneous iteration method to undamped vibration problems', *Int. J. Num. Meth. Engng.* 3, 13-24 (1971).
14. J. M. Ortega and H. F. Kaiser, 'The LL^T and QR methods for symmetric tri diagonal matrices', *Comp. J.* 6, 99-101 (1963).
15. B. N. Parlett and W. Kahan, 'On the convergence of a practical QR algorithm', Proc. IFIP Congress (1968).
16. G. Peters and J. H. Wilkinson, ' $Ax = \lambda Bx$ and the generalized eigenproblem', *SIAM, J. Num. Anal.* 7, 479-492 (1970).
17. M. F. Rubinstein, *Structural Systems—Statics, Dynamics and Stability*, Prentice-Hall, Englewood Cliffs, New Jersey, 1970.
18. H. Rutishauser, 'Computational aspects of F. L. Bauer's simultaneous iteration method', *Num. Math.* 13, 4-13 (1969).
19. J. H. Wilkinson, *The Algebraic Eigenvalue Problem*, Clarendon Press, Oxford, 1965.
20. O. C. Zienkiewicz, *The Finite Element Method in Engineering Science*, McGraw-Hill, London, 1971.

AN ACCELERATED SUBSPACE ITERATION METHOD

Klaus-Jürgen BATHE and Seshadri RAMASWAMY
Massachusetts Institute of Technology, Cambridge, MA 02139, U.S.A.

Received 17 July 1979

The subspace iteration method for solving symmetric eigenproblems in computational mechanics is considered. Effective procedures for accelerating the convergence of the basic subspace iteration method are presented. The accelerated subspace iteration method has been implemented and the results of some demonstrative sample solutions are presented and discussed.

1. Introduction

The analysis of a number of physical phenomena requires the solution of an eigenproblem. It is therefore natural that with the increased use of computational methods operating on discrete representations of physical problems the development of efficient algorithms for the calculation of eigenvalues and eigenvectors has attracted much attention [1]–[8]. In particular, the use of finite element and finite difference techniques on the digital computer can lead to large systems of equations, and the efficiency of an overall response analysis can depend to a significant degree on the effectiveness of the solution of the required eigenvalues and vectors.

In this paper we consider the solution of the smallest eigenvalues and corresponding eigenvectors of the generalized eigenproblem arising in dynamic analysis:

$$\mathbf{K}\boldsymbol{\phi} = \lambda\mathbf{M}\boldsymbol{\phi}, \quad (1)$$

where \mathbf{K} and \mathbf{M} are the stiffness and mass matrices of the discrete degree of freedom system, and $(\lambda_i, \boldsymbol{\phi}_i)$ is the i th eigenpair. If the order of \mathbf{K} and \mathbf{M} is n , we have n eigenpairs which we order as follows:

$$0 < \lambda_1 \leq \lambda_2 \leq \lambda_3 \leq \dots \leq \lambda_n, \\ \boldsymbol{\phi}_1, \boldsymbol{\phi}_2, \boldsymbol{\phi}_3, \dots, \boldsymbol{\phi}_n. \quad (2)$$

The solution for the lowest p eigenvalues and corresponding eigenvectors can be written as

$$\mathbf{K}\boldsymbol{\Phi} = \mathbf{M}\boldsymbol{\Phi}\boldsymbol{\Lambda}, \quad (3)$$

where the columns of $\boldsymbol{\Phi}$ contain the required eigenvectors, and $\boldsymbol{\Lambda}$ is a diagonal matrix with

the eigenvalues on its diagonal:

$$\Phi = [\phi_1, \dots, \phi_p], \quad \Lambda = \begin{bmatrix} \lambda_1 & & \\ & \dots & \\ & & \lambda_p \end{bmatrix}. \quad (4)$$

It should be noted that the eigenproblem given in eq. (1) also arises in heat transfer analysis, the analysis of associated field problems and buckling analysis.

Among the techniques for calculating the lowest p eigenvalues and corresponding eigenvectors of eq. (1) the subspace iteration method has proven to be efficient. This solution method—referred to in this paper as the *basic* subspace iteration method—consists of the following three steps [3], [7], [10]:

Step (1). Establish q starting iteration vectors, $q > p$, which span the starting subspace E_1 .

Step (2). Perform subspace iterations, in which simultaneous inverse iteration is used on the q vectors, and Ritz analysis is employed to extract optimum eigenvalue and eigenvector approximations at the end of each inverse iteration.

Step (3). After iteration convergence use the Sturm sequence check to verify that the required eigenvalues and corresponding eigenvectors have been obtained.

Considering step (1), the variable q is input by the user or $q = \min\{2p, p + 8\}$, and the starting iteration vectors are established as discussed in [7] or by using the Lanczos algorithm. Both procedures are briefly summarized in appendix A.

Consider next step (2) and store the starting iteration vectors in X_1 . The subspace iterations are performed as follows:

For $k = 1, 2, \dots$ iterate from subspace E_k to subspace E_{k+1} :

$$K\bar{X}_{k+1} = MX_k. \quad (5)$$

Calculate the projections of the matrices K and M onto E_{k+1} :

$$K_{k+1} = \bar{X}_{k+1}^t K \bar{X}_{k+1}, \quad (6)$$

$$M_{k+1} = \bar{X}_{k+1}^t M \bar{X}_{k+1}. \quad (7)$$

Solve for the eigensystem of the projected matrices:

$$K_{k+1}Q_{k+1} = M_{k+1}Q_{k+1}\Lambda_{k+1}. \quad (8)$$

Calculate an improved approximation to the eigenvectors:

$$X_{k+1} = \bar{X}_{k+1}Q_{k+1}. \quad (9)$$

Then, provided that the iteration vectors in X_1 are not orthogonal to one of the required eigenvectors (and assuming an appropriate ordering of the vectors), we have that the i th diagonal entry in Λ_{k+1} converges to λ_i and the i th vector in X_{k+1} converges to ϕ_i . In this iteration the ultimate rate of convergence of the i th iteration vector to ϕ_i is λ_i/λ_{q+1} , and the ultimate rate of convergence to the i th eigenvalue is $(\lambda_i/\lambda_{q+1})^2$. In the iteration, convergence is

measured on the eigenvalue approximations [7, p. 504],

$$tolc = \frac{|\lambda_i^{(k+1)} - \lambda_i^{(k)}|}{\lambda_i^{(k+1)}}, \quad (10)$$

where for convergence $tolc$ must be smaller than tol . This final convergence tolerance tol is typically equal to 10^{-6} , which yields a stable eigensolution and sufficient accuracy in the calculated eigenvalues and eigenvectors for practical analysis [7].

In this basic subspace iteration method, convergence has been achieved if $tolc \leq tol$ for $i = 1, \dots, p$ and the Sturm sequence check is passed. Considering the Sturm sequence check in step (3) above, the procedure to apply this check has been described in detail in [7]. The Sturm sequence check is very important in that it is the only means to make sure that indeed the required number of eigenpairs has been evaluated.

Considering the solution of problems for a relatively large number of eigenpairs, say $p > 50$, experience shows that the cost of solution using the above basic subspace iteration method rises rapidly as the number of eigenpairs considered is increased. This rapid increase in cost is due to a number of factors that can be neglected when the solution of only a few eigenpairs is required. An important point is that a relatively large number of subspace iterations may be required if the default value for q given above is employed. Namely, in this case, when p is large, the convergence rate to ϕ_p , equal to λ_p/λ_{q+1} , can be close to one. On the other hand, if q is increased, the numerical operations per subspace iteration are increased significantly. Another shortcoming of the basic subspace iterations with q large is that a relatively large number of iteration vectors is used throughout *all* subspace iterations in eqs. (5) to (9). Namely, convergence to the smallest eigenvalues is generally achieved in only a very few iterations, and the converged vectors plus the $(p+1)$ st to q th iteration vectors are only included in the additional iterations to provide solution stability and to accelerate the convergence to the larger required eigenvalues. A further important consideration pertains to the high-speed core and low-speed back-up storage requirements. As the number of iteration vectors q increases, the number of matrix blocks that need be used in an out-of-core solution can also increase significantly and the peripheral processing expenditures can be large. Finally, it is noted that the number of numerical operations required in the solution of the reduced eigenproblem in eq. (8) becomes significant when q is large and cannot be neglected in the operation count of the subspace iteration method. For these reasons the operation count given in [7, p. 507] is not applicable when q is large.

The above brief discussion shows that modifications to increase the effectiveness of the basic subspace iteration procedure are very desirable, in particular when the solution of a large number of eigenpairs is considered. The development of acceleration procedures to the subspace iteration method has been the subject of some earlier research [9]–[11]. In principle, a number of techniques can be employed, such as Aitken acceleration, overrelaxation, the use of Chebyshev polynomials and shifting; however, the difficulty is to provide a reliable and significantly more effective solution method, and such technique has not as yet been presented.

The objective in this paper is to describe an accelerated subspace iteration method that is reliable and significantly more effective than the basic scheme. We first discuss the theory and implementation of the acceleration procedures employed. These acceleration schemes have

been implemented and used in the solution of a large number of problems. To demonstrate the basic features of the solution method, we present some solution results in the paper and compare these with the results obtained using the determinant search method and the basic subspace iteration method [7]. We conclude that the new accelerated subspace iteration solution technique represents a very significant extension of the basic subspace iteration method.

2. Overrelaxation of iteration vectors

Overrelaxation techniques are commonly employed in iterative solution methods, and it can be expected that overrelaxation is also useful in the subspace iteration solution of eigenproblems. To incorporate overrelaxation into the subspace iterations, eqs. (5) to (8) remain unaltered, but the new iteration vectors X_{k+1} are obtained using instead of (9) the relation

$$X_{k+1} = X_k + (\bar{X}_{k+1} Q_{k+1} - X_k) \alpha, \quad (11)$$

where α is a diagonal matrix with its diagonal elements equal to individual vector overrelaxation factors α_i , $i = 1, \dots, q$, which are calculated as discussed below.

2.1. Preliminary considerations on vector overrelaxation

The use of overrelaxation of an iteration vector assumes that the vector has settled down and reached its asymptotic convergence rate. The overrelaxation factor is a function of this rate of convergence, and if the overrelaxation factor is chosen based on λ_{q+1} , the analysis in [10] gives

$$\alpha_i = \frac{1}{1 - \lambda_i / \lambda_{q+1}}. \quad (12)$$

It is therefore necessary to have a reliable scheme for the calculation of the vector convergence rate $\lambda_i / \lambda_{q+1}$. Such a scheme is the essence of our method of overrelaxation.

2.2. The overrelaxation method used

Assuming that some of the iteration vectors have reached their asymptotic rate of convergence and we have a reasonable approximation to the corresponding eigenvalues, our objective is to calculate an approximation to λ_{q+1} , so that eq. (12) can be employed to evaluate the overrelaxation factors. The approximation to λ_{q+1} is calculated effectively using the successive eigenvalue predictions obtained during the subspace iterations.

Considering the convergence to λ_i , let

$$r_i^{(k+1)} = \frac{\lambda_i^{(k+1)} - \lambda_i}{\lambda_i^{(k)} - \lambda_i}, \quad (13)$$

where thus

$$\lim_{k \rightarrow \infty} r_i^{(k+1)} = \left(\frac{\lambda_i}{\lambda_{q+1}} \right)^2. \quad (14)$$

Then we can say that, approximately,

$$r_i^{(k+1)} = \frac{|\lambda_i^{(k+1)} - \lambda_i^{(k)}|}{|\lambda_i^{(k)} - \lambda_i^{(k-1)}|}, \quad i = 1, \dots, p. \quad (15)$$

Depending on the iteration number, the convergence rate estimates in eq. (15) can be grossly in error and, due to finite precision arithmetic, will certainly be meaningless at or near convergence. However, the estimates are fairly reliable if the following two conditions are satisfied:

$$\left| \frac{r_i^{(k+1)} - r_i^{(k)}}{r_i^{(k+1)}} \right| \leq \text{tolr} \quad \text{and} \quad 10^{-3} \leq \text{tolc} \leq 10^{-10}, \quad (16)$$

where *tolr* is typically 0.2 to 0.35, and *tolc* is defined in eq. (10). In using the above tolerances and all tolerances specified in the discussion to follow, we assume that a computer with 14 or more digit arithmetic is employed (e.g. CDC machines in single precision arithmetic, IBM and UNIVAC machines in double precision arithmetic).

Assume that in iteration *l* there are some eigenvalue estimates (of the *p* eigenvalues to be calculated) for which the tests in eq. (16) are passed; then, using each of these eigenvalue estimates, we can calculate an approximation to λ_{q+1} :

$$\lambda_{q+1} \doteq \frac{\lambda_i^{(l+1)}}{\sqrt{r_i^{(l+1)}}} \quad (17)$$

and use as the best estimate for λ_{q+1} the average $\bar{\lambda}_{q+1}$ of all estimates ever calculated in the iterations.

The value $\bar{\lambda}_{q+1}$ is employed instead of λ_{q+1} in eq. (12) to evaluate the overrelaxation factor α_i .

3. Acceleration through shifting

The basic premise of using shifting procedures in the subspace iterations is that the rates of convergence to the required eigenpairs can be increased significantly and to such an extent as to outpay the added computational expense that is due to the additional triangular factorizations. It was shown earlier, when considering the solution of only a few eigenpairs, that for small-banded systems the determinant search algorithm is more effective than the basic subspace iteration method [7], and that for large-banded systems the subspace iteration method is more efficient. It can therefore be conjectured that, depending on the bandwidth of the system matrices and the number of eigenpairs to be calculated, some shifting procedure

that is similar to the one employed in the determinant search method should be effective in the subspace iteration method.

3.1. Preliminary considerations on matrix shifting

Considering shifting in the subspace iterations, it is most important to develop a stable and reliable solution scheme. A major difficulty in the use of shifting is that if a shift is on or very close to an eigenvalue, all iteration vectors immediately converge to the eigenvector corresponding to that eigenvalue. The vectors can then not be orthogonalized any more and the iteration is unstable. If the shift is very close to an eigenvalue, the last pivot element in the *LDL'* factorization of the coefficient matrix is small (compared to its original value) and the shift must be changed, but two serious situations can arise that are described qualitatively as follows:

- (1) If a shift is close but not very close to an eigenvalue (which is a situation in between the case of a shift "exactly" on an eigenvalue and the case of a shift far away from an eigenvalue), the attraction of an iteration vector to the shift may just be counterbalanced by the vector orthogonalization process. In such case, if the convergence tolerance employed is not high enough, an iteration vector is erroneously considered to have converged to an eigenvector.
- (2) Although an iteration vector may have converged already to a required eigenvector, if a shift is imposed, and this iteration vector is still included in the subspace iterations, it is possible that this iteration vector may deteriorate and suddenly converge to another eigenvector.

With due regard to these difficulties the shifting procedure presented below is a simple and stable algorithm to accelerate the convergence of the subspace iterations.

3.2. The shifting procedure used

Assume that the smallest r eigenvalues have already converged, i.e. we have $tolc \leq tol$ (using eq. (10)) for the approximations to the r smallest consecutive eigenvalues. The calculated r eigenvalue approximations the estimate for λ_{q+1} defined in section 2.2 as $\bar{\lambda}_{q+1}$ and the eigenvalue iterates that are converging to the higher eigenvalues ($i > r$) and satisfy eq. (10) with $tolc \leq 10^{-2}$ are employed to establish an appropriate algorithm for shifting in the subspace iterations.

In order that the iteration vectors continue to converge monotonically to the required p eigenvectors, the shift μ_s must satisfy the following condition:

$$\mu_s - \lambda_1 < \lambda_{q+1} - \mu_s, \quad (18)$$

which means that μ_s is in the left half of the eigenvalue spectrum λ_1 to λ_{q+1} . After shifting to μ_s the new convergence rates to the eigenvectors are $|\lambda_i - \mu_s|/|\lambda_{q+1} - \mu_s|$. To satisfy eq. (18) in a conservative manner, we use

$$\mu_s \leq \bar{\lambda}_1 + \frac{1}{3}(\bar{\lambda}_{q+1} - \bar{\lambda}_1), \quad (19)$$

where $\bar{\lambda}_1$ is the calculated approximation to λ_1 .

A second requirement for continued stability of the subspace iterations is that μ_s must be relatively far away from an eigenvalue. The shift μ_s is therefore chosen to lie midway between two well-spaced eigenvalue approximations, and these iterates must have converged to a tolerance (*tolc*) equal to 10^{-10} in eq. (10).

The criterion for shifting in the iterations is that the improvement in the convergence to the higher eigenvalues must outweigh the computational expense of performing a shift. Therefore, a shift is performed if the following condition is met:

$$\left[\begin{array}{l} \text{number of operations to} \\ \text{perform the shift} \end{array} \right] + \left[\begin{array}{l} \text{number of operations to} \\ \text{obtain convergence} \\ \text{after shifting} \end{array} \right] < \left[\begin{array}{l} \text{number of operations to} \\ \text{obtain convergence} \\ \text{without shifting} \end{array} \right]. \quad (20)$$

Let $\lambda_i^{(k+1)}$ be the latest estimate of λ_i with $\text{tolc} \leq 10^{-2}$ in eq. (10), where $r < i \leq p$, and let $\bar{\lambda}_{q+1}$ be the latest estimate for λ_{q+1} ; then we can estimate the convergence rate to λ_i as $d = (\lambda_i^{(k+1)}/\bar{\lambda}_{q+1})^2$. Also, let t be the number of additional iterations to reach convergence without shifting. We can estimate t using

$$d^t = \text{tol}_i, \quad (21)$$

where tol_i is the increase in accuracy still to be gained in the subspace iterations; here we have $\text{tol}_i = \text{tol}/\text{tolc}$. Hence

$$t = \frac{\log(\text{tol}_i)}{\log(d)}. \quad (22)$$

Using the information in eqs. (20)–(22), we can evaluate whether it is efficient to shift. Assume that a stable shift is given by μ_s (i.e. μ_s is chosen using eq. (19)); then the convergence rate \bar{d} to λ_i after shifting would be approximately

$$\bar{d} = \frac{(\lambda_i^{(k+1)} - \mu_s)^2}{(\bar{\lambda}_{q+1} - \mu_s)^2}. \quad (23)$$

Hence the number of subspace iterations required for convergence after shifting are approximately

$$\bar{t} = \frac{\log(\text{tol}_i)}{\log(\bar{d})}. \quad (24)$$

The above values for t and \bar{t} are calculated for all eigenvalue iterates $\lambda_i^{(k+1)}$, where $r < i \leq p$. The maximum difference between t and \bar{t} , given by $(t - \bar{t})_{\max}$, is then used in eq. (20). Thus a

where λ^* is the largest eigenvalue estimate calculated in the current subspace iteration, and $\bar{\lambda}_i$ represents the calculated approximation to λ_i . The number of Gram-Schmidt orthogonalizations thus performed is conservative.

Considering the selection of additional shifting, we note that once accurate approximations to the eigenvectors ϕ_1, \dots, ϕ_j have been calculated and stored on back-up storage, the smallest eigenvalue to be calculated next is λ_{j+1} , and hence eq. (19) is modified to

$$\mu_s \leq \bar{\lambda}_{j+1} + \frac{1}{3}(\bar{\lambda}_{q+j+1} - \bar{\lambda}_{j+1}), \quad (27)$$

where $\bar{\lambda}_{j+1}$ is the calculated approximation to λ_{j+1} .

This shifting strategy is used effectively if $q < p$, but to avoid convergence difficulties, the strategy is also best employed if q is only slightly larger than p . We thus recommend using the iteration vector replacement strategy when q is smaller than the default value quoted in section 1, i.e. when $q < \min\{2p, p + 8\}$.

4. Computer implementation

The solution scheme presented in the previous section has been implemented in the computer program SSPACE [7, p. 509]. The purpose of this section is to summarize how the solution procedures have been implemented in the program (see fig. 1).

4.1. Overrelaxation

Having calculated X_{k+1} in eq. (9), an overrelaxation is performed for an iteration vector if eq. (16) is satisfied. In the overrelaxation the iteration vectors from the previous iteration are read from back-up storage, and we calculate

$$X_{k+1} \leftarrow X_k + (X_{k+1} - X_k)\alpha. \quad (28)$$

4.2. Shifting

Considering the matrix shifting strategy, the initial shift is zero and then μ_s is increased with each shift. Based on the considerations in section 3.2, we assess after 4 subspace iterations at a shift whether it is effective to shift to a new position. Namely, about 4 subspace iterations are required for the iteration vectors to settle down after a shift, so that the analysis presented above is approximately applicable. Also, a shift is performed only if there is a saving of at least 3 subspace iterations, i.e. in addition to satisfying eq. (25), we must also have $(t - \bar{t})_{max} \geq 3$.

After 4 subspace iterations have been performed at the current shift the following procedure is employed to establish a *new* shift μ_s .

- (a) Calculate the convergence rates r_i of the eigenvalue iterates using eq. (15) at the end of each iteration, and calculate $\bar{\lambda}_{q+1}$ using eqs. (15) and (17).

(b) Establish the largest allowable shift μ_s . This shift is calculated as

$$\mu_s = \frac{\bar{\lambda}_s + \bar{\lambda}_{s-1}}{2}, \quad (29)$$

where $\bar{\lambda}_s$ is the calculated approximation to λ_s and λ_s is the largest eigenvalue for which all eigenvalue iterates, below and including λ_s , have converged to a tolerance of 10^{-10} using eq. (10). Check whether this shift satisfies eq. (19) (or eq. (27)) and also the condition

$$1.01\bar{\lambda}_{s-1} \leq \mu_s \leq 0.99\bar{\lambda}_s. \quad (30)$$

If either eq. (19) (or eq. (27)) or eq. (30) is not satisfied, decrease s (using $s \leftarrow s - 1$) until both conditions are met. It is next assessed whether shifting to μ_s is effective if the value of μ_s thus obtained is still larger than the current shift.

- (c) If only a few subspace iterations have been performed, reasonably accurate estimates for all λ_m , $s < m \leq p$, may not yet be attainable. Hence, to evaluate eqs. (21)–(25), we use only the eigenvalue iterates $\bar{\lambda}_m$ for which $tol \leq 10^{-2}$. In order that shifting to μ_s be performed, eq. (25) must be satisfied.
- (d) If a shift is performed, use the Sturm sequence information and error estimates on the calculated eigenpair approximations to establish whether all eigenvalues between the previous shift and the new shift have been obtained [7, p. 505]. Assume that j eigenvalues have been calculated between the previous and the current shift; then the following physical error norms [7, p. 413] should be small for all eigenpairs calculated:

$$\epsilon_i = \frac{\|\mathbf{K}\phi_i^{(t+1)} - \lambda_i^{(t+1)}\mathbf{M}\phi_i^{(t+1)}\|_2}{\|\mathbf{K}\phi_i^{(t+1)}\|_2}, \quad (31)$$

and j additional negative elements must be measured in \mathbf{D} , where

$$\mathbf{K} - \mu_s\mathbf{M} = \mathbf{LDL}^t. \quad (32)$$

In theory, it could happen that an eigenpair has been missed [7, p. 505]. However, in practice, such a situation is extremely rare and would always be detected; therefore, the solution procedure is a reliable analysis tool. Also, because the missing of an eigenpair is so rare, the recommended remedy is somewhat crude; namely, stop the solution and repeat with a larger number q of iteration vectors and possibly a tighter convergence tolerance tol [7].

Considering the case $q < \min\{2p, p + 8\}$, the matrix shifting strategy is as described above with one additional calculation procedure. Assume that the candidate shift is discarded based on eq. (25) and is the maximum value possible satisfying eq. (19) (or eq. (27)). In this case, all iteration vectors that correspond to the smallest eigenvalue iterates and that consecutively all satisfy eq. (10) to a tolerance of 10^{-10} are written on back-up storage and replaced by new starting iteration vectors. Further checking on whether additional matrix shifting is effective is then performed after four more subspace iterations.

Table 1. Analysis of the tridiagonal system ($p = 4$, $q = 8$)

	Accelerated scheme				
	Basic scheme	Standard starting subspace			Lanczos starting subspace
		Overrelaxation only	Shifting only	Overrelaxation and shifting	Overrelaxation and shifting
Number of iterations	49	35	31	23	20

5.2. Analysis of a piping system

Fig. 3 shows a computer plot of the piping system considered in this study. For this system the order n of the stiffness and mass matrices is 330, the mean half-bandwidth m_K of the stiffness matrix is 26, and a diagonal mass matrix was employed. The sixty smallest eigenvalues and corresponding eigenvectors were required.

Table 2 summarizes some relevant solution data corresponding to the various analyses performed.

Considering the solution with 68 iteration vectors ($q = 68$), the ratio $(\lambda_{60}/\lambda_{69})^2$ is equal to 0.3, resulting in rapid convergence using the basic scheme. In this case there is no reduction in the number of iterations and the required high speed storage using the accelerated method. However, considering the solution with $q = 20$ and $q = 4$, significantly less high speed storage is needed at no increase in central processor time. Since the average bandwidth of the stiffness matrix is small, the determinant search method is equally effective for this problem [7].

It is interesting to note that in the solution using the Lanczos starting subspace, with $q = 68$, after two iterations the first 34 eigenvalue iterates and after a total of only five iterations the smallest 45 eigenvalue iterates had converged to $tolc = 10^{-10}$. Since the converged iteration vectors are no longer included in the iterations (see section 3.2), about the same total solution

Table 2. Comparison of different solution strategies in the analysis of the piping system ($n = 330$, $m_K = 26$). Diagonal mass matrix was used (Computer used was CDC Cyber 175, $tol = 10^{-6}$)

p/q	Accelerated scheme						
	Basic scheme	Standard starting subspace			Lanczos starting subspace		Determinant search
		60/68	60/68	60/20	60/4	60/68	
Total number of subspace iterations	13	13	74	408	23	2	(5 + 6)*
Total high speed core storage used	42,494	42,494	17,870†	11,700†	42,494	64,094	12,490†
Solution time (CPU sec)	90	74	65	63	77	71	63

*Average number of factorizations and inverse iterations per eigenpair

†Additional secondary storage was required for storing converged eigenvectors

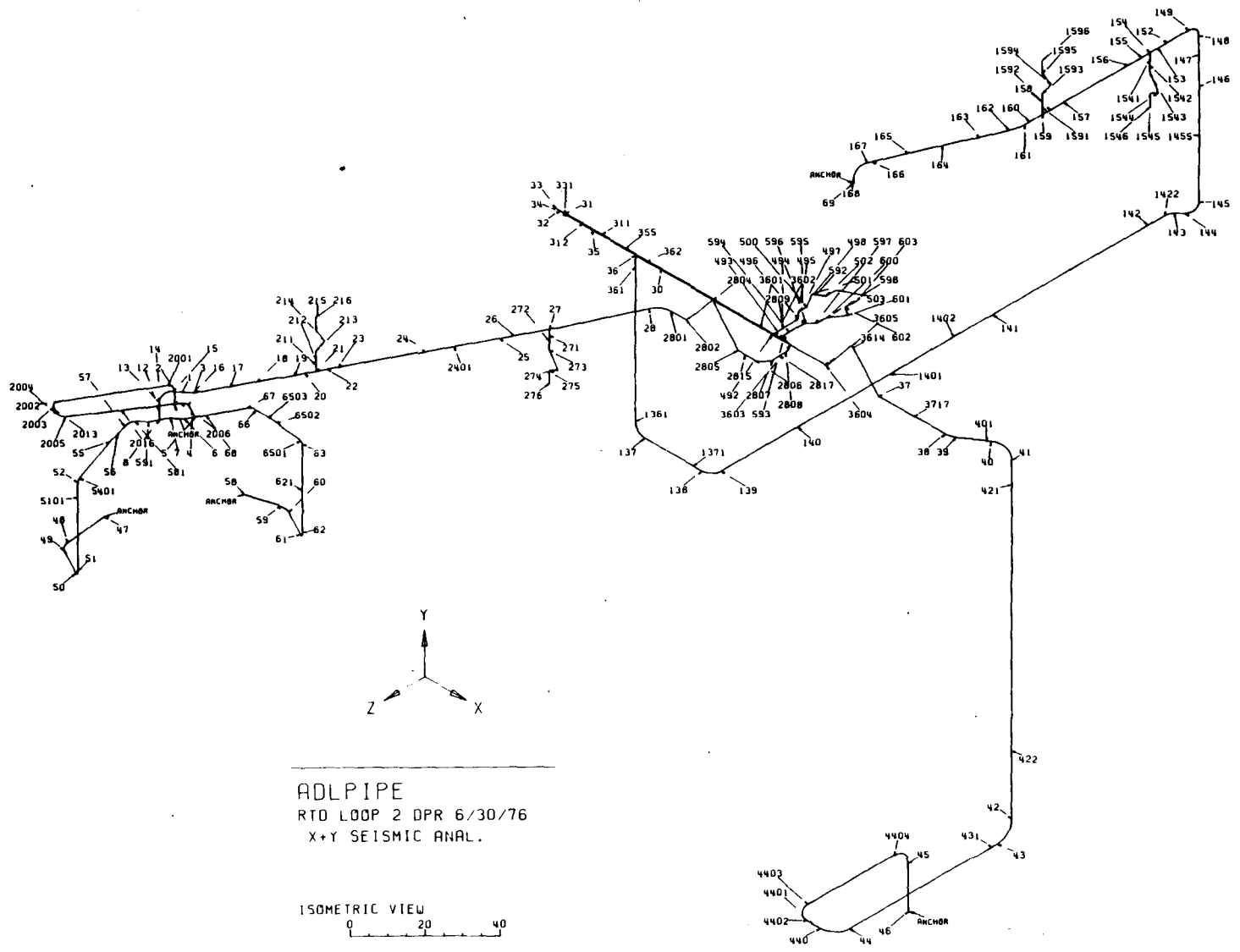


Fig. 3. Geometric view of piping system (order of matrices $n = 330$, mean half-bandwidth $m_K = 26$).

times are required using the "standard" and the Lanczos starting subspaces although more iterations are required using the Lanczos starting vectors.

Finally, table 3 summarizes the complete solution steps for the case $q = 20$. As seen from this table, a total of ten matrix shifts were performed in the solution, and the required sixty eigenpairs were calculated in bundles of 15, 13, 15, 5 and 12 each from five iteration vector sets.

5.3. Analysis of a building frame

The building frame shown in fig. 4 was earlier analyzed in [3]. We analyzed the same structure in this study to demonstrate some important features of the accelerated subspace iteration method. For this system $n = 468$ and $m_k = 91$, and a diagonal mass matrix was employed. The sixty smallest eigenvalues and corresponding eigenvectors were required.

Since the stiffness matrix has a relatively large bandwidth, a determinant search solution is not effective, and only subspace iteration solutions have been calculated.

Table 4 gives the characteristics of the solutions obtained. It is seen that the accelerated subspace iteration method yields a significantly more effective solution than the basic scheme. Table 5 summarizes the solution steps for the case $q = 20$.

In this analysis the Lanczos starting subspace was not employed because the stiffness matrix had to be processed in blocks due to high speed storage limitations [7]. The generation of the starting vectors using the Lanczos method in such a case requires considerable peripheral processing and is not effective when a large number of vectors need be calculated in the solution.

Table 3. Solution steps in the analysis of the piping system ($p = 60$, $q = 20$)

Iteration vector set numbers	Eigenpairs sought	Iterations performed with these vectors	Converged trial vectors simultaneously removed to back-up storage	Eigenpair approximations carried over to next step	Matrix shifts applied at $1/2(\lambda_i + \lambda_{i-1})$ based on convergence of λ_k			Calculation of λ_{q+1} (estimated value)		
					Iteration no.	i	k	$q + 1$	$\bar{\lambda}_{q+1}$	λ_{q+1}
1	1-20	1-17	1-15	16-20	5	1	14	21	24,501	40,373
			at iteration		9	4	17		29,738	
			17		13	11	17		32,847	
2	16-35	18-36	16-28	29-35	24	18	35	36	125,604	102,360
			at iteration		28	22	35		118,106	
			36		32	25	35		113,883	
3	29-48	37-52	29-43	44-48	40	31	44	49	182,623	254,685
			at iteration		44	34	46		227,682	
			52		48	41	46		232,584	
4	44-63	53-66	44-48	49-63	61	49	60	64	658,386	548,048
			at iteration							
5	49-68	67-73	49-60	74						
			at iteration							

Table 4. Comparison of different solution strategies in the analysis of the building frame ($n = 468$, $m_k = 91$). Diagonal mass matrix was used (Computer used was CDC Cyber 175, $tol = 10^{-6}$)

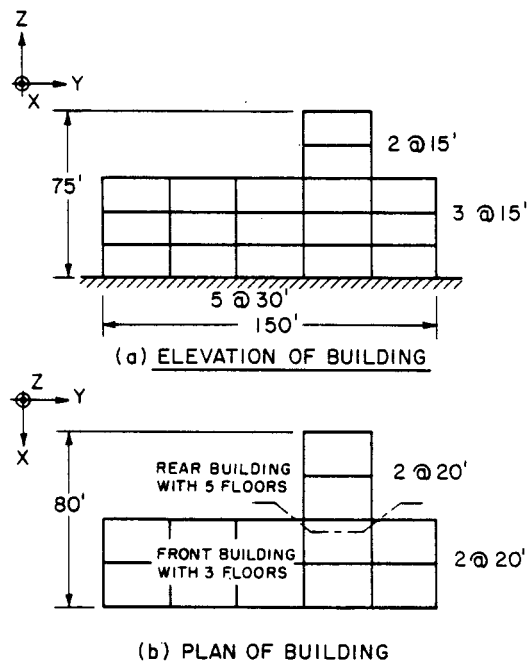
	Basic scheme	Accelerated scheme (standard starting subspace)	
		p/q	p/q
Total number of subspace iterations	47	60/68	80
Total high speed core storage used	66850*	60/68	55282†
Solution time (CPU sec)	570	60/20	209

*Stiffness matrix was stored out-of-core (4 blocks)

†Stiffness matrix was stored in-core, but additional secondary storage was required for storing converged iteration vectors

Table 5. Solution steps in the analysis of the building frame ($p = 60$, $q = 20$)

Iteration vector set numbers	Eigenpairs sought	Iterations performed with these vectors	Converged trial vectors simultaneously removed to back-up storage	Eigenpair approximations carried over to next set	Matrix shifts applied at $1/2(\lambda_i + \lambda_{i-1})$ based on convergence of λ_k			Calculation of λ_{q+1} (estimated value)		
					Iteration no.	i	k	$q+1$	$\hat{\lambda}_{q+1}$	λ_{q+1}
1	1-20	1-17	1-12 at iteration 17	13-20	9	6	15	21	9.59	11.58
					13	9	16			
2	13-32	18-37	13-27 at iteration 37	28-32	21	13	24	33	17.71	29.44
					25	17	30			
					29	24	32			
					33	25	32			
3	28-47	38-54	28-42 at iteration 54	43-47	42	29	34	48	41.51	86.12
					46	34	42			
					50	41	43			
4	43-62	55-72	43-48 at iteration 72	49-62	58	43	48	63	87.64	122.63
					64	46	59			
					68	47	60			
					68	47	60			
5	49-68	73-80	49-60 at iteration 80							

**DATA:**

YOUNG'S MODULUS=432000, MASS DENSITY=1.0
 COLUMNS IN FRONT BUILDING $A_1=3.0, I_1=I_2=I_3=1.0$
 COLUMNS IN REAR BUILDING $A_1=4.0, I_1=I_2=I_3=1.25$
 ALL BEAMS INTO X-DIRECTION $A_1=2.0, I_1=I_2=I_3=0.75$
 ALL BEAMS INTO Y-DIRECTION $A_1=3.0, I_1=I_2=I_3=1.0$
 UNITS : FT, KIP

Fig. 4. A three-dimensional building frame (order of matrices $n = 468$, mean half-bandwidth $m_K = 91$).

6. Conclusions

Effective strategies for accelerating the basic subspace iteration method in the calculation of the smallest eigenvalues and corresponding eigenvectors of generalized eigenproblems have been presented. The solution strategies have been implemented, and the results of some sample analyses are reported. Based on the theory used and the experience obtained with the accelerated subspace iteration method, we conclude that the technique can in some cases provide significantly more effective solutions than the basic method. The increase in solution effectiveness depends on the properties of the eigensolution sought, such as the number of eigenpairs to be calculated, the spreading of the eigenvalues and the order and bandwidths of the matrices. The accelerated solution scheme is in particular more effective than the basic subspace iteration method when the basic method converges only using relatively many iterations. Also, since the accelerated subspace iteration method can be employed with a small or large number of iteration vectors q , the method is more general than the basic method; e.g. the accelerated method can be applied effectively to the solution of eigenproblems in which the matrices have small or large bandwidths.

7. Acknowledgement

We would like to thank I.W. Dingwell of A.D. Little, Cambridge, Massachusetts for supplying the stiffness and mass matrices of the piping system considered in section 5.2. We are also thankful to Prof. B. Irons, University of Calgary, Canada, and Fred Peterson, Engineering/Analysis Corporation, Berkeley, California, for stimulating discussions on the subspace iteration method. Finally, we are grateful to the ADINA users group for supporting financially our research work in computational mechanics.

Appendix. Calculation of starting iteration vectors

Two procedures have been employed to generate the starting iteration vectors.

Using the "standard" procedure, the vectors are generated as described in [7, p. 501]. Briefly, the first starting iteration vector is a full unit vector, the next $q - 2$ vectors each are unit coordinate vectors with the unit entries corresponding to degrees of freedom with large mass and low stiffness values, and the q th starting iteration vector is a random vector. This procedure was always used in the basic subspace iteration method.

In the second procedure the Lanczos algorithm is employed to generate the starting iteration vectors [8]. This procedure is in general effective if q is considerably larger than p . Using this method, we proceed as follows:

Let

$$\bar{x}^t = \{1 \quad 1 \dots 1\} \quad (\text{with all elements } 1).$$

Calculate

$$\alpha^2 = \bar{x}^t M \bar{x},$$

and take the first starting iteration vector as

$$x_1 = \bar{x}/\alpha.$$

Now calculate the starting iteration vectors x_2, \dots, x_{q-1} , using the following equations (with $\beta_1 = 0$):

$$K \bar{x}_{i+1} = M x_i, \tag{A.1}$$

$$\alpha_i = \bar{x}_{i+1}^t M x_i, \tag{A.2}$$

$$\bar{x}_{i+1} = \bar{x}_{i+1} - \alpha_i x_i - \beta_i x_{i-1}, \tag{A.3}$$

$$\beta_{i+1}^2 = \bar{x}_{i+1}^t M \bar{x}_{i+1}, \tag{A.4}$$

$$x_{i+1} = \bar{x}_{i+1}/\beta_{i+1}. \tag{A.5}$$

The q th starting iteration vector is established using a random vector and orthogonalizing this vector to all vectors x_j , $j = 1, \dots, q - 1$.

Theoretically, the vectors \mathbf{x}_i , $i = 1, \dots, q$, that are generated by the above algorithm form an \mathbf{M} -orthonormal basis. However, in practice, the computed vectors are in general not orthogonal because of round-off errors. For this reason we orthogonalize the vectors \mathbf{x}_{i+1} obtained in eq. (A.5) to all previously computed vectors \mathbf{x}_j , $j = 1, \dots, i$.

Another consideration is that the generated vector \mathbf{x}_{i+1} would theoretically be a null vector if the starting vector \mathbf{x}_1 lies in an i -dimensional subspace of the operators \mathbf{K} and \mathbf{M} . Hence, we compute $\gamma_{i+1} = (\bar{\mathbf{x}}_{i+1}^t \mathbf{M} \bar{\mathbf{x}}_{i+1})^{1/2}$, and whenever the ratio β_{i+1}/γ_{i+1} is smaller than 10^{-4} , the computed vector \mathbf{x}_{i+1} is discarded. Then we use the $(i+1)$ st vector generated by the above "standard" procedure as the vector \mathbf{x}_{i+1} , orthogonalize it to all vectors \mathbf{x}_j , $j = 1, \dots, i$, and with β_{i+1} equal to zero we continue the recurrence algorithm in eqs. (A.1)–(A.5).

References

- [1] O.E. Brønlund, Eigenvalues of large matrices, Symposium on Finite Element Techniques at the Institut für Statik and Dynamik der Luft- und Raumfahrtskonstruktionen, Univ. Stuttgart, Jun. 1969.
- [2] K.K. Gupta, Solution of eigenvalue problems by the Sturm sequence method, *Int. J. Numer. Meths. Eng.* 4 (1972) 379–404.
- [3] K.J. Bathe, Solution methods for large generalized eigenvalue problems in structural engineering, Report UC SESM 71-20 (Civil Eng. Dep., Univ. California, Berkeley, CA, Nov. 1971).
- [4] P.S. Jensen, The solution of large symmetric eigenproblems by sectioning, *SIAM J. Numer. Anal.* 9 (1972) 534–545.
- [5] R.B. Corr and A. Jennings, A simultaneous iteration algorithm for symmetric eigenvalue problems, *Int. J. Numer. Meths. Eng.* 10 (1976) 647–663.
- [6] H.R. Schwarz, The eigenvalue problem $(\mathbf{A} - \lambda \mathbf{B})\mathbf{x} = \mathbf{o}$ for symmetric matrices of high order, *Comp. Meths. Appl. Mech. Eng.* 3 (1974) 11–28.
- [7] K.J. Bathe and E.L. Wilson, *Numerical methods in finite element analysis* (Prentice-Hall, Englewood Cliffs, NJ, 1976).
- [8] C.C. Paige, Computational variants of the Lanczos method for the eigenproblem, *J. Inst. Math. Appl.* 10 (1972) 373–381.
- [9] Y. Yamamoto and H. Ohtsubo, Subspace iteration accelerated by using Chebyshev polynomials for eigenvalue problems with symmetric matrices, *Int. J. Numer. Meths. Eng.* 10 (1976) 935–944.
- [10] K.J. Bathe, Convergence of subspace iteration, in: K.J. Bathe, J.T. Oden and W. Wunderlich (eds.), *Formulations and numerical algorithms in finite element analysis* (MIT Press, Cambridge, MA, 1977).
- [11] K.J. Bathe and S. Ramaswamy, Subspace iteration with shifting for solution of large eigensystems, Report AVL 82448-7 (Dept. Mech. Eng., MIT, Cambridge, MA, Dec. 1977).
- [12] K.J. Bathe, ADINA – a finite element program for automatic dynamic incremental nonlinear analysis, Report AVL 82448-1 (MIT, Cambridge, MA, May 1975 (rev. Dec. 1978)).

Part II Formulation and Implementation of Finite Elements and
Material Models for Nonlinear Analysis

An Assessment of Current Finite Element Analysis of Nonlinear
Problems in Solid Mechanics

Finite Element Formulation, Modeling, and Solution of Nonlinear
Dynamic Problems

Finite Element Formulations for Large Deformation Dynamic Analysis

Large Displacement Analysis of Three-Dimensional Beam Structures

A Geometric and Material Nonlinear Plate and Shell Element

A Simple and Effective Element for Analysis of General Shell
Structures

On Transient Analysis of Fluid-Structure Systems

Elastic-Plastic Large Deformation Static and Dynamic Analysis

On Finite Element Large Displacement and Elastic-Plastic Dynamic
Analysis of Shell Structures

On Some Current Procedures and Difficulties in Finite Element
Analysis of Elastic-Plastic Response

A Solution Procedure for Thermo-Elastic-Plastic and Creep
Problems

On Three-Dimensional Nonlinear Analysis of Concrete Structures

NONSAP - A Nonlinear Structural Analysis Program

Some Computational Capabilities for Nonlinear Finite Element
Analysis

Reprinted from:
NUMERICAL SOLUTION OF PARTIAL
DIFFERENTIAL EQUATIONS, III
© 1976
ACADEMIC PRESS, INC.
New York San Francisco London

AN ASSESSMENT OF CURRENT FINITE ELEMENT ANALYSIS OF
NONLINEAR PROBLEMS IN SOLID MECHANICS

Klaus-Jürgen Bathe*

1. Introduction

The finite element analysis of nonlinear problems in solid mechanics has acquired increasing attention. Presently, various large scale computer programs and smaller special purpose codes are used, that offer various analysis capabilities. However, although a large number of problems can already be solved effectively, all computer programs have serious limitations. The objective in this paper is to survey some important aspects of finite element solid mechanics nonlinear analysis, to point out the potential of the finite element method, and to identify some important present research areas with emphasis on numerical analysis procedures. In the presentation we consider what are believed to be the most effective finite element nonlinear analysis techniques presently in use.

The development of finite element nonlinear analysis procedures is based on knowledge in essentially three different disciplines; namely continuum mechanics, numerical analysis procedures and computer implementation. Figure 1 summarizes important areas in these three disciplines. Although the disciplines can be identified separately, an important point is that for the development of effective finite element nonlinear analysis techniques, it is necessary to take into account the

* Department of Mechanical Engineering, Massachusetts Institute of Technology.

interaction that exists between them. For example, the continuum mechanics formulation used in dynamic analysis must be amenable to the numerical time integration scheme that shall be employed, which in turn must be implemented in a cost effective manner on the computer. The objective in this paper is to discuss mainly the formulation of the finite element equations and the numerical procedures used for solution. However, when important, reference is briefly made to the computer implementation, and throughout the paper the important interaction between the areas summarized in Fig. 1 is emphasized.

The material presented in this paper is largely based on the experience gained during the development and use of the general purpose nonlinear static and dynamic finite element analysis computer program ADINA [1], which is a further development of program NONSAP [2] [3]. In order to enhance finite element nonlinear analysis procedures it is necessary, both, to develop new techniques, establish theoretical basis to the techniques used, and to test the procedures on actual difficult practical problems. In this way, the assumptions and limitations of the procedures are demonstrated and researchers are stimulated to improve and further develop the methods employed. It is for this reason that we shall discuss first the theory used and then present practical applications in order to emphasize the present capabilities and important research areas of nonlinear finite element analysis.

NONLINEAR PROBLEMS IN SOLID MECHANICS

A <u>CONTINUUM MECHANICS</u>	B <u>NUMERICAL METHODS</u>	C. <u>COMPUTER TECHNIQUES</u>
1. FORMULATION OF NONLINEAR EQUATIONS OF MOTION	1. NUMERICAL INTEGRATION IN SPACE	1. PROGRAMMING METHODS
2. DEVELOPMENT OF FINITE ELEMENT EQUATIONS	2. TIME INTEGRATION	2. USAGE OF AVAILABLE HARDWARE AND SOFTWARE
3. DEVELOPMENT OF MATERIAL MODELS	3. SOLUTION OF EQUATIONS	3. EFFICIENT PROGRAM ORGANIZATION
	4. CALCULATION OF EIGENSYSTEM	4. FLEXIBILITY FOR MODIFICATIONS

FIGURE 1 IMPORTANT DISCIPLINES IN THE DEVELOPMENT OF FINITE ELEMENT ANALYSIS PROCEDURES

2. Finite Element Formulations

The finite element formulation of nonlinear problems comprises the kinematic formulation of the problems using continuum mechanics principles, the identification of the constitutive relations, and finally the discretization of the equations using finite element procedures. We deal in the following with these individual aspects and discuss the important relations between them.

2.1 Continuum Mechanics Formulation

For the continuum mechanics formulation of nonlinear problems, there exist, in general, two approaches, namely using a Lagrangian (material) formulation or a Eulerian (spatial) formulation [4] [5] [6]. The important difference between the two approaches is that in the Lagrangian formulations attention is focussed on the material itself as it moves, whereas in the Eulerian formulations attention is focussed on what

happens at a specific spatial location. Eulerian formulations are used almost exclusively in fluid flow analysis, whereas Lagrangian descriptions are widely employed in finite element analysis of solid mechanics problems. In this context it may be noted that in some cases formulations have been termed Eulerian although material coordinates are used. Considering solid mechanics problems Lagrangian descriptions are generally employed, because the boundaries of the body under consideration change during the history of solution, and it is natural to use a description which follows the material of the body. In the following we summarize the important concepts of the Lagrangian formulation used in ADINA. The formulation has been presented in detail in references [7] and [8].

Consider a general body subjected to large displacements, large strains and linear or nonlinear constitutive relations. A schematic sketch of the body is shown in Fig. 2.

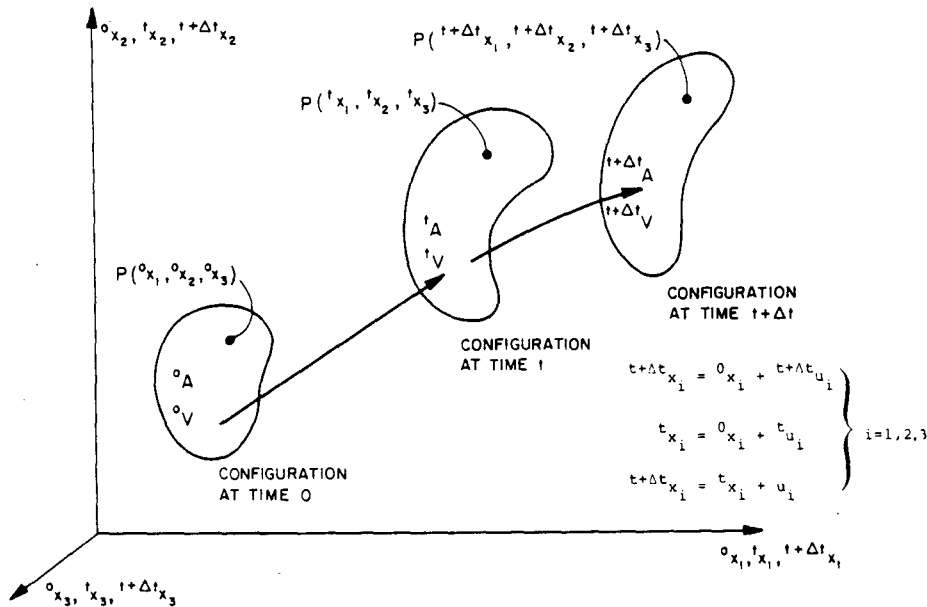


FIGURE 2 MOTION OF BODY IN CARTESIAN COORDINATE SYSTEM

To describe the motion of the body, we use rectangular Cartesian coordinates. The coordinates of a material particle are 0x_i at time 0, tx_i at time t , and ${}^{t+\Delta t}x_i$ at time $t+\Delta t$, $i = 1,2,3$. Thus, we have

$$(1) \quad {}^{t+\Delta t}x_i = {}^0x_i + {}^{t+\Delta t}u_i$$

$$(2) \quad {}^tx_i = {}^0x_i + {}^tu_i$$

where tu_i , ${}^{t+\Delta t}u_i$ are the Cartesian displacements of the particle at times t and $t+\Delta t$, respectively. We define the incremental displacements from times t to $t+\Delta t$ to be u_i , and hence

$$(3) \quad u_i = {}^{t+\Delta t}u_i - {}^tu_i$$

The governing equilibrium equations can be derived using the principle of virtual displacements. This principle is used to formulate a displacement-based finite element solution, which at present is regarded to be most effective. Consider that the solution of the body under static or dynamic loading is required for times $0, \Delta t, 2\Delta t, \dots, t, t+\Delta t, \dots$ and assume that the solution has been obtained up to time t . To calculate the solution for time $t+\Delta t$, in essence two different approaches can be followed that lead to explicit and implicit time integration. For explicit time integration the equilibrium equations are established at time t using a stress rate that is invariant with respect to body rotation [9] [10]. An important disadvantage of such formulations for general applications is that small time steps (load-steps in static analysis) must be used even though the constitutive relations may allow a much larger time step. The reason that small time steps must be employed in static

or dynamic analysis lies in that simple forward integration is employed. In dynamic analysis it is further necessary to use a small enough time step for integration stability.

Although not for all types of problems most effective, it is believed that a formulation in which the equilibrium of the body is considered at time $t+\Delta t$ is most efficient for general static and dynamic analysis. In dynamic analysis such formulation leads to implicit time integration, which using an appropriate integration operator is unconditionally stable in linear analysis. In nonlinear analysis, a control on the accuracy of solution is established by satisfying the equilibrium equations at time $t+\Delta t$ within a specified tolerance.

Considering the equilibrium of the body at time $t+\Delta t$, the principle of virtual displacements states the

$$(4) \quad \int_{t+\Delta t V} {}^{t+\Delta t} \tau_{ij} \delta {}^{t+\Delta t} e_{ij} {}^{t+\Delta t} dv = {}^{t+\Delta t} R$$

where

$$(5) \quad {}^{t+\Delta t} R = \int_{{}^0 A} {}^{t+\Delta t} t_k {}^0 \delta u_k da + \int_{{}^0 V} \rho {}^{t+\Delta t} f_k {}^0 \delta u_k dv$$

and ${}^{t+\Delta t} \tau_{ij}$ are the Cartesian components of the Cauchy stress tensor at time $t+\Delta t$, ${}^{t+\Delta t} t_k$ and ${}^{t+\Delta t} f_k$ are the Cartesian components of the surface traction and body force vectors at time $t+\Delta t$ referred to time 0, ${}^0 \rho$ is the specific mass of the material in the original configuration,

$$(6) \quad \delta {}^{t+\Delta t} e_{ij} = \frac{1}{2} ({}^{t+\Delta t} u_{i,j} + {}^{t+\Delta t} u_{j,i})$$

with ${}^{t+\Delta t} u_{l,m} = \frac{\partial u_l}{\partial {}^{t+\Delta t} u_m}$ and δu_k is a variation in

the current displacement components ${}^{t+\Delta t}u_k$. It should be noted that in Eq. (4) the internal virtual work is evaluated by integration over the volume at time $t+\Delta t$.

The virtual work principle given above is general and is used in linear, material and geometric nonlinear analysis. In small displacement and small strain analysis, the configuration of the body is assumed not to change and Eq. (4) can be used directly for the finite element solution. In this case Eq. (4) becomes

$$(7) \quad \int_{0_V} {}^{t+\Delta t}\sigma_{ij} \delta e_{ij}^0 dv = {}^{t+\Delta t}R$$

where ${}^{t+\Delta t}\sigma_{ij}$ are the Cartesian components of the small displacement stress tensor at time $t+\Delta t$, and e_{ij} are the Cartesian components of the infinitesimal strain increment tensor,

$$(8) \quad e_{ij} = \frac{1}{2} (u_{i,j} + u_{j,i}) .$$

The strain components are evaluated from the finite element displacement interpolations discussed in Section 2.3, and the stress components are obtained using

$$(9) \quad {}^{t+\Delta t}\sigma_{ij} = {}^t\sigma_{ij} + C_{ijrs} e_{rs}$$

where C_{ijrs} is the tangent constitutive tensor at time t . Substituting for ${}^{t+\Delta t}\sigma_{ij}$ from Eq. (9) into Eq. (7), we obtain the equation that is discretized in finite element analysis,

$$(10) \quad \int_{0V} C_{ijrs} e_{rs} \delta e_{ij} \, {}^0 dv = {}^{t+\Delta t} R - \int_{0V} {}^t \sigma_{ij} \delta e_{ij} \, {}^0 dv .$$

Considering now large displacement and large strain analysis, the configuration of the body changes continuously with the individual material particles being subjected to large rotations and stretches. Since the configuration at time $t+\Delta t$ is unknown, for solution the stress and strain variables are referred to a previously calculated known geometric configuration. A very general and effective formulation is the total Lagrangian formulation, in which the initial configuration of the body is used as reference. Using the relations

$$(11) \quad {}^{t+\Delta t} \tau_{sr} = \frac{{}^{t+\Delta t} \rho}{{}^0 \rho} {}^{t+\Delta t} x_{s,i} {}^{t+\Delta t} x_{r,j} {}^{t+\Delta t} S_{ij}$$

where ${}^{t+\Delta t} x_{s,i} = \partial {}^{t+\Delta t} x_s / \partial {}^0 x_i$, and

$$(12) \quad \delta {}^{t+\Delta t} e_{sr} = {}^{t+\Delta t} x_{i,s} {}^{t+\Delta t} x_{j,r} \delta {}^{t+\Delta t} e_{ij}$$

and

$$(13) \quad {}^0 \rho \, {}^0 dv = {}^{t+\Delta t} \rho \, {}^{t+\Delta t} dv$$

where ${}^{t+\Delta t} S_{ij}$ are the Cartesian components of the second Piola-Kirchhoff stress tensor and ${}^{t+\Delta t} e_{ij}$ are the Cartesian components of the Green-Lagrange strain tensor, we can express Eq. (4) as

$$(14) \quad \int_{0_V} {}^{t+\Delta t} S_{ij} \delta {}^{t+\Delta t} e_{ij} {}^0 dv = {}^{t+\Delta t} R .$$

The unknown stresses ${}^{t+\Delta t} S_{ij}$ can now be incrementally decomposed into known stresses ${}^t S_{ij}$ plus increments in stresses ${}^0 S_{ij}$. Then Eq. (4) can be rewritten and linearized as given in Table 1, to obtain

$$(15) \quad \int_{0_V} {}^0 C_{ijrs} {}^0 e_{rs} \delta {}^0 e_{ij} {}^0 dv + \int_{0_V} {}^t S_{ij} \delta {}^0 n_{ij} {}^0 dv \\ = {}^{t+\Delta t} R - \int_{0_V} {}^t S_{ij} \delta {}^0 e_{ij} {}^0 dv .$$

Instead of using the initial configuration at time 0, alternatively any other previously calculated configuration can be used. Specifically, if the configuration at time t is employed as reference the updated Lagrangian formulation also used in ADINA is obtained [1] [7] [8].

It must be noted that Eq. (14) is applicable to any magnitude of displacements and strains. However, Eq. (15) is the linearization of Eq. (14) about the configuration at time t and its solution only approximates the exact solution. If large nonlinearities are present within the individual time intervals, this linearization introduces large uncontrolled errors. In general, therefore, it is necessary to seek a more accurate solution within each interval of time, and such solution can frequently be obtained effectively using a modified Newton iteration. If we define

$$(16) \quad {}^{t+\Delta t} u_i(k) = {}^{t+\Delta t} u_i(k-1) + \Delta u_i(k)$$

where $t_{u_i}^{t+\Delta t(0)} = t_{u_i}$, the equation considered in the materially nonlinear only formulation is

$$(17) \int_{0_V} c_{ijrs} e_{rs}^{(k)} \delta e_{ij}^{(k)} dv = t_{\mathcal{R}}^{t+\Delta t} - \int_{0_V} t_{\sigma_{ij}}^{t+\Delta t(k-1)} \delta e_{ij}^{(k)} dv$$

$$/ k = 1, 2, \dots$$

and in the total Lagrangian formulation we use

$$(18) \int_{0_V} c_{ijrs} e_{rs}^{(k)} \delta e_{ij}^{(k)} dv + \int_{0_V} t_{S_{ij}}^t \delta \eta_{ij}^{(k)} dv$$

$$= t_{\mathcal{R}}^{t+\Delta t} - \int_{0_V} t_{S_{ij}}^{t+\Delta t(k-1)} \delta e_{ij}^{t+\Delta t(k-1)} dv$$

$$/ k = 1, 2, \dots$$

The important problem in using these equilibrium equations is the problem of convergence of the iteration in general analysis. The mathematical properties of the modified Newton iteration and experience show that convergence difficulties can generally be expected when the structure stiffens, which may be the result of a number of different physical phenomena. The result is that a very small time step may have to be used, and iteration may need to be dispensed with for economical reasons.

TABLE 1 TOTAL LAGRANGIAN FORMULATION

1. Equations of Motion

$$\int_{0V} {}^{t+\Delta t} S_{ij} \delta {}^{t+\Delta t} \epsilon_{ij} {}^0 dv = {}^{t+\Delta t} R$$

where

$${}^{t+\Delta t} S_{ij} = \frac{{}^0 \rho}{{}^{t+\Delta t} \rho} {}^0 x_{i,s} {}^{t+\Delta t} \tau_{sr} {}^0 x_{j,r};$$

$$\delta {}^{t+\Delta t} \epsilon_{ij} = \frac{1}{2} \delta ({}^{t+\Delta t} u_{i,j} + {}^{t+\Delta t} u_{j,i} + {}^{t+\Delta t} u_{k,i} {}^{t+\Delta t} u_{k,j}).$$

2. Incremental Decompositions

a. stresses

$${}^{t+\Delta t} S_{ij} = {}^t S_{ij} + \delta S_{ij}$$

b. strains

$${}^{t+\Delta t} \epsilon_{ij} = {}^t \epsilon_{ij} + \delta \epsilon_{ij}; \quad \delta \epsilon_{ij} = \delta e_{ij} + \delta \eta_{ij};$$

$$\delta e_{ij} = \frac{1}{2} ({}^0 u_{i,j} + {}^0 u_{j,i} + {}^t u_{k,i} {}^0 u_{k,j} + {}^0 u_{k,i} {}^t u_{k,j});$$

$$\delta \eta_{ij} = \frac{1}{2} ({}^0 u_{k,i} {}^0 u_{k,j}).$$

3. Equations of Motion with Incremental Decompositions

Noting that $\delta {}^{t+\Delta t} \epsilon_{ij} = \delta \epsilon_{ij}$ and ${}^0 S_{ij} = {}^0 C_{ijrs} {}^0 \epsilon_{rs}$

the equations of motion are

$$\int_{0V} {}^0 C_{ijrs} {}^0 \epsilon_{rs} \delta \epsilon_{ij} {}^0 dv + \int_{0V} {}^t S_{ij} \delta \eta_{ij} {}^0 dv = {}^{t+\Delta t} R$$

$$- \int_{0V} {}^t S_{ij} \delta e_{ij} {}^0 dv.$$

(cont.)

tensor relates 2nd Piola-Kirchhoff stresses to Green-Lagrange strains as is the case in hyperelasticity, the stress-strain law can directly be used in the formulation [11]. However, if the material law is defined in terms of Cauchy stresses, it need be transformed as discussed in detail in references [7] [10] [12]. These transformations can add significantly to the total solution cost and for this reason more effective stress-strain relationships are sought.

Considering the difficulties that are encountered in the analysis of nonlinear material behavior, as probably expected, solution difficulties generally increase as the material to be described becomes more complex. One important practical problem is excessive solution cost, because in history dependent analysis the constitutive relations can depend on many previously calculated variables and may be expensive to evaluate. Solution difficulties are also frequently encountered when discontinuities are present in the material behavior. This is, for example, the case in elastic-plastic analysis under cyclic loading conditions and in crack propagation analysis. Convergence difficulties are encountered when the material suddenly stiffens. In order to deal with such situations, the material discontinuity has been smeared over a small time domain, or simply iterations have not been carried out, well realizing that this way errors are introduced in the solution. As another means to obtain a solution artificial viscosity is used as described in Section 3.2.

2.3 Finite Element Discretization

During the course of nonlinear finite element analysis various different finite elements for different stress and strain conditions have been developed. However, considering general nonlinear analysis the discretization of the continuum mechanics equations using isoparametric and related elements

is considered to be most effective. In particular, the variable-number-nodes elements presented in [8] [9] [13] can be used very efficiently for the analysis of many problems.

In the isoparametric finite element discretization, the finite element equilibrium equations are obtained by interpolating the coordinates and displacements of the elements, using, respectively,

$$(19) \quad \left. \begin{aligned} 0x_j &= \sum_{k=1}^N h_k 0x_j^k ; & t_{x_j} &= \sum_{k=1}^N h_k t_{x_j}^k \\ t+\Delta t x_j &= \sum_{k=1}^N h_k t+\Delta t x_j^k \end{aligned} \right\} \begin{array}{l} j=1,2,3 \\ \text{as applicable} \end{array}$$

$$(20) \quad t_{u_j} = \sum_{k=1}^N h_k t_{u_j}^k ; \quad \Delta u_j = \sum_{k=1}^N h_k \Delta u_j^k \quad \begin{array}{l} j=1,2,3 \\ \text{as applicable} \end{array}$$

where $0x_j^k$ is the coordinate of nodal point k corresponding to direction j at time 0 , $t_{x_j}^k$, $t+\Delta t x_j^k$, $t_{u_j}^k$ and Δu_j^k are defined similarly, and N is the total number of nodal points of the element. The function h_k is the interpolation function corresponding to nodal point k .

Figures 3 and 4 show the variable-number-nodes elements presently used in program ADINA. The effectiveness of these elements lies in that any number of nodes between the minimum and the maximum number can be chosen. This way it is possible to model adequately a variety of structural configurations and continua using basically one element. In particular, it is possible to change from a coarse to a fine mesh always preserving displacement compatibility between elements. An important extension of the variable-number-nodes isoparametric elements would be the possibility of degenerating the elements partially or completely to superparametric elements as

NONLINEAR PROBLEMS IN SOLID MECHANICS

shown in Fig. 5. With the options of using a variable number of nodes and degenerate forms of the basic element, in essence one element can be used to model two and three-dimensional continua and thick and thin shell structures with full compatibility between element boundaries.

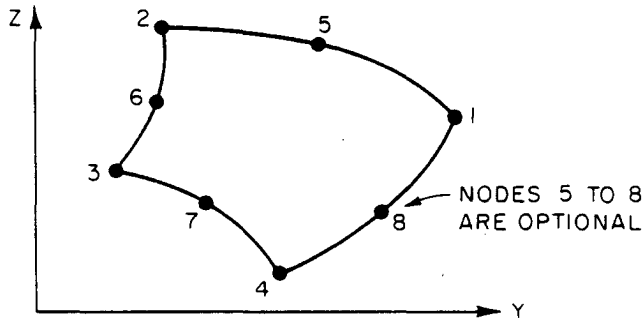


FIGURE 3 4 TO 8 VARIABLE - NUMBER - NODES
TWO-DIMENSIONAL PLANE STRESS,
PLANE STRAIN AND AXISYMMETRIC ELEMENTS

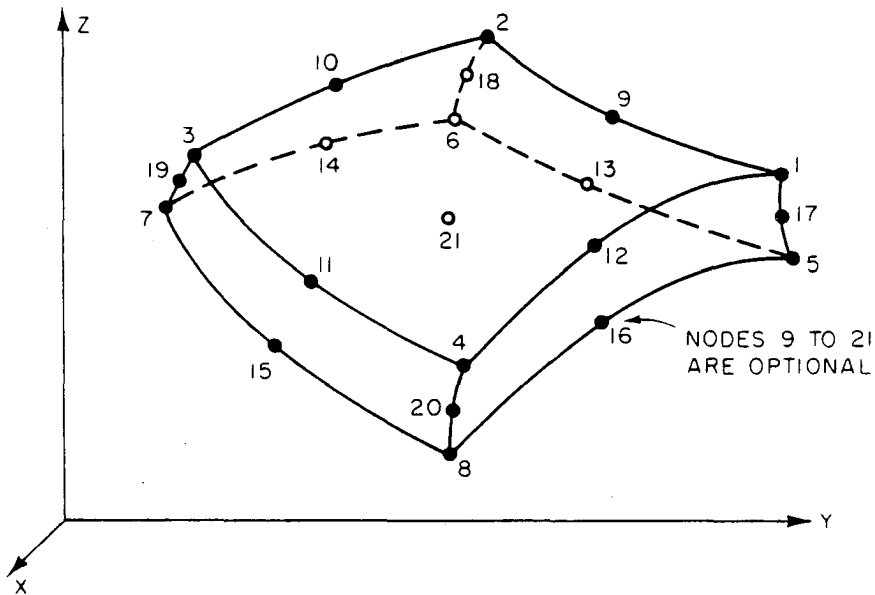
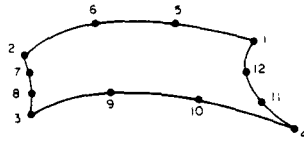


FIGURE 4 8 TO 21 VARIABLE - NUMBER - NODES
THREE - DIMENSIONAL SOLID
AND THICK SHELL ELEMENT

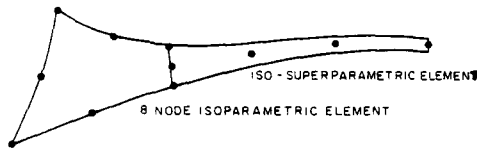
KLAUS-JÜRGEN BATHE



GENERAL 4 TO 12 NODE ELEMENT, ANY NODES FROM NUMBER 5 TO NUMBER 12 CAN BE OMITTED.



SUPERPARAMETRIC THIN SHELL ELEMENT



TYPICAL MODELLING USING AN ISOPARAMETRIC AND A DEGENERATE ELEMENT

FIGURE 5 TWO-DIMENSIONAL SHELL ELEMENTS

Once the interpolation functions for an element domain have been defined, the expressions in Eqs. (19) and (20) are used in Eqs. (17) and (18) to evaluate the finite element equilibrium equations. Realizing that in dynamic analysis body force components include inertia forces and damping forces, the equilibrium equations for a single element corresponding to Eq. (17) are

$$(21) \quad t_{K \Delta u}^{(k)} = t_{\Delta t_R}^{(k)} - t_{\Delta t_F}^{(k-1)} - C t_{\Delta t_U}^{(k)} - M t_{\Delta t_{\ddot{u}}}^{(k)}$$

$$k=1,2,\dots$$

Similarly, including large displacement and large strain effects we obtain for a single element using the total Lagrangian formulation

NONLINEAR PROBLEMS IN SOLID MECHANICS

$$(22) \left({}^t_{0L}K + {}^t_{0NL}K \right) \Delta u^{(k)} = {}^{t+\Delta t}R - {}^{t+\Delta t}F^{(k-1)} - C {}^{t+\Delta t}u^{(k)} - M {}^{t+\Delta t}\ddot{u}^{(k)}$$

$$k=1,2,\dots$$

where tK_L is the element linear strain stiffness matrix at time t when material nonlinear effects are considered only, ${}^t_{0L}K$ and ${}^t_{0NL}K$ are the linear and nonlinear strain stiffness matrices, ${}^{t+\Delta t}R$ is the vector of externally applied nodal point loads, ${}^{t+\Delta t}F^{(k-1)}$ is a vector of nodal point forces equivalent to the current element stresses, M and C are the mass and damping matrices and $\Delta u^{(k)}$ is a vector of nodal point displacement increments, with ${}^{t+\Delta t}u^{(k)} = {}^{t+\Delta t}u^{(k-1)} + \Delta u^{(k)}$. The vectors of nodal point accelerations and velocities are evaluated differently depending on the time integration scheme used (see Section 3.3). Table 2 summarizes the evaluation of the matrices. The calculation of the finite element matrices is given in more detail in references [7] and [8].

TABLE 2 FINITE ELEMENT MATRICES

ANALYSIS TYPE	INTEGRAL	MATRIX EVALUATION
IN ALL ANALYSES [†]	$\int_{0V} {}^0\rho \, {}^{t+\Delta t}\ddot{u}_k \, \delta u_k \, {}^0dv$	$M {}^{t+\Delta t}\ddot{u}$ $= {}^0\rho \left(\int_{0V} H^T H \, {}^0dv \right) {}^{t+\Delta t}\ddot{u}$
	${}^{t+\Delta t}R = \int_{0A} {}^{t+\Delta t}t_k \, \delta u_k \, {}^0da$ $+ \int_{0V} {}^0\rho \, {}^{t+\Delta t}f_k \, \delta u_k \, {}^0dv$	${}^{t+\Delta t}R = \int_{0A} H_S^T \, {}^{t+\Delta t}t \, {}^0da$ $+ {}^0\rho \int_{0V} H^T \, {}^{t+\Delta t}f \, {}^0dv$

(cont.)

continuum may individually be described by different kinematic formulations. Thus, nonlinear elements with material nonlinearities only or with combined material and geometric nonlinearities may be used in one finite element mesh to represent the actual continuum.

3. Numerical Methods

A most important part of finite element analysis is the use of effective numerical methods, firstly, to evaluate the required finite element matrices and, secondly, to calculate the solution of the equilibrium equations. In this section, the important numerical techniques used in nonlinear finite element analysis are surveyed with the objective to point out where significant improvements are needed.

3.1 Numerical Integration in Space

The evaluation of the finite element matrices as summarized in Table 2 must be performed using numerical integration. The technique widely used in isoparametric finite element analysis is Gauss quadrature [9] [15]. For example, the linear strain stiffness matrix in the total Lagrangian formulation is evaluated using

$$(23) \quad \int_{0_V} \mathbf{t}_{B_L}^T \mathbf{0}^C \mathbf{t}_{B_L} \mathbf{0}^i dv = \sum_i \alpha_i \mathbf{t}_{B_L}^{iT} \mathbf{0}^C \mathbf{t}_{B_L}^i$$

where α_i is a weighting factor and the summation is carried out over all integration points. Since the numerical effort is directly proportional to the number of integration points used, it is desirable to employ integration methods that minimize the number of integration points required for a given accuracy. Various integration schemes have been devised specifically for finite element analysis. Some success has

been reported using selective integration, in which different weighting factors are assigned to the different strain components. Although some excellent improvements in solution accuracy of some problems have been reported in linear analysis, the proposed techniques have not been evaluated to such an extent that they can be used with confidence in practical linear and nonlinear analysis.

It should be noted that in addition to ultimate convergence analyses, in particular, theoretical analyses are required that show under what conditions stable and for practical purposes sufficiently accurate solutions are obtained. Such guidelines are very difficult to establish when material and geometric nonlinearities are considered. However, for finite element analysis to be effective and reliable using a minimum number of integration points, rigorous guidelines for the choice of integration scheme and required order of integration are needed.

3.2 Solution of Static Equilibrium Equations

The equilibrium equations considered in static analysis are

$$(24) \quad t_{K \Delta u}^{(k)} = t_{\Delta t_R} - t_{\Delta t_F}^{(k-1)} \\ k=1,2,\dots$$

As discussed in Section 2.1, the above solution corresponds to a modified Newton iteration for the zero of the function f , where

$$(25) \quad f = t_{\Delta t_R} - t_{\Delta t_F}^{(\infty)}$$

The k 'th iteration in essence requires the evaluation of the vector $t_{\Delta t_F}^{(k-1)}$ and then the solution of a set of linear algebraic equations. These equations could be solved

using an iterative scheme or a direct method. Although probably not always most efficient, implementations of the basic Gauss elimination method are currently most effective for general applications [9]. An important advantage of Gauss elimination is that the number of numerical operations and hence the computer time required for the solution of the system of equations can be determined a priori, whereas using an iterative scheme such as the Gauss-Seidel method, the solution time can in general not be predicted accurately. It should also be noted that the direct solution solvers have been developed to be very efficient so that in many nonlinear analyses most of the computational effort is spent in the calculation of $t+\Delta t_F^{(k-1)}$ rather than in the solution of the equations.

The effectiveness of the direct equation solvers is largely a result of the specific storage scheme used and the specific implementation of the basic Gauss solution method. Namely, in the solution only the elements under the skyline of the matrix are considered as shown in Fig. 6 [1] [9] [16]. Although the number of operations required for the LDL^T or Cholesky factorization of a given matrix is predetermined, for a specific solution scheme, large reductions in the number of operations can frequently be obtained by rearranging the equations prior to the solution. It should be noted that for the compacted column storage reduction schemes, different algorithms than those developed for bandwidth minimization are required [17] [18].

KLAUS-JÜRGEN BATHE

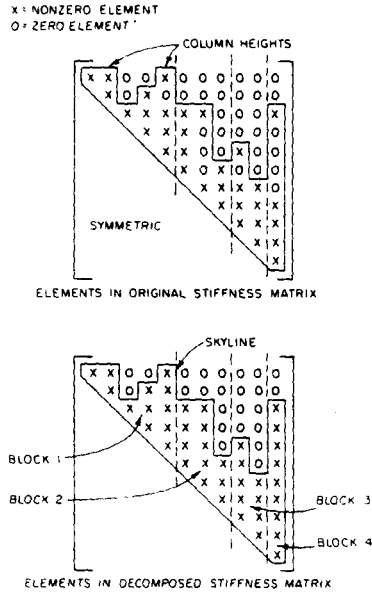


FIGURE 6 TYPICAL ELEMENT PATTERN IN A STIFFNESS MATRIX USING BLOCK STORAGE

The modified Newton iteration in Eq. (24) converges provided the correction $\Delta u^{(k)}$ is small enough, but relatively large corrections can be dealt with, if the first and second derivatives of f satisfy certain conditions. If a one degree of freedom system is considered, these conditions are that $f' < 0$ and $f'' \geq 0$. However, for multiple degree of freedom systems f represents a multiple dimension surface and the change in f corresponding to all components must be considered. In practice, those components that are subjected to the most significant changes will decide whether convergence within a specified tolerance will occur. The practical implications of these statements are that convergence difficulties can be expected if the finite element assemblage is stiffening under the applied load. The stiffening may be due to geometric nonlinear effects or changes in material properties.

If iteration divergence is encountered in practice, it frequently is effective to include in the analysis viscous effects in form of a damping matrix C , i.e. instead of Eq. (24) the following equilibrium relation is considered,

$$(26) \quad t_K \Delta u(k) = t+\Delta t_R - t+\Delta t_F(k-1) - C t+\Delta t_U(k)$$

$$k=1,2,\dots$$

where $t+\Delta t_U(k)$ is evaluated using a time integration scheme (see Section 3.3). The viscous nodal point forces prevent large sudden changes in displacements, and vanish once no more changes in displacements occur. Hence the static solution is obtained. In a number of static analyses with convergence difficulties, simply the Newmark time integration scheme was used with zero mass and small concentrated nodal damping values. These concentrated dampers were detected using engineering judgment.

Considering the difficulties in convergence, it is realized that a very important field is the development of solution strategies to speed up convergence in general analysis. The solution algorithms should detect convergence difficulties, and then choose appropriate measures to stabilize the solution. This can be achieved by means of automatic load step (time step) selection, over or under-relaxation, temporary modification of the equations or other measures. In addition to acceleration techniques for iteration convergence, also effective schemes for automatic load or time step selection are to be developed. It is in these areas that a great deal of research is still required in finite element analysis because very few generally applicable results have been obtained. Advances towards more effective solution strategies will only be possible by rigorous mathematical

analysis, if the solution methods are to be generally applicable and self-adaptive.

3.3 Solution of Dynamic Equilibrium Equations

In dynamic analysis including mass and damping effects the equations to be solved are

$$(27) \quad t_{K \Delta u}^{(k)} = t_{+\Delta t_R} - t_{+\Delta t_F}^{(k-1)} - c_{t+\Delta t} \dot{u}^{(k)} - M_{t+\Delta t} \ddot{u}^{(k)}$$

$$k=1,2,\dots$$

The solution to this system of equations is obtained using direct integration. As pointed out in Section 2.1, the equilibrium equations have been developed for use with an implicit integration method. The most effective implicit integration methods for general application are presently the Newmark method and Wilson θ -method [19] [20] [21] [22] [23]. The Houbolt method has similar characteristics of stability and accuracy as the Wilson method but the disadvantage that special starting strategies are required. Table 3 lists the assumptions used in these three methods. Although not included in the table, a great deal of potential appears to lie in the various stiffly stable methods [24] [25] [26].

TABLE 3 COMMON IMPLICIT DIRECT INTEGRATION METHODSHOUBOLT METHOD:

$${}^{t+\Delta t}\ddot{u} = \frac{1}{\Delta t^2} \left\{ 2{}^{t+\Delta t}u - 5{}^t u + 4{}^{t-\Delta t}u - {}^{t-2\Delta t}u \right\}$$

$${}^{t+\Delta t}\dot{u} = \frac{1}{6\Delta t} \left\{ 11{}^{t+\Delta t}u - 18{}^t u + 9{}^{t-\Delta t}u - 2{}^{t-2\Delta t}u \right\}$$

NEWMARK METHOD:

$${}^{t+\Delta t}\ddot{u} = \ddot{u} + \left\{ (1 - \delta)\ddot{u} + \delta{}^{t+\Delta t}\ddot{u} \right\} \Delta t$$

$${}^{t+\Delta t}u = u + \dot{u} \Delta t + \left\{ \left(\frac{1}{2} - \alpha \right) \ddot{u} + \alpha{}^{t+\Delta t}\ddot{u} \right\} \Delta t^2$$

WILSON θ - METHOD

$${}^{t+\theta\Delta t}\ddot{u} = \frac{6}{\theta^2 \Delta t^2} \left({}^{t+\theta\Delta t}u - u \right) - \frac{6}{\theta \Delta t} \dot{u} - 2\ddot{u}$$

$${}^{t+\theta\Delta t}\dot{u} = \frac{3}{\theta \Delta t} \left({}^{t+\theta\Delta t}u - u \right) - 2\dot{u} - \frac{\theta \Delta t}{2} \ddot{u}$$

In the computer program ADINA the Newmark method and Wilson θ -method are presently used, but it is expected that additional integration schemes will be implemented. Considering the various classes of problems that shall be solved using a general purpose finite element program, it is likely that a library of different integration methods should be provided. The important task is then to identify clearly for which classes of nonlinear problems each of the available operators is most effective. Indeed, it might well be that substantial advantages can be obtained by changing during the step-by-step

solution from one operator to another. At present, very little information other than engineering experience with specific nonlinear problems is available for the selection of an integration operator.

An important aspect is the generality of the integration algorithm used. Table 4 summarizes the dynamic step-by-step solution performed in program ADINA. Essentially one integration algorithm is used in which the constants are selected either to employ the Newmark method or the Wilson θ -method.

It should be noted from Table 4 that if no mass and damping effects are considered the step-by-step solution reduces to the solution of Eqs. (24) and (26) solved in static analysis. Therefore, the various solution aspects considering convergence and accuracy discussed in Section 3.2 are also applicable in dynamic analysis. However, it may be noted here that, as probably expected physically, the dynamic solution of a problem is more stable. This is mathematically demonstrated by the fact that the mass effects contribute to the effective stiffness of the system as shown in the calculation of t_K^c in Table 4. Convergence in the iteration is frequently assured provided the elements in the effective stiffness matrix are large enough, meaning in practical analysis that a small enough time step Δt has to be chosen (see Section 4).

It is interesting to note that until a few years ago almost all nonlinear dynamic finite element analysis has been performed without equilibrium iteration. Indeed, at present, it appears that the only general purpose computer programs that have specifically designed for equilibrium iteration in dynamic analysis are program ADINA and its forerunner NONSAP. This is the case, although the accurate solution of the equilibrium equations at each time step is even more important in dynamic analysis than in static analysis. Namely, any error

that is introduced into the dynamic step-by-step solution will accumulate and cannot be compensated for later, as in the solution of many static geometrically nonlinear elastic analyses.

TABLE 4 STEP-BY-STEP INTEGRATION IN ADINA

-- INITIAL CALCULATIONS --

1. Form linear stiffness matrix K , mass matrix M , and damping matrix C ; initialize 0u , ${}^0\dot{u}$, ${}^0\ddot{u}$.

2. Calculate the following constants:

$tol \leq 0.01$; $nitem \geq 3$; in static analysis $\theta = 1$ and go to 3.

Wilson θ -method: $\theta \geq 1.37$, usually $\theta = 1.4$, $\tau = \theta\Delta t$

$$a_0 = 6/\tau^2 \quad a_1 = 3/\tau \quad a_2 = 2a_1 \quad a_3 = 2$$

$$a_4 = 2 \quad a_5 = \tau/2 \quad a_6 = a_0/\theta \quad a_7 = -a_2/\theta$$

$$a_8 = 1 - 3/\theta \quad a_9 = \Delta t/2 \quad a_{10} = \Delta t^2/6$$

Newmark method: $\theta = 1.0$, $\delta \geq 0.50$, $\alpha \geq 0.25(0.5 + \delta)^2$, $\tau = \Delta t$

$$a_0 = 1/(\alpha\Delta t^2) \quad a_1 = \delta/(\alpha\Delta t) \quad a_2 = 1/(\alpha\Delta t) \quad a_3 = 1/(2\alpha) - 1$$

$$a_4 = \delta/\alpha - 1 \quad a_5 = \Delta t(\delta/\alpha - 2)/2 \quad a_6 = a_0 \quad a_7 = -a_2$$

$$a_8 = -a_3 \quad a_9 = \Delta t(1 - \delta) \quad a_{10} = \delta\Delta t$$

3. Form effective linear stiffness matrix: $\hat{K} = K + a_0M + a_1C$.

4. In linear analysis triangularize \hat{K} .

-- FOR EACH TIME STEP --

A. IN LINEAR ANALYSIS

(i) Form effective load vector

$${}^{t+\tau}\hat{R} = {}^tR + \theta({}^{t+\Delta t}R - {}^tR) + M(a_0 {}^tu + a_2 {}^t\dot{u} + a_3 {}^t\ddot{u}) \\ + C(a_1 {}^tu + a_4 {}^t\dot{u} + a_5 {}^t\ddot{u}) \cdot (\text{cont.})$$

TABLE 4 (cont.)

- A. (ii) Solve for displacement increments:

$$\hat{K} \hat{t}^{\tau} u = \hat{t}^{\tau} R ; u = \hat{t}^{\tau} u - t_u .$$

- (iii) Go to C .

- B. IN NONLINEAR ANALYSIS

- (i) If a new stiffness matrix is to be formed, update \hat{K} for nonlinear stiffness effects to obtain $\hat{t}^{\tau} \hat{K}$; triangularize $\hat{t}^{\tau} \hat{K}$:

$$\hat{t}^{\tau} \hat{K} = LDL^T .$$

- (ii) Form effective load vector:

$$\begin{aligned} \hat{t}^{\tau} \hat{R} = & t_R + \theta(t^{\Delta} t_{R-} - t_R) + M(a_2 t_{\dot{u}} + a_3 t_{\ddot{u}}) \\ & + C(a_4 t_{\dot{u}} + a_5 t_{\ddot{u}}) - t_F . \end{aligned}$$

- (iii) Solve for displacement increments using latest D , L factors:

$$LDL^T u = \hat{t}^{\tau} \hat{R} .$$

- (iv) If required, iterate for dynamic equilibrium; then initialize $u^{(0)} = u$, $i = 0$

- (a) $i = i + 1$.

- (b) Calculate (i-1)st approximation to accelerations, velocities, and displacements:

$$\hat{t}^{\tau} \ddot{u}^{(i-1)} = a_0 u^{(i-1)} - a_2 t_{\dot{u}} - a_3 t_{\ddot{u}} ;$$

$$\hat{t}^{\tau} \dot{u}^{(i-1)} = a_1 u^{(i-1)} - a_4 t_{\dot{u}} - a_5 t_{\ddot{u}} ;$$

$$\hat{t}^{\tau} u^{(i-1)} = u^{(i-1)} + t_u .$$

(cont.)

TABLE 4 (cont.)

- B. (iv) (c) Calculate (i-1)st effective out-of-balance loads:

$${}^{t+\tau_R}\hat{r}^{(i-1)} = {}^{t_R}r + \theta({}^{t+\Delta t}t_R - {}^{t_R}r) - M {}^{t+\tau_U}(i-1) \\ - C {}^{t+\tau_U}(i-1) - {}^{t+\tau_F}(i-1) .$$

- (d) Solve for i'th correction to displacement increments:

$$LDL^T \Delta u^{(i)} = {}^{t+\tau_R}\hat{r}^{(i-1)} .$$

- (e) Calculate new displacement increments:

$$u^{(i)} = u^{(i-1)} + \Delta u^{(i)} .$$

- (f) Iteration convergence if $\|\Delta u^{(i)}\|_2 / \|u^{(i)}\|_2 < tol$

$$+ \|u^{(i)}\|_2 < tol$$

If convergence: $u = u^{(i)}$ and go to C ;

If no convergence and $i < nitem$: go to (a); otherwise restart using new stiffness matrix and/or a smaller time step size.

C. CALCULATE NEW ACCELERATIONS, VELOCITIES, AND DISPLACEMENTS

Wilson θ -method:

$${}^{t+\Delta t}\ddot{u} = a_6 u + a_7 \dot{u} + a_8 \ddot{u}$$

$${}^{t+\Delta t}\dot{u} = \dot{u} + a_9 ({}^{t+\Delta t}\ddot{u} + \ddot{u})$$

$${}^{t+\Delta t}u = u + \Delta t \dot{u} + a_{10} ({}^{t+\Delta t}\ddot{u} + 2 \ddot{u})$$

Newmark method:

$${}^{t+\Delta t}\ddot{u} = a_6 u + a_7 \dot{u} + a_8 \ddot{u}$$

$${}^{t+\Delta t}\dot{u} = \dot{u} + a_9 \ddot{u} + a_{10} {}^{t+\Delta t}\ddot{u}$$

$${}^{t+\Delta t}u = u + u .$$

3.4 Solution of Eigenproblems

In nonlinear analysis of solid mechanics problems eigen-solutions are required at various occasions. A most frequently considered eigenproblem is the calculation of the smallest eigenvalues and corresponding eigenvectors of the finite element system. In this case the generalized eigenproblem considered is

$$(28) \quad \mathbf{t}_K \phi = \omega^2 \mathbf{M} \phi$$

and the solution is sought for the p lowest eigenvalues $0 < \omega_1^2 \leq \omega_2^2 \leq \dots \leq \omega_p^2$ and the corresponding eigenvectors $\phi_1, \phi_2, \dots, \phi_p$. The ω_i and the ϕ_i represent the free vibration frequencies and mode shapes of the finite element system at time t . The frequencies are used to estimate an appropriate time step Δt for the direct integration solution, and they are usually calculated at some representative time in order to take into account that they change during the solution.

Another important eigenproblem arises in linearized buckling analysis. This problem can be written in the form of Eq. (28) by introducing a shift [9].

A large number of different solution methods are available for the problem in Eq. (28) [9] [27]. However, considering that in finite element analysis large systems shall be solved on a routine basis, only a relatively few number of solution methods can be used, and indeed more effective solution techniques are still required. At present, for most practical finite element analyses the determinant search method and subspace iteration technique are considered to be most effective [9] [28]. These two solution methods have been described in detail earlier, and the only objective is here briefly summarized the subspace iteration method in order to point out the large additional potential in the technique.

In essence, the subspace iteration method consists of the following steps:

- (1) Establish q starting iteration vectors, $q > p$.
- (2) Use simultaneous inverse iteration on the q vectors and Ritz analysis to extract the "best" eigenvalue and eigenvector approximations from the q iteration vectors.
- (3) After iteration convergence use the Sturm sequence check to verify that the required eigenvalues and corresponding eigenvectors have been calculated.

The technique has been called subspace iteration method because the iteration is equivalent to iterating with a q -dimensional subspace, and should not be regarded as a simultaneous iteration with q individual iteration vectors. Let X_1 store the q linear independent starting iteration vectors, then the k 'th iteration step can be summarized as follows:

Iterate from the subspace E_k to the subspace E_{k+1} ,

$$(29) \quad {}^t_K \bar{X}_{k+1} = M X_k .$$

Calculate the projections of t_K and M onto E_{k+1} ,

$$(30) \quad K_{k+1} = \bar{X}_{k+1}^T {}^t_K \bar{X}_{k+1}$$

$$M_{k+1} = \bar{X}_{k+1}^T M \bar{X}_{k+1} .$$

Calculate the eigensystem of the projected stiffness and mass matrices,

$$(31) \quad K_{k+1} Q_{k+1} = M_{k+1} Q_{k+1} \omega_{k+1}^2 .$$

Evaluate new eigenvector approximations,

$$(32) \quad X_{k+1} = \bar{X}_{k+1} Q_{k+1} .$$

In Eqs. (31) and (32) the "best" eigenvalue and eigenvector approximations that can be obtained in the sense of a Ritz analysis are calculated, and provided that the starting vectors in X_1 are not orthogonal to the required eigenvectors convergence occurs to ϕ_1, \dots, ϕ_p and $\omega_1^2, \dots, \omega_p^2$.

It should be noted that the selection of the starting iteration vectors and the Sturm sequence check are considered important parts of the subspace iteration method. Namely, the closer the starting subspace is to the p -dimensional least dominant required subspace, the smaller will be the number of iterations required for convergence. Indeed, if q starting vectors can be established that span the least dominant p -dimensional subspace, convergence will occur in the first step of the iteration. Hence, one way to improve the effectiveness of the iteration, is to find algorithms that establish more effective starting iteration vectors. At present, the starting vectors are selected using the magnitudes of the diagonal elements in tK and M and, depending on the problem and the required eigensolution accuracy, of the order 10 iterations are required. In addition to improving the starting subspace, also reliable shift strategies and other acceleration techniques should further be investigated.

The last phase of the subspace iteration method consists of the Sturm sequence check, which assures that the required eigenvalues and vectors have indeed been obtained. This check can be relatively costly when a large banded system is considered and it is certainly desirable to develop equivalent more effective techniques.

The important point to emphasize is that, in theory, any order of eigenproblem of the form in Eq. (28) can be solved. However, in practice, restrictions on the order of the eigenproblem that can be considered are reached surprisingly fast,

mainly because of cost limitations. Therefore, additional research should be conducted to increase the effectiveness of the eigensolution of Eq. (28).

4. DEMONSTRATIVE SAMPLE SOLUTIONS

During the last years a large number of analysis results of nonlinear problems in solid mechanics have been obtained using various finite element computer programs [29]. But in almost all published material relatively little has been said about the practical difficulties encountered during the solutions. Apart from indicating the current capabilities and the potential of the finite element method for solving nonlinear problems, the primary objective in this section is to show some examples where the typical difficulties of nonlinear analysis described in the previous sections have been encountered. The analysis results used here for this purpose have been obtained using the computer programs ADINA [1] and SAP IV [13].

4.1 Static and Dynamic Large Displacement Analysis of a Cantilever Beam

A simple cantilever beam subjected to uniformly distributed loading was analyzed using the total Lagrangian formulation. The cantilever beam is shown in Fig. 7.

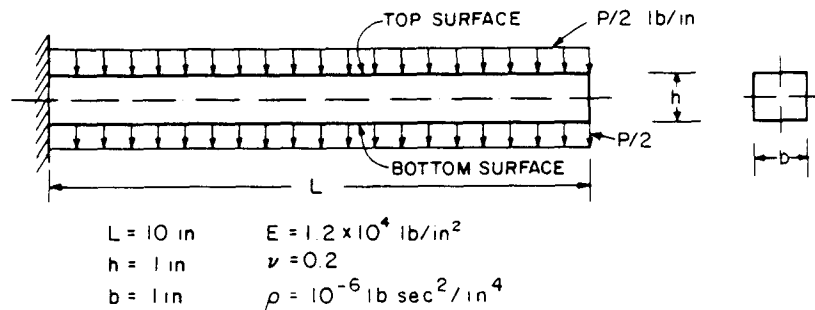


FIGURE 7 CANTILEVER UNDER UNIFORMLY DISTRIBUTED LOAD

For the finite element analysis the beam was idealized as an assemblage of 5 plane stress isoparametric elements.

This sample analysis demonstrates that excellent results can be obtained in some nonlinear static analyses, but a relatively large computational effort may be required. Figure 8 shows the calculated displacement response of the cantilever, when 100 equal load steps are used to apply the total load. The solution compares very well with the response predicted by Holden [30]. Although no attempt was made to optimize the solution cost, [8], a relatively large computational effort is required, in order to obtain accurate results, because the structure is stiffening with increasing displacements.

Considering next the dynamic behavior of the beam, the importance of equilibrium iterations in the dynamic analysis of this structure could be demonstrated. Figure 9 shows the displacement response predicted for an instantaneously applied pressure when two different values of solution time step Δt are used. It is noted that the response predicted with the three times larger time step is accurate provided equilibrium iterations are performed. If the step-by-step solution is used without equilibrium iterations errors accumulate, which in this case decrease the response significantly. In general, the calculated response would simply diverge from the actual response of the system, without the analyst knowing about the error accumulation. It is interesting to note that in the analysis with the larger time step an average of 4 iterations were required per time step, and that the dynamic analysis required a total computational effort which was of the same order as required in the static analysis.

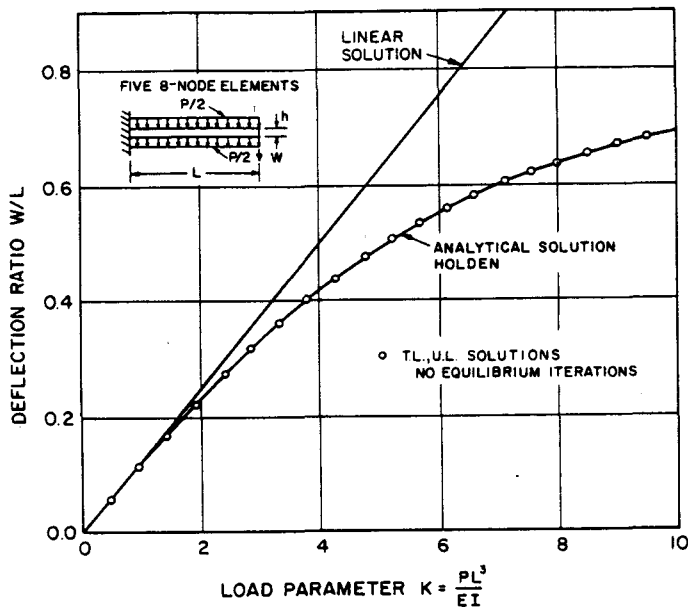


FIGURE 8 LARGE DISPLACEMENT ANALYSIS OF A CANTILEVER

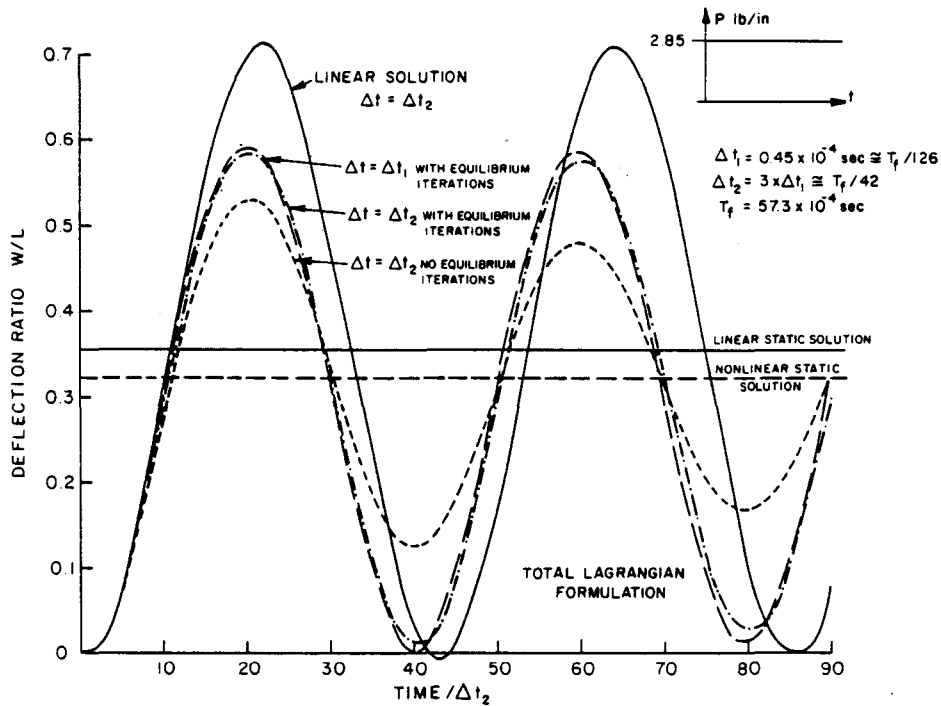


FIGURE 9 LARGE DISPLACEMENT DYNAMIC RESPONSE OF CANTILEVER UNDER UNIFORMLY DISTRIBUTED LOAD, NEWMARK METHOD $\delta=0.50$, $\alpha=0.25$

4.2 Elastic-Plastic Static Analysis of a Thick-Walled Cylinder

A very common computer program check-out problem is the elastic-plastic analysis of a thick-walled cylinder under internal pressure, because an accurate solution has been provided by Hodge and White [31]. To compare with their solution the finite element model shown in Fig. 10 was analyzed.

Figure 11 shows the predicted displacement response in the finite element analysis. It is observed that the finite element solution compares very well with the solution by Hodge and White. The reason for discussing this analysis here is to point out the difficulties that arise when unloading of the cylinder is considered. Namely, if at the unloading point the elastic-plastic stiffness matrix is used, the equilibrium iteration will not converge. In order to calculate in this finite element analysis the displacement response for loading and unloading the initial elastic stiffness matrix was used with equilibrium iterations in each load step. In this analysis good results have been obtained because of the special geometry and loading condition. In general, however, the use of the elastic stiffness matrix throughout an elastic-plastic analysis can introduce large uncontrolled errors.

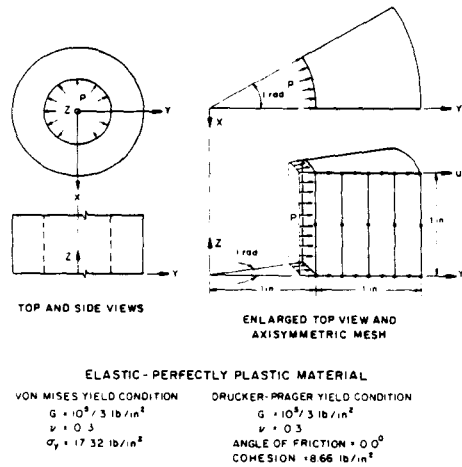


FIGURE 10 FINITE ELEMENT MESH OF THICK-WALLED CYLINDER

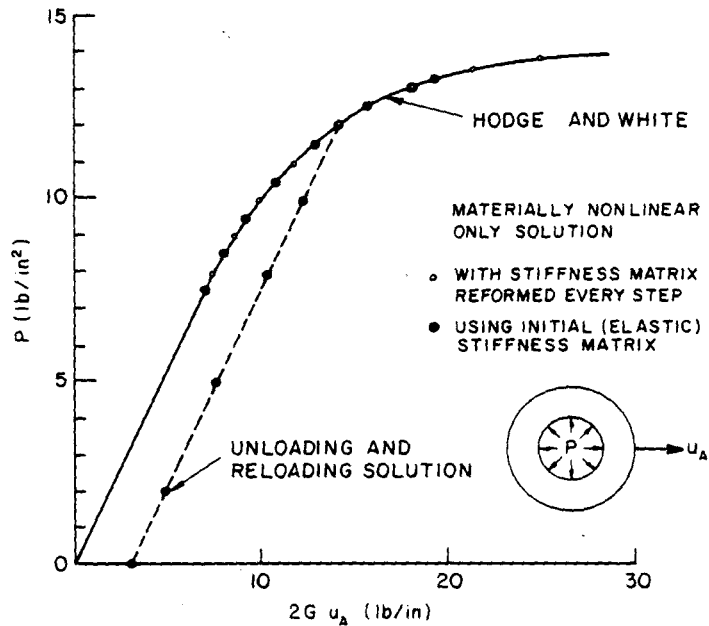


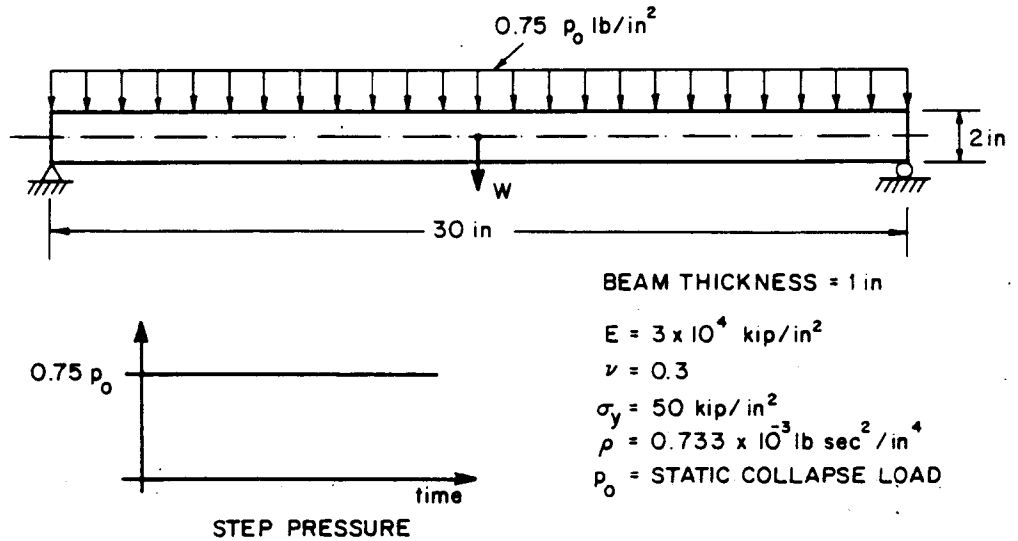
FIGURE 11 ELASTIC-PLASTIC DISPLACEMENT RESPONSE OF THICK-WALLED CYLINDER

4.3 Elastic-Plastic Dynamic Analysis of a Simply Supported Beam

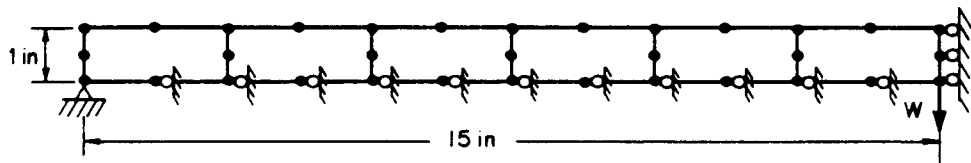
The simply supported beam shown in Fig. 12 was analyzed for the step loading indicated. The figure also gives the finite element idealization used in the analysis. The material of the beam was assumed to be elastic-perfectly plastic.

Figure 13 shows the calculated displacement response. The initial calculated displacement response is shown again in Fig. 14, but this time normalized with respect to the static elastic deflection of the beam subjected to p_0 . In the figure, also the displacement response predicted by Nagarajan and Popov is shown [32], who only presented the initial response and did not use equilibrium iterations. When the analysis was repeated with the time step used by Nagarajan and Popov and no equilibrium iterations close comparison with their results was obtained, as shown in Fig. 14. However, at

a later time the solution started to oscillate and diverge from the response given in Fig. 13, until finally the solution was meaningless. It can be concluded that the error accumulation was so severe that in effect the solution became unstable. The purpose of discussing this sample solution is to underline the importance of error control through equilibrium iterations in a dynamic analysis.



SIMPLY SUPPORTED BEAM AND APPLIED LOAD



FINITE ELEMENT IDEALIZATION, SIX 8 NODE ELEMENTS

FIGURE 12 ELASTIC-PLASTIC DYNAMIC ANALYSIS OF SIMPLY-SUPPORTED BEAM

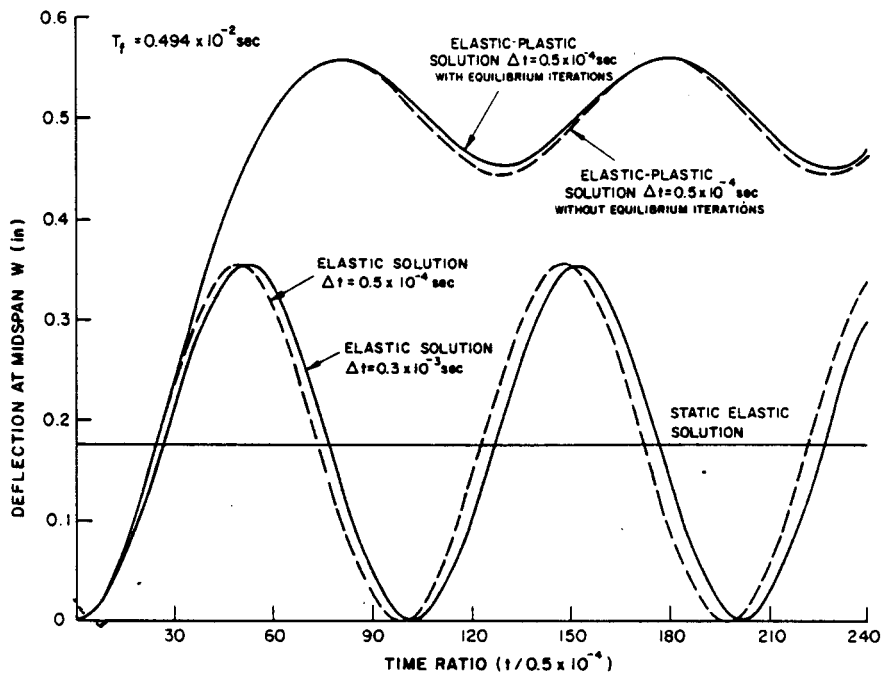


FIGURE 13 DYNAMIC SMALL DISPLACEMENT ELASTIC-PLASTIC RESPONSE OF SIMPLY SUPPORTED BEAM, NEWMARK METHOD, $\delta = 0.50$, $\alpha = 0.25$

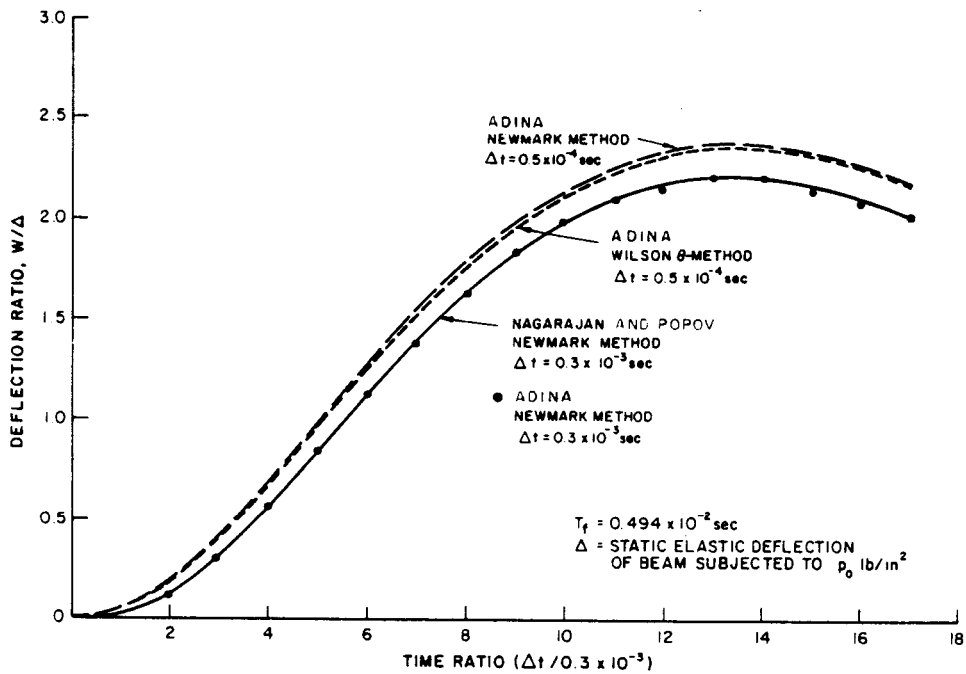


FIGURE 14 INITIAL ELASTIC-PLASTIC DISPLACEMENT RESPONSE OF SIMPLY SUPPORTED BEAM

4.4 Analysis of a Pipe Whip Problem

In the design of nuclear reactor piping equipment an important problem is the analysis of pipes that are subjected to high impact forces and impinge on displacement stops. The purpose of installing the displacement stops is to prevent the occurrence of large displacements in case of a pipe break.

Figures 15 and 16 show a simple finite element model of a cantilevered pipe and its displacement stop, which was analyzed using the program ADINA [33]. The behavior of the system is highly nonlinear, because the material of the pipe and the stop is assumed to be elastic-perfectly plastic and the stop introduces instantaneously a large stiffness into the system. The purpose of presenting this analysis is to indicate some present practical requirements in nonlinear analysis.

Figures 15 and 16 give the displacement and velocity response of the model. The response predicted for the pipe is compared with a solution obtained using the computer program HEMP using 720 zones [34], in which it was assumed that the stop is perfectly rigid. It is noted that the two solutions compare well, although only 6 elements have been used in the finite element analysis.

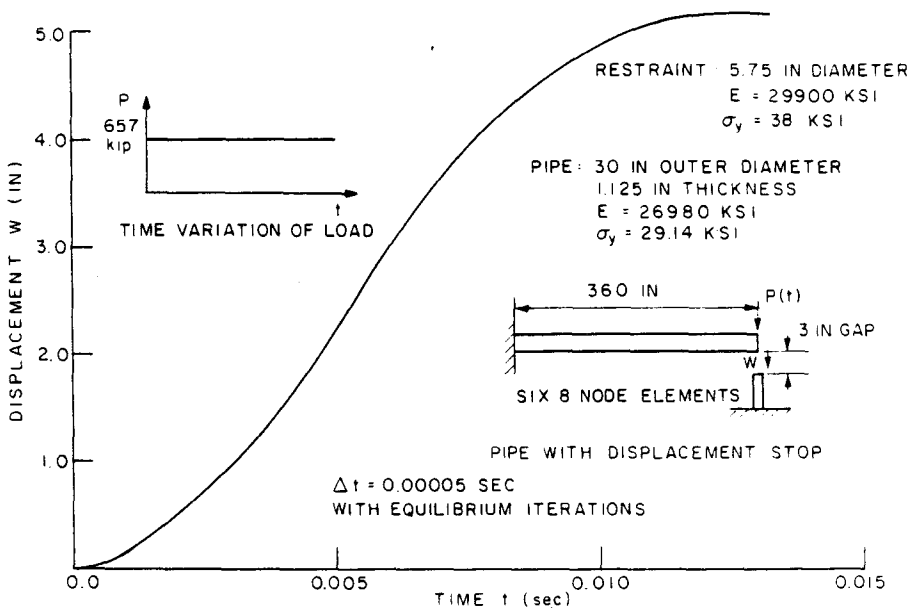


FIGURE 15 DISPLACEMENT RESPONSE OF PIPE WHIP MODEL USING ADINA, NEWMARK METHOD, $\delta = 0.50$, $\alpha = 0.25$

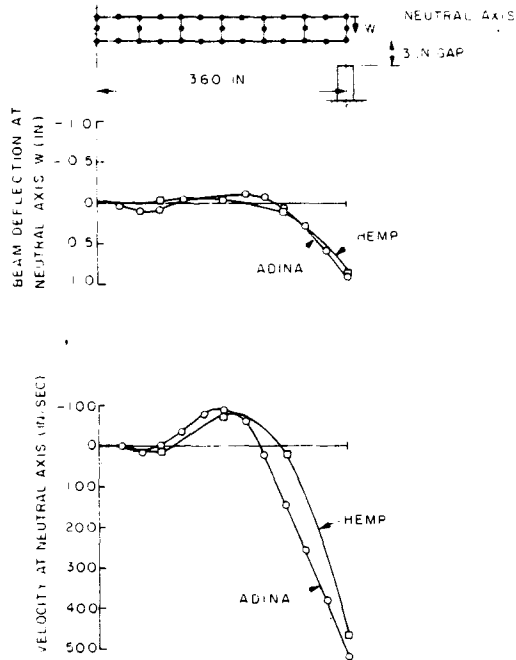


FIGURE 16 PIPE WHIP MODEL RESPONSE AT $t = 0.003$ SEC

4.5 Analysis of Tunnel Opening

In many important practical problems it is necessary to take into account the stiffness deterioration of the material under increasing load. The finite element method is much suited to the analysis of such problems.

Figure 17 shows a plane strain finite element model of a tunnel subjected to overburden pressure. In this analysis the variable-number-nodes elements have been used [8] [9], thus having complete displacement compatibility between elements. The material was characterized using the curve description model with tension cut-off to simulate the cracking of the material [8].

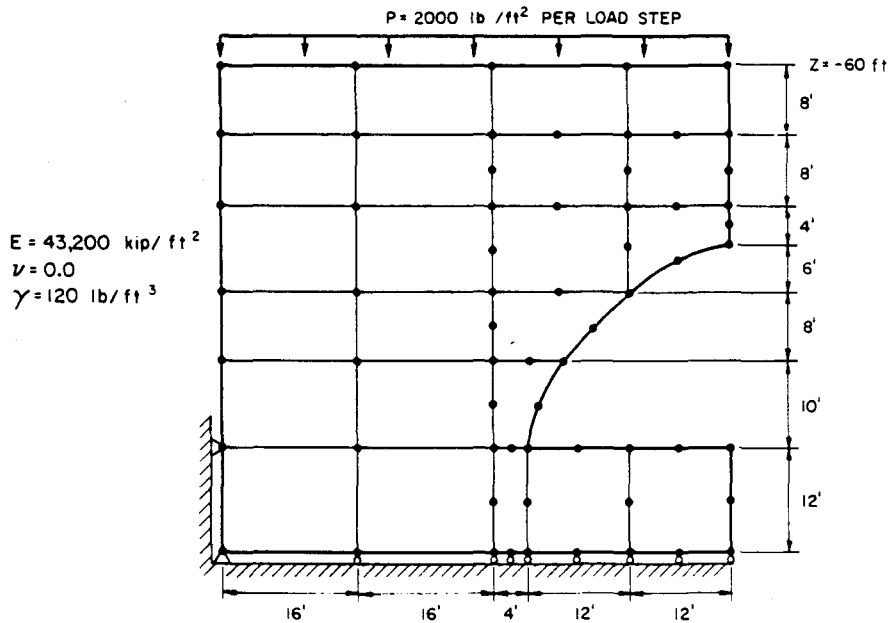


FIGURE 17 FINITE ELEMENT MESH FOR ANALYSIS OF UNDERGROUND OPENING

Figures 18 and 19 show the displacement response and crack distributions as a function of the overburden pressure. Accurate results can be obtained with this model provided small enough load steps are used and the material is loading. On the other hand, unloading conditions are difficult to analyze because the material is stiffening. Indeed, a great deal of additional research is still required to develop constitutive models that predict adequately stiffness deteriorating material response and are numerically stable and accurate under cyclic loading conditions.

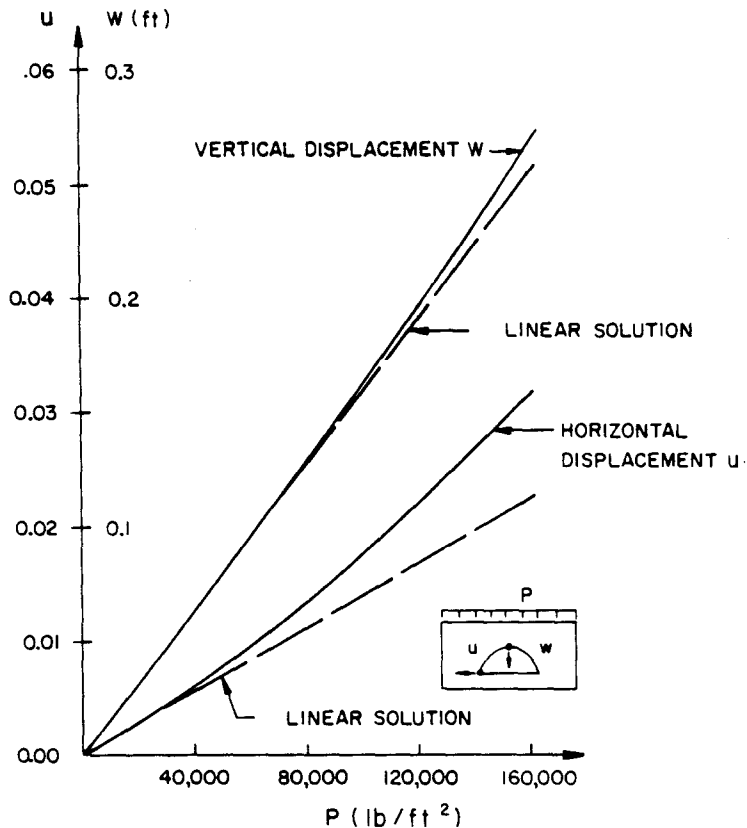


FIGURE 18 LOAD-DEFLECTION RESPONSE OF UNDERGROUND OPENING

KLAUS-JÜRGEN BATHE

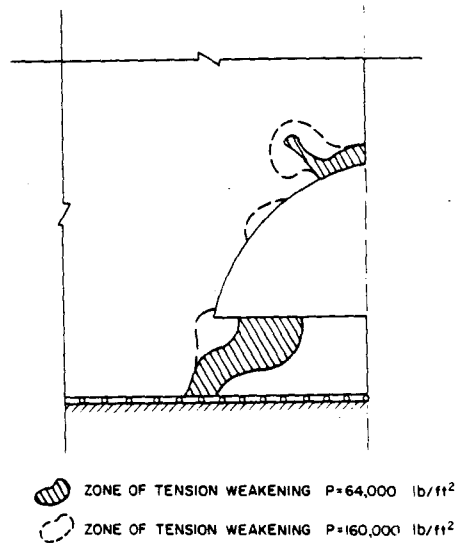


FIGURE 19 CRACKED REGIONS AROUND UNDERGROUND OPENING

4.6 Calculation of Frequencies and Mode Shapes

As was pointed out earlier a significant computational effort in finite element analysis is frequently expended in the calculation of eigenvalues and corresponding eigenvectors. To indicate the present capabilities and expense involved in the calculation of eigensystems, Table 5 summarizes the solution times for various problems using the subspace iteration method. In all cases the lowest frequencies and corresponding vibration mode shapes have been calculated. It is noted that very large finite element systems can already be solved without excessive cost, but that improvements in the efficiency of present eigensolution techniques are necessary, if very large systems shall be considered on a routine basis.

Table 5 CALCULATION OF FREQUENCIES AND MODE SHAPES
USING SUBSPACE ITERATION METHOD

SYSTEM	SYSTEM ORDER n	MAXIMUM HALF BANDWIDTH	NUMBER OF EIGENPAIRS	COMPUTER USED	CENTRAL PROCESSOR SECONDS
PIPING SYSTEM	566	12	28	CDC 6600	142
REACTOR BUILDING WITH FOUNDATION	1174	138	45	CDC 6600	890
DAM	2916	492	4	CDC 7600	495
WIND-TUNNEL	5952	216	10	CDC 7600	1000
3-DIM. BUILDING FRAME	468	156	4	CDC 6400	160

5. Conclusions

The objective in this paper was to survey present non-linear finite element analysis procedures with specific emphasis on the numerical techniques used. It is concluded that although already many practical problems can be solved effectively, there are a number of important research areas that require attention. The specific problems to be considered are, in essence, those of the stability, accuracy and cost of solution. Because of the inherent potential in the finite element method, major advances towards more effective solution strategies are anticipated, but it is concluded that an increasing amount of mathematical analysis will be required.

REFERENCES

1. Bathe, K. J., "ADINA - A Finite Element Program for Automatic Dynamic Incremental Nonlinear Analysis," Report No. 82448-1, Acoustics and Vibration Laboratory, Department of Mechanical Engineering, Massachusetts Institute of Technology, 1975.
2. Bathe, K. J., Wilson, E. L., and Iding R., "NONSAP - A Structural Analysis Program for Static and Dynamic Response of Nonlinear Systems," Report No. UCSESM 74-3, Department of Civil Engineering, University of California, Berkeley, February 1974.
3. Bathe, K. J., and Wilson, E. L., "NONSAP - A Nonlinear Structural Analysis Program," Nuclear Engineering and Design, Vol. 29, (1974).
4. Crandall, et al., Dynamics of Mechanical and Electro-mechanical Systems, McGraw-Hill, New York, 1967.
5. Malvern, L. E., Introduction to the Mechanics of a Continuous Medium, Prentice-Hall, Inc. Englewood Cliffs, New Jersey, 1969.
6. Washizu, K., Variational Methods in Elasticity and Plasticity, Pergamon Press, New York, 2nd edition, 1975.
7. Bathe, K. J., Ramm, E., and Wilson, E. L., "Finite Element Formulations for Large Deformation Dynamic Analysis," International Journal for Numerical Methods in Engineering, Vol. 9, 353-386.
8. Bathe, K. J., Ozdemir, H., and Wilson, E. L., "Static and Dynamic Geometric and Material Nonlinear Analysis," Report No. UCSESM 74-4, Department of Civil Engineering, University of California, Berkeley, February 1974.
9. Bathe, K. J., and Wilson, E. L., Numerical Methods in Finite Element Analysis, Prentice Hall, Englewood Cliffs, New Jersey, to appear 1976.
10. McMeeking, R. M., and Rice, J. R., "Finite Element Formulations for Problems of Large Elastic-Plastic Deformation," Technical Report, Nasa NGL 40-002-080/15, Division of Engineering, Brown University, Providence, R. I., May 1974.
11. Oden, J. T., Finite Elements of Nonlinear Continua, McGraw-Hill, 1972.
12. Bathe, K. J., and Ozdemir, H., "Elastic-Plastic Large Deformation Static and Dynamic Analysis," J. Computers and Structures, in press.
13. Bathe, K. J., Wilson, E. L., and Peterson, F. E., "SAP IV - A Structural Analysis Program for Static and Dynamic Response of Linear Systems," Report No. EERC 73-11, University of California, Berkeley, 1973.

NONLINEAR PROBLEMS IN SOLID MECHANICS

14. Clough, R. W., and Bathe, K. J., "Finite Element Analysis of Dynamic Response," 2nd U.S.-Japan Symposium, Berkeley, August 1972; *Advances in Computational Methods in Structural Mechanics and Design*, University of Alabama Press, Huntsville, Alabama, U.S.A.
15. Zienkiewicz, O. C., The Finite Element Method in Engineering Science, McGraw-Hill, London, 1971.
16. Mondkar, D. P. and Powell, G. H., "Large Capacity Equation Solver for Structural Analysis," *Computers and Structures*, Vol. 4 (1974), 699-728.
17. Rosen, R., "Matrix Bandwidth Minimization," *Proceedings National Conference A.C.M.* (1968), 585-595.
18. Cuthill, E. H., and McKee, J. M., "Reducing the Bandwidth of Sparse Symmetric Matrices," *Proceedings, National Conference A.C.M.* (1969), 151-172.
19. Newmark, N. M., "A Method of Computation for Structural Dynamics," *ASCE, Journal of Engineering Mechanics Division*, Vol. 85 (1959), 67-94.
20. Wilson, E. L., Farhoomand, I., and Bathe, K. J., "Non-linear Dynamic Analysis of Complex Structures," *International Journal of Earthquake Engineering and Structural Dynamics*, Vol. 1 (1973), 241-252.
21. Bathe, K. J., and Wilson, E. L., "Stability and Accuracy Analysis of Direct Integration Methods," *Earthquake Engineering and Structural Dynamics*, Vol. 1 (1973), 283-291.
22. Belytschko, T., and Schoeberle, D. F., "On the Unconditional Stability of an Implicit Algorithm for Nonlinear Structural Dynamics," to be published.
23. Houbolt, J. C., "A Recurrence Matrix Solution for the Dynamic Response of Elastic Aircraft," *Journal of Aeronautical Science*, Vol. 17 (1950), 540-550.
24. Gear, C. W., "The Automatic Integration of Stiff Ordinary Differential Equations," *Information Processing*, Vol. 68 (1969), 187-193.
25. Jain, M. K., and Srivastava, V. K., "Optimal Stiffly Stable Methods for Ordinary Differential Equations," Report 402, Department of Computer Sciences, University of Illinois, Urbana, June 1970.
26. Jensen, P. S., "Transient Analysis of Structures by Stiffly Stable Methods," *J. Computers and Structures*, Vol. 4 (May 1974), 615-626.
27. Wilkinson, J. H., The Algebraic Eigenvalue Problem, Clarendon Press, Oxford, 1965.
28. Bathe, K. J., and Wilson, E. L., "Solution Methods for Eigenvalue Problems in Structural Mechanics," *International Journal for Numerical Methods in Engineering*, Vol. 6 (1973), 213-226.

29. Marcal, P. V., "Survey of General Purpose Programs for Finite Element Analysis," 2nd U.S.-Japan Symposium, Berkeley, August 1972; Advances in Computational Methods in Structural Mechanics and Design, University of Alabama Press, Huntsville, Alabama, U.S.A.
30. Holden, J. T., "On the Finite Deflections of Thin Beams," Int. J. Solids Struct., Vol. 8 (1972), 1051-1055.
31. Hodge, P. G., and White, G. H., "A Quantitative Comparison of Flow and Deformation Theories of Plasticity," J. Appl. Mech., Vol. 17 (1950), 180-184.
32. Nagarajan, S., and Popov, E. P., "Elastic-Plastic Dynamic Analysis of Axisymmetric Solids," Report No. UC SESM 73-9, Department of Civil Engineering, University of California, Berkeley, 1973.
33. Dunder, V. and Ma, S. M., Private Communication, Bechtel Int. Corp., San Francisco, California, 1975.
34. Wilkins, M. L., "Calculation of Elastic-Plastic Flow," Report UCRL-7322, Rev. I, Lawrence Radiation Laboratory, University of California, Livermore, Ca. 1969.

Finite Element Formulation, Modeling, and Solution of Nonlinear Dynamic Problems

Klaus-Jürgen Bathe

ABSTRACT

Finite element procedures for analysis of nonlinear dynamic problems in solid and structural mechanics and fluid-structure interaction are surveyed and assessed. Effective finite element formulations for highly nonlinear continuum and structural mechanics problems are summarized, modeling considerations for analysis of structural dynamics and wave propagation problems are described, and time integration procedures for the solution of the equations of motion are discussed. Some demonstrative analysis results are given that indicate the present state-of-the-art in nonlinear dynamic analysis.

1. INTRODUCTION

During recent years an increasing demand for nonlinear dynamic analysis of various engineering problems has developed, and, correspondingly, a relatively large amount of research effort has been devoted to the development of efficient solution procedures for problems in nonlinear dynamics. The increasing importance of nonlinear analysis is largely due to the emphasis placed by agencies on realistic modeling and accurate analysis of critical structural components as arise, for example, in the safety deliberations of strategic structures and nuclear reactor components, and the design of satellites. At present some nonlinear dynamic problems can already be solved quite efficiently and with confidence, but most problems are still difficult and computationally very expensive to analyze, or cannot be solved at all.

In general, dynamic problems can be classified as wave propagation problems or structural vibration problems. An effective and accurate nonlinear finite element analysis of either type of problem is based on the use of appropriate kinematic formulations, constitutive models, time integration schemes, and most importantly on the use of an appropriate finite element model of the system under consideration. The finite element model and the time integration step to be chosen for the analysis of a problem depend on the type of loading, the geometry, and the material conditions. The complexity of practical nonlinear dynamic analysis lies in the interdependency between the various important analysis considerations, and the difficulties in establishing appropriate finite element meshes and integration time steps.

The objective in this paper is to survey and assess what are believed to be at present the most effective finite element procedures for analysis of nonlinear dynamic problems in solid and structural mechanics, and fluid-structure interaction. In the first part of the paper the general finite element formulation of nonlinear dynamic problems is presented. Continuum and structural mechanics problems are considered with large displacement, large strain and material nonlinearities. Also briefly summarized are the time integration schemes used, and a mode superposition method which is effective for problems that contain local nonlinearities only.

In the second part of the paper the finite element modeling of nonlinear dynamic problems is presented. The use of lumped versus consistent mass idealization, the choice and required number of elements and degrees of freedom, and the selection of appropriate time steps in the solution of structural dynamics and wave propagation problems are discussed.

Of particular concern in the analysis of nonlinear dynamic problems is the stability and accuracy of the step-by-step solution. In the third part of the paper some important stability and accuracy characteristics of the time integration methods in use are described, and the importance of these characteristics in practical nonlinear analysis is emphasized. Finally, in the last part of the paper, the analyses of a number of problems are presented. The description

of these analyses and the results obtained demonstrate the use of the finite element modeling and solution procedures discussed in the paper, and indicate the present state-of-the-art in the analysis of nonlinear dynamic problems.

2. FINITE ELEMENT FORMULATION AND SOLUTION

The use of effective finite element formulations and solution procedures is of main importance in the analysis of nonlinear dynamic problems. Indeed, whether in practice, the analysis of a problem is deemed possible or not can depend to a large degree on the selection of the appropriate finite element formulation and solution procedures.

2.1 Formulation of Nonlinear Dynamic Problems

The solution of general nonlinear dynamic problems is at present most efficiently obtained using isoparametric displacement-based finite element discretization. Assume that in an incremental analysis of a general body as shown in Fig. 1, the solution has been obtained from time 0 to time t , and that the solution is required for time $t+\Delta t$. For the analysis we use the principle of virtual displacements to express the equilibrium of the body in a stationary Cartesian coordinate system; in explicit time integration the equilibrium is considered at time t [1, 2],

$$\int_{t_V} t_{\tau_{ij}} \delta_t e_{ij} t dv = t_R \quad (1)$$

where $t_{\tau_{ij}}$ is a Cartesian component of the Cauchy stress tensor at time t , " δ " means "variation in", $t e_{ij}$ is a Cartesian component of the infinitesimal strain tensor referred to the configuration at time t ,

$$t e_{ij} = \frac{1}{2} \left(\frac{\partial u_i}{\partial t_{x_j}} + \frac{\partial u_j}{\partial t_{x_i}} \right) ; \quad t_{x_i} = {}^0 x_i + t_{u_i} \quad (2)$$

and t_R is the virtual work of the externally applied loads and inertia forces.

In implicit time integration the equilibrium of the body is considered at time $t+\Delta t$,

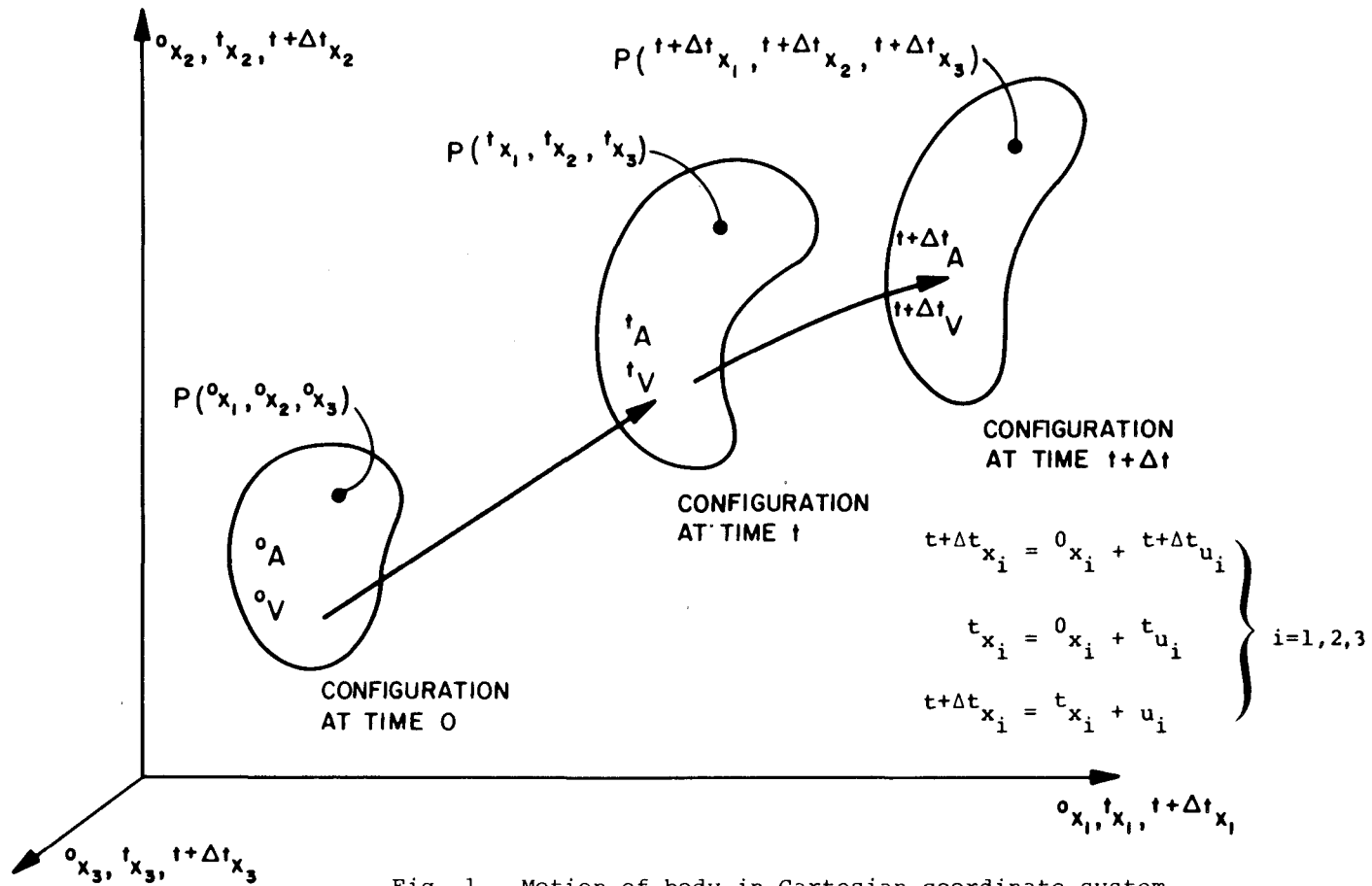


Fig. 1. Motion of body in Cartesian coordinate system.

$$\int_{t+\Delta t_V}^{t+\Delta t} \tau_{ij} \delta_{t+\Delta t} \epsilon_{ij} dv = t+\Delta t R \quad (3)$$

where the variables are defined as in Eq. (1) but corresponding to time $t+\Delta t$.

For solution by finite element discretization we recognize that Eq. (1) can be solved directly, because the configuration and static and kinematic variables of the body at time t are known. Substituting the finite element interpolations (see Section 2.2) into Eq. (1) we obtain for a single element or an element assemblage (the element assemblage process is carried out using the direct stiffness method) [1],

$$\underline{M} \ddot{\underline{U}} = \underline{t}_R - \underline{t}_F \quad (4)$$

where

\underline{M} = mass matrix,

\underline{t}_R = vector of externally applied nodal loads at time t ,

\underline{t}_F = vector of nodal point forces that are equivalent to the element stresses at time t ,

\underline{U} = vector of nodal point accelerations at time t .

Equation (4) is used directly to calculate the displacements and stresses at time $t+\Delta t$ using an explicit time integration scheme (see Section 2.3).

Considering next the solution of Eq. (3) we recognize that the configuration of the body at time $t+\Delta t$ is unknown and that, therefore, the static and kinematic variables must first be referred to a known, previously calculated, configuration. A very effective and general formulation is the total Lagrangian formulation [3-6] in which the initial configuration of the body is used as reference, and Eq. (3) reduces to

$$\int_{0_V}^{t+\Delta t} {}_0S_{ij} \delta {}_0\epsilon_{ij} dv = t+\Delta t R \quad (5)$$

where ${}_0S_{ij}^{t+\Delta t}$ is a Cartesian component of the 2nd Piola-Kirchhoff stress tensor and ${}_0\epsilon_{ij}^{t+\Delta t}$ is a Cartesian

component of the Green-Lagrange strain tensor. The unknown stresses and strains can now be incrementally decomposed, and Eq. (5) can be linearized as given in [4-6]. Then the solution of the linearized incremental equation results in an approximation to the solution of Eq. (5). If large nonlinearities are present within the individual time intervals, the linearization can introduce significant uncontrolled errors. In general, therefore, it is necessary to seek a more accurate solution within each interval of time, and such solution can be obtained effectively using a Newton-type iteration [7]. If we define

$$t+\Delta t u_i^{(k)} = t+\Delta t u_i^{(k-1)} + \Delta u_i^{(k)} \quad (6)$$

where $t+\Delta t u_i^{(0)} = t u_i$, a Newton-type iteration obtained by linearization of Eq. (5) is

$$\begin{aligned} \int_{0_V} {}_0 C_{ijrs} \Delta {}_0 e_{rs}^{(k)} \delta {}_0 e_{ij}^{(k)} {}_0 dv + \int_{0_V} {}^\tau S_{ij} \delta \Delta {}_0 \eta_{ij}^{(k)} {}_0 dv \\ = t+\Delta t R - \int_{0_V} t+\Delta t S_{ij}^{(k-1)} \delta t+\Delta t \epsilon_{ij}^{(k-1)} {}_0 dv \end{aligned} \quad (7)$$

/k = 1, 2, ...

where in the Newton iteration τ corresponds to $t+\Delta t$ and iteration $(k-1)$, and in the modified Newton iteration τ corresponds to t or any previously considered time.

The finite element discretization of Eq. (7) gives [4]

$$\underline{M} t+\Delta t \ddot{\underline{U}}^{(k)} + {}^\tau \underline{K} \Delta \underline{U}^{(k)} = t+\Delta t \underline{R} - t+\Delta t \underline{F}^{(k-1)} \quad (8)$$

/k = 1, 2, ...

where damping forces could be included in the usual way [1]. In Eq. (8) ${}^\tau \underline{K}$ is the stiffness matrix of the finite element discretization and the other variables are analogous to those used in Eq. (4).

An important concern in using Eq. (8) is the problem of convergence of the iteration in general analysis, as discussed in Section 4.

2.2 Element Displacement Interpolations

In the formulation of the finite element equilibrium equations we assumed that the element displacement interpolation functions are known, so that the displacement and strain-displacement interpolation matrices can be constructed. In the development of finite element matrices it is convenient to distinguish between continuum elements and structural elements.

In the formulation of isoparametric continuum elements the solution variables are the displacements u , v and w for one, two and three-dimensional elements, respectively, and the following interpolations are employed [4-6], for the coordinates,

$$\begin{aligned}
 {}^0x_j &= \sum_{k=1}^N h_k {}^0x_j^k & ; & & t_{x_j} &= \sum_{k=1}^N h_k t_{x_j}^k \\
 {}^{t+\Delta t}x_j &= \sum_{k=1}^N h_k {}^{t+\Delta t}x_j^k & & & & & \quad (9)
 \end{aligned}$$

/j = 1,2,3
as applicable

for the displacements,

$$\begin{aligned}
 t_{u_j} &= \sum_{k=1}^N h_k t_{u_j}^k & ; & & u_j &= \sum_{k=1}^N h_k u_j^k & \quad (10)
 \end{aligned}$$

/j = 1,2,3
as applicable

where ${}^0x_j^k$ is the coordinate of nodal point k corresponding to direction j at time 0, $t_{x_j}^k$, ${}^{t+\Delta t}x_j^k$, $t_{u_j}^k$ and u_j^k are defined similarly, and N is the total number of nodal points of the element. The function h_k is the interpolation function corresponding to nodal point k .

Figures 2 and 3 show variable-number-nodes continuum elements that can be employed efficiently in analysis. The effectiveness of these elements lies in that any number of nodes between the minimum and the maximum number can be chosen [1]. This way it is possible to model adequately a

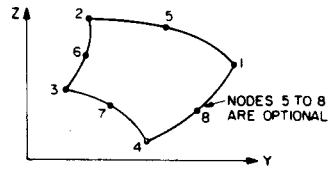


Fig. 2. Two-dimensional continuum element.

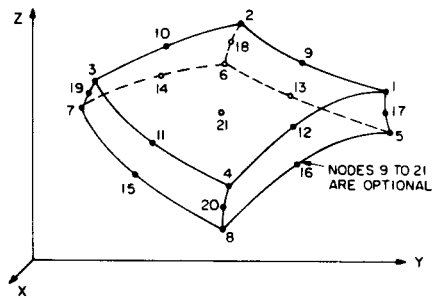
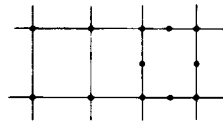
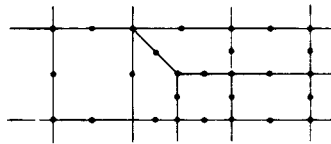


Fig. 3. Three-dimensional continuum element.



(a) Transition from 4-node to 8-node elements.



(b) Transition from coarse to fine mesh.

Fig. 4. Compatible element lay-outs.

variety of structural configurations and continua using basically one element. In particular, it is possible to change from a coarse to a fine mesh always preserving displacement compatibility between elements, as shown in Fig. 4.

The continuum elements can be employed to model solid or fluid continua, where it is assumed that the fluid undergoes relatively small deformations when using the T.L. formulation [8], in the analysis of field problems, and in the analysis of some structural configurations. However, in the analysis of beam structures, piping configurations, plates and shells it is usually more effective to employ a structural element [9, 10]. Two basic assumptions are employed in the formulation of isoparametric structural elements. Firstly, it is assumed that normals to the mid-surface of a structural member remain straight during deformation (but not necessarily normal to the mid-surface) and, secondly, it is assumed that the stresses normal to the mid-surface can be neglected and do not contribute to the structural response.

The assumption on the displacement behavior of the normals directly makes it possible to interpolate the geometry of the structural elements at time t . For a three-dimensional bending element we have, Fig. 5,

$$t_{x_i} = \sum_{k=1}^N h_k t_{x_i}^k + \frac{t}{2} \sum_{k=1}^N a_k h_k t_{V_{ti}}^k + \frac{s}{2} \sum_{k=1}^N b_k h_k t_{V_{si}}^k \quad (11)$$

/i = 1,2,3

and for a plate or shell element we have,

$$t_{x_i} = \sum_{k=1}^N h_k t_{x_i}^k + \frac{t}{2} \sum_{k=1}^N a_k h_k t_{V_{ni}}^k \quad (12)$$

/i = 1,2,3

where

$$t_{x_i} = \text{Cartesian coordinate of any point in the element at time } t,$$

$$h_k(r), h_k(r,s) = \text{isoparametric interpolation functions,}$$

$$t_{x_i}^k = \text{Cartesian coordinate of nodal point } k \text{ at time } t,$$

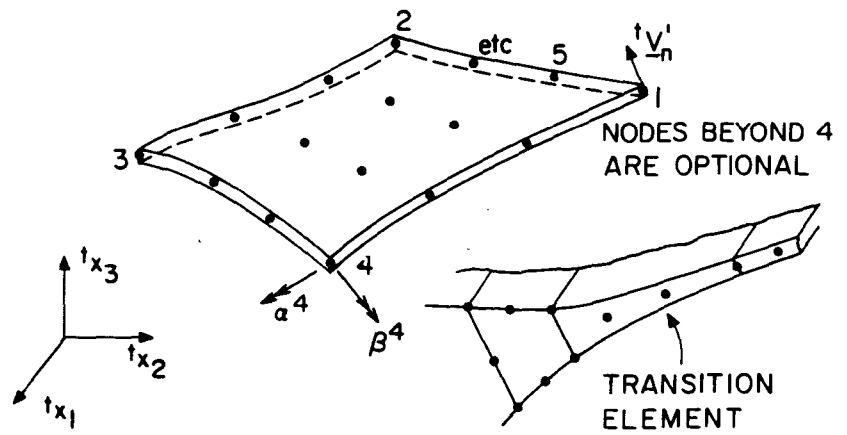
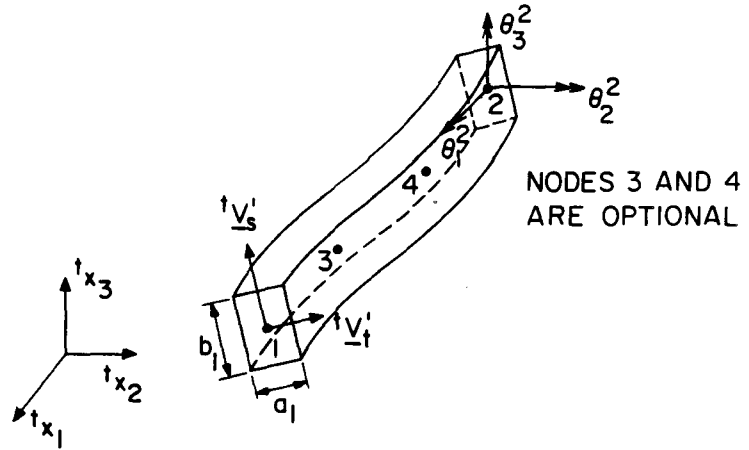


Fig. 5. Structural elements.

$$\begin{aligned}
 a_k &= \text{thickness of element in } t \text{ direction,} \\
 b_k &= \text{thickness of element in } s \text{ direction,} \\
 t_{V_{si}}^k, t_{V_{ti}}^k, t_{V_{ni}}^k &= \text{component } i \text{ of unit vector,} \\
 & \quad t_{\underline{V}_{-s}}^k, t_{\underline{V}_{-t}}^k, t_{\underline{V}_{-n}}^k, \text{ at nodal point } k \text{ at time } t.
 \end{aligned}$$

Also, in Eqs. (11) and (12) the variable N is equal to the number of nodes of the element. Considering the three-dimensional bending element we note that the interpolation for a three-dimensional truss element is obtained by not including the last two terms in Eq. (11).

To obtain an expression for the incremental displacements, consider the evaluation of u_i ($\Delta u_i^{(k)}$ would be obtained in an analogous manner). We have

$$u_i = {}^{t+\Delta t}x_i - {}^t x_i \quad (13)$$

and substituting from Eqs. (11) and (12) we obtain for the three-dimensional bending element,

$$\begin{aligned}
 u_i &= \sum_{k=1}^N h_k u_i^k + \frac{t}{2} \sum_{k=1}^N a_k h_k v_{ti}^k \\
 & \quad + \frac{s}{2} \sum_{k=1}^N b_k h_k v_{si}^k \quad /i = 1,2,3 \quad (14)
 \end{aligned}$$

and for the plate and shell element

$$u_i = \sum_{k=1}^N h_k u_i^k + \frac{t}{2} \sum_{k=1}^N a_k h_k v_{ni}^k \quad /i = 1,2,3 \quad (15)$$

where

$$\begin{aligned}
 v_{ti}^k &= {}^{t+\Delta t}v_{ti}^k - {}^t v_{ti}^k \\
 v_{ni}^k &= {}^{t+\Delta t}v_{ni}^k - {}^t v_{ni}^k \\
 v_{si}^k &= {}^{t+\Delta t}v_{si}^k - {}^t v_{si}^k
 \end{aligned} \quad ; \quad (16)$$

For the finite element solution we express the components v_{ti}^k , v_{si}^k , v_{ni}^k in terms of rotation increments. To do so we use the vectors \underline{v}_t^k , \underline{v}_s^k , and \underline{v}_n^k corresponding to the configuration at time t which are known (the initial vectors $0_{\underline{v}_t}^k$, $0_{\underline{v}_s}^k$, $0_{\underline{v}_n}^k$ corresponding to the configuration at time 0 are defined and input to the analysis). Then we have approximately (for small changes in \underline{v}_t^k , \underline{v}_s^k and \underline{v}_n^k),

$$\underline{v}_t^k = \underline{\theta}^k \times \underline{v}_t^k ; \quad \underline{v}_s^k = \underline{\theta}^k \times \underline{v}_s^k ; \quad \underline{v}_n^k = -\underline{v}_2^k \alpha^k + \underline{v}_1^k \beta^k \quad (17)$$

where $\underline{\theta}^k$ lists the incremental rotations θ_1^k , θ_2^k , and θ_3^k , and α^k and β^k are incremental rotations about vectors \underline{v}_1^k and \underline{v}_2^k that are normal to \underline{v}_n^k [9].

As pointed out in Section 2.1, in the linearization of the nonlinear response equations, approximate values for the incremental displacement and rotational quantities are calculated. These values correspond to the first iteration in the solution of the nonlinear equations of motion. The corrections to the incremental displacements and rotations are then interpolated in the same way as the incremental quantities, until convergence of the iteration.

The effectiveness of the structural element formulation given above lies in that it is a natural extension of the continuum element formulation with the basic assumptions of beam, plate and shell theory. The elements can be employed with a variable number of nodes, and can thus model a large number of structural configurations. Also, special transition elements as illustrated in Fig. 5 can be employed to enable a fully compatible transition between structural and continuum elements [9, 10].

2.3 Time Integration Schemes

For the solution of the dynamic equilibrium equations a time integration scheme must be employed. In explicit time integration, solution of Eq. (4), the central difference method can be employed effectively; and in implicit time integration, solution of Eq. (8), the Newmark method is very efficient in general analysis. The basic assumptions

employed using these techniques are [1,11]:
central difference method,

$$\ddot{\underline{u}} = (\underline{u}^{t+\Delta t} - 2\underline{u}^t + \underline{u}^{t-\Delta t}) / (\Delta t)^2 \quad (18)$$

$$\dot{\underline{u}} = (\underline{u}^{t+\Delta t} - \underline{u}^{t-\Delta t}) / (2\Delta t) \quad (19)$$

Newmark method,

$$\underline{u}^{t+\Delta t} = \underline{u}^t + \{(1 - \delta) \dot{\underline{u}}^t + \delta \dot{\underline{u}}^{t+\Delta t}\} \Delta t \quad (20)$$

$$\underline{u}^{t+\Delta t} = \underline{u}^t + \dot{\underline{u}}^t \Delta t + \left\{ \left(\frac{1}{2} - \alpha \right) \ddot{\underline{u}}^t + \alpha \ddot{\underline{u}}^{t+\Delta t} \right\} \Delta t^2 \quad (21)$$

where α and δ are parameters that are selected to obtain best stability and accuracy characteristics of the integration scheme. Table 1 summarizes the efficient use of the central difference method and the Newmark method in a computer program.

Considering implicit methods for the time integration, also the Houbolt method, the Wilson θ -method and the Park method are used significantly [12-14], and for a specific nonlinear analysis these techniques may display some solution advantages [15]. In addition, the use of simultaneous explicit and implicit time integration for different parts of finite element systems has been proposed and used with success [16].

2.4 Solution Using Mode Superposition

The required computations in solving Eq. (8) by direct integration can in the analysis of some problems be reduced significantly using mode superposition. Basically, mode superposition analysis consists of a transformation from the element nodal point degrees of freedom to the generalized degrees of freedom of the vibration mode shapes [1]. Since the dynamic equilibrium equations in the basis of the mode shape vectors decouple (assuming proportional damping) mode superposition analysis can be very effective in linear analysis if only some vibration modes are excited by the loading. In nonlinear analysis the vibration mode shapes and frequencies change, and to obtain decoupled modal response equations the free vibration mode shapes of the system at time τ need

TABLE 1 SUMMARY OF STEP-BY-STEP TIME INTEGRATION

DYNAMIC ANALYSIS USING THE NEWMARK METHOD (implicit time integration), OR THE CENTRAL DIFFERENCE METHOD (explicit time integration)

--- INITIAL CALCULATIONS ---

1. Form linear stiffness matrix \underline{K} , mass matrix \underline{M} and damping matrix \underline{C} , whichever applicable; Calculate the following constants:

Newmark method: $\delta \geq 0.50$, $\alpha \geq 0.25 (0.5 + \delta)^2$

$$a_0 = 1/(\alpha \Delta t^2) \quad a_1 = \delta/(\alpha \Delta t) \quad a_2 = 1/(\alpha \Delta t) \quad a_3 = 1/(2\alpha) - 1$$

$$a_4 = \delta/\alpha - 1 \quad a_5 = \Delta t(\delta/\alpha - 2)/2 \quad a_6 = -a_2 \quad a_7 = -a_3$$

$$a_8 = \Delta t(1 - \delta) \quad a_9 = \delta \Delta t$$

Central difference method:

$$a_0 = 1/\Delta t^2 \quad a_1 = 1/(2\Delta t) \quad a_2 = 2a_0 \quad a_3 = 1/a_2$$

2. Initialize ${}^0\underline{U}$, ${}^0\dot{\underline{U}}$, ${}^0\ddot{\underline{U}}$;

For central difference method only, calculate $\Delta t \underline{U}$ from initial conditions:

$$\Delta t \underline{U} = {}^0\underline{U} + \Delta t {}^0\dot{\underline{U}} + a_3 {}^0\ddot{\underline{U}}$$

3. Form effective linear coefficient matrix;

in implicit time integration: $\hat{\underline{K}} = \underline{K} + a_0 \underline{M} + a_1 \underline{C}$

in explicit time integration: $\hat{\underline{M}} = a_0 \underline{M} + a_1 \underline{C}$

--- FOR EACH TIME STEP ---

- (i) In implicit time integration if a new stiffness matrix is to be formed, update $\hat{\underline{K}}$ for nonlinear stiffness effects to obtain $\underline{t}_{\underline{K}}$; triangularize $\underline{t}_{\underline{K}}$:

$$\underline{t}_{\underline{K}} = \underline{L} \underline{D} \underline{L}^T$$

- (ii) Form effective load vector;
in implicit time integration:

$$\underline{t}^{+\Delta t} \underline{\hat{R}} = \underline{t}^{+\Delta t} \underline{R} + \underline{M}(a_2 \underline{\dot{U}} + a_3 \underline{\ddot{U}}) + \underline{C}(a_4 \underline{\dot{U}} + a_5 \underline{\ddot{U}}) - \underline{t}_{\underline{F}}$$

in explicit time integration:

$$\underline{\hat{R}} = \underline{t}_{\underline{R}} + a_2 \underline{M}(\underline{t}_{\underline{U}} - \underline{t}^{-\Delta t} \underline{U}) + \underline{\hat{M}} \underline{t}^{-\Delta t} \underline{U} - \underline{t}_{\underline{F}}$$

- (iii) Solve for displacement increments:

in implicit time integration using latest \underline{D} , \underline{L} factors:

$$\underline{L} \underline{D} \underline{L}^T \underline{U} = \underline{t}^{+\Delta t} \underline{\hat{R}}$$

in explicit time integration:

$$\underline{\hat{M}} \underline{t}^{+\Delta t} \underline{U} = \underline{\hat{R}}$$

- (iv) In implicit time integration iterate for dynamic equilibrium:

$$\underline{U}^{(0)} = \underline{U}, i = 0; \text{ then}$$

(a) $i = i + 1$

TABLE 1 SUMMARY OF STEP-BY-STEP TIME INTEGRATION (Cont.)

- (b) Calculate (i-1)st approximation to accelerations, velocities, and displacements:

$${}^{t+\Delta t}\ddot{\underline{U}}^{(i-1)} = a_0 \underline{U}^{(i-1)} - a_2 \dot{\underline{U}}^t - a_3 \ddot{\underline{U}}^t$$

$${}^{t+\Delta t}\dot{\underline{U}}^{(i-1)} = a_1 \underline{U}^{(i-1)} - a_4 \dot{\underline{U}}^t - a_5 \ddot{\underline{U}}^t$$

$${}^{t+\Delta t}\underline{U}^{(i-1)} = \underline{U}^{(i-1)} + \dot{\underline{U}}^t \Delta t$$

- (c) Calculate (i-1)st effective out-of-balance loads:

$${}^{t+\Delta t}\hat{\underline{R}}^{(i-1)} = {}^{t+\Delta t}\underline{R} - \underline{M} {}^{t+\Delta t}\ddot{\underline{U}}^{(i-1)} - \underline{C} \dot{\underline{U}}^{(i-1)} - {}^{t+\Delta t}\underline{F}^{(i-1)}$$

- (d) Solve for *i*th correction to displacement increments:

$$\underline{L} \underline{D} \underline{L}^T \Delta \underline{U}^{(i)} = {}^{t+\Delta t}\hat{\underline{R}}^{(i-1)}$$

- (e) Calculate new displacement increments:

$$\underline{U}^{(i)} = \underline{U}^{(i-1)} + \Delta \underline{U}^{(i)}$$

- (f) Check for iteration convergence. If convergence: $\underline{U} = \underline{U}^{(i)}$ and go to (v);

If no convergence and $(i) < (\text{number of allowable iterations})$ go to (a); otherwise restart using new stiffness matrix reformation strategy and/or a smaller time step size.

- (v) Calculate new accelerations, velocities, and displacements;

Newmark Method:

$${}^{t+\Delta t}\ddot{\underline{U}} = a_0 \underline{U} + a_6 \dot{\underline{U}}^t + a_7 \ddot{\underline{U}}^t$$

$$t+\Delta t \dot{\underline{u}} = t \dot{\underline{u}} + a_8 \underline{t \ddot{u}} + a_9 \underline{t+\Delta t \ddot{u}}$$

$$t+\Delta t \underline{u} = t \underline{u} + \underline{u}$$

Central Difference Method:

$$t \dot{\underline{u}} = a_1 (t+\Delta t \underline{u} - t-\Delta t \underline{u})$$

$$t \ddot{\underline{u}} = a_0 (t+\Delta t \underline{u} - 2t \underline{u} + t-\Delta t \underline{u})$$

to be used in the transformation. The calculation of the vibration mode shapes and frequencies at time τ , when these quantities have been calculated at a previous time, can be achieved economically using the subspace iteration method [1]; however, the complete mode superposition analysis of nonlinear dynamic response is generally only effective when the solution can be obtained without updating the stiffness matrix [17, 18]. In this case, the governing finite element equilibrium equations for the solution of the response at time $t+\Delta t$ are

$$\underline{M} \ddot{\underline{U}}(k) + \underline{K} \Delta \underline{U}(k) = \underline{R}(k) - \underline{F}(k-1) \quad (22)$$

/k=1,2,...

where \underline{K} is the stiffness matrix corresponding to the configuration at time 0. In the mode superposition analysis we use

$$\underline{U} = \sum_{i=r}^s \underline{\phi}_i x_i \quad (23)$$

where x_i is the i th generalized modal displacement at time $t+\Delta t$, and

$$\underline{K} \underline{\phi}_i = \omega_i^2 \underline{M} \underline{\phi}_i \quad ; \quad i = r, \dots, s \quad (24)$$

that is, $(\omega_i, \underline{\phi}_i)$ are free vibration frequencies (rad/sec) and mode shape vectors of the system at time 0. Using Eq. (23) in the usual way, Eq. (22) is transformed to a set of equations in the generalized modal displacements [1],

$$\ddot{\underline{X}}(k) + \underline{\Omega}^2 \Delta \underline{X}(k) = \underline{\Phi}^T (\underline{R}(k) - \underline{F}(k-1)) \quad (25)$$

/k=1,2,...

where

$$\underline{\Omega}^2 = \begin{bmatrix} \omega_r^2 & & \\ & \ddots & \\ & & \omega_s^2 \end{bmatrix}; \quad \underline{\Phi} = [\underline{\phi}_r, \dots, \underline{\phi}_s]; \quad \underline{X} = \begin{bmatrix} x_r \\ \vdots \\ x_s \end{bmatrix} \quad (26)$$

Equation (25) can be solved effectively using the Newmark method. The algorithm is analogous to the procedure

presented in Section 2.3 [18].

The use of the mode superposition solution in Eqs. (23) to (26) is effective if only a few mode shapes need to be considered in the analysis and if the system is only locally nonlinear. Such conditions are, for example, encountered in earthquake response analysis, and in the analysis of vibration excitation problems.

3. FINITE ELEMENT MODELING FOR DYNAMIC ANALYSIS

In order to obtain an effective finite element solution of a nonlinear dynamic problem, it is imperative that an appropriate finite element model of the actual physical problem is employed. The finite element model is established differently depending on whether a structural dynamics or a wave propagation problem is solved [1].

3.1 Modeling of Structural Dynamics Problems

The basic consideration in the selection of an appropriate finite element model of a structural dynamics problem is that only the lowest modes (or only a few intermediate modes) of a physical system are being excited by the load vector. Thus, if a Fourier analysis of the dynamic load input shows that only frequencies below ω_u are contained in the loading, the finite element mesh should represent accurately the frequencies to about $4\omega_u$ of the actual system. There is no need to represent the higher frequencies of the actual system accurately in the finite element system, because the dynamic response contribution in those frequencies is negligible as illustrated in Fig. 6 [1, 19]. For values of ω_L/ω_F smaller than 0.25, a static response is measured and this response is directly included in the direct integration step-by-step dynamic response calculations.

The complete procedure for the modeling of a structural vibration problem is therefore:

- (1) Identify the frequencies contained in the loading, using a Fourier analysis if necessary.
- (2) Choose a finite element mesh that accurately represents all frequencies up to about four times the highest frequency ω_u contained in the loading.

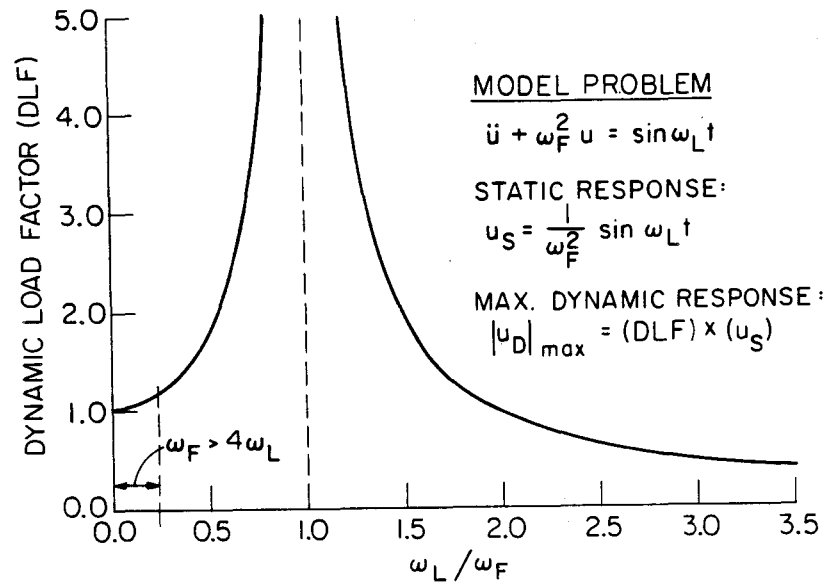
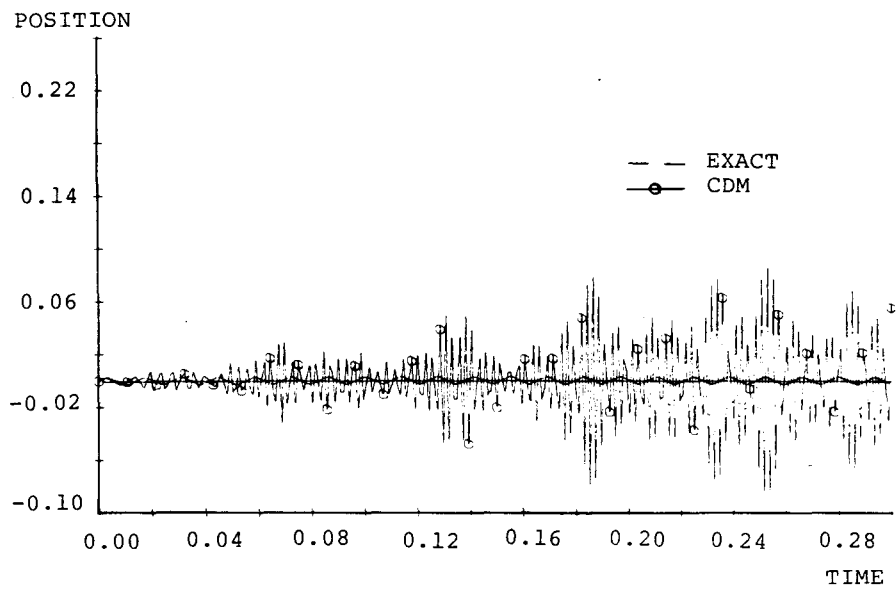


Fig. 6. Dynamic load factor.

Fig. 7. Response of 900:1 bilinear elastic system
(see Fig. 8(a); $K_2 = 9 \times 10^8$, $\dot{x}_0 = 0.955$).

- (3) Perform the direct integration analysis. The time step Δt for this solution should equal about $\frac{1}{20} T_u$, where $T_u = 2\pi/\omega_u$, or be smaller for stability reasons, as discussed in Section 4.

When analyzing a structural dynamics problem, in most cases, an implicit time integration is most effective. In this integration the time step Δt need generally only be $\frac{1}{20} T_u$, and not smaller, unless convergence problems are encountered in the iteration for the solution at time $t+\Delta t$ (see Section 4.2). If an implicit time integration is employed, it is important to operate on a finite element system that is of the smallest order possible. Namely, the analysis involves factorizations of effective stiffness matrices and vector forward reductions and back-substitutions (see Table 1), with each factorization requiring in essence $\frac{1}{2} Nm^2$ and each vector solution requiring $2Nm$ operations, where N = total number of degrees of freedom and m = effective half-bandwidth of the coefficient matrix. However, the bandwidth varies roughly proportionally with N , and the computational effort in the calculation of the element matrices and their assemblage into the total stiffness matrix, ${}^T\mathbf{K}$, and force vector ${}^t\mathbf{F}$, varies about linearly with N . Therefore, depending on the fraction of total computational effort spent in the setting up of the equations and their solution, the total analysis cost will vary a little more than linearly to almost cubically with the number of degrees of freedom employed in the finite element mesh. In addition, it must be noted that the analysis increases significantly in cost if an out-of-core solution is required.

For the solution cost reasons given above, it is frequently effective to use in implicit time integration higher-order finite elements, for example, the 8 and 20 node elements of Figs. 2 and 3 in two- and three-dimensional analysis, respectively, and a consistent mass idealization. The higher-order elements are effective in the representation of bending behavior, but need generally be employed with a consistent load vector, so that the mid-side and the corner nodes are subjected to their appropriate load contributions

in the analysis.

The observation that the use of higher-order elements can be effective with implicit time integration in the analysis of structural dynamics problems is consistent with the fact that higher-order elements have generally been found to be efficient in static analysis, and structural dynamics problems can be thought of as "static problems including inertia effects." If, on the other hand, the finite element idealization is so large that a multiple block out-of-core solution is necessary with a large bandwidth it can be more efficient to use explicit time integration with a lumped mass matrix, in which case no effective stiffness matrices are assembled and triangularized (see Table 1), but a smaller time step Δt must generally be employed in the solution (see Section 4.1).

In the above discussion we assumed that the time step Δt is constant, but the same considerations may be used to establish a varying time step considering that the frequencies of the system vary in nonlinear analysis.

3.2 Modeling of Wave Propagation Problems

The major difference between a structural dynamics problem and a wave propagation problem can be understood to be that in a wave propagation problem a large number of frequencies (and possibly all from 0 to infinity) are excited in the system. It follows that one way to analyze a wave propagation problem is to use the procedure given in Section 3.1, with a sufficiently high cut-off frequency ω_u to obtain enough solution accuracy. The difficulties are in identifying the cut-off frequency to be used and in establishing a corresponding finite element model.

Instead of using the considerations outlined in Section 3.1 to obtain an appropriate finite element mesh for the analysis of a wave propagation problem, it is generally more effective to employ the concepts used in finite difference analysis and the method of characteristics in order to establish an appropriate finite element mesh and time step Δt for the analysis [20].

If we assume that the wave length is L_w , the total

time for the wave to travel past a point is

$$t_w = \frac{L_w}{c} \quad (27)$$

where c is the wave speed. Assuming that n time steps are necessary to represent the wave, we use

$$\Delta t = \frac{t_w}{n} \quad (28)$$

and the "length" of a finite element should be

$$L_e = c \Delta t \quad (29)$$

Using Eqs. (27) to (29) and the central difference method in a one-dimensional analysis with lumped mass idealization (for example, in the analysis of a truss element assemblage) results into the exact solution, because the spatial and temporal discretization is equivalent to the use of the method of characteristics (see Section 5.1). In this case L_e would simply be the length of the two-noded elements (assumed to be all equal).

In more complex two- and three-dimensional analyses, the exact solution is generally not obtained, and L_e must be chosen depending on whether the central difference method or an implicit method is employed for solution. If the explicit central difference method is used, a lumped mass matrix should be employed and in this case low-order finite elements are probably most effective, for example the 4 and 8 node elements of Figs. 2 and 3 in two- and three-dimensional analysis, respectively. In this case L_e is equal to the smallest distance between any two of the nodes of the mesh employed. On the other hand, if an implicit unconditionally stable time integration method is used, L_e should be equal to the smallest distance between any two of the nodes that lie in the direction of the wave travel. If material nonlinearities are also included and higher-order elements are used, L_e is best chosen as the smallest distance between integration points that lie in the direction of the wave travel (see Section 5.3). In this case it should also be noted that it is best to choose for the wave speed c the largest possible wave speed that can occur during the

response calculations.

Some demonstrative sample solutions that illustrate the modeling procedures discussed in this section are given in Section 5.

4. SOME STABILITY AND ACCURACY CONSIDERATIONS

The stability and accuracy characteristics of the common time integrationschemes used in finite element analysis have been discussed extensively for the case of linear dynamic analysis [1]. The conclusions reached in those investigations are also useful in nonlinear analysis, if it is realized that the frequencies and mode shapes change during the response calculations, and that the stability properties applicable to a linear analysis may not be directly applicable in a nonlinear solution [14].

4.1 Explicit Time Integration

In explicit time integration using the central difference method it is important to note that the time step Δt is selected using Eqs. (28) and (29), where the wave speed changes with time. Therefore, to obtain a stable solution Δt may have to be adjusted during the time integration, and any reduction in Δt should be carried out in a conservative manner, so that with certainty the time integration is stable at all times.

To emphasize the importance of the above point, consider an analysis in which the time step is always smaller than the critical time step except for a few successive solution steps, and for these solution steps the time step Δt is just slightly larger than the critical time step. In such case, the analysis results may not show an "obvious" solution instability, but instead a significant solution error is accumulated over the solution steps for which the time step size was larger than the critical value for stability. This situation can arise, for example, in the analysis of a stiffening system as demonstrated by the simple analysis in Fig. 7. Namely, it is noted that the response prediction for the single degree-of-freedom system considered in Fig. 7 does not grow without bound. Hence, if this single degree-

of-freedom system would correspond to the higher frequency of a larger finite element model, a significant error accumulation must be expected without an obvious blow-up of the solution. This response characteristic is quite different from what is observed in linear analysis, where the solution quickly blows up if the time step is larger than the critical time step size for stability.

4.2 Implicit Time Integration

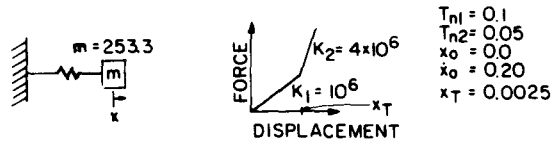
Considering the use of implicit time integration methods, such as the Newmark, Wilson, Houbolt or Park methods, the time step size is chosen such that the response in all modes that are excited significantly is integrated accurately. Therefore, the time step may be much larger than the smallest period in the finite element system. However, in the integration using the implicit techniques it is usually necessary to iterate for dynamic equilibrium in order to assure a stable and accurate solution [5, 21], and if convergence difficulties arise in this iteration a smaller time step has to be chosen. In the iteration of Eq. (8) convergence may be measured using [15],

$$\frac{\| \underline{t+\Delta t} \underline{R} - \underline{t+\Delta t} \underline{F}^{(k-1)} - \underline{M} \underline{t+\Delta t} \underline{\ddot{U}}^{(k-1)} \|_2}{\| \underline{t} \underline{R} - \underline{t-\Delta t} \underline{F} - \underline{M} \underline{t-\Delta t} \underline{\ddot{U}} \|_2^{(\max)}} \leq \text{RTOL} \quad (30a)$$

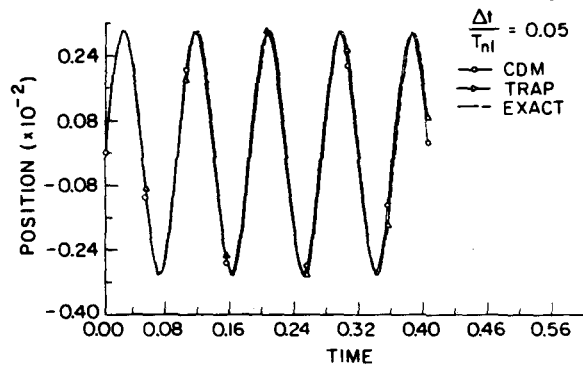
and

$$\frac{\Delta \underline{U}^{(k)T} (\underline{t+\Delta t} \underline{R} - \underline{t+\Delta t} \underline{F}^{(k-1)} - \underline{M} \underline{t+\Delta t} \underline{\ddot{U}}^{(k-1)})}{\Delta \underline{U}^{(1)T} (\underline{t+\Delta t} \underline{R} - \underline{t} \underline{F} - \underline{M} \underline{t} \underline{\ddot{U}})} \leq \text{ETOL} \quad (30b)$$

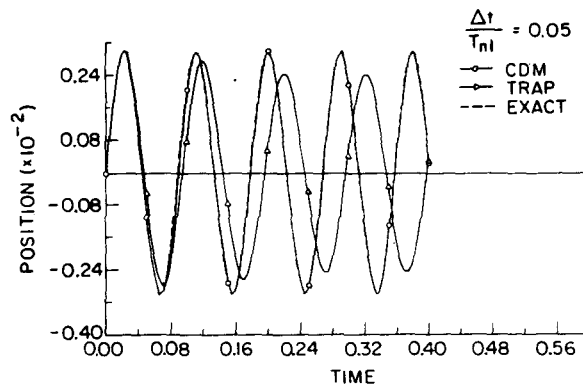
where RTOL is a force tolerance, and ETOL is an energy tolerance. To assure an accurate solution both criteria above may have to be satisfied. To illustrate the effect of iterating in a simple nonlinear dynamic analysis, the response of a single degree-of-freedom system as predicted with and without iteration is shown in Fig. 8. It is seen that without iteration a large error accumulation occurs. Additional sample results that demonstrate the importance of iteration for a stable and accurate solution are given in Sections 5.3,



(a) 4:1 bilinear elastic system. Material law is symmetric with respect to the origin.



(b) Response of system. Update and iterate.



(c) Response of system. Stiffness matrix updated. No equilibrium iterations performed.

Fig. 8. Response of 4:1 bilinear elastic system.

5.4 and 5.5.

Since it can be important to iterate in a nonlinear dynamic analysis using implicit time integration, rapid convergence in this iteration is desirable. Convergence is assured and fast, provided the time step is small enough, however for a larger time step, convergence difficulties can be encountered [7]. In such case the use of an acceleration technique, or possibly a reduction in the time step size may be required [15].

5. DEMONSTRATIVE SAMPLE SOLUTIONS

During the last few years a large number of nonlinear dynamic analyses have been performed using various computer programs. The objective in this section is to report on some analyses that demonstrate the application of the procedures discussed in the previous sections. The analyses have been performed using the ADINA computer program with the time integration schemes summarized in Table 1 [22].

5.1 Linear Analysis of a Rigidly-Contained Water Column

A simple axisymmetric water column idealized using 4-node continuum elements as shown in Fig. 9 was analyzed for a step pressure applied at its free end [8]. Lumped and consistent mass idealizations were employed in this analysis, and the objective was to study the accuracy with which the response of the water column is predicted.

Figure 9 shows the calculated longitudinal displacements at the free end of the column and compares these displacements with the analytical solution. It is seen that using implicit time integration (Newmark method) the free-end displacements in the consistent mass analysis were predicted accurately for a time period that included 6 wave reflections, whereas the lumped mass analysis results are inaccurate.

Considering the analysis of the problem using the explicit central difference time integration method with a lumped mass matrix idealization, because this is a one-dimensional wave propagation problem, the exact solution is obtained using the time step in Eq. (29).

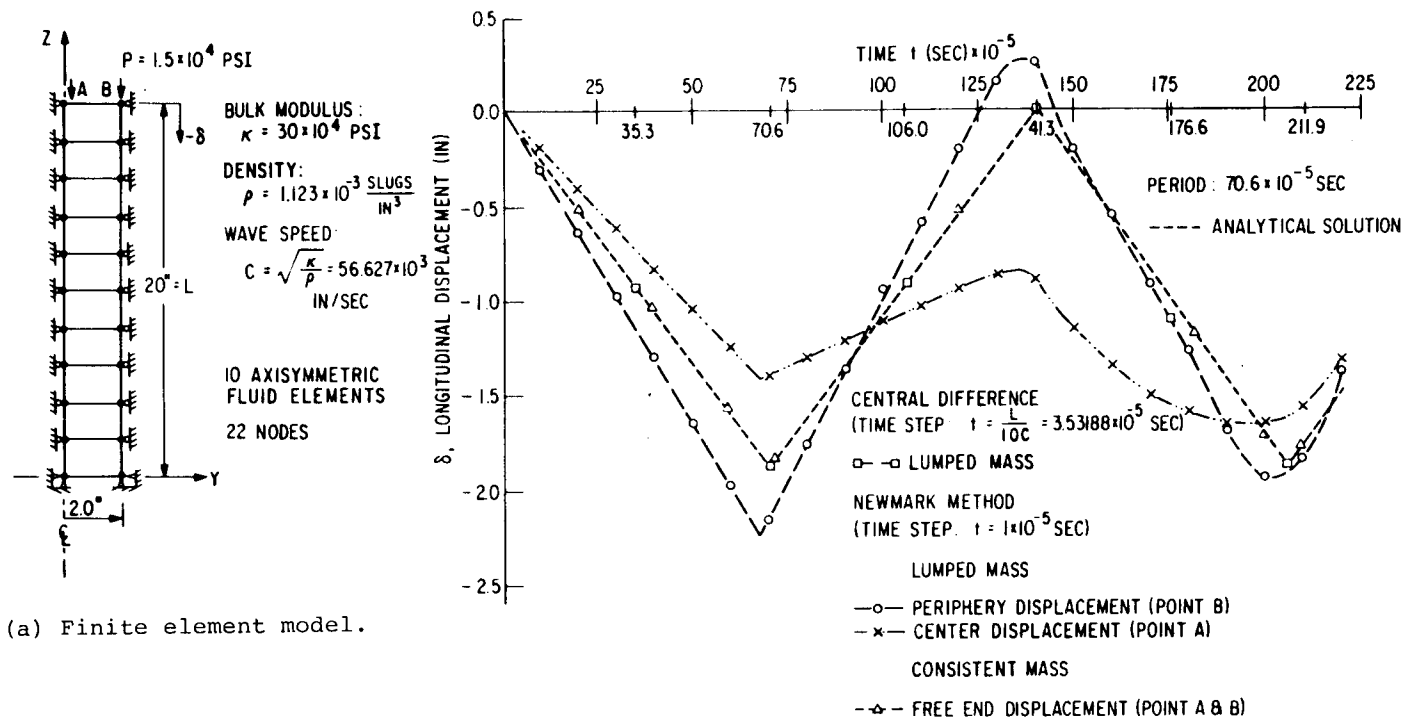


Fig. 9. Dynamic analysis of rigidly contained water column.

5.2 Linear Analysis of a Two-Dimensional Wave Propagation Problem

The wave propagation produced by a suddenly applied strip load to an infinite elastic half space was analyzed. Figure 10 depicts the finite element idealization employed for the analysis and the loading applied.

Fig. 11 shows the stress response at point A (indicated in Fig. 10) calculated using ADINA and an analytical solution [23]. The analysis was performed using lumped and consistent mass approximations and for the time integration the central difference method and Newmark method were used. It is seen that with this finite element mesh and time step selection accurate results have been obtained.

5.3 Nonlinear Transient Analysis of a Pipe Test

The water-filled straight piping configuration shown in Fig. 12 was analyzed for its dynamic response when subjected to a pressure pulse at its end [8]. The finite element model employed in the analysis is shown in Fig. 12. The elastic-plastic response of this pipe was experimentally assessed as reported in [24].

In this analysis, a consistent mass matrix was employed and the time integration was carried out using the Newmark method. The time step was changed to half its size at the time the pulse entered the nickel pipe so that the pulse front would pass through a solid element in about three time steps. The effective stiffness matrix used in this analysis was reformed only at times $t = 1.905, 2.302, \text{ and } 3.435$ msec. However, to take into account the elastic-plastic response of the pipe, equilibrium iterations were used at each time step once the pulse reached the nickel pipe. The equilibrium iterations were found to be necessary for a stable solution, although an average of only 1 to 2 iterations per time step were carried out.

Figure 13 shows the calculated pressures and hoop strains at various locations along the pipe as a function of time and compares the ADINA results with the experimental data. It is noted that in general the calculated response

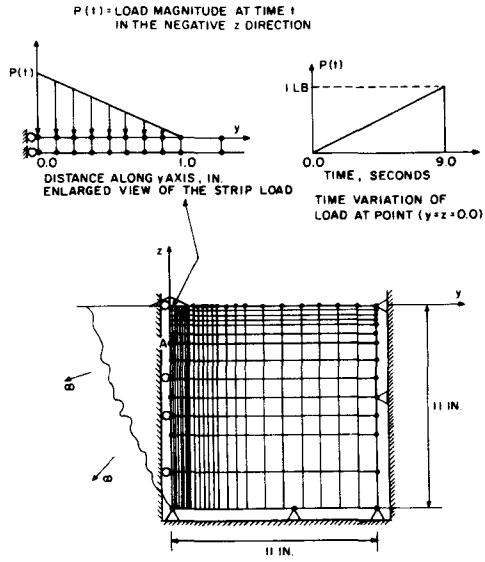


Fig. 10. Finite element analysis of infinite elastic half space.

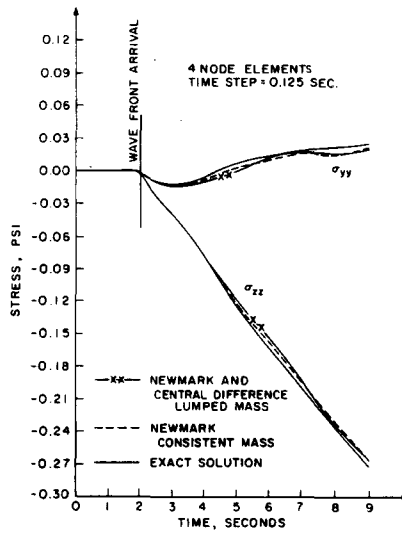
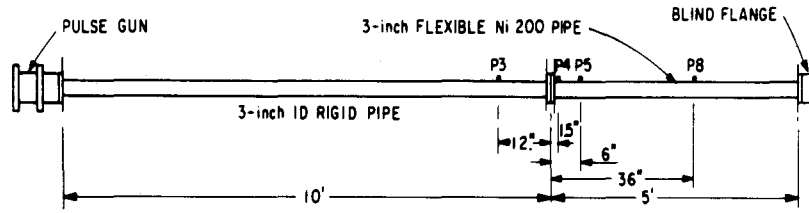


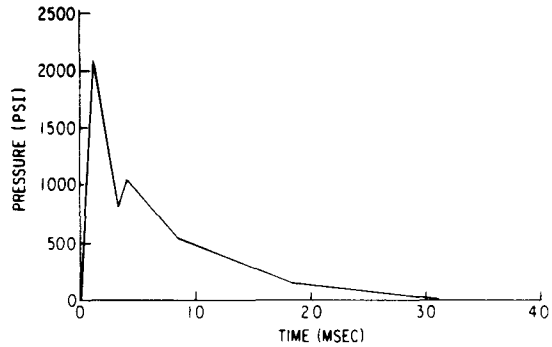
Fig. 11. Stresses at point A ($z = -2.0, y = 0.0$) on centerline.



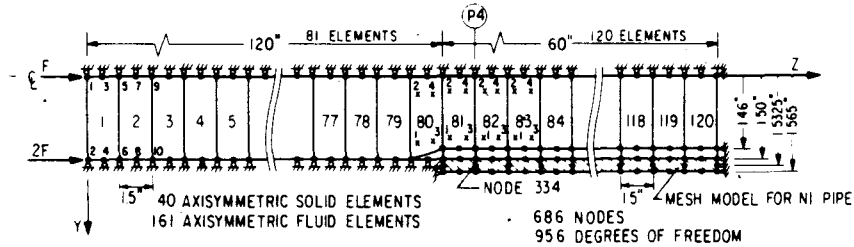
STRAIGHT PIPE TEST CONFIGURATION

MATERIAL PROPERTIES:

NICKEL 200	
E - YOUNG'S MODULUS	30×10^6 PSI
E_T - TANGENT MODULUS	73.7×10^4 PSI
ν - POISSON'S RATIO	.30
ρ_1 - DENSITY	8.31×10^{-4} SLUG-FT ³ /IN ³
σ_0 - YIELD STRESS	12.8×10^3 PSI
WATER	
κ - BULK MODULUS	32×10^4 PSI
ρ_w - DENSITY	9.36×10^{-5} SLUG-FT ³ /IN ³



PRESSURE PULSE INPUT IN FINITE ELEMENT ANALYSIS



TIME STEP: $\Delta t = \begin{cases} 1.5 \times 10^{-5} \text{ SEC} & 0 \leq t \leq 1.905 \text{ MSEC} \\ 75 \times 10^{-5} \text{ SEC} & 1.905 \leq t \leq 4.560 \text{ MSEC} \end{cases}$

EQUILIBRIUM ITERATION EVERY STEP
FOR $t \geq 2.092 \text{ MSEC}$

INTEGRATION ORDER: SOLID ELEMENTS 3*3
FLUID ELEMENTS 2*2

STIFFNESS REFORMED AT RESTARTS ONLY
(i.e., $t = 1.905, 2.302, \text{ and } 3.435 \text{ MSEC}$)

PRESSURE P AT VARIOUS AXIAL LOCATIONS OBTAINED BY AVERAGING PRESSURES AT INTEGRATION POINTS
4*2 OF ADJACENT ELEMENTS (e.g., $P_4 = (P_{d1} + P_{d2})/2$ WHERE P_4 IS THE PRESSURE AT 1.5 IN INTO NICKEL PIPE)

HOOP STRAIN ϵ_θ IN THE NICKEL PIPE AT VARIOUS AXIAL LOCATIONS OBTAINED BY $\epsilon_\theta = u/r$ WHERE
 u IS THE RADIAL DISPLACEMENT OF A MIDSIDE NODE AND r IS THE INITIAL RADIAL LOCATION
OF THE MIDSIDE NODE (e.g., $\epsilon_\theta = u^{334}/1.5325$ HOOP STRAIN 1.5 IN INTO NICKEL PIPE).

PRESSURE LOAD APPLIED TO NODES 1 AND 2

CONSISTENT MASS **NEWMARK INTEGRATION**
SMALL DISPLACEMENTS

Fig. 12. Finite element model of pipe test.

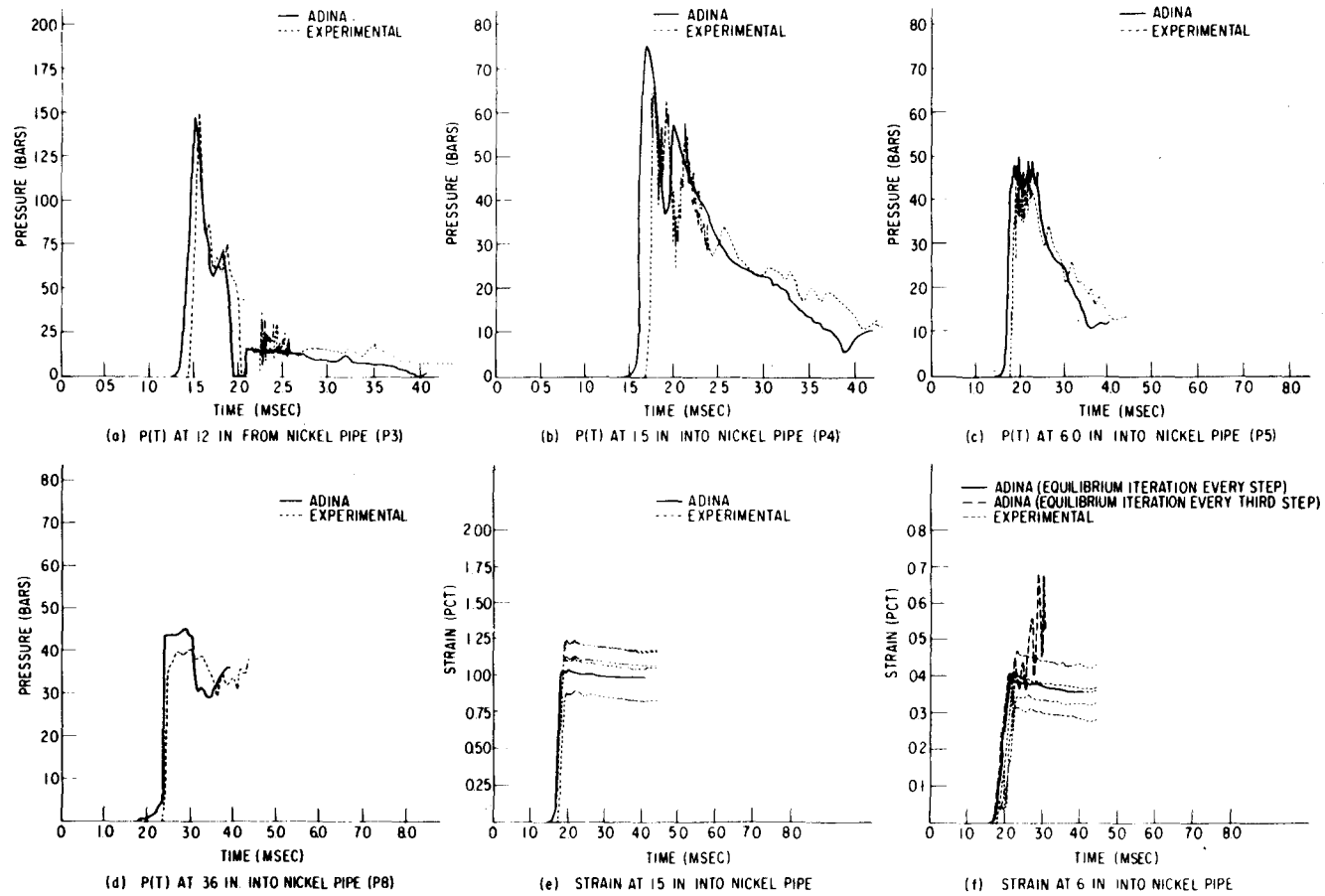


Fig. 13. Pressures and strains in pipe test.

compares well with the experimentally observed response.

It may be noted that the consistent mass idealization and implicit time integration employed in this analysis were effective, because using higher-order isoparametric elements only relatively few elements needed to be employed, the half band-width of the stiffness and mass matrices was small and a relatively large time step could be used in the time integration.

5.4 Nonlinear Transient Analysis of a Pipe Whip Problem

Figure 14 shows a simple model of a cantilevered pipe, subjected to an instantaneously applied tip load. The tip of the cantilever is restrained to undergo very large displacements by a stop with a gap. Such system is generally analyzed using direct integration [5], but we include here the response predicted when using the mode superposition analysis technique described in Section 2.4. Figure 14 shows that the response is predicted accurately in the analysis, when using in the mode superposition analysis only the first two modes of the structure and a time step of $\Delta t=0.0001$ sec.

5.5 Nonlinear Transient Analysis of a Cantilever Beam

A simple cantilever beam subjected to a uniformly distributed loading was analyzed for its large displacement dynamic response. Figure 15 shows the finite element model employed, the applied loading, and the predicted response.

The analysis was performed using two different time step sizes, as shown in Fig. 15. It is noted that the response predicted with the larger time step is accurate provided equilibrium iterations are performed. If the step-by-step solution is used without equilibrium iterations errors accumulate, which in this case decrease the response significantly. In general, the calculated response would simply diverge from the actual response of the system, without the analyst knowing about the error accumulation. It is interesting to note that in the analysis with the larger time step an average of only 4 iterations were required per time step.

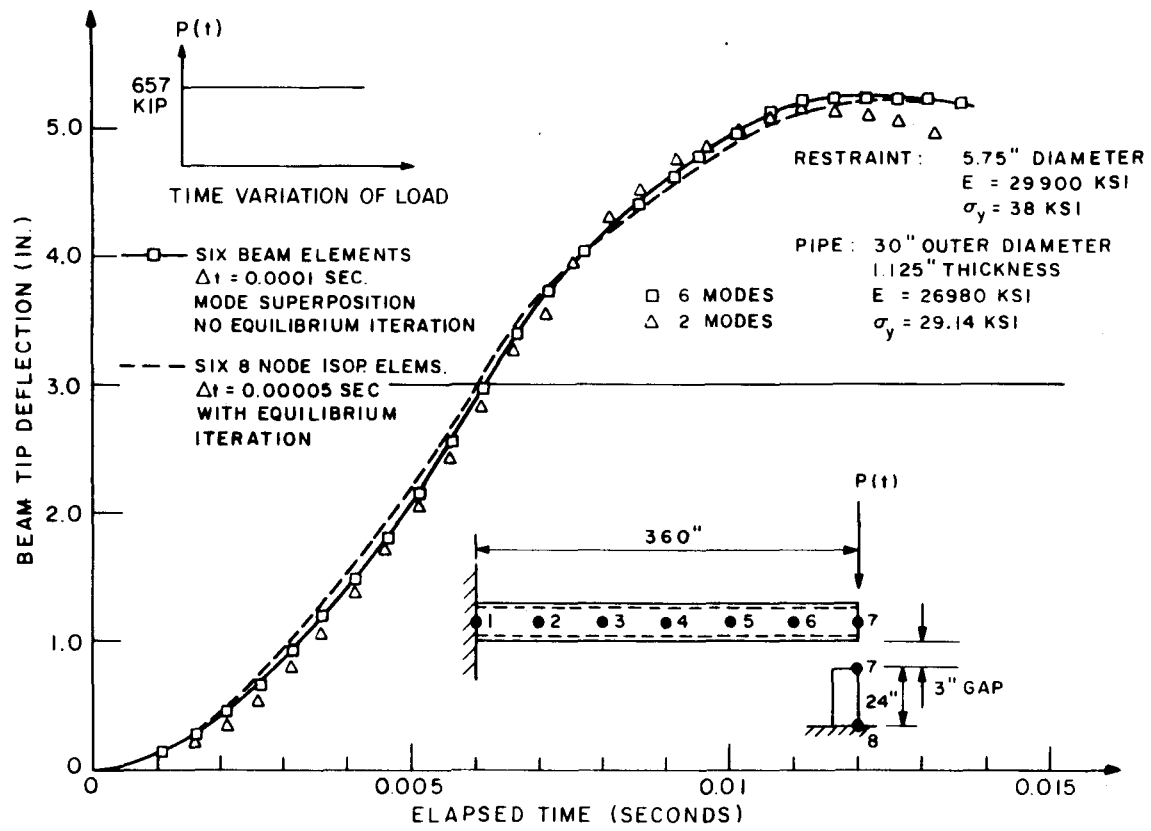


Fig. 14. Analysis of pipe whip problem.

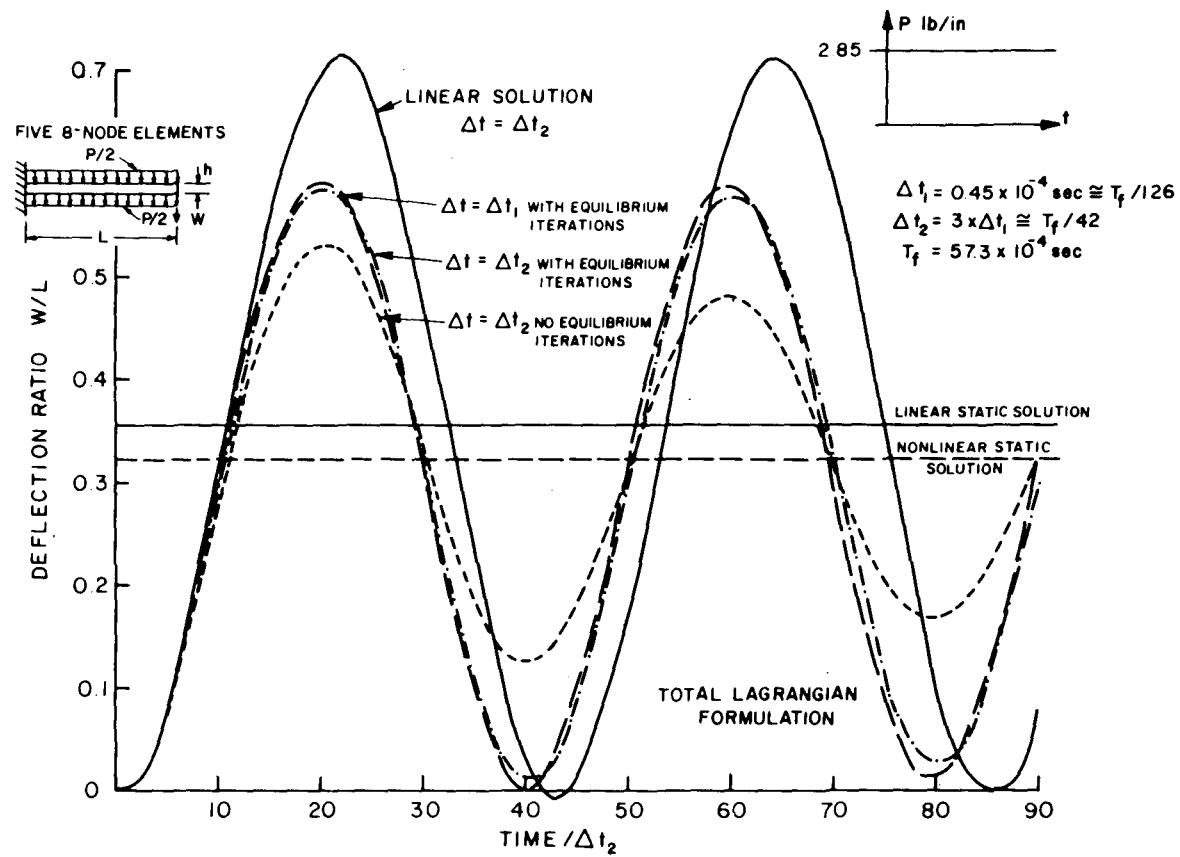


Fig. 15. Large displacement dynamic response of cantilever under uniformly distributed load, Newmark method, $\delta = 0.50$, $\alpha = 0.25$.

5.6 Elastic-Plastic Large Displacement Dynamic Analysis of a Spherical Cap

The dynamic response of the spherical cap in Fig. 16 subjected to a distributed step pressure $p = 600 \text{ lb/in}^2$ was calculated. The material was assumed to obey the von Mises yield condition with linear isotropic hardening. Figure 16 shows the dynamic response of the cap predicted using the Newmark time integration scheme in linear analysis, materially nonlinear only analysis, i.e., assuming small displacements and small strains, and combined geometric and material nonlinear analysis. In the fully nonlinear analysis the solution was obtained using the T.L. formulation.

The solutions in the figure demonstrate the effect of including different degrees of nonlinearities. It is observed that the materially nonlinear only solution differs a great deal from the linear elastic response, and that the effect of large displacements is also significant. The decrease in amplitude of vibration and increase in the mean deflection of the shell when nonlinearities are taken into account should be noted.

6. CONCLUSIONS

The use of the current finite element capabilities for nonlinear dynamic analysis of solids, structures, and fluid-structure systems requires the selection of appropriate finite element idealizations and effective numerical techniques. The objective in this paper was to survey the important considerations that lead to an efficient nonlinear dynamic finite element analysis using the current state-of-the-art analysis techniques. It is concluded that some nonlinear dynamic problems can already be analyzed quite effectively, but major improvements in the solution techniques are greatly needed to obtain more stable, accurate, and cost-effective solutions.

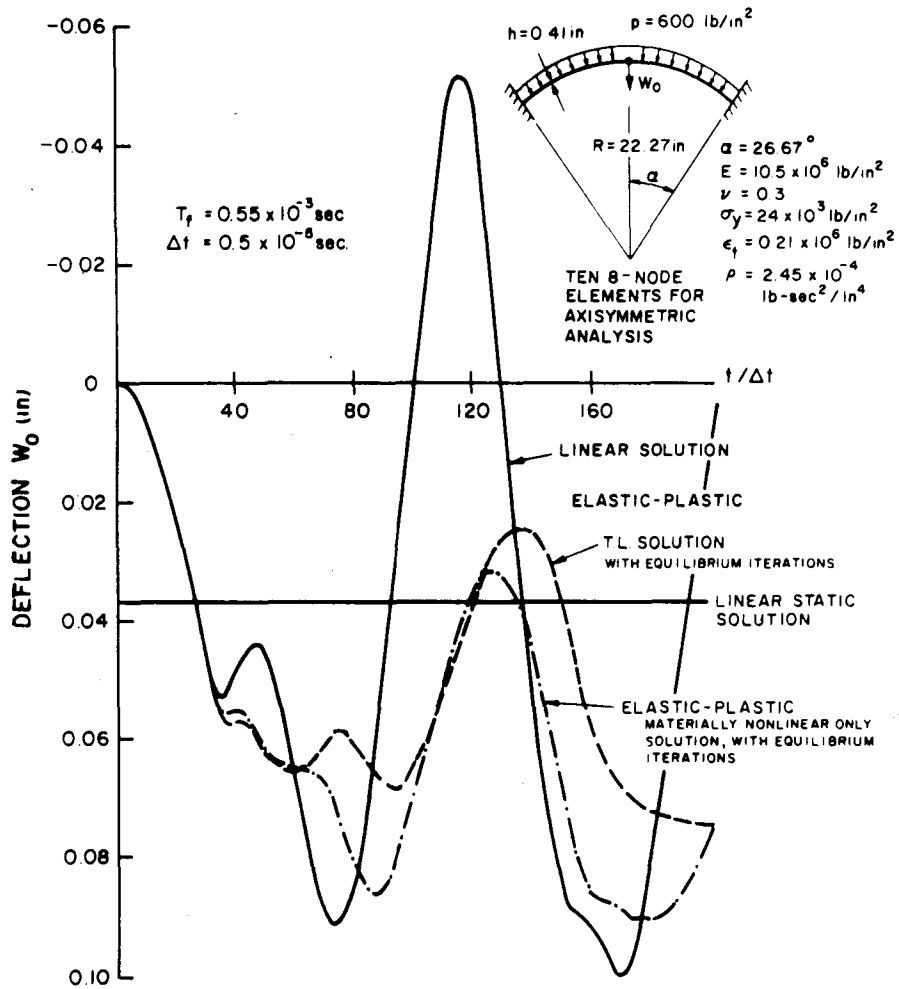


Fig. 16. Large displacement dynamic elastic-plastic analysis of spherical cap, Newmark method, $\delta = 0.50$, $\alpha = 0.25$.

REFERENCES

1. Bathe, K.J., and Wilson, E.L., Numerical Methods in Finite Element Analysis, Prentice-Hall, Inc., Englewood Cliffs, New Jersey, 1976.
2. Malvern, L.E., Introduction to the Mechanics of a Continuous Medium, Prentice-Hall, Inc., Englewood Cliffs, New Jersey, 1969.
3. Oden, J.T., Finite Elements of Nonlinear Continua, McGraw-Hill, New York, N.Y., 1972.
4. Bathe, K.J., Ramm, E., and Wilson, E.L., "Finite Element Formulations for Large Deformation Dynamic Analysis," International Journal for Numerical Methods in Engineering, Vol. 9, 353-386, 1975.
5. Bathe, K.J., "An Assessment of Current Finite Element Analysis of Nonlinear Problems in Solid Mechanics," Numerical Solution of Partial Differential Equations, Academic Press, 1976.
6. Bathe, K.J., "Static and Dynamic Geometric and Material Nonlinear Analysis using ADINA," Report 82448-2, Acoustics and Vibration Laboratory Report, Department of Mechanical Engineering, M.I.T., May 1976 (rev. May 1977).
7. Dahlquist, E., and Björck, Å., Numerical Methods, Prentice-Hall, Inc., Englewood Cliffs, New Jersey, 1974.
8. Bathe, K.J., and Hahn, W., "On Transient Analysis of Fluid-Structure Systems," J. Computers and Structures, Vol. 10, pp. 383-391, 1978.
9. Bathe, K.J., and Bolourchi, S., "A Geometric and Material Nonlinear Plate Element," submitted for publication.
10. Bolourchi, S., and Bathe, K.J., "Geometric and Material Nonlinear Analysis of General Shell Structures," in preparation.
11. Newmark, N.M., "A Method of Computation for Structural Dynamics," ASCE, Journal of Engineering Mechanics Division, Vol. 85 (1959), pp. 67-94.
12. Houbolt, J.C., "A Recurrence Matrix Solution for the Dynamic Response of Elastic Aircraft," Journal of Aeronautical Science, Vol. 17 (1950), pp. 540-550.

13. Wilson, E.L., Farhoomand, I., and Bathe, K.J., "Non-linear Dynamic Analysis of Complex Structures," *International Journal of Earthquake Engineering and Structural Dynamics*, Vol. 1 (1973), pp. 241- 252.
14. Park, K.C., "An Improved Stiffly Stable Method for Direct Integration of Nonlinear Structural Dynamics;" *Journal of Applied Mechanics*, Vol. 97, pp. 464-470, 1975.
15. Bathe, K.J., and Cimento, A., "On the Time Integration of Nonlinear Dynamic Response," *Proceedings, GAMM/GAMNI Conference, Paris, Nov. 1978.*
16. Belytschko, T., and Mullen, R., "Mesh Partitions of Explicit-Implicit Time Integration," Formulations and Computational Algorithms in Finite Element Analysis, Bathe, K.J., Oden, J.T., and Wunderlich. W., (eds.), M.I.T. Press, 1977.
17. Nickell, R.E., "Nonlinear Dynamics by Mode Superposition," *J. Computer Methods in Applied Mechanics and Engineering*, Vol. 7, pp. 107-129, 1976.
18. Bathe, K.J., Ramaswamy, S., and Sonnad, V., "On Analysis of Nonlinear Dynamic Response using Mode Superposition," in preparation.
19. Clough, R.W., and Penzien, J., Dynamics of Structures, McGraw-Hill, New York, N.Y., 1975.
20. Crandall, S.H., Engineering Analysis, McGraw-Hill, 1956.
21. Belytschko, T., and Schoeberle, D.F., "On the Unconditional Stability of an Implicit Algorithm for Nonlinear Structural Dynamics," *Journal of Applied Mechanics*, Vol. 97, pp. 865-869, Dec. 1975.
22. Bathe, K.J., "ADINA - A Finite Element Program for Automatic Dynamic Incremental Nonlinear Analysis," Report No. 82448-1, Acoustics and Vibration Laboratory, Department of Mechanical Engineering, M.I.T., 1975 (revised Nov. 1978).
23. Achenbach, J.D., Wave Propagation in Elastic Solids, North-Holland Pub. Co., Amsterdam, 1975.

24. Romander, C.M., Cagliostro, D.J., and Florence, A.L., "Experiments on the Response of Flexible Piping Systems to Internal Pressure Pulses," SRI Project PYD-1960, Stanford Research Institute, Menlo Park, California, April 1976.

ACKNOWLEDGEMENT

Much of the work reported in this paper has been supported financially by the ADINA users group. We gratefully acknowledge this support.

Department of Mechanical Engineering
Massachusetts Institute of Technology
Cambridge, Massachusetts 02139 U.S.A.

FINITE ELEMENT FORMULATIONS FOR LARGE DEFORMATION DYNAMIC ANALYSIS

KLAUS-JÜRGEN BATHE*

Civil Engineering Department, University of California, Berkeley, California, U.S.A.

EKKEHARD RAMM†

University of Stuttgart, West Germany

EDWARD L. WILSON‡

Civil Engineering Department, University of California, Berkeley, California, U.S.A.

SUMMARY

Starting from continuum mechanics principles, finite element incremental formulations for non-linear static and dynamic analysis are reviewed and derived. The aim in this paper is a consistent summary, comparison, and evaluation of the formulations which have been implemented in the search for the most effective procedure. The general formulations include large displacements, large strains and material non-linearities. For specific static and dynamic analyses in this paper, elastic, hyperelastic (rubber-like) and hypoelastic elastic-plastic materials are considered. The numerical solution of the continuum mechanics equations is achieved using isoparametric finite element discretization. The specific matrices which need be calculated in the formulations are presented and discussed. To demonstrate the applicability and the important differences in the formulations, the solution of static and dynamic problems involving large displacements and large strains are presented.

INTRODUCTION

In non-linear dynamic finite element analysis involving large displacements, large strains and material non-linearities, it is necessary to resort to an incremental formulation of the equations of motion. Various formulations are used in practice (see References). Some procedures are general and others are restricted to account for material non-linearities only, or for large displacements but not for large strains, or the formulation may only be applicable to certain types of elements. Limited results have been obtained in dynamic non-linear analysis involving large displacements and large strains.

Currently, the general purpose non-linear finite element analysis program NONSAP is being developed at the University of California, Berkeley.² An important aspect in the development of the program is to assess which general finite element formulation should be implemented.

In dynamic analysis numerical time integration of the finite element equations of motion is required. Extensive research is currently being devoted towards the development of stable and accurate integration schemes.^{1,5,20,31} However, it need be realized that a proper evaluation and use of an integration method is only possible if a consistent non-linear finite element formulation is used.

* Assistant Research Engineer.

† Research Fellow of Deutsche Forschungsgemeinschaft. Formerly Visiting Scholar, University of California.

‡ Professor.

Received 18 February 1974

The earliest non-linear finite element analyses were essentially based on extensions of linear analyses and have been developed for specific applications (for a comprehensive list of References, see the books by Oden³³ and Zienkiewicz⁴³). The procedures were primarily developed on an intuitive basis in order to obtain solutions to the specific problems considered. However, to provide general analysis capabilities using isoparametric (and related) elements a general formulation need be used. The isoparametric finite element discretization procedure has proved to be very effective in many applications, and lately it has been shown that general non-linear formulations based on principles of continuum mechanics can be efficiently implemented.

Basically, two different approaches have been pursued in incremental non-linear finite element analysis. In the first, static and kinematic variables are referred to an updated configuration in each load step. This procedure is generally called Eulerian, moving co-ordinate or updated formulation. Murray and Wilson,²⁸ Felippa,⁹ Yaghmai,³⁹ Yaghmai and Popov,⁴⁰ Farhoomand,⁸ Sharifi and Popov,³⁵ Yamada,⁴¹ Stricklin and many others,³⁸ Heifitz and Costantino,¹⁵ Belytschko and Hsieh⁶ have presented some form of this formulation.

In the second approach, which is generally called Lagrangian formulation, all static and kinematic variables are referred to the initial configuration. This procedure is used by Oden,^{32,33} Marcal,²⁶ Hibbitt *et al.*,¹⁶ Larsen,²² McNamara,³⁰ Sharifi and Yates,³⁶ Stricklin and many others,^{37,38} Haug and Powell.¹³ A survey paper of the Lagrangian formulation in static analysis was presented by Hibbitt *et al.*,¹⁶ where it is stated that additional research is required for use of an equivalently consistent updated formulation.

It is apparent that with the different formulations available, in the development of a general purpose non-linear dynamic analysis program a decision need be made on the procedure to be used. An important consideration is that using any formulation based on continuum mechanics principles, in which all non-linear effects are included, the same results should be obtained in the analyses. Stricklin and many others, discussed a moving co-ordinate formulation and a Lagrangian formulation and pointed out that the latter is more general and computationally more efficient.³⁸ Yamada compared an Eulerian and Lagrangian formulation and predicted for a simple truss structure a maximum difference of about 25 per cent in the displacements.⁴¹ Dupuis and many others, analyzed arches using the Lagrangian and an updated formulation and also calculated a much different response by either formulation.⁷

The purpose of this paper is to present and compare in detail the general formulations that have been implemented in program NONSAP, and to show their general applicability in non-linear static and dynamic analysis. The formulations are termed total Lagrangian and updated Lagrangian formulations and they are based on the work of the authors cited above. For specific solutions in this paper, elastic, hyperelastic, and hypoelastic materials are considered.

The procedures are derived from the basic principle of virtual work and are valid for non-linear material behaviour, large displacements and large strains. It is pointed out that, in theory, there is no difference in the formulations. Any differences in the numerical results arise from the fact that different descriptions of material behaviour are assumed, and if the material constants are transformed appropriately, identical numerical results are obtained. Therefore, the question of which formulation should be used merely depends on the relative numerical effectiveness of the methods. In the paper specific attention is directed to the numerical efficiency of either formulation.

To demonstrate the applicability and the important differences in the formulations, the numerical operations required for solution are studied and a variety of sample solutions are presented. These include the large displacement static and dynamic analysis of a cantilever, the large displacement and large strain static and dynamic analysis of a rubber-like material and the static and dynamic, elastic and elastic-plastic large displacement analysis of arches and shells.

FORMULATION OF THE CONTINUUM MECHANICS INCREMENTAL EQUATIONS OF MOTION

Consider the motion of a body in a Cartesian co-ordinate system as shown in Figure 1. The aim is to evaluate the equilibrium positions of the body at the discrete time points $0, \Delta t, 2\Delta t, 3\Delta t, \dots$, where Δt is an increment in time. Assume that the solution for the kinematic and static variables for all time steps from time 0 to time t , inclusive, have been solved, and that the solution for time $t + \Delta t$ is required next. It is noted that the solution process for the next required equilibrium position is typical and would be applied repetitively until the complete solution path has been solved.

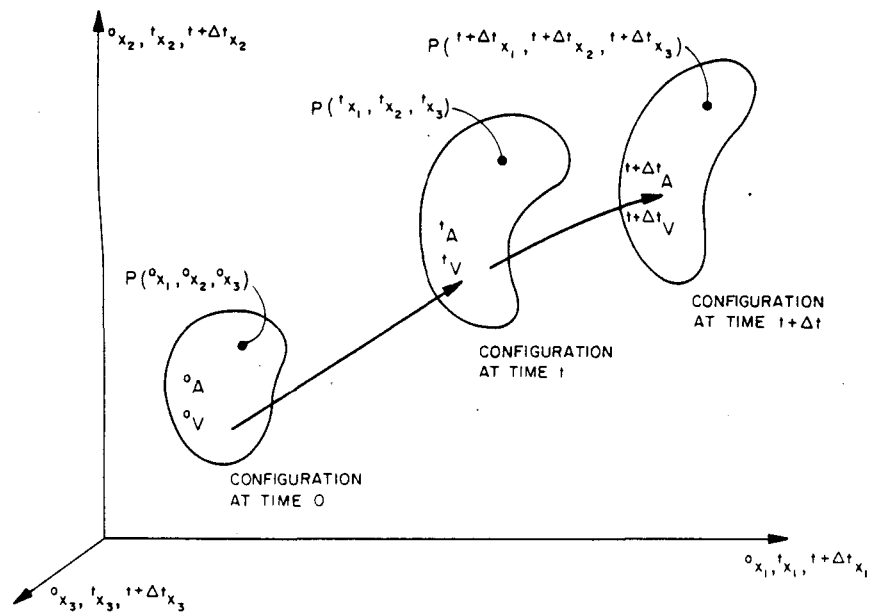


Figure 1. Motion of body in Cartesian co-ordinate system

Nomenclature

It is useful at this point to lay out the notation which will be employed.

The motion of the body is considered in a fixed Cartesian co-ordinate system, Figure 1, in which all kinematic and static variables are defined.

The co-ordinates describing the configuration of the body at time 0 are ${}^0x_1, {}^0x_2, {}^0x_3$, at time t are ${}^tx_1, {}^tx_2, {}^tx_3$, and at time $t + \Delta t$ are ${}^{t+\Delta t}x_1, {}^{t+\Delta t}x_2, {}^{t+\Delta t}x_3$, where the left superscripts refer to the configuration of the body and the subscripts to the co-ordinate axes.

The notation for the displacements of the body is similar to the notation for the co-ordinates: at time t the displacements are ${}^tu_i, i = 1, 2, 3$ and at time $t + \Delta t$ the displacements are ${}^{t+\Delta t}u_i, i = 1, 2, 3$; therefore

$$\left. \begin{aligned} {}^tx_i &= {}^0x_i + {}^tu_i \\ {}^{t+\Delta t}x_i &= {}^0x_i + {}^{t+\Delta t}u_i \end{aligned} \right\} \quad i = 1, 2, 3$$

The unknown increments in the displacements from time t to $t + \Delta t$ are denoted as

$$u_i = {}^{t+\Delta t}u_i - {}^tu_i; \quad i = 1, 2, 3$$

During motion of the body, its volume, surface area, mass density, stresses and strains are changing continuously. The specific mass, area and volume of the body at times 0, t and $t + \Delta t$ are denoted by ${}^0\rho, {}^t\rho, {}^{t+\Delta t}\rho; {}^0A, {}^tA, {}^{t+\Delta t}A$; and ${}^0V, {}^tV, {}^{t+\Delta t}V$; respectively.

Since the configuration of the body at time $t + \Delta t$ is not known, the applied forces, stresses and strains are referred to a known equilibrium configuration. In analogy to the notation used for co-ordinates and displacements a left superscript indicates in which configuration the quantity (body force, surface traction, stress, ...) occurs; in addition, a left subscript indicates with respect to which configuration the quantity is measured.

The surface and body force components per unit mass at time $t + \Delta t$, but measured in configuration t , are ${}^{t+\Delta t}t_k, {}^{t+\Delta t}f_k, k = 1, 2, 3$.

Considering stresses, the Cartesian components of the Cauchy stress tensor at time $t + \Delta t$ are denoted by ${}^{t+\Delta t}\tau_{ij}$ (since Cauchy stresses are always referred to the configuration in which they do occur ${}^{t+\Delta t}\tau_{ij} \equiv {}^{t+\Delta t}t_{ij}$), and the Cartesian components of the 2nd Piola–Kirchhoff stress tensor corresponding to the configuration at time $t + \Delta t$ but measured in configuration at time t are denoted by ${}^{t+\Delta t}S_{ij}$.

Considering strains, the Cartesian components of Cauchy's infinitesimal strain tensor referred to the configuration at time $t + \Delta t$ are denoted by ${}_{t+\Delta t}e_{ij}$; and the Cartesian components of the Green–Lagrange strain tensor using the displacements from the configuration at time t to the configuration at time $t + \Delta t$, and referred to the configuration at time t are denoted by ${}^{t+\Delta t}e_{ij}$.

The reference configurations, which will be used for applied forces, Kirchhoff–Piola stresses and Green–Lagrange strains, are those at time 0 and at time t .

In the formulation of the governing equilibrium equations derivatives of displacements and co-ordinates need be considered. In the notation adopted, a comma denotes differentiation with respect to the co-ordinate following, and the left time subscripts indicate the configuration in which this co-ordinate is measured: thus, for example,

$${}^{t+\Delta t}u_{i,j} = \frac{\partial {}^{t+\Delta t}u_i}{\partial x_j} \quad \text{and} \quad {}_{t+\Delta t}x_{m,n} = \frac{\partial x_m}{\partial x_n}$$

Principle of virtual displacements

With the notation having been explained briefly, consider again the body in Figure 1. Since the solution is known at all discrete time points 0, $\Delta t, 2\Delta t, \dots, t$, the basic aim of the formulation is to establish an equation of virtual work from which the unknown static and kinematic variables in the configuration at time $t + \Delta t$ can be solved. Since the isoparametric displacement based finite element procedure shall be employed for numerical solution, the principle of virtual displacements is used to express the equilibrium of the body in the configuration at time $t + \Delta t$. The principle of virtual displacements requires that

$$\int_{{}^{t+\Delta t}V} {}^{t+\Delta t}\tau_{ij} \delta {}_{t+\Delta t}e_{ij} {}^{t+\Delta t}dV = {}^{t+\Delta t}\mathcal{R} \quad (1)$$

where ${}^{t+\Delta t}\mathcal{R}$ is the external virtual work expression,

$${}^{t+\Delta t}\mathcal{R} = \int_{{}^{t+\Delta t}A} {}^{t+\Delta t}t_k \delta u_k {}^{t+\Delta t}da + \int_{{}^{t+\Delta t}V} {}^{t+\Delta t}\rho {}^{t+\Delta t}f_k \delta u_k {}^{t+\Delta t}dV \quad (2)$$

In equations (1) and (2) δu_k is a (virtual) variation in the current displacement components ${}^{t+\Delta t}u_k$, and $\delta {}_{t+\Delta t}e_{ij}$ are the corresponding (virtual) variations in strains, i.e.

$$\delta {}_{t+\Delta t}e_{ij} = \delta \frac{1}{2} ({}_{t+\Delta t}u_{i,j} + {}_{t+\Delta t}u_{j,i})$$

It need be noted that in equation (1) and the equations to follow the summation convention of tensor notation is implied.

Equation (1) cannot be solved directly since the configuration at time $t + \Delta t$ is unknown. A solution can be obtained by referring all variables to a known previously calculated equilibrium configuration. For this purpose, in principle, any one of the already calculated equilibrium configurations could be used. In practice, however, the choice lies essentially between two different formulations, namely, the total Lagrangian formulation (T.L.) and the updated Lagrangian (U.L.) formulation, which are presented in the following sections.

Total Lagrangian formulation

The formulation called here total Lagrangian (T.L.) formulation is generally referred to as Lagrangian formulation and has been used a great deal in static analysis.^{14,16,26,38}

In the formulation all variables in equations (1) and (2) are referred to the initial configuration at time 0 of the body. The applied forces in equation (2) are evaluated using

$$\left. \begin{aligned} {}^{t+\Delta t}t_k \, {}^{t+\Delta t}da &= {}^{t+\Delta t}t_k \, {}^0da: \\ {}^{t+\Delta t}\rho \, {}^{t+\Delta t}f_k \, {}^{t+\Delta t}dv &= {}^0\rho \, {}^{t+\Delta t}f_k \, {}^0dv \end{aligned} \right\} \quad (3)$$

where it is assumed that the direction and magnitude of the forces ${}^{t+\Delta t}t_k$ and ${}^0\rho \, {}^{t+\Delta t}f_k$ are independent of the specific configuration at time $t + \Delta t$. Loading conditions that depend on the deformations will be considered later.

The volume integral of Cauchy stresses times variations in infinitesimal strains in equation (1) can be transformed to give²⁵

$$\int_{{}^{t+\Delta t}V} {}^{t+\Delta t}\tau_{ij} \delta {}^{t+\Delta t}e_{ij} \, {}^{t+\Delta t}dv = \int_{{}^0V} {}^{t+\Delta t}S_{ij} \delta {}^{t+\Delta t}e_{ij} \, {}^0dv \quad (4)$$

where ${}^{t+\Delta t}S_{ij}$ = Cartesian components of the 2nd Piola-Kirchhoff stress tensor corresponding to the configuration at time $t + \Delta t$ but measured in the configuration at time 0.

$${}^{t+\Delta t}S_{ij} = \frac{{}^0\rho}{{}^{t+\Delta t}\rho} {}^{t+\Delta t}X_{i,s} \, {}^{t+\Delta t}\tau_{sr} \, {}^{t+\Delta t}X_{j,r} \quad (5)$$

and $\delta {}^{t+\Delta t}e_{ij}$ = variations in the Cartesian components of the Green-Lagrange strain tensor in the configuration at time $t + \Delta t$, referred to the configuration at time 0.

$$\delta {}^{t+\Delta t}e_{ij} = \delta \frac{1}{2} ({}^{t+\Delta t}u_{i,j} + {}^{t+\Delta t}u_{j,i} + {}^{t+\Delta t}u_{k,i} \, {}^{t+\Delta t}u_{k,j}) \quad (6)$$

It should be noted that the integral of Piola-Kirchhoff stresses times variations in the Green-Lagrange strains is defined over the initial configuration at time 0 of the body.

Substituting the relations in equations (3) and (4) into equations (1) and (2), the following equilibrium equation for the body in the configuration at time $t + \Delta t$ but referred to the configuration at time 0 is obtained,

$$\int_{{}^0V} {}^{t+\Delta t}S_{ij} \delta {}^{t+\Delta t}e_{ij} \, {}^0dv = {}^{t+\Delta t}\mathcal{A} \quad (7)$$

where ${}^{t+\Delta t}\mathcal{R}$ is now calculated using

$${}^{t+\Delta t}\mathcal{R} = \int_{o_A} {}^{t+\Delta t}t_k \delta u_k \, {}^0da + \int_{o_V} {}^0\rho {}^{t+\Delta t}f_k \delta u_k \, {}^0dv \quad (8)$$

Since the stresses ${}^{t+\Delta t}S_{ij}$ and strains ${}^{t+\Delta t}\varepsilon_{ij}$ are unknown, for solution, the following incremental decompositions are used

$${}^{t+\Delta t}S_{ij} = {}^tS_{ij} + {}_0S_{ij} \quad (9)$$

$${}^{t+\Delta t}\varepsilon_{ij} = {}^t\varepsilon_{ij} + {}_0\varepsilon_{ij} \quad (10)$$

where ${}^tS_{ij}$ and ${}^t\varepsilon_{ij}$ are the known 2nd Piola–Kirchhoff stresses and Green–Lagrange strains in the configuration at time t . Using the displacement definition of the Green–Lagrange strain tensor, it follows from equation (10) that $\delta {}^{t+\Delta t}\varepsilon_{ij} = \delta {}_0\varepsilon_{ij}$ and

$${}_0\varepsilon_{ij} = {}_0e_{ij} + {}_0\eta_{ij} \quad (11)$$

where

$${}_0e_{ij} = \frac{1}{2}({}_0u_{i,j} + {}_0u_{j,i} + {}^t u_{k,i} {}_0u_{k,j} + {}_0u_{k,i} {}^t u_{k,j}) \quad (12)$$

$${}_0\eta_{ij} = \frac{1}{2} {}_0u_{k,i} {}_0u_{k,j} \quad (13)$$

The incremental 2nd Piola–Kirchhoff stresses ${}_0S_{ij}$ are related to the incremental Green–Lagrange strains ${}_0\varepsilon_{ij}$ using the constitutive tensor ${}_0C_{ijrs}$, i.e.

$${}_0S_{ij} = {}_0C_{ijrs} {}_0\varepsilon_{rs} \quad (14)$$

Equation (7) can now be written as

$$\int_{o_V} {}_0C_{ijrs} {}_0\varepsilon_{rs} \delta {}_0\varepsilon_{ij} \, {}^0dv + \int_{o_V} {}^tS_{ij} \delta {}_0\eta_{ij} \, {}^0dv = {}^{t+\Delta t}\mathcal{R} - \int_{o_V} {}^tS_{ij} \delta {}_0e_{ij} \, {}^0dv \quad (15)$$

which represents a non-linear equation for the incremental displacements u_i .

Updated Lagrangian formulation

Most updated formulations previously used are approximate in that they are restricted to small strains or even constant strain conditions within each finite element used for numerical solution.^{6,28} However, Yaghmai introduced a general procedure, and the U.L. formulation given here is largely based on his work.³⁹

In the U.L. formulation all variables in equations (1) and (2) are referred to the configuration at time t , i.e. the updated configuration of the body. By an analogous procedure to the derivation of the T.L. formulation, equation (1) is in this case transformed to

$$\int_{t_V} {}^{t+\Delta t}S_{ij} \delta {}^{t+\Delta t}\varepsilon_{ij} \, {}^t dv = {}^{t+\Delta t}\mathcal{R} \quad (16)$$

where ${}^{t+\Delta t}S_{ij}$ = Cartesian components of the 2nd Piola–Kirchhoff stress tensor and ${}^{t+\Delta t}\varepsilon_{ij}$ = Cartesian components of the Green–Lagrange strain tensor from the configuration at time t to the configuration at time $t + \Delta t$ and referred to the configuration at time t . The quantities ${}^{t+\Delta t}S_{ij}$ and ${}^{t+\Delta t}\varepsilon_{ij}$ are defined by equations (5) and (6), respectively, if the superscript and subscript '0' is replaced by 't' and displacements are measured from the configuration at time t . Since deformation independent loading is considered ${}^{t+\Delta t}\mathcal{R}$ is evaluated as in the T.L. formulation.

The incremental stress decomposition used in this case is

$${}^{t+\Delta t}S_{ij} = {}^t\tau_{ij} + {}^tS_{ij} \quad (17)$$

where ${}^t\tau_{ij}$ = Cartesian components of the Cauchy stress tensor and ${}^tS_{ij}$ = Cartesian components of the 2nd Piola–Kirchhoff stress increment tensor referred to the configuration at time t . Considering the strain increments ${}^{t+\Delta t}\varepsilon_{ij}$, the following relations hold

$${}^{t+\Delta t}\varepsilon_{ij} = {}^t\varepsilon_{ij} \quad (18)$$

$${}^t\varepsilon_{ij} = {}^te_{ij} + {}^t\eta_{ij} \quad (19)$$

where

$${}^te_{ij} = \frac{1}{2}({}^tu_{i,j} + {}^tu_{j,i}) \quad (20)$$

$${}^t\eta_{ij} = \frac{1}{2}{}^tu_{k,i}{}^tu_{k,j} \quad (21)$$

The constitutive relation between stress and strain increments used now is

$${}^tS_{ij} = {}^tC_{ijrs}{}^t\varepsilon_{rs} \quad (22)$$

and equation (16) can be rewritten as

$$\int_{tV} {}^tC_{ijrs}{}^t\varepsilon_{rs} \delta_t \varepsilon_{ij} {}^t dv + \int_{tV} {}^t\tau_{ij} \delta_t \eta_{ij} {}^t dv = {}^{t+\Delta t}\mathcal{R} - \int_{tV} {}^t\tau_{ij} \delta_t e_{ij} {}^t dv \quad (23)$$

which, as equation (15), is a non-linear equation in the incremental displacements u_i .

Linearization of equilibrium equations

It should be noted that equations (15) and (23) are, theoretically, equivalent and provided the appropriate constitutive relations are used, the equations yield identical solutions. However, as will be seen, the finite element matrices established for solution are different.

The solution of equation (15) and of equation (23) cannot be calculated directly, since they are nonlinear in the displacement increments. Approximate solutions can be obtained by assuming that in equation (15) ${}^0\varepsilon_{ij} = {}^0e_{ij}$ and in equation (23) ${}^t\varepsilon_{ij} = {}^te_{ij}$. This means that, in addition to using $\delta_0 \varepsilon_{ij} = \delta_0 e_{ij}$ and $\delta_t \varepsilon_{ij} = \delta_t e_{ij}$, respectively, the incremental constitutive relations employed are

$${}^0S_{ij} = {}^0C_{ijrs}{}^0e_{rs} \quad (24)$$

and

$${}^tS_{ij} = {}^tC_{ijrs}{}^te_{rs} \quad (25)$$

FINITE ELEMENT SOLUTION

In the T.L. formulation the approximate equilibrium equation to be solved is

$$\int_{{}^0V} {}^0C_{ijrs}{}^0e_{rs} \delta_0 e_{ij} {}^0 dv + \int_{{}^0V} {}^0S_{ij} \delta_0 \eta_{ij} {}^0 dv = {}^{t+\Delta t}\mathcal{R} - \int_{{}^0V} {}^0S_{ij} \delta_0 e_{ij} {}^0 dv \quad (26)$$

whereas in the U.L. formulation the equation is

$$\int_{{}^tV} {}^tC_{ijrs}{}^te_{rs} \delta_t e_{ij} {}^t dv + \int_{{}^tV} {}^t\tau_{ij} \delta_t \eta_{ij} {}^t dv = {}^{t+\Delta t}\mathcal{R} - \int_{{}^tV} {}^t\tau_{ij} \delta_t e_{ij} {}^t dv \quad (27)$$

Equations (26) and (27) are linear equations in the incremental displacements and are used as the basis for isoparametric finite element analysis.^{32,43} Referring to the standard procedures for assembling the structure matrices, attention need only be given to the derivation of the matrices corresponding to a single element.

Finite element matrices

In the isoparametric element solution the co-ordinates and displacements are interpolated using

$$\left. \begin{aligned} {}^0x_i &= \sum_{k=1}^N h_k {}^0x_i^k; & {}^t x_i &= \sum_{k=1}^N h_k {}^t x_i^k \\ & & {}^{t+\Delta t} x_i &= \sum_{k=1}^N h_k {}^{t+\Delta t} x_i^k \end{aligned} \right\} \quad i = 1, 2, 3 \quad (28)$$

$${}^t u_i = \sum_{k=1}^N h_k {}^t u_i^k; \quad u_i = \sum_{k=1}^N h_k u_i^k \quad i = 1, 2, 3 \quad (29)$$

where ${}^t x_i^k$ is the co-ordinate of nodal point k corresponding to direction i at time t , ${}^t u_i^k$ is defined similarly to ${}^t x_i^k$, h_k is the interpolation function corresponding to nodal point k , and N is the number of element nodal points.⁴³

Using equations (28) and (29) to evaluate the displacement derivatives required in the integrals, equation (26) becomes, considering a single element

$$({}^t \mathbf{K}_L + {}^t \mathbf{K}_{NL}) \mathbf{u} = {}^{t+\Delta t} \mathbf{R} - {}^t \mathbf{F} \quad (30)$$

where ${}^t \mathbf{K}_L \mathbf{u}$, ${}^t \mathbf{K}_{NL} \mathbf{u}$ and ${}^t \mathbf{F}$ are obtained from the finite element evaluation of $\int_{0V} {}_0 C_{ijrs} {}_0 e_{rs} \times \delta_0 e_{ij} {}^0 dv$, $\int_{0V} {}^t S_{ij} \delta_0 \eta_{ij} {}^0 dv$, and $\int_{0V} {}^t S_{ij} \delta_0 e_{ij} {}^0 dv$, respectively, i.e.

$${}^t \mathbf{K}_L = \int_{0V} {}^t \mathbf{B}_L^T {}_0 \mathbf{C} {}^t \mathbf{B}_L {}^0 dv \quad (31)$$

$${}^t \mathbf{K}_{NL} = \int_{0V} {}^t \mathbf{B}_{NL}^T {}^t \mathbf{S} {}^t \mathbf{B}_{NL} {}^0 dv \quad (32)$$

$${}^t \mathbf{F} = \int_{0V} {}^t \mathbf{B}_L^T {}^t \hat{\mathbf{S}} {}^0 dv \quad (33)$$

The vector ${}^{t+\Delta t} \mathbf{R}$ in equation (30) is obtained from the finite element evaluation of equation (8) in the usual way.⁴³ In the above equations, ${}^t \mathbf{B}_L$ and ${}^t \mathbf{B}_{NL}$ are linear and non-linear strain-displacement transformation matrices, ${}_0 \mathbf{C}$ is the incremental material property matrix, ${}^t \mathbf{S}$ is a matrix of 2nd Piola-Kirchhoff stresses, and ${}^t \hat{\mathbf{S}}$ is a vector of these stresses. All matrix elements correspond to the configuration at time t and are defined with respect to the configuration at time 0.

Similarly, the finite element solution of equation (27), which was obtained using the U.L. formulation, results into

$$({}^t \mathbf{K}_L + {}^t \mathbf{K}_{NL}) \mathbf{u} = {}^{t+\Delta t} \mathbf{R} - {}^t \mathbf{F} \quad (34)$$

where

$${}^t \mathbf{K}_L = \int_{tV} {}^t \mathbf{B}_{L,t}^T {}^t \mathbf{C} {}^t \mathbf{B}_{L,t} {}^t dt \quad (35)$$

$${}^t\mathbf{K}_{NL} = \int_{tV} {}^t\mathbf{B}_{NL}^T {}^t\boldsymbol{\tau} {}^t\mathbf{B}_{NL} {}^t dv \tag{36}$$

and

$${}^t\mathbf{F} = \int_{tV} {}^t\mathbf{B}_L^T {}^t\hat{\boldsymbol{\tau}} {}^t dv \tag{37}$$

In Equations (35) to (37) the elements of the linear and non-linear strain-displacement transformation matrices ${}^t\mathbf{B}_L$ and ${}^t\mathbf{B}_{NL}$, respectively, and the elements of the incremental material property matrix ${}^t\mathbf{C}$ correspond to and are defined with respect to the configuration at time t , ${}^t\boldsymbol{\tau}$ is a matrix and ${}^t\hat{\boldsymbol{\tau}}$ is a vector of Cauchy stresses in the configuration at time t .

It should be noted that the elements of the matrices in equations (30) to (37) are functions of the natural element co-ordinates and that the volume integrations are performed using a co-ordinate change from Cartesian to natural co-ordinates.^{4,3} Table I gives the strain-displacement and stress matrices used for two-dimensional (plane stress, plane strain and axisymmetric) analysis in the U.L. and T.L. formulations. Figure 2 shows the 4 to 8 variable-number-nodes element that has been used in the sample solutions.³

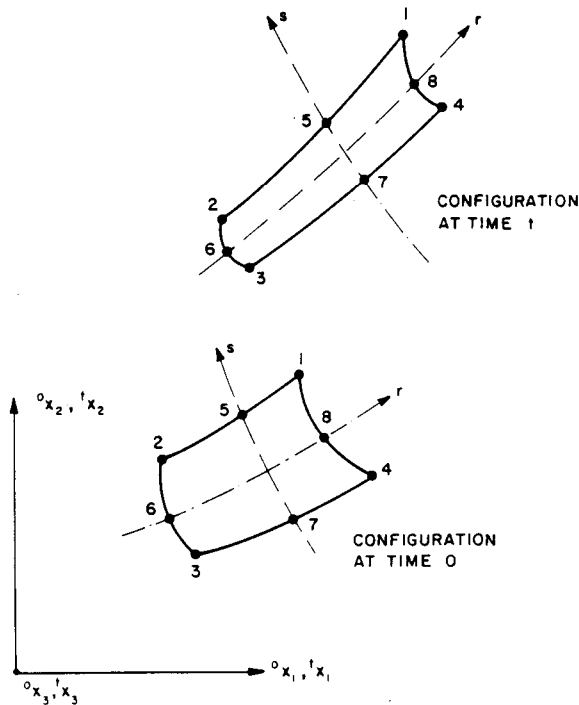


Figure 2. Two-dimensional element shown in the global ${}^t x_1 - {}^t x_2$ plane

Dynamic analysis

In dynamic analysis, the applied body forces include inertia forces. Assuming that the mass of the body considered is preserved, the mass matrix can in both formulations be evaluated prior to the time integration using the initial configuration at time 0 as reference. Employing the standard finite element formulation to evaluate the element mass matrix,^{4,3} the incremental equilibrium equation for a single element in the T.L. formulation is

$$({}_0^t\mathbf{K}_L + {}_0^t\mathbf{K}_{NL})\mathbf{u} = {}^{t+\Delta t}\mathbf{R} - {}_0^t\mathbf{F} - \mathbf{M} {}^{t+\Delta t}\ddot{\mathbf{u}} \tag{38}$$

Table I. Matrices used in two-dimensional analysis

*Total Lagrangian formulation**Incremental strains*

$${}^0\varepsilon_{11} = {}^0u_{1,1} + {}^i u_{1,1} {}^0u_{1,1} + {}^i u_{2,1} {}^0u_{2,1} + \frac{1}{2}[({}^0u_{1,1})^2 + ({}^0u_{2,1})^2]$$

$${}^0\varepsilon_{22} = {}^0u_{2,2} + {}^i u_{1,2} {}^0u_{1,2} + {}^i u_{2,2} {}^0u_{2,2} + \frac{1}{2}[({}^0u_{1,2})^2 + ({}^0u_{2,2})^2]$$

$${}^0\varepsilon_{12} = \frac{1}{2}[{}^0u_{1,2} + {}^0u_{2,1}] + \frac{1}{2}[{}^i u_{1,1} {}^0u_{1,2} + {}^i u_{2,1} {}^0u_{2,2} + {}^i u_{1,2} {}^0u_{1,1} + {}^i u_{2,2} {}^0u_{2,1}] + \frac{1}{2}[{}^0u_{1,1} {}^0u_{1,2} + {}^0u_{2,1} {}^0u_{2,2}]$$

$${}^0\varepsilon_{33} = \frac{u_1}{{}^0x_1} + \frac{{}^i u_1 u_1}{{}^0x_1)^2} + \frac{1}{2} \left(\frac{u_1}{{}^0x_1} \right)^2 \quad (\text{axisymmetric analysis})$$

where

$${}^0u_{i,j} = \frac{\partial u_i}{\partial {}^0x_j}; \quad {}^i u_{i,j} = \frac{\partial^i u_i}{\partial {}^0x_j}$$

Linear strain-displacement transformation matrix

Using

$${}^0e = {}^i B_L u$$

where

$${}^0e^T = [{}^0e_{11} \quad {}^0e_{22} \quad 2{}^0e_{12} \quad {}^0e_{33}]; \quad u^T = [u_1^1 u_2^1 u_1^2 u_2^2 \dots u_1^N u_2^N]$$

and

$${}^i B_L = {}^i B_{L0} + {}^i B_{L1}$$

$${}^i B_{L0} = \begin{bmatrix} {}^0h_{1,1} & 0 & {}^0h_{2,1} & 0 & {}^0h_{3,1} & 0 & \dots & {}^0h_{N,1} & 0 \\ 0 & {}^0h_{1,2} & 0 & {}^0h_{2,2} & 0 & {}^0h_{3,2} & \dots & 0 & {}^0h_{N,2} \\ {}^0h_{1,2} & {}^0h_{1,1} & {}^0h_{2,2} & {}^0h_{2,1} & {}^0h_{3,2} & {}^0h_{3,1} & \dots & {}^0h_{N,2} & {}^0h_{N,1} \\ \frac{h_1}{{}^0\bar{x}_1} & 0 & \frac{h_2}{{}^0\bar{x}_1} & 0 & \frac{h_3}{{}^0\bar{x}_1} & 0 & \dots & \frac{h_N}{{}^0\bar{x}_1} & 0 \end{bmatrix}$$

where

$${}^0h_{k,j} = \frac{\partial h_k}{\partial {}^0x_j}; \quad u_j^k = {}^{i+\Delta t} u_j^k - {}^i u_j^k; \quad {}^0\bar{x}_1 = \sum_{k=1}^N h_k {}^0x_1^k; \quad N = \text{number of nodes}$$

and

$${}^i B_{L1} = \begin{bmatrix} l_{11} {}^0h_{1,1} & l_{21} {}^0h_{1,1} & l_{11} {}^0h_{2,1} & l_{21} {}^0h_{2,1} \\ l_{12} {}^0h_{1,2} & l_{22} {}^0h_{1,2} & l_{12} {}^0h_{2,2} & l_{22} {}^0h_{2,2} \\ (l_{11} {}^0h_{1,2} + l_{12} {}^0h_{1,1}) & (l_{21} {}^0h_{1,2} + l_{22} {}^0h_{1,1}) & (l_{11} {}^0h_{2,2} + l_{12} {}^0h_{2,1}) & (l_{21} {}^0h_{2,2} + l_{22} {}^0h_{2,1}) \\ l_{33} \frac{h_1}{{}^0\bar{x}_1} & 0 & l_{33} \frac{h_2}{{}^0\bar{x}_1} & 0 \\ \dots & \dots & l_{11} {}^0h_{N,1} & l_{21} {}^0h_{N,1} \\ \dots & \dots & l_{12} {}^0h_{N,2} & l_{22} {}^0h_{N,2} \\ \dots & \dots & (l_{11} {}^0h_{N,2} + l_{12} {}^0h_{N,1}) & (l_{21} {}^0h_{N,2} + l_{22} {}^0h_{N,1}) \\ \dots & \dots & l_{33} \frac{h_N}{{}^0\bar{x}_1} & 0 \end{bmatrix}$$

Table I—continued

where

$$l_{11} = \sum_{k=1}^N {}_0h_{k,1} {}'u_1^k; \quad l_{22} = \sum_{k=1}^N {}_0h_{k,2} {}'u_2^k; \quad l_{21} = \sum_{k=1}^N {}_0h_{k,1} {}'u_2^k;$$

$$l_{12} = \sum_{k=1}^N {}_0h_{k,2} {}'u_1^k; \quad l_{33} = \left(\sum_{k=1}^N h_k {}'u_1^k \right) / {}_0\bar{x}_1$$

Non-linear strain-displacement transformation matrix

$${}^i\mathbf{B}_{NL} = \begin{bmatrix} {}_0h_{1,1} & 0 & {}_0h_{2,1} & 0 & {}_0h_{3,1} & 0 & \dots & {}_0h_{N,1} & 0 \\ {}_0h_{1,2} & 0 & {}_0h_{2,2} & 0 & {}_0h_{3,2} & 0 & \dots & {}_0h_{N,2} & 0 \\ 0 & {}_0h_{1,1} & 0 & {}_0h_{2,1} & 0 & {}_0h_{3,1} & \dots & 0 & {}_0h_{N,1} \\ 0 & {}_0h_{1,2} & 0 & {}_0h_{2,2} & 0 & {}_0h_{3,2} & \dots & 0 & {}_0h_{N,2} \\ \frac{h_1}{{}_0\bar{x}_1} & 0 & \frac{h_2}{{}_0\bar{x}_1} & 0 & \frac{h_3}{{}_0\bar{x}_1} & 0 & \dots & \frac{h_N}{{}_0\bar{x}_1} & 0 \end{bmatrix}$$

2nd Piola-Kirchhoff stress matrix and vector

$${}^i\mathbf{S} = \begin{bmatrix} {}^iS_{11} & {}^iS_{12} & 0 & 0 & 0 \\ {}^iS_{21} & {}^iS_{22} & 0 & 0 & 0 \\ 0 & 0 & {}^iS_{11} & {}^iS_{12} & 0 \\ 0 & 0 & {}^iS_{21} & {}^iS_{22} & 0 \\ 0 & 0 & 0 & 0 & {}^iS_{33} \end{bmatrix}; \quad {}^i\hat{\mathbf{S}} = \begin{bmatrix} {}^iS_{11} \\ {}^iS_{22} \\ {}^iS_{12} \\ {}^iS_{33} \end{bmatrix}$$

Updated Lagrangian formulation

Incremental strains

$${}_i e_{11} = {}_i u_{1,1} + \frac{1}{2} [({}_i u_{1,1})^2 + ({}_i u_{2,1})^2]$$

$${}_i e_{22} = {}_i u_{2,2} + \frac{1}{2} [({}_i u_{1,2})^2 + ({}_i u_{2,2})^2]$$

$${}_i e_{12} = \frac{1}{2} [{}_i u_{1,2} + {}_i u_{2,1}] + \frac{1}{2} [{}_i u_{1,1} {}_i u_{1,2} + {}_i u_{2,1} {}_i u_{2,2}]$$

$${}_i e_{33} = \frac{u_1}{{}_i x_1} + \frac{1}{2} \left(\frac{u_1}{{}_i x_1} \right)^2 \quad (\text{axisymmetric analysis})$$

where

$${}_i u_{i,j} = \frac{\partial u_i}{\partial {}^i x_j}$$

Linear strain-displacement transformation matrix

Using

$${}_i \mathbf{e} = {}^i\mathbf{B}_L \mathbf{u}$$

where

$${}_i \mathbf{e}^T = [{}_i e_{11}, {}_i e_{22}, 2{}_i e_{12}, {}_i e_{33}]; \quad \mathbf{u}^T = [u_1^1 u_2^1 u_1^2 u_2^2 \dots u_1^N u_2^N]$$

$${}^i\mathbf{B}_L = \begin{bmatrix} {}_i h_{1,1} & 0 & {}_i h_{2,1} & 0 & {}_i h_{3,1} & 0 & \dots & {}_i h_{N,1} & 0 \\ 0 & {}_i h_{1,2} & 0 & {}_i h_{2,2} & 0 & {}_i h_{3,2} & \dots & 0 & {}_i h_{N,2} \\ {}_i h_{1,2} & {}_i h_{1,1} & {}_i h_{2,2} & {}_i h_{2,1} & {}_i h_{3,2} & {}_i h_{3,1} & \dots & {}_i h_{N,2} & {}_i h_{N,1} \\ \frac{h_1}{{}_i \bar{x}_1} & 0 & \frac{h_2}{{}_i \bar{x}_1} & 0 & \frac{h_3}{{}_i \bar{x}_1} & 0 & \dots & \frac{h_N}{{}_i \bar{x}_1} & 0 \end{bmatrix}$$

Table 1—continued

where

$$h_{k,j} = \frac{\partial h_k}{\partial x_j}; \quad u_j^k = {}^{t+\Delta t}u_j^k - {}^t u_j^k; \quad \bar{x}_1 = \sum_{k=1}^N h_k {}^t x_1^k; \quad N = \text{number of nodes}$$

Non-linear strain-displacement transformation matrix

$${}^t \mathbf{B}_{NL} = \begin{bmatrix} {}^t h_{1,1} & 0 & {}^t h_{2,1} & 0 & {}^t h_{3,1} & 0 & \dots & {}^t h_{N,1} & 0 \\ {}^t h_{1,2} & 0 & {}^t h_{2,2} & 0 & {}^t h_{3,2} & 0 & \dots & {}^t h_{N,2} & 0 \\ 0 & {}^t h_{1,1} & 0 & {}^t h_{2,1} & 0 & {}^t h_{3,1} & \dots & 0 & {}^t h_{N,1} \\ 0 & {}^t h_{1,2} & 0 & {}^t h_{2,2} & 0 & {}^t h_{3,2} & \dots & 0 & {}^t h_{N,2} \\ \frac{h_1}{\bar{x}_1} & 0 & \frac{h_2}{\bar{x}_1} & 0 & \frac{h_3}{\bar{x}_1} & 0 & \dots & \frac{h_N}{\bar{x}_1} & 0 \end{bmatrix}$$

Cauchy stress matrix and stress vector

$${}^t \boldsymbol{\tau} = \begin{bmatrix} {}^t \tau_{11} & {}^t \tau_{12} & 0 & 0 & 0 \\ {}^t \tau_{21} & {}^t \tau_{22} & 0 & 0 & 0 \\ 0 & 0 & {}^t \tau_{11} & {}^t \tau_{12} & 0 \\ 0 & 0 & {}^t \tau_{21} & {}^t \tau_{22} & 0 \\ 0 & 0 & 0 & 0 & {}^t \tau_{33} \end{bmatrix}; \quad {}^t \hat{\boldsymbol{\tau}} = \begin{bmatrix} {}^t \tau_{11} \\ {}^t \tau_{22} \\ {}^t \tau_{12} \\ {}^t \tau_{33} \end{bmatrix}$$

and in the U.L. formulation this equation is

$$({}^t \mathbf{K}_L + {}^t \mathbf{K}_{NL}) \mathbf{u} = {}^{t+\Delta t} \mathbf{R} - {}^t \mathbf{F} - \mathbf{M} {}^{t+\Delta t} \ddot{\mathbf{u}} \quad (39)$$

where ${}^{t+\Delta t} \ddot{\mathbf{u}}$ is a vector of the element nodal point accelerations at time $t + \Delta t$, and \mathbf{M} is the element mass matrix calculated at time 0. In integrations (38) and (39), damping effects defined by a matrix \mathbf{C} have been ignored.⁴

Equilibrium iteration

It is important to realize that equations (38) and (39) are only approximations to the actual equations to be solved in each time step, i.e. equations (7) and (16), respectively. Depending on the non-linearities in the system, the linearization of equations (15) and (23) may introduce errors which ultimately result into solution instability. For this reason it may be necessary to iterate in each load step until, within the necessary assumptions on the variation of the material constants and the numerical time integration, equations (7) and (16) are satisfied to a required tolerance. The equation used in the T.L. formulation is

$$({}_0^t \mathbf{K}_L + {}_0^t \mathbf{K}_{NL}) \Delta \mathbf{u}^{(i)} = {}^{t+\Delta t} \mathbf{R} - {}^{t+\Delta t} \mathbf{F}^{(i-1)} - \mathbf{M} {}^{t+\Delta t} \ddot{\mathbf{u}}^{(i)} \quad i = 1, 2, 3 \dots \quad (40)$$

where ${}^{t+\Delta t} \mathbf{u}^{(i)} = {}^{t+\Delta t} \mathbf{u}^{(i-1)} + \Delta \mathbf{u}^{(i)}$.

It should be noted that for $i = 1$ equation (40) corresponds to equation (38), i.e. $\Delta \mathbf{u}^{(1)} = \mathbf{u}$, ${}^{t+\Delta t} \ddot{\mathbf{u}}^{(1)} = {}^{t+\Delta t} \ddot{\mathbf{u}}$, ${}^{t+\Delta t} \mathbf{u}^{(0)} = {}^t \mathbf{u}$, and ${}^{t+\Delta t} \mathbf{F}^{(0)} = {}^t \mathbf{F}$.

The calculation of the acceleration approximation ${}^{t+\Delta t} \ddot{\mathbf{u}}^{(i)}$ depends on the time integration scheme used.

The vector of nodal point forces equivalent to the element stresses, ${}^{t+\Delta t} \mathbf{F}^{(i)}$, is the finite element evaluation of $\int_{\text{vol}} {}^{t+\Delta t} S_{ij}^{(i)} \delta_0^t c_{ij}^{(i)} dV$, where the superscript (i) shows that stresses and strains are evaluated using ${}^{t+\Delta t} \mathbf{u}^{(i)}$. Since $\delta_0^t c_{ij}^{(i)} = \frac{1}{2} (\delta_0^t u_{i,j} + \delta_0^t u_{j,i} + {}^{t+\Delta t} u_{k,i} \delta_0^t u_{k,j} + {}^{t+\Delta t} u_{k,j} \delta_0^t u_{k,i})$, the

nodal point forces are

$${}^{t+\Delta t}{}_0\mathbf{F}^{(i)} = \int_{0V} {}^{t+\Delta t}{}_0\mathbf{B}_L^{(i)T} {}^{t+\Delta t}{}_0\hat{\mathbf{S}}^{(i)} dV \quad (41)$$

in which the matrices ${}^{t+\Delta t}{}_0\mathbf{B}_L^{(i)}$ and ${}^{t+\Delta t}{}_0\hat{\mathbf{S}}^{(i)}$ correspond to the matrices ${}_0\mathbf{B}_L$ and ${}_0\hat{\mathbf{S}}$ in Table I, but are defined for time $t + \Delta t$ and iteration (i), respectively.

In the U.L. formulation the equation used for a single element with equilibrium iteration is

$$({}^t\mathbf{K}_L + {}^t\mathbf{K}_{NL}) \Delta \mathbf{u}^{(i)} = {}^{t+\Delta t}\mathbf{R} - {}^{t+\Delta t}{}_{t+\Delta t}\mathbf{F}^{(i-1)} - \mathbf{M} {}^{t+\Delta t}\ddot{\mathbf{u}}^{(i)} \quad i = 1, 2, 3, \dots \quad (42)$$

in which the i th displacement and acceleration approximations are calculated as above and ${}^{t+\Delta t}{}_{t+\Delta t}\mathbf{F}^{(i)}$ is the finite element evaluation of

$$\int_{{}^{t+\Delta t}V^{(i)}} {}^{t+\Delta t}{}_{t+\Delta t}\tau_{ij}^{(i)} \delta_{t+\Delta t} e_{ij}^{(i)} {}^{t+\Delta t}dV^{(i)}; \quad \text{i.e.} \quad {}^{t+\Delta t}{}_{t+\Delta t}\mathbf{F}^{(i)} = \int_{{}^{t+\Delta t}V^{(i)}} {}^{t+\Delta t}{}_L\mathbf{B}_L^{(i)T} {}^{t+\Delta t}\hat{\boldsymbol{\tau}}^{(i)} {}^{t+\Delta t}dV^{(i)} \quad (43)$$

where ${}^{t+\Delta t}{}_L\mathbf{B}_L^{(i)}$ and ${}^{t+\Delta t}\hat{\boldsymbol{\tau}}^{(i)}$ correspond to the matrices ${}_L\mathbf{B}_L$ and $\hat{\boldsymbol{\tau}}$ in Table I, respectively, but are defined for time $t + \Delta t$ and iteration (i), respectively.

It may be noted that the equilibrium iterations correspond to a modified Newton iteration within each load step.⁴³ Table II summarizes the step-by-step algorithm used. For details on the Wilson θ and Newmark integration schemes see References 4, 5, 31.

Table II. Summary of step-by-step integration

Initial calculations

1. Form mass matrix \mathbf{M} ; initialize ${}^0\mathbf{u}$, ${}^0\dot{\mathbf{u}}$, ${}^0\ddot{\mathbf{u}}$
2. Calculate the following constants:
 - tol ≤ 0.01 ; nitem ≥ 3 ; in static analysis $\theta = 1$ and go to A.
 - Wilson θ method: $\theta \geq 1.37$, usually $\theta = 1.4$, $\tau = \theta \Delta t$
 - $a_0 = 6/\tau^2$ $a_1 = 6/\tau$ $a_2 = 2$
 - $a_3 = a_0/\theta$ $a_4 = -a_1/\theta$ $a_5 = 1 - 3/\theta$
 - $a_6 = \Delta t/2$ $a_7 = \Delta t^2/6$
 - Newmark method: $\theta = 1.0$, $\delta \geq 0.50$, $\alpha \geq 0.25(0.5 + \delta)^2$, $\tau = \Delta t$
 - $a_0 = 1/(\alpha \Delta t^2)$ $a_1 = 1/(\alpha \Delta t)$ $a_2 = 1/(2\alpha) - 1$
 - $a_3 = a_0$ $a_4 = -a_1$ $a_5 = -a_2$
 - $a_6 = \Delta t(1 - \delta)$ $a_7 = \delta \Delta t$
3. Calculate mass contribution to effective stiffness matrix: $\hat{\mathbf{K}} = a_0\mathbf{M}$

For each time step

A. *Calculation of Displacement increment*

- (i) If a new stiffness matrix is to be formed, calculate and triangularize ${}^t\hat{\mathbf{K}}$:

$${}^t\hat{\mathbf{K}} = {}^t\mathbf{K} + \hat{\mathbf{K}}; \quad {}^t\hat{\mathbf{K}} = \mathbf{LDL}^T$$

- (ii) Form effective load vector:

$${}^{t+\tau}\hat{\mathbf{R}} = {}^t\mathbf{R} + \theta({}^{t+\tau}\mathbf{R} - {}^t\mathbf{R}) + \mathbf{M}(a_1{}^t\dot{\mathbf{u}} + a_2{}^t\ddot{\mathbf{u}}) - {}^t\mathbf{F}$$

Table II—continued

(iii) Solve for displacement increments using latest \mathbf{D} , \mathbf{L} factors:

$$\mathbf{LDL}^T \mathbf{u} = {}^{t+\tau} \hat{\mathbf{R}}$$

(iv) If required, iterate for dynamic equilibrium; then initialize $\mathbf{u}^{(0)} = \mathbf{u}$, $i = 0$

(a) $i = i + 1$

(b) Calculate $(i-1)$ st approximation to accelerations and displacements:

$${}^{t+\tau} \ddot{\mathbf{u}}^{(i-1)} = a_0 \mathbf{u}^{(i-1)} - a_1 {}^t \dot{\mathbf{u}} - a_2 {}^t \ddot{\mathbf{u}}; \quad {}^{t+\tau} \mathbf{u}^{(i-1)} = {}^t \mathbf{u} + \mathbf{u}^{(i-1)}$$

(c) Calculate $(i-1)$ st effective out-of-balance loads:

$${}^{t+\tau} \hat{\mathbf{R}}^{(i-1)} = {}^t \mathbf{R} + \theta ({}^{t+\Delta t} \mathbf{R} - {}^t \mathbf{R}) - \mathbf{M} ({}^{t+\tau} \ddot{\mathbf{u}}^{(i-1)} - {}^{t+\tau} \mathbf{F}^{(i-1)})$$

(d) Solve for i th correction to displacement increments:

$$\mathbf{LDL}^T \Delta \mathbf{u}^{(i)} = {}^{t+\tau} \hat{\mathbf{R}}^{(i-1)}$$

(e) Calculate new displacement increments:

$$\mathbf{u}^{(i)} = \mathbf{u}^{(i-1)} + \Delta \mathbf{u}^{(i)}$$

(f) Iteration convergence if $\|\Delta \mathbf{u}^{(i)}\|_2 / \|\mathbf{u}^{(i)} + {}^t \mathbf{u}\|_2 < \text{tol}$

If convergence: $\mathbf{u} = \mathbf{u}^{(i)}$ and go to B;

If no convergence and $i < \text{nitem}$: go to (a); otherwise restart using new stiffness matrix and/or a smaller time step size.

B. Calculate new accelerations, velocities and displacements

Wilson θ method:

$${}^{t+\Delta t} \ddot{\mathbf{u}} = a_3 \mathbf{u} + a_4 {}^t \dot{\mathbf{u}} + a_5 {}^t \ddot{\mathbf{u}}$$

$${}^{t+\Delta t} \dot{\mathbf{u}} = {}^t \dot{\mathbf{u}} + a_6 ({}^{t+\Delta t} \ddot{\mathbf{u}} + {}^t \ddot{\mathbf{u}})$$

$${}^{t+\Delta t} \mathbf{u} = {}^t \mathbf{u} + \Delta t {}^t \dot{\mathbf{u}} + a_7 ({}^{t+\Delta t} \ddot{\mathbf{u}} + 2 {}^t \ddot{\mathbf{u}})$$

Newmark method:

$${}^{t+\Delta t} \ddot{\mathbf{u}} = a_3 \mathbf{u} + a_4 {}^t \dot{\mathbf{u}} + a_5 {}^t \ddot{\mathbf{u}}$$

$${}^{t+\Delta t} \dot{\mathbf{u}} = {}^t \dot{\mathbf{u}} + a_6 {}^t \ddot{\mathbf{u}} + a_7 {}^{t+\Delta t} \ddot{\mathbf{u}}$$

$${}^{t+\Delta t} \mathbf{u} = {}^t \mathbf{u} + \mathbf{u}$$

CONSTITUTIVE RELATIONS

An important aspect in the solution of non-linear problems is the calculation of the constitutive tensors, which define the stress-strain matrices in the finite element evaluations. In the isoparametric finite element discretization it is necessary to evaluate the stress-strain matrices at the element integration points, and they are required for the calculation of the element stiffness matrices and stress vectors.

Linear elasticity and hyperelasticity

Elastic and hyperelastic materials are relatively easy to deal with in practical analyses. In the T.L. formulation the stress-strain relations are¹¹

$${}^t S_{ij} = {}^t C_{ijrs} {}^t \epsilon_{rs} \quad (44)$$

where ${}^t S_{ij}$ is the 2nd Piola–Kirchhoff stress tensor, ${}^t \epsilon_{rs}$ is the Green–Lagrange strain tensor and ${}^t C_{ijrs}$ is the material property tensor in the configuration at time t . The relation in equation (44)

can be written for all configurations at time $0, \Delta t, 2\Delta t, \dots$. In the U.L. formulation the constitutive relation equivalent to equation (44) is

$${}^t\tau_{ij} = {}^tC_{ijrs} {}^t\varepsilon_{rs} \quad (45)$$

in which ${}^t\tau_{ij}$ is the Cauchy stress tensor, ${}^t\varepsilon_{rs}$ is the Almansi strain tensor and ${}^tC_{ijrs}$ is the material property tensor at time t .

Considering linear elasticity ${}^0C_{ijrs}$ and ${}^tC_{ijrs}$ are both constant and defined in terms of the Young's moduli and Poisson's ratios of the material. However, it should be noted that specifying constant ${}^tC_{ijrs}$ is equivalent to using a material tensor ${}^0C_{ijrs}$, which is deformation dependent, and *vice versa*; namely the following relations exist

$${}^0C_{mnpq} = \frac{{}^0\rho}{{}^t\rho} {}^0x_{m,i} {}^0x_{n,j} {}^tC_{ijrs} {}^0x_{p,r} {}^0x_{q,s} \quad (46)$$

$${}^tC_{mnpq} = \frac{{}^t\rho}{{}^0\rho} {}^t x_{m,i} {}^t x_{n,j} {}^0C_{ijrs} {}^t x_{p,r} {}^t x_{q,s} \quad (47)$$

The constitutive relations in equations (44) and (45) are used in the evaluation of the element stress matrices and stress vectors (see Table I), i.e. total 2nd Piola–Kirchhoff and Cauchy stresses are calculated directly from total Green–Lagrange and Almansi strains, respectively. However, in the calculation of the linear strain stiffness matrices at time t , tangent material property tensors are required. In the T.L. and U.L. formulations the relations considered are ${}^0S_{ij} = {}^0C_{ijrs} {}^0\varepsilon_{rs}$ and ${}^tS_{ij} = {}^tC_{ijrs} {}^t\varepsilon_{rs}$, respectively, in which, for linear elasticity,

$${}^0C_{ijrs} = {}^0S_{ijrs} \quad (48)$$

$${}^tC_{ijrs} = {}^tS_{ijrs} \quad (49)$$

Considering hyperelasticity the stress-strain relations are derived from the strain energy function.^{11,19,33} In this study the constitutive relations defining ${}^0S_{ij}$ and ${}^0C_{ijrs}$ in terms of the Green–Lagrange strain at time t for a rubber-like material in plane stress conditions have been derived.^{4,19} Therefore, to use the U.L. formulation, it is necessary to transform ${}^0S_{ij}$ and ${}^0C_{ijrs}$ to ${}^t\tau_{ij}$ and ${}^tC_{ijrs}$, respectively, as expressed in equations (5) and (47).

It is important to note that in the analysis of elastic and hyperelastic materials identical numerical results are obtained using the T.L. and U.L. formulations provided the material tensors are related as given in equations (46) and (47). Also, since the material constants are independent of the history of solution, analysis errors result only from the isoparametric finite element formulation and the time integration scheme, provided equilibrium iterations are performed. Therefore, in the analysis of elastic and hyperelastic materials the analysis errors are quite similar to those in small displacement linear elastic analysis.

Hypoelasticity including elastoplasticity

For hypoelastic materials the constitutive tensors relate increments in stresses to increments in deformations.¹¹ Since the constitutive relations depend, in general, on the stress and strain history, the use of a material law corresponding to the T.L. or the U.L. formulation must depend to a large degree on the possibility of performing experiments to obtain the appropriate material constants. In this context it should be noted that a great deal of additional research is still required to formulate and evaluate appropriate material constants for hypoelastic materials, in particular, for the identification of large strain behaviour.^{19,22,23} Although the formulations presented below are applicable to large strain conditions, in actual practical analysis the material law is

most likely to be defined only for small strains.⁴ An important such case here included is the elastic-plastic material behaviour characterized using the flow theory, which can be used in the analysis of large displacement but small strain problems.

Using the T.L. formulation, hypoelastic material behaviour can be described using equation (14), i.e.

$${}_0S_{ij} = {}_0C_{ijrs} {}_0e_{rs} \quad (14)$$

in which ${}_0C_{ijrs}$ depends on the history of the Green-Lagrange strains and 2nd Piola-Kirchhoff stresses. The stresses at time $t + \Delta t$ are calculated using equation (9), i.e.

$${}^{t+\Delta t}{}_0S_{ij} = {}^tS_{ij} + {}_0S_{ij} \quad (9)$$

In the analysis using equations (14) and (9) it is assumed that the material tensor ${}_0C_{ijrs}$ is evaluated in the same way as in small displacement analysis, but the stress and strain variables of the T.L. formulation are used to define the history of the material. A main advantage of adopting this material description is that it is relatively simple to use. Namely, assume that a subroutine to calculate the material law in small displacement analysis has been written; then the same program would also calculate ${}_0C_{ijrs}$ in large displacement analysis by simply using Green-Lagrange strains and 2nd Piola-Kirchhoff stresses to define the stress and strain history.^{10,22}

Similarly to equation (14), in the U.L. formulation hypoelastic material behaviour may be described using equation (22), i.e.

$${}^tS_{ij} = {}^tC_{ijrs} {}^te_{rs} \quad (22)$$

in which ${}^tC_{ijrs}$ is defined by the history of Cauchy stresses and the accumulation of the instantaneous plastic strain increments. The constitutive relation in equation (22) may be more appealing than the T.L. material law in equation (14) since physical stress components are used to define the material constants, and ${}^te_{rs}$ approximated by ${}^te_{rs}$ can kinematically be understood to be the addition of elastic and plastic strain increments, just as in small displacement analysis. Having calculated ${}^tS_{ij}$ from the relation ${}^tS_{ij} = C_{ijrs} e_{rs}$, the Cauchy stresses at time $t + \Delta t$ are obtained using equation (17), i.e.

$${}^{t+\Delta t}{}^tS_{ij} = {}^t\tau_{ij} + {}^tS_{ij} \quad (17)$$

and the transformation

$${}^{t+\Delta t}{}^t\tau_{sr} = \frac{{}^{t+\Delta t}\rho}{{}^t\rho} {}^{t+\Delta t}x_{s,i} {}^{t+\Delta t}S_{ij} {}^{t+\Delta t}x_{r,j} \quad (50)$$

A third possibility is to characterize the material behaviour using a stress rate which is defined with respect to the current moving co-ordinates within the time interval t to $t + \Delta t$.^{11,15,16,23} The stress rate used must be invariant with respect to rigid body rotations, and one possibility is to use the Jaumann stress rate, which, at time t , is defined as

$${}^t\tau_{ij}^{\nabla} = \frac{D}{Dt} {}^t\tau_{ij} - {}^t\tau_{ip} {}^t\Omega_{pj} - {}^t\tau_{jp} {}^t\Omega_{pi} \quad (51)$$

where D/Dt denotes time derivative with tx_i , $i = 1, 2, 3$, kept constant,

$${}^t\tau_{ij}^{\nabla} = {}^tC_{ijrs} \frac{D}{Dt} {}^te_{rs} \quad (52)$$

and ${}^t\Omega_{pj}$ are the Cartesian components of the spin tensor,

$${}^t\Omega_{pj} = \frac{1}{2} \frac{D}{Dt} ({}^t u_{j,p} - {}^t u_{p,j}) \quad (53)$$

Equations (51) to (53) need to be considered in the evaluation of the tangent stiffness matrix and in the calculation of the current stress conditions. The constitutive tensor relating the Jaumann stress rate tensor ${}^t\tau_{ij}^{\nabla}$ to the incremental strain rate tensor $(D/Dt)_t e_{rs}$ is calculated in the same way as in small displacement analysis, but using Cauchy stresses to define the history of the material. In the evaluation of the linear strain tangent stiffness matrix, instead of equation (22), the following approximate relation may be used,

$$D^t\tau_{ij} = {}_t C_{ijrs} {}_t e_{rs} \quad (54)$$

where D signifies 'discrete increment in', and therefore $D_t e_{rs} \equiv {}_t e_{rs}$. Considering the calculation of Cauchy stresses at time $t + \Delta t$, ${}^{t+\Delta t}\tau_{ij}$, it is important to use equations (51) to (53) in small enough increments of time. In elastic-plastic analysis it is in any case necessary to evaluate the stress increments by numerical integration of the elastic-plastic material law times the strain increments, and it is efficient to include equation (51) in this integration.

In this study the T.L. material description using equations (14) and (9) and the U.L. material descriptions given in equations (22), (17), (50) and in equations (51) to (54) have been implemented. The U.L. formulations will be referred to as U.L. with transformation, U.L.(T), and U.L. with Jaumann stress rate, U.L.(J), respectively. The calculation of the elastic-plastic material constants and stress vectors in the T.L., U.L.(T) and U.L.(J) formulations is presented in detail in Reference 4.

In the above enumeration it was assumed that the solution procedure, namely the T.L. or U.L. formulation, is chosen according to the definition of the constitutive tensor. Since the constitutive tensor is dependent on stress and strain quantities, it is expedient to use the specific incremental finite element formulation, for which the material law is defined. If this is not done, it is necessary to evaluate the required stress and strain quantities for the calculation of the material constants and transform the constitutive relations using equation (46) or equation (47).

DEFORMATION DEPENDENT LOADING

So far it has been assumed that the loads are independent of the configuration of the body. In practice, therefore, the external loads for each step can be calculated and stored on back-up storage before the actual time integration is carried out. However, when the structure undergoes large displacements or large strains it may be necessary to consider the externally applied loads to be configuration dependent.

An important type of loading, which may need to be considered as deformation dependent, is pressure loading.³³ In this case the loading to be used in the T.L. formulation is

$${}^{t+\Delta t}t_k^0 da = -\frac{{}^0\rho}{{}^{t+\Delta t}\rho} {}^{t+\Delta t}p_{{}^{t+\Delta t}x_{i,k}} {}^0n_i^0 da \quad (55)$$

and in the U.L. formulation

$${}^{t+\Delta t}t_k^t da = -\frac{{}^t\rho}{{}^{t+\Delta t}\rho} {}^{t+\Delta t}p_{{}^{t+\Delta t}x_{i,k}} {}^t n_i^t da \quad (56)$$

where ${}^t n_i$ = component i of the normal n in the configuration at time t , and similarly for time 0, and ${}^{t+\Delta t}p$ = surface pressure in the configuration at time $t + \Delta t$. Equation (55) can be written

in the form

$${}^{t+\Delta t}t_k^0 da = -\frac{{}^0\rho}{{}^{t+\Delta t}\rho} {}^{t+\Delta t}p {}^0x_{i,k} {}^0n_i {}^0da + \frac{{}^0\rho}{{}^{t+\Delta t}\rho} {}^{t+\Delta t}p {}^0x_{i,j} {}^{t+\Delta t}u_{j,k} {}^0n_i {}^0da \quad (57)$$

and similarly equation (56) becomes

$${}^{t+\Delta t}t_k^t da = -\frac{{}^t\rho}{{}^{t+\Delta t}\rho} {}^{t+\Delta t}p {}^t n_k^t da + \frac{{}^t\rho}{{}^{t+\Delta t}\rho} {}^{t+\Delta t}p {}^{t+\Delta t}u_{i,k} {}^t n_i^t da \quad (58)$$

where in both formulations the first integral enters the load vector and, assuming that ${}^{t+\Delta t}u_{i,k} \doteq {}^t u_{i,k}$, the second integral contributes to the system tangent stiffness matrix. It should be noted that this is a non-symmetric contribution to the stiffness matrix, and is therefore, in practice, computationally inefficient to handle. Using equilibrium iterations, it appears more efficient, at least when pressures are reasonably small, to neglect the contribution of the pressure loads to the stiffness matrix. In the iteration the loads are then evaluated as

$$-\frac{{}^0\rho}{{}^{t+\Delta t}\rho^{(j)}} {}^{t+\Delta t}p \frac{\partial^0 x_i}{\partial {}^{t+\Delta t}x_k^{(j)}} {}^0n_i {}^0da \quad \text{and} \quad -{}^{t+\Delta t}p {}^{t+\Delta t}n_k^{(j)} {}^{t+\Delta t}da^{(j)}$$

in the T.L. and U.L. formulations, respectively, where the right superscript (j) indicates the configuration of the iteration. It is seen that although the same approximations are involved in both formulations, the U.L. formulation requires less numerical operations and seems more natural to use.

SAMPLE SOLUTIONS

All solutions presented in the following have been obtained using the algorithm presented in Table II, in which the selected parameters were $\text{tol} = 0.001$, $\text{nitem} = 15$, $\theta = 1.4$, $\delta = 0.50$ and $\alpha = 0.25$. No attempt was made to optimize the solution times by selecting the most effective load step increments. In the dynamic analyses, nearly always one or two equilibrium iterations were sufficient in each time step and the computer time used was in all analyses rather small.

The time step used in an analysis is denoted by Δt and was selected as a reasonable fraction of the fundamental period, T_f , of the structure at time 0. In all dynamic analyses zero initial conditions on the displacements, velocities and accelerations were assumed.

For the finite element discretization 4- or 8-node two-dimensional elements have been employed (Figure 2). The material properties given have always been assumed to be defined corresponding to the specific formulation used for solution.

Large displacement static and dynamic analysis of a cantilever

The cantilever in Figure 3 under uniformly distributed load was analyzed using the T.L. and U.L. formulations. The cantilever was idealized using five 8-node plane stress elements.

Static solutions were obtained for the loading retaining its vertical direction, and for the loading remaining perpendicular to the top and bottom surfaces of the cantilever, i.e. deformation dependent follower loading. In the finite element solution the follower loading can be defined by specifying the direction of the nodal loads to pass through two nodal points, the co-ordinates of which are updated in each load step. In this specific analysis, the top and bottom surface nodal points of the cantilever have been used to define the direction of the loading. In addition to the U.L. and T.L. formulations also the U.L.(T) and U.L.(J) formulations have been used in the solution for deformation independent loading, in order to assess the accuracy that may be

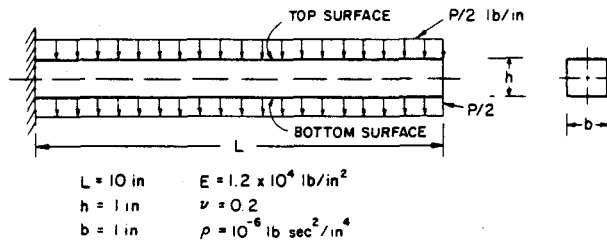


Figure 3. Cantilever under uniformly distributed load

expected in elastic-plastic analysis. It is seen that, to the precision possible to show in Figure 4, the T.L., U.L., U.L.(T) and U.L.(J) solutions predict the same response (although the same E and ν have been used in each analysis, Figure 3) and that excellent agreement has been obtained with an analytical solution reported by Holden.¹⁷

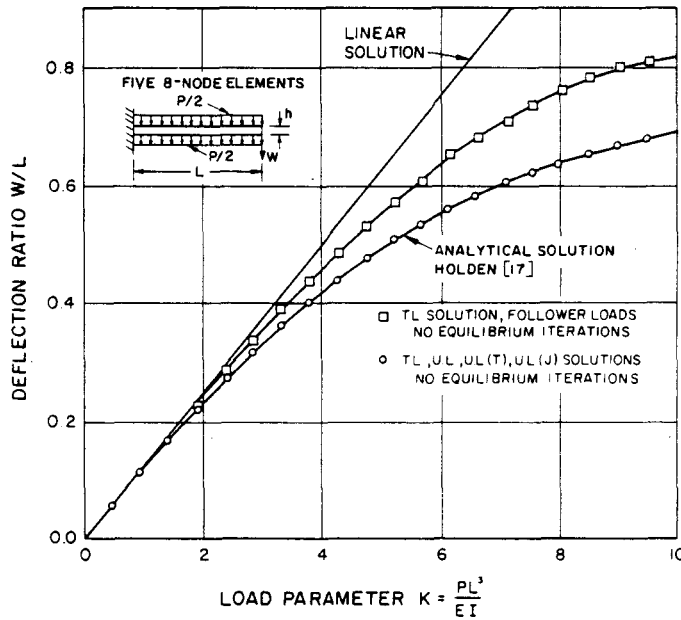


Figure 4. Large deflection analysis of cantilever under uniformly distributed load

For the dynamic analysis the T.L. formulation was selected. Figure 5 shows the results obtained using the Newmark integration scheme. It is seen that the solution predicted using a time step $\Delta t \cong T_f/42$, where T_f is the fundamental period of the cantilever, is significantly different from the solution obtained with the smaller time step $\Delta t \cong T_f/126$, unless equilibrium iterations are used. An average of 4 iterations per time step were required. The analysis therefore shows the importance of using equilibrium iterations in the response calculations of this structure, unless a small time step, Δt , is used.

It should be noted that a main characteristic of the cantilever is that the structure stiffens with increasing displacement, which, as shown in Figure 5, results in a substantial decrease in amplitude and effective period of vibration. It is the stiffening of a structure that can result in convergence difficulties in equilibrium iteration.⁴

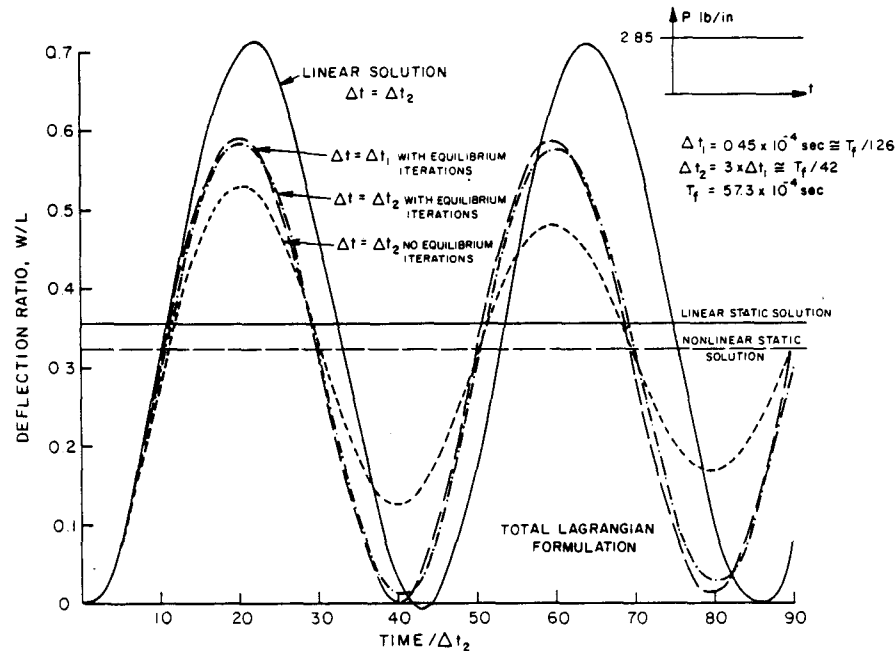


Figure 5. Large displacement dynamic response of cantilever under uniformly distributed load, Newmark method $\delta = 0.50$, $\alpha = 0.25$

Static large displacement analysis of a spherical shell

The clamped shallow spherical shell in Figure 6 subjected to uniform pressure was analyzed using a finite element idealization of eight 8-node elements.

Figure 6 shows the load deflection curve predicted using the T.L. formulation. In the analysis, 36 load steps with an average of about 3 to 4 equilibrium iterations in each step were used. The results are compared with an analytical solution of Kornishin and Isanbaeva,²¹ and a finite element solution of Yeh.⁴² As shown, good agreement between the different solutions has been obtained. Since equilibrium iterations were performed in the present solution, the oscillating behaviour at the beginning of the post-buckling range in Yeh's solution was not obtained.

The U.L. formulation gave almost indistinguishable results to those of the T.L. formulation.

Static and dynamic large displacement analysis of a second spherical shell

The spherical shell subjected to a concentrated apex load shown in Figure 7 was analyzed for static and dynamic response.

Figure 7 shows the static load-deflection response predicted in this study and by Stricklin³⁷ and Mescall.²⁷ Good agreement between the different solutions has been obtained. In the present solutions, the T.L. and U.L. formulations were used and no equilibrium iterations have been performed. In addition, to assess the accuracy that may be obtained in elastic-plastic analysis, the U.L.(T) and U.L.(J) formulations have been used. Figure 8 compares the T.L. response predictions with two U.L.(T) and U.L.(J) solutions. It is seen that the U.L.(T) and U.L.(J) solutions approach the T.L. solution as the load steps become smaller.

The dynamic response calculated using the Wilson θ integration method when the apex load is applied as a step load is shown in Figure 9. It is observed that for this problem the differences between the solutions using equilibrium iteration and not iterating for equilibrium are small.

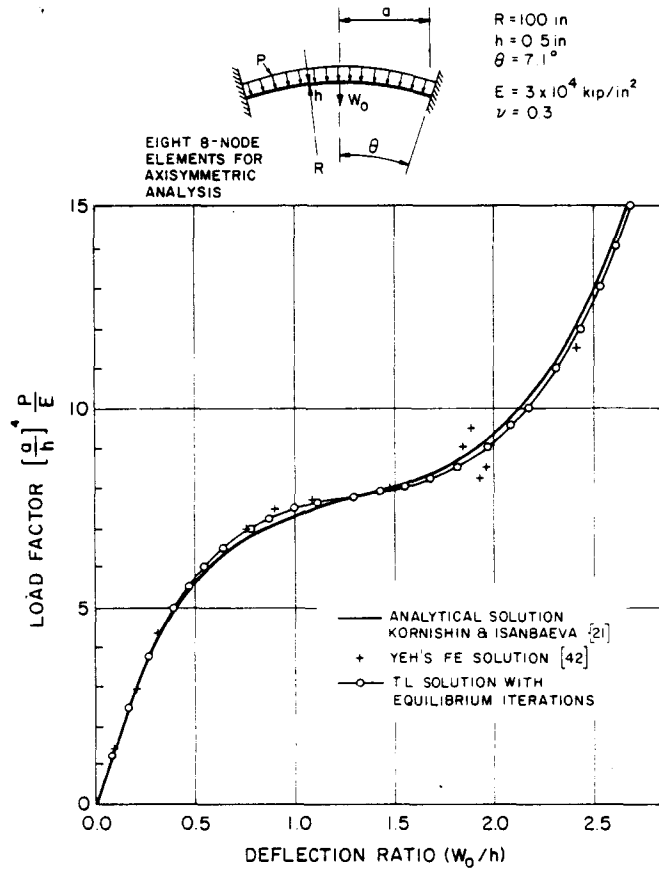


Figure 6. Load-deflection curve for a shallow spherical shell

The much larger response and effective period predicted in the non-linear analysis is a result of the softening behaviour of the structure with increasing load. It should be noted that in the analysis of this highly non-linear shell no difficulties were encountered using the Wilson or the Newmark integration methods, and practically identical results were obtained.⁴

Large displacement static buckling analysis of an arch

The clamped circular arch shown in Figure 10 was analyzed for buckling due to a single static load using the T.L. and U.L. formulations with equilibrium iterations.

Figure 10 shows the calculated load-deflection curve of the arch. The differences in the displacements calculated using the U.L. and T.L. formulations were less than two per cent. The solutions were obtained using 28 load steps with an average of two to three equilibrium iterations per step.

The same arch was also analyzed by Mallet and Berke, who used four 'equilibrium-based' elements.²⁴ Dupuis and many others, analyzed the arch with curved beam elements, and used this example to demonstrate the convergence of their Lagrangian and 'updated' formulations.⁷ In the latter formulation only the nodal points were updated, but not the geometry within the elements. As shown in Figure 10, the results are very sensitive to the number of elements used and are not satisfactory. Dupuis and many others, also compared the calculated results with

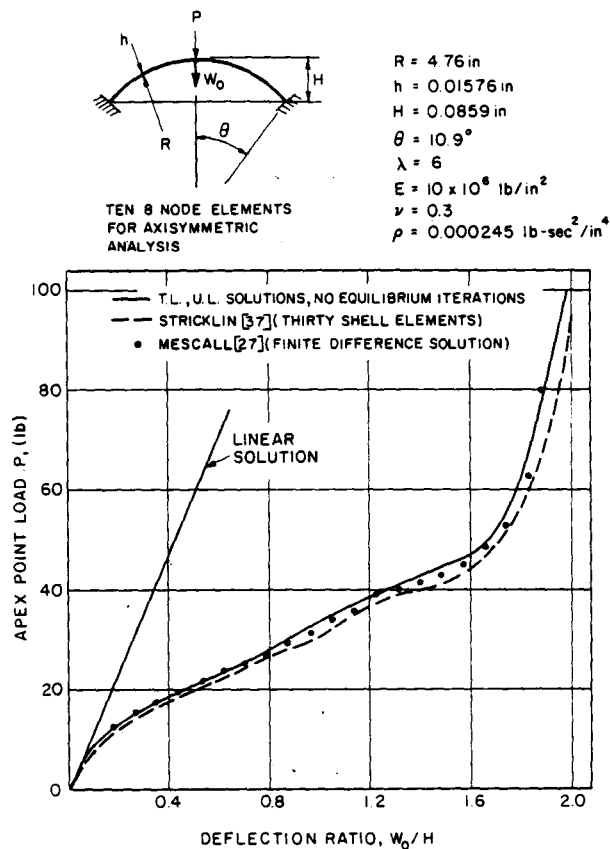


Figure 7. Load-deflection curves for spherical shell

experimental results by Gjelsvik and Bodner,¹² whose predicted buckling load is about 10 per cent lower than that calculated by Mallet. However, it need be realized that an arch with a parameter $\lambda = 11.6$ is already influenced by antisymmetric buckling modes, which, although possible in the experiment, have not been taken account of in the analyses.³⁴ The results obtained in this study are therefore satisfactory.

Elastic dynamic snap buckling of a second arch

A dynamic buckling analysis of the circular arch shown in Figure 11 was carried out. The material of the arch was assumed to be isotropic linear elastic.

In the analyses the T.L. formulation was used. The uniformly distributed pressure load was applied as a step load. The time step to fundamental period ratio, $\Delta t/T_f$, was approximately 1/70.

The arch is an example of Humphreys' analytical and experimental investigation, who solved the governing differential equation using an analogue computer.¹⁸ Humphreys concluded that the buckling load of this arch is not influenced by antisymmetric modes.

Figure 12 shows the displacement response predicted in this study using the Wilson θ integration scheme. The solution obtained by Humphreys is also shown. In the Figure, the deflection ratio Δ defined as

$$\Delta = \frac{\text{average normal deflection } w}{\text{average rise of arch} = H/2}$$

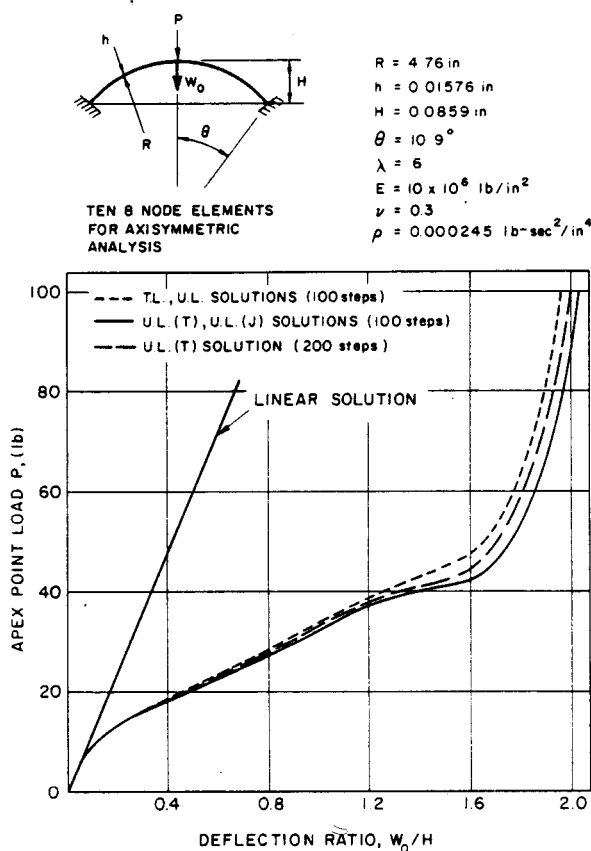


Figure 8. Load-deflection curves for spherical shell

is used. The dynamic buckling of the arch occurs at that load level at which a sudden increase in the deflection ratio Δ is measured. Figure 12 shows that at $p_0 = 0.190$ the arch oscillates about a position of approximately $\Delta = 0.25$, and that at $p_0 = 0.200$ the arch first snaps through, and then oscillates about a position of approximately $\Delta = 2.5$. Therefore, the buckling load predicted here lies between $p_0 = 0.190$ and $p_0 = 0.200$, which is about five per cent lower than that predicted by Humphreys.

It should be noted that for a load larger than the buckling load, i.e. for $p_0 = 0.25$, the maximum response increases only little. The results for $p_0 = 0.250$ are in essential agreement with Humphreys' results, where the slightly larger response agrees with the observation that a smaller buckling load was predicted in this study. The discrepancies in the results can arise from approximations in either analysis. Humphreys' series solution is based on the assumption of shallowness, i.e. q and w are measured vertically, and in the series solution only a finite number of terms have been included.

It is noted that in a practical analysis damping should be included and a longer time range may be considered as well.

Large displacement and large strain static and dynamic analysis of a rubber sheet with a hole

A plane stress analysis of the rubber sheet shown in Figure 13 was carried out. The purpose of this analysis was to test the capability of predicting static and dynamic large strain response.

The material of the rubber sheet was assumed to be of Mooney-Rivlin type. The specific material constants used for the hyperelastic incompressible material were $C_1 = 25$ psi, $C_2 =$

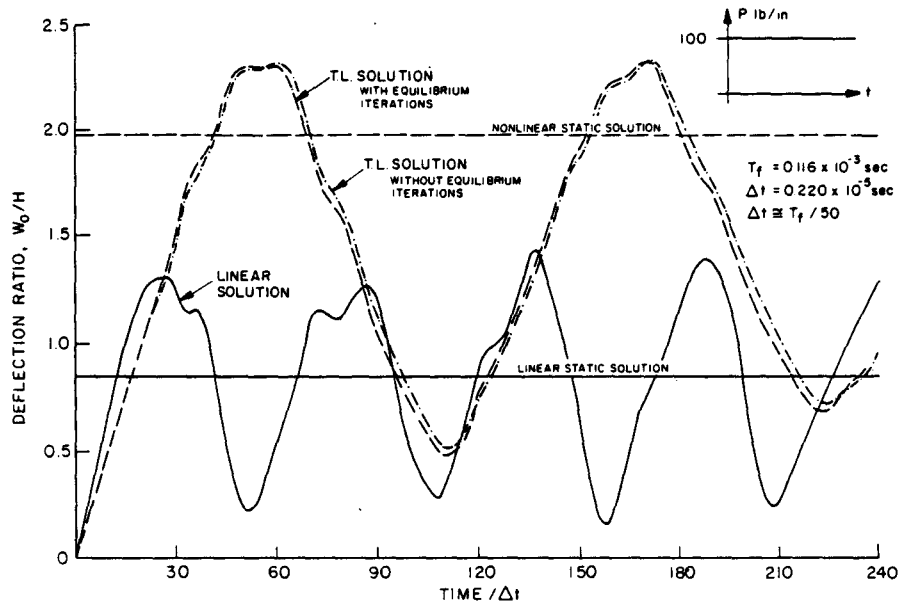


Figure 9. Non-linear dynamic response of spherical shell. Wilson θ method. $\theta = 1.4$

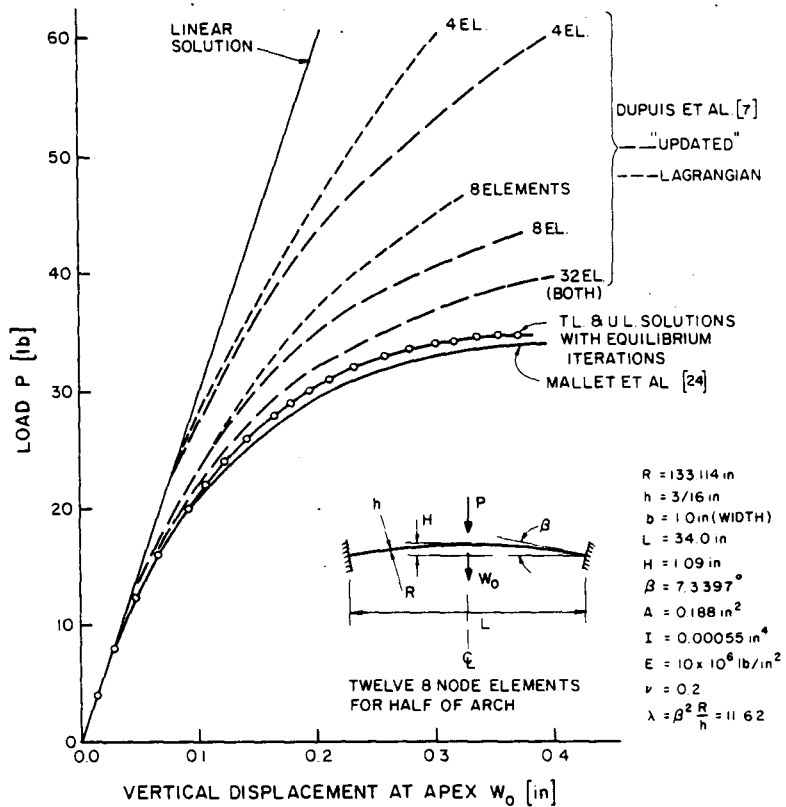


Figure 10. Load-deflection curve for a shallow arch under concentrated load

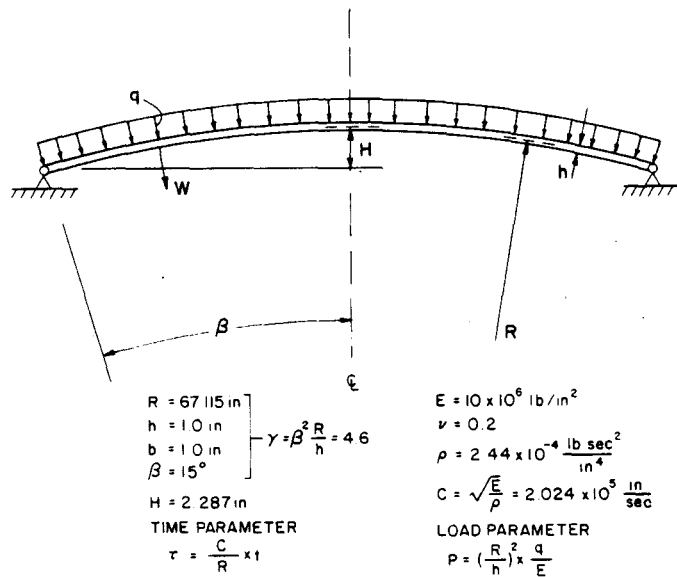


Figure 11. Simply supported shallow arch

7 psi. These constants are based on an analytical and experimental investigation of the rubber sheet by Iding.¹⁹ The finite element mesh used in the analysis is presented in Figure 13.

Figure 14 shows the static load deflection curves for different points on the sheet. Only five equal load increments with an average of four equilibrium iterations have been used to reach the final load position with a displacement of more than 11 in at point B. At this stage Green-Lagrange strains of more than 4.5 are measured, see Figure 15. The results obtained are in

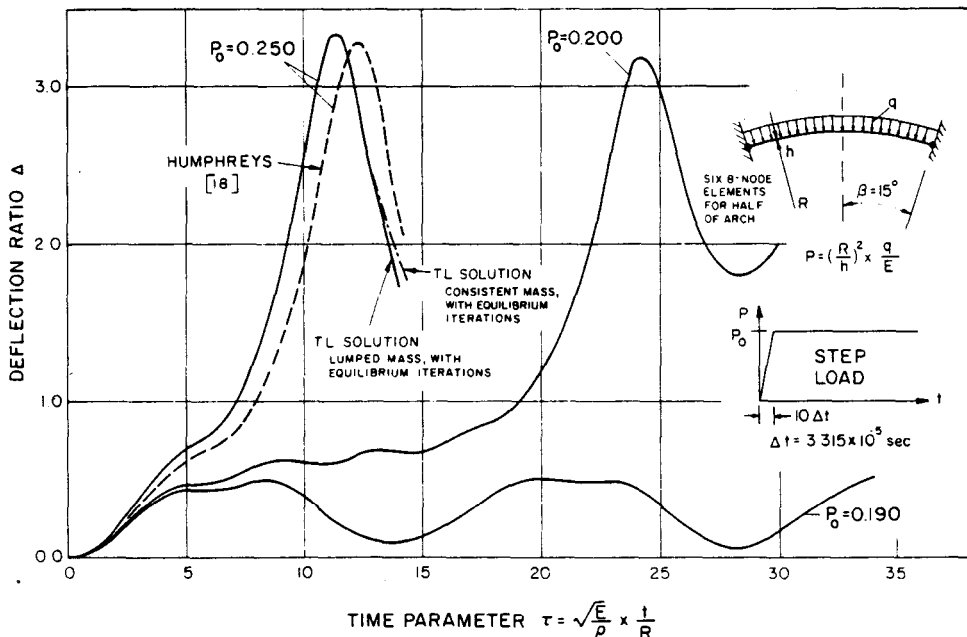


Figure 12. Dynamic snap-through of a shallow circular arch Wilson θ method. $\theta = 1.4$

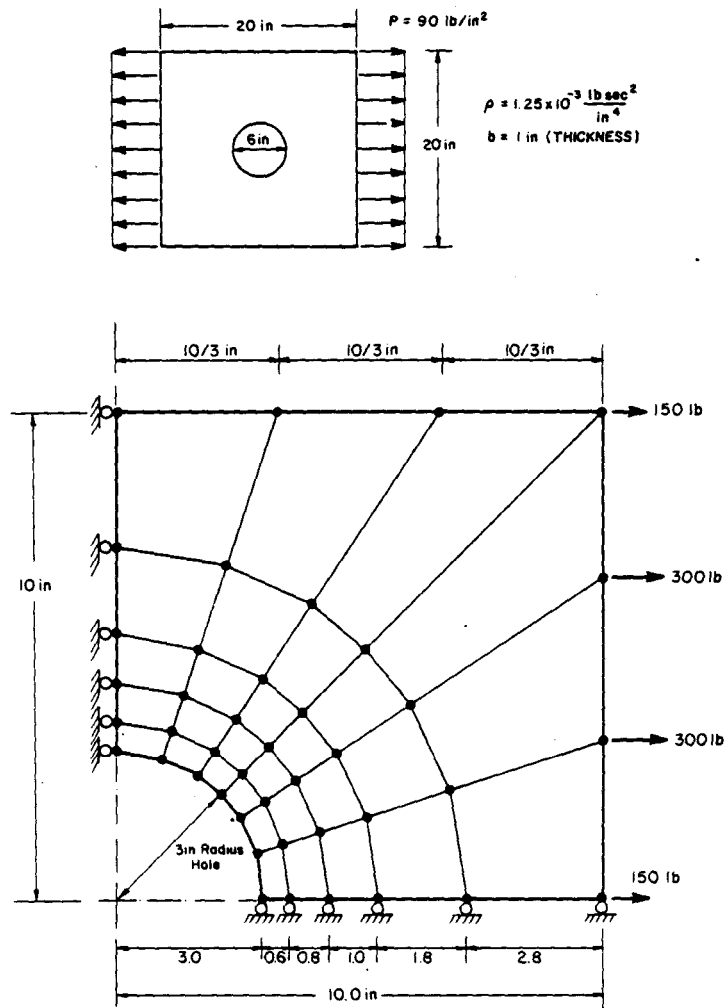


Figure 13. Finite element mesh of rubber sheet with hole

excellent agreement with those of Iding. The results of Iding have been obtained with the computer program developed in Reference 19, but are not given in the Reference.

The dynamic analysis was performed for the step load shown in Figure 16 using the Wilson θ and Newmark integration schemes with $\Delta t/T_f \cong 120$.

Figure 16 compares the displacement response predicted using the two integration methods. As is seen, practically the same response was calculated using the Wilson θ and the Newmark methods. In addition, it should be noted that identical solutions have been obtained using either integration scheme and an interval of stiffness reformation of 10, 5 or 1 time steps (see Table II). This should be expected, since the solution is unique for the selected time step Δt .

Elastic-plastic large displacement dynamic analysis of a third spherical shell

The dynamic response of the spherical shell in Figure 17 subjected to a distributed step pressure $p = 600 \text{ lb/in}^2$ was calculated. The material was assumed to obey the von Mises yield condition with linear isotropic hardening. The purpose of this analysis was to compare the results obtained

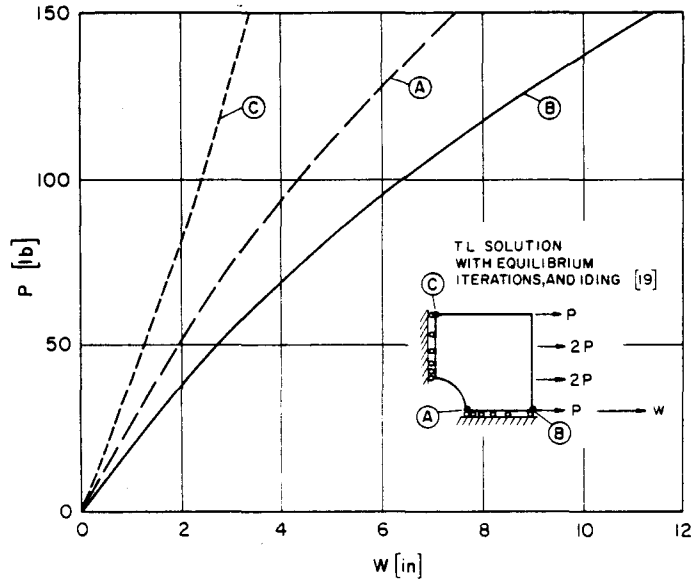


Figure 14. Static load-deflection curve for a rubber sheet with hole

using the various non-linear large displacement formulations available for elastic-plastic response calculations.

Figure 17 shows the dynamic response of the cap predicted using the Newmark time integration scheme in linear analysis, materially non-linear only analysis, i.e. assuming small displacements and small strains, and combined geometrically and materially non-linear analysis. In the fully non-linear analysis the solutions using the T.L., U.L.(T) and U.L.(J) formulations have been obtained. It is observed that all three formulations predict essentially the same response. The reason for obtaining almost identical solutions lies partly in that the mathematical representation of the yield function is almost the same in the 2nd Piola-Kirchhoff stress space and the Cauchy stress space. Namely, in problems of small strains but large rotations, such as in the

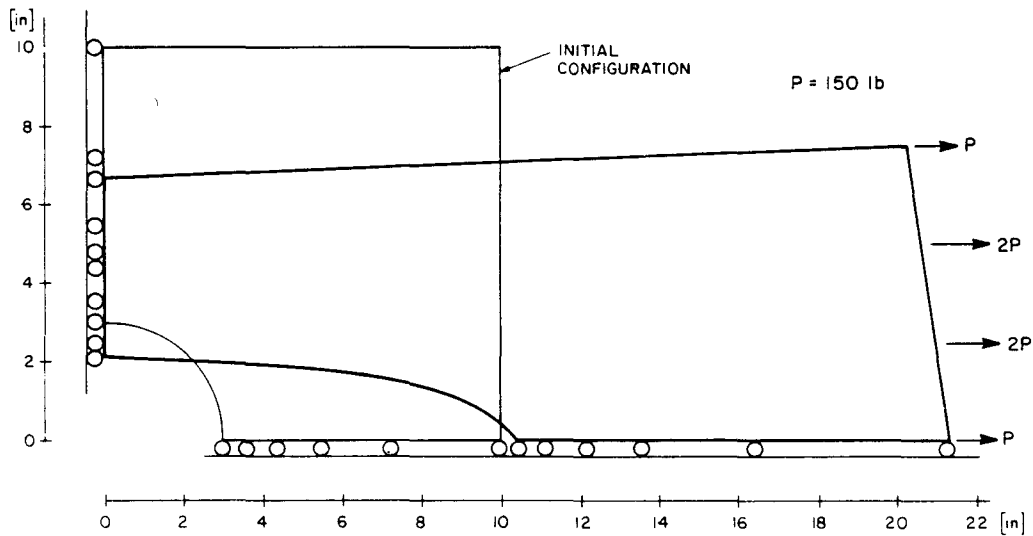


Figure 15. Deformed configuration drawn to scale of rubber sheet with hole (static analysis)

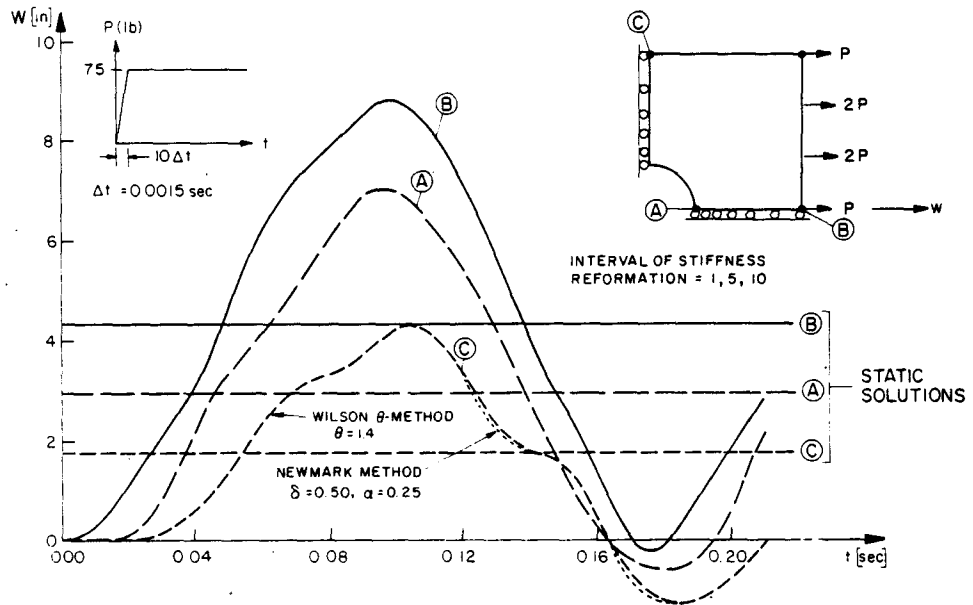


Figure 16. Displacements versus time for rubber sheet with hole. T.L. solution with equilibrium iterations

analysis of shells, the physical components of the Cauchy stress tensor in rotated (surface) co-ordinates are approximately equal to the Cartesian components of the 2nd Piola-Kirchhoff stress tensor.

The solutions in Figure 17 demonstrate the effect of including different degrees of non-linearities. It is observed that the materially non-linear only solution differs a great deal from the linear elastic response, and that the effect of large displacements is also significant. The decrease in amplitude of vibration and increase in the mean deflection of the shell when non-linearities are taken into account should be noted.

The response of the cap was also calculated using the Wilson θ method, which gave practically the same results.⁴

A comparison of the results obtained in this study with those calculated by Nagarajan²⁹ is given in Figure 18. Nagarajan used degenerate isoparametric elements, in which it is assumed that the transverse normal stresses are negligibly small. This assumption affects the effective stress patterns which control plastic loading and contributes to the different response predicted in his study.

CONCLUSIONS

The objective in this paper was to review, derive and evaluate finite element formulations for general non-linear static and dynamic analysis which have been implemented in the search for the most effective procedure.³ The formulations have been derived from general principles of continuum mechanics and include material, large displacement and large strain non-linearities. The conceptual difference between the formulations is the reference configuration that is used for the linearization of the incremental equations of motion. In the T.L. formulation the initial configuration is used as reference, whereas in the U.L. formulations, the reference configuration corresponds to the last calculated configuration.

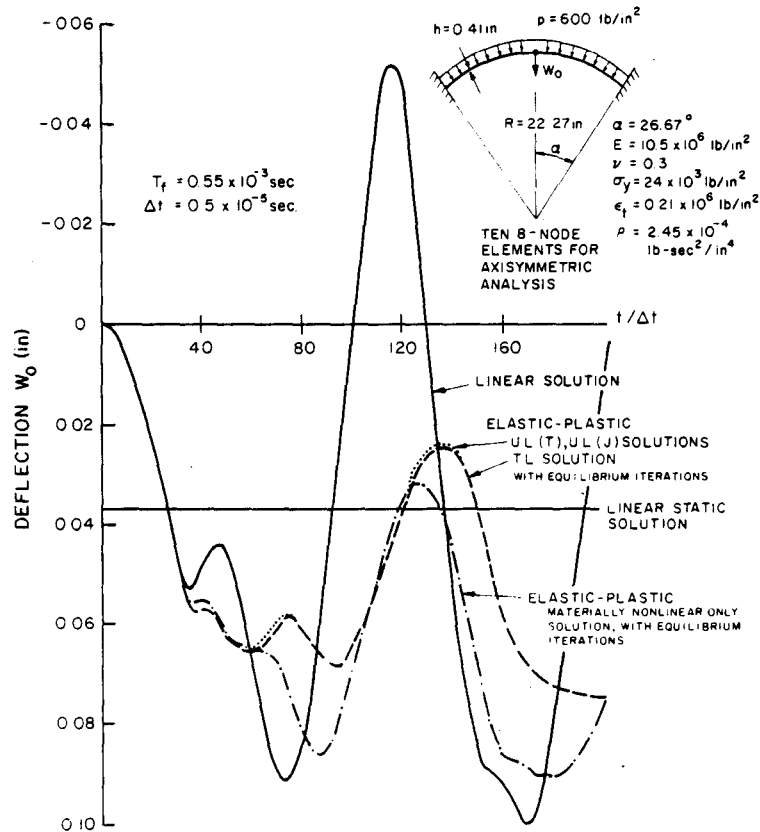


Figure 17. Large displacement dynamic elastic-plastic analysis of spherical cap. Newmark method. $\delta = 0.50$, $\alpha = 0.25$

A first important observation is that provided the constitutive tensors are defined appropriately, all formulations give the same numerical results. The only advantage of using one formulation rather than the others is its better numerical effectiveness. Theory and sample analyses show that in small strain but large displacement analyses the differences which arise by using the same material constants in the formulations—because, for instance, a clear definition of the constants may not be available—can be expected to be small.

With regard to the numerical operations required, Table I shows that all matrices of the formulations have corresponding patterns of zero elements, except for the linear strain-displacement transformation matrices. In the T.L. formulation, this matrix is full, because of the initial displacement effect in the linear strain terms. Therefore, the calculation of the element matrices requires less time in the U.L. formulations.

An advantage of the T.L. formulation is that the derivatives of the interpolation functions are with respect to the initial configuration, and therefore need only be formed once, if they are stored on back-up storage for use in all load steps. However, in practice, the use of tape or disc to store and retrieve the required derivatives in each step may be more costly than simply to recalculate them, and, in particular, the required storage is a problem size governing factor since saturation of back-up storage may be reached. Auxiliary storage considerations are particularly important, if a considerable amount of stress and strain history need to be stored already.

It should be noted that the U.L. formulations are quite different from the moving co-ordinate formulation presented in the survey paper by Stricklin and many others,¹⁸ and the updated

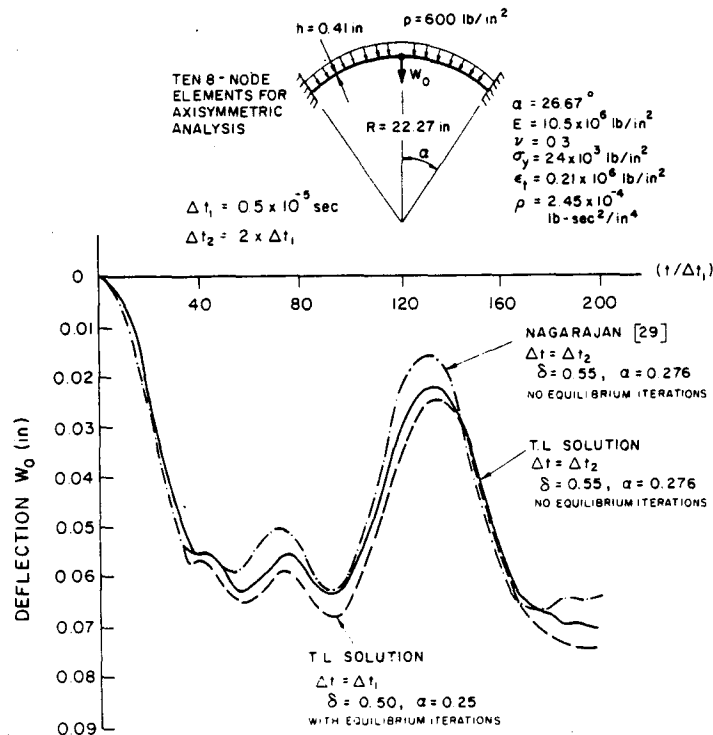


Figure 18. Large displacement dynamic elastic-plastic analysis of spherical cap. Newmark method

formulation, which was used in the comparative study by Dupuis and many others.⁷ The incremental moving co-ordinate formulation surveyed by Stricklin and many others,^{38,10,35} was stated to be restricted to small strains and have distinct computational disadvantages. These conclusions do not apply to the U.L. formulations used here. The 'updated' formulation employed by Dupuis and many others, in their comparative study of this formulation versus a Lagrangian formulation did not give satisfactory results.⁷ However, using the U.L. formulation with isoparametric elements as presented in this paper, the results are as good as those obtained using the T.L. formulation. The only errors are due to the numerical solution of the governing continuum mechanics equations.

In general, using both the T.L. and the U.L. formulations equilibrium iterations should be performed in order to ensure an accurate solution and possibly dispense with the calculation of a new non-linear stiffness matrix in each load step. If no equilibrium iterations are carried out, the linearization can introduce uncontrolled large errors. In the elastic and hyperelastic analyses presented here, it was possible to calculate the stresses in the configuration at time $t + \Delta t$ directly from the corresponding total strains. Therefore, the non-linear finite element equations have been solved 'exactly' within the assumptions of the time integration scheme and the convergence limit of the iteration. In path dependent problems this is not possible and total stresses are calculated by adding increments in stresses.

An important consideration in path dependent problems is the definition and calculation of the constitutive tensors, which depends on the stress and strain history. A great deal of additional research is still required to identify various materials. Using the T.L. formulation, the effort to implement a non-linear constitutive relation can, in some cases, be less than in the U.L. formulation; however, the appropriate material constants need be available. It is the ease of implementing

a new material law in a general non-linear analysis program that makes the T.L. formulation very attractive.

In conclusion, both the U.L. or T.L. formulations can effectively be used in a general non-linear analysis program. It depends largely on the program design and the material constants available which formulation is most effective.

APPENDIX

Notation

The following convention for tensor and vector subscripts and superscripts is employed:

A left superscript denotes the time of the configuration in which the quantity occurs.

A left subscript can have two different meanings. If the quantity considered is a derivative, the left subscript denotes the time of the configuration, in which the co-ordinate is measured with respect to which is differentiated. Otherwise the left subscript denotes the time of the configuration in which the quantity is measured.

Right lower case subscripts denote the components of a tensor or vector. Components are referred to a fixed Cartesian co-ordinate system; $i, j, \dots = 1, 2, 3$. Differentiation is denoted by a right lower case subscript following a comma, with the subscript indicating the co-ordinate with respect to which is differentiated.

- ${}^0A, {}^tA, {}^{t+\Delta t}A$ = Area of body in configuration at time 0, $t, t + \Delta t$
- ${}^0C_{ijrs}, {}^tC_{ijrs}$ = Component of constitutive tensor at time t referred to configuration at time 0, t
- ${}_0C_{ijrs}, {}_tC_{ijrs}$ = Component of tangent constitutive tensor at time t referred to configuration at time 0, t
- ${}^{t+\Delta t}f_i, {}^{t+\Delta t}f_i$ = Component of body force vector per unit mass in configuration at time $t + \Delta t$ referred to configuration at time 0, $t + \Delta t$
- h_k = Finite element interpolation function associated with nodal point k
- (i) = Superscript indicating number of iteration
- ${}^0n_i, {}^t n_i, {}^{t+\Delta t}n_i$ = Component of surface normal in configuration at time 0, $t, t + \Delta t$
- ${}^{t+\Delta t}p$ = Pressure load at time $t + \Delta t$
- ${}^{t+\Delta t}\mathcal{W}$ = External virtual work expression corresponding to configuration at time $t + \Delta t$, defined in equation (8)
- r, s = Natural element co-ordinates
- ${}^0S_{ij}, {}^{t+\Delta t}S_{ij}$ = Component of 2nd Piola–Kirchhoff stress tensor in configuration at time $t, t + \Delta t$ referred to configuration at time 0
- ${}^{t+\Delta t}{}_tS_{ij}$ = Component of 2nd Piola–Kirchhoff stress tensor in configuration at time $t + \Delta t$ referred to configuration at time t
- ${}_0S_{ij}, {}_tS_{ij}$ = Component of 2nd Piola–Kirchhoff stress increment at time $t, t + \Delta t$
- $t, t + \Delta t$ = time t and $t + \Delta t$, before and after time increment Δt
- ${}^{t+\Delta t}{}_0t_i, {}^{t+\Delta t}{}_t t_i$ = Component of surface traction vector in configuration at time $t + \Delta t$, referred to configuration at time 0, $t + \Delta t$
- ${}^t u_i, {}^{t+\Delta t} u_i$ = Component of displacement vector from initial position at time 0 to configuration at time $t, t + \Delta t$
- u_i = Increment in displacement component, $u_i = {}^{t+\Delta t}u_i - {}^t u_i$
- ${}^t u_i^k$ = Displacement component of nodal point k in configuration at time t
- u_i^k = Increment in ${}^t u_i^k$

- ${}^0u_{i,j}, {}^{t+\Delta t}u_{i,j}$ = Derivative of displacement component to configuration at time $t, t + \Delta t$ with respect to co-ordinate 0x_j
 ${}^0u_{i,j}, {}^t u_{i,j}, {}^{t+\Delta t}u_{i,j}$ = Derivative of displacement increment with respect to co-ordinate ${}^0x_j, {}^t x_j, {}^{t+\Delta t}x_j$
 ${}^0V, {}^t V, {}^{t+\Delta t}V$ = Volume of body in configuration at time $0, t, t + \Delta t$
 ${}^0x_j, {}^t x_j, {}^{t+\Delta t}x_j$ = Cartesian co-ordinate in configuration at time $0, t, t + \Delta t$
 ${}^0x_i^k, {}^t x_i^k, {}^{t+\Delta t}x_i^k$ = Cartesian co-ordinate of nodal point k in configuration at time $0, t, t + \Delta t$
 ${}^0x_{i,j}, {}^t x_{i,j}$ = Derivative of co-ordinate in configuration at time $0, t$ with respect to co-ordinate ${}^t x_j, {}^0x_j$
 δ = Denoting 'variation in'
 ${}^{t+\Delta t}\epsilon_{ij}, {}^t \epsilon_{ij}$ = Component of Almansi strain tensor in configuration at time $t + \Delta t, t$, referred to configuration at time 0
 ${}^{t+\Delta t}{}_0\epsilon_{ij}, {}^t{}_0\epsilon_{ij}$ = Component of Green-Lagrange strain tensor in configuration at time $t + \Delta t, t$, referred to configuration at time 0
 ${}^{t+\Delta t}{}_t\epsilon_{ij}$ = Component of Green-Lagrange strain tensor in configuration at time $t + \Delta t$, referred to configuration at time t (i.e. using displacements from the configuration at time t to the configuration at time $t + \Delta t$)
 ${}^0e_{ij}, {}^t e_{ij}$ = Component of strain increment tensor (Green-Lagrange) referred to configuration at time $0, t$
 ${}^0e_{ij}, {}^t e_{ij}$ = Linear part of strain increment ${}^0e_{ij}, {}^t e_{ij}$
 ${}^0n_{ij}, {}^t n_{ij}$ = Non-linear part of strain increment ${}^0e_{ij}, {}^t e_{ij}$
 ${}^t \Omega_{pi}$ = Component of spin tensor in configuration at time t
 ${}^0\rho, {}^t \rho, {}^{t+\Delta t}\rho$ = Specific mass of body in configuration at time $0, t, t + \Delta t$
 ${}^t \tau_{ij}, {}^{t+\Delta t}\tau_{ij}$ = Component of Cauchy stress tensor in configuration at time $t, t + \Delta t$
 ${}^t \tau_{ij}^{\nabla}$ = Component of Jaumann stress rate tensor in configuration at time t

Matrices

- ${}^0\mathbf{B}_L, {}^t \mathbf{B}_L$ = Linear strain-displacement matrix in configuration at time t referred to configuration at time $0, t$
 ${}^0\mathbf{B}_{NL}, {}^t \mathbf{B}_{NL}$ = Non-linear strain-displacement matrix in configuration at time t referred to configuration at time $0, t$
 ${}^0\mathbf{C}, {}^t \mathbf{C}$ = Tangent material property matrix at time t and referred to configuration at time $0, t$
 ${}^0\mathbf{F}, {}^t \mathbf{F}$ = Vector of nodal point forces in configuration at time t (referred to configuration at time $0, t$)
 ${}^0\mathbf{K}_L, {}^t \mathbf{K}_L$ = Linear strain stiffness matrix in configuration at time t (referred to configuration at time $0, t$)
 ${}^0\mathbf{K}_{NL}, {}^t \mathbf{K}_{NL}$ = Non-linear strain stiffness matrix in configuration at time t (referred to configuration at time $0, t$)
 \mathbf{M} = Mass matrix
 ${}^{t+\Delta t}\mathbf{R}$ = Vector of external loads in configuration at time $t + \Delta t$
 ${}^0\mathbf{S}, {}^t \mathbf{S}$ = 2nd Piola-Kirchhoff stress matrix and vector in configuration at time t and referred to configuration at time 0
 ${}^t \boldsymbol{\tau}, {}^t \hat{\boldsymbol{\tau}}$ = Cauchy stress matrix and vector in configuration at time t
 ${}^t \mathbf{u}, {}^{t+\Delta t}\mathbf{u}$ = Vector of displacements at time $t, t + \Delta t$
 \mathbf{u} = Vector of incremental displacements at time t

REFERENCES

1. J. H. Argyris, P. C. Dunne and T. Angelopoulos, 'Nonlinear oscillations using the finite element technique', *Computer Meth. Appl. Mech. Engng.*, **2**, 203-250 (1973).
2. K. J. Bathe and E. L. Wilson, 'NONSAP—A general finite element program for nonlinear dynamic analysis of complex structures', Paper M3/1, *Proc. 2nd Int. Conf. Struct. Mech. Reactor Technology*, Berlin (1973).
3. K. J. Bathe, E. L. Wilson and R. H. Iding, 'NONSAP—A structural analysis program for static and dynamic response of nonlinear systems', *SESM Report No. 74-3*, Dept. of Civ. Engng, Univ. of California, Berkeley (1974).
4. K. J. Bathe, H. Ozdemir and E. L. Wilson, 'Static and dynamic geometric and material nonlinear analysis', *SESM Report No. 74-4*, Dept. Civ. Engng, Univ. of California, Berkeley (1974).
5. K. J. Bathe and E. L. Wilson, 'Stability and accuracy analysis of direct integration methods', *Int. J. Earthq. Engng Struct. Dyn.*, **1**, 283-291 (1973).
6. T. Belytschko and B. J. Hsieh, 'Nonlinear transient analysis of shells and solids of revolution by convected elements', *AIAA paper No. 73-359*, *AIAA/ASME/SAE 14th Structures, Struct. Dyn. Materials Conf.*, Williamsburg, Virginia (1973).
7. G. A. Dupuis, H. D. Hibbitt, S. F. McNamara and P. V. Marcal, 'Nonlinear material and geometric behavior of shell structures', *Computers Struct.*, **1**, 223-239 (1971).
8. I. Farhoomand, 'Nonlinear dynamic stress analysis of two-dimensional solids', *Ph.D. Dissertation*, Univ. of California, Berkeley, 1970.
9. C. A. Felippa, 'Refined finite element analysis of linear and nonlinear two-dimensional structures', *SESM Report No. 66-22*, Dept. Civ. Engng, Univ. of California, Berkeley (1966).
10. C. A. Felippa and P. Sharifi, 'Computer implementation of nonlinear finite element analysis', *Proc. Symp. ASME*, Detroit (1973).
11. Y. C. Fung, *Foundations of Solid Mechanics*, Prentice-Hall, Englewood Cliffs, N.J., 1965.
12. A. Gjelsvik and S. R. Bodner, 'The energy criterion and snap buckling of arches', *J. Engng Mech. Div., ASCE*, **88**, 87-134 (1962).
13. E. Haug and G. H. Powell, 'Finite element analysis of nonlinear membrane structures', *SESM Report No. 72-7*, Dept. of Civ. Engng, Univ. of California, Berkeley (1972).
14. B. J. Hartz and N. D. Nathar, 'Finite element formulation of geometrically nonlinear problems of elasticity', *Recent Advances in Matrix Methods of Structural Analysis and Design*, 1st Japan-U.S. Seminar Matrix Meth. Struct. Analysis and Design, Univ. of Alabama Press, 415-440 (1971).
15. J. H. Heifitz and C. J. Costantino, 'Dynamic response of nonlinear media at large strains', *J. Engng Mech. Div., ASCE*, **98**, 1511-1527 (1972).
16. H. D. Hibbitt, P. V. Marcal and J. R. Rice, 'Finite element formulation for problems of large strain and large displacements', *Int. J. Solids Struct.*, **6**, 1069-1086 (1970).
17. J. T. Holden, 'On the finite deflections of thin beams', *Int. J. Solids Struct.*, **8**, 1051-1055 (1972).
18. J. S. Humphreys, 'On dynamic snap buckling of shallow arches', *AIAA J.*, **4**, 878-886 (1966).
19. R. H. Iding, 'Identification of nonlinear materials by finite element methods', *SESM Report No. 73-4*, Dept. of Civ. Engng, Univ. of California, Berkeley (1973).
20. P. S. Jensen, 'Transient analysis of structures by stiffly stable methods', *Computers Struct.*, **4**, 615-626 (1974).
21. H. S. Kornishin and F. S. Isanbaeva, *Flexible Plates and Panels*, (in Russian), Nauka, Moscow, 1968.
22. P. K. Larsen, 'Large displacement analysis of shells of revolution, including creep, plasticity and viscoelasticity', *SESM Report No. 71-22*, Dept. of Civ. Engng, Univ. of California, Berkeley (1971).
23. E. H. Lee, 'Elastic-plastic deformation at finite strains', *J. Appl. Mech., Trans. ASME*, **38** (1969).
24. R. H. Mallet and L. Berke, 'Automated method for the large deflection and instability analysis of 3-dimensional truss and frame assemblies', *AFFDL-TR-66-102* (1966).
25. L. E. Malvern, *Introduction to the Mechanics of a Continuum Medium*, Prentice-Hall, Englewood Cliffs, N.J., 1969.
26. P. V. Marcal, 'The effect of initial displacements on problems of large deflection and stability', *Tech. Report ARPA E54*, Brown University, Division of Engineering (1967).
27. J. F. Mescall, 'Large deflection of spherical shells under concentrated loads', *J. Appl. Mech.*, **32**, 936-938 (1965).
28. D. W. Murray and E. L. Wilson, 'Finite element large deflection analysis of plates', *J. Engng Mech. Div., ASCE*, **94**, 143-165 (1965).
29. S. Nagarajan, 'Nonlinear static and dynamic analysis of shells of revolution under axisymmetric loading', *SESM Report No. 73-11*, Dept. of Civ. Engng, Univ. of California, Berkeley (1973).
30. J. F. McNamara, 'Incremental stiffness method for finite element analysis of the nonlinear dynamic problem', *Ph.D. Thesis*, Dept. of Civ. Engng, Brown University, 1972.
31. R. E. Nickell, 'Direct integration methods in structural dynamics', *J. Engng Mech. Div., ASCE*, **99**, 303-317 (1973).
32. J. T. Oden, 'Finite element applications in nonlinear structural analysis', *Proc. Symp. Application Finite Element Meth. Civ. Engng*, Nashville, Tenn. (1969).
33. J. T. Oden, *Finite Elements of Nonlinear Continua*, McGraw-Hill, New York, 1972.
34. H. Schreyer and E. P. Masur, 'Buckling of shallow arches', *J. Engng Mech. Div., ASCE*, **92**, 1-19 (1966).
35. P. Sharifi and E. P. Popov, 'Nonlinear buckling analysis of sandwich arches', *J. Engng Mech. Div., ASCE*, **97**, 1397-1412 (1970).

36. P. Sharifi and D. N. Yates, 'Nonlinear thermo-elastic-plastic and creep analysis by the finite element method', *AIAA Paper No. 73-358, AIAA/ASME/SAE 14th Structures, Struct. Dyn. Materials Conf.*, Williamsburg, Virginia (1973).
37. J. A. Stricklin, 'Geometrically nonlinear static and dynamic analysis of shells of revolution', *High Speed Computing Elastic Struct., Proc. Symp. IUTAM*, Univ. of Liege, 383-411.
38. J. A. Stricklin, W. A. Von Riesenmann, J. R. Tillerson and W. E. Haisler, 'Static geometric and material nonlinear analysis', *Advances in Computational Methods in Computational Methods in Structural Mechanics and Design*, 2nd U.S.-Japan Seminar Matrix Meth. Struct. Analysis and Design, Univ. of Alabama Press, 301-324 (1972).
39. S. Yaghmai, 'Incremental analysis of large deformations in mechanics of solids with applications to axisymmetric shells of revolution', *SESM Report No. 69-17*, Dept. of Civ. Engng, Univ. of California, Berkeley (1968).
40. S. Yaghmai and E. P. Popov, 'Incremental analysis of large deflections of shells of revolution', *Int. J. Solids Struct.* 7, 1375-1393 (1971).
41. Y. Yamada, 'Incremental formulation for problems with geometric and material nonlinearities', *Advances in Computational Methods in Structural Mechanics and Design*, 2nd U.S.-Japan Seminar Matrix Meth. Struct. Analysis Design, Univ. of Alabama Press, 325-355 (1972).
42. C. H. Yeh, 'Large deflection dynamic analysis of thin shells using the finite element method', *SESM Report No. 70-78*, Dept. of Civ. Engng, Univ. of California (1970).
43. O. C. Zienkiewicz, *The Finite Element Method in Engineering Science*, McGraw-Hill, London, 1971.

LARGE DISPLACEMENT ANALYSIS OF THREE-DIMENSIONAL BEAM STRUCTURES

KLAUS-JÜRGEN BATHE† AND SAÏD BOLOURCHI‡

Department of Mechanical Engineering, Massachusetts Institute of Technology, Massachusetts, U.S.A.

SUMMARY

An updated Lagrangian and a total Lagrangian formulation of a three-dimensional beam element are presented for large displacement and large rotation analysis. It is shown that the two formulations yield identical element stiffness matrices and nodal point force vectors, and that the updated Lagrangian formulation is computationally more effective. This formulation has been implemented and the results of some sample analyses are given.

INTRODUCTION

The possibility of practical static and dynamic nonlinear analysis of structures has during recent years progressed substantially, due to the effective use of digital computers operating on finite element representations of the structures. To enable general nonlinear analysis the development of versatile geometric and material nonlinear finite elements is in much need, and among these elements the use of an effective three-dimensional beam element is very important.

Since the first applications of computers to nonlinear analysis of structures, various nonlinear beam elements have been presented.¹⁻¹¹ The large number of publications on nonlinear analysis of beam structures is, at least partially, due to the fact that various kinematic nonlinear formulations can be employed, and that at this time it is not clear which formulation is most effective. The difficulty of obtaining effective solutions is particularly pronounced in the analysis of three-dimensional beam structures. Namely, considering a beam element it is noted that a general three-dimensional nonlinear beam formulation is not a simple extension of a two-dimensional formulation, because in three-dimensional analysis large rotations have to be accounted for that are not vector quantities.

In the development of a geometrically nonlinear beam element, basically an updated Lagrangian or a total Lagrangian formulation can be employed.^{12,13} These formulations must be implemented using appropriate displacement interpolation functions. Considering the choice of these functions it is recognized that for a beam of constant cross-section in small displacement analysis the Hermitian functions should be employed to interpolate the transverse bending displacements, and linear interpolation must be used to interpolate the torsional and longitudinal displacements. Therefore, in the search for a beam element that can undergo large rotations (with small strains), it is natural to employ the same functions but referred to the beam convected co-ordinate axes. In this way the usual beam kinematic assumptions are used referred to the current beam geometry.

† Associate Professor of Mechanical Engineering.

‡ Research Assistant.

Considering the formulation of a large displacement beam element, once specific beam assumptions have been made and the interpolation functions have been selected, basically the same element stiffness matrices and nodal point force vectors should be calculated using any one formulation. Therefore, the response predicted using different formulations must be the same, if the same number of beam elements are employed to model a structure. Indeed, the choice for a total Lagrangian or an updated Lagrangian formulation should be decided only by the relative numerical effectiveness of the formulations. However, considering large displacement beam formulations using the Hermitian interpolations to describe bending deformations and linear interpolations to specify axial and torsional displacements, a moving co-ordinate formulation appears quite natural. Namely, in a total Lagrangian formulation for large rotation analysis, the fact that the different displacement components are interpolated using different order polynomials establishes an interpolation directionality that requires special attention.

In another approach to formulate a beam element that includes large rotation effects, the transverse displacements, axial displacements and the rotations are interpolated independently. If the same interpolation functions are employed for all these kinematic variables, the problem of interpolation directionality under large rotations does not arise in the total Lagrangian formulation.¹⁴ However, to obtain the same accuracy as with the beam elements based on Hermitian functions, in this element formulation about twice as many degrees of freedom are needed. It can be concluded that, for straight beams, it is more efficient to employ the conventional beam interpolation functions, but to formulate more general and curved beam elements the independent interpolation of displacements and rotations is effective.

The objective in this paper is to present two consistent large rotation nonlinear three-dimensional beam formulations: an updated Lagrangian (U.L.) and a total Lagrangian (T.L.) formulation. The formulations are derived from the continuum mechanics based Lagrangian incremental equilibrium equations.¹² The beam elements are assumed to be straight, and the conventional beam displacement functions are employed to express the displacements of the elements in convected co-ordinates. In the paper the two formulations are evaluated, and it is shown that the governing incremental equilibrium equations of the beam elements are identical but that the updated Lagrangian-based element is computationally more effective. This element is a very efficient three-dimensional nonlinear beam element. The element has been implemented for use in elastic, elastic-plastic, static and dynamic analysis and in the paper a few demonstrative sample solutions are presented.

INCREMENTAL T.L. AND U.L. CONTINUUM MECHANICS FORMULATIONS

The beam element formulations are based on the general incremental T.L. and U.L. continuum mechanics equations,¹² which are briefly summarized below.

Consider the motion of a body in a fixed Cartesian co-ordinate system, as shown in Figure 1. Assume that the solutions measured in the co-ordinate system corresponding to all time points $0, \Delta t, 2\Delta t, \dots, t$ are known. It is required to solve for the unknown static and kinematic variables in the configuration at time $t + \Delta t$. In static analysis and implicit time integration the equilibrium of the body at time $t + \Delta t$ is expressed and used to solve for the static and kinematic variables corresponding to time $t + \Delta t$. On the other hand, in explicit time integration, the equilibrium at time t is employed to solve for the displacements at time $t + \Delta t$.^{12,15}

Total Lagrangian (T.L.) formulation

In the total Lagrangian formulation all static and kinematic variables are referred to the initial configuration at time 0. Considering the equilibrium of the body at time $t + \Delta t$, the principle of

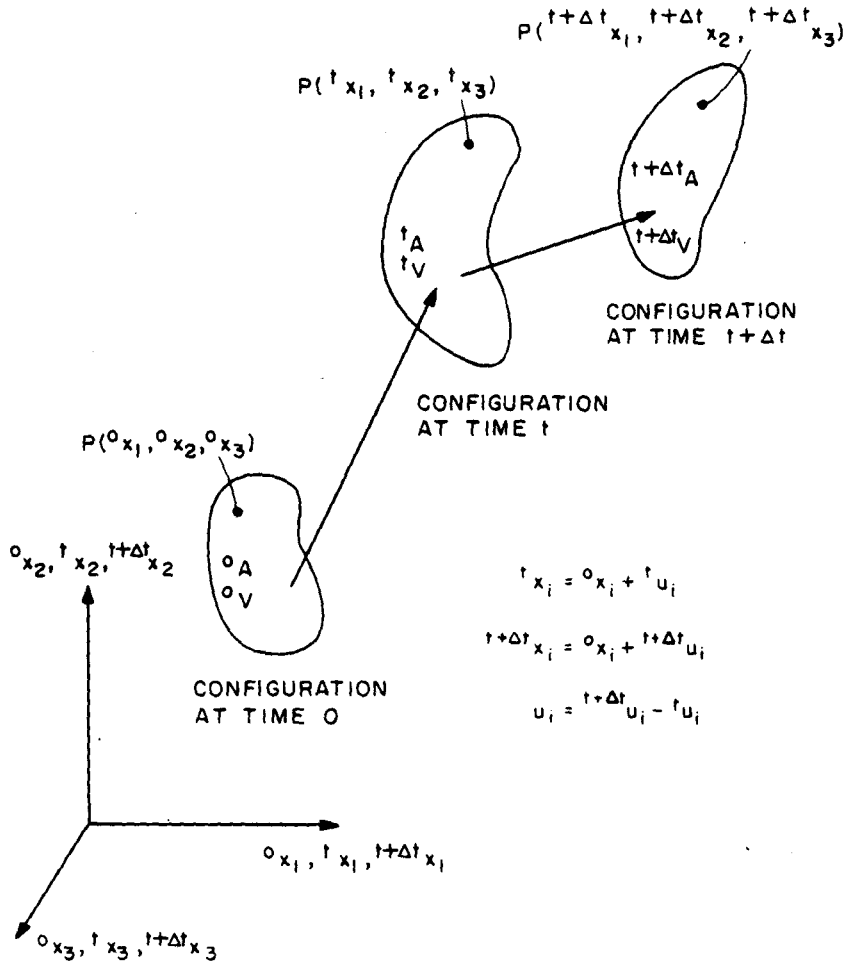


Figure 1. Motion of body in Cartesian co-ordinate system

virtual displacements gives

$$\int_{0V} {}^{t+\Delta t} S_{ij} \delta {}^{t+\Delta t} {}_0 \epsilon_{ij} {}^0 dv = {}^{t+\Delta t} \mathcal{R} \quad (1)$$

where ${}^{t+\Delta t} \mathcal{R}$ is the total external virtual work expression due to the surface tractions with components ${}^{t+\Delta t} {}_0 t_k$, and body forces with components ${}^{t+\Delta t} {}_0 f_k$,

$${}^{t+\Delta t} \mathcal{R} = \int_{0A} {}^{t+\Delta t} {}_0 t_k \delta u_k {}^0 da + \int_{0V} {}^0 \rho {}^{t+\Delta t} {}_0 f_k \delta u_k {}^0 dv \quad (2)$$

In equations (1) and (2), δu_k is a (virtual) variation in the current displacement components ${}^{t+\Delta t} u_k$, $\delta {}^{t+\Delta t} {}_0 \epsilon_{ij}$ is a (virtual) variation in the Cartesian components of the Green-Lagrange strain tensor in the configuration at time $t + \Delta t$ referred to the initial configuration, and ${}^{t+\Delta t} {}_0 S_{ij}$ are the Cartesian components of the 2nd Piola-Kirchhoff stress tensor in the configuration $t + \Delta t$ and

measured in the configuration at time 0:

$${}^{t+\Delta t}{}_0\varepsilon_{ij} = \frac{1}{2}({}^{t+\Delta t}{}_0u_{i,j} + {}^{t+\Delta t}{}_0u_{j,i} + {}^{t+\Delta t}{}_0u_{k,i} {}^{t+\Delta t}{}_0u_{k,j}) \quad (3)$$

$${}^{t+\Delta t}{}_0S_{ij} = \frac{\rho}{t+\Delta t} \frac{\rho}{\rho} {}^{t+\Delta t}{}_0x_{i,k} {}^{t+\Delta t}{}_0\tau_{kl} {}^{t+\Delta t}{}_0x_{j,l} \quad (4)$$

where ${}^{t+\Delta t}{}_0x_{i,j} = \partial^0 x_i / \partial^{t+\Delta t} x_j$ and the ${}^{t+\Delta t}{}_0\tau_{kl}$ are the components of the Cauchy stress tensor at time $t + \Delta t$.

In dynamic analysis the body force components in equation (2) include the mass inertia effects.¹²

Since the stresses ${}^{t+\Delta t}{}_0S_{ij}$ and strains ${}^{t+\Delta t}{}_0\varepsilon_{ij}$ are unknown, for solution the following incremental decompositions are used:

$${}^{t+\Delta t}{}_0S_{ij} = {}^t_0S_{ij} + {}_0S_{ij} \quad (5)$$

$${}^{t+\Delta t}{}_0\varepsilon_{ij} = {}^t_0\varepsilon_{ij} + {}_0\varepsilon_{ij} \quad (6)$$

where ${}^t_0S_{ij}$ and ${}^t_0\varepsilon_{ij}$ are the known 2nd Piola–Kirchhoff stresses and Green–Lagrange strains in the configuration at time t . It follows from equation (6) that $\delta^{t+\Delta t}{}_0\varepsilon_{ij} = \delta_0\varepsilon_{ij}$. The strain increment components can be separated into linear and nonlinear parts

$${}_0\varepsilon_{ij} = {}_0e_{ij} + {}_0\eta_{ij} \quad (7)$$

where

$${}_0e_{ij} = \frac{1}{2}[({}_0u_{i,j} + {}_0u_{j,i}) + ({}_0u_{k,i} {}_0u_{k,j} + {}_0u_{k,j} {}_0u_{k,i})] \quad (8)$$

and

$${}_0\eta_{ij} = \frac{1}{2}({}_0u_{k,i} {}_0u_{k,j}) \quad (9)$$

Finally, the constitutive relations with tensor components ${}_0C_{ijrs}$ can be used to relate incremental 2nd Piola–Kirchhoff stresses to incremental Green–Lagrange strains

$${}_0S_{ij} = {}_0C_{ijrs} {}_0e_{rs} \quad (10)$$

Using equations (5)–(10), equation (1) can now be transformed to

$$\int_{0V} {}_0C_{ijrs} {}_0e_{rs} \delta_0\varepsilon_{ij} {}^0dv + \int_{0V} {}^t_0S_{ij} \delta_0\eta_{ij} {}^0dv = {}^{t+\Delta t}\mathcal{R} - \int_{0V} {}^t_0S_{ij} \delta_0e_{ij} {}^0dv \quad (11)$$

Equation (11) is nonlinear in the incremental displacements u_i , and can be linearized by using the approximations ${}_0S_{ij} = {}_0C_{ijrs} {}_0e_{rs}$ and $\delta_0\varepsilon_{ij} = \delta_0e_{ij}$. We thus obtain

$$\int_{0V} {}_0C_{ijrs} {}_0e_{rs} \delta_0e_{ij} {}^0dv + \int_{0V} {}^t_0S_{ij} \delta_0\eta_{ij} {}^0dv = {}^{t+\Delta t}\mathcal{R} - \int_{0V} {}^t_0S_{ij} \delta_0e_{ij} {}^0dv \quad (12)$$

which is a linear equation in the incremental displacements.

Equation (12) is employed in static analysis or implicit time integration. In explicit time integration, equation (1) is used corresponding to time t .

Updated Lagrangian (U.L.) formulation

In the U.L. formulation the same incremental stress and strain decompositions as in the T.L. formulation are employed, but all variables are referred to the configuration at time t , i.e. the last known configuration. Thus, corresponding to equation (12), the linearized equilibrium equation

is in the U.L. formulation

$$\int_{t_V} {}^t C_{ijrs} {}^t e_{rs} \delta {}^t e_{ij} {}^t dv + \int_{t_V} {}^t \tau_{ij} \delta {}^t \eta_{ij} {}^t dv = {}^{t+\Delta t} \mathcal{R} - \int_{t_V} {}^t \tau_{ij} \delta {}^t e_{ij} {}^t dv \quad (13)$$

where the ${}^t \tau_{ij}$ are the Cartesian components of the Cauchy stress tensor at time t ; e_{ij} and η_{ij} are the Cartesian components of the linear and nonlinear strain increments, respectively, and the ${}^t C_{ijrs}$ are the components of the tangent constitutive tensor relating small strain increments to the corresponding stress increments.

U.L. AND T.L. FORMULATIONS OF BEAM ELEMENT

The general three-dimensional straight beam element is formulated based on the continuum mechanics theory summarized above. The element has two nodes with 6 degrees-of-freedom per node, and can transmit an axial force, two shear forces, two bending moments and a torque. Figure 2 shows a typical beam element.

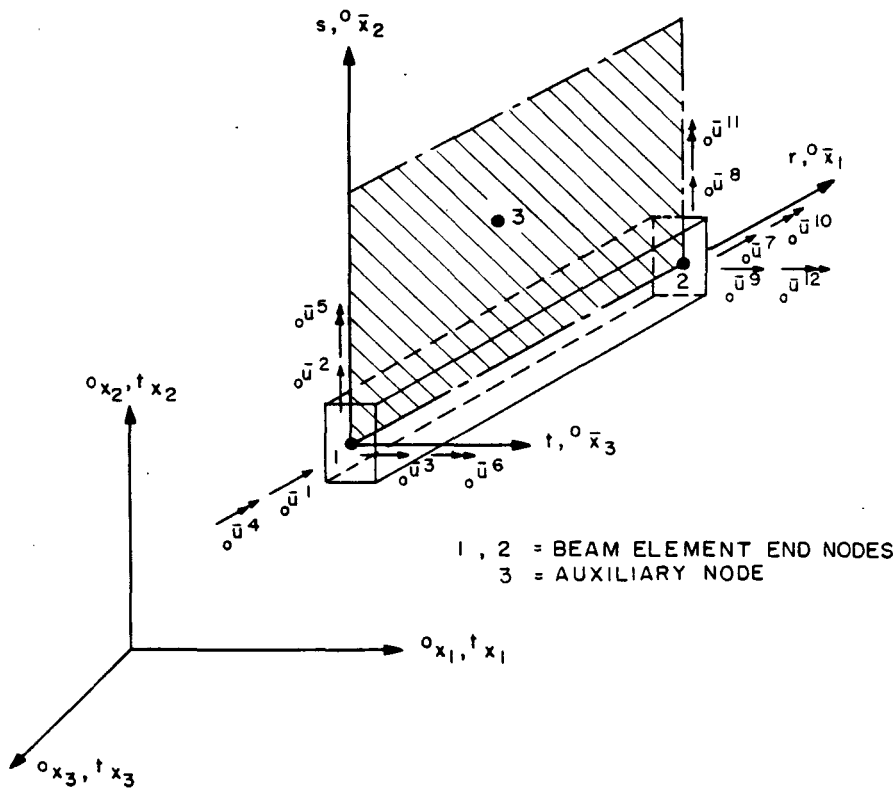


Figure 2. Schematic view of the three-dimensional beam element local co-ordinate axes

The element is assumed to be straight and of constant cross-section. It is assumed that plane sections of the beam element remain plane during deformation, but not necessarily perpendicular to the neutral axis, i.e. a constant shear is allowed. The element can undergo large deflections and rotations, but small strains are assumed. Thus, the cross-sectional area and the length of the beam element do not change during deformation.

The principal moment of inertia axes of the beam element define the local co-ordinate system r, s, t , as shown in Figure 2. The two end nodes of the element, 1 and 2, plus a third auxiliary

node, 3, are used to define these axes, where it should be noted that in the computations the r - s plane is defined by nodes 1, 2 and 3.

Incremental equilibrium equations

In equations (12) and (13) the incremental equilibrium equations of a body in motion are given corresponding to the global co-ordinate system ${}^T x_i$, $\tau = 0$ or t . Considering a typical beam element it is more effective to first evaluate the finite element matrices corresponding to the local principal axes ${}^T \bar{x}_i$ of the element (see Figure 3), and then transform the resulting matrices to correspond to the global Cartesian co-ordinate axes prior to the element assemblage process.¹⁶

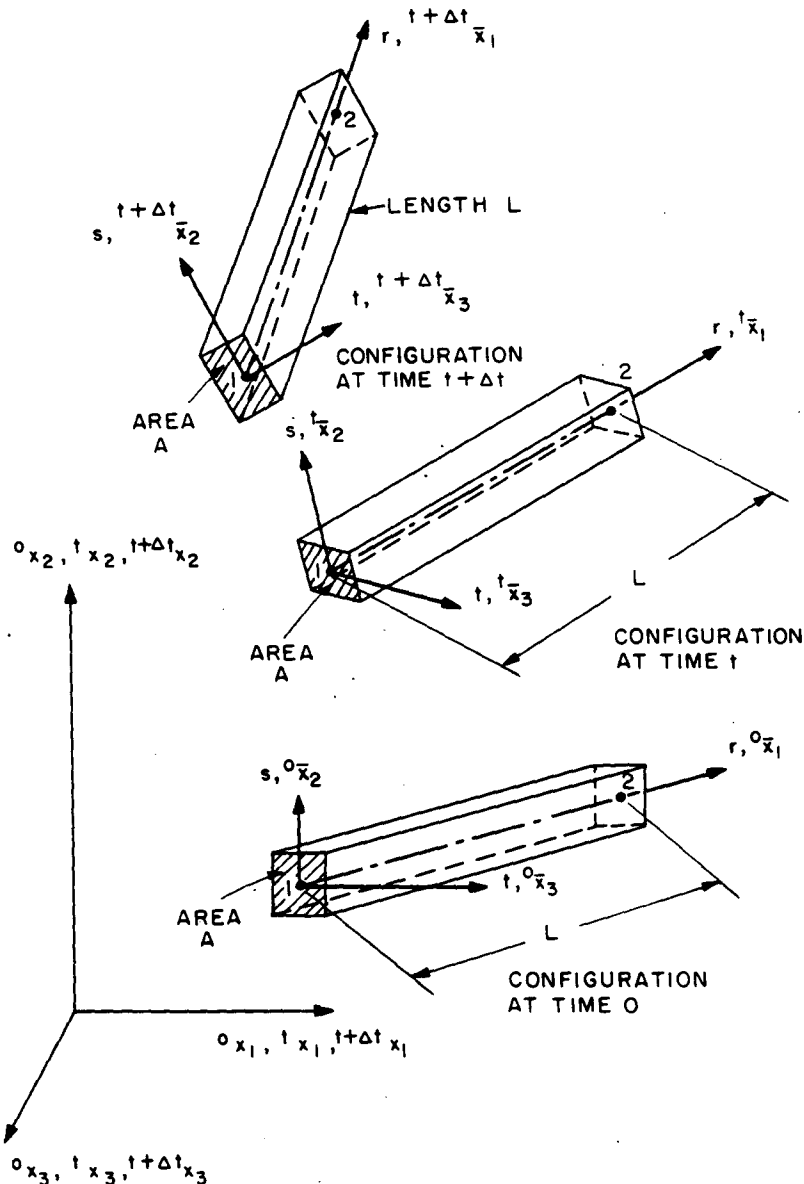


Figure 3. Motion of the three-dimensional beam element and its local co-ordinate axes shown in global co-ordinate system.

The finite element matrices corresponding to the axes $\tau \bar{x}_i$ are simply obtained by measuring all static and kinematic quantities in this co-ordinate system. These new quantities are denoted by a bar placed over them. Thus, using equations (12) and (13) we obtain for a single beam element, using the *U.L. formulation* and considering only static analysis

$$({}^t\mathbf{K}_L + {}^t\mathbf{K}_{NL})\mathbf{u} = {}^{t+\Delta t}\mathbf{R} - {}^t\mathbf{F} \tag{14}$$

and using the *T.L. formulation* and considering only static analysis

$$({}_0\mathbf{K}_L + {}_0\mathbf{K}_{NL})\mathbf{u} = {}^{t+\Delta t}\mathbf{R} - {}_0\mathbf{F} \tag{15}$$

where ${}_0\mathbf{K}_L, {}^t\mathbf{K}_L$ are linear strain incremental stiffness matrices; ${}_0\mathbf{K}_{NL}, {}^t\mathbf{K}_{NL}$ are nonlinear strain (geometric or initial stress) incremental stiffness matrices; ${}^{t+\Delta t}\mathbf{R}$ is the vector of externally applied element nodal loads at time $t + \Delta t$; ${}_0\mathbf{F}, {}^t\mathbf{F}$ are vectors of nodal point forces equivalent to the element stresses at time t ; and \mathbf{u} is the vector of incremental nodal displacements.

In dynamic analysis using implicit time integration the inertia forces corresponding to time $t + \Delta t$ are added to the left-hand sides of equations (14) and (15), whereas in dynamic analysis using explicit time integration the stiffness effect is not included, the inertia forces corresponding to time t are added to the left-hand sides of equations (14) and (15), and the applied external loads correspond to time t .

The element matrices in equations (14) and (15) are evaluated using the displacement interpolation functions of the beam element. Table I summarizes these calculations. The following notation is used in Table I with all quantities referred to the co-ordinate systems $\tau \bar{x}_i$, $\tau = 0$ or t :

- ${}_0\bar{\mathbf{B}}_L, {}^t\bar{\mathbf{B}}_L$ = linear strain–displacement transformation matrices
- ${}_0\bar{\mathbf{B}}_{NL}, {}^t\bar{\mathbf{B}}_{NL}$ = nonlinear strain–displacement transformation matrices
- ${}_0\bar{\mathbf{C}}, {}^t\bar{\mathbf{C}}$ = incremental stress–strain material property matrices
- ${}^t\bar{\boldsymbol{\tau}}, {}^t\bar{\boldsymbol{\tau}}$ = matrix and vector of Cauchy stresses
- ${}_0\bar{\mathbf{S}}, {}_0\bar{\mathbf{S}}$ = matrix and vector of 2nd Piola–Kirchhoff stresses.

Table I. Finite element matrices

Total Lagrangian formulation	$\int_V {}_0\bar{\mathbf{C}}_{ijrs} {}_0\bar{e}_{rs} \delta_0 \bar{e}_{ij} dv$	${}_0\bar{\mathbf{K}}_L {}_0\bar{\mathbf{u}} = \left(\int_V {}_0\bar{\mathbf{B}}_L^T {}_0\bar{\mathbf{C}} {}_0\bar{\mathbf{B}}_L dv \right) {}_0\bar{\mathbf{u}}$
	$\int_V {}_0\bar{\mathbf{S}}_{ij} \delta_0 \bar{\eta}_{ij} dv$	${}_0\bar{\mathbf{K}}_{NL} {}_0\bar{\mathbf{u}} = \left(\int_V {}_0\bar{\mathbf{B}}_{NL}^T {}_0\bar{\mathbf{S}} {}_0\bar{\mathbf{B}}_{NL} dv \right) {}_0\bar{\mathbf{u}}$
	$\int_V {}_0\bar{\mathbf{S}}_{ij} \delta_0 \bar{e}_{ij} dv$	${}_0\bar{\mathbf{F}} = \int_V {}_0\bar{\mathbf{B}}_L^T {}_0\bar{\mathbf{S}} dv$
Updated Lagrangian formulation	$\int_V {}^t\bar{\mathbf{C}}_{ijrs} {}^t\bar{e}_{rs} \delta_t \bar{e}_{ij} dv$	${}^t\bar{\mathbf{K}}_L {}^t\bar{\mathbf{u}} = \left(\int_V {}^t\bar{\mathbf{B}}_L^T {}^t\bar{\mathbf{C}} {}^t\bar{\mathbf{B}}_L dv \right) {}^t\bar{\mathbf{u}}$
	$\int_V {}^t\bar{\boldsymbol{\tau}}_{ij} \delta_t \bar{\eta}_{ij} dv$	${}^t\bar{\mathbf{K}}_{NL} {}^t\bar{\mathbf{u}} = \left(\int_V {}^t\bar{\mathbf{B}}_{NL}^T {}^t\bar{\boldsymbol{\tau}} {}^t\bar{\mathbf{B}}_{NL} dv \right) {}^t\bar{\mathbf{u}}$
	$\int_V {}^t\bar{\boldsymbol{\tau}}_{ij} \delta_t \bar{e}_{ij} dv$	${}^t\bar{\mathbf{F}} = \int_V {}^t\bar{\mathbf{B}}_L^T {}^t\bar{\boldsymbol{\tau}} dv$

It should be noted that the elements of the stress matrices and vectors in the T.L. and the U.L. formulations are equal, because small strain conditions are assumed.

Interpolation functions for incremental displacements

To describe the motion of the beam elements the incremental displacement field within the elements as a function of the incremental nodal point displacement components is required,

$${}^t\bar{u}_i = \sum_{k=1}^N h_k^i {}^t\bar{u}^k \quad (16)$$

where the h_k^i are the interpolation functions corresponding to the local axes ${}^t\bar{x}_i$, and the ${}^t\bar{u}^k$ are the nodal point displacement increments measured in the local axes at time t (see Figure 3).

The interpolation functions in equation (16) are constructed assuming cubic bending displacement variations and a linear variation in the axial and torsional displacements. In order to include shear effects, constant shear deformations can be included. Using the usual beam incremental nodal displacements (these are shown for time 0 in Figure 2) and leaving the shear deformations as independent variables, we obtain the incremental displacement interpolation functions given in Table II. In this table the variable N in equation (16) is equal to 12 if no shear deformations are included; otherwise N is equal to 14. If shear deformations are included the element stiffness matrices and nodal point force vectors are of order 14, and are reduced to order 12 by static condensation prior to the element assemblage process.

Strain-displacement transformation matrices in the U.L. formulation

The kinematic assumptions used in defining the interpolation functions of Table II hold for small strains, small rigid body incremental rotations in each solution step, but any size translational displacements. These assumptions are appropriate for the updated Lagrangian formulation of beams, because the kinematic variables are linearized about the last-known body position.

Using the interpolation functions in Table II, the strain-displacement matrices of the U.L. formulation can directly be evaluated. Table III(B) summarizes the calculation of the matrices ${}^t\bar{\mathbf{B}}_L$ and ${}^t\bar{\mathbf{B}}_{NL}$ that are required to evaluate the tangent stiffness matrix and nodal point force vector of an element corresponding to co-ordinate axes ${}^t\bar{x}_i$ ($i = 1, 2, 3$). The element matrices have to be transformed to the global co-ordinate system prior to their assemblage into a system of beam elements.

Strain-displacement transformation matrices in the T.L. formulation

In the discussion of the total Lagrangian formulation and the comparative study of the total and updated Lagrangian formulations we do not include, for clarity, the effect of shear deformations. Referring to the definitions in Figures 2 and 3, the displacement increments within the element at time t measured in the local axes at time 0 are related to the nodal point displacement increments of the element in its local axes using

$${}^0\bar{u}_i = \sum_{k=1}^{12} {}^0h_k^i {}^0\bar{u}^k \quad (17)$$

where the ${}^0\bar{u}^k$ are the element nodal point displacement increments at time t , but measured in the ${}^0\bar{x}_i$ ($i = 1, 2, 3$) co-ordinate system. The functions ${}^0h_k^i$ ($i = 1, 2, 3$) are the interpolation

Table II. Beam interpolation functions

We define:

$$\begin{aligned} \psi_1 &= \frac{r}{L} - \left(\frac{r}{L}\right)^2; & \psi_2 &= 1 - 4\frac{r}{L} + 3\left(\frac{r}{L}\right)^2; & \psi_3 &= 2\frac{r}{L} - 3\left(\frac{r}{L}\right)^2 \\ \psi_4 &= 1 - 3\left(\frac{r}{L}\right)^2 + 2\left(\frac{r}{L}\right)^3; & \psi_5 &= \frac{r}{L} - 2\left(\frac{r}{L}\right)^2 + \left(\frac{r}{L}\right)^3 \\ \psi_6 &= 3\left(\frac{r}{L}\right)^2 - 2\left(\frac{r}{L}\right)^3; & \psi_7 &= \frac{r}{L} - 3\left(\frac{r}{L}\right)^2 + 2\left(\frac{r}{L}\right)^3 \end{aligned}$$

Incremental displacement interpolation matrix

$${}^i\bar{\mathbf{H}} = \begin{bmatrix} {}^i\mathbf{h}^1 \\ {}^i\mathbf{h}^2 \\ {}^i\mathbf{h}^3 \end{bmatrix} =$$

$$\begin{bmatrix} 1 - \frac{r}{L} & 6\psi_1 \frac{s}{L} & 6\psi_1 \frac{t}{L} & 0 & \psi_2 t & -\psi_2 s & \frac{r}{L} \\ 0 & \psi_4 & 0 & -\left(1 - \frac{r}{L}\right)t & 0 & \psi_5 L & 0 \\ 0 & 0 & \psi_4 & \left(1 - \frac{r}{L}\right)s & -\psi_5 L & 0 & 0 \\ -6\psi_1 \frac{s}{L} & -6\psi_1 \frac{t}{L} & 0 & -\psi_3 t & \psi_3 s & -(1 - 6\psi_1)t & (1 - 6\psi_1)s \\ \psi_6 & 0 & -\frac{r}{L}t & 0 & -\psi_1 r & 0 & (r - \psi_7 L) \\ 0 & \psi_6 & \frac{r}{L}s & \psi_1 r & 0 & (r - \psi_7 L) & 0 \end{bmatrix}$$

where

L = length of the beam element

${}^i\mathbf{h}^i$ = vector of interpolation functions in ${}^i\bar{x}_i$ direction

r, s, t = beam convected co-ordinate axes (see Figure 3)

The incremental displacement vector is

$${}^i\bar{\mathbf{u}}^T = [{}^i\bar{u}^1, {}^i\bar{u}^2, \dots, {}^i\bar{u}^{12}, {}^i\bar{u}^{13}, {}^i\bar{u}^{14}]$$

where ${}^i\bar{u}^{13} \equiv \beta_1$, ${}^i\bar{u}^{14} \equiv \beta_2$ (shear deformations)

functions corresponding to the convected axes r, s, t and measured in the co-ordinate system ${}^0\bar{x}_j$ ($j = 1, 2, 3$).

The interpolation functions ${}^0h_k^i$ are obtained using

$${}^0h_k^i = \sum_{m=1}^3 \sum_{n=1}^{12} {}^i\bar{\mathbf{R}}_{im} h_n^m {}^0\bar{\mathbf{R}}_{nk} \tag{18}$$

Table III. Matrices used in beam analysis

A. TOTAL LAGRANGIAN FORMULATION

1. Incremental strains

$${}^0\bar{\epsilon}_{ij} = {}^0\bar{\epsilon}_{ij} + {}^0\bar{\eta}_{ij}$$

$${}^0\bar{\epsilon}_{11} = {}^0\bar{u}_{1,1} + {}^0\bar{u}'_{1,1} {}^0\bar{u}_{1,1} + {}^0\bar{u}'_{2,1} {}^0\bar{u}_{2,1} + {}^0\bar{u}'_{3,1} {}^0\bar{u}_{3,1} + \frac{1}{2}[({}^0\bar{u}_{1,1})^2 + ({}^0\bar{u}_{2,1})^2 + ({}^0\bar{u}_{3,1})^2]$$

$${}^0\bar{\epsilon}_{12} = \frac{1}{2}\{[{}^0\bar{u}_{1,2} + {}^0\bar{u}'_{2,1}] + [{}^0\bar{u}'_{1,1} {}^0\bar{u}_{1,2} + {}^0\bar{u}'_{2,1} {}^0\bar{u}_{2,2} + {}^0\bar{u}'_{3,1} {}^0\bar{u}_{3,2} + {}^0\bar{u}'_{1,2} {}^0\bar{u}_{1,1} + {}^0\bar{u}'_{2,2} {}^0\bar{u}_{2,1} + {}^0\bar{u}'_{3,2} {}^0\bar{u}_{3,1}]\}$$

$$+ \frac{1}{2}[{}^0\bar{u}'_{1,1} {}^0\bar{u}_{1,2} + {}^0\bar{u}'_{2,1} {}^0\bar{u}_{2,2} + {}^0\bar{u}'_{3,1} {}^0\bar{u}_{3,2}]$$

$${}^0\bar{\epsilon}_{13} = \frac{1}{2}\{[{}^0\bar{u}_{1,3} + {}^0\bar{u}'_{3,1}] + [{}^0\bar{u}'_{1,1} {}^0\bar{u}_{1,3} + {}^0\bar{u}'_{2,1} {}^0\bar{u}_{2,3} + {}^0\bar{u}'_{3,1} {}^0\bar{u}_{3,3} + {}^0\bar{u}'_{1,3} {}^0\bar{u}_{1,1} + {}^0\bar{u}'_{2,3} {}^0\bar{u}_{2,1} + {}^0\bar{u}'_{3,3} {}^0\bar{u}_{3,1}]\}$$

$$+ \frac{1}{2}[{}^0\bar{u}'_{1,1} {}^0\bar{u}_{1,3} + {}^0\bar{u}'_{2,1} {}^0\bar{u}_{2,3} + {}^0\bar{u}'_{3,1} {}^0\bar{u}_{3,3}]$$

where

$${}^0\bar{u}_{i,j} = \frac{\partial {}^0\bar{u}_i}{\partial {}^0\bar{x}_j}; \quad {}^0\bar{u}'_{i,j} = \frac{\partial {}^0\bar{u}'_i}{\partial {}^0\bar{x}_j}; \quad {}^0\bar{x}_1 \equiv r, \quad {}^0\bar{x}_2 \equiv s, \quad {}^0\bar{x}_3 \equiv t$$

2. Linear strain-displacement transformation matrix

Using

$${}^0\bar{\epsilon} = {}^0\bar{\mathbf{B}}_L {}^0\bar{\mathbf{u}}; \quad {}^0\bar{\mathbf{u}} = {}^0\mathbf{R}\mathbf{u}$$

where

${}^0\bar{\mathbf{u}}$ = vector of incremental nodal displacements measured in ${}^0\bar{x}_i$ ($i = 1, 2, 3$) co-ordinate system

\mathbf{u} = vector of incremental nodal displacements in global co-ordinate system

${}^0\mathbf{R}$ = transformation matrix

and

$${}^0\bar{\epsilon}^T = [{}^0\bar{\epsilon}_{11} \quad 2{}^0\bar{\epsilon}_{12} \quad 2{}^0\bar{\epsilon}_{13}]; \quad {}^0\bar{\mathbf{u}}^T = [{}^0\bar{u}^1 \quad {}^0\bar{u}^2 \quad {}^0\bar{u}^3 \quad \dots \quad {}^0\bar{u}^{12}]$$

$${}^0\bar{\mathbf{B}}_L = {}^0\bar{\mathbf{B}}_{L0} + {}^0\bar{\mathbf{B}}_{L1}$$

where

$${}^0\bar{\mathbf{B}}_{L0} = \begin{bmatrix} {}^0h^1_{1,1} & {}^0h^1_{2,1} & {}^0h^1_{3,1} & \dots & {}^0h^1_{12,1} \\ ({}^0h^1_{1,2} + {}^0h^2_{1,1}) & ({}^0h^1_{2,2} + {}^0h^2_{2,1}) & ({}^0h^1_{3,2} + {}^0h^2_{3,1}) & \dots & ({}^0h^1_{12,2} + {}^0h^2_{12,1}) \\ ({}^0h^1_{1,3} + {}^0h^3_{1,1}) & ({}^0h^1_{2,3} + {}^0h^3_{2,1}) & ({}^0h^1_{3,3} + {}^0h^3_{3,1}) & \dots & ({}^0h^1_{12,3} + {}^0h^3_{12,1}) \end{bmatrix}$$

and

$${}^0\bar{\mathbf{B}}_{L1} = \begin{bmatrix} (l_{11} {}^0h^1_{1,1} + l_{21} {}^0h^2_{1,1} + l_{31} {}^0h^3_{1,1}) \\ (l_{11} {}^0h^1_{1,2} + l_{12} {}^0h^1_{1,1} + l_{21} {}^0h^2_{1,2} + l_{22} {}^0h^2_{1,1} + l_{31} {}^0h^3_{1,2} + l_{32} {}^0h^3_{1,1}) \\ (l_{11} {}^0h^1_{1,3} + l_{13} {}^0h^1_{1,1} + l_{21} {}^0h^2_{1,3} + l_{23} {}^0h^2_{1,1} + l_{31} {}^0h^3_{1,3} + l_{33} {}^0h^3_{1,1}) \\ \\ (l_{11} {}^0h^1_{2,1} + l_{21} {}^0h^2_{2,1} + l_{31} {}^0h^3_{2,1}) \dots \\ (l_{11} {}^0h^1_{2,2} + l_{12} {}^0h^1_{2,1} + l_{21} {}^0h^2_{2,2} + l_{22} {}^0h^2_{2,1} + l_{31} {}^0h^3_{2,2} + l_{32} {}^0h^3_{2,1}) \dots \\ (l_{11} {}^0h^1_{2,3} + l_{13} {}^0h^1_{2,1} + l_{21} {}^0h^2_{2,3} + l_{23} {}^0h^2_{2,1} + l_{31} {}^0h^3_{2,3} + l_{33} {}^0h^3_{2,1}) \dots \\ \\ \dots (l_{11} {}^0h^1_{12,1} + l_{21} {}^0h^2_{12,1} + l_{31} {}^0h^3_{12,1}) \\ \dots (l_{11} {}^0h^1_{12,2} + l_{12} {}^0h^1_{12,1} + l_{21} {}^0h^2_{12,2} + l_{22} {}^0h^2_{12,1} + l_{31} {}^0h^3_{12,2} + l_{32} {}^0h^3_{12,1}) \\ \dots (l_{11} {}^0h^1_{12,3} + l_{13} {}^0h^1_{12,1} + l_{21} {}^0h^2_{12,3} + l_{23} {}^0h^2_{12,1} + l_{31} {}^0h^3_{12,3} + l_{33} {}^0h^3_{12,1}) \end{bmatrix}$$

Table III—continued

where

$$l_{ij} = \frac{\partial \bar{u}_i}{\partial \bar{x}_j}$$

3. Nonlinear strain-displacement transformation matrix

$${}^0\bar{\mathbf{B}}_{NL} = \begin{bmatrix} {}^0h_{1,1}^1 & {}^0h_{2,1}^1 & {}^0h_{3,1}^1 & \dots & {}^0h_{12,1}^1 \\ {}^0h_{1,1}^2 & {}^0h_{2,1}^2 & {}^0h_{3,1}^2 & \dots & {}^0h_{12,1}^2 \\ {}^0h_{1,1}^3 & {}^0h_{2,1}^3 & {}^0h_{3,1}^3 & \dots & {}^0h_{12,1}^3 \\ {}^0h_{1,2}^1 & {}^0h_{2,2}^1 & {}^0h_{3,2}^1 & \dots & {}^0h_{12,2}^1 \\ {}^0h_{1,2}^2 & {}^0h_{2,2}^2 & {}^0h_{3,2}^2 & \dots & {}^0h_{12,2}^2 \\ {}^0h_{1,2}^3 & {}^0h_{2,2}^3 & {}^0h_{3,2}^3 & \dots & {}^0h_{12,2}^3 \\ {}^0h_{1,3}^1 & {}^0h_{2,3}^1 & {}^0h_{3,3}^1 & \dots & {}^0h_{12,3}^1 \\ {}^0h_{1,3}^2 & {}^0h_{2,3}^2 & {}^0h_{3,3}^2 & \dots & {}^0h_{12,3}^2 \\ {}^0h_{1,3}^3 & {}^0h_{2,3}^3 & {}^0h_{3,3}^3 & \dots & {}^0h_{12,3}^3 \end{bmatrix}$$

4. 2nd Piola-Kirchhoff stress matrix and vector

$${}^0\bar{\mathbf{S}} = \begin{bmatrix} {}^0\bar{\mathbf{S}}_{11}\mathbf{I}_3 & \text{symmetric} \\ {}^0\bar{\mathbf{S}}_{12}\mathbf{I}_3 & \mathbf{0} \\ {}^0\bar{\mathbf{S}}_{13}\mathbf{I}_3 & \mathbf{0} & \mathbf{0} \end{bmatrix}; \quad {}^0\bar{\mathbf{S}} = \begin{bmatrix} {}^0\bar{\mathbf{S}}_{11} \\ {}^0\bar{\mathbf{S}}_{12} \\ {}^0\bar{\mathbf{S}}_{13} \end{bmatrix}$$

where \mathbf{I}_3 is a 3×3 identity matrix.

B. UPDATED LAGRANGIAN FORMULATION

1. Incremental strains

$$\begin{aligned} {}_i\bar{\epsilon}_{ij} &= {}_i\bar{\epsilon}_{ij} + {}_i\bar{\eta}_{ij} \\ {}_i\bar{\epsilon}_{11} &= {}_i\bar{u}_{1,1} + \frac{1}{2}[({}_i\bar{u}_{1,1})^2 + ({}_i\bar{u}_{2,1})^2 + ({}_i\bar{u}_{3,1})^2] \\ {}_i\bar{\epsilon}_{12} &= \frac{1}{2}[{}_i\bar{u}_{1,2} + {}_i\bar{u}_{2,1}] + \frac{1}{2}[{}_i\bar{u}_{1,1}{}_i\bar{u}_{1,2} + {}_i\bar{u}_{3,1}{}_i\bar{u}_{3,2}] \\ {}_i\bar{\epsilon}_{13} &= \frac{1}{2}[{}_i\bar{u}_{1,3} + {}_i\bar{u}_{3,1}] + \frac{1}{2}[{}_i\bar{u}_{1,1}{}_i\bar{u}_{1,3} + {}_i\bar{u}_{2,1}{}_i\bar{u}_{2,3}] \end{aligned}$$

where

$${}_i\bar{u}_{i,j} = \frac{\partial {}_i\bar{u}_i}{\partial {}_i\bar{x}_j}; \quad {}_i\bar{x}_j \quad (j = 1, 2, 3) \equiv r, s, t$$

2. Linear strain-displacement transformation matrix

Using

$${}_i\bar{\mathbf{e}} = {}^i\bar{\mathbf{B}}_L \cdot {}_i\bar{\mathbf{u}}$$

where

$${}_i\bar{\mathbf{e}}^T = [{}_i\bar{\epsilon}_{11} \quad 2{}_i\bar{\epsilon}_{12} \quad 2{}_i\bar{\epsilon}_{13}]$$

and

$${}_i\bar{\mathbf{u}} = {}^i\mathbf{R} \mathbf{u}$$

In order to evaluate the strain increments it is also necessary to calculate the derivatives of the total displacements. The kinematics of the rigid body rotations of the beam give

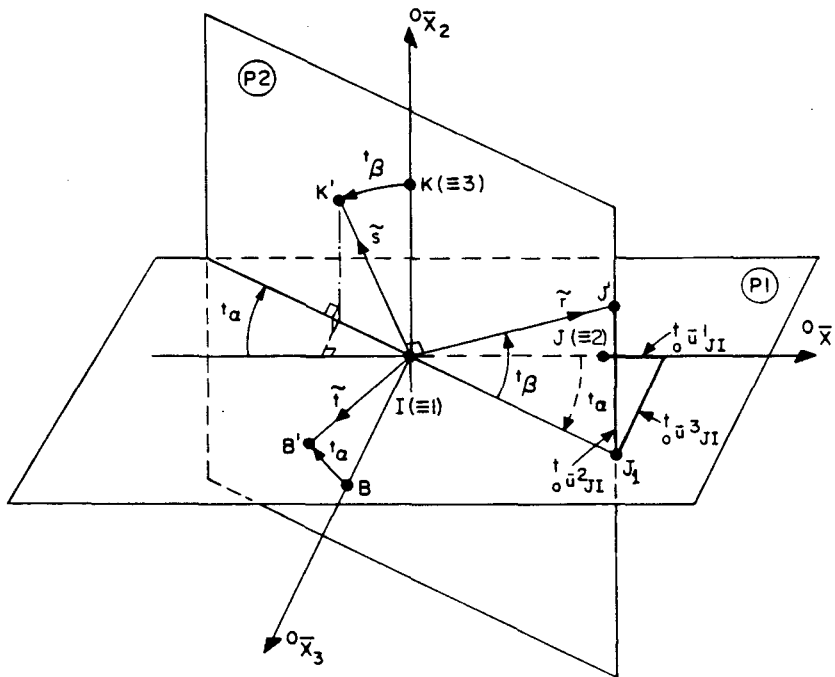
$${}^t_0\bar{u}_{i,j} = {}^t\bar{R}_{ij} - \delta_{ij} \quad \begin{matrix} (i = 1, 2, 3) \\ (j = 1, 2, 3) \end{matrix} \quad (20)$$

where the ${}^t\bar{R}_{ij}$ are the direction cosines of the ${}^t\bar{x}_i$ axes with respect to the ${}^0\bar{x}_j$ axes, as defined in equation (23), and δ_{ij} is the Kronecker delta.

Transformation between current and original beam co-ordinate axes

In the U.L. and T.L. formulations a transformation matrix ${}^t\bar{\mathbf{R}}$ that relates displacements measured in the current configuration to displacements measured in the original configuration is needed.

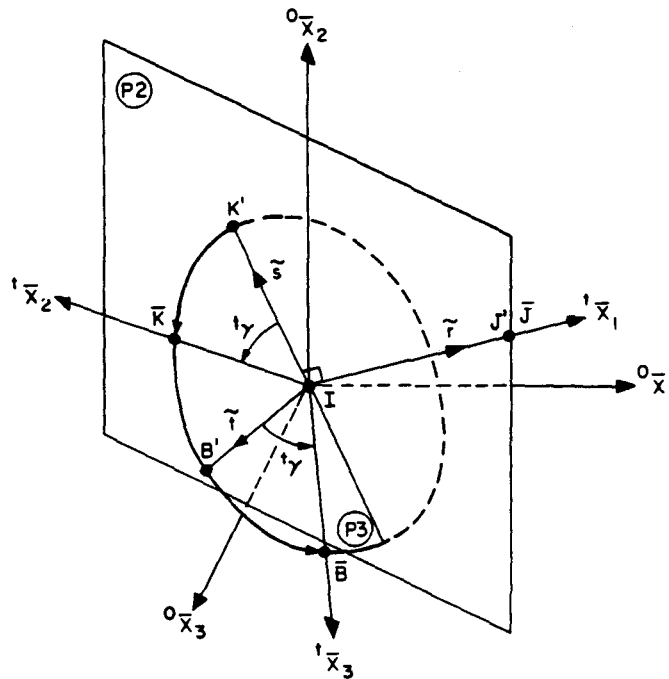
The ${}^t\bar{\mathbf{R}}$ transformation matrix is evaluated using Euler angles which define the rotations of the beam. These angles are shown in Figures 4(a) and 4(b). To arrive at the information given in this illustration it is required first to evaluate the relative translational displacements of nodes



${}^t\alpha$ = ROTATION OF COORDINATE AXES ABOUT ${}^0\bar{x}_2$ AXIS
 $({}^0\bar{x}_1, {}^0\bar{x}_2, {}^0\bar{x}_3)$ TO $(\bar{I}\bar{J}_1, {}^0\bar{x}_2, \bar{t})$
 ${}^t\beta$ = ROTATION OF COORDINATE AXES ABOUT \bar{t} AXIS
 $(\bar{I}\bar{J}_1, {}^0\bar{x}_2, \bar{t})$ TO $(\bar{t}, \bar{s}, \bar{t})$

PLANE P1 IS PERPENDICULAR TO PLANE P2

Figure 4(a). Rotation of beam element co-ordinate axes in large displacement analysis (first step).



γ = ROTATION OF COORDINATE AXES ABOUT \tilde{r} AXIS
 $(\tilde{r}, \tilde{s}, \tilde{y})$ TO $({}^1\bar{x}_1, {}^1\bar{x}_2, {}^1\bar{x}_3)$

PLANE P3 IS PERPENDICULAR TO \tilde{r} AXIS

Figure 4(b). Rotation of beam element co-ordinate axes in large displacement analysis (final step).

1 and 2 measured in the beam original co-ordinate system. Denoting for clarity nodes 1 and 2 as nodes I and J , these relative displacements are evaluated as

$${}^i\bar{u}_{JI}^i = {}^0R_{ij}({}^i u^{j+6} - {}^i u^j) \quad \left(\begin{array}{l} i = 1, 2, 3 \\ \text{sum on } j = 1, 2, 3 \end{array} \right) \quad (21)$$

where the ${}^i u^k$ are the element nodal point displacements measured in the global co-ordinate system, and the ${}^0R_{ij}$ are components of the matrix ${}^0\mathbf{R}$ that transforms the global nodal point displacements to the element local axes at time 0.

The components of the matrix ${}^i\bar{\mathbf{R}}$ are then constructed from the direction cosines of the axes ${}^i\bar{x}_i$ ($i = 1, 2, 3$) with respect to the axes ${}^0\bar{x}_j$ ($j = 1, 2, 3$). We have

$${}^i\bar{\mathbf{R}} = \begin{bmatrix} {}^i\bar{\mathbf{R}} & & 0 \\ & {}^i\bar{\mathbf{R}} & \\ 0 & & {}^i\bar{\mathbf{R}} \end{bmatrix} \quad (22)$$

where ${}^i\bar{\mathbf{R}}$ is a matrix of order 3×3 ,

$${}^i\bar{\mathbf{R}} = {}^i\bar{\mathbf{R}}^a {}^i\bar{\mathbf{R}}^d \quad (23)$$

In equation (23) ${}^t\bar{\mathbf{R}}^d$ is the transformation matrix due to the relative translational displacements of nodes J and I , and ${}^t\bar{\mathbf{R}}^a$ is the transformation matrix that takes into account the axial rotation of the beam.

The components of the matrix ${}^t\bar{\mathbf{R}}^d$ are the direction cosines of the axes $\tilde{r}, \tilde{s}, \tilde{t}$ with respect to ${}^0\bar{x}_i$ ($i = 1, 2, 3$). These components are

$${}^t\bar{\mathbf{R}}^d = \begin{bmatrix} \cos({}^t\alpha) \cos({}^t\beta) & \sin({}^t\beta) & \sin({}^t\alpha) \cos({}^t\beta) \\ -\cos({}^t\alpha) \sin({}^t\beta) & \cos({}^t\beta) & -\sin({}^t\alpha) \sin({}^t\beta) \\ -\sin({}^t\alpha) & 0 & \cos({}^t\alpha) \end{bmatrix} \quad (24)$$

where the angle ${}^t\alpha$ represents the rotation about the (negative) ${}^0\bar{x}_2$ axis

$$\cos({}^t\alpha) = \frac{{}^0L + {}^t\bar{u}_{JI}^1}{{}^t\bar{L}_1} \quad (25)$$

and 0L is the original length of the beam,

$${}^t\bar{L}_1 = \{({}^0L + {}^t\bar{u}_{JI}^1)^2 + ({}^t\bar{u}_{JI}^3)^2\}^{1/2} \quad (26)$$

The angle ${}^t\beta$ represents the rotation about the positive \tilde{t} direction;

$$\sin({}^t\beta) = \frac{{}^t\bar{u}_{JI}^2}{{}^tL} \quad (27)$$

where

$${}^tL = \{({}^t\bar{L}_1)^2 + ({}^t\bar{u}_{JI}^2)^2\}^{1/2} \quad (28)$$

The components of the ${}^t\bar{\mathbf{R}}^a$ matrix, which are the direction cosines between ${}^t\bar{x}_i$ ($i = 1, 2, 3$) and the $\tilde{r}, \tilde{s}, \tilde{t}$ axes are computed using

$${}^t\bar{\mathbf{R}}^a = \begin{bmatrix} 1 & 0 & 0 \\ 0 & \cos({}^t\gamma) & \sin({}^t\gamma) \\ 0 & -\sin({}^t\gamma) & \cos({}^t\gamma) \end{bmatrix} \quad (29)$$

where ${}^t\gamma$ is the rigid body rotation of the beam about the \tilde{r} -axis in the configuration at time t . This angle is calculated using

$$\begin{aligned} \gamma &= \frac{1}{2}\{({}^t\bar{u}^4 + {}^t\bar{u}^{10})\} \\ &= \frac{1}{2}\{{}^t\bar{\mathbf{R}}_{11}^d ({}^0\bar{u}^4 + {}^0\bar{u}^{10}) + {}^t\bar{\mathbf{R}}_{12}^d ({}^0\bar{u}^5 + {}^0\bar{u}^{11}) + {}^t\bar{\mathbf{R}}_{13}^d ({}^0\bar{u}^6 + {}^0\bar{u}^{12})\} \end{aligned} \quad (30)$$

and then

$${}^t\gamma = {}^{t-\Delta t}\gamma + \gamma \quad (31)$$

Substituting the relations in equations (23)–(31) into equation (22) we obtain the transformation matrix between the beam local axes at times t and 0 .

Calculation of beam element stresses

In the development of the incremental U.L. and T.L. equilibrium equations corresponding to time t , we assumed that the stress components corresponding to the configuration at time t are known (see Table I). The solution of the incremental equations (14) and (15) will then yield nodal point displacement increments, from which the corresponding stress increments must be calculated. These stress increments are added to the stress components at time t to obtain the stress components corresponding to time $t + \Delta t$.

To evaluate the stress increments accurately it is realized that the tangent approximation in the strain-displacement relation for the normal strain, as employed in the ${}^i\bar{\mathbf{B}}_L$ and ${}^0\bar{\mathbf{B}}_L$ matrices, does not yield an increment in normal strain if the element deflects transversely without bending. However, for large displacement analysis, the corresponding extension of the element is taken into account in the incremental strains using in the U.L. formulation

$${}^i\bar{e}_{1i} = \sum_{\substack{j=2 \\ j \neq 7}}^N {}^i\bar{\mathbf{B}}_{L_{ij}} \bar{u}^j + ({}^i\bar{e}_{11} - {}^{i-\Delta t}\bar{e}_{11})\delta_{1i} \quad (32)$$

where the ${}^i\bar{\mathbf{B}}_{L_{ij}}$ are the components of the linear strain-displacement matrix given in Table III(B) and δ_{ij} is the Kronecker delta; also

$${}^i\bar{e}_{11} = ({}^iL - {}^0L)/{}^0L$$

Using the T.L. formulation the corresponding calculations are

$${}^0\bar{e}_{1i} = \sum_{j=1}^{12} {}^0\bar{\mathbf{B}}_{L_{ij}} {}^0\bar{u}^j + ({}^i\bar{e}_{11} - {}^{i-\Delta t}\bar{e}_{11})\delta_{1i} \quad (33)$$

where the constraints

$${}^0\bar{u}^1 = ({}^i\bar{\mathbf{R}}_{12} {}^0\bar{u}^2 + {}^i\bar{\mathbf{R}}_{13} {}^0\bar{u}^3)/{}^i\bar{\mathbf{R}}_{11}; \quad {}^0\bar{u}^7 = ({}^i\bar{\mathbf{R}}_{12} {}^0\bar{u}^8 + {}^i\bar{\mathbf{R}}_{13} {}^0\bar{u}^9)/{}^i\bar{\mathbf{R}}_{11} \quad (34)$$

should be imposed to evaluate the appropriate normal strains.

With the incremental strains known, the corresponding stress increments can be calculated as usual.¹⁵ In general large displacement and elastic-plastic analysis, the stiffness matrices and nodal point force vectors must be evaluated using numerical integration. Also, to improve the solution accuracy it may be necessary to employ equilibrium iterations in the incremental solution. The iterative equations are directly obtained from equations (14) and (15) in the usual manner.¹²

COMPARISON OF T.L. AND U.L. FORMULATIONS

In the T.L. formulation the reference co-ordinate system used is given by the element principal axes of inertia in the configuration at time 0, ${}^0\bar{x}_i$ ($i = 1, 2, 3$). Therefore, the complete stiffness matrix (including the linear and nonlinear strain stiffness matrices), the nodal point force vector and the local displacement increments are referred to this co-ordinate system and must be transformed to the global co-ordinate system 0x_i ($i = 1, 2, 3$):

$$\begin{aligned} {}^0\mathbf{K} &= {}^0\mathbf{R}^T {}^i\bar{\mathbf{K}} {}^0\mathbf{R} \\ {}^0\mathbf{F} &= {}^0\mathbf{R}^T {}^i\bar{\mathbf{F}} \\ \mathbf{u} &= {}^0\mathbf{R}^T {}^0\bar{\mathbf{u}} \end{aligned} \quad (35)$$

where ${}^0\mathbf{R}$ is the transformation matrix that expresses the nodal point displacements measured in the beam local co-ordinate system ${}^0\bar{x}_i$ ($i = 1, 2, 3$) in terms of the global nodal point displacements.

The reference co-ordinate system used in the U.L. formulation is defined by the principal axes of the beam element in the position at time t , i.e. ${}^t\bar{x}_i$ ($i = 1, 2, 3$). Therefore, the local stiffness matrix and the nodal point force vector are referred to this co-ordinate system. These

matrices are transformed to the global co-ordinate system using

$$\begin{aligned} {}^i\mathbf{K} &= {}^i\mathbf{R}^T {}^i\bar{\mathbf{K}} {}^i\mathbf{R} \\ {}^i\mathbf{F} &= {}^i\mathbf{R}^T {}^i\bar{\mathbf{F}} \\ \mathbf{u} &= {}^i\mathbf{R}^T \bar{\mathbf{u}} \\ {}^i\mathbf{R} &= {}^i\bar{\mathbf{R}} {}^0\mathbf{R} \end{aligned} \quad (36)$$

where ${}^i\bar{\mathbf{R}}$ is the transformation matrix relating the co-ordinate systems ${}^i\bar{x}_i$ and ${}^0\bar{x}_i$ ($i = 1, 2, 3$), as defined in equation (22).

The principal difference between the U.L. and the T.L. formulations is that in the T.L. formulation the transformation on the interpolation functions in equation (18) is carried out to refer the displacement interpolations to the original configuration, and the ${}^0\bar{\mathbf{B}}_{L1}$ matrix is included in the calculations. The transformations on the interpolation functions and the use of the ${}^0\bar{\mathbf{B}}_{L1}$ matrix in the T.L. formulation together are equivalent to the additional transformation matrix ${}^i\bar{\mathbf{R}}$ that is employed in equation (36) in the U.L. formulation. Indeed, as shown in more detail in the Appendix, using these formulations the same element stiffness matrices and nodal point force vectors are obtained.

Although the same final element stiffness matrices and nodal point force vectors are generated in the two formulations, it is noted that using numerical integration the transformation on the interpolation functions in equation (18) and the evaluation of the ${}^0\bar{\mathbf{B}}_{L1}$ matrix is carried out at each integration point. Therefore, the U.L. formulation is computationally more effective.

SAMPLE SOLUTIONS

The updated Lagrangian-based beam element was implemented in the computer program ADINA¹⁷ and a number of sample analyses were carried out. We report here the results of some of the analyses. In these analyses the beam linear strain stiffness matrices ${}^i\bar{\mathbf{K}}_L$ were evaluated in closed form, and the nonlinear strain stiffness matrices ${}^i\bar{\mathbf{K}}_{NL}$ and force vectors ${}^i\bar{\mathbf{F}}$ (see Table I) were evaluated using Newton-Cotes integration¹⁶. Also, in all analyses beam shear deformations were neglected.

Large deflection analysis of a shallow arch

The clamped circular arch with a single static load at the apex was analysed for buckling using the beam element, as shown in Figure 5. The material of the arch was assumed to be isotropic linear elastic. One half of the arch was idealized using 6, 12 and 18 equal beam elements. The same arch was also analysed using eight six-node isoparametric elements with 2×2 Gauss integration.

This arch was also analysed by Mallet and Berke, who used four 'equilibrium-based' elements.¹⁰ Dupuis *et al.*¹¹ analysed the same arch using curved beam elements, and used this example to demonstrate the convergence of their 'Lagrangian' and 'updated' formulations.

Figure 5 shows the predicted load-deflection curve of the arch. It is observed that in this analysis the use of the beam elements is quite effective.

Large deflection and rotation analyses of a cantilever beam

The objective in this analysis was to investigate the performance of the beam element in large displacement and rotation problems. Two problems were analysed. First, a large deflection and

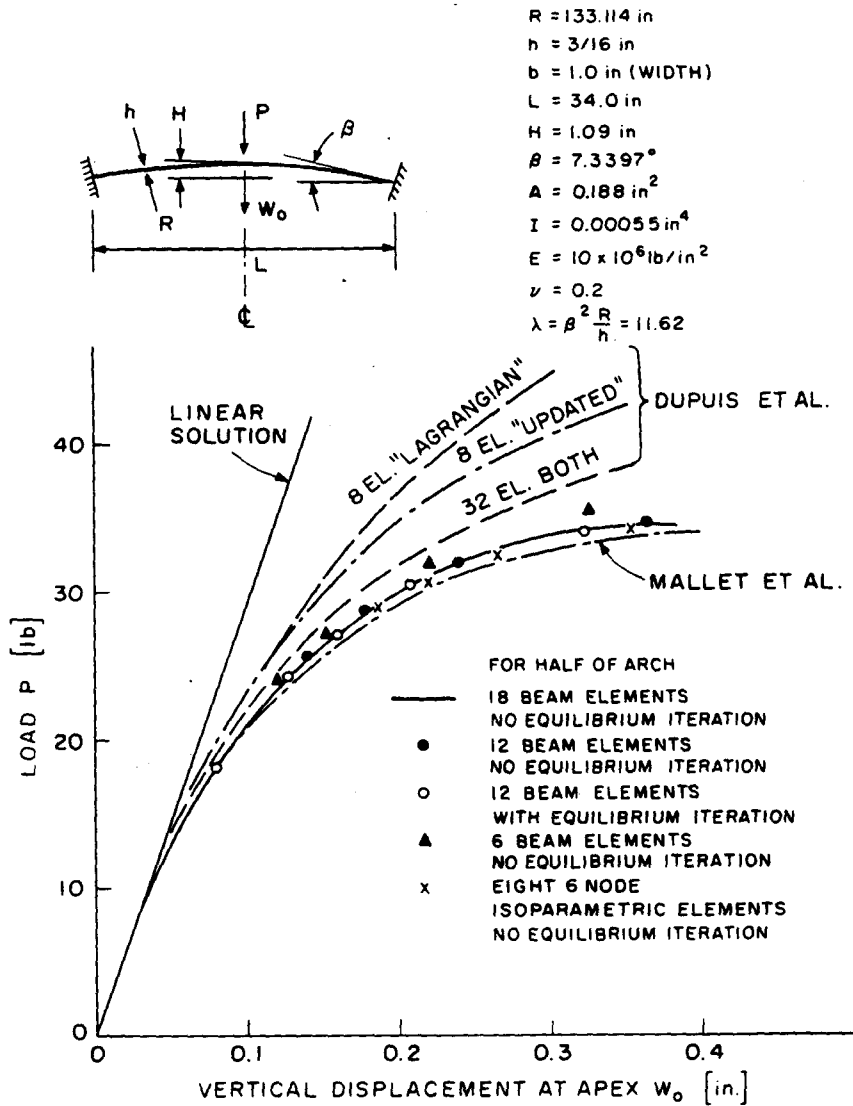


Figure 5. Large deflection analysis of shallow arch under concentrated load.

moderate rotation analysis of a clamped cantilever with a concentrated end load was carried out as shown in Figure 6. The second problem was the large displacement and large rotation analysis of a cantilever beam subjected to a concentrated end moment (Figure 7).

In the cantilever analysis subjected to the concentrated tip load, the objective was to demonstrate the effects of the aspect ratio of an element on its performance in the geometric nonlinear range. Figure 6 shows the response predicted by ADINA using four different models and an analytical solution.⁹ It is noted that the cantilever models using beam elements and two-dimensional isoparametric elements (2×2 Gauss integration), with an aspect ratio of 2, predict responses quite close to the analytical solution, and that the performance of the

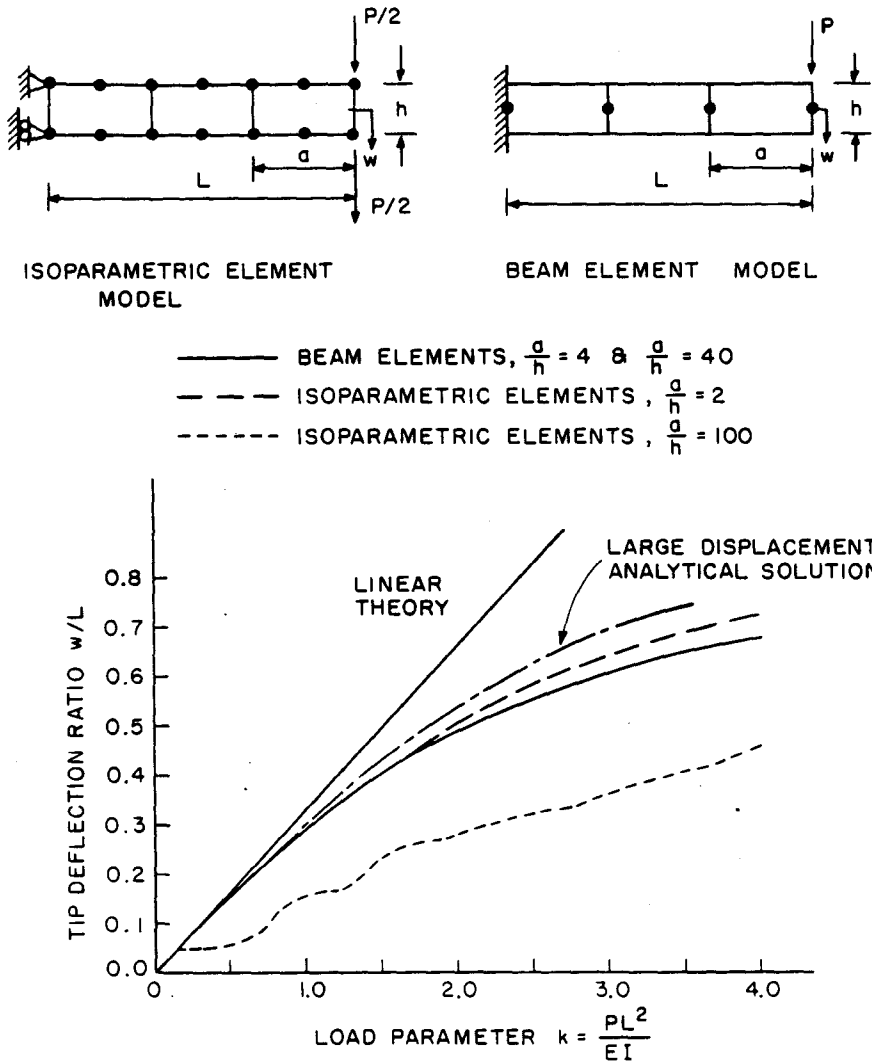


Figure 6. Large deflection analysis of a cantilever subjected to a concentrated load.

beam element does not change with its aspect ratio. However, as is well known, the predicted response using two-dimensional isoparametric elements deviates from the analytical solution with increasing element aspect ratios.

Figure 7 shows the results obtained in the analysis of the cantilever subjected to an end moment. The cantilever was modelled using 5 and 20 beam elements. The figure shows that the predicted response compares well with the analytical solution up to 90 degrees rotation.¹⁸ It is also seen that as the number of elements increases the numerically predicted response improves. This increase in accuracy is due to the fact that the geometry of the deformed cantilever is defined more accurately with a larger number of elements.

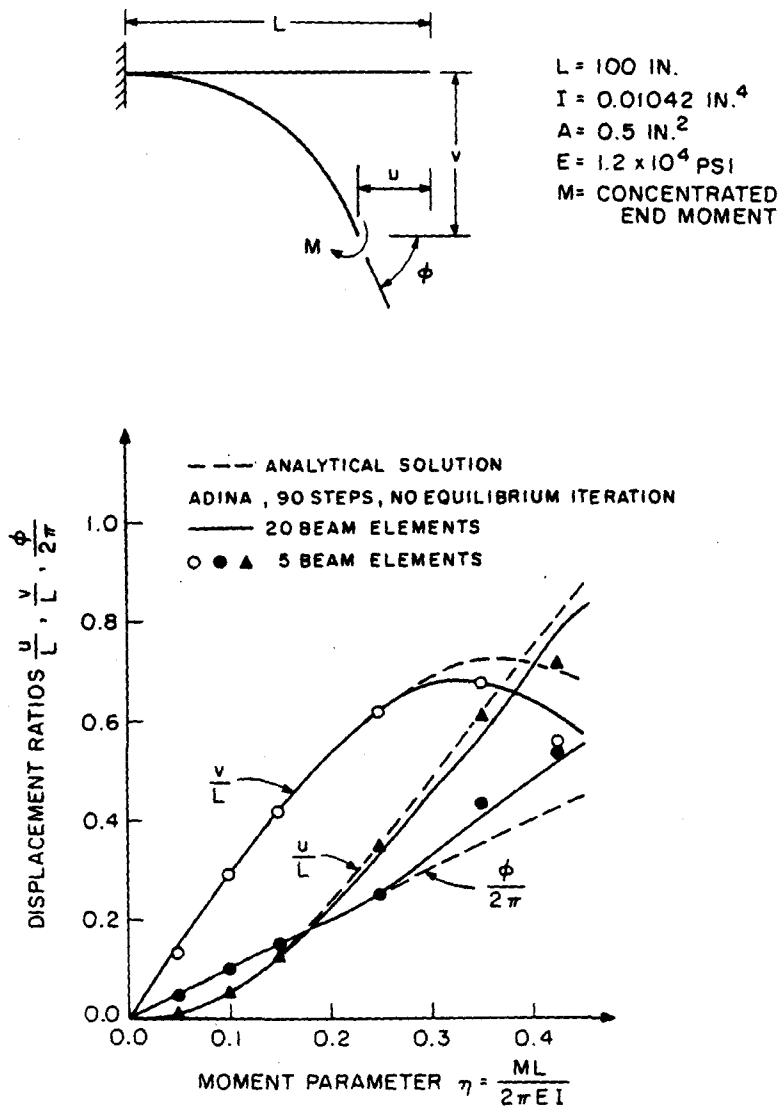


Figure 7. Moment-deflection curve.

Large displacement three-dimensional analysis of a 45-degree bend

The large displacement response of a cantilever 45-degree bend subjected to a concentrated end load, as shown in Figure 8, was calculated. The bend has an average radius of 100 in, cross-sectional area 1 in^2 and lies in the X - Y plane. The concentrated tip load is applied into the Z -direction.

The bend was idealized using 8 equal straight beam elements and 16 sixteen-node three-dimensional solid elements. For the beam elements the Newton-Cotes formula of order $3 \times 3 \times 3$ was used and, for the isoparametric elements, Gauss integration of order $2 \times 2 \times 2$ was employed.¹⁶ The material was assumed to be linear elastic.

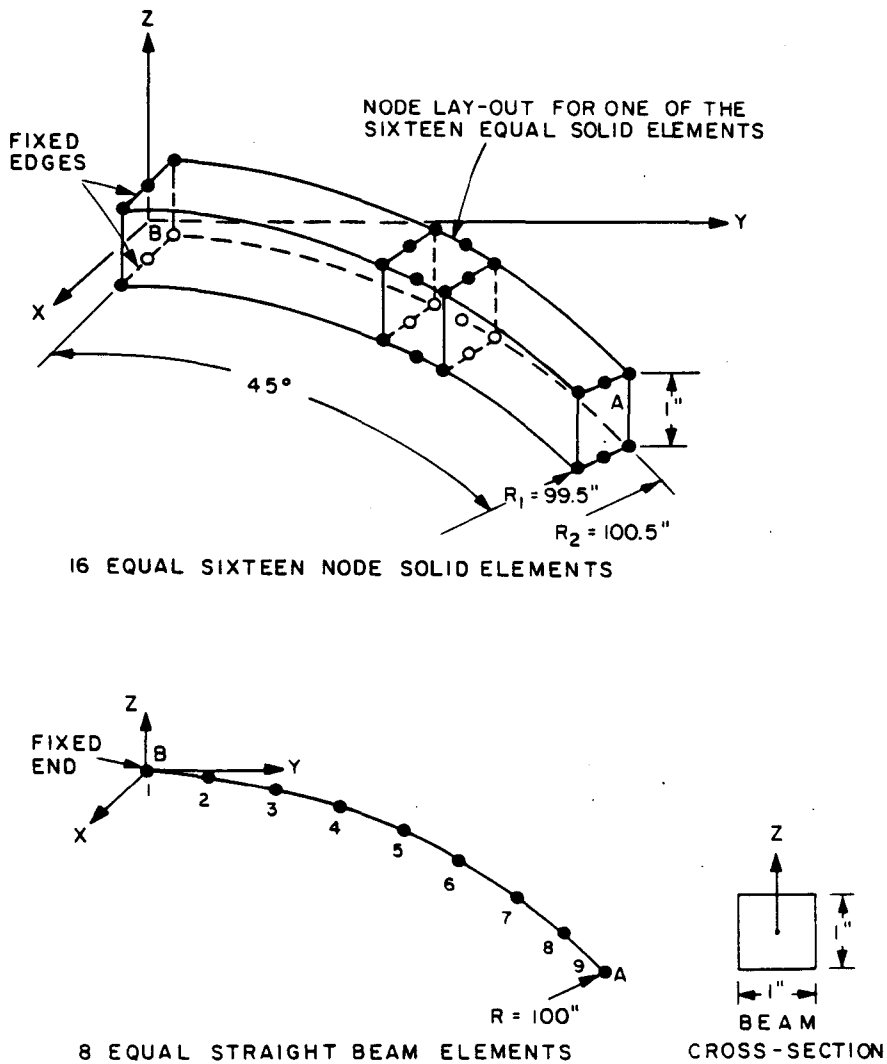


Figure 8. Finite element modelling of a 45-degree circular bend.

Figure 9 shows the tip deflection predicted by ADINA using the two finite element models. To the accuracy that can be shown in the illustration, the same response is predicted using the beam element idealization and the isoparametric element discretization. The deflected shapes of the bend at various load levels are shown in Figure 10.

CONCLUSIONS

To develop capabilities for large displacement and large rotation analysis of beam structures, an updated Lagrangian and a total Lagrangian formulation of a geometric nonlinear beam element

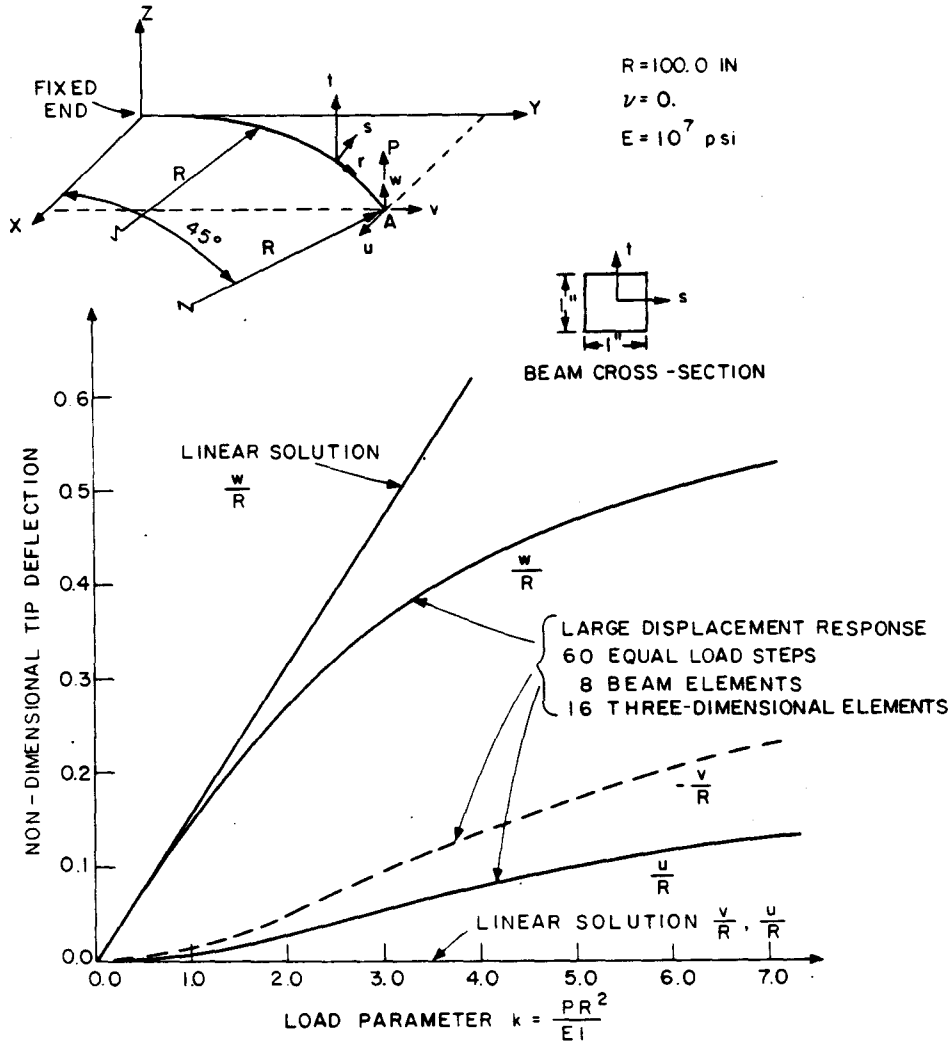


Figure 9. Three-dimensional large deflection analysis of a 45-degree circular bend.

have been presented. The incremental displacement fields within the straight two-noded beam element are defined using the usual beam displacement functions. It has been shown that the two formulations yield identical element stiffness matrices and nodal point force vectors, and that the updated Lagrangian formulation is computationally more effective. This formulation can be used efficiently for the general nonlinear analysis of beam structures.

ACKNOWLEDGEMENT

The work reported in this paper has been supported financially by the ADINA users group. We would like to acknowledge gratefully this support.

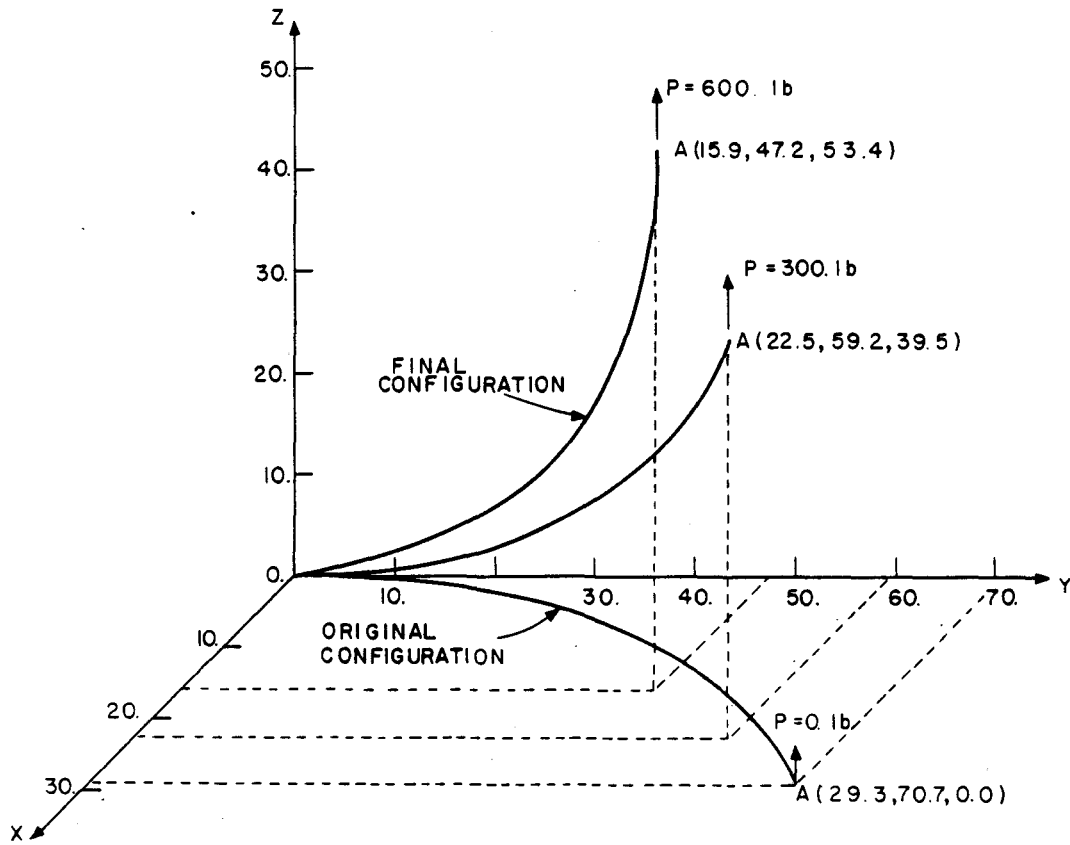


Figure 10. Deformed configurations of a 45-degree circular bend.

APPENDIX: DETAILED COMPARISON OF BEAM T.L. AND U.L. FORMULATIONS

In the text we showed that the U.L. formulation is more effective than the T.L. formulation for beam analysis. The objective in this appendix is to compare the T.L. and U.L. formulations presented in detail. Assume that the beam is deformed to the configuration at time t , as shown in Figure 3. It is shown in this appendix that all element matrices are identical in both formulations.

Linear strain stiffness matrices

Consider first the *T.L. formulation*. The initial displacement effect is taken into account using equation (20). Thus we have corresponding to Table III(A)

$$l_{ij} = {}^t\bar{R}_{ij} - \delta_{ij} \quad \begin{matrix} (i = 1, 2, 3) \\ (j = 1, 2, 3) \end{matrix} \quad (37)$$

The ${}^t\bar{R}_{ij}$ are the direction cosines of the ${}^t\bar{x}_i$ axes with respect to the ${}^0\bar{x}_i$ axes defined in equation (23), and δ_{ij} is the Kronecker delta. Using equation (37) the ${}^0\bar{\mathbf{B}}_{L1}$ matrix defined in Table III(A) is

$${}^0\bar{\mathbf{B}}_{L1} = \begin{bmatrix} ({}^t\bar{R}_{11} - 1) {}^0\mathbf{h}_{,1}^1 + {}^t\bar{R}_{21} {}^0\mathbf{h}_{,1}^2 + {}^t\bar{R}_{31} {}^0\mathbf{h}_{,1}^3 \\ ({}^t\bar{R}_{11} - 1) {}^0\mathbf{h}_{,2}^1 + {}^t\bar{R}_{12} {}^0\mathbf{h}_{,1}^1 + {}^t\bar{R}_{21} {}^0\mathbf{h}_{,2}^2 + ({}^t\bar{R}_{22} - 1) {}^0\mathbf{h}_{,2}^2 + {}^t\bar{R}_{31} {}^0\mathbf{h}_{,2}^3 + {}^t\bar{R}_{32} {}^0\mathbf{h}_{,1}^3 \\ ({}^t\bar{R}_{11} - 1) {}^0\mathbf{h}_{,3}^1 + {}^t\bar{R}_{13} {}^0\mathbf{h}_{,1}^1 + {}^t\bar{R}_{21} {}^0\mathbf{h}_{,3}^2 + {}^t\bar{R}_{23} {}^0\mathbf{h}_{,1}^2 + {}^t\bar{R}_{31} {}^0\mathbf{h}_{,3}^3 + ({}^t\bar{R}_{33} - 1) {}^0\mathbf{h}_{,1}^3 \end{bmatrix} \quad (38)$$

where (not considering shear deformations)

$${}^0\mathbf{h}^i_j = [{}^0h^i_{1,j} \ 0h^i_{2,j} \ \dots \ 0h^i_{12,j}] \tag{39}$$

Adding the ${}^i\bar{\mathbf{B}}_{L1}$ matrix of equation (38) to the matrix ${}^i\bar{\mathbf{B}}_{L0}$ defined in Table III(A) yields the linear strain-displacement matrix,

$${}^i\bar{\mathbf{B}}_L = \begin{bmatrix} {}^i\bar{\mathbf{R}}_{11} & {}^i\bar{\mathbf{R}}_{21} & {}^i\bar{\mathbf{R}}_{31} & 0 & 0 & 0 & 0 & 0 & 0 \\ {}^i\bar{\mathbf{R}}_{12} & {}^i\bar{\mathbf{R}}_{22} & {}^i\bar{\mathbf{R}}_{32} & {}^i\bar{\mathbf{R}}_{11} & {}^i\bar{\mathbf{R}}_{21} & {}^i\bar{\mathbf{R}}_{31} & 0 & 0 & 0 \\ {}^i\bar{\mathbf{R}}_{13} & {}^i\bar{\mathbf{R}}_{23} & {}^i\bar{\mathbf{R}}_{33} & 0 & 0 & 0 & {}^i\bar{\mathbf{R}}_{11} & {}^i\bar{\mathbf{R}}_{21} & {}^i\bar{\mathbf{R}}_{31} \end{bmatrix} \begin{bmatrix} {}^0\mathbf{H}_{,1} \\ {}^0\mathbf{H}_{,2} \\ {}^0\mathbf{H}_{,3} \end{bmatrix} \tag{40}$$

where we define

$${}^r\mathbf{H}_{,i} = \begin{bmatrix} {}^r\mathbf{h}^1_{,i} \\ {}^r\mathbf{h}^2_{,i} \\ {}^r\mathbf{h}^3_{,i} \end{bmatrix} \quad (\tau = 0, t) \tag{41}$$

The derivatives of the interpolation functions ${}^0h^i_k$ defined in equation (18) are

$${}^0h^i_{k,j} = \sum_{m=1}^3 \sum_{n=1}^{12} {}^i\bar{\mathbf{R}}_{im} {}^r\mathbf{h}^m_{n,i} {}^i\bar{\mathbf{R}}_{nk} \quad \begin{matrix} (i = 1, 2, 3) \\ (j = 1, 2, 3) \end{matrix} \tag{42}$$

where the incremental interpolation functions ${}^r\mathbf{h}^m$ are defined in Table III. Equations (42) may be rewritten in matrix form

$$\begin{bmatrix} {}^0\mathbf{H}_{,1} \\ {}^0\mathbf{H}_{,2} \\ {}^0\mathbf{H}_{,3} \end{bmatrix} = \begin{bmatrix} {}^i\bar{\mathbf{R}} & \mathbf{0} & \mathbf{0} \\ \mathbf{0} & {}^i\bar{\mathbf{R}} & \mathbf{0} \\ \mathbf{0} & \mathbf{0} & {}^i\bar{\mathbf{R}} \end{bmatrix} \begin{bmatrix} {}^r\mathbf{H}_{,1} \\ {}^r\mathbf{H}_{,2} \\ {}^r\mathbf{H}_{,3} \end{bmatrix} {}^i\bar{\mathbf{R}} \tag{43}$$

where ${}^i\bar{\mathbf{R}}$ and ${}^i\bar{\mathbf{R}}$ are defined in equations (22) and (23), respectively. Substituting equations (43) into equation (40) and simplifying gives,

$${}^i\bar{\mathbf{B}}_L = \begin{bmatrix} {}^r\mathbf{h}^1_{,1} \\ ({}^r\mathbf{h}^2_{,1} + {}^r\mathbf{h}^1_{,2}) \\ ({}^r\mathbf{h}^3_{,1} + {}^r\mathbf{h}^1_{,3}) \end{bmatrix} {}^i\bar{\mathbf{R}} \tag{44}$$

In the *U.L. formulation* the geometric linear strain-displacement matrix is given in Table III(B)

$${}^i\bar{\mathbf{B}}_L = \begin{bmatrix} {}^r\mathbf{h}^1_{,1} \\ ({}^r\mathbf{h}^2_{,1} + {}^r\mathbf{h}^1_{,2}) \\ ({}^r\mathbf{h}^3_{,1} + {}^r\mathbf{h}^1_{,3}) \end{bmatrix} \tag{45}$$

Comparing equations (44) and (45) yields

$${}^i\bar{\mathbf{B}}_L = {}^i\bar{\mathbf{B}}_L {}^i\bar{\mathbf{R}} \tag{46}$$

Substituting the above relation into Table I to evaluate the linear strain stiffness matrices in both formulations, and comparing, we obtain

$${}^i\bar{\mathbf{K}}_L = {}^i\bar{\mathbf{R}}^T {}^i\bar{\mathbf{K}}_L {}^i\bar{\mathbf{R}} \tag{47}$$

Therefore the two formulations lead to identical linear-strain stiffness matrices corresponding to the global co-ordinate system.

Nodal point force vectors

The components of the Cauchy stress tensor referred to the ${}^i x_i$ axes are numerically equal to the components of the 2nd Piola–Kirchhoff stress tensor referred to the ${}^0 x_i$ axes, i.e. the stress vectors ${}^i \hat{\tau}$ and ${}^0 \hat{S}$ [as defined in Table III] are equal. It follows from equation (46), Table I and the above fact that the nodal point force vectors corresponding to the global axes are equal in both formulations.

Nonlinear strain stiffness matrices

The nonlinear strain–displacement matrix in the *T.L. formulation* is defined in Table III(A):

$${}^0 \bar{\mathbf{B}}_{NL} = \begin{bmatrix} {}^0 \mathbf{H}_{,1} \\ {}^0 \mathbf{H}_{,2} \\ {}^0 \mathbf{H}_{,3} \end{bmatrix} \tag{48}$$

Substituting equation (43) into (48) gives

$${}^0 \bar{\mathbf{B}}_{NL} = \begin{bmatrix} {}^i \bar{\mathbf{R}} & \mathbf{0} & \mathbf{0} \\ \mathbf{0} & {}^i \bar{\mathbf{R}} & \mathbf{0} \\ \mathbf{0} & \mathbf{0} & {}^i \bar{\mathbf{R}} \end{bmatrix} \begin{bmatrix} {}^i \mathbf{H}_{,1} \\ {}^i \mathbf{H}_{,2} \\ {}^i \mathbf{H}_{,3} \end{bmatrix} {}^i \bar{\mathbf{R}} \tag{49}$$

The geometric nonlinear stiffness matrix is evaluated as defined in Table I,

$${}^0 \bar{\mathbf{K}}_{NL} = {}^i \bar{\mathbf{R}}^T \left\{ \int_V \begin{bmatrix} {}^i \mathbf{H}_{,1} \\ {}^i \mathbf{H}_{,2} \\ {}^i \mathbf{H}_{,3} \end{bmatrix}^T \begin{bmatrix} {}^i \bar{\mathbf{R}} & \mathbf{0} & \mathbf{0} \\ \mathbf{0} & {}^i \bar{\mathbf{R}} & \mathbf{0} \\ \mathbf{0} & \mathbf{0} & {}^i \bar{\mathbf{R}} \end{bmatrix}^T {}^0 \bar{\mathbf{S}} \right. \tag{50}$$

$$\left. \begin{bmatrix} {}^i \bar{\mathbf{R}} & \mathbf{0} & \mathbf{0} \\ \mathbf{0} & {}^i \bar{\mathbf{R}} & \mathbf{0} \\ \mathbf{0} & \mathbf{0} & {}^i \bar{\mathbf{R}} \end{bmatrix} \begin{bmatrix} {}^i \mathbf{H}_{,1} \\ {}^i \mathbf{H}_{,2} \\ {}^i \mathbf{H}_{,3} \end{bmatrix} dv \right\} {}^i \bar{\mathbf{R}}$$

where the 2nd Piola–Kirchhoff stress matrix is given in Table III(A). We also have

$$\begin{bmatrix} {}^i \bar{\mathbf{R}} & \mathbf{0} & \mathbf{0} \\ \mathbf{0} & {}^i \bar{\mathbf{R}} & \mathbf{0} \\ \mathbf{0} & \mathbf{0} & {}^i \bar{\mathbf{R}} \end{bmatrix}^T {}^0 \bar{\mathbf{S}} \begin{bmatrix} {}^i \bar{\mathbf{R}} & \mathbf{0} & \mathbf{0} \\ \mathbf{0} & {}^i \bar{\mathbf{R}} & \mathbf{0} \\ \mathbf{0} & \mathbf{0} & {}^i \bar{\mathbf{R}} \end{bmatrix} = {}^0 \bar{\mathbf{S}} \tag{51}$$

and the ${}^i \mathbf{h}_{,2}^2$ and ${}^i \mathbf{h}_{,3}^3$ are null vectors. Thus equation (50) can be written as

$${}^0 \bar{\mathbf{K}}_{NL} = {}^i \bar{\mathbf{R}}^T \left\{ \int_V {}^i \bar{\mathbf{B}}_{NL}^T {}^0 \bar{\mathbf{S}} {}^i \bar{\mathbf{B}}_{NL} dv \right\} {}^i \bar{\mathbf{R}} \tag{52}$$

where the matrix ${}^i \bar{\mathbf{B}}_{NL}$ is defined in Table III(B), and

$${}^0 \bar{\mathbf{S}} = \begin{bmatrix} {}^i \bar{S}_{11} & & & & & & & \\ 0 & {}^i \bar{S}_{11} & & & & & & \\ 0 & 0 & {}^i \bar{S}_{11} & & & & & \\ {}^i \bar{S}_{12} & 0 & 0 & 0 & & & & \\ 0 & 0 & {}^i \bar{S}_{12} & 0 & 0 & & & \\ {}^i \bar{S}_{13} & 0 & 0 & 0 & 0 & 0 & & \\ 0 & {}^i \bar{S}_{13} & 0 & 0 & 0 & 0 & 0 & 0 \end{bmatrix} \tag{53}$$

Symmetric

The geometric nonlinear stiffness matrix based on the *U.L. formulation* is evaluated by using the matrices of Table III,

$${}^i\bar{\mathbf{K}}_{NL} = \int_V {}^i\bar{\mathbf{B}}_{NL}^T {}^i\bar{\boldsymbol{\tau}} {}^i\bar{\mathbf{B}}_{NL} dV \quad (54)$$

Since the stress vectors ${}^i\bar{\boldsymbol{\tau}}$ and ${}^i_0\hat{\mathbf{S}}$ are numerically identical for the beam element we have

$${}^i_0\bar{\mathbf{K}}_{NL} = {}^i\bar{\mathbf{R}}^T {}^i\bar{\mathbf{K}}_{NL} {}^i\bar{\mathbf{R}} \quad (55)$$

Therefore the two formulations lead to identical nonlinear strain stiffness matrices corresponding to the global co-ordinate system.

REFERENCES

1. J. H. Argyris and P. C. Dunne, 'A simple theory of geometrical stiffness with application to beam and shell problems', *2nd Int. Symp. Computing Meth. Appl. Sci. & Engng*, Versailles, France (1975); *ISD-Report No. 183*, Univ. of Stuttgart (1975).
2. Z. P. Bazant and M. E. Nimeiri, 'Large-deflection spatial buckling of thin-walled beams and frames', *ASCE, J. Eng. Mech. Div.*, 10247-10281 (1973).
3. C. Oran and A. Kassimaili, 'Large deflection of framed structures under static and dynamic loads', *Comp. & Struct.* 6, 536-547 (1976).
4. R. W. H. Wu and E. A. Witmer, 'Nonlinear transient responses of structures by the spatial finite element method', *AIAA J.* 11(8), 1110-1117 (1973).
5. T. Y. Yang, 'Matrix displacement solution to elastica problems of beams and frames', *Int. J. Sol. Struct.* 9, 828-842 (1973).
6. C. Orean, 'Tangent stiffness in plane frames', *J. Struct. Div., ASCE*, 99 (ST6), 973-985 (1973).
7. T. Belytschko, L. Schwer and M. J. Klein, 'Large displacement transient analysis of space frames', *Int. J. Num. meth. Engng*, 11, 65-84 (1977).
8. S. Ranganath and R. J. Clifton, 'Finite deflection dynamics of elastic beams', *Int. J. Sol. Struct.* 10, 557-568 (1974).
9. J. T. Holden, 'On the finite deflections of thin beams', *Int. J. Sol. Struct.* 8, 1051-1055 (1972).
10. R. H. Mallet and L. Berke, 'Automated method for the large deflection and instability analysis of three-dimensional truss and frame assemblies', *AFFDL-TR-66-102*, (1966).
11. G. A. Dupuis, H. D. Hibbitt, S. F. McNamara and P. V. Marcal, 'Nonlinear material and geometric behavior of shell structures', *Comp. & Struct.* 1, 223-239 (1971).
12. K. J. Bathe, E. Ramm and E. L. Wilson, 'Finite element formulations for large deformation dynamic analysis', *Int. J. num. Meth. Engng*, 9, 353-386 (1975).
13. K. J. Bathe, 'An assessment of current finite element analysis of nonlinear problems in solid mechanics', *Symp. Num. Solutions of Partial Diff. Eqns*, Univ. Maryland (1975).
14. K. J. Bathe, 'Finite element formulation, modeling and solution of nonlinear dynamic problems', in *Numerical Methods for Partial Differential Equations* (Ed. S. V. Parter), Academic Press, 1979.
15. K. J. Bathe, 'Static and dynamic geometric and material nonlinear analysis using ADINA', *Report 82448-2*, Acoustics and Vibration Lab., Mechanical Engineering Dept., MIT (1977).
16. K. J. Bathe and E. L. Wilson, *Numerical Methods in Finite Element Analysis*, Prentice-Hall, Englewood Cliffs, N.J., 1976.
17. K. J. Bathe, 'ADINA - A finite element program for automatic dynamic incremental nonlinear analysis', *Report 82448-1*, Acoustics and Vibration Lab., Mechanical Engineering Dept., MIT (1977).
18. E. Ramm, 'A plate/shell element for large deflections and rotations', in *Formulations and Computational Algorithms in Finite Element Analysis*, (Eds. K. J. Bathe, J. T. Oden and W. Wunderlich), MIT Press, 1977.

A GEOMETRIC AND MATERIAL NONLINEAR PLATE AND SHELL ELEMENT

KLAUS-JÜRGEN BATHE and SAÏD BOLOURCHI

Department of Mechanical Engineering, Massachusetts Institute of Technology, Cambridge, MA 02139,
U.S.A.

(Received 13 June 1979)

Abstract—A displacement-based versatile and effective finite element is presented for linear and geometric and material nonlinear analysis of plates and shells. The element is formulated by interpolating the element geometry using the mid-surface nodal point coordinates and mid-surface nodal point normals. A total and an updated Lagrangian formulation are presented, that allow very large displacements and rotations. In linear analysis of plates, the element reduces to well-established plate bending elements based on classical plate theory, whereas in linear analysis of shells and geometrically nonlinear analysis of plates and shells by use of the element, in essence, a very general shell theory is employed. The element has been implemented as a variable-number-nodes element and can also be employed as a fully compatible transition element to model shell intersections and shell-solid regions. In the paper various sample solutions are presented that illustrate the effectiveness of the element in practical analysis.

1. INTRODUCTION

The analysis of plate and shell structures is of considerable interest in various areas of structural mechanics. It is, therefore, natural that with the development of the finite element method a large number of different finite elements have been formulated for the analysis of plate and shell problems. In these developments, basically two approaches have been followed: firstly, what may be called a classical procedure and, secondly, an approach in which displacement/rotation isoparametric elements are employed.

In the first approach a classical concept is employed, in which a plate or shell theory is used as the starting point of the finite element formulation. This plate or shell theory has been developed from the three-dimensional field equations by incorporating various assumptions appropriate to the structural behavior. Using variational formulations based on these theories various finite element models have been developed; namely, displacement, hybrid, and mixed formulations [1-5].

In the second approach, isoparametric elements with independent rotational and displacement degrees of freedom are employed. This procedure was originally introduced by Ahmad *et al.* [6] for the linear analysis of moderately thick and thin shells, and has recently been applied also to the nonlinear analysis of shells by Ramm [7] and Kråkeland [8].

The basic ideas for the development of the displacement/rotation isoparametric elements evolved from the difficulties that are encountered when using the usual displacement isoparametric elements in the analysis of plates and shells. Firstly, computational difficulties can result when these isoparametric elements are very thin, because the stiffness coefficients corresponding to the transverse displacement degrees

of freedom are considerably larger than those corresponding to the longitudinal displacements. Secondly, errors are introduced in the analysis because erroneous strain energy corresponding to the normal stresses in the thickness direction is included. These two difficulties are overcome in the approach introduced by Ahmad *et al.*, because it is assumed that the normal to the shell surface remains straight and does not extend, and the normal stresses in the direction of the shell thickness are ignored in the element formulation.

The conceptual advantage of the displacement/rotation isoparametric elements is their inherent generality, which is analogous to the generality of the isoparametric elements in the analysis of two- and three-dimensional continuum problems. In contrast to the classical approach, no specific classical plate or shell theory is employed; instead, the geometry and the displacement field of the structure are directly discretized and interpolated as in the analysis of continuum problems. This approach is equivalent to using a general shell theory and can be employed efficiently for the analysis of general structural configurations by using variable-number-nodes elements [9, 10].

The objective in this paper is to present the formulation, implementation and application of a general variable-number-nodes rotation/displacement isoparametric element for linear and geometric and material nonlinear analysis of plates and shells. This element has been developed to be employed in much the same way as the variable-number-nodes isoparametric continuum elements and can directly be connected to these elements. The underlying philosophy of the development was that it is user-effective to be able to analyze various types of structures with what is basically a single element that is effective in linear

analysis and geometric and material nonlinear analysis [11, 12].

The concepts of the formulation of the shell element are those used earlier by Ahmad *et al.* for linear elastic analysis, and Ramm and Kråkeland for nonlinear analysis [6–8]. However, the actual effective usage of those concepts depends on the details of the formulation and implementation, and the element presented in this paper is in a number of important aspects, that are discussed in the paper, more general and more effective than the shell elements published earlier. These aspects include the choice of effective rotational degrees of freedom; the use of quadrilateral or triangular, low or high-order elements for geometric and/or materially nonlinear analysis; the use of a special transition element to model structural intersections, and the use of the element in the analysis of stiffened plates and shells.

In the paper, we first present the large displacement formulation of the variable-number-nodes element. Starting from the basic continuum mechanics virtual work theorem an updated Lagrangian (U. L.) and a total Lagrangian (T. L.) formulation are presented, that allow very large displacements and rotations, and materially nonlinear conditions. Considering linear analysis we point out that the simplest elements (the three-node triangular and four node-quadrilateral plate elements) of the variable-number-nodes element are the elements considered by Hughes *et al.* using the Mindlin plate theory [13].

Next we describe some important aspects pertaining to the formulation, implementation and usage of the element. In the practical analysis of shell structures it is important that a shell element can be employed to model arbitrary and complex geometries with variable shell thickness, cut-outs, discrete reinforcing and eccentric stiffeners and branches and intersections. In the paper we show how the element can be employed to model such analysis complexities using special transition elements and compatible three-dimensional bending elements. Also, it is pointed out that using higher-order shell elements no reduced integration need be employed.

Finally, we present in the paper the results of a number of sample analyses that demonstrate the versatility and effectiveness of the element. First, solutions are presented to some simple problems merely to demonstrate some important features of the element: its high accuracy without reduced integration and its use in the analysis of stiffened shells and shell intersections are illustrated, and the results of a convergence study using various nodal point configurations are given. In this convergence study the shell element was used as a parabolic and cubic, quadrilateral and triangular element. Next, the solution results of some highly nonlinear problems are given and discussed, and based on the experiences with the element it is concluded that the shell element presented in this paper is highly effective and versatile for the practical analysis of general shell structures.

2. FORMULATIONS OF THE SHELL ELEMENT

Consider the large displacement motion of a general body as a function of time and assume that the solutions for the static and kinematic variables are

known for the discrete time points, $0, \Delta t, 2\Delta t, \dots, t$. The basic aim of the analysis is to establish an equation of virtual work from which the unknown static and kinematic variables in the configuration at time $t + \Delta t$ can be solved. Since the displacement-based finite element procedure shall be employed for numerical solution, we use the principle of virtual displacements to express the equilibrium of the body.

In order to solve for the static and kinematic variables of the body at time $t + \Delta t$, in essence, two different formulations can be employed [14]. In the total Lagrangian (T. L.) formulation all static and kinematic variables are referred to the initial configuration at time 0. The updated Lagrangian (U. L.) formulation is based on the same procedures that are used in the T. L. formulation, but in the solution all static and kinematic variables are referred to the last calculated configuration at time t . Various applications of both formulations in the analysis of continuum problems are presented in [14, 15], where it was shown, in particular, that both the T. L. and U. L. formulations include all nonlinear effects due to large displacements, large strains and material nonlinearities. The only advantage of using one formulation rather than the other is that it may yield a more effective numerical solution.

In the following sections, we develop the governing equations for the geometric and material nonlinear analysis of shell structures. In the discussion, we develop first the matrix expressions that describe the nonlinear kinematic behavior of the shell element, and we discuss afterwards briefly the use of appropriate constitutive relations.

2.1 Updated Lagrangian formulation

In the U. L. formulation the virtual work principle expressing the equilibrium and compatibility requirements of the body at time $t + \Delta t$ is [14]

$$\int_V {}^{t+\Delta t}S_{ij} \delta {}^{t+\Delta t}\epsilon_{ij} {}^{t+\Delta t}dv = {}^{t+\Delta t}\mathcal{R} \quad (1)$$

where the ${}^{t+\Delta t}S_{ij}$ and the ${}^{t+\Delta t}\epsilon_{ij}$ are the components of the 2nd Piola–Kirchhoff stress tensor and Green–Lagrange strain tensor (both referred to the configuration at time t), respectively; ${}^{t+\Delta t}\mathcal{R}$ is the external virtual work due to surface tractions and body forces, and δ means “variation in”.

Equation (1) represents a nonlinear equation in the unknown static and kinematic variables of the body at time $t + \Delta t$. Using our usual notation, Table 1 summarizes the linearization and solution of eqn (1) by the modified Newton–Raphson iteration.

Geometry and displacement interpolations

The updated Lagrangian formulation in Table 1 was used in [14, 15] to obtain finite element solution schemes for solid continua using isoparametric elements with displacement degrees of freedom only. In our derivation of an effective shell element we follow the work presented earlier, but use displacement and rotational degrees of freedom. Referring to Figs 1 and

Table 1. Updated Lagrangian formulation

1. Equation of Motion	Notation
$\int_{\mathcal{V}} {}^{t+\Delta t} S_{ij} \delta {}^{t+\Delta t} e_{ij} {}^t dv = {}^{t+\Delta t} \mathcal{R}$	${}^{t+\Delta t} x_i = {}^t x_i + u_i$
where	${}^{t+\Delta t} x_{i,s} = \frac{\partial {}^t x_i}{\partial {}^{t+\Delta t} x_s}$
${}^{t+\Delta t} S_{ij} = \frac{{}^t \rho}{{}^{t+\Delta t} \rho} {}^{t+\Delta t} x_{i,s} {}^{t+\Delta t} \tau_{sr} + {}^t S_{j,r}$	${}^t u_{i,j} = \frac{\partial u_i}{\partial {}^t x_j}$
${}^{t+\Delta t} e_{ij} = \frac{1}{2} (u_{i,j} + u_{j,i} + u_{k,i} u_{k,j})$	
2. Incremental decompositions	
a. stresses	
${}^{t+\Delta t} S_{ij} = {}^t \tau_{ij} + {}^t S_{ij}$	
b. strains	
${}^{t+\Delta t} e_{ij} = {}^t e_{ij}; \quad {}^t e_{ij} = {}^t e_{ij} + {}^t \eta_{ij}$	
${}^t e_{ij} = \frac{1}{2} (u_{i,j} + u_{j,i}); \quad {}^t \eta_{ij} = \frac{1}{2} u_{k,i} u_{k,j}$	
3. Equation of motion with incremental decompositions	
Noting that ${}^t S_{ij} = {}^t C_{ijrs} e_{rs}$ the equation of motion is	
$\int_{\mathcal{V}} {}^t C_{ijrs} e_{rs} \delta {}^t e_{ij} {}^t dv + \int_{\mathcal{V}} {}^t \tau_{ij} \delta {}^t \eta_{ij} {}^t dv = {}^{t+\Delta t} \mathcal{R} - \int_{\mathcal{V}} {}^t \tau_{ij} \delta {}^t e_{ij} {}^t dv$	
4. Linearization of equation of motion	
Using the approximations ${}^t S_{ij} = {}^t C_{ijrs} e_{rs}$, $\delta {}^t e_{ij} = \delta {}^t e_{ij}$ we obtain as approximate equation of motion	
$\int_{\mathcal{V}} {}^t C_{ijrs} e_{rs} \delta {}^t e_{ij} {}^t dv + \int_{\mathcal{V}} {}^t \tau_{ij} \delta {}^t \eta_{ij} {}^t dv = {}^{t+\Delta t} \mathcal{R} - \int_{\mathcal{V}} {}^t \tau_{ij} \delta {}^t e_{ij} {}^t dv$	
5. Equilibrium iteration (modified Newton–Raphson iteration)	
$\int_{\mathcal{V}} {}^t C_{ijrs} \Delta {}^t e_{rs} \delta \Delta {}^t e_{ij} {}^t dv + \int_{\mathcal{V}} {}^t \tau_{ij} \delta \Delta {}^t \eta_{ij} {}^t dv = {}^{t+\Delta t} \mathcal{R} - \int_{\mathcal{V}} {}^{t+\Delta t} \tau_{ij}^{(i-1)} \delta {}^{t+\Delta t} e_{ij}^{(i-1)} {}^{t+\Delta t} dv^{(i-1)}$	
6. Finite element discretization (for a single element)	
$\left\{ \int_{\mathcal{V}} {}^t \mathbf{B}_L^T {}^t \mathbf{C} {}^t \mathbf{B}_L {}^t dv + \int_{\mathcal{V}} {}^t \mathbf{B}_{NL}^T {}^t \boldsymbol{\tau} {}^t \mathbf{B}_{NL} {}^t dv \right\} \Delta \mathbf{u}^{(i)} = {}^{t+\Delta t} \mathbf{R} - \int_{\mathcal{V}} {}^{t+\Delta t} \mathbf{B}_L^{(i-1)T} {}^{t+\Delta t} \hat{\boldsymbol{\tau}}^{(i-1)} {}^{t+\Delta t} dv^{(i-1)}$	
${}^{t+\Delta t} \mathbf{u}^{(i)} = {}^{t+\Delta t} \mathbf{u}^{(i-1)} + \Delta \mathbf{u}^{(i)}$	

2. the geometry of the variable-number-nodes shell element at time “ t ” is interpolated using

$${}^t x_i = \sum_{k=1}^N h_k {}^t x_i^k + \frac{t}{2} \sum_{k=1}^N a_k h_k {}^t V_{ni}^k \quad (2)$$

where

${}^t x_i$ = Cartesian coordinate of any point in the element at time t ;

$h_k(r, s)$ = isoparametric interpolation functions;

${}^t x_i^k$ = Cartesian coordinate of nodal point k at

time t ;

t_k = thickness of plate (in t direction) at nodal point k ;

${}^t V_{ni}^k$ = component i of unit normal vector, ${}^t \mathbf{V}_n^k$, to the surface of the plate at nodal point k and time t .

Also, in eqn (2), the isoparametric element coordinates are r, s and t and N is the number of nodes of the element.

To obtain an expression for u_i , we use

$$u_i = {}^{t+\Delta t} x_i - {}^t x_i \quad (3)$$

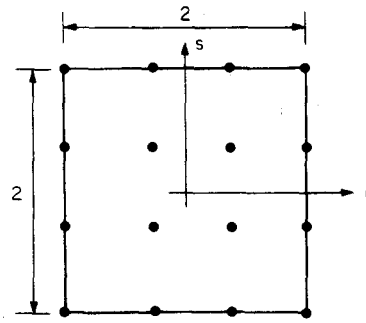
and substitute from eqn (2)

$$u_i = \sum_{k=1}^N h_k u_i^k + \frac{t}{2} \sum_{k=1}^N a_k h_k V_{ni}^k \quad (4)$$

where

$$V_{ni}^k = {}^{t+\Delta t} V_{ni}^k - {}^t V_{ni}^k \quad (5)$$

For the finite element solution we express the components V_{ni}^k in terms of rotations. To do so we use the vector ${}^t \mathbf{V}_n^k$ corresponding to the configuration at time t which is known. The vector ${}^t \mathbf{V}_n^k$ does not pertain to an element but to the nodal point k , and ${}^0 \mathbf{V}_n^k$ is input



16-NODE PARENT ELEMENT WITH CUBIC INTERPOLATION

SOME DERIVED ELEMENTS:

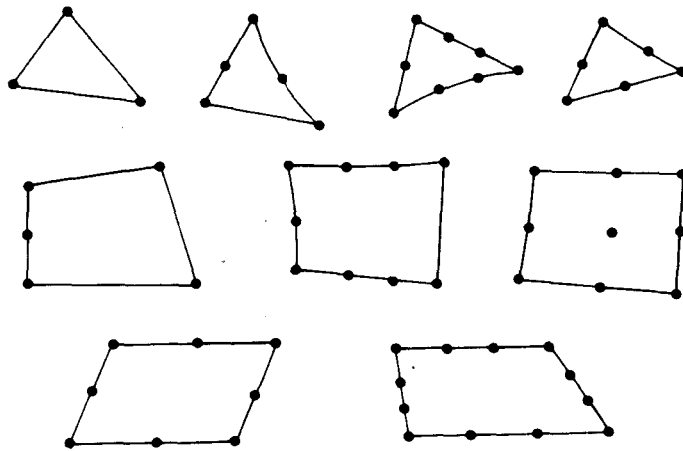


Fig. 1. Variable-number-nodes shell element.

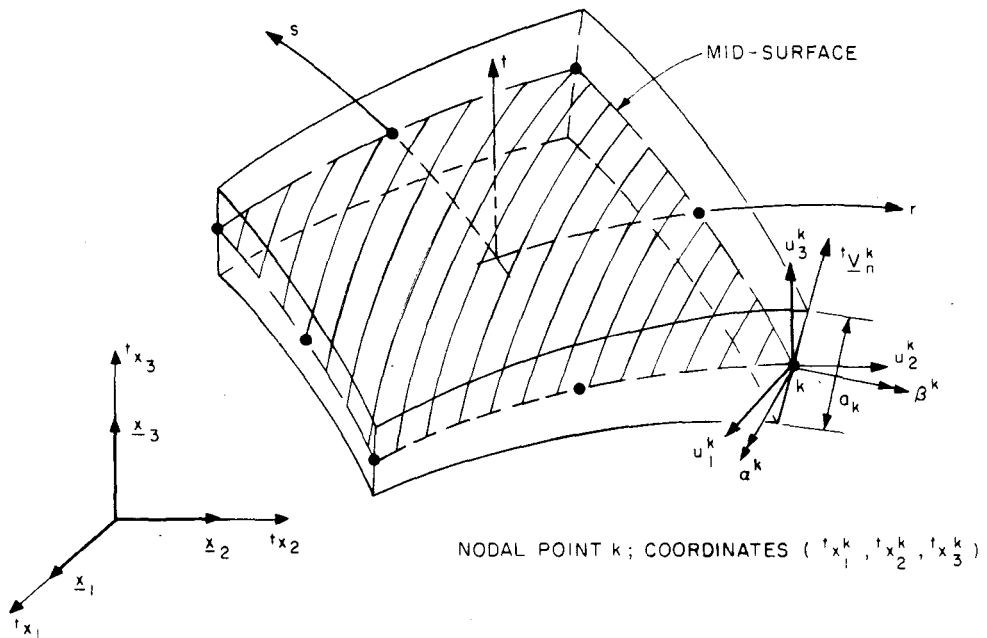


Fig. 2. Quadrilateral shell element in configuration at time t .

prior to the incremental analysis. Thus, all shell elements meeting at the nodal point k of a shell surface have the same vector as mid-surface normal as illustrated in Fig. 3.

When defining the normal at a nodal point it may be that the assumption of a single normal is inappropriate at the intersection of shell surfaces. These intersections can be modeled using a different nodal point (with the same coordinates) corresponding to each shell surface and constraint equations to couple the nodal degrees of freedom [11], or, more effectively, using transition elements (see Section 3.4).

To express the components V_{ni}^k in terms of rotation angles, we first define two unit vectors V_1^k and V_2^k that are orthogonal to V_n^k (see Fig. 4),

$$V_1^k = (x_3 \times V_n^k) / |x_3 \times V_n^k| \quad (6)$$

where we set V_1^k equal to x_3 if V_n^k is parallel to x_3 , and

$$V_2^k = V_n^k \times V_1^k. \quad (7)$$

Let α^k and β^k be the rotations of the normal vector about the vectors V_1^k and V_2^k from the configuration at time t to the configuration at time $t + \Delta t$, then we have approximately (for small incremental angles α^k and β^k)

$$V_n^k = -V_2^k \alpha^k + V_1^k \beta^k. \quad (8)$$

Substituting from eqn (8) into eqn (4) we thus obtain the incremental internal element displacements in terms of the nodal point incremental displacements and rotations

$$u_i = \sum_{k=1}^N h_k u_i^k + \frac{t}{2} \sum_{k=1}^N a_k h_k [-V_{2i}^k \alpha^k + V_{1i}^k \beta^k]. \quad (9)$$

The finite element solution will yield the nodal point variables u_i^k , α^k and β^k , which can then be employed to evaluate accurately ${}^{t+\Delta t}V_n^k$,

$${}^{t+\Delta t}V_n^k = {}^tV_n^k + \int_{\alpha^k, \beta^k} -{}^tV_2^k d\alpha^k + {}^tV_1^k d\beta^k. \quad (10)$$

If α^k and β^k are small, the integration in eqn (10) can be carried out to sufficient accuracy using the Euler method [9],

$${}^{t+\Delta t}V_n^k = {}^tV_n^k - {}^tV_2^k \alpha^k + {}^tV_1^k \beta^k \quad (11)$$

which corresponds to the assumption employed in eqn (8).

Calculation of element matrices

Considering a single shell element, as summarized in Table 1, the linear strain-displacement transformation matrix, tL , the nonlinear strain-displacement matrix, ${}^tB_{NL}$, the stress matrix, ${}^t\tau$, and the stress vector, ${}^t\bar{t}$, are required.

To evaluate the strain-displacement matrices we obtain from eqn (9)

$$\begin{bmatrix} u_{i,r} \\ u_{i,s} \\ u_{i,t} \end{bmatrix} = \sum_{k=1}^N \begin{bmatrix} h_{k,r} [1 & {}^t g_{1i}^k & {}^t g_{2i}^k] \\ h_{k,s} [1 & {}^t g_{1i}^k & {}^t g_{2i}^k] \\ h_k [0 & {}^t g_{1i}^k & {}^t g_{2i}^k] \end{bmatrix} \begin{bmatrix} u_i^k \\ \alpha^k \\ \beta^k \end{bmatrix} \quad (12)$$

where we use the notation

$$\begin{aligned} {}^t g_{1i}^k &= -\frac{1}{2} a_k {}^t V_{2i}^k \\ {}^t g_{2i}^k &= \frac{1}{2} a_k {}^t V_{1i}^k. \end{aligned} \quad (13)$$

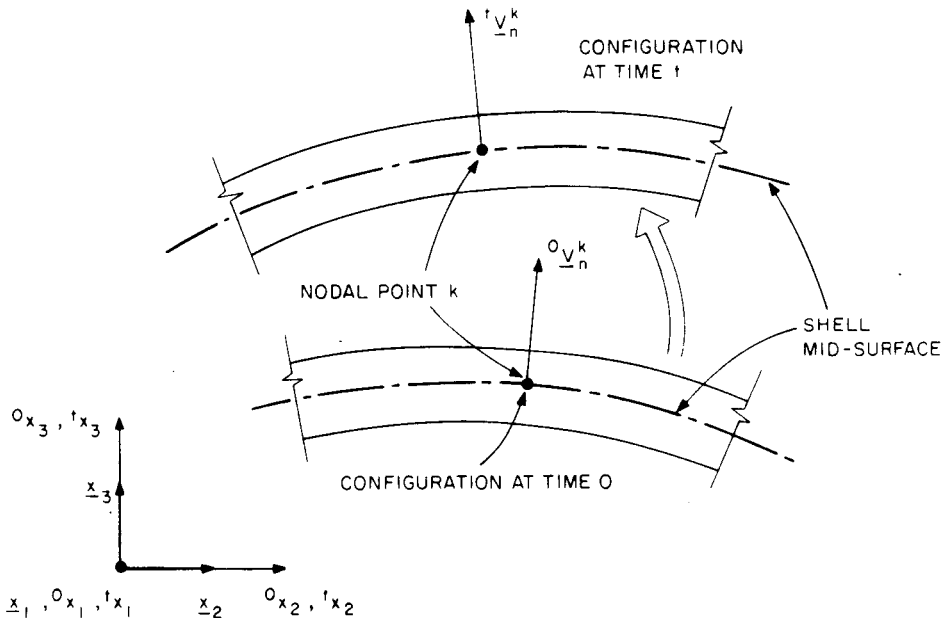


Fig. 3. Normal to shell mid-surface.

Table 3. Total Lagrangian formulation

1. Equation of motion	Notation
$\int_{0V} {}^{t+\Delta t} S_{ij} \delta^{t+\Delta t} {}_0^e \varepsilon_{ij} {}^0 dv = {}^{t+\Delta t} \mathcal{R}$	${}^{t+\Delta t} x_i = {}^0 x_i + {}^{t+\Delta t} u_i$
${}_{0V}$	${}^{t+\Delta t} x_{j,r} = \frac{\partial {}^0 x_j}{\partial {}^{t+\Delta t} x_r}$
<p>where</p> ${}^{t+\Delta t} S_{ij} = \frac{\partial \rho}{\partial {}^{t+\Delta t} \rho} {}^{t+\Delta t} x_{i,s} {}^{t+\Delta t} \tau_{sr} + \frac{\partial \rho}{\partial {}^{t+\Delta t} \rho} {}^{t+\Delta t} x_{j,r}$ ${}^{t+\Delta t} \varepsilon_{ij} = \frac{1}{2} ({}^{t+\Delta t} u_{i,j} + {}^{t+\Delta t} u_{j,i} + {}^{t+\Delta t} u_{k,i} {}^{t+\Delta t} u_{k,j})$	${}^{t+\Delta t} u_{i,j} = \frac{\partial {}^{t+\Delta t} u_i}{\partial {}^0 x_j}$
<p>2. Incremental decompositions</p> <p>a. stresses</p> ${}^{t+\Delta t} S_{ij} = {}_0^t S_{ij} + {}_0 S_{ij}$ <p>b. strains</p> ${}^{t+\Delta t} \varepsilon_{ij} = {}_0^t \varepsilon_{ij} + {}_0 \varepsilon_{ij}; \quad {}_0 \varepsilon_{ij} = {}_0 e_{ij} + {}_0 \eta_{ij}$ ${}_0 e_{ij} = \frac{1}{2} ({}_0 u_{i,j} + {}_0 u_{j,i} + {}_0 u_{k,i} {}_0 u_{k,j} + {}_0 u_{k,i} {}_0 u_{k,j}); \quad {}_0 \eta_{ij} = \frac{1}{2} {}_0 u_{k,i} {}_0 u_{k,j}$	
<p>3. Equation of motion with incremental decompositions</p> <p>Noting that $\delta^{t+\Delta t} {}_0^e \varepsilon_{ij} = \delta_0 \varepsilon_{ij}$ and ${}_0 S_{ij} = {}_0 C_{ijrs} {}_0 e_{rs}$ the equation of motion is</p> $\int_{0V} {}_0 C_{ijrs} {}_0 e_{rs} \delta_0 \varepsilon_{ij} {}^0 dv + \int_{0V} {}_0^t S_{ij} \delta_0 \eta_{ij} {}^0 dv = {}^{t+\Delta t} \mathcal{R} - \int_{0V} {}_0^t S_{ij} \delta_0 \varepsilon_{ij} {}^0 dv$	
<p>4. Linearization of equation of motion</p> <p>Using the approximations ${}_0 S_{ij} = {}_0 C_{ijrs} {}_0 e_{rs}$, $\delta_0 \varepsilon_{ij} = \delta_0 e_{ij}$ we obtain as approximate equation of motion</p> $\int_{0V} {}_0 C_{ijrs} {}_0 e_{rs} \delta_0 e_{ij} {}^0 dv + \int_{0V} {}_0^t S_{ij} \delta_0 \eta_{ij} {}^0 dv = {}^{t+\Delta t} \mathcal{R} - \int_{0V} {}_0^t S_{ij} \delta_0 e_{ij} {}^0 dv$	
<p>5. Equilibrium iteration (modified Newton-Raphson iteration)</p> $\int_{0V} {}_0 C_{ijrs} \Delta_0 e_{rs} \delta \Delta_0 e_{ij} {}^0 dv + \int_{0V} {}_0^t S_{ij} \delta \Delta_0 \eta_{ij} {}^0 dv = {}^{t+\Delta t} \mathcal{R} - \int_{0V} {}^{t+\Delta t} S_{ij}^{(i-1)} \delta^{t+\Delta t} e_{ij}^{(i-1)} {}^0 dv$	
<p>6. Finite element discretization (for a single element)</p> $\left\{ \int_{0V} {}_0^t \mathbf{B}_{L,0}^T \mathbf{C}_0 \mathbf{B}_{L,0} {}^0 dv + \int_{0V} {}_0^t \mathbf{B}_{NL,0}^T \mathbf{S}_0 \mathbf{B}_{NL,0} {}^0 dv \right\} \Delta \mathbf{u}^{(i)} = {}^{t+\Delta t} \mathbf{R} - \int_{0V} {}^{t+\Delta t} \mathbf{B}_{L,0}^{(i-1)T} {}^{t+\Delta t} \mathbf{S}_0^{(i-1)} {}^0 dv$ ${}^{t+\Delta t} \mathbf{u}^{(i)} = {}^{t+\Delta t} \mathbf{u}^{(i-1)} + \Delta \mathbf{u}^{(i)}$	

used in Tables 1 and 3. To obtain this tensor with the shell assumption that the stress normal to the shell is zero, we use the usual three-dimensional constitutive relations corresponding to the r , s and t directions, impose the condition that the normal stress is zero and then transform the modified constitutive relations to correspond to the Cartesian coordinate axes. Here, it should be noted that if the element is employed to model a plate which is flat initially, but not necessarily aligned with the global coordinate system, in geometrically linear analysis and when using the T. L. formulation only one transformation matrix to calculate the constitutive matrix need be established for each element.

3. SOME IMPORTANT FEATURES OF THE ELEMENT

The variable-number-nodes shell element is a very versatile element. In this section we summarize some of its pertinent theoretical and practical features.

3.1 Interpolation functions

As shown in Fig. 1, the element can have a minimum of three nodes and a maximum of sixteen nodes, in which case the functions $h_k(r, s)$ are the usual Lagrangian cubic interpolation functions. The interpolation functions of an N -node element are basically constructed using the procedure in [9, p. 130], and more specific details are given in [10].

3.2 Comparison of element with elements based on plate theory

In the previous section, we presented the formulation of a general shell element for large displacement and rotation analysis. Both, the U. L. and the T. L. formulations reduce as usual to a linear analysis in the first step of the incremental solution.

In the linear analysis of plates, the element is identical to those discussed by Ahmad *et al.* [6], Zienkiewicz [2], and Hughes *et al.* [13]. Ahmad, Irons and Zienkiewicz used the formulation employed in this paper, whereas Hughes *et al.* employed the Mindlin plate theory that includes shear deformations to obtain the stiffness matrix of the four-node quadrilateral element and then studied element improvements by selective integration.

The important point is that in linear analysis of plates, therefore, the shell element is based on classical plate theory including shear deformations and all element matrices can also be derived using this theory. Considering large displacement analysis, the basic assumptions of the linear plate theory are still employed, but the element matrices are calculated using general nonlinear continuum mechanics equations with no assumptions on the magnitude of the plate displacements and rotations. This approach is equivalent to using a general nonlinear shell theory.

3.3 Numerical integration

To evaluate the element matrices, it is necessary, in general, to employ numerical integration. In this study, we employed for the quadrilateral elements the usual Gauss integration used in isoparametric finite element analysis, and for the triangular elements the integration formulas proposed by Cowper [16], the order of integration being dependent on the order of interpolation employed [9, p.165] and whether elastic or elastic-plastic material conditions are modeled. It should be noted that with the higher-order elements no reduced integration is necessary to obtain accurate solutions (see Section 4.1). This observation is important; namely, in general shell analysis reduced integration in the evaluation of an element stiffness matrix must be employed with care and, in practice, is still best avoided. Using reduced or selective integration the difficulties are that, for all possible geometric shapes, the finite element must not contain small spurious eigenvalues (or develop such eigenvalues in the incremental solution), and the element must satisfy all convergence requirements and display good accuracy characteristics. The precise effect of using reduced integration in general large displacement analysis is very difficult to assess and has not yet been established. Furthermore, considering materially nonlinear analysis, a higher-order integration may be desirable anyway, in order to capture the variation in the constitutive relations.

3.4 Use of top and bottom displacement nodes

In the analysis of an actual shell structure, it may be necessary to model shell intersections and shell to solid transitions. These geometric regions can be modeled effectively without the use of constraint equations using transition elements, which have mid-surface nodes to couple into other shell elements and top and

bottom nodes to connect to each other or to the usual three-dimensional isoparametric elements (see Fig. 5). The interpolation functions corresponding to the top and bottom nodes are the usual functions used in three-dimensional analysis, and the interpolation functions associated with the mid-surface nodes are those of the shell element.

3.5 Element description

To describe an assemblage of variable-number-nodes shell elements the following input is required:

- (i) the shell nodal point coordinates;
- (ii) the shell mid-surface normals, ${}^0V_n^k$ at all mid-surface nodes;
- (iii) the shell thickness, a_k , at all mid-surface nodes; one thickness is defined at each mid-surface node;
- (iv) the material properties of the elements.

3.6 Formulation of a compatible bending element

The procedure of the shell element formulation presented in Section 2 can also be employed to formulate a three-dimensional bending element. Assuming a rectangular solid cross-section as shown in Fig. 6, we use in the formulation instead of eqn (2)

$${}^t x_i = \sum_{k=1}^N h_k {}^t x_i^k + \frac{t}{2} \sum_{k=1}^N a_k h_k {}^t V_{ti}^k + \frac{s}{2} \sum_{k=1}^N b_k h_k {}^t V_{si}^k \quad (20)$$

where all variables are defined as in eqn (2), but the function h_k is now an interpolation function in r only, and

a_k = thickness of element in t -direction at nodal point k ,

b_k = thickness of element in s -direction at nodal point k ,

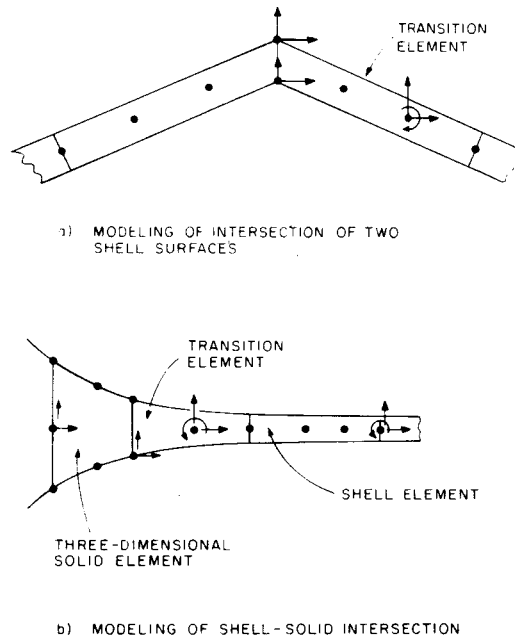


Fig. 5. Some applications of the transition element.

Table 4. Matrices used in total Lagrangian formulation

1. Linear Strain-Displacement Transformation Matrix

$${}^0\mathbf{e} = {}^0\mathbf{B}_L \mathbf{u}; \quad \delta\mathbf{B}_L = {}^0\mathbf{B}_{L0} + \delta\mathbf{B}_{L1}$$

$${}^0\mathbf{e}^T = [{}^0e_{11} \quad {}^0e_{22} \quad {}^0e_{33} \quad 2{}^0e_{12} \quad 2{}^0e_{13} \quad 2{}^0e_{23}]$$

$$\mathbf{u}^T = [u_1^1 \quad u_2^1 \quad u_3^1 \quad \alpha^1 \quad \beta^1 : u_1^2 \quad u_2^2 \quad \dots : u_1^N \quad u_2^N \quad u_3^N \quad \alpha^N \quad \beta^N]$$

$${}^0\mathbf{B}_{L0} = \begin{bmatrix} {}^0h_{k,1} & 0 & 0 & {}^t g_{110}^k G_1^k & {}^t g_{210}^k G_1^k \\ 0 & {}^0h_{k,2} & 0 & {}^t g_{120}^k G_2^k & {}^t g_{220}^k G_2^k \\ 0 & 0 & {}^0h_{k,3} & {}^t g_{130}^k G_3^k & {}^t g_{230}^k G_3^k \\ \dots & \dots & \dots & \dots & \dots \\ {}^0h_{k,2} & {}^0h_{k,1} & 0 & ({}^t g_{110}^k G_2^k + {}^t g_{120}^k G_1^k) & ({}^t g_{210}^k G_2^k + {}^t g_{220}^k G_1^k) \\ {}^0h_{k,3} & 0 & {}^0h_{k,1} & ({}^t g_{110}^k G_3^k + {}^t g_{130}^k G_1^k) & ({}^t g_{210}^k G_3^k + {}^t g_{230}^k G_1^k) \\ 0 & {}^0h_{k,3} & {}^0h_{k,2} & ({}^t g_{120}^k G_3^k + {}^t g_{130}^k G_2^k) & ({}^t g_{220}^k G_3^k + {}^t g_{230}^k G_2^k) \end{bmatrix}$$

for nodal point k

$${}^0\mathbf{B}_{L1} = \begin{bmatrix} l_{110}^k h_{k,1} & l_{210}^k h_{k,1} & l_{310}^k h_{k,1} & \phi_{110}^k G_1^k & \phi_{210}^k G_1^k \\ l_{120}^k h_{k,2} & l_{220}^k h_{k,2} & l_{320}^k h_{k,2} & \phi_{120}^k G_2^k & \phi_{220}^k G_2^k \\ l_{130}^k h_{k,3} & l_{230}^k h_{k,3} & l_{330}^k h_{k,3} & \phi_{130}^k G_3^k & \phi_{230}^k G_3^k \\ \dots & \dots & \dots & \dots & \dots \\ (l_{110}^k h_{k,2} + l_{120}^k h_{k,1})(l_{210}^k h_{k,2} + l_{220}^k h_{k,1})(l_{310}^k h_{k,2} + l_{320}^k h_{k,1})(\phi_{120}^k G_1^k + \phi_{110}^k G_2^k)(\phi_{220}^k G_1^k + \phi_{210}^k G_2^k) \\ (l_{110}^k h_{k,3} + l_{130}^k h_{k,1})(l_{210}^k h_{k,3} + l_{230}^k h_{k,1})(l_{310}^k h_{k,3} + l_{330}^k h_{k,1})(\phi_{130}^k G_1^k + \phi_{110}^k G_3^k)(\phi_{230}^k G_1^k + \phi_{210}^k G_3^k) \\ (l_{120}^k h_{k,3} + l_{130}^k h_{k,2})(l_{220}^k h_{k,3} + l_{230}^k h_{k,2})(l_{320}^k h_{k,3} + l_{330}^k h_{k,2})(\phi_{130}^k G_2^k + \phi_{120}^k G_3^k)(\phi_{230}^k G_2^k + \phi_{220}^k G_3^k) \end{bmatrix}$$

for nodal point k

where

$$l_{ij} = \frac{\partial^i u_i}{\partial^0 x_j}; \quad \phi_{ij}^k = \sum_{m=1}^3 {}^t g_{im}^k l_{mj}$$

2. Nonlinear strain-displacement transformation matrix

$${}^0\mathbf{B}_{NL} = \begin{bmatrix} {}^0h_{k,1} & 0 & 0 & {}^t g_{110}^k G_1^k & {}^t g_{210}^k G_1^k \\ 0 & {}^0h_{k,1} & 0 & {}^t g_{120}^k G_1^k & {}^t g_{220}^k G_1^k \\ 0 & 0 & {}^0h_{k,1} & {}^t g_{130}^k G_1^k & {}^t g_{230}^k G_1^k \\ \dots & \dots & \dots & \dots & \dots \\ {}^0h_{k,2} & 0 & 0 & {}^t g_{110}^k G_2^k & {}^t g_{210}^k G_2^k \\ 0 & {}^0h_{k,2} & 0 & {}^t g_{120}^k G_2^k & {}^t g_{220}^k G_2^k \\ 0 & 0 & {}^0h_{k,2} & {}^t g_{130}^k G_2^k & {}^t g_{230}^k G_2^k \\ \dots & \dots & \dots & \dots & \dots \\ {}^0h_{k,3} & 0 & 0 & {}^t g_{110}^k G_3^k & {}^t g_{210}^k G_3^k \\ 0 & {}^0h_{k,3} & 0 & {}^t g_{120}^k G_3^k & {}^t g_{220}^k G_3^k \\ 0 & 0 & {}^0h_{k,3} & {}^t g_{130}^k G_3^k & {}^t g_{230}^k G_3^k \end{bmatrix}$$

for nodal point k

3. Stress matrix

$${}^0\mathbf{S} = \begin{bmatrix} {}^0S_{11}\mathbf{I}_3 & \text{Symm.} \\ {}^0S_{12}\mathbf{I}_3 & {}^0S_{22}\mathbf{I}_3 \\ {}^0S_{13}\mathbf{I}_3 & {}^0S_{23}\mathbf{I}_3 & {}^0S_{33}\mathbf{I}_3 \end{bmatrix}$$

where

$$\mathbf{I}_3 = \begin{bmatrix} 1 & 0 & 0 \\ 0 & 1 & 0 \\ 0 & 0 & 1 \end{bmatrix}$$

4. Stress vector

$${}^0\mathbf{S}^T = [{}^0S_{11} \quad {}^0S_{22} \quad {}^0S_{33} \quad {}^0S_{12} \quad {}^0S_{13} \quad {}^0S_{23}]$$

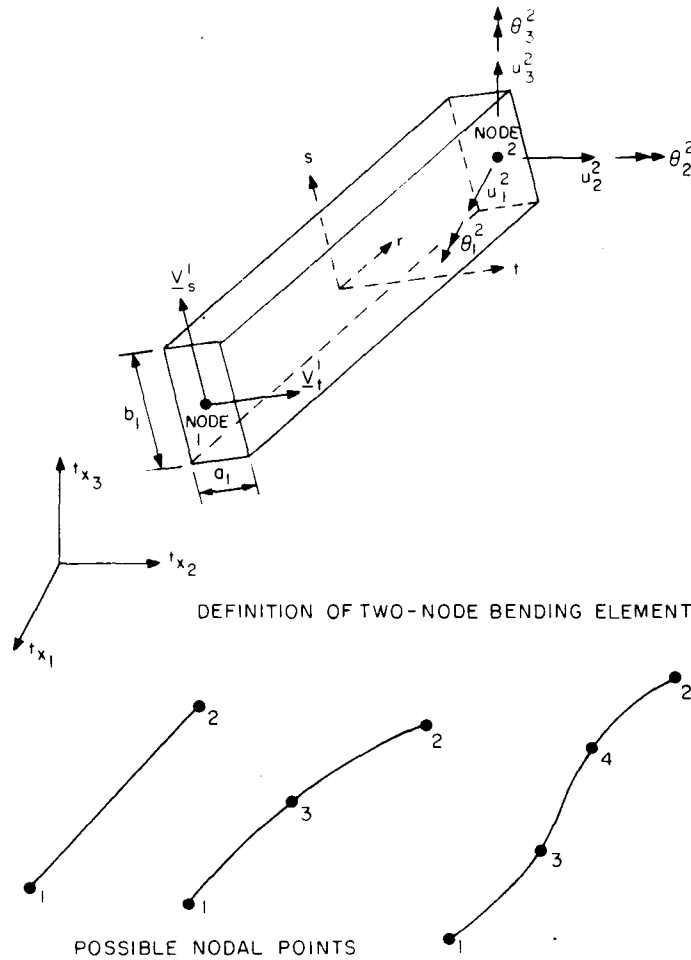


Fig. 6. Three-dimensional bending element.

${}^tV_{ti}^k$ = component i of unit normal vector, ${}^tV_t^k$, in t -direction,

${}^tV_{si}^k$ = component i of unit normal vector, ${}^tV_s^k$, in s -direction, and N is the number of nodes of the element, $N = 2, 3$ or 4 .

Using eqn (20) in the same way as eqn (2) for the shell element, the bending element matrices corresponding to the six degrees of freedom per node shown in Fig. 6 can directly be calculated. Since the same interpolation functions are employed for this element as in the formulation of the shell element, the bending and shell elements are compatible and can be used together effectively to model stiffened plates and shells as illustrated in Section 4.1.

4. SAMPLE SOLUTIONS

The variable-number-nodes element has been implemented in the computer program ADINA, and we present here the results of a selection of sample analyses. In Section 4.1 we report on some very simple analyses merely to illustrate the modeling capabilities with the element.

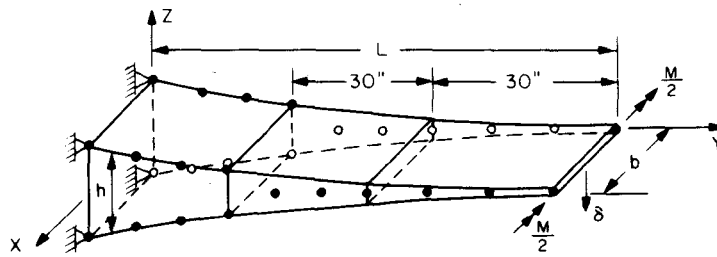
4.1 Linear analyses of three cantilevers

Three simple cantilevers were analyzed using the shell element. The results of the analysis of a uniform

cantilever subjected to a tip transverse load are listed in Table 5. These results show that the cubic element can be employed without selective or reduced integration with very large aspect ratios, and the element does not display the stiffening effect that is observed with the low-order elements [2].

The objective in reporting on the second cantilever analysis is to demonstrate the use of the transition element between solid and shell elements. Figure 7 shows the tapered cantilever analyzed, the model employed and the analysis results. In this analysis, a transition element was employed to model the transition region between the relatively thick root and thin tip of the structure. The transition element can be very useful in the analysis of some practical shell structures for which shell-solid regions must be included in the analysis (e.g. analysis of arch dams and foundations, turbine blades mounted on a shaft) and in the modeling of shell intersections and branches.

The third cantilever analysis illustrates the use of the shell element in conjunction with the three-dimensional bending element in the analysis of stiffened plates and shells. Figure 8 shows the cantilever, the plate model used and the response predicted. The analysis results compare well with the solution calculated using elementary beam theory.



$$E = 3.0 \times 10^7 \text{ PSI}$$

$$\nu = 0$$

$$L = 100 \text{ IN}$$

$$b = 10 \text{ IN}$$

$$h = 10 / (1 + 9 \frac{y}{L}) \text{ IN}$$

δ = CALCULATED TIP DEFLECTION

δ_{TH} = THEORETICAL TIP DEFLECTION
(NO SHEAR DEFORMATION INCLUDED)

M = CONCENTRATED END MOMENT

GAUSS INTEGRATION ORDER = $3 \times 2 \times 2$

STRESSES (AT INTEGRATION POINTS)

LOCATION		$\frac{\sigma_{Th} - \sigma}{\sigma_{Th}}$
Y	Z	
3.3811	2.2133	0.0375
15.0	1.2284	-0.0044
26.6190	0.8501	0.0375
33.3811	0.7209	0.0013
45.0	0.5716	-0.0001
56.6190	0.4736	0.0013
64.5081	0.4242	0.0006
80.0	0.3520	-0.0001
95.4919	0.3009	0.0005

$$\frac{\delta_{Th} - \delta}{\delta_{Th}} = 0.0022$$

Fig. 7. Linear analysis of a tapered cantilever.

4.2 Linear analysis of a cylindrical shell

The thin cylindrical shell shown in Fig. 9 was analyzed for its static response. The cylinder is freely supported at its ends and is loaded by two centrally located and diametrically opposed concentrated forces. Using the double symmetry of the structure and the loading, only one-eighth of the cylinder was analyzed.

This structural problem was employed to study the convergence of the shell element when using different element nodal configurations and increasing the number of elements.

Figures 10 and 11 show some displacements and stresses predicted in the finite element analyses. For comparison also the analytical solution is shown [17]. Figure 10 gives the ratios of the calculated and the theoretical displacements for w_C and u_D , see Fig. 9. It is seen that, as expected, using the lower-order integration in the finite element analyses, in general, the displacements are predicted more accurately. However, Fig. 10 also shows that using the cubic element with high-order integration the displacements converge rapidly as the number of elements used in the idealization is increased. Figure 11 shows that for the 6

$\times 6$ element idealizations, the stress distributions are predicted accurately using the 8-node element with $2 \times 2 \times 2$ Gauss integration and the 16-node element with $4 \times 4 \times 2$ Gauss integration.

4.3 Large displacement/rotation analysis of a cantilever

A cantilever subjected to a concentrated end moment was idealized using one 8-node cubic element. Figure 12 shows the load deflection curves for different displacement/rotation variables. The predicted response shows excellent agreement with the analytical solution [7].

4.4 Elastic-plastic instability analysis of a column

The column shown in Fig. 13 was analyzed for its large displacement elastic-plastic response. Two different finite element idealizations were employed in the study. Namely, one model using six quadratic shell elements (using $2 \times 2 \times 2$ Gauss integration) and another model using twenty-five 6-node isoparametric two-dimensional elements (with 4×4 Gauss integration).

Figure 13 shows the calculated response of the column using the two finite element idealizations. It is

Table 5. Effect of aspect ratio in linear analysis of a cantilever subjected to a transverse tip load

L = Length of cantilever (along r -direction).
 a = Thickness (along t -direction).
 a = Width (along s -direction).
 I = Second moment of area
 E = Young's modulus
 P = Applied tip load
 δ = Computed tip deflection
 δ_{TH} = Theoretical tip deflection = $\frac{PL^3}{3EI}$

$\nu = 0$

One 8-node cubic shell element to model the cantilever.
 (Gauss integration orders $4 \times 2 \times 2$ along r, s and t -directions)

Aspect ratio L/a	$(\delta - \delta_{TH})/\delta_{TH}$
10	0.00500
100	0.00005
1,000	0.00000
10,000	-0.00001

The errors in calculated stresses are less than 0.003 % in all cases.

seen that the predicted collapse load is slightly higher using the two-dimensional element model.

4.5 Large deflection analysis of a diamond structure

A diamond structure constructed of four equal length bars and loaded as shown in Fig. 14 was analyzed using 6-node quadratic shell elements. Using the symmetry of the structure and its loading only one quarter of the structure (one of the beams) was modeled. The finite element model used and the predicted load deflection response of the structure are shown in Fig. 14. The predicted response shows excellent agreement with the analytical solution [18].

Figure 15 shows various equilibrium positions of the structure predicted at different load levels. The deformed shapes of the structure compare very closely to the shapes calculated in [18].

4.6 Large displacement analysis of an elastic simply-supported plate

The simply supported square plate subjected to a uniformly distributed pressure shown in Fig. 16 was analyzed for its large deflection response. One single 16-node shell element was used to model one quarter of the plate. The total Lagrangian formulation was employed.

Figure 16 shows the displacement response predicted in the finite element analysis. The computed displacement response is very close to the solutions given by Levy [19], where the effect of using different assumptions on the plate edge in-plane displacements should be noted.

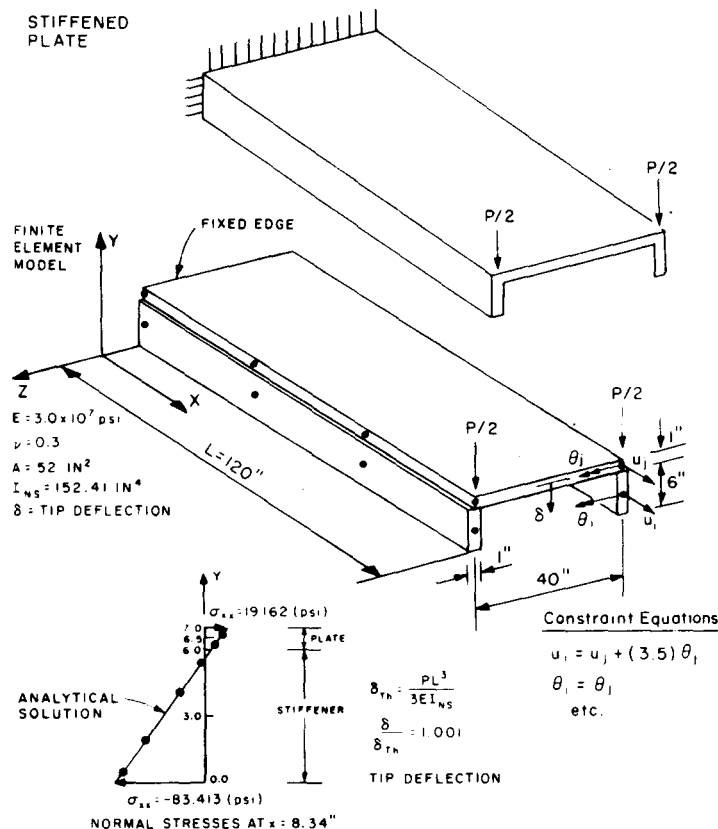


Fig. 8. Linear analysis of a stiffened plate.

TYPE OF ELEMENTS	INTEGRATION ORDER	SYMBOL	TYPE OF ELEMENTS	INTEGRATION ORDER	SYMBOL
8 NODES	3 x 3 x 2	—○—	12 NODES	4 x 4 x 2	---▽---
	2 x 2 x 2	—●—		3 x 3 x 2	---▼---
9 NODES	3 x 3 x 2	---□---	16 NODES	4 x 4 x 2	---◇---
	2 x 2 x 2	---■---		3 x 3 x 2	---◆---
6 NODES (TRIANGLE)	7 x 2	---x---			

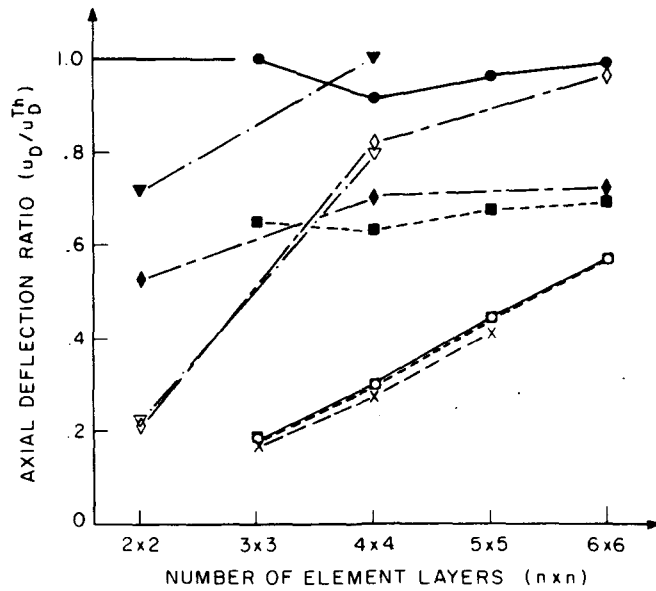
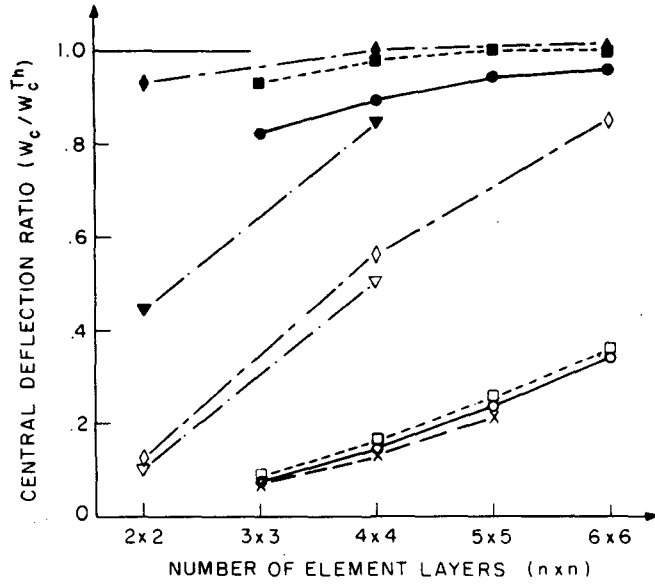


Fig. 10. Pinched cylindrical shell, convergence study of displacements.

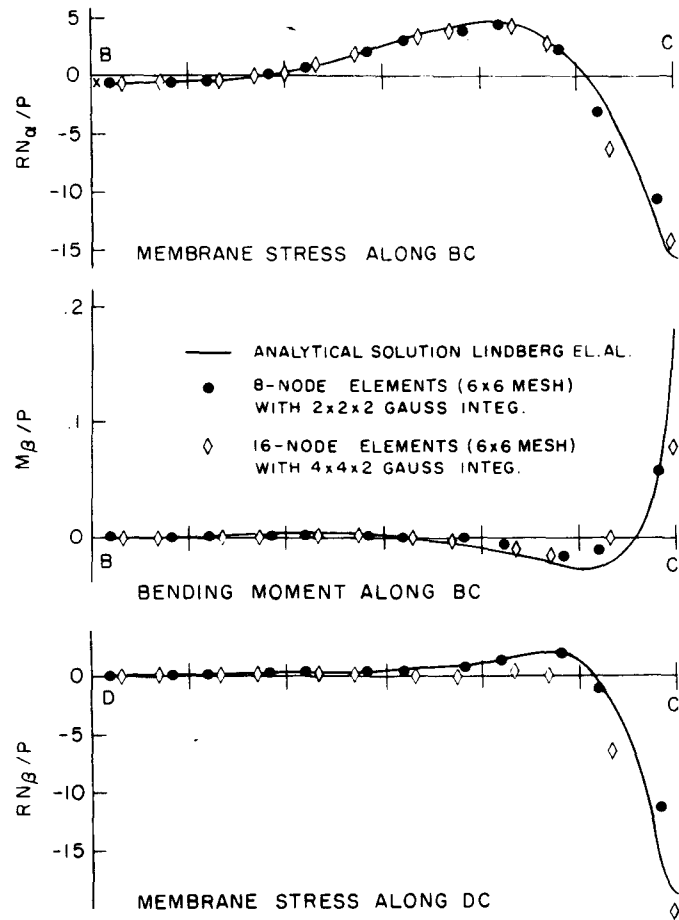


Fig. 11. Pinched cylindrical shell, stress distribution (the element stresses have been calculated in the finite element solutions at the integration points that are closest to the section considered).

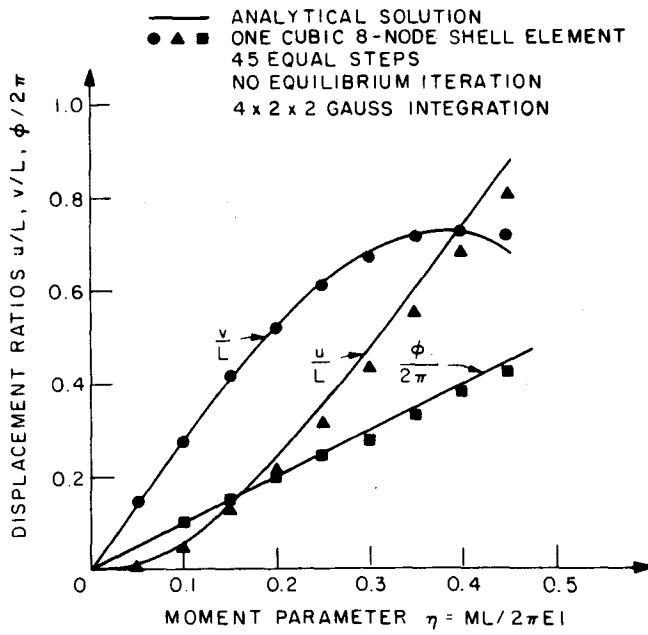
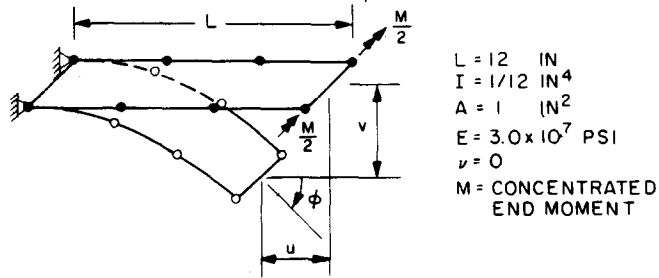


Fig. 12. Large deflection response of a cantilever subjected to an end moment.

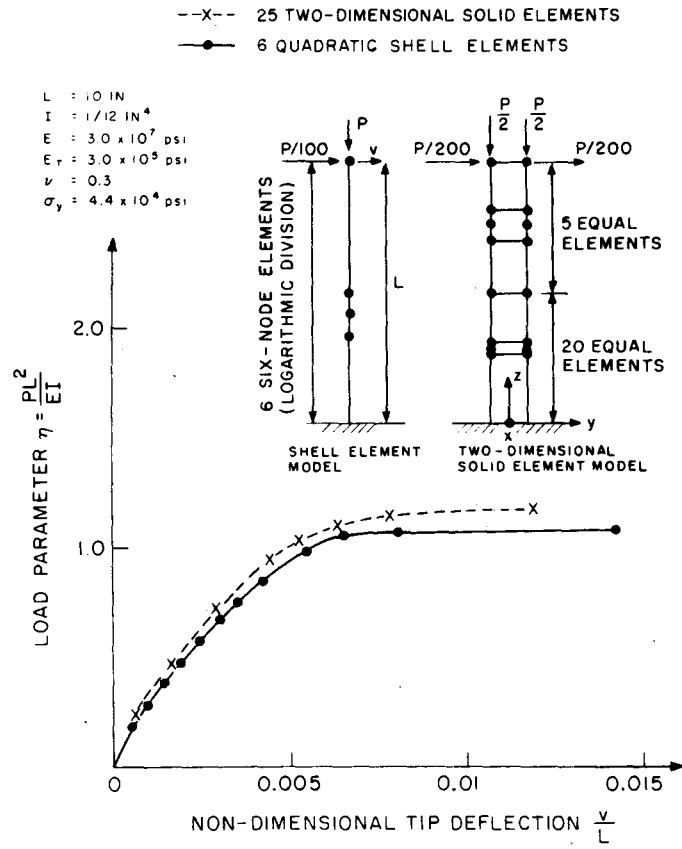


Fig. 13. Elastic-plastic instability analysis of a column.

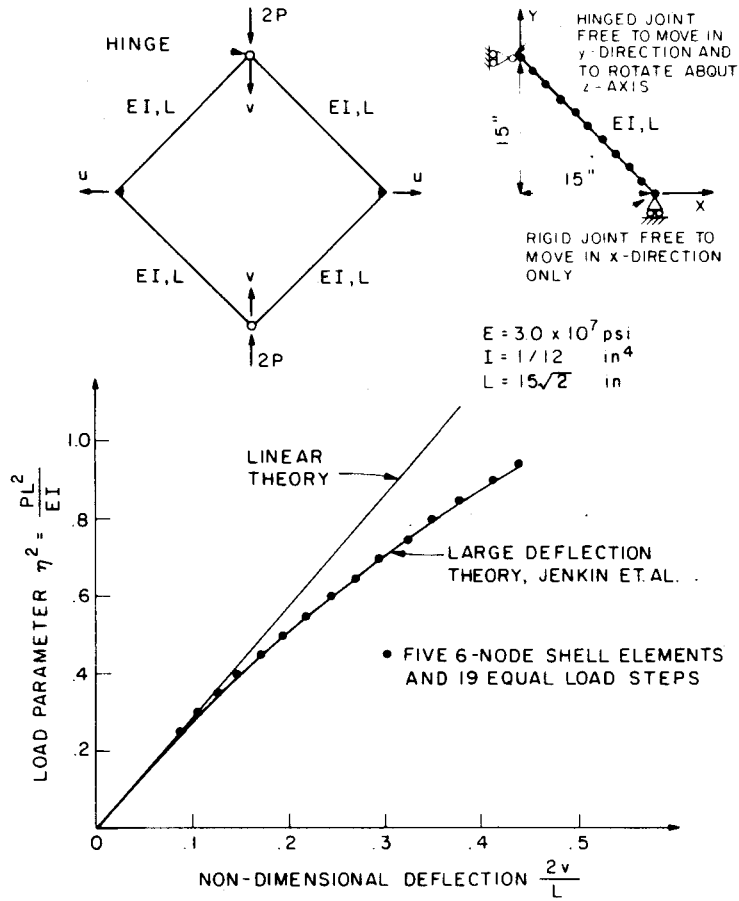
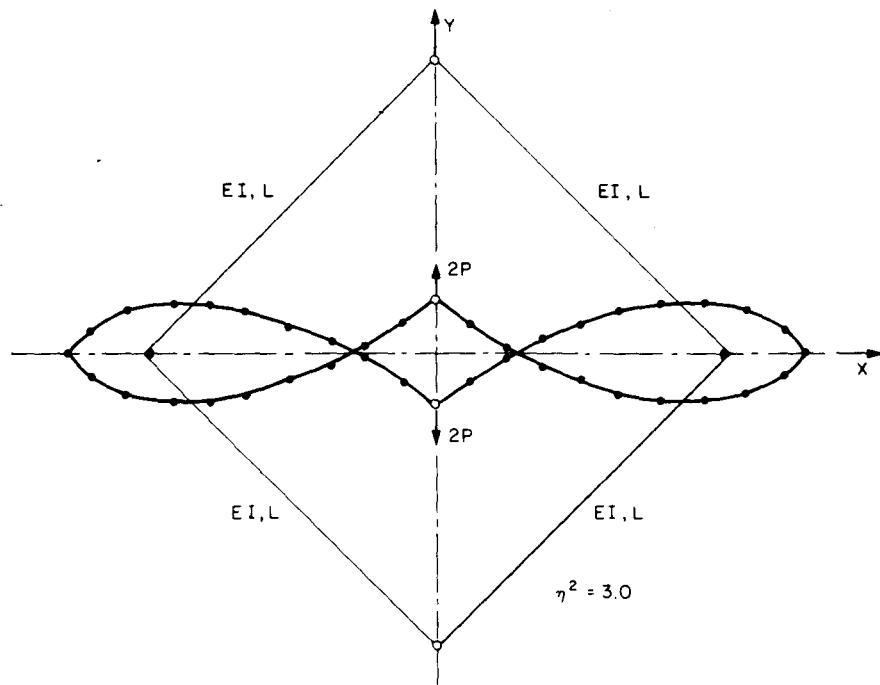
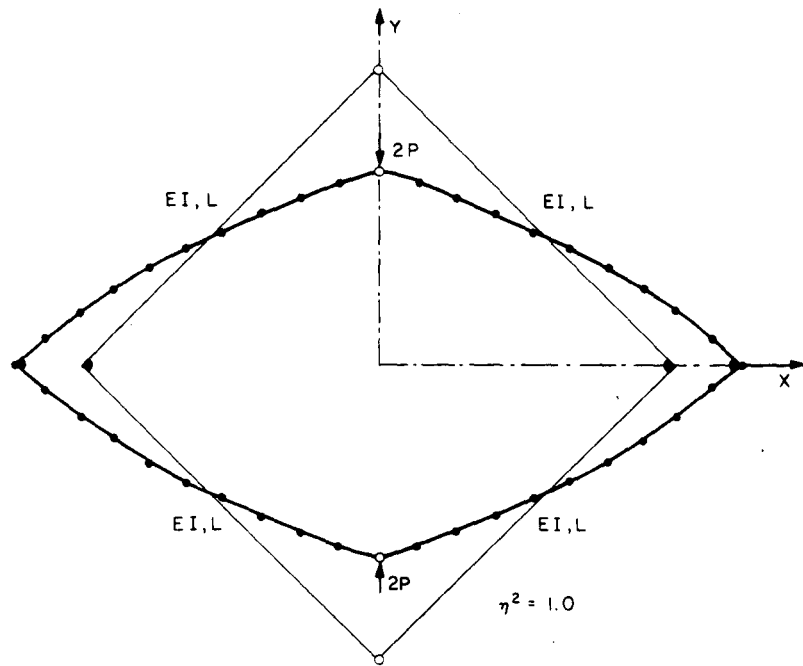


Fig. 14. Load-deflection curve for a diamond structure.



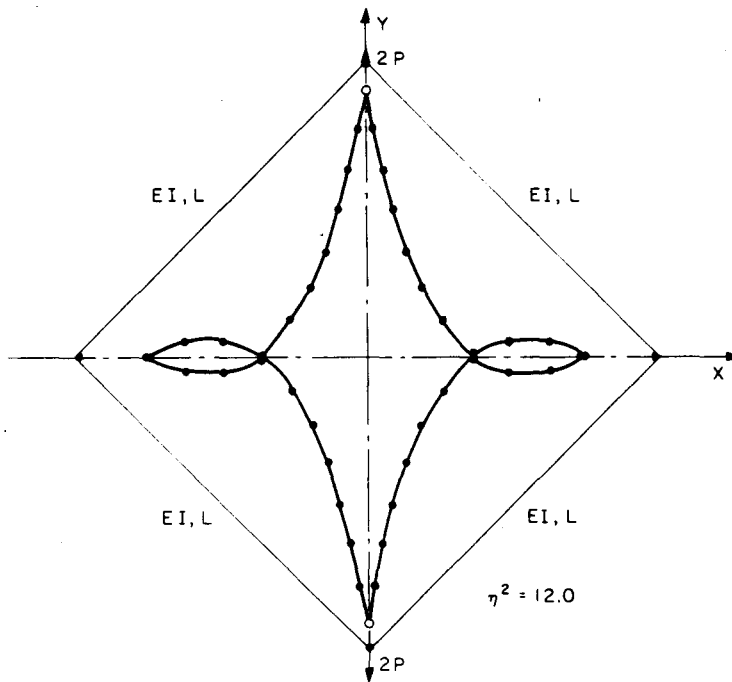


Fig. 15. Deformed shapes of the diamond structure for different values of the loading parameter $\eta^2 = PL^2/EI$.

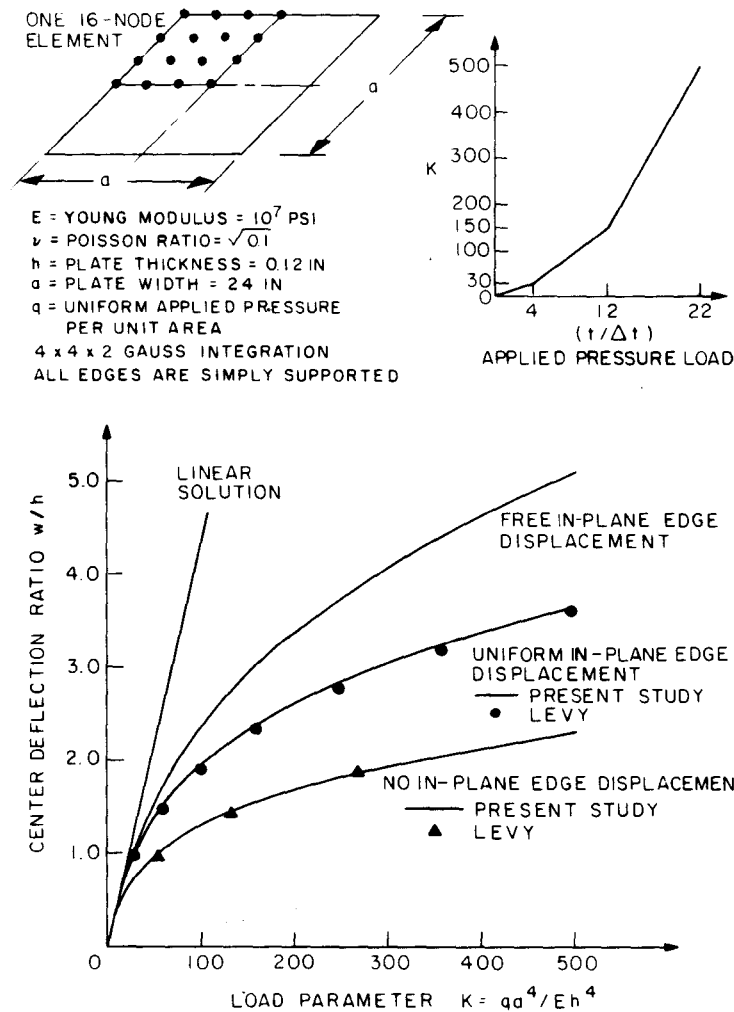


Fig. 16. Large deflection analysis of a simply-supported square plate subjected to pressure loading.

4.7 Elastic-plastic dynamic analysis of a simply supported plate

A dynamic analysis of a simply supported square plate subjected to lateral pressure loading was carried out. The Newmark time integration method was used with the time step increment $\Delta t = T_f/48$, where T_f is the fundamental period of the linear elastic plate. Nine 8-node quadratic plate elements were used to model one quarter of the plate. In a first analysis an elastic and in a second analysis an elastic-perfectly-plastic material was assumed.

Figure 17 shows the predicted response for both material property assumptions, and compares the calculated response with a solution given by Liu and Lin [20].

4.8 Large displacement analysis of two shells

The large displacement response of two shells was calculated. Using symmetry conditions, the shells shown in Figs 18 and 19 were modeled with only one 16-node cubic element. The predicted transverse displacements under the loads are compared in the figures with the solutions of Leicester [21] and Horrigmoe [22]. It is seen that the one cubic element

idealizations used in this study yield accurate displacement predictions.

5. CONCLUSIONS

The efficient practical finite element nonlinear analysis of shells requires the use of a shell finite element that is accurate, reliable, and versatile. In this paper a shell element has been presented that is very effective in those respects. The shell element can have a variable number of nodes, it can be employed as a transition element to model shell intersections or shell to continuum transition regions, and it can be used with a compatible bending element to model stiffened shells. The element can be employed in material and geometric nonlinear analysis of plates and general shells in which very large displacements and rotations can be measured. The results of various sample solutions have been given in the paper to indicate the accuracy that is obtained using various element nodal configurations and integration orders.

Considering further work on the element, it is desirable that possibilities of improving the element performance in the general analysis of shells using special numerical integration schemes be investigated.

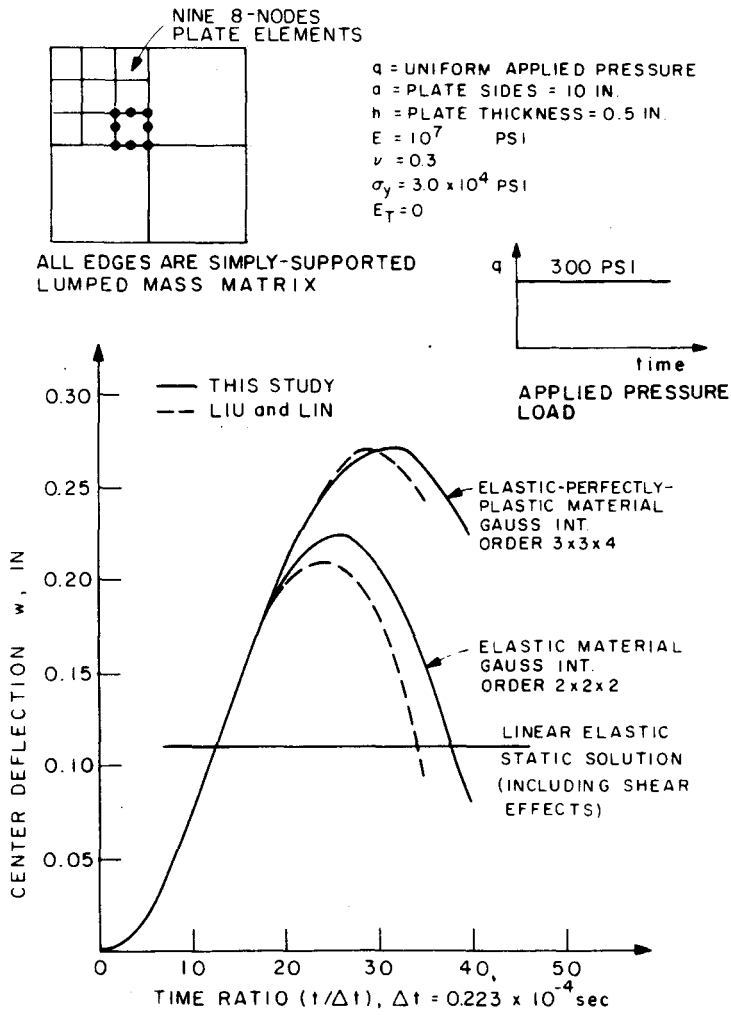


Fig. 17. Elastic and elastic-plastic dynamic response of a simply-supported square plate.

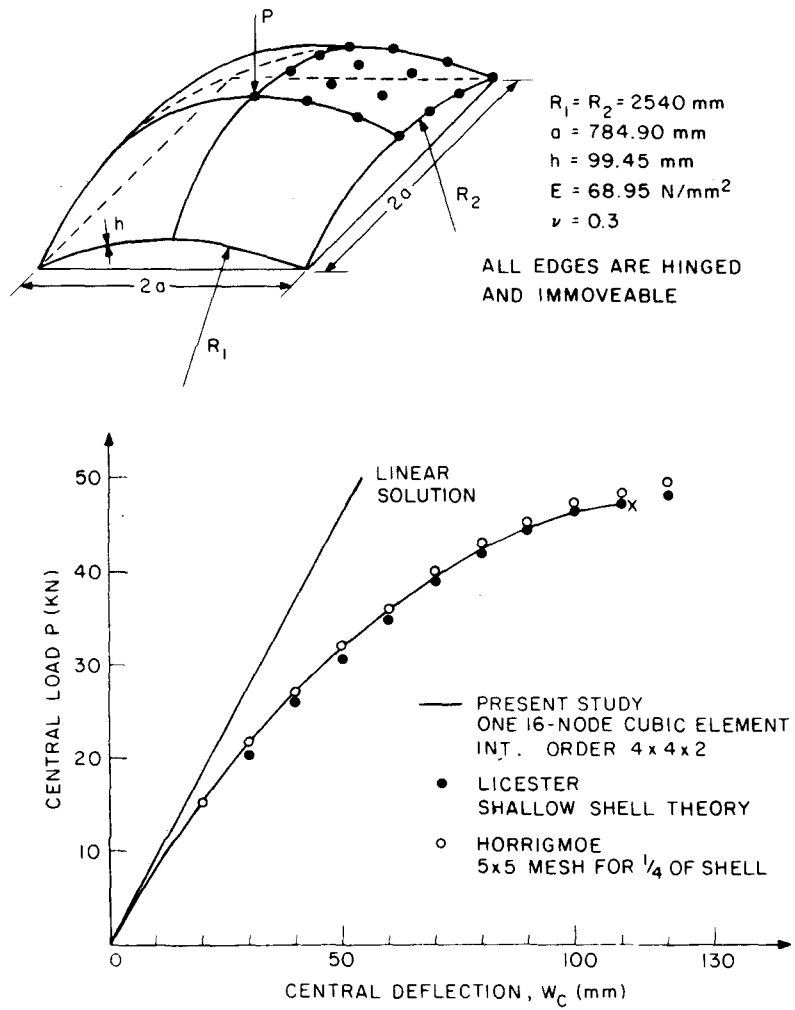


Fig. 18. Central deflection of a hinged spherical shell.

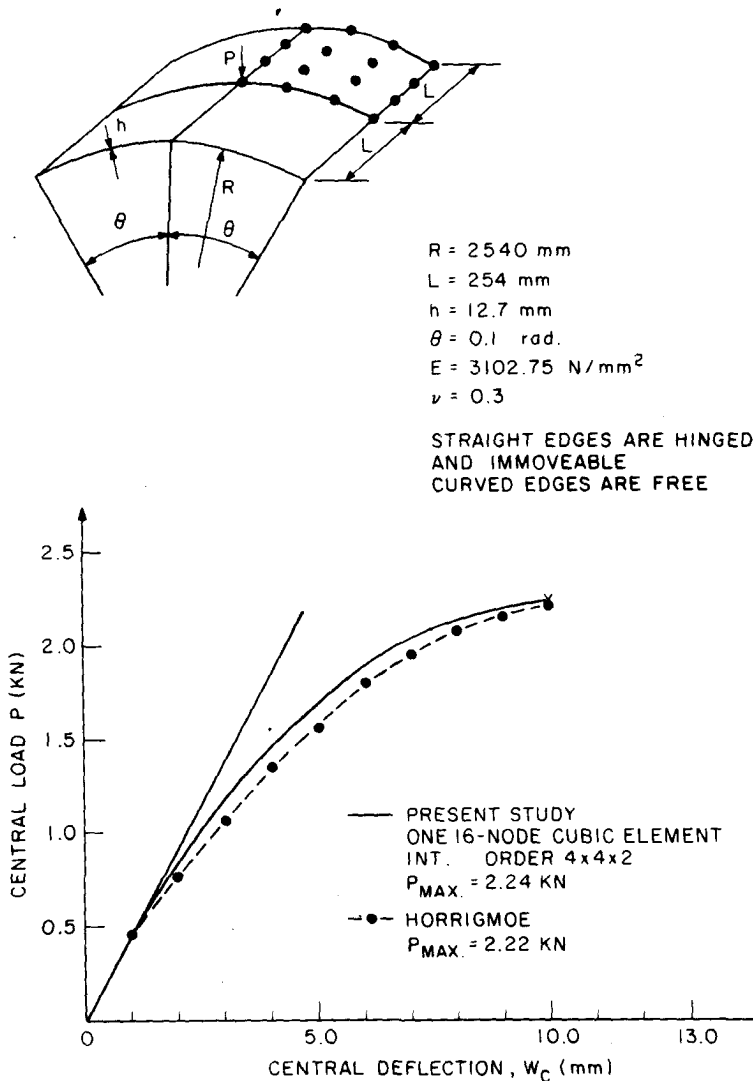


Fig. 19. Central deflection of a hinged cylindrical shell.

The difficulties lie in that such schemes must be put on a firm theoretical foundation and should be generally applicable and reliable in linear, and geometric and material nonlinear analysis.

Acknowledgement—The work reported in this paper has been supported financially by the ADINA users group. We gratefully acknowledge this support.

REFERENCES

1. R. H. Gallagher, *Finite Element Analysis Fundamentals*. Prentice-Hall, Englewood Cliffs, New Jersey (1973).
2. O. C. Zienkiewicz, *The Finite Element Method*. McGraw-Hill (1976).
3. R. H. Gallagher, Shell Elements, in Proc. of World Congress on Finite Elements in Struct. Mech., Vol. 1, Bournemouth, England (1975).
4. T. H. H. Pian and P. Boland, Formulation of large deflection shell analysis by assumed stress finite element method. in *Formulations and Computational Algorithms in Finite Element Analysis* (Edited by K. J. Bathe, J. T. Oden, and W. Wunderlich), M.I.T. Press, Massachusetts (1977).
5. A. K. Noor and S. J. Hartley, Nonlinear shell analysis via mixed isoparametric elements. *Comput. Structures* 7, 615-626 (1977).
6. S. Ahmad, B. M. Irons and O. C. Zienkiewicz, Analysis of thick and thin shell structures by curved elements. *Int. J. Num. Meth. Engng.* 2, 419-451 (1970).
7. E. Ramm, A plate/shell element for large deflections and rotations, in *Formulations and Computational Algorithms in Finite Element Analysis*, Bathe, K. J., Oden, J. T., and Wunderlich, W., (eds.), M.I.T. Press (1977).
8. B. Kråkeland, Large displacement analysis of shells considering elastic-plastic and elasto-viscoplastic materials. Report No. 776, The Norwegian Institute of Technology, The University of Trondheim, Norway (Dec. 1977).
9. K. J. Bathe and E. L. Wilson, *Numerical Methods in Finite Element Analysis*. Prentice-Hall, Englewood Cliffs, New Jersey (1976).
10. S. Bolourchi, On finite element nonlinear analysis of general shell structures. Ph.D. Thesis, Mechanical Engineering Department, M.I.T., Massachusetts (1979).
11. K. J. Bathe, ADINA—A finite element program for automatic dynamic incremental nonlinear analysis. Acoustics and Vibration Lab. Report 82448-1, Dept. of Mechanical Engineering, M.I.T., Massachusetts (Sept. 1975. rev. Dec. 1978).

12. K. J. Bathe, S. Bolourchi, S. Ramaswamy and M. D. Snyder, Some computational capabilities for nonlinear finite element analysis. *J. Nuclear Engng Design* **46**, 429-455 (1978).
13. T. J. R. Hughes, R. L. Taylor and W. Kanoknukulchai, A simple and efficient finite element for plate bending. *Int. J. Num. Meth. Engng* **9**, 353-386 (1975).
14. K. J. Bathe, E. Ramm and E. L. Wilson, Finite element formulations for large deformation dynamic analysis. *Int. J. Num. Meth. Engng* **9**, 353-386 (1975).
15. K. J. Bathe, Static and dynamic geometric and material nonlinear analysis using ADINA., Acoustics and Vibration Lab. Report 82448-2, Dept. of Mechanical Engineering, M.I.T., Massachusetts (May 1976, rev. May 1977).
16. G. R. Cowper, Gaussian quadrilateral formulas for triangles. *Int. J. Num. Meth. Engng* **7**, 405-410 (1973).
17. G. M. Lindberg, M. D. Olson and G. R. Cowper, New developments in the finite element analysis of shells. National Research Council of Canada Quarterly Bulletin of the Division of Mechanical Engineering and the National Aeronautical Establishment, Vol. 4, 1-38 (1969).
18. J. A. Jenkins, T. B. Seitz and J. S. Przemieniecki, Large deflections of diamond-shaped frames., *Int. J. Solids Structures* **2**, 591-603 (1966).
19. S. Levy, Bending of rectangular plates with large deflections. Technical Notes, National Advisory Committees for Aeronautics, No. 846 (1942).
20. S. C. Liu and T. H. Lin, Elastic-plastic dynamic analysis of structures using known elastic solutions. *Int. J. Earthquake Eng. and Struct. Dynamics*, **7**, 147-159 (1979).
21. R. H. Leicester, Finite deformations of shallow shells. *ASCE* **94**, EM6, 1409-1423 (1968).
22. G. Horrigmoe, Finite element instability analysis of free-form shells. Report No. 77-2, The Norwegian Institute of Technology, The University of Trondheim, Norway (May 1977).

A SIMPLE AND EFFECTIVE ELEMENT FOR ANALYSIS OF GENERAL SHELL STRUCTURES

KLAUS-JÜRGEN BATHE and LEE-WING HO

Department of Mechanical Engineering, Massachusetts Institute of Technology, Cambridge, MA 02139, U.S.A.

Abstract—A simple flat three-node triangular shell element for linear and nonlinear analysis is presented. The element stiffness matrix with 6 degrees-of-freedom per node is obtained by superimposing its bending and membrane stiffness matrices. An updated Lagrangian formulation is used for large displacement analysis. The application of the element to the analysis of various linear and nonlinear problems is demonstrated.

1. INTRODUCTION

Two approaches have basically been employed in the recent efforts on the development of general shell analysis capabilities [1, 2]:

- High-order isoparametric elements based on degenerating fully three-dimensional stress conditions have been proposed.

- Low-order simple elements that are basically obtained by superimposing plate bending and membrane stiffnesses have been developed.

The higher-order isoparametric elements are very versatile (they can be employed as transition elements [2, 3]) and are quite effective, but they can be costly in use. The element stiffness matrix is relatively large in size and a sufficiently high enough integration order must be used to avoid the introduction of spurious zero energy modes.

The premise of the simple low-order elements lies in that their related matrices can be formed inexpensively. Thus, even when a large number of elements are required to model a complex structure, the overall analysis effort may still be less than with the use of the higher-order isoparametric shell elements. Also, the direct use of stress resultants (moments, membrane forces) may not only decrease the cost of analysis, but also facilitates the interpretation of the computed results.

Various simple low-order elements have been proposed recently [4-8]. When evaluating these elements for practical analysis, we believe that the following three criteria should be considered:

(1) The element should yield accurate solutions when modeling any shell geometry and under all boundary and loading conditions. In particular, the element should exactly contain the required 6 zero rigid modes, so that reliable results can always be expected. The theory of the element formulation must be well-understood and should not contain any "numerical fudge factors".

(2) We should be able to use the element in the modeling of general shell structures with beam stiffeners, cut-outs, intersections, and so on.

(3) The element should be cost-effective in linear as well as in nonlinear, static and dynamic analysis. In nonlinear analysis, the element should be applicable to large displacement, large rotation, and materially nonlinear conditions.

Considering the above criteria we want to emphasize that the reliability aspect in (1) is the most important. Yet, a considerable number of elements that have been published do not satisfy this criterion. Such element developments represent interesting research, but should not be used in actual engineering analyses, because the generated analysis results cannot be interpreted with confidence.

The objective in this paper is to present a shell element that is simple and effective and that has been developed with due regard to the above requirements. The element is shown schematically in Fig. 1. We observe that the element is flat and has 3 nodes with 6 degrees of freedom per node. The total element stiffness matrix is formulated by superimposing—in the way some of the earliest shell elements were formulated [9]—a plane stress membrane stiffness K_M , a bending stiffness K_B and an in-plane rotational stiffness K_{θ_z} . In the next section we discuss the derivation of these stiffness matrices for linear analysis. The updated Lagrangian formulation used in large displacement analysis is then presented in Section 3 and finally in Section 4 we present the results obtained in various demonstrative sample analyses.

2. FORMULATION OF ELEMENT FOR INFINITESIMAL DISPLACEMENT ANALYSIS

Since the complete stiffness matrix of the element is obtained by the direct superposition of K_M , K_B and K_{θ_z} , we can discuss the formulation of these matrices independently.

2.1 Membrane stiffness matrix

The element membrane stiffness K_M is simply the constant strain plane stress stiffness matrix of a 3-node element.

2.2 Bending stiffness matrix

The bending stiffness matrix is formulated using the Mindlin theory of plates with shear deformations included. Using the variables defined in Fig. 2, the displacement components of a point with coordinates x , y , z are in this theory [8]

$$u = z\beta_x(x, y); v = -z\beta_y(x, y); \text{ and } w = w(x, y) \quad (1)$$

where w is the transversal displacement, β_x and β_y are the rotations of the normal to the undeformed middle surface about the y and x axes, respectively.

The bending strains vary linearly through the thickness

$$\epsilon_b = z\kappa \quad (2)$$

where κ is the three component vector of curvatures

$$\kappa = \begin{bmatrix} \beta_{x,x} \\ -\beta_{y,y} \\ \beta_{x,y} - \beta_{y,x} \end{bmatrix} \quad (3)$$

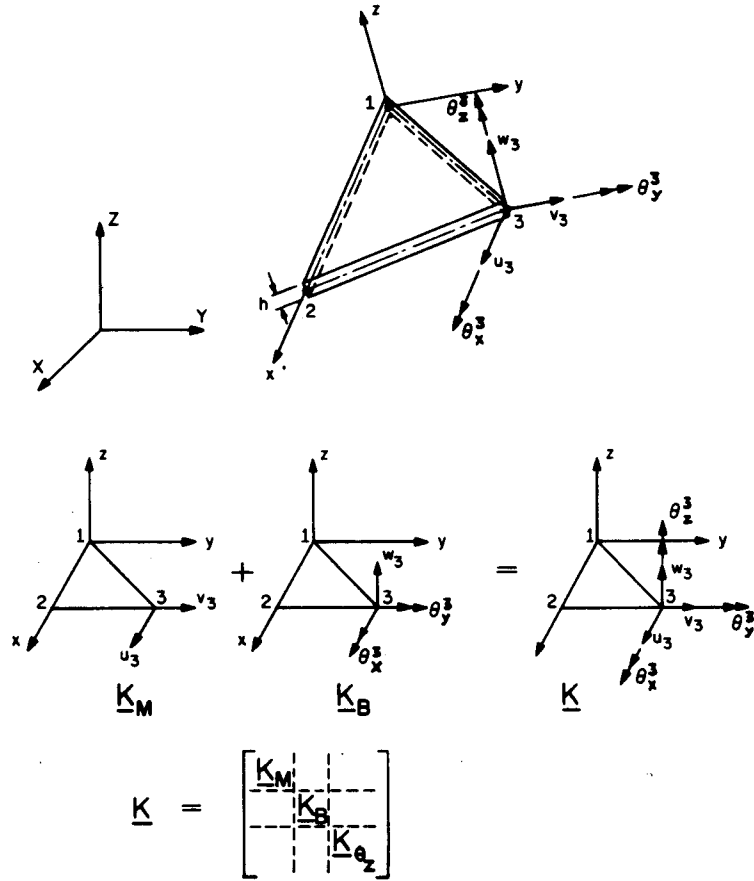


Fig. 1. The shell element.

and the transverse shear strains are constant through the thickness,

$$\gamma = \begin{bmatrix} w_{,y} - \beta_y \\ w_{,x} + \beta_x \end{bmatrix} \quad (4)$$

As in the Krichhoff plate theory, the state of stress in

the plate is defined with plane stress assumption, i.e. $\sigma_z = 0$. The stress-strain relations for a particular layer are:

$$\sigma_b = \begin{bmatrix} \sigma_x \\ \sigma_y \\ \tau_{xy} \end{bmatrix} = z C \kappa \quad (5)$$

and

$$\sigma_s = \begin{bmatrix} \tau_{yz} \\ \tau_{zx} \end{bmatrix} = C_s \gamma \quad (6)$$

where the matrices C and C_s are the elasticity matrices in plane stress and shear deformations, respectively [1, 2].

With the kinematics as given by eqns (1)-(4) and the material descriptions given by eqns (5) and (6) the strain energy is

$$\mathcal{U} = \mathcal{U}_b + \mathcal{U}_s \quad (7)$$

where

$$\mathcal{U}_b = \frac{1}{2} \int_A \kappa^T D_b \kappa dA \quad (8)$$

$$\mathcal{U}_s = \frac{1}{2} \int_A \gamma^T D_s \gamma dA \quad (9)$$

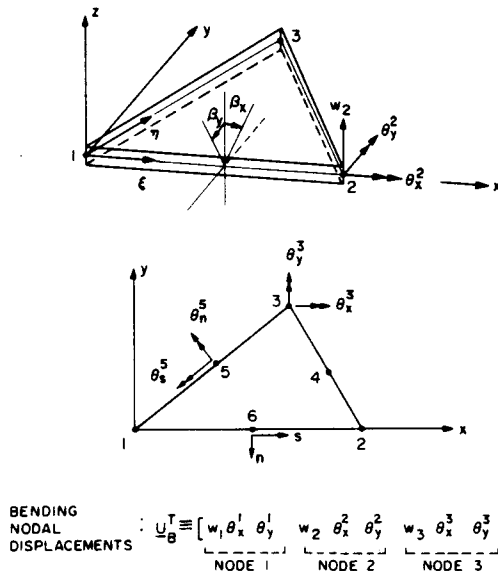


Fig. 2. Notation used in calculation of bending stiffness matrix.

BENDING NODAL DISPLACEMENTS : $U_B^T \equiv [\underbrace{w_1 \theta_x^1 \theta_y^1}_{\text{NODE 1}} \quad \underbrace{w_2 \theta_x^2 \theta_y^2}_{\text{NODE 2}} \quad \underbrace{w_3 \theta_x^3 \theta_y^3}_{\text{NODE 3}}]$

and

$$D_b = \int_{-h/2}^{h/2} C z^2 dz \quad (10)$$

$$D_s = k \int_{-h/2}^{h/2} C_s dz. \quad (11)$$

The variables u_b and u_s represent the bending and transverse shear contributions, respectively, and k in eqn (11) is a shear correction factor to account for the non-uniformity of the transverse shear stresses through the plate thickness.

In eqns (8) and (9) the matrices D_b and D_s are functions of the thickness of the plate, h , and of the elastic properties of the different layers; the variable A is the area of the middle surface of the plate. For the important practical case of an isotropic homogeneous plate of constant thickness we have

$$D_b = \frac{Eh^3}{12(1-\nu^2)} \begin{bmatrix} 1 & \nu & 0 \\ \text{(sym)} & 1 & 0 \\ & & \frac{1-\nu}{2} \end{bmatrix}; D_s = \frac{Ehk}{2(1+\nu)} \begin{bmatrix} 1 & 0 \\ 0 & 1 \end{bmatrix}. \quad (12)$$

The variables E and ν in eqn (12) are the Young's modulus and Poisson's ratio, and k is usually taken as 5/6.

By definition, the bending moments M and shear forces Q are obtained by integration of the stresses through the thickness:

$$M = \begin{bmatrix} M_x \\ M_y \\ M_{xy} \end{bmatrix} = \int_{-h/2}^{h/2} \sigma z dz = D_b \kappa \quad (13)$$

and

$$Q = \begin{bmatrix} Q_y \\ Q_x \end{bmatrix} = k \int_{-h/2}^{h/2} \sigma_s dz = D_s \gamma. \quad (14)$$

For thin plates the transverse shear strains are small and therefore the transverse shear strain energy u_s is negligible compared to the bending energy. The finite element model based on the energies in eqns (7)–(9) must be able to represent this constraint. Therefore, the stiffness matrix of the element for the analysis of thin plates is based only on the expression,

$$u = \frac{1}{2} \int_A \kappa^T D_b \kappa dA \quad (15)$$

and this results in a discrete-Kirchhoff-theory (DKT) element formulation.

Equation (15) contains only the first derivatives of β_x and β_y , and hence it is relatively easy to establish interpolation functions that satisfy the compatibility requirements. However, since β_x, β_y are the only variables in eqn (15), it is necessary to relate the rotations of the normal to the middle surface to the transverse displacement w (which does not appear in eqn (15)). We use that β_x and β_y vary quadratically over the element, i.e.

$$\beta_x = \sum_{i=1}^6 h_i \theta_{y,i}; \beta_y = \sum_{i=1}^6 h_i \theta_{x,i} \quad (16)$$

where $\theta_{x,i}$ and $\theta_{y,i}$ are the nodal values at the corners and at the mid-points of the sides (see Fig. 2), and then we used the following constraints:

- (1) the Kirchhoff hypothesis is imposed at:
 - (a) the corner nodes

$$\gamma = \begin{bmatrix} w_{,y} - \beta_y \\ w_{,x} + \beta_x \end{bmatrix} = 0 \quad \text{at nodes 1, 2 and 3} \quad (17)$$

- (b) the mid-points of the sides (defined anticlockwise around the element boundary),

$$w_{,s} - \beta_s = 0 \quad k = 4, 5, 6; \quad (18)$$

- (2) the variation of w along the sides is cubic, i.e.

$$w_{,s} \Big|_{\text{at node } k} = -\frac{3}{2l_{ij}} w_i - \frac{1}{4} w_{,s} \Big|_{\text{at node } i} + \frac{3}{2l_{ij}} w_j - \frac{1}{4} w_{,s} \Big|_{\text{at node } j} \quad (19)$$

with k denoting the mid-node of side ij and l_{ij} equal to the length of the side ij ; and

- (3) a linear variation of β_n is imposed along the sides, i.e.

$$\beta_n^k = \frac{1}{2} (\beta_n^i + \beta_n^j) \quad (20)$$

where $k = 4, 5, 6$ denotes the mid-points of the element sides. Using eqns (16)–(20) we obtain [8]

$$\begin{aligned} \beta_x &= H_x^T(\xi, \eta) U_B \\ \beta_y &= H_y^T(\xi, \eta) U_B \end{aligned} \quad (21)$$

where the H_x and H_y are nine component vectors of new shape functions, and ξ, η are the natural elements coordinates.

The evaluation of the stiffness matrix now follows the standard procedures of the finite element displacement method. We have

$$\kappa = B_B U_B \quad (22)$$

where B_B is the strain-displacement transformation matrix,

$$B_B(\xi, \eta) = \frac{1}{2A} \begin{bmatrix} y_3 H_{x,\xi}^T & & \\ -x_3 H_{y,\xi}^T + x_2 H_{y,\eta}^T & & \\ -x_3 H_{x,\xi}^T + x_2 H_{x,\eta}^T + y_3 H_{y,\xi}^T & & \end{bmatrix}. \quad (23)$$

The bending stiffness matrix of the element is then

$$K_B = 2A \int_0^1 \int_0^{1-\eta} B_B^T D_b B_B d\xi d\eta. \quad (24)$$

If the thickness and the material properties are constant over the element, the exact integration of K_B is obtained using three numerical integration points located at the mid-points of the edges or inside because the integral involves only quadratic terms.

Once the nodal displacements have been calculated, the bending moments M at any point in the element can be obtained

$$M(\xi, \eta) = D_b B_B(\xi, \eta) U_B \quad (25)$$

where

$$\begin{aligned} x &= \xi x_2 + \eta x_3 \\ y &= \eta y_3. \end{aligned} \tag{26}$$

2.2 In-plane rotation stiffness

The superposition of K_M and K_B in a three-dimensional space yields an element stiffness matrix that in a local coordinate system has zero in-plane rotational stiffness. The value of K_{θ} , equal to 10^{-4} times the smallest bending stiffness is thus added into this degree-of-freedom to obtain 6 stiffness degrees-of-freedom per node. This value is chosen to remove the in-plane rotational singularity from the element stiffness matrix when the local x - y - z axes coincide with the global X - Y - Z axes.

3. FORMULATION FOR LARGE DISPLACEMENT ANALYSIS

The formulation of the element for large displacement analysis follows closely the developments presented in [10]. In that work we studied an updated and a total Lagrangian formulation of a beam element that was based on Hermitian interpolation of the bending displacements and linear interpolation of the longitudinal and torsional displacements. We concluded in that study that the use of both formulations yields in an analysis identically the same numerical results, but that the updated Lagrangian formulation requires less computations. For the same reasons, considering the 3-node shell element, which is also based on different interpolations for the bending and membrane displacements, an updated Lagrangian formulation will be more effective.

3.1 Governing equilibrium equations

The application of the principle of virtual displacements to an element yields in the incremental large displacement analysis [2]

$$(\mathbf{K}_L + \mathbf{K}_{NL})\Delta\mathbf{U}^{(i)} = \mathbf{R}^{t+\Delta t} - \mathbf{F}^{t+\Delta t(i-1)} \tag{27}$$

where \mathbf{K}_L and \mathbf{K}_{NL} are the linear and nonlinear strain stiffness matrices, $\mathbf{R}^{t+\Delta t}$ is the load vector corresponding to the external loads at time $t + \Delta t$, $\mathbf{F}^{t+\Delta t(i-1)}$ is a vector of nodal point forces corresponding to the element stresses at time $t + \Delta t$ and iteration $(i - 1)$, and

$$\mathbf{U}^{t+\Delta t(i)} = \mathbf{U}^{t+\Delta t(i-1)} + \Delta\mathbf{U}^{(i)}. \tag{28}$$

In eqn (27) we consider the equilibrium equations of a single element from which the equilibrium equations of an assemblage of elements can be obtained using standard procedures [2]. Also, the updated Lagrangian formulation is used because the reference configuration (denoted by left subscripts) corresponds to the times at which the quantities are calculated (denoted by the left superscripts).

Figure 3 shows schematically an element undergoing large displacements, and defines the coordinate systems and displacements used in the calculation of the stiffness matrix and force vector. We note that the global coordinate system X, Y, Z is stationary and that the total and incremental nodal point displacements and rotations are evaluated in this coordinate system. In addition, we consider body-attached coordinate systems. The stiffness

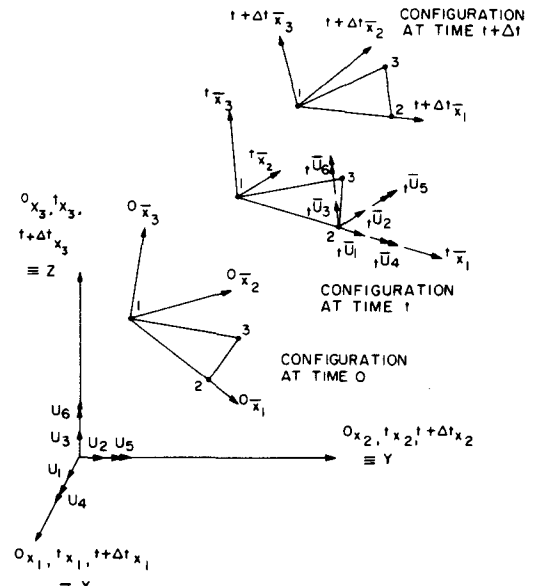


Fig. 3. Large displacement motion of the element.

matrix and force vector of the element corresponding to the global stationary coordinate system are evaluated by calculating these matrices first in the current body-attached coordinate frame. Since small strain but large rotation conditions are assumed, the membrane and bending contributions can—in the body-attached coordinate system—be evaluated separately much in the same way as in linear analysis. The matrices are then transformed to the global coordinate frame. In the following sections we, therefore, only need to discuss how the bending and membrane stiffness matrices and the corresponding nodal point force vectors are calculated in the body-attached coordinate system.

3.2 Membrane force vector and stiffness matrix

The membrane displacements at any time τ yield the membrane forces corresponding to that time. Let \mathbf{U}_M^τ be the total membrane displacements at time τ in the plane of the element as shown in Fig. 4. These displacements are calculated from the difference in the local element coordinates at times equal to τ and zero. The element internal membrane forces, \mathbf{N} , are then calculated as in linear analysis. Using the strain-displacement matrix corresponding to the original element configuration,

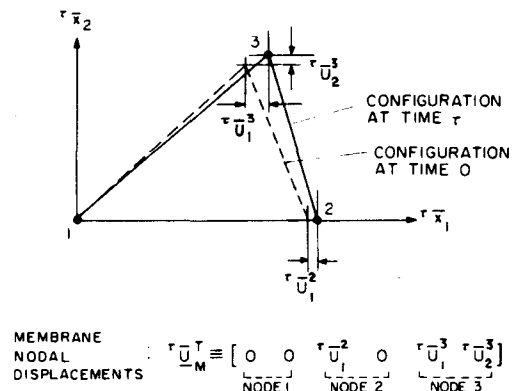


Fig. 4. Element membrane displacements.

B_M , and the displacements shown in Fig. 4, we have

$$\bar{N} = h C B_M^T \bar{U}_M \quad (29)$$

where the bar over a quantity signifies that it is defined in the local coordinate system.

The nodal point force vector corresponding to the internal membrane forces is then

$$\bar{F} = \int_A B_M^T \bar{N} dA. \quad (30)$$

The linear strain stiffness matrix in the local coordinate system is calculated as in linear analysis,

$$\bar{K}_{LM} = \bar{K}_M \quad (31)$$

and the nonlinear strain stiffness matrix is

$$\bar{K}_{NLM} = \int_A B_{NL}^T \hat{N} B_{NL} dA \quad (32)$$

where B_{NL} and \hat{N} are given in Appendix A.

3.3 Bending force vector and stiffness matrix

Whereas the membrane internal element forces are calculated from the total membrane displacements at time τ , the element bending moments are calculated by incrementation, i.e. we have

$$\bar{M} = \tau - \Delta t \bar{M} + \tau - \Delta t \bar{M}. \quad (33)$$

The incremental bending moments are obtained from the local curvature increments,

$$\tau - \Delta t \bar{\kappa} = B_B \tau - \Delta t \bar{U}_B \quad (34)$$

$$\tau - \Delta t \bar{M} = D_B \tau - \Delta t \bar{\kappa} \quad (35)$$

where B_B is the constant generalized strain-displacement matrix defined in eqn (23), and $\tau - \Delta t \bar{U}_B$ is a vector storing the bending displacement increments from the configuration at time $\tau - \Delta t$.

The nodal point force vector corresponding to the element bending moments is then

$$\bar{F}_B = \int_A B_B^T \bar{M} dA. \quad (36)$$

Considering the element stiffness matrix, the linear strain stiffness matrix is evaluated as in linear analysis

$$\bar{K}_{LB} = K_B \quad (37)$$

and the effect of the nonlinear strain stiffness matrix is neglected. This assumption is appropriate because the bending effect is relatively small, and only an approximate stiffness matrix is required in the analysis.

The above calculations (eqns (33)–(35)) assume that the incremental displacements are small, and the bending distortions of the element can be neglected in the evaluation of the generalized strain-displacement matrix.

4. SAMPLE SOLUTIONS

To indicate the applicability and effectiveness of the element we present in this section the results obtained in

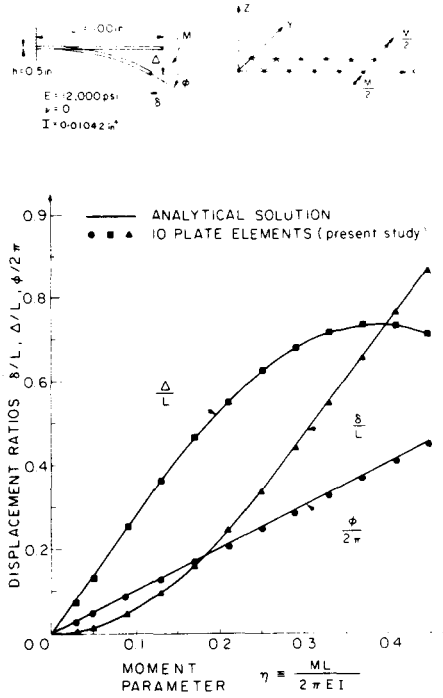


Fig. 5. Large deflection response of a cantilever.

the analyses of some problems. Tests of the element in the linear analysis of plates have been presented in [8].

4.1 Large deflection and rotation analysis of a cantilever

The cantilever shown in Fig. 5 was analyzed for its large deflection response. Five layers of elements were used in the analysis. This is a problem that is frequently used to study the characteristics of an element [6, 10].

Figure 5 shows the predicted response in the analysis and the response calculated analytically. We observe good correspondence between the two solutions.

4.2 Analysis of a pinched cylindrical shell

The structure analyzed and a typical finite element idealization used are shown in Fig. 6. In the figure the 10×10 mesh used is shown, but the analysis was also carried out with 4×4 , 6×6 , 8×8 and 16×16 mesh topologies. Figures 7–9 give calculated displacement and stress resultant distributions along the lines DC, BC and AD of the shell, respectively. It is seen that the finite element predictions converge rapidly to the analytical solution [11] as a reasonable number of shell elements is employed in the structural idealization. Table 1 sum-

Table 1. Total solution times in analysis of pinched cylindrical shell (on a CDC Cyber 175)

Grid	Solution time (sec.)
4x4	1.00
6x6	1.86
8x8	3.19
10x10	5.73
16x16	21.94

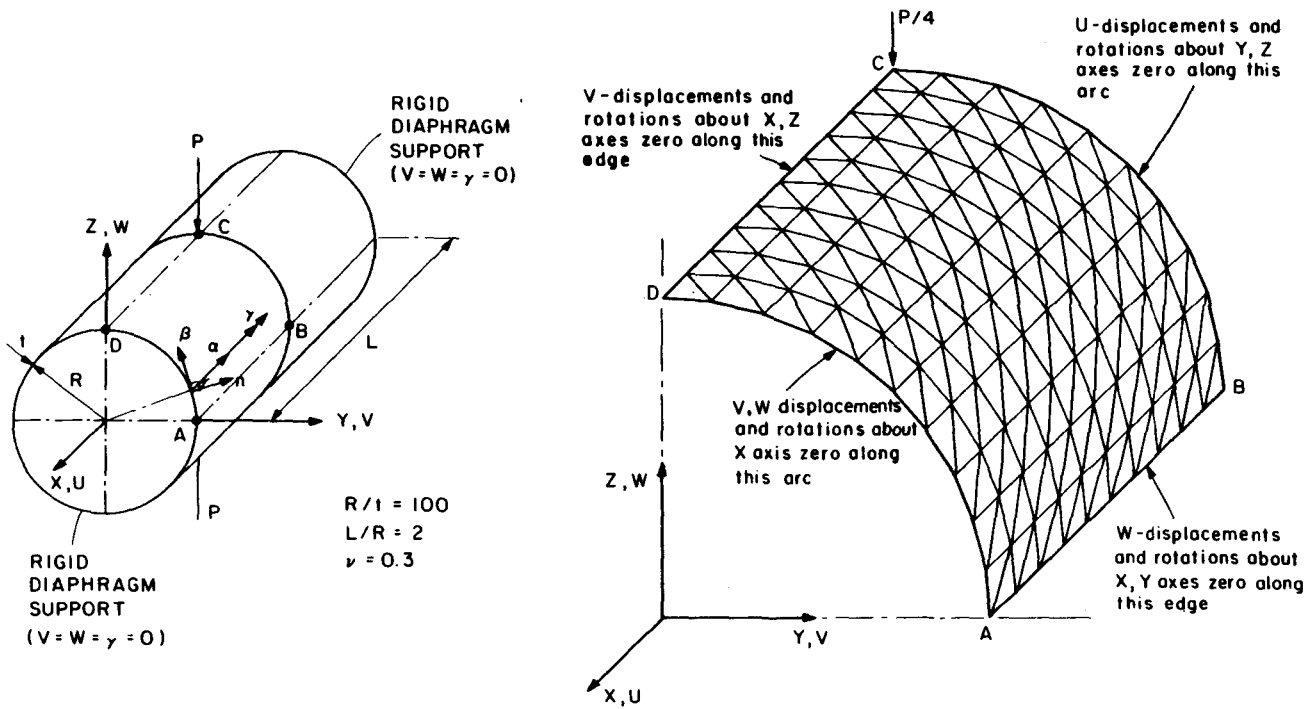


Fig. 6. Analysis of a pinched cylindrical shell structure.

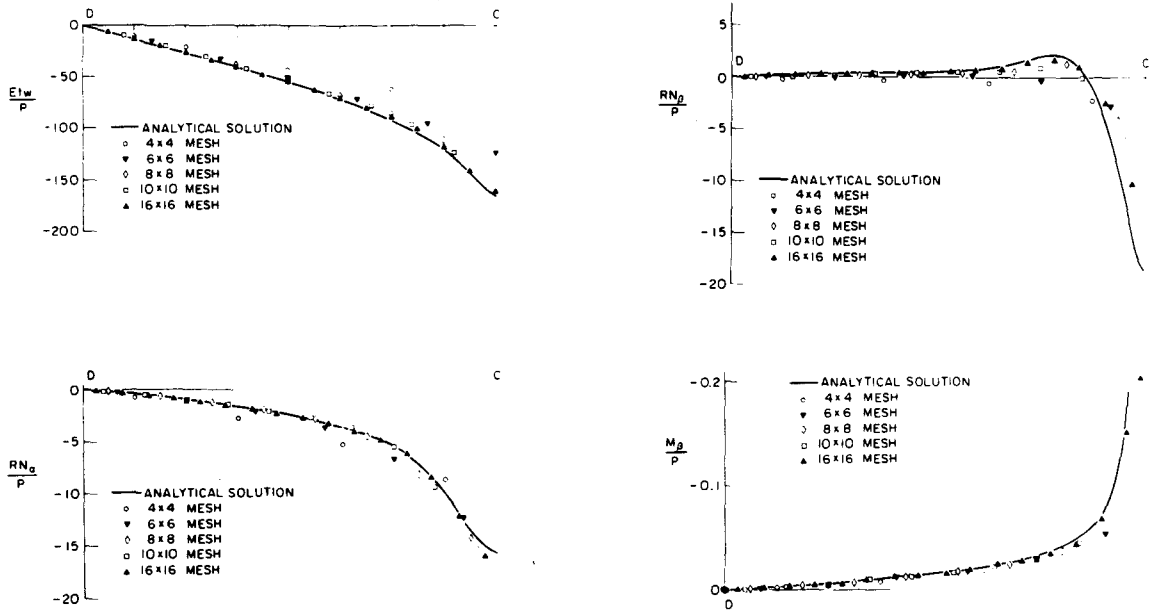


Fig. 7. Predicted displacement and stress distributions along DC of shell in Fig. 6.

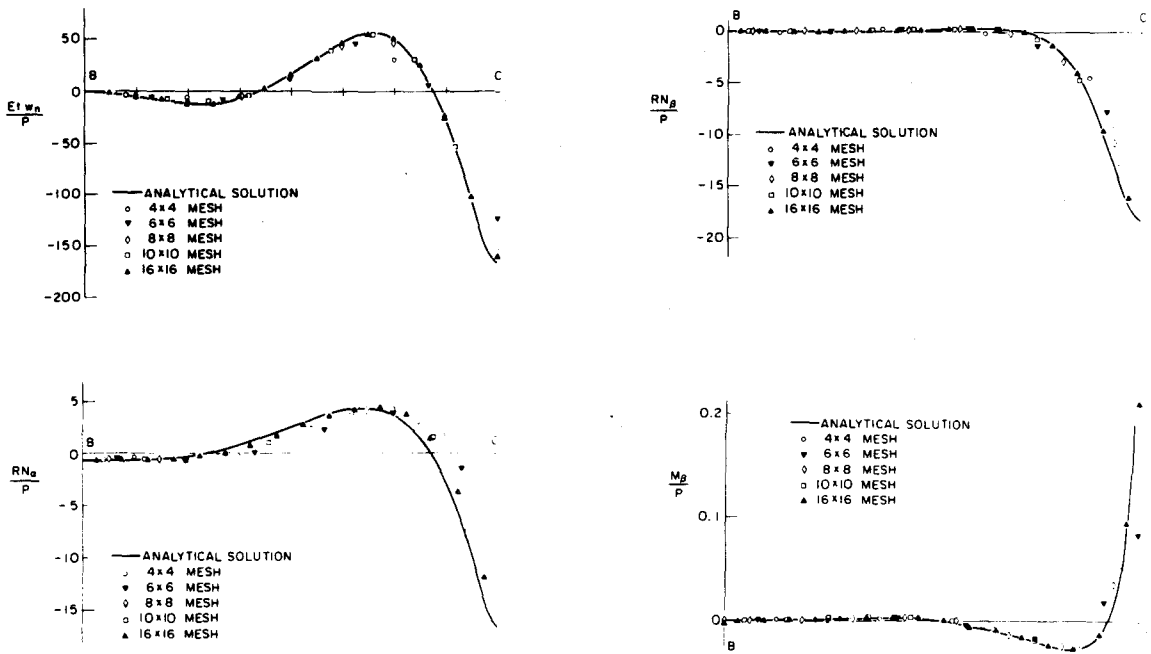


Fig. 8. Predicted displacement and stress distributions along BC of shell in Fig. 6.

marizes the solution times used in the analysis of the shell structure.

4.3 Large displacement analysis of a simply-supported plate

The plate was subjected to a uniform pressure loading q . Figure 10 shows the finite element idealization used for the plate and the response predicted. In a first analysis, the edges were constrained not to move in the plane of the plate, and in a second analysis, the u and v edge dis-

placements were left free. The predicted responses in these analyses are compared in Fig. 10 with other solutions reported earlier [12, 3].

4.4 Large displacement analysis of a spherical shell

The shell described in Fig. 11 was analyzed for its large displacement response using a 5×5 mesh. Figure 12 shows the response predicted when the shell is subjected to the concentrated apex load. The post-buckling response was calculated by adding a stiffness of 12,000 lb/in

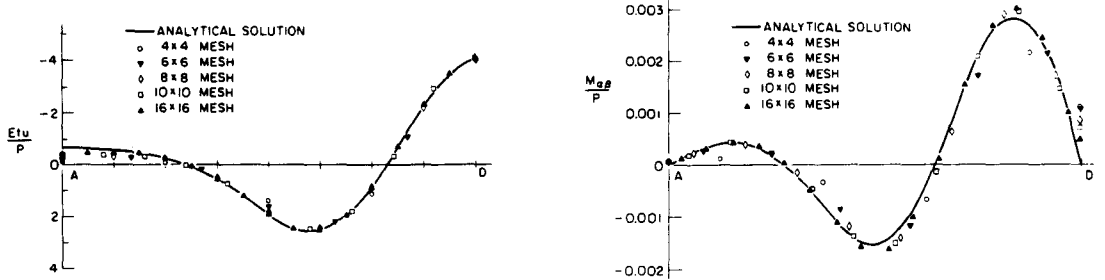


Fig. 9. Predicted displacement and stress distributions along AD of shell in Fig. 6.

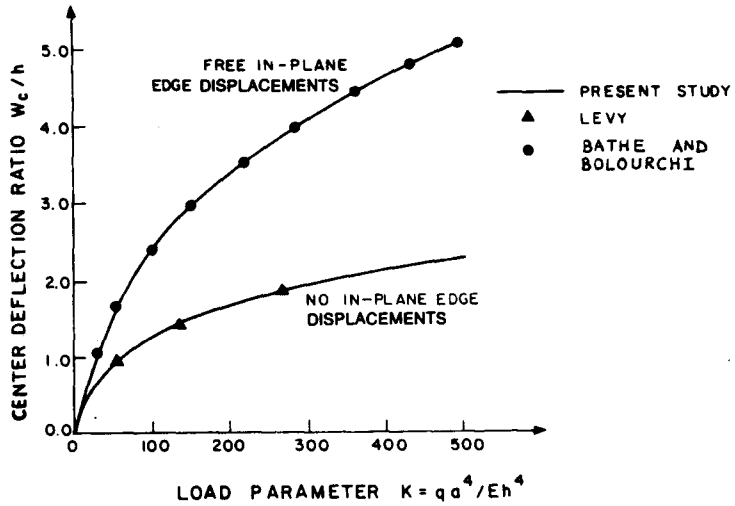
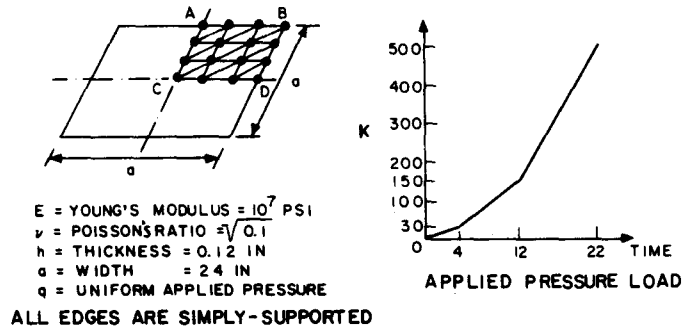


Fig. 10. Analysis of a simply-supported plate.

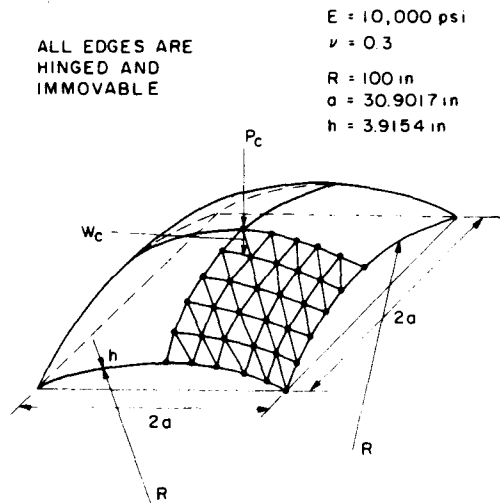


Fig. 11. Spherical shell subjected to apex load.

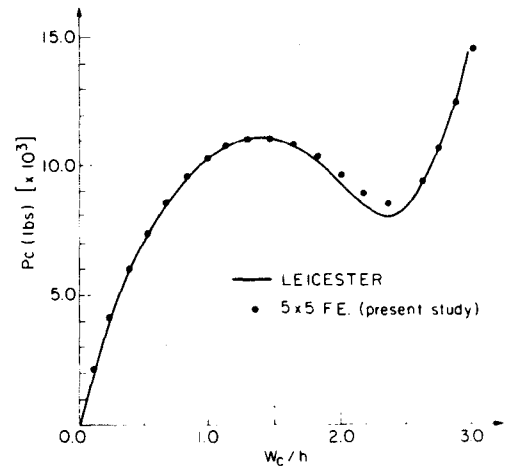


Fig. 12. Displacement response of spherical shell in Fig. 11.

to the w_c degree-of-freedom. This stiffness renders the stiffness matrix of the total structure positive-definite throughout the response history.

The result obtained in the finite element analysis is compared in Fig. 12 with the solution reported by Leicester [13, 14].

CONCLUDING REMARKS

The objective in this paper was to present a simple and effective 3-node triangular plate/shell element. The element is easy to use and very versatile. It is also reliable because the element stiffness matrix is integrated exactly: hence, the element contains no spurious zero energy modes. The element has excellent bending characteristics but a shortcoming is that the membrane forces are assumed to be constant. Therefore, it is still desirable to improve the element membrane behavior.

We have tested the element in various applications and some solution results are presented in the paper. Our experiences with the element show that it complements in a very effective way the higher-order isoparametric shell elements also available in ADINA.

Acknowledgement—We gratefully acknowledge the financial support of the ADINA users group.

REFERENCES

1. O. C. Zienkiewicz, *The Finite Element Method*. McGraw-Hill, New York (1977).
2. K. J. Bathe, *Finite Element Procedures in Engineering Analysis*, Prentice-Hall, Englewood Cliffs, New Jersey, in press.
3. K. J. Bathe and S. Bolourchi, A geometric and material nonlinear plate and shell element. *Comput. Structures* 11, 23-48 (1979).
4. T. J. R. Hughes, R. L. Taylor and W. Kanoknukulchai, A simple and efficient finite element for plate bending. *Int. J. Numer. Meth. Engng* 11, 1529-1543 (1977).
5. O. C. Zienkiewicz, J. Bauer, K. Morgan and E. Onate, A simple and efficient element for axisymmetric shells. *Int. J. Numer. Meth. Engng* 11, 1545-1558 (1977).

$$B_{NL} = \frac{1}{2A} \begin{bmatrix} -\bar{x}_2^3 & 0 & 0 & \bar{x}_2^3 & 0 & 0 & 0 & 0 & 0 \\ \bar{x}_1^{32} & 0 & 0 & -\bar{x}_1^3 & 0 & 0 & \bar{x}_1^2 & 0 & 0 \\ 0 & -\bar{x}_2^3 & 0 & 0 & \bar{x}_2^3 & 0 & 0 & 0 & 0 \\ 0 & \bar{x}_1^{32} & 0 & 0 & -\bar{x}_1^3 & 0 & 0 & \bar{x}_1^2 & 0 \\ 0 & 0 & -\bar{x}_2^3 & 0 & 0 & \bar{x}_2^3 & 0 & 0 & 0 \\ 0 & 0 & \bar{x}_1^{32} & 0 & 0 & -\bar{x}_1^3 & 0 & 0 & \bar{x}_1^2 \end{bmatrix}$$

6. J. H. Argyris, P. C. Dunne, G. A. Malejannakis and E. Schelkle, A simple triangular facet shell element with applications to linear and non-linear equilibrium and elastic stability problems. *Comput. Meth. Appl. Mech. Engng* 10, 371-403 (1977).
7. K. J. Bathe and L. W. Ho, Some results in the analysis of thin shell structures. In *Nonlinear Finite Element Analysis in Structural Mechanics* (Edited by W. Wunderlich et al.). Springer-Verlag, Berlin (1981).

8. J. L. Batoz, K. J. Bathe and L. W. Ho, A study of three-node triangular plate bending elements. *Int. J. Numer. Meth. Engng*, 15, 1771-1812 (1980).
9. R. W. Clough and E. L. Wilson, Dynamic finite element analysis of arbitrary thin shells. *Comput. Structures* 1, 33-56 (1971).
10. K. J. Bathe and S. Bolourchi, Large displacement analysis of three-dimensional beam structures. *Int. J. Numer. Meth. Engng* 14, 861-986 (1979).
11. G. M. Lindberg, M. D. Olson and G. R. Cowper, New developments in the finite element analysis of shells. *National Research Council of Canada, Quart. Bull. Div. Mech. Engng and the National Aeronautical Establishment*, Vol. 4, pp. 1-38, 1969.
12. S. Levy, Bending of rectangular plates with large deflections. *Tech. Notes, NACA*, No 846 (1942).
13. R. H. Leicester, Finite deformations of shallow shells. *Proc. ASCE* 94(EM6), 1409-1423 (1968).
14. G. S. Dhatt, Instability of thin shells by the finite element method. *IASS Symp. for Folded Plates and Prismatic Structures*, Vienna, 1970.

APPENDIX A

Calculation of nonlinear strain stiffness matrix

Let \bar{N}_1 , \bar{N}_2 and \bar{N}_{12} be the membrane force components given in eqn (29), and

$$\hat{N} = \begin{bmatrix} \bar{N}^* \\ \bar{N}^* \\ \bar{N}^* \end{bmatrix}$$

where

$$\bar{N}^* = \begin{bmatrix} \bar{N}_1 & \bar{N}_{12} \\ \bar{N}_{12} & \bar{N}_2 \end{bmatrix}$$

Then corresponding to the displacement vector \bar{U}^* ,

$$\bar{U}^{*T} = [\bar{U}_1^1 \ \bar{U}_2^1 \ \bar{U}_3^1 \ \bar{U}_1^2 \ \bar{U}_2^2 \ \bar{U}_3^2 \ \bar{U}_1^3 \ \bar{U}_2^3 \ \bar{U}_3^3]$$

we have

where \bar{x}_1^k is the \bar{x}_1 -coordinate of node k and

$$\bar{x}_1^{\#} = \bar{x}_1^i - \bar{x}_1^j, \text{ etc.}$$

Note that the small strain assumption allows the following approximation:

$$\bar{x}_1^k \cong {}^0\bar{x}_1^k \cong \bar{x}_1^k,$$

that is, the undeformed local coordinates are used for all τ .

ON TRANSIENT ANALYSIS OF FLUID-STRUCTURE SYSTEMS

K. J. BATHE and W. F. HAHN

Department of Mechanical Engineering, Massachusetts Institute of Technology, Cambridge, MA 02139, U.S.A.

(Received 12 May 1978)

Abstract—Finite element procedures for the dynamic analysis of fluid-structure systems are presented and evaluated. The fluid is assumed to be inviscid and compressible and is described using an updated Lagrangian formulation. Variable-number-nodes isoparametric two- and three-dimensional elements with lumped or consistent mass idealization are employed in the finite element discretization, and the incremental dynamic equilibrium equations are solved using explicit or implicit time integration. The solution procedures are applied to the analysis of a number of fluid-structure problems including the nonlinear transient analysis of a pipe test.

1. INTRODUCTION

The accurate and efficient transient analysis of fluid-structure problems has during recent years attracted much research effort [1-5]. Fluid-structure problems need to be considered in various engineering disciplines, and to a great deal in reactor safety deliberations [1]. In this paper we consider the response of fluid-structure systems in which the fluid can be idealized as being inviscid and compressible, and we focus particular attention on the analysis of problems in which the fluid transmits a significant amount of energy in a relatively short time duration (such as might occur under accident conditions).

An obvious approximate procedure to analyze a fluid-structure problem is to perform the complete analysis in two steps: first, the fluid response is calculated assuming that the structure is rigid; and then the structural response is predicted that is due to the calculated fluid pressures. In most cases this analysis approach will (probably) yield a conservative estimate of the structural deformations. Thus, a drawback of this decoupling of the fluid and the structural analysis is that a substantial overdesign may be reached. On the other hand, this procedure of analysis may yield an unsound design if significant resonance between the fluid and the structure occurs.

A decoupled analysis of the fluid and the structural response is somewhat a natural engineering solution, because, historically, finite difference analysis procedures are employed for analysis of fluid response and finite element procedures are used for structural analysis. Thus, it is natural to employ a finite difference-based computer program to perform the fluid analysis and a finite element program to predict the structural response.

Recognizing the serious deficiency of a decoupled analysis, emphasis has been directed in recent years towards the development of solution algorithms that can be employed to directly analyze the coupled response of fluid-structure systems. In the search for effective solution procedures the versatility and generality of the finite element method for structural analysis and the close relationship between finite difference and finite element procedures suggest that it be very effective to include fluid elements in the finite element programs. These elements can then be directly employed together with structural elements to model fluid-structure systems. At present, some solution capabilities are available, but the programs use only lower-order fluid elements, are

restricted to two-dimensional analysis, and, in general, lack versatility with regard to explicit and implicit time integration and lumped and consistent mass idealizations [1].

The objective of this paper is to report on our recent developments of solution capabilities for fluid-structure interaction problems. In the paper, first the Lagrangian formulation of the inviscid and compressible variable-number-nodes 3-8 two-dimensional and 4-21 three-dimensional isoparametric fluid elements is briefly summarized [6]. These elements have been implemented in the computer program ADINA [7]. The elements can undergo large displacements, they can be employed with implicit (Newmark or Wilson- θ methods) or explicit (central difference method) time integration schemes, and lumped or consistent mass idealizations. Next, the elements, time integration schemes and modeling considerations that lead to either a lumped or consistent mass idealization are discussed. Finally, a number of demonstrative sample solutions are presented. Here, the analysis of a fluid pressure pulse propagating in a pipe section and leading to elastic-plastic structural response is discussed in detail with regard to the finite element modeling and the time integration scheme employed.

2. CALCULATION OF FLUID FINITE ELEMENTS

The objective in this work was to develop a fluid-structure analysis capability that can be employed in the analysis of problems in which no gross fluid motion occurs. For these types of problems a Lagrangian formulation is effective. The fluid elements can then be employed in conjunction with structural elements that are also based on Lagrangian descriptions. The following two basic assumptions have been used in the formulation of the fluid elements:

1. The fluid is compressible and inviscid.
2. Interaction between mechanical and thermal processes is negligible; thus only the mechanical equations are needed to describe the fluid response.

Using a Lagrangian formulation, in principle, a total or updated Lagrangian formulation can be employed, but considering the numerical operations required for fluid systems, an updated Lagrangian (U.L.) formulation is more effective [8].

2.1 Continuum mechanics formulation

Consider a body of fluid undergoing large deformations and assume that the solutions are known at all

discrete time points $0, \Delta t, 2\Delta t, \dots t$. The basic aim of the formulation is to establish an equation of virtual work from which the unknown static and kinematic variables in the configuration at time $t + \Delta t$ can be solved. Since the displacement-based finite element procedure shall be employed for numerical solution, we use the principle of virtual displacements to express the equilibrium of the fluid body. In explicit time integration equilibrium is considered at time t [6]

$$\int_{V} -{}^t p \delta_t e_{ii} {}^t dv = {}^t \mathcal{R} \quad (1)$$

whereas in implicit time integration equilibrium is considered at time $t + \Delta t$,

$$\int_{V} -{}^{t+\Delta t} p \delta_{t+\Delta t} e_{ii} {}^{t+\Delta t} dv = {}^{t+\Delta t} \mathcal{R} \quad (2)$$

In eqn (1) ${}^t p$ is the pressure at time t , $\delta_t e_{ii}$ is a virtual variation of the volumetric strain at time t ,

$$\delta_t e_{ii} \equiv \delta \frac{\partial u_i}{\partial x_i} \quad (\text{sum on } i) \quad (3)$$

${}^t V$ is the volume at time t and ${}^t \mathcal{R}$ is the external virtual work corresponding to time t , and includes the effect of body, surface and inertial forces [8]. The quantities in eqn (2) are defined analogously.

Equations (1) and (2) contain the momentum balance and continuity equations used in analytical fluid mechanics [9]. In addition we also use the constitutive relation

$${}^t p = -{}^t \alpha \Delta V / V_0 \quad (4)$$

where ΔV is the total volume change of a differential volume V_0 and ${}^t \alpha$ is a variable that may be pressure dependent. Using eqn (4) we can directly employ eqn (1) in transient analysis. For static analysis or implicit time integration we linearize eqn (2) as summarized in Table 1 and obtain [8, 9],

$$\int_{V} {}^t \kappa e_{ij} \delta_t e_{ij} {}^t dv - \int_{V} {}^t p \delta_t \eta_{ii} {}^t dv = {}^{t+\Delta t} \mathcal{R} + \int_{V} {}^t p \delta_t e_{ii} {}^t dv \quad (5)$$

where ${}^t p$ is evaluated using eqn (4) and ${}^t \kappa$ is the tangent fluid bulk modulus.

The linearization used to arrive at eqn (5) introduces errors in the solution which may be large if the time step is relatively large. In order to reduce solution errors and in some cases instabilities (see sample problem 4.4) equilibrium iterations are used. In this case, we employ the following equation to solve for the incremental displacements [10]

$$\begin{aligned} & \int_{V} {}^t \kappa \Delta_t e_{ij}^{(k)} \delta_t e_{ij} {}^t dv - \int_{V} {}^t p \delta \Delta_t \eta_{ii}^{(k)} {}^t dv \\ & = {}^{t+\Delta t} \mathcal{R} + \int_{V} {}^{t+\Delta t} p^{(k-1)} \delta_{t+\Delta t} e_{ii}^{(k-1)} {}^{t+\Delta t} dv^{(k-1)} \end{aligned} \quad (6)$$

$k = 1, 2, \dots$

where

$${}^{t+\Delta t} u_i^{(k)} = {}^{t+\Delta t} u_i^{(k-1)} + \Delta u_i^{(k)}$$

and eqn (6) reduces to eqn (5) when $k = 1$.

Table 1. Updated Lagrangian formulation of fluid elements

1. Equation of motion

$$\int_{V} -{}^{t+\Delta t} p \delta_{t+\Delta t} e_{ii} {}^{t+\Delta t} dv = {}^{t+\Delta t} \mathcal{R}$$

or

$$\int_{V} {}^{t+\Delta t} S_{ij} \delta {}^{t+\Delta t} e_{ij} {}^t dv = {}^{t+\Delta t} \mathcal{R}$$

where

$${}^{t+\Delta t} S_{ij} = \frac{{}^t p}{{}^{t+\Delta t} \rho} \frac{\partial x_{i,r}}{\partial x_{j,r}} - {}^{t+\Delta t} p \frac{\partial x_{i,r}}{\partial x_{j,r}};$$

$$\delta {}^{t+\Delta t} e_{ij} = \delta \frac{1}{2} ({}^t u_{i,j} + {}^t u_{j,i} + {}^t u_{k,i} {}^t u_{k,j})$$

2. Incremental decompositions

(a) Stresses

$${}^{t+\Delta t} S_{ij} = -{}^t p \delta_{ij} + {}^t S_{ij}; \quad \delta_{ij} = \text{Kronecker delta.}$$

(b) Strains

$${}^{t+\Delta t} e_{ij} = {}^t e_{ij}; \quad {}^t e_{ij} = e_{ij} + {}^t \eta_{ij}$$

$${}^t e_{ij} = \frac{1}{2} ({}^t u_{i,j} + {}^t u_{j,i}); \quad {}^t \eta_{ij} = \frac{1}{2} ({}^t u_{k,i} {}^t u_{k,j})$$

3. Equation of motion with incremental decompositions

Substituting from (a) and (b) into the equation of motion we obtain

$$\int_{V} {}^t S_{ij} \delta_t e_{ij} {}^t dv - \int_{V} {}^t p \delta_t \eta_{ii} {}^t dv = {}^{t+\Delta t} \mathcal{R} + \int_{V} {}^t p \delta_t e_{ii} {}^t dv.$$

4. Linearization of equation of motion

Using the approximations ${}^t S_{ij} = {}^t \kappa e_{ij} \delta_{ij}$, $\delta_t e_{ij} = \delta_t e_{ij}$ we obtain an approximate equation of motion

$$\int_{V} {}^t \kappa e_{ij} \delta_t e_{ij} {}^t dv - \int_{V} {}^t p \delta_t \eta_{ii} {}^t dv = {}^{t+\Delta t} \mathcal{R} + \int_{V} {}^t p \delta_t e_{ii} {}^t dv.$$

2.2 Finite element discretization

Using isoparametric finite element discretization, the basic assumptions for an element are [6]

$$\begin{aligned} {}^t x_i &= \sum_{k=1}^N h_k {}^t x_i^k & i = 1, 2, 3 \text{ depending on} \\ {}^t u_i &= \sum_{k=1}^N h_k {}^t u_i^k & \text{one, two or three-} \\ \Delta u_i &= \sum_{k=1}^N h_k \Delta u_i^k & \text{dimensional analysis,} \\ & & \text{respectively} \end{aligned} \quad (7)$$

where N is the number of nodes of the element considered, the h_k are the element interpolation functions, and the ${}^t x_i^k$, ${}^t u_i^k$ and Δu_i^k are the coordinates, displacements and incremental displacements of nodal point k at time t .

Substituting the relations in eqn (7) into eqns (1) and (6) and including the effect of inertia forces, we obtain the governing finite element equations in explicit time integration,

$$\mathbf{M}^t \ddot{\mathbf{u}} = \mathbf{R} - \mathbf{F} \quad (8)$$

and in implicit time integration

$$\mathbf{M}^{t+\Delta t} \ddot{\mathbf{u}}^{(i)} + ({}^t \mathbf{K}_L + {}^t \mathbf{K}_{NL}) \Delta \mathbf{u}^{(i)} = {}^{t+\Delta t} \mathbf{R} - {}^{t+\Delta t} \mathbf{F}^{(i-1)} \quad (9)$$

where the first iteration, $i = 1$, corresponds to the solution of eqn (5).

In eqns (8) and (9) we have

- \mathbf{M} = time independent lumped or consistent mass matrix
- ${}^i\mathbf{K}_L, {}^i\mathbf{K}_{NL}$ = linear, nonlinear strain (tangent) stiffness matrix in the configuration at time t
- ${}^i\ddot{\mathbf{u}}, {}^{t+\Delta t}\ddot{\mathbf{u}}$ = vector of nodal point accelerations in the configuration at time $t, t + \Delta t$
- $\Delta \mathbf{u}$ = vector of incremental nodal point displacements
- ${}^i\mathbf{R}, {}^{t+\Delta t}\mathbf{R}$ = vector of external loads at time $t, t + \Delta t$
- ${}^i\mathbf{F}, {}^{t+\Delta t}\mathbf{F}$ = vector of nodal point forces at time $t, t + \Delta t$ and the superscript (i) indicates i th iteration.

The matrices in eqns (8) and (9) are defined in Table 2 for a single element using the following notation:

- \mathbf{H} = displacement transformation matrix
- \mathbf{H}^S = surface displacement transformation matrix
- ${}^i\mathbf{V}$ = dilatation-displacement transformation matrix
- ${}^i\mathbf{B}_{NL}$ = nonlinear strain-displacement transformation matrix
- ${}^{t+\Delta t}\mathbf{t}, {}^{t+\Delta t}\mathbf{f}$ = traction and body force vectors.

The displacement transformation matrices and force vectors are defined as usual [6, 10], and Table 3 gives the matrices ${}^i\mathbf{V}$ and ${}^i\mathbf{B}_{NK}$ for the two and three dimensional fluid elements.

Using the above formulation, the 4-8 and 8-21 variable-number nodes elements (shown in Fig. 1 [6]) with lumped or consistent mass assumptions have been implemented in ADINA for two- and three-dimensional analysis, respectively. The lumped mass matrix of an element is calculated by simply allocating $1/N$ times the total element mass (where N = number of nodes) to the nodal degrees of freedom.

We may note that the continuum mechanics equations of motion (eqns 1 and 2) are valid for general displacements. However, considering the finite element equations of motion severe mesh distortions that are due to large

Table 2. Finite element matrices

Integral	Matrix evaluation
$\int_{0v} {}^0\rho {}^{t+\Delta t}\ddot{u}_k \delta u_k^0 dv$	$\mathbf{M} {}^{t+\Delta t}\ddot{\mathbf{u}} = {}^0\rho \left(\int_{0v} \mathbf{H}^T \mathbf{H}^0 dv \right) {}^{t+\Delta t}\ddot{\mathbf{u}}$ (consistent mass)
${}^{t+\Delta t}\mathcal{Q} = \int_{0A} {}^{t+\Delta t}\delta_i^0 t_k \delta u_k^0 da$ $+ \int_{0v} {}^0\rho {}^{t+\Delta t}\delta_i^0 f_k \delta u_k^0 dv$	${}^{t+\Delta t}\mathbf{R} = \int_{0A} \mathbf{H}^{ST} {}^{t+\Delta t}\mathbf{t}^0 da$ $+ {}^0\rho \int_{0v} \mathbf{H}^T {}^{t+\Delta t}\mathbf{f}^0 dv$
$\int_{IV} {}^i\kappa_i e_{ii} \delta_i e_{ij}^i dv$	${}^i\mathbf{K}_L \mathbf{u} = \left(\int_{IV} {}^i\kappa_i {}^i\mathbf{V}^T {}^i\mathbf{V}^i dv \right) \mathbf{u}$
$\int_{IV} -{}^i p \delta_i \eta_{ii}^i dv$	${}^i\mathbf{K}_{NL} \mathbf{u} = \left(\int_{IV} -{}^i p {}^i\mathbf{B}_{NL}^T {}^i\mathbf{B}_{NL}^i dv \right) \mathbf{u}$
$\int_{IV} -{}^i p \delta_i e_{ii}^i dv$	${}^i\mathbf{F} = \int_{IV} -{}^i p {}^i\mathbf{V}^T dv$

Table 3. Linear and nonlinear strain-displacement transformation matrices

Two-dimensional analysis

Dilatation-displacement transformation vector:

$${}^i\mathbf{V} = \left[\left(h_{1,1} + \frac{h_1}{{}^i\bar{x}_1} \right), h_{1,2} \left(h_{2,1} + \frac{h_2}{{}^i\bar{x}_1} \right), \dots, \left(h_{N,1} + \frac{h_N}{{}^i\bar{x}_1} \right), h_{N,2} \right]$$

where

$${}^i\bar{x}_1 = \sum_{j=1}^N h_j {}^i x_j^j$$

Nonlinear strain-displacement transformation matrix:

$${}^i\mathbf{B}_{NL} = \begin{bmatrix} {}^i h_{1,1} & 0 & {}^i h_{2,1} & \dots & {}^i h_{N,1} & 0 \\ {}^i h_{1,2} & 0 & {}^i h_{2,2} & \dots & {}^i h_{N,2} & 0 \\ 0 & {}^i h_{1,1} & 0 & \dots & 0 & {}^i h_{N,1} \\ 0 & {}^i h_{1,2} & 0 & \dots & 0 & {}^i h_{N,2} \\ \frac{h_1}{{}^i\bar{x}_1} & 0 & \frac{h_2}{{}^i\bar{x}_1} & \dots & \frac{h_N}{{}^i\bar{x}_1} & 0 \end{bmatrix}$$

($\frac{h_i}{{}^i\bar{x}_1}$ is included only in axisymmetric analysis)

Three-dimensional analysis

Dilatation-displacement transformation vector

$${}^i\mathbf{V} = [h_{1,1}, h_{1,2}, h_{1,3}, h_{2,1}, \dots, h_{N,1}, h_{N,2}, h_{N,3}]$$

Nonlinear strain-displacement transformation matrix:

$${}^i\mathbf{B}_{NL} = \begin{bmatrix} {}^i\bar{\mathbf{B}}_{NL} & 0 & 0 \\ 0 & {}^i\bar{\mathbf{B}}_{NL} & 0 \\ 0 & 0 & {}^i\bar{\mathbf{B}}_{NL} \end{bmatrix}; \quad \mathbf{0} = \begin{bmatrix} 0 \\ 0 \\ 0 \end{bmatrix}$$

$${}^i\bar{\mathbf{B}}_{NL} = \begin{bmatrix} {}^i h_{1,1} & 0 & 0 & {}^i h_{2,1} & 0 & 0 & \dots & {}^i h_{N,1} \\ {}^i h_{1,2} & 0 & 0 & {}^i h_{2,2} & 0 & 0 & \dots & {}^i h_{N,2} \\ {}^i h_{1,3} & 0 & 0 & {}^i h_{2,3} & 0 & 0 & \dots & {}^i h_{N,3} \end{bmatrix}$$

displacements reduce the accuracy of a finite element solution. In order to preserve solution accuracy rezoning would have to be used which is not considered in this study.

2.3 Analysis of fluid finite elements

The variable-number-nodes fluid elements shown in Fig. 1 are compatible with the solid elements available in ADINA. This compatibility is important because higher-order isoparametric solid elements have proven to be significantly more effective than lower-order elements in analysis of problems with significant bending response and would naturally be employed with high-order fluid elements. However, to model the complete fluid domain appropriately, the basic characteristics of the fluid elements need to be known.

The basic characteristics of a fluid element are displayed by the element eigenvalues and eigenvectors [6]. Figure 2 summarizes the eigensystem of a 4-node two-dimensional element. The figure shows that, as reported earlier, using reduced Gauss integration (1 point integration) for the 4-node element the hourglass patterns correspond to zero eigenvalues. Various attempts have been made to remove the instability of the hourglass deformation modes without increasing the computational expense significantly, but it is believed to be best to use 2×2 Gauss integration. Indeed, the formulation-consistent removal of the hourglass instability using 2×2

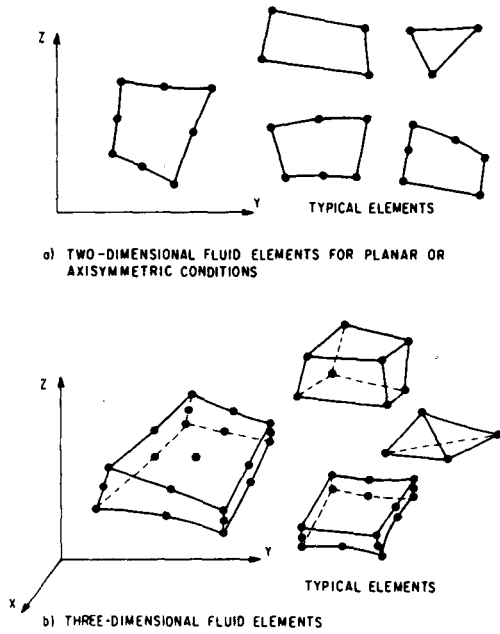
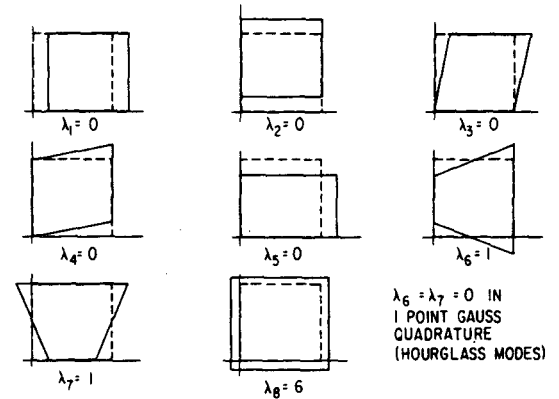


Fig. 1. Fluid elements in ADINA.

Gauss quadrature is an advantage of a finite element formulation over a finite difference analysis.

Figure 2 also gives the number of zero eigenvalues of the 8-node two-dimensional and 8 and 20-node three-dimensional elements. As for the 4-node two-dimensional element, reduced integration introduces additional zero eigenvalues that can result in solution instabilities in the analysis of a fluid-structure system.

Of particular interest is the analysis of fluid-filled pipes. If the geometry and loading are axisymmetric, these fluid-structure systems can be modeled using the axisymmetric elements, and the question is whether higher or lower-order elements should be employed. It is well-known that in axisymmetric analysis of solids, higher-order isoparametric elements need be employed for accurate prediction of stresses. The same conclusion is reached for the fluid elements. Figure 3 shows the



(a) EIGENVALUES AND EIGENVECTORS OF 4-NODE TWO-DIMENSIONAL PLANE FLUID ELEMENT, EXACT INTEGRATION

INTEGRATION ORDER	NO. OF ZERO EIGENVALUES / NO. OF dof		THREE-DIMENSIONAL	
	4-NODE	8-NODE	8-NODE	20-NODE
2 x 2	5 / 8	12 / 16	17 / 24	52 / 60
3 x 3		10 / 16		43 / 60

(b) NUMBER OF ZERO STRAIN ENERGY MODES FOR FLUID ELEMENTS (INCLUDING RIGID BODY MODES)

Fig. 2. Eigensystems of two and three-dimensional fluid elements.

stresses calculated in axisymmetric plane strain fluid-solid models with a varying bulk modulus in the fluid and compares the results with theoretical values.

The use of higher-order fluid and solid elements in transient analysis requires that a distinct choice be made on the use of a lumped or consistent mass idealization. If 4-node two-dimensional elements (and 8-node three-dimensional elements) are employed it is probably most effective to use a lumped mass model. Not only is the computational expense less when using a lumped mass matrix but the similarity between the finite element equations and the finite difference equations (in some cases these are the equations used in the method of characteristics) requires the use of a lumped mass matrix for best solution accuracy[11]. On the other hand,

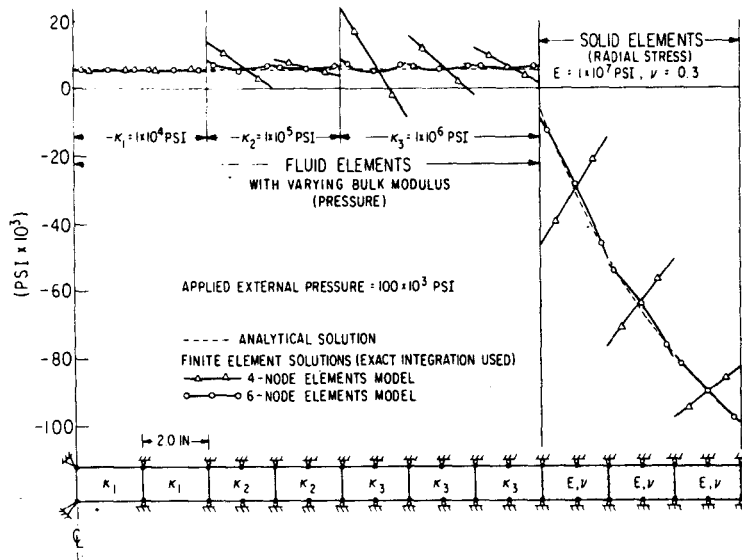


Fig. 3. Analysis of axisymmetric plane strain fluid-structure model, 4-node vs 6-node elements.

considering the use of higher-order elements, a lumped mass characterization leads to spurious oscillations that arise because a lumped mass distribution does not represent a consistent loading on the elements. Since it is the objective to employ as few higher-order elements as possible to model the fluid-structure domain, a consistent mass idealization is in most cases desirable.

3. TIME INTEGRATION

In ADINA, the central difference method is employed in explicit time integration and the Newmark method or the Wilson- θ method can be used in implicit time integration[6]. Using implicit time integration a lumped or consistent mass matrix can be employed, but in explicit time integration only a lumped mass idealization can be specified. Table 1 in [7] summarizes the complete solution algorithm employed.

The stability and accuracy characteristics and the computational details of using these techniques in linear analysis have been summarized in [6]. Considering general nonlinear analysis the main difficulty is to assure the stability of a time integration solution. In explicit time integration the solution is simply marched forward, and it may be difficult to identify an instability that manifests itself only as a significant error accumulation over a few time steps. On the other hand, using an implicit time integration method, in each time step the incremental equilibrium equations are solved and equilibrium iterations can be performed on the solution quantities. These equilibrium iterations are equivalent to an energy balance check and can be very important to assure a stable and accurate solution (see sample problem 4.4).

4. SAMPLE SOLUTIONS

The sample analyses presented in this section have been performed using the computer program ADINA in which the fluid elements discussed in this paper have been implemented.

4.1 Analysis of rigidly-contained water column

A simple axisymmetric water column idealized using 4-node elements as shown in Fig. 4 was analyzed for a

step pressure applied at its free end. Lumped and consistent mass idealizations were employed in this analysis, and the objective was to study the accuracy with which the response of the water column is predicted.

Figure 4 shows the calculated longitudinal displacements at the free end of the column and compares these displacements with the analytical solution. It is seen that using implicit time integration (Newmark method) the free-end displacements in the consistent mass analysis were predicted accurately for a time period that included 6 wave reflections, whereas the lumped mass analysis results are inaccurate.

Because of the simplicity of the problem the method of characteristics shows that in this analysis the exact solution can be calculated using the central difference explicit solution method[11]. To obtain the exact solution the pressure and lumped mass idealizations must be such that the displacements are uniform over the column cross section and $\Delta t = \Delta L/c$, where c is the wave velocity and ΔL is the length of an element.

4.2 Static analysis of an assemblage of concentric fluid-filled cylinders

Five concentric fluid-filled cylinders were analyzed for a load applied on a stiff cap. This same problem was studied by Munro and Piekarski[12]. Figure 5 shows the finite element model employed and the predicted fluid pressures. The finite element solution is compared with the approximate analysis results of Munro and Piekarski.

4.3 Transient analysis of a water-filled copper tube

The dynamic response of a water-filled copper tube subjected to an impact loading was analyzed. The structure, the loading and the finite element model employed are shown in Fig. 6. This problem was also analyzed by Walker and Phillips[13], who established governing differential equations based on a number of assumptions and solved these equations using the method of characteristics.

Two finite element analyses were performed: a lumped mass and a consistent mass idealization was used. The mass allocation employed in the lumped mass analysis is

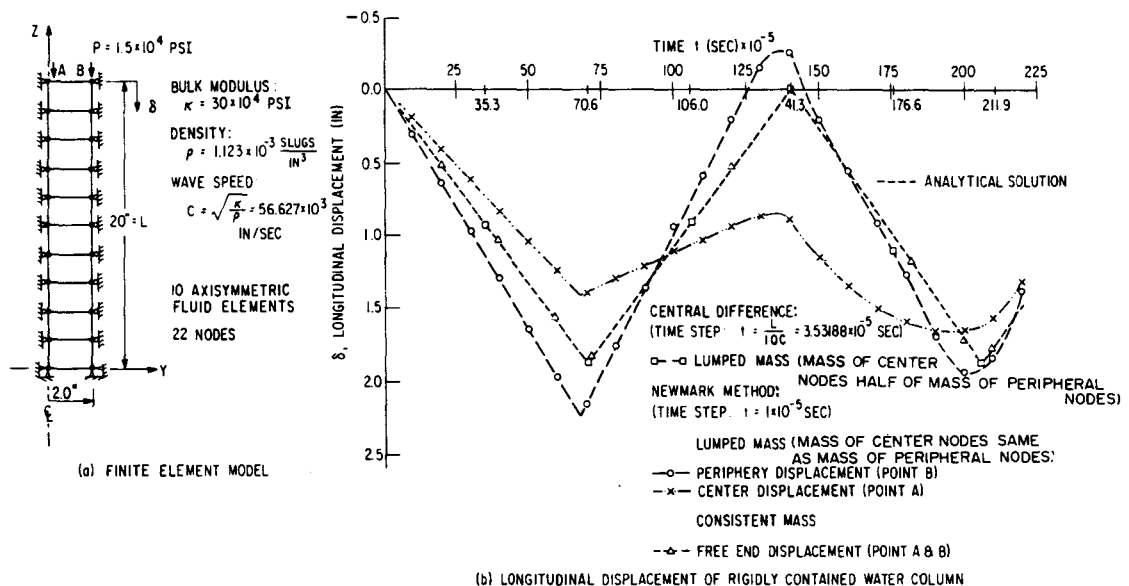


Fig. 4. Longitudinal displacement of free end of rigidly contained water column under pressure step load.

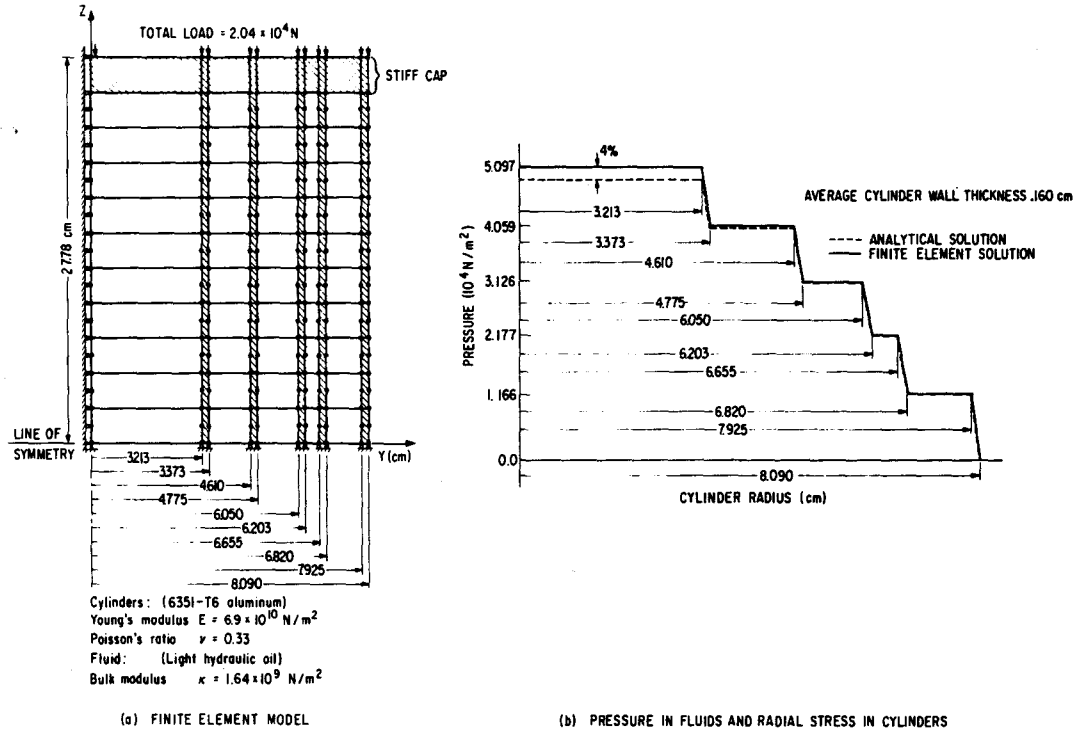
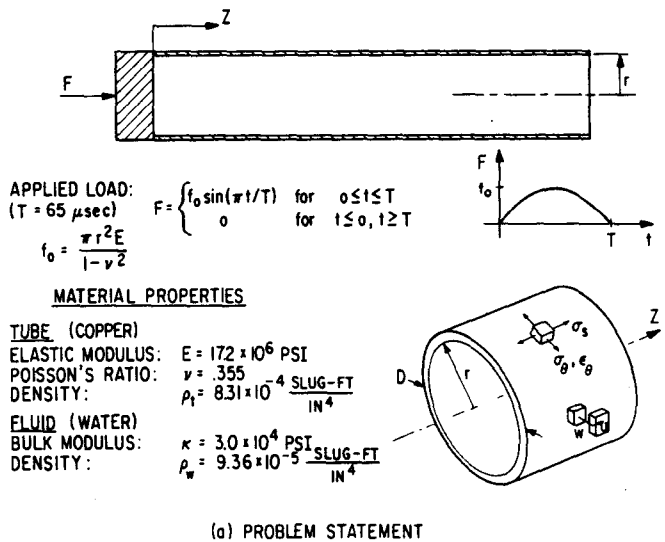
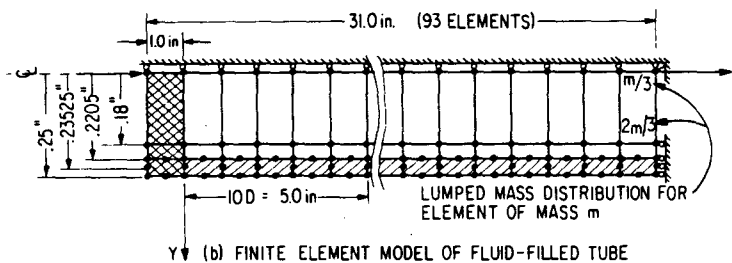


Fig. 5. Static analysis of fluid-filled concentric cylinders.



(a) PROBLEM STATEMENT



(b) FINITE ELEMENT MODEL OF FLUID-FILLED TUBE

Fig. 6. Analysis of water-filled copper tube.

shown in Fig. 6. This distribution of mass corresponds to the assumption used by Walker and Phillips. It should be noted that a thin layer of elements was used at the tube wall in order to "release" the axial displacements of the fluid.

In both finite element analyses the Newmark method was employed with a time step $1 \mu\text{sec}$, i.e. 65 time steps correspond to the pulse length. The length of the elements (axial direction) was about 1/10th of the pulse length. The aspect ratio of the elements was very high (1:34).

Figures 7 and 8 show the response of the system at $Z = 5\text{in}$ (see Fig. 6) as predicted in this study and by Walker and Phillips. It is seen that for $t < 100 \mu\text{sec}$ the finite element solutions correspond reasonably well with the results of Walker and Phillips, but relatively large solution discrepancies are observed at larger times. These solution discrepancies are due to the different assumptions employed in the analyses. Since no experimental or "exact analytical" results are available, it is difficult to assess the actual accuracy of the different models. However, considering the finite element solution results it is seen that the consistent mass model predicts a somewhat smoother response for the hoop strain than does the lumped mass model and gives also results that

compare somewhat better with the response predicted in [13].

4.4 Nonlinear transient analysis of a pipe test

The experience gained in the above analysis was used to analyze the water-filled straight piping configuration shown in Fig. 9 subjected to a pressure pulse at its end. The elastic-plastic response of this pipe was experimentally assessed as reported in [14]. Figure 9 shows also the finite element model employed in the analysis.

In this analysis, a consistent mass matrix was employed and the time integration was carried out using the Newmark method. The time step was changed to half its size at the time the pulse entered the nickel pipe so that the pulse front would pass through a solid element in about three time steps. The effective stiffness matrix used in this analysis was reformed only at time $t = 1.905, 2.302, \text{ and } 3.435 \text{ msec}$. However, to take into account the elastic-plastic response of the pipe, equilibrium iterations were used at each time step once the pulse reached the nickel pipe. The equilibrium iterations (energy balance check) were found to be necessary for a stable solution, although an average of only 1 to 2 iterations per time step were carried out.

Figure 10 shows the calculated pressures and hoop

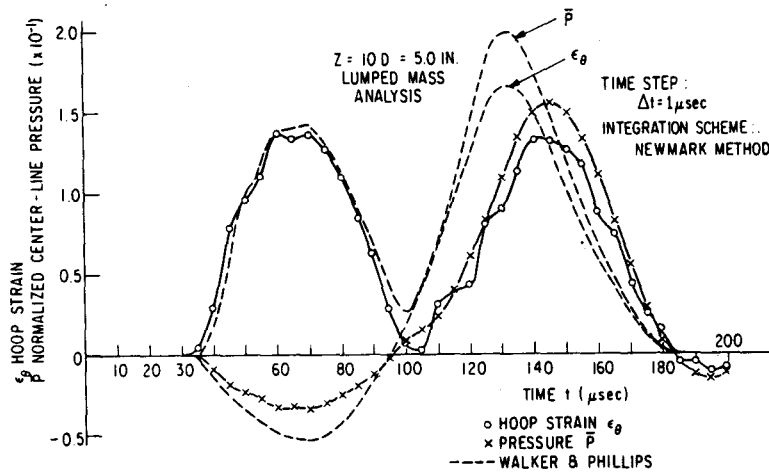


Fig. 7. Response of water-filled copper tube to half sine pulse of 65 μsec duration.

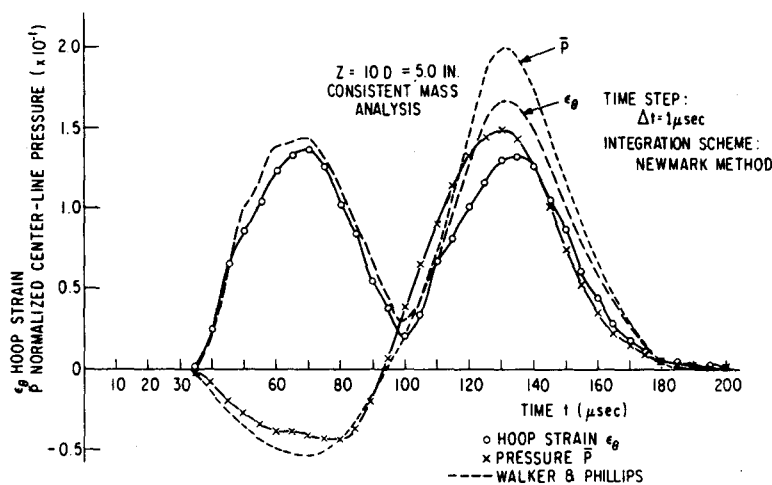
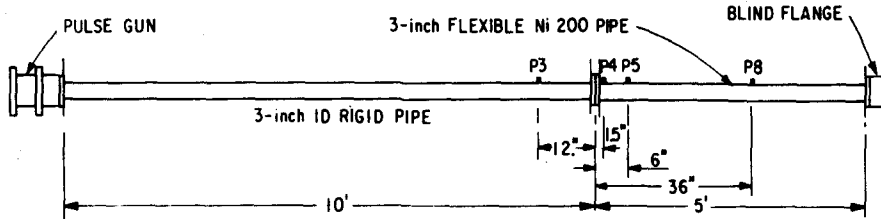


Fig. 8. Response of water-filled copper tube to half sine pulse of 65 μsec duration.

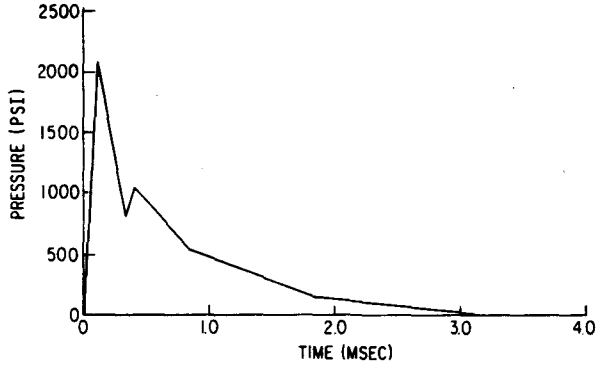


(a) STRAIGHT PIPE TEST CONFIGURATION

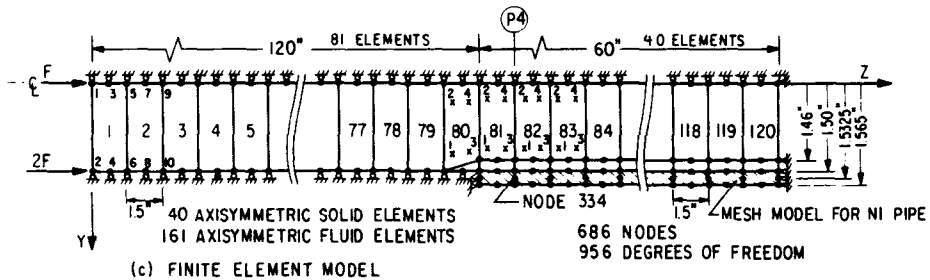
MATERIAL PROPERTIES:

NICKEL 200
 E - YOUNG'S MODULUS 30×10^6 PSI
 E_T - TANGENT MODULUS 73.7×10^4 PSI
 ν - POISSON'S RATIO .30
 ρ_f - DENSITY 8.31×10^{-4} SLUG-FT/IN³
 σ_0 - YIELD STRESS 12.8×10^3 PSI

WATER
 κ - BULK MODULUS 32×10^4 PSI
 ρ_w - DENSITY 9.36×10^{-5} SLUG-FT/IN³



(b) PRESSURE PULSE INPUT IN FINITE ELEMENT ANALYSIS



(c) FINITE ELEMENT MODEL

TIME STEP: $\Delta t = \begin{cases} 1.5 \times 10^{-5} \text{ SEC} & 0 \leq t \leq 1.905 \text{ MSEC} \\ 7.5 \times 10^{-6} \text{ SEC} & 1.905 \leq t \leq 4.560 \text{ MSEC} \end{cases}$

EQUILIBRIUM ITERATION: EVERY STEP FOR $t \geq 2.092 \text{ MSEC}$

INTEGRATION ORDER: SOLID ELEMENTS: 3x3
 FLUID ELEMENTS: 2x2

STIFFNESS REFORMED AT RESTARTS ONLY (i.e., $t = 1.905, 2.302, \text{ and } 3.435 \text{ MSEC}$)

PRESSURE P AT VARIOUS AXIAL LOCATIONS OBTAINED BY AVERAGING PRESSURES AT INTEGRATION POINTS
 4/82 OF ADJACENT ELEMENTS (e.g., $P_4 = (P_{81} + P_{82}) / 2$ WHERE P_4 IS THE PRESSURE AT 1.5 IN. INTO NICKEL PIPE)

HOOP STRAIN ϵ_θ IN THE NICKEL PIPE AT VARIOUS AXIAL LOCATIONS OBTAINED BY $\epsilon_\theta = u/r$ WHERE u IS THE RADIAL DISPLACEMENT OF A MIDSIDE NODE AND r IS THE INITIAL RADIAL LOCATION OF THE MIDSIDE NODE (e.g., $\epsilon_\theta = u^{334} / 1.5325$ HOOP STRAIN 1.5 IN. INTO NICKEL PIPE)

PRESSURE LOAD APPLIED TO NODES 1 AND 2

CONSISTENT MASS **NEWMARK INTEGRATION**
SMALL DISPLACEMENTS

Fig. 9. Finite element model of straight pipe test.

strains at various locations along the pipe as a function of time and compares the ADINA results with the experimental data. It is noted that in general the calculated response compares well with the experimentally observed response.

5. CONCLUSIONS

The transient analysis of fluid-structure systems presents a great deal of difficulties because an appropriate structural and fluid representation together with effective numerical procedures must be employed. In this paper, the fluid is assumed to be inviscid and compressible, an updated Lagrangian formulation is used to describe the fluid motion, isoparametric finite element discretization is employed with lumped or consistent mass idealizations and the incremental equilibrium equa-

tions are solved using explicit or implicit time integration. The solution capabilities have been implemented in the ADINA computer program, and the solution results of various sample analyses are presented.

The study performed here indicates that higher-order isoparametric finite elements can be effective in the representation of the fluid. Depending on the discretization used, the elements may have to be employed with a consistent mass idealization and implicit time integration.

Considering nonlinear analysis, it can be important that equilibrium iterations be performed in order to prevent solution instability. In some analyses only very few iterations are needed to greatly improve the solution accuracy (see Section 4.4).

Since there does not exist a single analysis approach

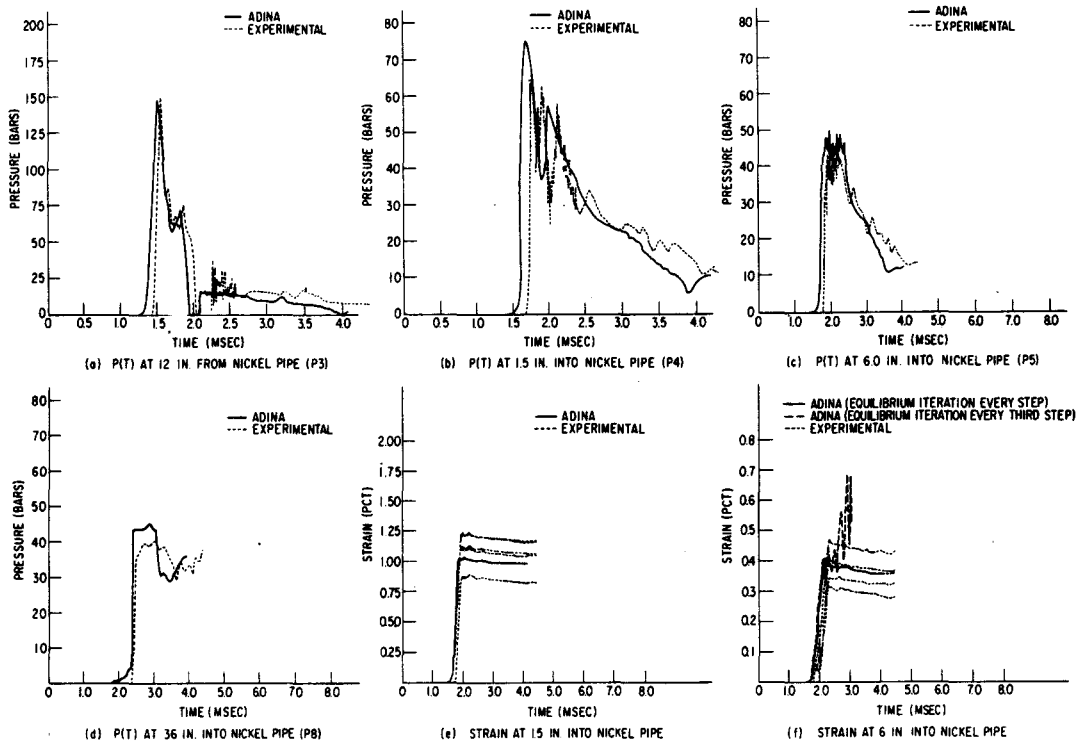


Fig. 10. Pulse propagation in water filled straight pipe system.

that is always most effective for the analysis of fluid-structure problems, it is deemed best at this time to have versatile computational capabilities available. This way, different finite element discretizations, mass idealizations and time integration procedures can be chosen for an effective solution to a particular problem. In this paper much emphasis has been placed on the use of higher-order isoparametric finite elements, consistent mass idealization and implicit time integration. However, it need be noted that these techniques have been employed primarily in two-dimensional analysis and can be prohibitively expensive in three-dimensional response calculations.

Acknowledgements—The work reported in this paper has been supported financially by the Nuclear Regulatory Commission contract No. AT(49-24)-0366 and the ADINA users group. We would like to acknowledge gratefully this support.

REFERENCES

1. T. Belytschko, Methods and programs for analysis of fluid-structure systems. *J. Nuclear Engng and Design* **42**, 41-52 (1977).
2. T. Belytschko, *Transient Analysis, Structural Mechanics Computer Programs* (Edited by W. Pilkey et al.), pp. 255-275. University Press of Virginia (1974).
3. J. M. Kennedy and T. Belytschko, Energy source and fluid representation in a structural response code—STRAW. Argonne Natl Lab. *Rep. ANL-8140* (May 1975).
4. U. W. Chang and J. Gvildys. REXCO-HEP: A two-dimensional computer code for calculating the primary system response in fast reactors. Argonne Natl Lab. *Rep. ANL-75-19* (June 1975).
5. R. Hofmann, STEALTH, A Lagrangian explicit finite difference code for solids, structural and thermohydraulic analysis. *Electric Power Res. Instit.* Vol. 1-4, Palo Alto, California (June 1976).
6. K. J. Bathe and E. L. Wilson, *Numerical Methods in Finite Element Analysis*. Prentice-Hall, Englewood Cliffs, New Jersey (1976).
7. K. J. Bathe, ADINA-A finite element program for automatic dynamic incremental nonlinear analysis. Acoustics and Vibration Lab., *Rep. 82448-1*, Department of Mechanical Engineering, M.I.T. (Sept. 1975, revised May 1977).
8. K. J. Bathe, E. Ramm and E. L. Wilson, Finite element formulations for large deformation dynamic analysis. *Int. J. Num. Meth. Engng* **9**, 353-386 (1975).
9. L. E. Malvern *Introduction to the Mechanics of a Continuous Medium*. Prentice-Hall, Englewood Cliffs, New Jersey (1969).
10. K. J. Bathe, Static and dynamic geometric and material nonlinear analysis using ADINA. Acoustics and Vibration Lab., *Rep. 82448-2*, Dept. of Mechanical Engng, M.I.T. (May 1976, revised May 1977).
11. S. H. Crandall, *Engineering Analysis-A Survey of Numerical Procedures*. McGraw-Hill, New York (1956).
12. M. Munro and K. Piekarski, Stress-induced radial pressure gradients in liquid-filled multiple concentric cylinders. *J. App. Mech.* **44**(2) 218-221 (1977).
13. J. S. Walker and J. W. Phillips, Pulse propagation in fluid-filled tubes. *J. Appl. Mech.* **44**(1), 31-35 (1977).
14. C. M. Romander, D. J. Cagliostro and A. L. Florence, Experiments on the response of flexible piping systems to internal pressure pulses. *SRI Project PVD-1960*, Stanford Research Institute, Menlo Park, California (April 1976).

ELASTIC-PLASTIC LARGE DEFORMATION STATIC AND DYNAMIC ANALYSIS

KLAUS-JÜRGEN BATHE

Dept. of Mechanical Engineering, Massachusetts Institute of Technology, Cambridge, MA 02139, U.S.A.

and

HALUK OZDEMIR

Civil Engineering Department, University of California, Berkeley, CA 94720, U.S.A.

(Received 28 February 1975)

Abstract—The problem of formulating and numerically implementing finite element elastic-plastic large deformation analysis is considered. In general, formulations can use different kinematic descriptions and assumptions in the material law, and analysis results can vary by a large amount. In this paper, starting from continuum mechanics principles, two consistent formulations for elastic-plastic large deformation analysis are presented in which either the initial configuration or the current configuration is used for the description of static and kinematic variables. The differences between the formulations are clearly identified and it is established that, depending on the elastic-plastic material description, identical numerical results can be obtained. If, in practice, certain constitutive transformations are not included, the differences in the analysis results are relatively small in large displacement but small strain problems. The formulations have been implemented and representative sample analyses of large deformation response of beams and shells are presented.

NOMENCLATURE

The following convention for tensor and vector subscripts and superscripts is employed:

A left superscript denotes the time of the configuration in which the quantity occurs.

A left subscript can have two different meanings. If the quantity considered is a derivative, the left subscript denotes the time of the configuration, in which the coordinate is measured with respect to which is differentiated. Otherwise the left subscript denotes the time of the configuration in which the quantity is measured.

Right lower case subscripts denote the components of a tensor or vector. Components are referred to a fixed Cartesian coordinate system; $i, j, \dots = 1, 2, 3$. Differentiation is denoted by a right lower case subscript following a comma, with the subscript indicating the coordinate with respect to which is differentiated.

- 0A = Area of body in configuration at time 0
- $^0C_{ijrs}, ^tC_{ijrs}$ = Component of tangent constitutive tensor at time t referred to configuration at time 0, t (superscript E indicating elastic)
- ${}^{t+\Delta t}f_i$ = Component of body force vector per unit mass in configuration at time $t + \Delta t$ referred to configuration at time 0.
- F = Yield function.
- h_k = Finite element interpolation function associated with nodal point k .
- (i) = Superscript indicating number of iteration.
- ${}^{t+\Delta t}\mathcal{R}$ = External virtual work expression corresponding to configuration at time $t + \Delta t$, defined in equation (2).
- ${}^{t+\Delta t}S_{ij}, {}^tS_{ij}$ = Component of 2nd Piola-Kirchhoff stress tensor in configuration at time $t + \Delta t$ referred to configuration at time 0, t .
- $^0S_{ij}, ^tS_{ij}$ = Component of 2nd Piola-Kirchhoff stress increment at time t .
- $t, t + \Delta t$ = time t and $t + \Delta t$, before and after time increment Δt .
- ${}^{t+\Delta t}t_i$ = Component of surface traction vector in configuration at time $t + \Delta t$, referred to configuration at time 0.
- ${}^t u_i, {}^{t+\Delta t} u_i$ = Component of displacement vector from initial position at time 0 to configuration at time $t, t + \Delta t$.

- u_i = Increment in displacement component, $u_i = {}^{t+\Delta t} u_i - {}^t u_i$.
- Δu_i = Correction to displacement increment u_i .
- ${}^t u_i^k$ = Displacement component of nodal point k in configuration at time t .
- ${}^0 u_{i,j}, {}^{t+\Delta t} u_{i,j}$ = Derivative of displacement component in configuration at time $t, t + \Delta t$ with respect to coordinate ${}^0 x_j$.
- ${}^0 u_{i,j}, {}^t u_{i,j}, {}^{t+\Delta t} u_{i,j}$ = Derivative of displacement increment with respect to coordinate ${}^0 x_j, {}^t x_j, {}^{t+\Delta t} x_j$.
- ${}^0 V, {}^t V, {}^{t+\Delta t} V$ = Volume of body in configuration at time 0, $t, t + \Delta t$.
- ${}^0 x_i, {}^t x_i, {}^{t+\Delta t} x_i$ = Cartesian coordinate in configuration at time 0, $t, t + \Delta t$.
- ${}^0 x_i^k, {}^t x_i^k, {}^{t+\Delta t} x_i^k$ = Cartesian coordinate of nodal point k in configuration at time 0, $t, t + \Delta t$.
- ${}^0 x_{i,j}, {}^{t+\Delta t} x_{i,j}$ = Derivative of coordinate in configuration at time 0, $t + \Delta t$ with respect to coordinate ${}^t x_j, {}^{t+\Delta t} x_j$.
- ${}^{t+\Delta t} \epsilon_{ij}, {}^t \epsilon_{ij}$ = Component of Green-Lagrange strain tensor in the configuration at time $t + \Delta t, t$, referred to the configuration at time 0.
- ${}^t \epsilon_{ij}^p$ = Component of total plastic strain tensor at time t in total Lagrangian formulation.
- ${}^{t+\Delta t} \epsilon_{ij}$ = Component of Green-Lagrange strain tensor in the configuration at time $t + \Delta t$, referred to the configuration at time t (i.e. using displacements from the configuration at time t to the configuration at time $t + \Delta t$).
- ${}^0 \epsilon_{ij}, {}^t \epsilon_{ij}$ = Component of strain increment tensor referred to configuration at time 0, t .
- ${}^0 e_{ij}, {}^t e_{ij}$ = Linear part of strain increment ${}^0 \epsilon_{ij}, {}^t \epsilon_{ij}$.
- ${}^0 \eta_{ij}, {}^t \eta_{ij}$ = Nonlinear part of strain increment ${}^0 \epsilon_{ij}, {}^t \epsilon_{ij}$.
- ${}^0 \rho, {}^t \rho, {}^{t+\Delta t} \rho$ = Specific mass of body in configuration at time 0, $t, t + \Delta t$.
- ${}^t \tau_{ij}, {}^{t+\Delta t} \tau_{ij}$ = Component of Cauchy stress tensor in configuration at time $t, t + \Delta t$.
- λ = Constant of proportionality at time t .

Matrices

- ${}^0 B_{i..}, {}^t B_{i..}$ = Linear strain-displacement matrix in configuration at time t referred to configuration at time 0, t .
- ${}^0 B_{Ni..}, {}^t B_{Ni..}$ = Nonlinear strain-displacement matrix in con-

figuration at time t referred to configuration at time 0, t .

${}^0C, {}^tC$ = Tangent material property matrix at time t and referred to configuration at time 0, t

${}^0F, {}^tF$ = Vector of nodal point forces in configuration at time t referred to configuration at time 0, t .

${}^0K_L, {}^tK_L$ = Linear strain stiffness matrix in configuration at time t referred to configuration at time 0, t .

${}^0K_{NL}, {}^tK_{NL}$ = Nonlinear strain stiffness matrix in configuration at time t referred to configuration at time 0, t .

M = Mass matrix.

${}^{t+\Delta t}R$ = Vector of external loads in configuration at time $t + \Delta t$.

${}^0S, {}^tS$ = 2nd Piola-Kirchhoff stress matrix and vector in configuration at time t and referred to configuration at time 0.

${}^t\tau, {}^t\hat{\tau}$ = Cauchy stress matrix and vector in configuration at time t .

${}^t u, {}^{t+\Delta t} u$ = Vector of displacements at time $t, t + \Delta t$.

u = Vector of incremental displacements at time t .

Δu = Vector of corrections to u .

INTRODUCTION

The importance of investigating the elastic-plastic dynamic behavior of structural components for adequate design is being recognized to an increasing extent. In the analysis of some problems, large deformation effects can be neglected, but in other cases geometry changes significantly influence the predicted response.

Lately, the finite element method has proven to be very effective in linear analysis and solutions have also been obtained to some complex nonlinear problems. However, much research is now underway to improve the continuum mechanics, material and finite element formulations, the numerical integration procedures and computer program implementations.

The specific problem considered in this paper is the formulation and implementation of incremental finite element equations of motion for large deformation elastic-plastic dynamic analysis. It is assumed that isoparametric finite element discretization and an implicit time integration scheme shall be used, because these techniques are believed to be most effective for a wide range of problems.

Considering the formulation of the incremental finite element equilibrium equations, using an implicit time integration procedure all static and kinematic variables must be referred to a known equilibrium configuration. In practice the choice lies between using the initial configuration or the last calculated configuration as reference. For elastic-plastic analysis, Hibbitt, Marcal and Rice[9], Larsen[11], McNamara and Marcal[13], Stricklin *et al.*[21], Sharifi and Yates[19], Felippa and Sharifi[6] and Nagarajan[16] have used the initial configuration. However, Hibbitt *et al.* pointed out that it may be more effective to employ the current configuration as reference[9]. Larsen[11] and Felippa and Sharifi[6] rejected the idea of updating the reference configuration without giving details about a possible implementation. Murray and Wilson[15], Yaghmai[22] and Yaghmai and Popov[23] updated the reference configuration in static analysis, and Belytschko and Hsieh[5] in dynamic analysis using an explicit time integration scheme. Considering the different procedures currently in use, an important question is under what conditions, if at all, the same numerical results are obtained.

The objective in this paper is to present in detail two formulations in which either the initial configuration or the last calculated configuration is used for reference. These formulations have been termed total Lagrangian and updated Lagrangian formulations and have been described in detail earlier for elastic analysis[3,4]. An important feature to be discussed is that provided the constitutive relations are defined appropriately, identical numerical results are obtained using the two formulations and indeed the same finite element matrices are employed. If, however, the appropriate constitutive transformations are not included, the differences can be expected to be small in case large displacement but small strain response is considered. The formulations have been implemented and various sample solutions are described in the paper.

CONTINUUM MECHANICS FORMULATION

Consider the motion of a general body such as shown in Fig. 1 and assume that the solution has been obtained for the time points 0, $\Delta t, 2\Delta t, \dots, t$. The basic aim is to establish an equation from which the unknown static and kinematic variables in the configuration at time $t + \Delta t$ can be solved. Because it is the objective to use a displacement-based finite element procedure with an implicit time integration scheme, the principle of virtual displacements is used to express the equilibrium of the body in the configuration at time $t + \Delta t$. Using the notation in Fig. 1, the principle of virtual displacements requires

$$\int_{V^{t+\Delta t}} {}^{t+\Delta t}\tau_{ij} \delta_{i+\Delta t} e_{ij} {}^{t+\Delta t} dv = {}^{t+\Delta t}R \quad (1)$$

where

$${}^{t+\Delta t}R = \int_{A} {}^{t+\Delta t}t_k \delta u_k {}^0 da + \int_{V} {}^0\rho {}^{t+\Delta t}f_k \delta u_k {}^0 dv \quad (2)$$

and ${}^{t+\Delta t}\tau_{ij}$ are Cartesian components of the Cauchy stress tensor at time $t + \Delta t$, and ${}^{t+\Delta t}t_k$ and ${}^{t+\Delta t}f_k$ are surface tractions and body force components at time $t + \Delta t$, but referred to time 0. Also, δ denotes 'variation in', δu_k is a variation in the current displacement components ${}^{t+\Delta t}u_k$ and

$$\delta_{i+\Delta t} e_{ij} = \delta \frac{1}{2} ({}_{i+\Delta t}u_{i,j} + {}_{i+\Delta t}u_{j,i}) \quad (3)$$

where

$${}_{i+\Delta t}u_{i,m} = \frac{\partial u_i}{\partial {}^{t+\Delta t}x_m}$$

It should be noted that in a dynamic analysis the body force components include mass inertia effects.

Using an implicit time integration procedure equation (1) cannot be solved directly, because the configuration at time $t + \Delta t$ is unknown. For solution the equation is recast into a form in which all variables are referred to a previously calculated equilibrium configuration. In this form the equilibrium relation can be linearized and be employed effectively in a Newton iteration[7].

In principle, any one of the already calculated equilibrium configurations could be used as a reference configuration. However, in practice the choice lies essentially between two formulations which have been termed total Lagrangian (T.L.) and updated Lagrangian (U.L.) formulations[3,4]. In the T.L. solution all static and kinematic variables are referred to the initial

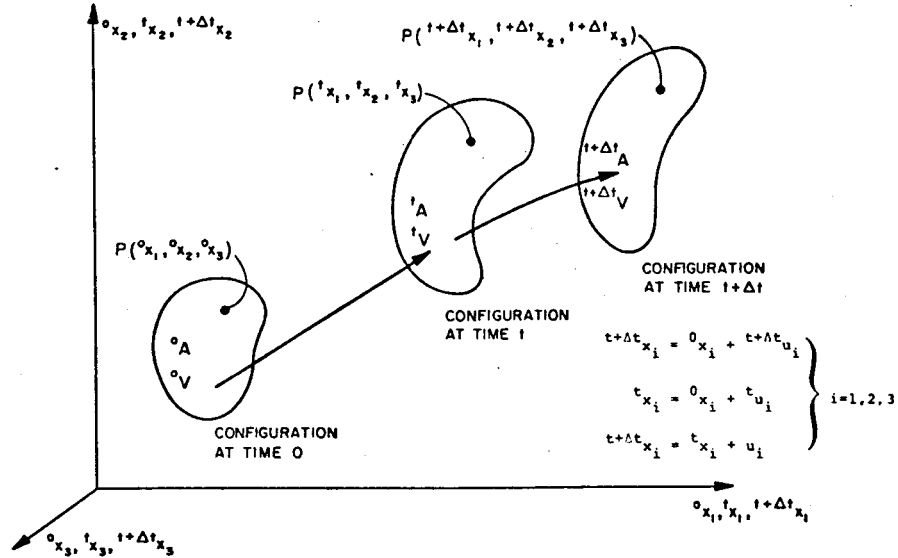


Fig. 1. Motion of body in Cartesian coordinate system.

configuration at time 0. The U.L. formulation is based on the same procedures that are used in the T.L. formulation, but in the solution all static and kinematic variables are referred to the configuration at time t .

Using the T.L. formulation, equation (1) is transformed to [8, 12, 18],

$$\int_{oV} {}^{t+\Delta t} S_{ij} \delta {}^{t+\Delta t} {}^0 \epsilon_{ij} {}^0 dv = {}^{t+\Delta t} \mathcal{R} \quad (4)$$

where ${}^{t+\Delta t} S_{ij}$ are components of the 2nd Piola-Kirchhoff stress tensor and ${}^{t+\Delta t} {}^0 \epsilon_{ij}$ are components of the Green-Lagrange strain tensor using the displacements ${}^{t+\Delta t} u_k$. Similarly, in the U.L. formulation equation (1) becomes

$$\int_{tV} {}^{t+\Delta t} S_{ij} \delta {}^{t+\Delta t} {}_t \epsilon_{ij} {}^t dv = {}^{t+\Delta t} \mathcal{R} \quad (5)$$

As pointed out above the objective is to linearize the equations of motion. Tables 1 and 2 summarize the relations used to arrive at the linearized equations of motion in the T.L. and the U.L. formulations. As shown in the tables, the linearized equilibrium equations are in the T.L. formulation

$$\int_{oV} {}^0 C_{ijrs} {}^0 e_{rs} \delta {}^0 \epsilon_{ij} {}^0 dv + \int_{oV} {}^0 S_{ij} \delta {}^0 \eta_{ij} {}^0 dv = {}^{t+\Delta t} \mathcal{R} - \int_{oV} {}^0 S_{ij} \delta {}^0 \epsilon_{ij} {}^0 dv \quad (6)$$

and in the U.L. formulation

$$\int_{tV} {}_t C_{ijrs} {}_t e_{rs} \delta {}_t \epsilon_{ij} {}^t dv + \int_{tV} {}_t \tau_{ij} \delta {}_t \eta_{ij} {}^t dv = {}^{t+\Delta t} \mathcal{R} - \int_{tV} {}_t \tau_{ij} \delta {}_t \epsilon_{ij} {}^t dv \quad (7)$$

where ${}^0 C_{ijrs}$ and ${}_t C_{ijrs}$ are the incremental material property tensors in the configuration at time t and referred to the configurations at times 0 and t , respectively.

It need be noted that in equations (6, 7) ${}^0 S_{ij}$ and ${}_t \tau_{ij}$ are given 2nd Piola-Kirchhoff and Cauchy stresses acting in the configuration at time t ; and ${}^0 e_{ij}$, ${}^0 \eta_{ij}$ and ${}_t e_{ij}$, ${}_t \eta_{ij}$ are the linear and nonlinear incremental strains referred to the configurations at times 0 and t , respectively.

Having linearized equation (1) about the equilibrium configuration at time t , a modified Newton iteration is employed effectively to evaluate an accurate solution. Defining for the k 'th iteration

$${}^{t+\Delta t} u_i^{(k)} = {}^{t+\Delta t} u_i^{(k-1)} + \Delta u_i^{(k)} \quad (8)$$

where ${}^{t+\Delta t} u_i^{(0)} = {}^t u_i$, the equation considered in the T.L. formulation is

$$\int_{oV} {}^0 C_{ijrs} {}^0 e_{rs}^{(k)} \delta {}^0 \epsilon_{ij}^{(k)} {}^0 dv + \int_{oV} {}^0 S_{ij} \delta {}^0 \eta_{ij}^{(k)} {}^0 dv = {}^{t+\Delta t} \mathcal{R} - \int_{oV} {}^{t+\Delta t} {}^0 S_{ij}^{(k-1)} \delta {}^{t+\Delta t} {}^0 \epsilon_{ij}^{(k-1)} {}^0 dv \quad k = 1, 2, \dots \quad (9)$$

where ${}^0 e_{ij}^{(k)}$ and ${}^0 \eta_{ij}^{(k)}$ are evaluated as given in Table 1 but using $\Delta u_i^{(k)}$ instead of u_i ; and ${}^{t+\Delta t} {}^0 S_{ij}^{(k-1)}$ and ${}^{t+\Delta t} {}^0 \epsilon_{ij}^{(k-1)}$ are the stresses and strains calculated using ${}^{t+\Delta t} u_i^{(k-1)}$. Similarly, using the U.L. formulation the equation considered is

$$\int_{tV} {}_t C_{ijrs} {}_t e_{rs}^{(k)} \delta {}_t \epsilon_{ij}^{(k)} {}^t dv + \int_{tV} {}_t \tau_{ij} \delta {}_t \eta_{ij}^{(k)} {}^t dv = {}^{t+\Delta t} \mathcal{R} - \int_{t-\Delta t, V^{(k-1)}} {}^{t+\Delta t} {}_t \tau_{ij}^{(k-1)} \delta {}_t \epsilon_{ij}^{(k-1)} {}^{t+\Delta t} dv \quad k = 1, 2, \dots \quad (10)$$

It need be noted that for $k = 1$ equations (9, 10) reduce to equations (6, 7), respectively.

FINITE ELEMENT SOLUTION

For the finite element solution of equations (9, 10) isoparametric elements have been employed [24]. In the isoparametric finite element solution the coordinates and

Table 1. Total Lagrangian formulation

1. Equations of motion

$$\int_{\mathcal{V}} {}^{t+\Delta t} {}_0^t S_{ij} \delta {}^{t+\Delta t} {}_0^t \epsilon_{ij} {}^0 dV = {}^{t+\Delta t} \mathcal{R}$$

where

$${}^{t+\Delta t} {}_0^t S_{ij} = \frac{\rho}{t-\Delta t} {}^{t+\Delta t} x_{i,r} {}^{t+\Delta t} \tau_{rj} {}^{t-\Delta t} x_{j,r}$$

$$\delta {}^{t+\Delta t} {}_0^t \epsilon_{ij} = \delta \frac{1}{2} ({}^{t-\Delta t} {}_0^t u_{i,j} + {}^{t+\Delta t} {}_0^t u_{j,i} + {}^{t+\Delta t} {}_0^t u_{k,i} {}^{t+\Delta t} {}_0^t u_{k,j})$$

2. Incremental decompositions

(a) Stresses

$${}^{t+\Delta t} {}_0^t S_{ij} = {}_i^t S_{ij} + {}_0^t S_{ij}$$

(b) Strains

$${}^{t+\Delta t} {}_0^t \epsilon_{ij} = {}_i^t \epsilon_{ij} + {}_0^t \epsilon_{ij}; \quad {}_0^t \epsilon_{ij} = {}_0^t e_{ij} + {}_0^t \eta_{ij}$$

$${}_0^t \epsilon_{ij} = \frac{1}{2} ({}_0^t u_{i,j} + {}_0^t u_{j,i} + {}_0^t u_{k,i} {}_0^t u_{k,j} + {}_0^t u_{k,i} {}_0^t u_{k,j}); \quad {}_0^t \eta_{ij} = \frac{1}{2} ({}_0^t u_{k,i} {}_0^t u_{k,j})$$

3. Equations of motion with incremental decompositions

Noting that $\delta {}^{t+\Delta t} {}_0^t \epsilon_{ij} = \delta {}_0^t \epsilon_{ij}$ and ${}_0^t S_{ij} = {}_0^t C_{ijrs} {}_0^t \epsilon_{rs}$ the equations of motion are

$$\int_{\mathcal{V}} {}_0^t C_{ijrs} {}_0^t \epsilon_{rs} \delta {}_0^t \epsilon_{ij} {}^0 dV + \int_{\mathcal{V}} {}_i^t S_{ij} \delta {}_0^t \eta_{ij} {}^0 dV = {}^{t+\Delta t} \mathcal{R} - \int_{\mathcal{V}} {}_i^t S_{ij} \delta {}_0^t e_{ij} {}^0 dV$$

4. Linearization of equations of motion

Using the approximations ${}_0^t S_{ij} = {}_0^t C_{ijrs} {}_0^t e_{rs}$, $\delta {}_0^t \epsilon_{ij} = \delta {}_0^t e_{ij}$ we obtain as approximate equations of motion

$$\int_{\mathcal{V}} {}_0^t C_{ijrs} {}_0^t e_{rs} \delta {}_0^t e_{ij} {}^0 dV + \int_{\mathcal{V}} {}_i^t S_{ij} \delta {}_0^t \eta_{ij} {}^0 dV = {}^{t+\Delta t} \mathcal{R} - \int_{\mathcal{V}} {}_i^t S_{ij} \delta {}_0^t e_{ij} {}^0 dV$$

Table 2. Updated Lagrangian formulation

1. Equations of motion

$$\int_{\mathcal{V}} {}^{t+\Delta t} {}_t^t S_{ij} \delta {}^{t+\Delta t} {}_t^t \epsilon_{ij} {}^t dV = {}^{t+\Delta t} \mathcal{R}$$

where

$${}^{t+\Delta t} {}_t^t S_{ij} = \frac{\rho}{t-\Delta t} {}^{t+\Delta t} x_{i,r} {}^{t+\Delta t} \tau_{rj} {}^{t-\Delta t} x_{j,r}$$

$$\delta {}^{t+\Delta t} {}_t^t \epsilon_{ij} = \delta \frac{1}{2} ({}^t u_{i,j} + {}^t u_{j,i} + {}^t u_{k,i} {}^t u_{k,j})$$

2. Incremental decompositions

(a) Stresses

$${}^{t+\Delta t} {}_t^t S_{ij} = {}^t \tau_{ij} + {}_t^t S_{ij}$$

(b) Strains

$${}^{t+\Delta t} {}_t^t \epsilon_{ij} = {}^t \epsilon_{ij}; \quad {}^t \epsilon_{ij} = {}^t e_{ij} + {}^t \eta_{ij}$$

$${}^t \epsilon_{ij} = \frac{1}{2} ({}^t u_{i,j} + {}^t u_{j,i}); \quad {}^t \eta_{ij} = \frac{1}{2} ({}^t u_{k,i} {}^t u_{k,j})$$

3. Equations of motion with incremental decompositions

Noting that ${}^t S_{ij} = {}^t C_{ijrs} {}^t \epsilon_{rs}$ the equations of motion are

$$\int_{\mathcal{V}} {}^t C_{ijrs} {}^t \epsilon_{rs} \delta {}^t \epsilon_{ij} {}^t dV + \int_{\mathcal{V}} {}^t \tau_{ij} \delta {}^t \eta_{ij} {}^t dV = {}^{t+\Delta t} \mathcal{R} - \int_{\mathcal{V}} {}^t \tau_{ij} \delta {}^t e_{ij} {}^t dV$$

4. Linearization of equations of motion

Using the approximations ${}^t S_{ij} = {}^t C_{ijrs} {}^t e_{rs}$, $\delta {}^t \epsilon_{ij} = \delta {}^t e_{ij}$ we obtain as approximate equations of motion

$$\int_{\mathcal{V}} {}^t C_{ijrs} {}^t e_{rs} \delta {}^t e_{ij} {}^t dV + \int_{\mathcal{V}} {}^t \tau_{ij} \delta {}^t \eta_{ij} {}^t dV = {}^{t+\Delta t} \mathcal{R} - \int_{\mathcal{V}} {}^t \tau_{ij} \delta {}^t e_{ij} {}^t dV$$

displacements of an element are interpolated using

$$\left. \begin{aligned} {}^0x_j &= \sum_{k=1}^N h_k {}^0x_j^k; \quad {}^t x_j = \sum_{k=1}^N h_k {}^t x_j^k \\ {}^{t+\Delta t}x_j &= \sum_{k=1}^N h_k {}^{t+\Delta t}x_j^k \end{aligned} \right\} j = 1, 2, 3 \quad (11)$$

$${}^t u_j = \sum_{k=1}^N h_k {}^t u_j^k; \quad \Delta u_j = \sum_{k=1}^N h_k \Delta u_j^k \quad j = 1, 2, 3 \quad (12)$$

where ${}^0x_j^k$ is the coordinate of nodal point k corresponding to direction j at time 0, ${}^t x_j^k$, ${}^{t+\Delta t}x_j^k$, ${}^t u_j^k$ and Δu_j^k are defined similarly, h_k is the interpolation function corresponding to nodal point k , and N is the number of nodal points of the element. Using these interpolations to evaluate equations (9, 10) and taking into account that in dynamic analysis the body force components include inertia forces, the matrix equilibrium equation for a single element is in the T.L. formulation

$$({}^0K_L + {}^0K_{NL})\Delta u^{(k)} = {}^{t+\Delta t}R - {}^{t+\Delta t}{}_0F^{(k-1)} - M {}^{t+\Delta t}\ddot{u}^{(k)} \quad k = 1, 2, 3 \dots \quad (13)$$

where 0K_L and ${}^0K_{NL}$ are the linear and nonlinear strain stiffness matrices, ${}^{t+\Delta t}R$ is the vector of externally applied nodal point loads, ${}^{t+\Delta t}{}_0F^{(k-1)}$ is a vector of nodal point forces equivalent to the current element stresses, M is the mass matrix and $\Delta u^{(k)}$ is a vector of nodal point displacement increments, with ${}^{t+\Delta t}u^{(k)} = {}^{t+\Delta t}u^{(k-1)} + \Delta u^{(k)}$. The vector of nodal point accelerations is evaluated differently depending on the time integration scheme used.

Considering next the U.L. formulation the equilibrium

equations to be solved are

$$\begin{aligned} ({}^tK_L + {}^tK_{NL})\Delta u^{(k)} &= {}^{t+\Delta t}R \\ &- {}^{t+\Delta t}{}_tF^{(k-1)} - M {}^{t+\Delta t}\ddot{u}^{(k)} \quad k = 1, 2, 3 \dots \end{aligned} \quad (14)$$

in which matrices equivalent to those in equation (13) are used. Table 3 summarizes the matrix evaluations. The strain-displacement and stress matrices used in Table 3 have been defined in [3, 4].

Once the matrices corresponding to a single element have been calculated, the equilibrium equations corresponding to an assemblage of elements are obtained using standard procedures [24]. These equations are

$$({}^tK_L + {}^tK_{NL})\Delta u^{(k)} = {}^{t+\Delta t}R - {}^{t+\Delta t}{}_tF^{(k-1)} - M {}^{t+\Delta t}\ddot{u}^{(k)} \quad k = 1, 2, 3 \dots \quad (15)$$

where the left subscript indicating whether the T.L. or U.L. formulation is used has been omitted, because equation [15] is applicable to an assemblage of elements that individually may be described by either formulation. For the numerical solution of equation (15) the Newmark scheme and Wilson θ method have been employed [1, 17]. Table 4 summarizes the integration procedures. It should be noted that because implicit numerical time integration is used, the step-by-step algorithm reduces to a static analysis when inertia effects are not considered.

ELASTIC-PLASTIC CONSTITUTIVE RELATIONS

Comparing the U.L. and T.L. formulations in Tables 1 and 2, it is noted that the formulations are analogous and, in fact, the only theoretical difference between the two

Table 3. Evaluation of integrals

Integral	Matrix evaluation
In all analyses	
$\int_{\sigma_V} {}^0\rho \quad {}^{t+\Delta t}\ddot{u}_k \quad \delta u_k \quad {}^0dv$	$M \quad {}^{t+\Delta t}\ddot{u} = {}^0\rho \left(\int_{\sigma_V} H^T H \quad {}^0dv \right) \quad {}^{t+\Delta t}\ddot{u}$
${}^{t+\Delta t}R = \int_{\sigma_A} {}^{t+\Delta t}{}_0t_k \quad \delta u_k \quad {}^0da$	${}^{t+\Delta t}R = \int_{\sigma_A} H_S^T \quad {}^{t+\Delta t}{}_0t \quad {}^0da$
$+ \int_{\sigma_V} {}^0\rho \quad {}^{t+\Delta t}{}_0f_k \quad \delta u_k \quad {}^0dv$	$+ {}^0\rho \int_{\sigma_V} H^T \quad {}^{t+\Delta t}{}_0f \quad {}^0dv$
Total Lagrangian formulation	
$\int_{\sigma_V} {}^0C_{ijrs} \quad {}^0e_{rs}^{(k)} \quad \delta_i e_{ij}^{(k)} \quad {}^0dv$	${}^0K_L \Delta u^{(k)} = \left(\int_{\sigma_V} {}^0B_L^T \quad {}^0C \quad {}^0B_L \quad {}^0dv \right) \Delta u^{(k)}$
$\int_{\sigma_V} {}^0S_{ij} \quad \delta \eta_{ij}^{(k)} \quad {}^0dv$	${}^0K_{NL} \Delta u^{(k)} = \left(\int_{\sigma_V} {}^0B_{NL}^T \quad {}^0S \quad {}^0B_{NL} \quad {}^0dv \right) \Delta u^{(k)}$
$\int_{\sigma_V} {}^{t+\Delta t}{}_0S_{ij}^{(k-1)} \quad \delta \left({}^{t+\Delta t}{}_0e_{ij}^{(k-1)} \right) \quad {}^0dv$	${}^{t+\Delta t}{}_0F^{(k-1)} = \int_{\sigma_V} {}^{t+\Delta t}{}_0B_L^T \quad ({}^{k-1})^T \quad {}^{t+\Delta t}{}_0S^{(k-1)} \quad {}^0dv$
Updated Lagrangian formulation	
$\int_{i_V} {}^tC_{ijrs} \quad {}^te_{rs}^{(k)} \quad \delta_i e_{ij}^{(k)} \quad {}^tdv$	${}^tK_L \Delta u^{(k)} = \left(\int_{i_V} {}^tB_L^T \quad {}^tC \quad {}^tB_L \quad {}^tdv \right) \Delta u^{(k)}$
$\int_{i_V} {}^t\tau_{ij} \quad \delta \eta_{ij}^{(k)} \quad {}^tdv$	${}^tK_{NL} \Delta u^{(k)} = \left(\int_{i_V} {}^tB_{NL}^T \quad {}^t\tau \quad {}^tB_{NL} \quad {}^tdv \right) \Delta u^{(k)}$
$\int_{i-\Delta v, (k-1)} {}^{t+\Delta t}{}_i\tau_{ij}^{(k-1)} \quad \delta_{i+\Delta t} e_{ij}^{(k-1)} \quad {}^{t+\Delta t}dv^{(k-1)}$	${}^{t+\Delta t}{}_iF^{(k-1)}$
	$= \int_{i-\Delta v, (k-1)} {}^{t+\Delta t}{}_iB_L^T \quad ({}^{k-1})^T \quad {}^{t+\Delta t}{}_i\tau^{(k-1)} \quad {}^{t+\Delta t}dv^{(k-1)}$

Table 4. Summary of step-by-step integration

Initial calculations	
1. Form mass matrix M ; initialize ${}^0\mathbf{u}$, ${}^0\dot{\mathbf{u}}$, ${}^0\ddot{\mathbf{u}}$.	
2. Calculate the following constants: tol ≤ 0.01 ; nitem ≥ 3 ; in static analysis $\theta = 1$ and go to A. Wilson θ method: $\theta \geq 1.37$, usually $\theta = 1.4$, $\tau = \theta \Delta t$	
$a_0 = 6/\tau^2$ $a_1 = 6/\tau$ $a_2 = 2$ $a_3 = a_0/\theta$ $a_4 = -a_1/\theta$ $a_5 = 1 - 3/\theta$	
$a_6 = \Delta t/2$ $a_7 = \Delta t^2/6$	
Newmark method: $\theta = 1.0$, $\delta \geq 0.50$, $\alpha \geq 0.25 (0.5 + \delta)^2$, $\tau = \Delta t$	
$a_0 = 1/(\alpha \Delta t^2)$ $a_1 = 1/(\alpha \Delta t)$ $a_2 = 1/(2\alpha) - 1$ $a_3 = a_0$ $a_4 = -a_1$ $a_5 = -a_2$	
$a_6 = \Delta t(1 - \delta)$ $a_7 = \delta \Delta t$	
3. Calculate mass contribution to effective stiffness matrix: $\hat{\mathbf{K}} = a_0 M$	
For each timestep	
(A) Calculation of displacement increment	
(i) If a new stiffness matrix is to be formed, calculate and triangularize ${}^i\hat{\mathbf{K}}$	
	${}^i\hat{\mathbf{K}} = \mathbf{LDL}^T$
(ii) Form effective load vector:	
	${}^{i+1}\hat{\mathbf{R}} = {}^i\mathbf{R} + \theta({}^{i+\Delta t}\mathbf{R} - {}^i\mathbf{R}) + M(a_1 {}^i\dot{\mathbf{u}} + a_2 {}^i\ddot{\mathbf{u}}) - {}^i\mathbf{F}$
(iii) Solve for displacement increments using latest D, L factors:	
	$\mathbf{LDL}^T \mathbf{u} = {}^{i+1}\hat{\mathbf{R}}$
(iv) If required, iterate for dynamic equilibrium: then initialize $\mathbf{u}^{(0)} = \mathbf{u}$, $i = 0$	
(a) $i = i + 1$.	
(b) Calculate $(i - 1)$ st approximation to accelerations and displacements:	
	${}^{i+1}\ddot{\mathbf{u}}^{(i-1)} = a_0 \mathbf{u}^{(i-1)} - a_1 {}^i\dot{\mathbf{u}} - a_2 {}^i\ddot{\mathbf{u}}$; ${}^{i+1}\mathbf{u}^{(i-1)} = {}^i\mathbf{u} + \mathbf{u}^{(i-1)}$
(c) Calculate $(i - 1)$ st effective out-of-balance loads:	
	${}^{i+1}\hat{\mathbf{R}}^{(i-1)} = {}^i\mathbf{R} + \theta({}^{i+\Delta t}\mathbf{R} - {}^i\mathbf{R}) - M({}^{i+1}\ddot{\mathbf{u}}^{(i-1)} - {}^{i+1}\mathbf{F}^{(i-1)})$
(d) Solve for i 'th correction to displacement increments:	
	$\mathbf{LDL}^T \Delta \mathbf{u}^{(i)} = {}^{i+1}\hat{\mathbf{R}}^{(i-1)}$
(e) Calculate new displacement increments:	
	$\mathbf{u}^{(i)} = \mathbf{u}^{(i-1)} + \Delta \mathbf{u}^{(i)}$
(f) Iteration convergence if $\ \Delta \mathbf{u}^{(i)}\ _2 / \ \mathbf{u}^{(i)}\ _2 + \ \mathbf{u}^{(i)}\ _2 < \text{tol}$.	
If convergence: $\mathbf{u} = \mathbf{u}^{(i)}$ and go to B;	
If no convergence and $i < \text{nitem}$: go to (a); otherwise restart using new stiffness matrix and/or a smaller time step size	
(B) Calculate new accelerations, velocities and displacements	
Wilson θ -method:	
	${}^{i+\Delta t}\ddot{\mathbf{u}} = a_3 \mathbf{u} + a_4 {}^i\dot{\mathbf{u}} + a_5 {}^i\ddot{\mathbf{u}}$
	${}^{i+\Delta t}\dot{\mathbf{u}} = {}^i\dot{\mathbf{u}} + a_6({}^{i+\Delta t}\ddot{\mathbf{u}} + {}^i\ddot{\mathbf{u}})$
	${}^{i+\Delta t}\mathbf{u} = {}^i\mathbf{u} + \Delta t {}^i\dot{\mathbf{u}} + a_7({}^{i+\Delta t}\ddot{\mathbf{u}} + {}^i\ddot{\mathbf{u}})$
Newmark method:	
	${}^{i+\Delta t}\ddot{\mathbf{u}} = a_3 \mathbf{u} + a_4 {}^i\dot{\mathbf{u}} + a_5 {}^i\ddot{\mathbf{u}}$
	${}^{i+\Delta t}\dot{\mathbf{u}} = {}^i\dot{\mathbf{u}} + a_6({}^{i+\Delta t}\ddot{\mathbf{u}} + a_7 {}^{i-\Delta t}\ddot{\mathbf{u}})$
	${}^{i+\Delta t}\mathbf{u} = {}^i\mathbf{u} + \mathbf{u}$

formulations lies in the choice of different reference configurations for kinematic and static variables. Indeed, if in the numerical solution the appropriate constitutive tensors are used, the evaluation of the corresponding integrals in equations (6, 7) results into the same matrices and thus identical response is predicted using either formulation. The conditions for obtaining the same equations are that the stresses must be related as given in Tables 1 and 2 and the relation between the constitutive tensors must be as follows,

$${}_0C_{mnpq} = \frac{\rho}{\rho} \frac{\partial x_{m,i}}{\partial x_{m,i}} \frac{\partial x_{n,j}}{\partial x_{n,j}} \frac{\partial x_{p,r}}{\partial x_{p,r}} \frac{\partial x_{q,s}}{\partial x_{q,s}} \quad (16)$$

$${}_tC_{mnpq} = \frac{\rho}{\rho} \frac{\partial x_{m,i}}{\partial x_{m,i}} \frac{\partial x_{n,j}}{\partial x_{n,j}} \frac{\partial x_{p,r}}{\partial x_{p,r}} \frac{\partial x_{q,s}}{\partial x_{q,s}} \quad (17)$$

where

$$\frac{\partial x_{i,j}}{\partial x_{i,j}} = \frac{\partial x_i}{\partial x_j}$$

These relations are precisely the kinematic transformations required for the integrals in equations (6, 7) to be identical. Any differences in response calculations would then lie in the definition of ${}_tC_{ijrs}$ or ${}_0C_{ijrs}$. However, in practice, the transformations in equations (16, 17) add to the total computational effort required for solution. Therefore, the aim is to formulate the elastic-plastic constitutive relations directly corresponding to the specific kinematic nonlinear formulation used, and the following two constitutive formulations have been implemented and evaluated in this work. The basic ingredients of the constitutive relations are those used in small displacement analysis; namely, in addition to the elastic stress-strain relations, the following assumptions are employed: (1) a yield condition, which specifies the state of multiaxial stress corresponding to start of plastic flow; (2) a flow rule relating plastic strain increments to the current stresses and stress increments subsequent to yielding; and (3) a hardening rule, which specifies how the yield condition is modified during plastic flow [8].

Total Lagrangian formulation

For an elastic-plastic material, the constitutive relations depend on the complete stress and strain history. At any time between the discrete time points t and $t + \Delta t$ the elastic-plastic material behavior is therefore described in the T.L. formulation using

$$d_0S_{ij} = {}_0C_{ijrs} d_0e_{rs} \quad (18)$$

where d_0S_{ij} and d_0e_{rs} are differential increments in 2nd Piola-Kirchhoff stresses and Green-Lagrange strains, respectively, and ${}_0C_{ijrs}$ is the elastic-plastic constitutive tensor at the current stress and strain conditions. Referring to Tables 1 and 3 and equation (13), it is noted that in the calculation of the linear strain stiffness matrix tK_L , the following approximate relation is employed

$${}_0S_{ij} = {}_0C_{ijrs} {}_0e_{rs} \quad (19)$$

where ${}_0e_{rs}$ is the linear part of ${}_0e_{rs}$, and ${}_0C_{ijrs}$ is the stress-strain relation at time t . However, in the equilibrium iterations the total incremental strains are calculated using

$${}_0e_{rs}^{(k)} = {}^{t+\Delta t}{}_0e_{rs}^{(k)} - {}^t{}_0e_{rs} \quad (20)$$

and then, because ${}_0C_{ijrs}$ is a function of the stresses and strains,

$${}_0S_{ij}^{(k)} = \int_0^{t+\Delta t} {}_0C_{ijrs} d_0e_{rs} \quad (21)$$

To evaluate the integral in equation (21) Euler's method has been used [7]. The stresses corresponding to ${}^{t+\Delta t}{}_0e_{rs}^{(k)}$ are then

$${}^{t+\Delta t}{}_0S_{ij}^{(k)} = {}^t{}_0S_{ij} + {}_0S_{ij}^{(k)} \quad (22)$$

The above description shows that basically the material tensor ${}_0C_{ijrs}$ need be evaluated for a given stress and strain state. Consider the calculation of ${}_0C_{ijrs}$ corresponding to ${}^t{}_0e_{ij}$ and ${}^t{}_0S_{ij}$. In the investigation carried out isothermal and elastic-perfectly plastic or isotropic hardening conditions have been assumed. In this case the initial and subsequent yield condition is

$$F({}^t{}_0S_{ij}, {}^t\kappa) = 0 \quad (23)$$

where ${}^t\kappa$ is a hardening parameter that depends on the total plastic strains ${}^t{}_0e_{ij}^p$. The total plastic strain is obtained by addition of the incremental plastic strains $d_0e_{ij}^p$,

$$d_0e_{ij}^p = d_0e_{ij} - d_0e_{ij}^E \quad (24)$$

where $d_0e_{ij}^E$ is the elastic part of the differential increment in strain d_0e_{ij} . Assuming an associated flow rule

$$d_0e_{ij}^p = {}^t\lambda \frac{\partial F}{\partial {}^t{}_0S_{ij}} \quad (25)$$

and because $F = 0$ during plastic deformation

$$\frac{\partial F}{\partial {}^t{}_0S_{ij}} d_0S_{ij} + \frac{\partial F}{\partial {}^t\kappa} d_0e_{ij}^p = 0 \quad (26)$$

The stress increments are calculated using

$$d_0S_{ij} = {}_0C_{ijrs}^E d_0e_{rs}^E \quad (27)$$

where ${}_0C_{ijrs}^E$ is a component of the elasticity tensor relating 2nd Piola-Kirchhoff stresses to Green-Lagrange strains [3].

Equations (23-27) enable the calculation of the components of the constitutive tensor ${}_0C_{ijrs}$ in equation (18) in the usual way [8],

$${}_0C_{ijrs} = {}_0C_{ijrs}^E - \frac{{}_0C_{ijmn}^E \frac{\partial F}{\partial {}^t{}_0S_{mn}} {}_0C_{rnpq}^E \frac{\partial F}{\partial {}^t{}_0S_{pq}}}{\frac{\partial F}{\partial {}^t{}_0e_{mn}^p} \frac{\partial F}{\partial {}^t{}_0S_{mn}} + {}_0C_{lprq}^E \frac{\partial F}{\partial {}^t{}_0S_{lj}} \frac{\partial F}{\partial {}^t{}_0S_{pq}}} \quad (28)$$

It may be noted that once ${}^{t+\Delta t}{}_0S_{ij}^{(k)}$ has been evaluated and the iteration converged, Cauchy stresses are calculated as given in Table 1 whenever stress output is required.

Updated Lagrangian formulation

In the U.L. formulation the elastic-plastic material response is described using

$$d_tS_{ij} = {}_tC_{ijrs} d_te_{rs} \quad (29)$$

where d_tS_{ij} and d_te_{rs} are differential increments in the 2nd

Piola-Kirchhoff stress referred to the configuration at time t and the linear part of ${}^t\epsilon_{rs}$, respectively. In analogy to the T.L. formulation, in the calculation of the linear strain stiffness matrix tK_L , the relation used is

$${}^tS_{ij} = {}^tC_{ijrs} {}^t e_{rs} \quad (30)$$

A main difference appears in the calculation of stresses. The solution of equation (14) yields $\Delta u_i^{(k)}$ and thus corresponding strain components ${}^t e_{rs}^{(k)}$ can be calculated and

$${}^tS_{ij}^{(k)} = \int_0^{\Delta u_i^{(k)}} {}^tC_{ijrs} d {}^t e_{rs} \quad (31)$$

where ${}^tC_{ijrs}$ is a function of the current total stress and strain conditions. Cauchy stresses are then evaluated using

$${}^{t+\Delta t}S_{ij}^{(k)} = {}^t\tau_{ij} + {}^tS_{ij}^{(k)} \quad (32)$$

and

$${}^{t+\Delta t}\tau_{ij}^{(k)} = \frac{{}^{t+\Delta t}\rho^{(k)}}{\rho} ({}^{t+\Delta t}\tau_{ij}^{(k)} + {}^{t+\Delta t}S_{ij}^{(k)} - {}^{t+\Delta t}\tau_{ij}^{(k)}) \quad (33)$$

The calculation of the constitutive relations is carried out as in the T.L. formulation but using Cauchy stresses and the small displacement strain increments ${}^t e_{rs}$. It should be noted that in the evaluation total plastic strains are obtained by addition of the plastic components of ${}^t e_{rs}$ occurring in each time step. The U.L. formulation is therefore quite similar to the calculation of elastic-plastic constitutive relations in small displacement analysis, but to take large displacements into account the transformation in equation (33) is used for stress calculations.

Comparison of formulations

On comparing the evaluation of the elastic-plastic constitutive relations in the U.L. and T.L. formulations, it is noted that different basic assumptions are used. In the T.L. formulation the elastic properties, the yield function and flow rule are defined in the 2nd Piola-Kirchhoff stress space whereas in the U.L. formulation the Cauchy stress space is employed. Under large displacement and large strain conditions, it would therefore be necessary to specify the appropriate elasticity constants, yield stresses and hardening constants. If the same material constants were used large differences between the response predicted using the T.L. and U.L. formulations would, in general, be observed. However, if only moderate deformations are considered the response predicted using the U.L. and T.L. formulations can be expected not to differ a great deal. Namely, for moderate deformations

$${}^t\tau_{ij} = {}^tS_{ij} + o({}^t u_{k,l}) {}^tS_{k,l} \quad (34)$$

where o signifies 'of order'. But then considering the calculation of the elastic-plastic incremental constitutive relations, it is noted that products of stresses are employed and hence the differences in the elements of the stress-strain matrices used in the T.L. and U.L. formulations will be small.

Considering the implementation of the two formulations, it is noted that the T.L. formulation is programmed more easily. Namely, in this case large displacement analysis is a simple extension of small displacement analysis in that the same subroutine which calculates the

material matrix in small displacement analysis can be used without modification for large displacement conditions. It is only necessary to work with 2nd Piola-Kirchhoff stresses and Green-Lagrange strains instead of conventional small displacement strains and stresses.

SAMPLE SOLUTIONS

To implement the T.L. and U.L. formulations described above program NONSAP was employed [2]. The program is available with the T.L. formulation for elastic-plastic analysis and thus had to be modified for the U.L. formulation.

Static large displacement analysis of a cantilever

The cantilever in Fig. 2 was analyzed for a uniformly distributed load using five 8-node plane stress isoparametric elements. The material of the cantilever was assumed to be isotropic and linear elastic. An analytical solution for the response of the cantilever was given by Holden [10].

The purpose of this analysis was to compare the Holden solution with the response predicted using the T.L. and U.L. formulations. Since the beam is elastic, to prevent plastic response the yield stress of the material was selected sufficiently high. It should be noted that in this case the same material constants have been employed in both formulations.

The response of the cantilever using the T.L. and U.L. formulations and 100 equal load steps is shown in Fig. 3, in which Holden's solution is also given. It is seen that for the accuracy with which the response can be presented in the figure all three solutions are identical.

In order to observe the effect of the load step size the analysis was repeated using only five equal load steps. Fig. 4 shows the calculated response. In this case the displacement response predicted using the two formula-

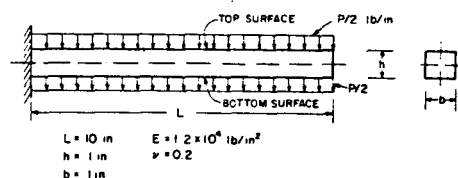


Fig. 2. Cantilever under uniformly distributed load.

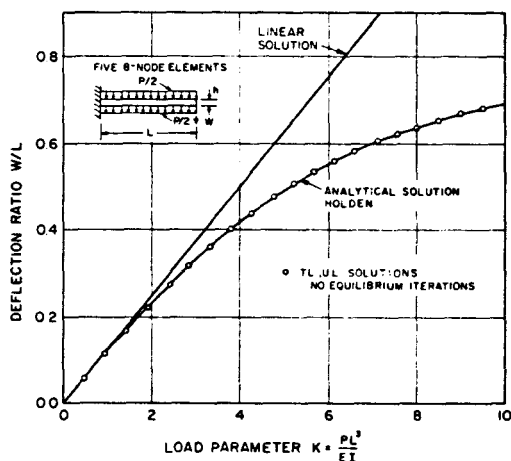


Fig. 3. Large displacement analysis of a cantilever.

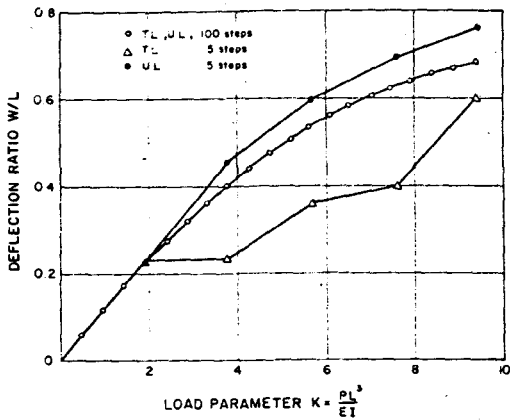


Fig. 4. Large displacement analysis of a cantilever, comparison of nonlinear formulations.

tions is significantly different, because the incremental solution using either formulation was not obtained accurately.

Static large displacement analysis of a spherical shell

The elastic spherical shell shown in Fig. 5 was analyzed for its static response due to a concentrated apex load. The shell was idealized using the 8-node isoparametric elements. The same shell was also analyzed by Stricklin[20] and Mescall[14], and the objective was to compare those solutions with the response predicted in this study. As in the analysis of the cantilever, because the shell is assumed to remain elastic, the yield stress of the material was selected sufficiently high and in both formulations the same material constants have been used.

Figures 5 and 6 show the response predicted by Stricklin, Mescall and in this study. Taking into account that this shell behaves highly nonlinear, good agreement between the different solutions is observed. It should be noted that the difference between the U.L. and T.L. solutions becomes smaller as the number of load steps is increased.

Dynamic large displacement analysis of a second spherical shell

The dynamic response of the spherical cap shown in Fig. 7 was investigated. The shell was subjected to a distributed step pressure $p = 600 \text{ lb/in}^2$. The material was assumed to obey the von Mises yield condition with linear isotropic hardening. The objective in the analysis was to compare the response predicted using the U.L. and T.L. formulations.

Figure 7 shows the response calculated using the Newmark time integration scheme. In this analysis the difference between the response predicted using the T.L. and U.L. formulations is very small indeed. (It should be noted that in this analysis using the U.L. formulation 2nd Piola-Kirchhoff stresses referred to the configuration at time t instead of Cauchy stresses have been used to define ϵ_{vir} in equation (31).) In order to observe the effect of elastic-plastic behavior and the additional effect due to large displacements on the response, a linear analysis and an analysis including only the nonlinear material effects were carried out. As shown in Fig. 7 the material and geometric nonlinear effects are very significant. A comparison of the results obtained in this study with the response predicted by Nagarajan, who used degenerate

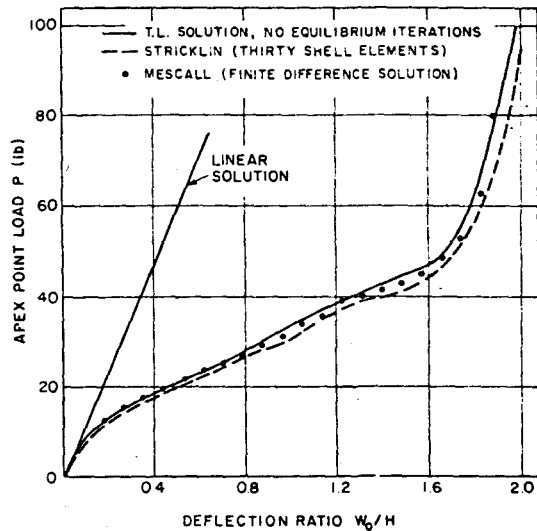
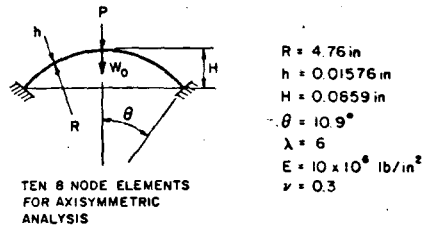


Fig. 5. Load-deflection curves for spherical shell.

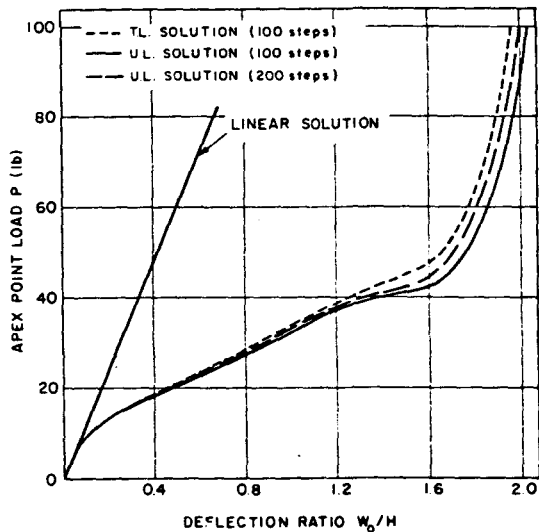
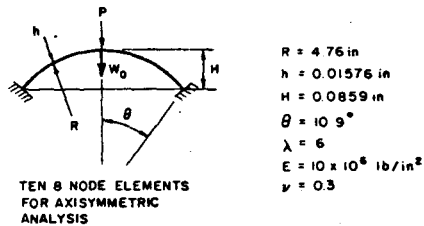


Fig. 6. Load-deflection curves for spherical shell.

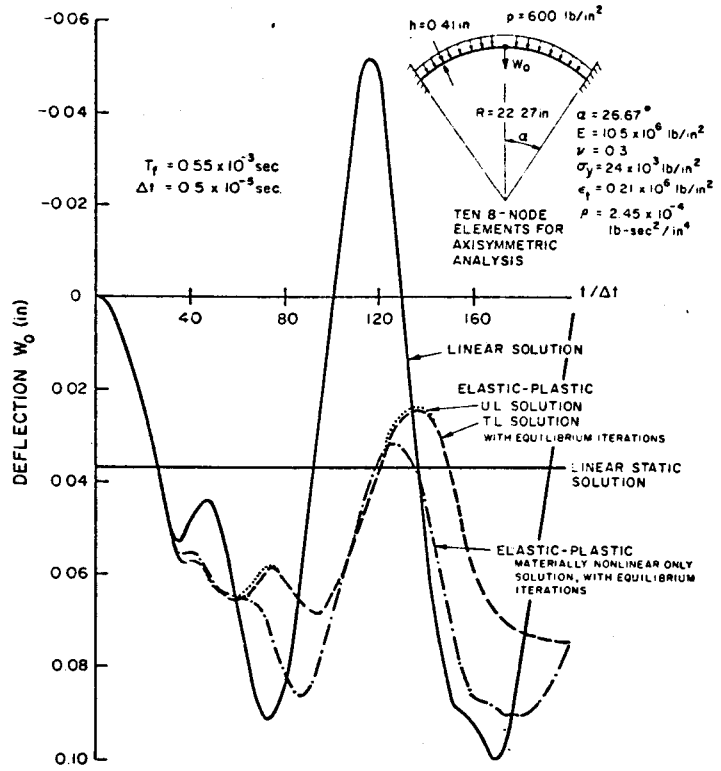


Fig. 7. Large displacement dynamic elastic-plastic analysis of spherical cap, Newmark method, $\delta = 0.50, \alpha = 0.25$.

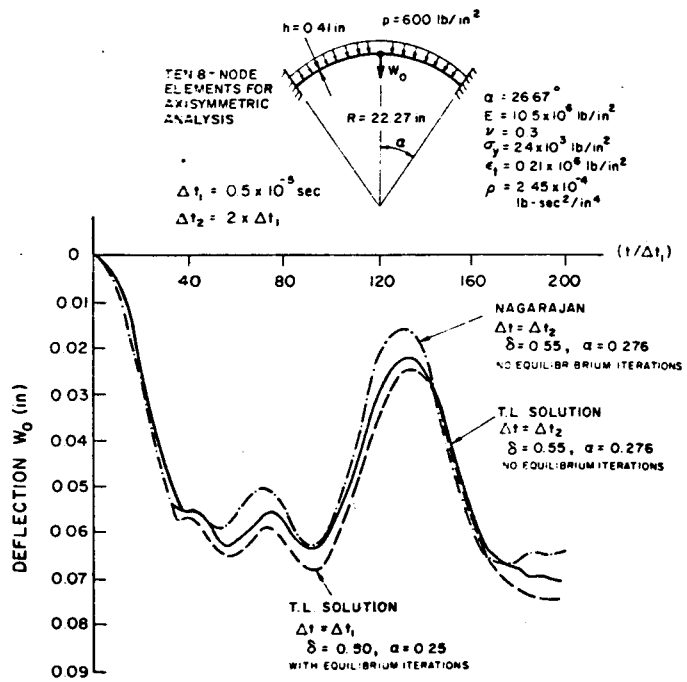


Fig. 8. Large displacement dynamic elastic-plastic analysis of spherical cap, Newmark method.

isoparametric elements and $\alpha = 0.276$, $\delta = 0.55$ in the Newmark method is given in Fig. 8[16].

The objective in this work was to study the T.L. and U.L. incremental formulations for elastic-plastic analysis. However, since the errors in dynamic response calculations are also due to the numerical time integration scheme used, it is also of interest to compare the solutions presented in Fig. 7 with solutions obtained using the Wilson θ -method for time integration. These results are given in Fig. 9.

SUMMARY AND CONCLUSIONS

In the analysis of geometrically nonlinear static or dynamic response using an implicit time integration method, it is necessary to employ a known configuration as reference for stresses and strains. Corresponding to the choice of reference configuration different stress and strain measures must be used. In elastic-plastic analysis the constitutive relations depend on stresses and strains, and an important problem is how to define the material behavior in conjunction with the specific kinematic formulation used.

In this paper two consistent and effective formulations for elastic-plastic analysis have been presented and compared. In the total Lagrangian formulation all static and kinematic variables are referred to the initial configuration whereas in the updated Lagrangian formulation the last calculated configuration is used as reference. It is pointed out that provided the same material description is employed and the appropriate kinematic transformations are carried out identical numerical results are obtained by either formulation. On the other hand, if the constitutive relations are defined directly for each

formulation, as given in the paper, because such material descriptions are numerically more effective, differences will be relatively small provided "moderate" deformations are considered. Since the implementation of the total Lagrangian formulation is simplest, it appears that this formulation is most attractive.

The updated and total Lagrangian formulations have been implemented and in the paper the large deformation response of a cantilever and two shells as predicted using the formulations has been presented.

REFERENCES

1. K. J. Bathe and E. L. Wilson, Stability and accuracy analysis of direct integration methods, *Int. J. Earthquake Engng Struct. Dynamics*, 1, 283-291 (1973).
2. K. J. Bathe, E. L. Wilson and R. H. Iding, NONSAP—A structural analysis program for static and dynamic response of nonlinear systems, Report No. UCSESM 74-3, Department of Civil Engineering, University of California, Berkeley (1974).
3. K. J. Bathe, E. Ramm and E. L. Wilson, Finite element formulations for large displacement and large strain analysis, Report No. UCSESM 73-14, Department of Civil Engineering, University of California, Berkeley (Sept. 1973).
4. K. J. Bathe, E. Ramm and E. L. Wilson, Finite element formulations for large deformation dynamic analysis, *Int. J. Num. Meth. Engng*, 9, 353-386 (1975).
5. T. Belytschko and B. J. Hsieh, Nonlinear transient analysis of shells and solids of revolution by convected elements, AIAA paper No. 73-359, AIAA-ASME/SAE 14th Structures, Structural Dynamics and Materials Conference, Williamsburg, Virginia, (March, 1973).
6. C. A. Felippa and P. Sharifi, Computer implementation of nonlinear finite element analysis, *Proc. Symp. ASME, Detroit* (November, 1973).

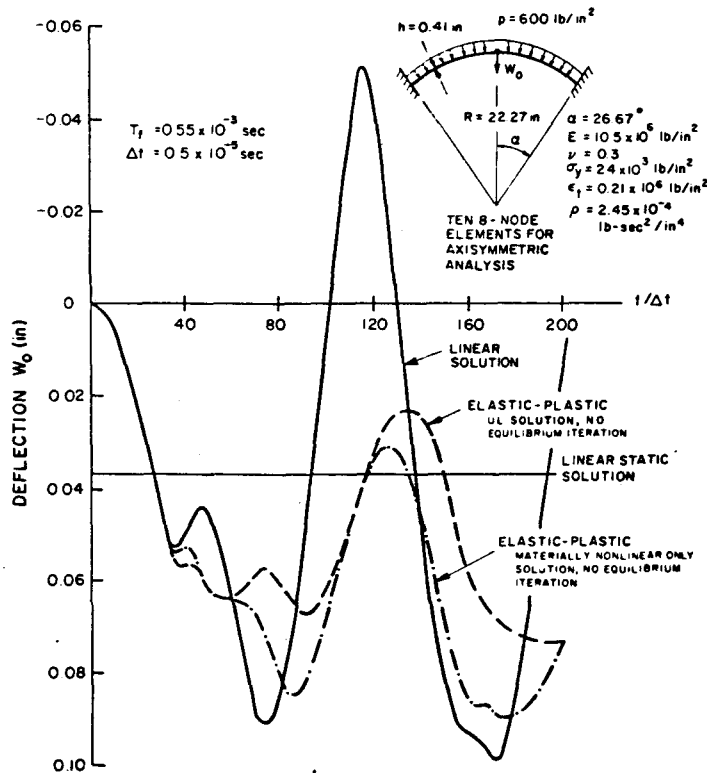


Fig. 9. Large displacement dynamic elastic-plastic analysis of spherical cap, Wilson θ -method, $\theta = 1.4$.

7. C. E. Fröberg, *Introduction to Numerical Analysis*, Addison-Wesley, Reading, Mass.
8. Y. C. Fung, *Foundations of Solid Mechanics*, Prentice-Hall, Englewood Cliffs, New Jersey (1965).
9. H. D. Hibbitt, P. V. Marcal and J. R. Rice, Finite element formulation for problems of large strain and large displacements, *Int. J. Solids Struct.* 6, 1069-1086 (1970).
10. J. T. Holden, On the finite deflections of thin beams, *Int. J. Solids Struct.* 8, 1051-1055 (1972).
11. P. K. Larsen, Large displacement analysis of shells of revolution, including creep, plasticity and viscoelasticity, Report No. UCSESM 71-22, Department of Civil Engineering, University of California, Berkeley (1971).
12. L. E. Malvern, *Introduction to the Mechanics of a Continuous Medium*, Prentice-Hall, Englewood Cliffs, New Jersey, (1969).
13. J. F. McNamara and P. V. Marcal, Incremental stiffness method for finite element analysis of the nonlinear dynamic problem, In *Numerical and Computer Methods in Structural Mechanics*, Fenves, Perrone, Robinson and Schnobrich, (Eds.) Academic Press, New York (1973).
14. J. F. Mescall, Large deflections of spherical shells under concentrated loads, *J. Appl. Mech.* 32, 936-938 (1965).
15. D. W. Murray and E. L. Wilson, Finite element large deflection analysis of plates, *ASCE, J. Engng. Mech. Div.* 95, 143-165 (1969).
16. S. Nagarajan, Nonlinear static and dynamic analysis of shells of revolution under axisymmetric loading, Report No. UCSESM 73-11, Department of Civil Engineering, University of California, Berkeley (1973).
17. R. E. Nickell, Direct integration methods in structural dynamics, *ASCE, J. Engng. Mech. Div.* 99, 303-317, (1973).
18. J. T. Oden, *Finite Elements of Nonlinear Continua*, McGraw-Hill, New York (1972).
19. P. Sharifi and D. N. Yates, Nonlinear thermo-elastic-plastic and creep analysis by the finite element method, AIAA Paper No. 73-358, AIAA/ASME/SAE 14th Structures, Structural Dynamics and Materials Conference, Williamsburg, Virginia (March, 1973).
20. J. A. Stricklin, Geometrically nonlinear static and dynamic analysis of shells of revolution, High speed computing of elastic structures, *Proc. Symp. IUTAM*, University of Liege, pp. 383-411 (August, 1970).
21. J. A. Stricklin, W. A. Von Riesenmann, J. R. Tillerson and W. E. Haisler, Static geometric and material nonlinear analysis, *Advances in Computational Methods in Structural Mechanics and Design*, 2nd U.S.-Japan Seminar in Matrix Methods of Structural Analysis and Design, University of Alabama Press pp. 301-324 (1972).
22. S. Yaghmai, Incremental analysis of large deformations in mechanics of solids with applications to axisymmetric shells of revolution, Report No. UCSESM 68-17, Department of Civil Engineering, University of California, Berkeley (1968).
23. S. Yaghmai and E. P. Popov, Incremental analysis of large deflections of shells of revolution, *Int. J. Solids Struct.* 7, 1375-1393 (1971).
24. O. C. Zienkiewicz, *The Finite Element Method in Engineering Science*, McGraw-Hill, London (1971).

ON FINITE ELEMENT LARGE DISPLACEMENT AND ELASTIC-PLASTIC DYNAMIC ANALYSIS OF SHELL STRUCTURES

TAIRO ISHIZAKI

Kure Research Laboratory, Babcock Hitachi K.K. Takara-machi, Kure, Hiroshima 737, Japan

and

KLAUS-JÜRGEN BATHE

Department of Mechanical Engineering, Massachusetts Institute of Technology, Cambridge, MA 02139, U.S.A.

(Received 17 December 1979; received for publication 11 February 1980)

Abstract—Finite element procedures for nonlinear dynamic analysis of shell structures are presented and assessed. Geometric and material nonlinear conditions are considered. Some results are presented that demonstrate current applicabilities of finite element procedures to the nonlinear dynamic analysis of two-dimensional shell problems. The nonlinear response of a shallow cap, an impulsively loaded cylindrical shell and a complete spherical shell is predicted. In the analyses the effects of various finite element modeling characteristics are investigated. Finally, solutions of the static and dynamic large displacement elastic-plastic analysis of a complete spherical shell subjected to external pressure are reported. The effect of initial imperfections on the static and dynamic buckling behavior of this shell is presented and discussed.

1. INTRODUCTION

The calculation of the nonlinear dynamic response of shell structures including instability or buckling phenomena has received considerable attention in recent years and much literature has appeared on this subject [1-25]. The elastic dynamic buckling of spherical caps was solved using the Galerkin method [2], finite difference methods [3-5] and finite element methods [6-8]. The dynamic response of spherical caps and domes subjected to large external loads that cause plastic deformations was analyzed using finite element methods [6-10], and the analysis of dynamic buckling of some cylindrical shells was performed using analogue computers [11], finite difference methods [12-15], and finite element methods [8, 16, 17]. The dynamic buckling of hemispheres and complete spherical shells was discussed in references [13, 18] and [19-21], respectively. The results of these studies showed that initial shell imperfections have the effect of reducing the dynamic buckling loads, as well as the static buckling loads [1, 5, 22-25].

It is not our intention in this paper to survey all the work that has been performed on dynamic shell buckling (and the list of reports referred to above is by no means a complete reference list on this subject), but based on the previous work performed it is concluded that to calculate the dynamic buckling load of a shell using numerical methods, an evaluation of the transient response of the shell for various load levels is required [5]. Furthermore, based on the experiences obtained with finite element procedures, these techniques appear to be much suited for the calculation of dynamic buckling loads.

Considering the use of the finite element method for the analysis of nonlinear dynamic problems, it is necessary to employ consistent and stable finite element formulations. A shell structure may undergo large displacements and large strains; hence, the finite element procedures must be based on large deformation kinematic formulations and appropriate constitutive equations. Also, for the dynamic analysis, numerical time integration of the finite element equations of motion is necessary. Here, it is important that a time integration scheme be used that is stable and accurate, since otherwise buckling loads are predicted numerically that are

physically non-existent. Also, the appropriate use of these techniques is not straight-forward and is generally based on much solution experience.

The objective of this paper is to demonstrate the application of some state-of-the-art finite element analysis procedures to the nonlinear dynamic analysis of shell structures, and thus contribute to the body of knowledge available for the proper finite element modeling of the problems considered. In addition, the solutions obtained summarize the static and dynamic large deflection and instability characteristics of some important shell structures.

In the first part of the paper, the general finite element formulations used for the nonlinear dynamic analyses are presented. The incremental kinematic formulations include large displacements and large strains. Also, the time integration and the equilibrium iteration schemes employed are briefly summarized.

In the second part of the paper, the finite element formulations that have been discussed earlier are applied to the nonlinear large displacement and elastic-plastic dynamic analysis of three different two-dimensional shells: a spherical cap subjected to an external step pressure, an infinitely long cylinder subjected to an impulse, and a complete spherical shell subjected to uniform external pressure. These analyses have been performed to identify the effects of some important modeling variables used, such as the number of finite elements, the mass idealization, the number of Gauss integration points, the time step size Δt , and the use of equilibrium iteration. The finite element solutions obtained are compared in some cases with other finite element results reported elsewhere and experimental predictions.

In the last part of the paper, further analysis results of the complete spherical shell with and without initial imperfections are reported. The shell is subjected to uniform external pressure and was analyzed for its large displacement elastic-plastic static and dynamic response. The results of the analysis show the static and dynamic characteristics of the shell when different levels of geometric imperfections are assumed. The shell instability characteristics identified in this paper should be valuable in the design of some spherical shell structures.

2. SUMMARY OF THE FINITE ELEMENT PROCEDURES USED

In the finite element analysis of shell structures it is most important to employ consistent kinematic continuum and finite element formulations, appropriate constitutive relations and stable and accurate procedures for the solution of the finite element equations.

2.1 Incremental equations of motion

As previously summarized [6, 7], for large displacement elastic-plastic analysis, basically two different kinematic formulations can be employed, i.e. the total Lagrangian (T.L.) and the updated Lagrangian Jaumann (U.L.J.) formulations can be used.

Total Lagrangian formulation. The principle of virtual displacements for the T.L. formulation is

$$\int_{0V} {}^{t+\Delta t} \delta {}^0 S_{ij} \delta {}^{t+\Delta t} \epsilon_{ij} dV = {}^{t+\Delta t} \mathcal{R} \quad (1)$$

where 0V is the volume of the body at time 0, ${}^{t+\Delta t} S_{ij}$ is the 2nd Piola-Kirchhoff stress tensor at time $t + \Delta t$ referred to the configuration at time 0, ${}^{t+\Delta t} \epsilon_{ij}$ is the Green-Lagrange strain tensor at time $t + \Delta t$ referred to the configuration at time 0, and ${}^{t+\Delta t} \mathcal{R}$ is the external virtual work at time $t + \Delta t$.

Linearizing eqn (1) about the state at time t the governing continuum mechanics equations are,

$$\begin{aligned} \int_{0V} {}^0 C_{ijrs} \delta {}^0 e_{rs} \delta {}^0 e_{ij} dV + \int_{0V} {}^0 S_{ij} \delta {}^0 \eta_{ij} dV \\ = {}^{t+\Delta t} \mathcal{R} - \int_{0V} {}^t S_{ij} \delta {}^0 e_{ij} dV \end{aligned} \quad (2)$$

and

$${}^{t+\Delta t} \epsilon_{rs} = {}^t \epsilon_{rs} + {}^0 \epsilon_{rs} \quad (3)$$

$$+ \int_0^{t+\Delta t} {}^0 C_{ijrs} d {}^0 \epsilon_{rs} \quad (4)$$

where the total Green-Lagrange strains corresponding to time $t + \Delta t$ are calculated from the total nodal-point displacements. This formulation can be employed effectively for large displacement but small strain elastic-plastic analysis [6].

Updated Lagrangian Jaumann stress formulation. In the U.L.J. formulation, all variables are referred to the configuration at time t , i.e. the updated configuration of the body. In this case the principle of virtual displacements used is

$$\int_{tV} {}^{t+\Delta t} \delta {}^t S_{ij} \delta {}^{t+\Delta t} \epsilon_{ij} dV = {}^{t+\Delta t} \mathcal{R} \quad (5)$$

where tV is the volume of the body at time t , ${}^{t+\Delta t} S_{ij}$ is the 2nd Piola-Kirchhoff stress tensor at time $t + \Delta t$ referred to the configuration at time t and ${}^{t+\Delta t} \epsilon_{ij}$ is the Green-Lagrange strain tensor at time $t + \Delta t$ referred to the configuration at time t .

Proceeding as in the T.L. formulation, the governing linearized continuum mechanics equation is in the U.L.J. formulation,

$$\begin{aligned} \int_{tV} {}^t C_{ijrs} \delta {}^t e_{rs} \delta {}^t e_{ij} dV + \int_{tV} {}^t \tau_{ij} \delta {}^t \eta_{ij} dV \\ = {}^{t+\Delta t} \mathcal{R} - \int_{tV} {}^t \tau_{ij} \delta {}^t e_{ij} dV. \end{aligned} \quad (6)$$

This formulation can directly be employed for large displacement and large strain elastic-plastic analysis provided the Young's modulus and strain hardening modulus corresponding to the Cauchy stress and logarithmic (true) strain increments are used instead of the usual small displacement quantities [26, 27]. With this constitutive tensor, the solution of eqn (6) yields an increment of displacements and hence an increment of strains, after which the stresses corresponding to time $t + \Delta t$ are calculated.

The large strain formulation accounts for rigid body rotations on the current stresses using

$${}^{\nabla} \tau_{ij} = {}^t \dot{\tau}_{ij} - {}^t \tau_{ip} {}^t \Omega_{pj} - {}^t \tau_{jp} {}^t \Omega_{pi} \quad (7)$$

where ${}^{\nabla} \tau_{ij}$ is the Jaumann stress rate tensor at time t , ${}^t \dot{\tau}_{ij}$ is the time derivative of the Cauchy stress tensor at time t and ${}^t \Omega_{ij}$ is the spin tensor. The Jaumann stress rate tensor is evaluated using

$${}^{\nabla} \tau_{ij} = {}^t C_{ijrs} {}^t \dot{e}_{rs} \quad (8)$$

where ${}^t \dot{e}_{rs}$ is the rate of strain increment. Integrating eqn (8) over the time increment Δt , which is assumed to be small, and using eqn (7), we obtain as an approximation to the Cauchy stresses at time $t + \Delta t$

$$\begin{aligned} {}^{t+\Delta t} \tau_{ij} = {}^t \tau_{ij} + \int_t^{t+\Delta t} {}^t C_{ijrs} d {}^t e_{rs} \\ + {}^t \tau_{ip} {}^t \Omega_{pj} \Delta t + {}^t \tau_{jp} {}^t \Omega_{pi} \Delta t. \end{aligned} \quad (9)$$

Considering elastic-plastic analysis the integration in eqn (9) with all the ingredients of the elastic-plastic formulation chosen can be performed effectively using an Euler method or the trapezoidal rule.

2.2 Finite element formulations

The finite element implementation of eqn (2) in the T.L. formulation can be written in matrix form, for a single finite element, as

$$({}^0 \mathbf{K}_L + {}^0 \mathbf{K}_{NL}) \mathbf{U} = {}^{t+\Delta t} \mathbf{R} - {}^0 \mathbf{F} \quad (10)$$

where ${}^0 \mathbf{K}_L$ and ${}^0 \mathbf{K}_{NL}$ are the linear and nonlinear strain stiffness matrices, \mathbf{U} is the vector of incremental nodal-point displacements, ${}^{t+\Delta t} \mathbf{R}$ is the external nodal-point force vector and ${}^0 \mathbf{F}$ is the vector of nodal-point forces equivalent to the element stresses. Considering eqns (2) and (10), the integrals of eqn (2) are approximated in eqn (10) as follows:

$${}^0 \mathbf{K}_L = \int_{0V} {}^0 \mathbf{B}_L^T {}^0 \mathbf{C} {}^0 \mathbf{B}_L dV; \quad {}^0 \mathbf{K}_{NL} = \int_{0V} {}^0 \mathbf{B}_{NL}^T {}^0 \mathbf{S} {}^0 \mathbf{B}_{NL} dV \quad (11)$$

$${}^0 \mathbf{F} = \int_{0V} {}^0 \mathbf{B}_L^T {}^0 \hat{\mathbf{S}} dV \quad (12)$$

where ${}^0 \mathbf{B}_L$ and ${}^0 \mathbf{B}_{NL}$ are the linear and nonlinear strain-displacement transformation matrices, ${}^0 \mathbf{C}$ is the incremental stress-strain material property matrix, and ${}^0 \mathbf{S}$ and ${}^0 \hat{\mathbf{S}}$ are a matrix and a vector of 2nd Piola-Kirchhoff

stresses. Once the matrices corresponding to a single element have been calculated, they are assembled into the complete system matrices in the usual manner [28].

Similarly, the finite element implementation of eqn (4), which was obtained using the U.L.J. formulation, is

$$({}^i\mathbf{K}_L + {}^i\mathbf{K}_{NL})\mathbf{U} = {}^{t+\Delta t}\mathbf{R} - {}^t\mathbf{F} \quad (13)$$

where

$${}^i\mathbf{K}_L = \int_{V} {}^i\mathbf{B}_L^T \mathbf{C} {}^i\mathbf{B}_L dV; \quad {}^i\mathbf{K}_{NL} = \int_{V} {}^i\mathbf{B}_{NL}^T {}^t\boldsymbol{\tau} {}^i\mathbf{B}_{NL} dV \quad (14)$$

$${}^t\mathbf{F} = \int_{V} {}^i\mathbf{B}_L^T {}^t\hat{\boldsymbol{\tau}} dV \quad (15)$$

where ${}^i\mathbf{B}_L$ and ${}^i\mathbf{B}_{NL}$ are the linear and nonlinear strain-displacement transformation matrices, \mathbf{C} is the incremental stress-strain material property matrix and ${}^t\boldsymbol{\tau}$ and ${}^t\hat{\boldsymbol{\tau}}$ are a matrix and vector of Cauchy stresses.

2.3 Deformation-dependent pressure loading

So far the external loads, which resulted in the load vector in eqns (10) and (13), have been assumed to be independent of the configuration of the body. However, when shell structures undergo large displacements, it is necessary to consider the externally applied pressures to be configuration-dependent. The vector of nodal-point forces equivalent to the applied pressure at time $t + \Delta t$, ${}^{t+\Delta t}\mathbf{p}$, can then be evaluated approximately using

$${}^{t+\Delta t}\mathbf{R}_p = \int_{A} {}^i\mathbf{H}^T {}^{t+\Delta t}\mathbf{p} dA \quad (16)$$

where A is the area and ${}^i\mathbf{H}^s$ is the matrix of surface displacement interpolation functions at time t .

2.4 Time integration

Considering dynamic analysis, using an implicit time integration scheme, the external loads in eqns (10) and (13) include the d'Alembert forces at time $t + \Delta t$. The equilibrium equations of a pressure loaded shell discretized in finite element analysis, as above, can be written generally as follows [6, 7],

$${}^t\mathbf{K}\mathbf{U} = {}^{t+\Delta t}\mathbf{R}_p - {}^t\mathbf{F} - \mathbf{M} {}^{t+\Delta t}\ddot{\mathbf{U}} \quad (17)$$

where ${}^t\mathbf{K}$ is the stiffness matrix at time t , \mathbf{M} is the mass matrix and ${}^{t+\Delta t}\ddot{\mathbf{U}}$ is the vector of nodal-point accelerations at time $t + \Delta t$.

Using the trapezoidal rule of time integration, the following assumptions are employed,

$${}^{t+\Delta t}\mathbf{U} = {}^t\mathbf{U} + \frac{\Delta t}{2} ({}^t\dot{\mathbf{U}} + {}^{t+\Delta t}\dot{\mathbf{U}}) \quad (18)$$

$${}^{t+\Delta t}\dot{\mathbf{U}} = {}^t\dot{\mathbf{U}} + \frac{\Delta t}{2} ({}^t\ddot{\mathbf{U}} + {}^{t+\Delta t}\ddot{\mathbf{U}}). \quad (19)$$

From the above equations, we obtain

$${}^{t+\Delta t}\ddot{\mathbf{U}} = \frac{4}{(\Delta t)^2} ({}^{t+\Delta t}\mathbf{U} - {}^t\mathbf{U}) - \frac{4}{\Delta t} {}^t\dot{\mathbf{U}} - {}^t\ddot{\mathbf{U}} \quad (20)$$

and substituting into eqn (17) we obtain

$${}^t\hat{\mathbf{K}}\mathbf{U} = {}^{t+\Delta t}\hat{\mathbf{R}} - {}^t\mathbf{F} \quad (21)$$

where

$${}^t\hat{\mathbf{K}} = {}^t\mathbf{K} + \frac{4}{(\Delta t)^2} \mathbf{M}; \quad \mathbf{U} = {}^{t+\Delta t}\mathbf{U} - {}^t\mathbf{U} \quad (22)$$

$${}^{t+\Delta t}\hat{\mathbf{R}} = {}^{t+\Delta t}\mathbf{R}_p + \mathbf{M} \left[\frac{4}{\Delta t} {}^t\dot{\mathbf{U}} + {}^t\ddot{\mathbf{U}} \right]. \quad (23)$$

By solving eqn (21) we obtain the increment of nodal-point displacements, \mathbf{U} , and then the velocities and accelerations at time $t + \Delta t$, ${}^{t+\Delta t}\dot{\mathbf{U}}$ and ${}^{t+\Delta t}\ddot{\mathbf{U}}$, are obtained using eqns (19) and (20).

2.5 Equilibrium iteration

The step-by-step solution of the nonlinear response of a shell can in general only be performed accurately using equilibrium iterations during a time increment [7, 29, 30],

$${}^{\tau}\hat{\mathbf{K}} \Delta \mathbf{U}^{(i)} = {}^{t+\Delta t}\hat{\mathbf{R}}^{(i-1)} - {}^{t+\Delta t}\mathbf{F}^{(i-1)}. \quad (24)$$

where ${}^{\tau}\hat{\mathbf{K}}$ is the effective stiffness matrix corresponding to time τ ,

$${}^{t+\Delta t}\mathbf{U}^{(i)} = {}^{t+\Delta t}\mathbf{U}^{(i-1)} + \Delta \mathbf{U}^{(i)} \quad (25)$$

$${}^{t+\Delta t}\hat{\mathbf{R}}^{(i-1)} = {}^{t+\Delta t}\mathbf{R}_p^{(i-1)} - \mathbf{M} \left[\frac{4}{(\Delta t)^2} ({}^{t+\Delta t}\mathbf{U}^{(i-1)} - {}^t\mathbf{U}) - \frac{4}{\Delta t} {}^t\dot{\mathbf{U}} - {}^t\ddot{\mathbf{U}} \right] \quad (26)$$

and

$${}^{t+\Delta t}\mathbf{R}_p^{(i-1)} = \int_{A} {}^i\mathbf{H}^s (i-1)^T {}^{t+\Delta t}\mathbf{p} dA. \quad (27)$$

Furthermore, in the T.L. formulation,

$${}^{t+\Delta t}\mathbf{F}^{(i-1)} = \int_{V} {}^{t+\Delta t}{}_{\delta} \mathbf{B}_L^{(i-1)T} {}^{t+\Delta t}{}_{\delta} \hat{\boldsymbol{\sigma}}^{(i-1)} dV \quad (28)$$

and in the U.L.J. formulation,

$${}^{t+\Delta t}\mathbf{F}^{(i-1)} = \int_{V} {}^i\mathbf{B}_L^{(i-1)T} {}^{t+\Delta t}{}_{\delta} \hat{\boldsymbol{\tau}}^{(i-1)} dV. \quad (29)$$

In the equilibrium iteration of eqn (24), the modified Newton method may be used. In this method, the coefficient matrix, ${}^{\tau}\hat{\mathbf{K}}$, is constant during iteration and " τ " is equal to " t ." However, when a time increment is not sufficiently small, the modified Newton method may display slow convergence or even divergence.

The BFGS (Broydon-Fletcher-Goldfarb-Shanno) method, in which the coefficient matrix is modified to improve the convergence, is frequently more effective than the modified Newton method [30, 31]. The basic equations used in the BFGS method are

$$\Delta \mathbf{U}^{(i)} = ({}^{\tau}\hat{\mathbf{K}}^{-1})^{(i-1)} ({}^{t+\Delta t}\hat{\mathbf{R}}^{(i-1)} - {}^{t+\Delta t}\mathbf{F}^{(i-1)}) \quad (30)$$

and

$${}^{t+\Delta t}\mathbf{U}^{(i)} = {}^{t+\Delta t}\mathbf{U}^{(i-1)} + \beta \Delta \mathbf{U}^{(i)} \quad (31)$$

where β is a scalar that is evaluated to satisfy the condition

$$\Delta U^{(i)T} ({}^{t+\Delta t} \hat{\mathbf{R}}^{(i)} - {}^{t+\Delta t} \mathbf{F}^{(i)}) \leq \text{STOL} [\Delta U^{(i)T} ({}^{t+\Delta t} \hat{\mathbf{R}}^{(i-1)} - {}^{t+\Delta t} \mathbf{F}^{(i-1)})] \quad (32)$$

with STOL a tolerance. The coefficient matrix in eqn (30) is evaluated as follows,

$$({}^t \hat{\mathbf{K}}^{-1})^{(i-1)} = \mathbf{A}^{(i-1)T} ({}^t \hat{\mathbf{K}}^{-1})^{(i-2)} \mathbf{A}^{(i-1)} \quad (33)$$

where the matrices $\mathbf{A}^{(i-1)}$ are of the simple form

$$\mathbf{A}^{(i-1)} = (\mathbf{I} + \mathbf{v}^{(i-1)} \mathbf{w}^{(i-1)T}) \quad (34)$$

with the vectors $\mathbf{v}^{(i-1)}$ and $\mathbf{w}^{(i-1)}$ given by the calculated nodal-point displacements and forces.

Effective convergence criteria for the equilibrium iterations are [30],

$$\frac{\|{}^{t+\Delta t} \mathbf{R}_p^{(i-1)} - {}^{t+\Delta t} \mathbf{F}^{(i-1)} - \mathbf{M}^{t+\Delta t} \ddot{\mathbf{U}}^{(i-1)}\|_2}{\|{}^t \mathbf{R}_p - {}^t \mathbf{F} - \mathbf{M} {}^t \ddot{\mathbf{U}}\|_2^{(\max)}} \leq \epsilon_F \quad (35)$$

and

$$\frac{\Delta U^{(i)T} ({}^{t+\Delta t} \mathbf{R}_p^{(i-1)} - {}^{t+\Delta t} \mathbf{F}^{(i-1)} - \mathbf{M}^{t+\Delta t} \ddot{\mathbf{U}}^{(i-1)})}{\Delta U^{(i)T} ({}^{t+\Delta t} \mathbf{R}_p - {}^t \mathbf{F} - \mathbf{M} {}^t \ddot{\mathbf{U}})} \leq \epsilon_E \quad (36)$$

where ϵ_F is an out-of-balance force tolerance and ϵ_E is an energy tolerance. In eqn (35) the superscript (max) denotes the maximum value ever calculated during the solution, and $\|\mathbf{a}\|_2$ is the Euclidean norm of vector \mathbf{a} .

Both convergence criteria, eqns (35) and (36), have to be satisfied for the termination of the iteration.

3. ANALYSES OF THREE SHELL STRUCTURES

Except for the deformation-dependent pressure load option (which we had to implement during this study), the finite element procedures summarized in the previous sections are available in the computer program ADINA [32], and we have used this program for the nonlinear dynamic analysis of the shell structures described in the following sections. In all analyses equilibrium iterations were performed with $\epsilon_F = 0.1$ and $\epsilon_E = 0.001$ in eqns (35) and (36), unless otherwise stated. In general, the modified Newton method was used, but when convergence difficulties were encountered the BFGS method was employed. To model the elastic-plastic conditions in all analyses the Prandtl-Reuss equations were used with the von Mises yield condition and isotropic strain-hardening.

3.1 Analysis of a spherical cap

In order to identify the applicability of the finite element procedures discussed in the previous section, the nonlinear dynamic analysis of a spherical cap subjected to a uniformly distributed external step pressure was performed using different finite element models and solution variables.

The cap dimensions and material properties are given in Fig. 1. Ten equal 8-node axisymmetric elements were used to discretize the cap from its apex to the fixed support with one element through the thickness.

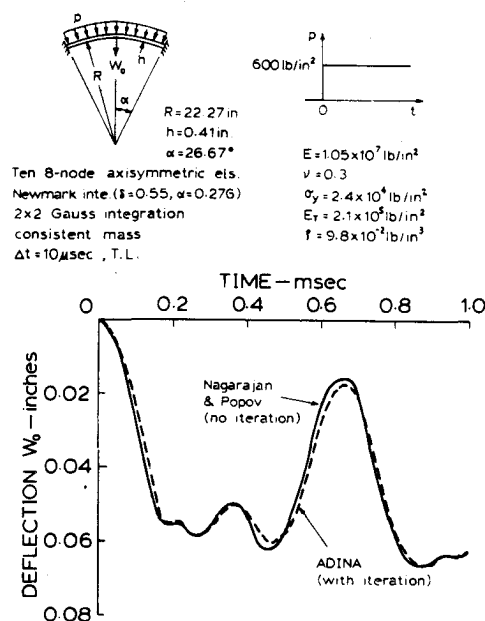


Fig. 1. Dynamic elastic-plastic response of a spherical cap, p deformation independent.

Figure 1 shows the dynamic response of the spherical cap predicted with 2×2 Gauss integration [28], a consistent mass matrix assumption, equilibrium iterations using the BFGS method, the Newmark time integration scheme ($\delta = 0.55$, $\alpha = 0.276$) with $\Delta t = 1.0 \times 10^{-5}$ sec and using the T.L. formulation. Also shown is the finite element solution calculated by Nagarajan and Popov [9].

The effects of using a lumped mass idealization, different Gauss integration orders and different tolerances in the equilibrium iterations are shown in Figs. 2-4. Based on the results obtained in this analysis, and previous experiences, we used in all the following analyses a consistent mass idealization and 2×2 Gauss integration.

3.2 Analysis of a cylindrical shell

In this study, the nonlinear dynamic response of an impulsively loaded cylindrical shell was calculated and the results were compared with experimental and

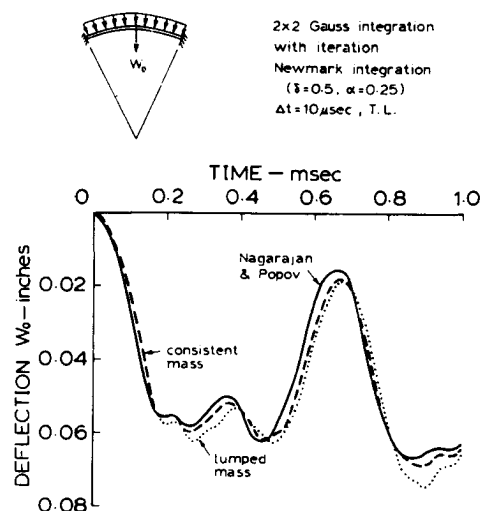


Fig. 2. Response of the cap using consistent and lumped mass idealization.

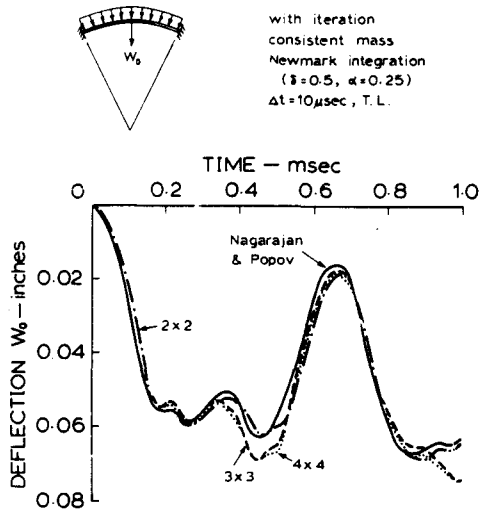


Fig. 3. Effect of numbers of Gauss integration points on the cap response predicted.

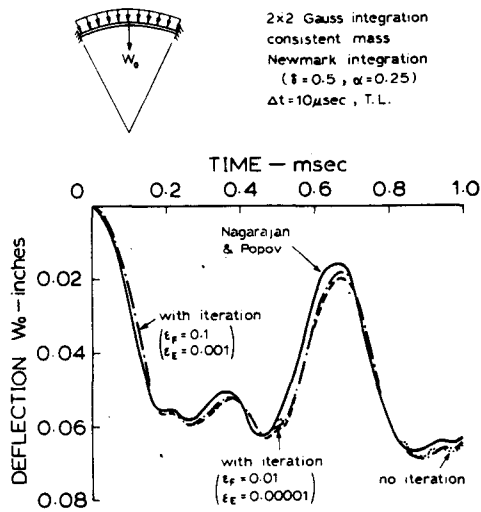


Fig. 4. Effect of equilibrium tolerance on the cap response predicted.

numerical results obtained by Lindberg and Kennedy[17].

The cylindrical shell is shown in Fig. 5. The material is 6061-T6 aluminum. An impulse, uniform in axial direction, was applied to the shell with a circumferential variation of a cosine curve, as shown in Fig. 5. This loading was expressed by the following initial inward radial velocity, $\dot{w}_i(\phi)$ [in/sec],

$$\dot{w}_i(\phi) = 1327 + 2079 \cos \phi + 835 \cos 2\phi - 172 \cos 4\phi \quad (37)$$

where ϕ is the circumferential angle.

In our finite element analysis one half of the cross-section of the cylindrical shell was idealized using sixty 8-node isoparametric plane strain elements, with one element layer modeling the thickness of the shell.

A plot of the radial displacement at $\phi = 15^\circ$ as a function of time is shown in Fig. 5. Also shown are experimental results and the finite element solution obtained by Lindberg and Kennedy. The ADINA solutions based on the T.L. and U.L.J. formulations show good agreement with the experimental results. The effect of large strain is small, because the U.L.J. formulation including the large strain effect predicts almost the same response as the T.L. formulation. Figures 6 and 7 show the circumferential strain vs time at $\phi = 0$ and the peak circumferential strain measured during the complete response history as a function of the angle ϕ , respectively. It is observed that the peak strain is (locally) about 4%, which represents the limit of a small-strain assumption[26].

3.3 Analysis of a complete spherical shell

Axisymmetric static and dynamic analyses of the complete spherical shell shown in Fig. 8 with initial imperfections were performed. The finite element model used is also given in the figure. As shown, the complete spherical shell was idealized using twenty 8-node axisymmetric elements, with one element layer through the shell thickness. An initial geometric imperfection in the form of a function $w_i(\phi)$ was assumed. This imperfection was proportional to the static elastic buckling mode[23, 24],

$$w_i(\phi) = \delta h P_{18}(\cos \phi) \quad (38)$$

where ϕ is the angle measured from the pole of the

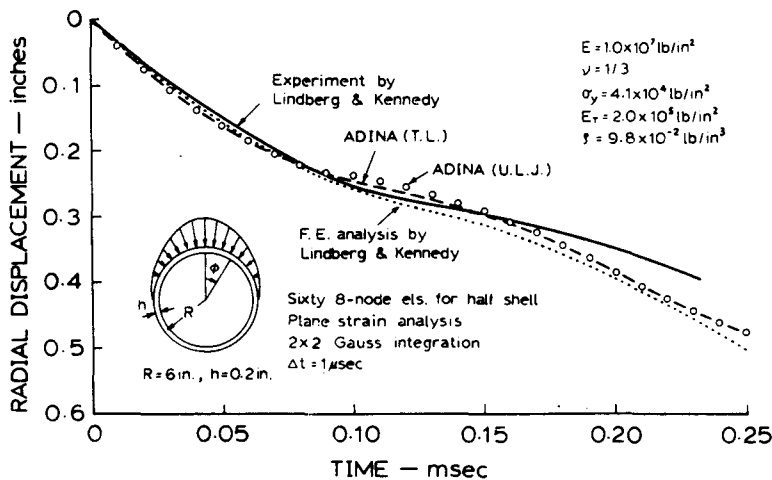


Fig. 5. Radial displacement of a cylindrical shell at $\phi = 15^\circ$.

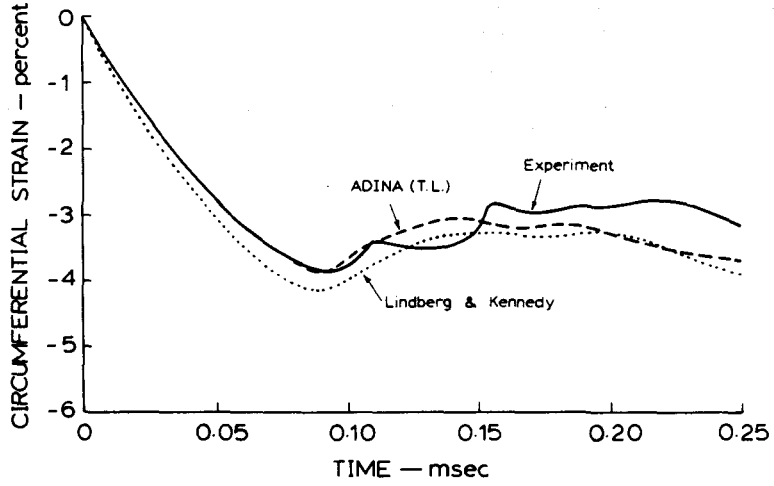


Fig. 6. Circumferential strain of the cylindrical shell at $\phi = 0^\circ$.

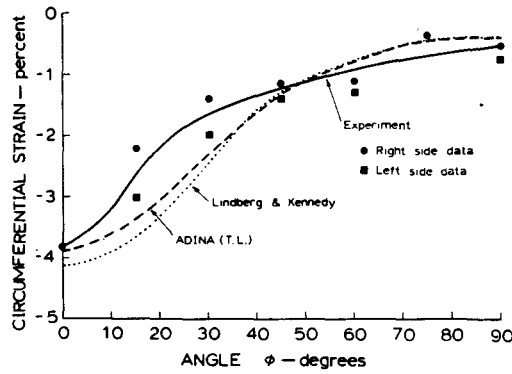
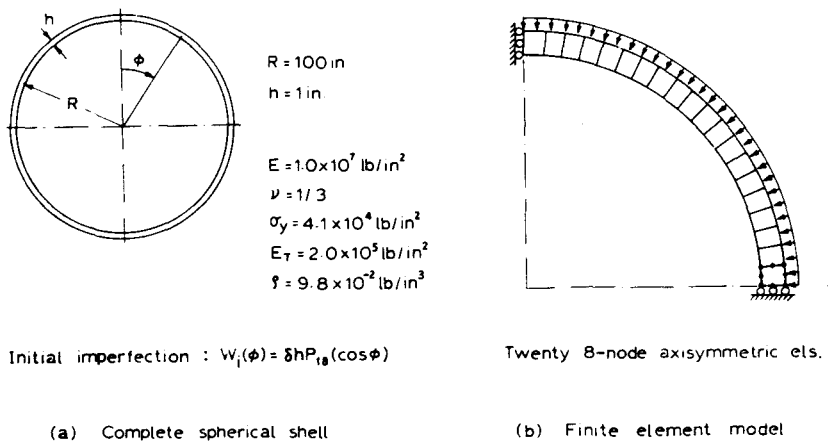


Fig. 7. Peak strain distribution in the cylindrical shell.



Initial imperfection : $W_1(\phi) = \delta h P_{18}(\cos \phi)$

Twenty 8-node axisymmetric els.

(a) Complete spherical shell

(b) Finite element model

Fig. 8. Spherical shell and finite element model considered, p deformation dependent.

complete spherical shell, δ is the amplitude of the imperfection, h is the shell thickness and $P_{18}(\cos \phi)$ is the Legendre polynomial of order 18. These initial imperfections were specified in the analysis by changing the nodal-point coordinates of the finite element model. The time increment, $\Delta\tau$, for dynamic analysis was 0.05 where

τ is the following nondimensionalized time

$$\tau = \sqrt{\left(\frac{E}{\rho R^2}\right)} t. \tag{39}$$

The static response of a perfect shell ($\delta = 0$) cor-

responding to elastic small displacement assumptions (E), elastic-plastic small displacement assumptions (E-P), elastic large displacement assumptions using the T.L. formulation (E, T.L.) and elastic-plastic large displacement assumptions using the T.L. formulation (E-P, T.L.) are compared in Fig. 9. The pressure is nondimensionalized with respect to the classical elastic static buckling pressure p_{cr} ,

$$p_{cr} = \frac{2E}{[3(1-\nu^2)]^{1/2}} \left(\frac{h}{R}\right)^2 \quad (40)$$

As expected the elastic small displacement analysis (E) does not predict buckling of the shell. The analysis assuming elastic-plastic small displacements (E-P) does also not predict buckling, but at the load level equal to $0.67 p_{cr}$ (which is close to the analytical yield pressure 0.673) the displacements suddenly increase at the larger rate because the complete shell is plastic. The (E, T.L.) and (E-P, T.L.) formulations predicted buckling of the shell as shown in Fig. 9 because, although a perfect shell was to be analyzed (case $\delta = 0$), considering the finite element model the coordinates of the nodal-points were only specified to 4 digit accuracy which is equivalent to a very small geometry imperfection in the analysis. As shown in Fig. 9 the predicted elastic buckling load is very close to the classical value given by eqn (40).

Figure 10 shows the static response of the shell with an imperfection of δ equal to 0.1. In this case, the (E, T.L.) analysis results show that the elastic buckling

load is $0.599 p_{cr}$. When plastic deformations are included, the (E-P, T.L.) analysis predicts that the shell buckles at the pressure $0.503 p_{cr}$. The distribution of the inward radial displacement obtained by the (E-P, T.L.) static analysis is shown in Fig. 11. It should be noted that the displacement distribution has the same form as the specified initial imperfection expressed by the Legendre polynomial of order 18, and that the displacement at $\phi = 0$, where the geometric imperfection was maximum, becomes very large.

The dynamic response of the perfect shell ($\delta = 0$) and the imperfect shell ($\delta = 0.1$) is shown in Fig. 12 and 13.

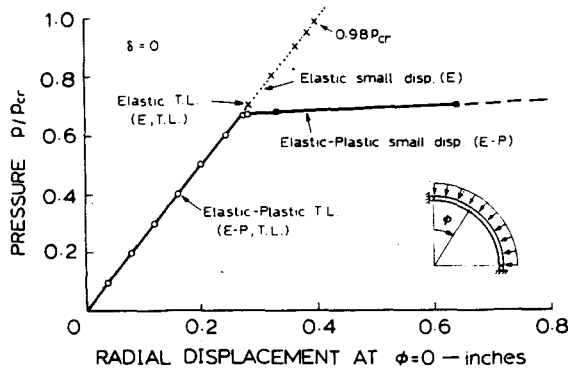


Fig. 9. Static response of a perfect ($\delta = 0$) complete spherical shell under uniform external pressure.

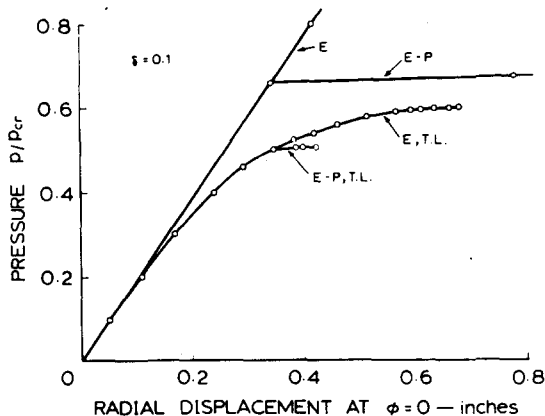


Fig. 10. Static response of an imperfect ($\delta = 0.1$) complete spherical shell under uniform external pressure.

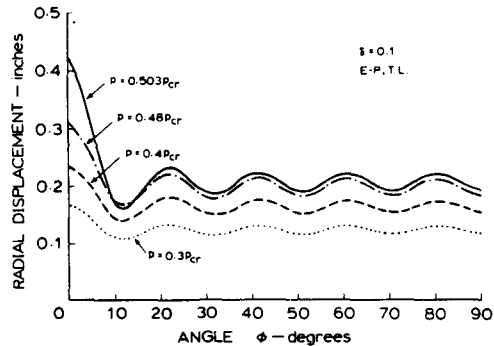


Fig. 11. Distribution of radial displacement of the imperfect ($\delta = 0.1$) complete spherical shell.

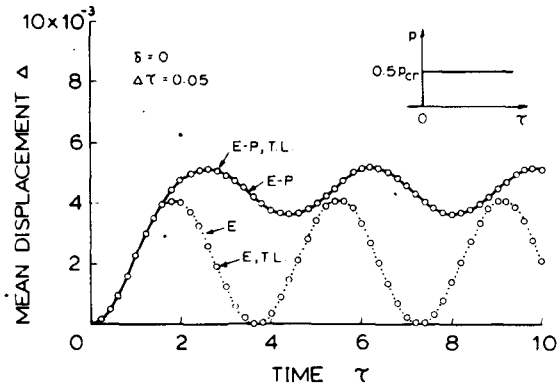


Fig. 12. Dynamic response of the perfect ($\delta = 0$) complete spherical shell under step external pressure.

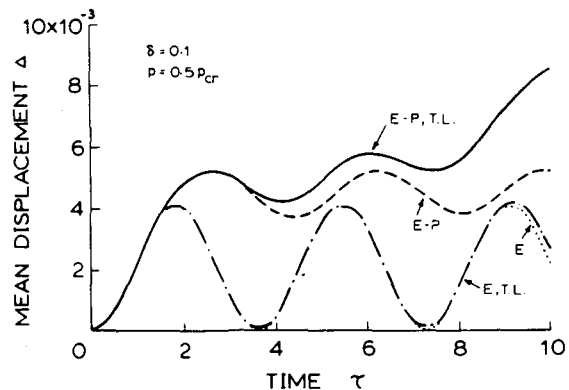


Fig. 13. Dynamic response of the imperfect ($\delta = 0.1$) complete spherical shell under step external pressure.

Both shells were subjected to a step pressure of $0.5 p_{cr}$ of infinite duration. The predicted response is given in terms of the mean displacement Δ vs the nondimensionalized time τ , where

$$\Delta = \frac{\text{volume generated by the shell deformation}}{\text{shell volume}} \quad (41)$$

This mean displacement measure was employed in earlier investigations on the static and dynamic behavior of axisymmetric shells and was, in particular, employed to measure the buckling of an elastic cap[5].

Considering the analysis of the perfect shell, the predicted dynamic response assuming small displacements and large displacements (T.L. formulation) were the same to the accuracy that can be shown. The elastic analyses, (E) and (E, T.L.), show that the shell vibrates steadily and Δ becomes 0 after each cycle. The plastic analysis results, (E-P) and (E-P, T.L.), show the typical characteristics of elastic-plastic behavior; namely, the period and amplitude of vibration are larger and smaller, respectively, than in elastic conditions, and there is a permanent displacement set when considering plastic conditions.

In Fig. 13 the analysis results of the imperfect shell are presented. It is found that the imperfect shell is unstable, as predicted by the (E, T.L.) and (E-P, T.L.) analyses because the peak displacement is increased cycle by cycle.

The distributions of radial displacement obtained by the (E-P, T.L.) analysis are shown in Fig. 14. As in the static response shown in Fig. 11, the displacement at $\phi = 0$ becomes very large with increasing time.

A comparison of solution results using the T.L. formulation and the U.L.J. formulation is shown in Fig. 15. Also shown is the sensitivity of the analysis results to the number of finite elements and the time step used. The pressure was selected to be $0.4 p_{cr}$, because, as shown in the next section, the shell is just unstable under this pressure. Therefore, the predicted response should be sensitive to the finite element modeling used. As shown in Fig. 15, the U.L.J. formulation predicts somewhat smaller displacements than the T.L. formulation, but in both cases the unstable response of the shell is predicted.

In the dynamic buckling analyses to be discussed in the next section, the T.L. formulation was employed in the large displacement calculations. For large displace-

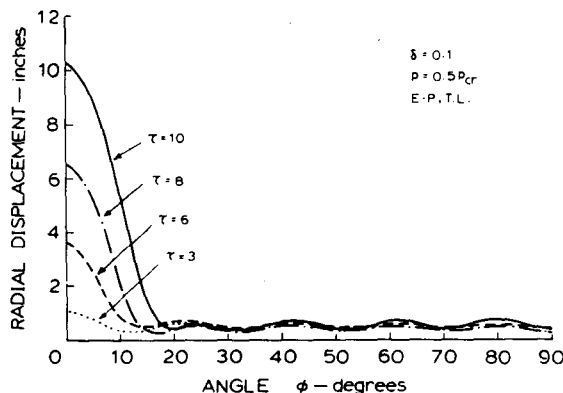


Fig. 14. Distribution of radial displacement of the imperfect ($\delta = 0.1$) complete spherical shell under step external pressure.

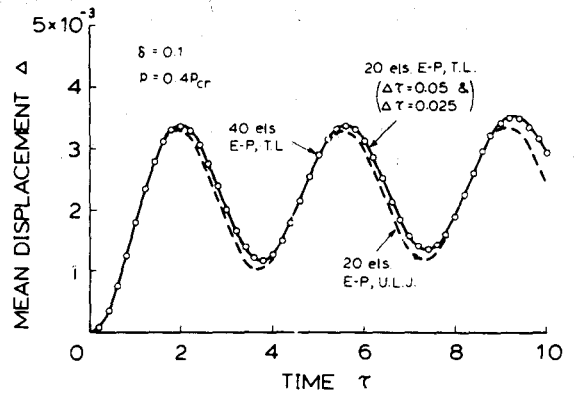


Fig. 15. Elastic-plastic dynamic response of the imperfect ($\delta = 0.1$) complete spherical shell under step external pressure.

ment but small strain elastic-plastic analysis this formulation is effective, because considering the kinematics only, the increment in displacements can be large (provided the equilibrium iteration converges), whereas using the U.L.J. formulation of eqns (6)–(9), the time (or displacement) increment must be relatively small.

Figure 15 also shows that the model of forty elements predicts the same response as the model of twenty elements. Therefore, it can be concluded that the model of twenty elements is appropriate for the analysis of this problem. The results also show that the time step $\Delta\tau = 0.05$ is sufficiently small.

4. ELASTIC-PLASTIC ANALYSIS OF THE AXISYMMETRIC BUCKLING BEHAVIOR OF THE COMPLETE SPHERICAL SHELL

The analyses described in the previous sections were performed in order to verify the numerical procedures and models used for the nonlinear elastic-plastic analysis of shell structures, and to obtain familiarity with the analysis difficulties of the complete spherical shell. The objective in this section is to report on some detailed buckling behavior characteristics that were predicted for the complete spherical shell considered in Section 3.3. In the analyses the 20 finite element model with the (E-P, T.L.) formulation was used. The loading on the shell was as before the uniform external pressure, and in the dynamic analyses the pressure was applied as a step function of infinite duration.

The elastic-plastic static axisymmetric buckling behavior of the complete spherical shell is shown in Fig. 16. This analysis includes only axisymmetric deformations, hence the buckling load is equal to the limit load. As shown in Fig. 16, the limit load is reduced significantly by the existence of the initial imperfections and the deformations at the limit load are larger for greater initial imperfections. In all these analyses the limit loads were detected by the sign change of the determinant of the tangent stiffness matrix from positive to negative.

The static limit load can be determined by a single incremental step-by-step solution. On the other hand, to calculate the dynamic elastic-plastic buckling load of a shell the transient response for various load levels must be calculated. Figures 17–20 give the dynamic response of the complete spherical shell with various amplitudes of imperfections under the step pressure. Figure 21 summarizes the results shown in Figs. 17–20 and shows

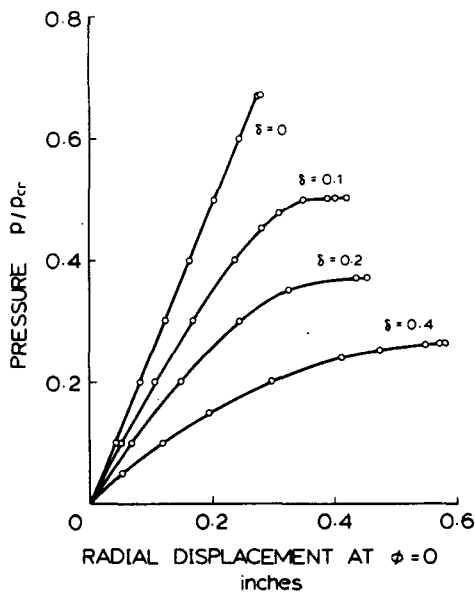


Fig. 16. Elastic-plastic static buckling behavior of the complete spherical shell with various levels of initial imperfection.

the imperfection sensitivity of the shell when subjected to dynamic loading. The static buckling loads are also shown in order to be able to compare the imperfection sensitivities in static and dynamic buckling. As shown in this figure, the dynamic buckling load is significantly smaller than the static buckling load for $0 < \delta < 0.2$, but the difference in the buckling loads becomes small when δ is greater than 0.2. These results are similar to the analysis results reported by Kao and Perrone, who considered the static and dynamic elastic buckling of shallow caps[5].

6. CONCLUSIONS

The nonlinear static and dynamic analysis of a shell structure is in general still difficult to perform, and considering a general shell a nonlinear dynamic buckling analysis is frequently beyond the current state-of-the-art. In this paper some finite element procedures for nonlinear static and dynamic analysis have been briefly summarized. These analysis techniques are available in

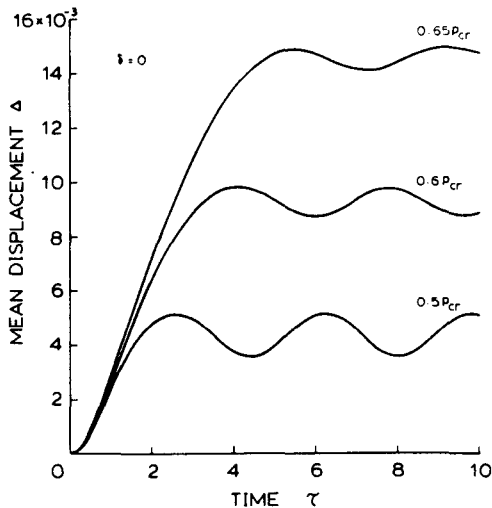


Fig. 17. Elastic-plastic dynamic response of the perfect ($\delta = 0$) complete spherical shell.

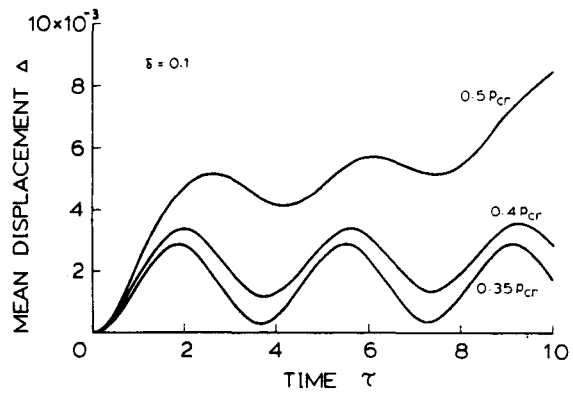


Fig. 18. Elastic-plastic dynamic response of the imperfect ($\delta = 0.1$) complete spherical shell.

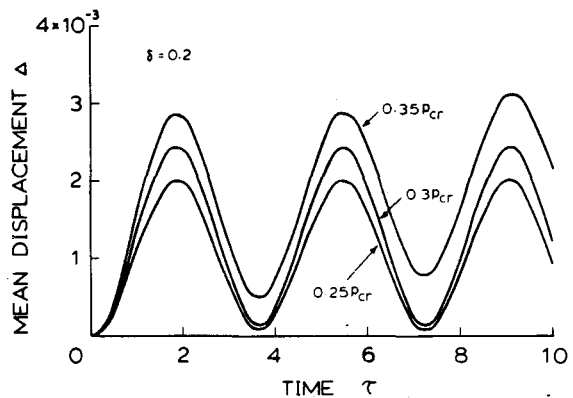


Fig. 19. Elastic-plastic dynamic response of the imperfect ($\delta = 0.2$) complete spherical shell.

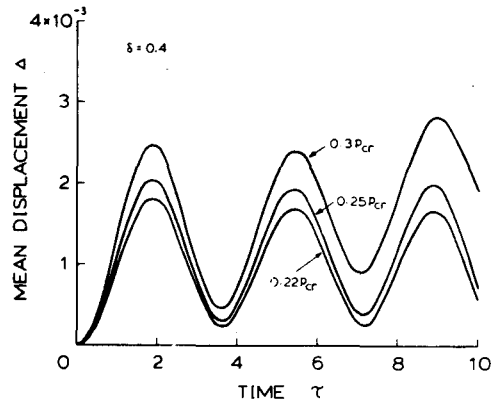


Fig. 20. Elastic-plastic dynamic response of the imperfect ($\delta = 0.4$) complete spherical shell.

the computer program ADINA, but much difficulty can lie in their appropriate use for a complex nonlinear dynamic solution; namely, it is most important to select an appropriate finite element model for a specific analysis. The discussions and results presented in this paper suggest some finite element modeling procedures and show that the techniques can be employed effectively for elastic-plastic and large displacement studies of two-dimensional shell structures. The computer times required to analyze the two-dimensional shells considered in the paper were in all cases relatively small.

Finally, it shall be noted that although further research

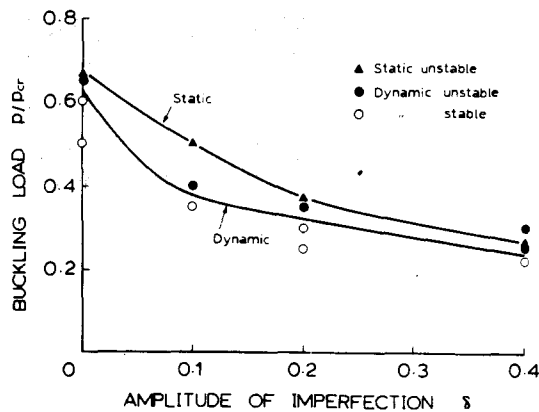


Fig. 21. Effect of initial imperfections on the elastic-plastic buckling load of the complete spherical shell.

is still desirable to increase the effectiveness of finite element two-dimensional shell analysis procedures, much additional research and development efforts are still needed before we can analyze general three-dimensional shell structures [33–35] with about the same confidence and at a reasonable cost.

Acknowledgements—We would like to thank Prof. N. Jones, Department of Ocean Engineering, M.I.T., for valuable discussions on the buckling of shells. We are grateful to the ADINA users group for the financial support of our computational work.

REFERENCES

- J. H. Argyris and P. C. Dunne, Nonlinear and post-buckling analysis of structures. In *Formulations and Computational Algorithms in Finite Element Analysis* (Edited by K. J. Bathe, J. T. Oden and W. Wunderlich). M.I.T. Press, Cambridge, Massachusetts (1977).
- B. Budiansky and R. S. Roth, Axisymmetric dynamic buckling of clamped shallow spherical shells. *TN D-1510, NASA*, 1962, pp. 597–606.
- R. R. Archer and C. G. Lange, Nonlinear dynamic behavior of shallow spherical shells. *AIAA J.* **3**(12), 2313–2317 (1965).
- W. B. Stephens, Computer program for static and dynamic analysis of symmetrically loaded orthotropic shells of revolution. *TN D-6158, NASA* (1970).
- R. Kao and N. Perrone, Dynamic buckling of axisymmetric spherical caps with initial imperfections. *Comp. Structures* **9**, 463–473 (1978).
- K. J. Bathe, E. Ramm and E. L. Wilson, Finite element formulations for large deformation dynamic analysis. *Int. J. Num. Meth. Engng* **9**, 353–386 (1975).
- K. J. Bathe, Static and dynamic geometric and material nonlinear analysis using ADINA. *Rep. 82448-2, Acoustics and Vibration Laboratory, M.I.T.*, May 1976. (rev. May 1977).
- S. Klein, The nonlinear dynamic analysis of shells of revolution with asymmetric properties by the finite element method. *J. Pressure Vessel Tech.* **97**(3), 163–171 (1975).
- S. Nagarajan and E. P. Popov, Nonlinear dynamic analysis of axisymmetric shells. *Int. J. Num. Meth. Engng* **9**, 535–550 (1975).
- M. Harzmann, Comparison of calculated static and dynamic collapse pressure of clamped spherical domes. *AIAA J.* **12**(4), 568–570 (1974).
- J. N. Goodier and I. K. McIvor, The elastic cylindrical shell under nearly uniform radial impulse. *J. Appl. Mech.* **31**(2), 259–266 (1964).
- J. W. Leech, E. A. Witmer and T. H. H. Pian, Numerical calculation technique for large elastic-plastic transient deformation of thin shells. *AIAA J.* **6**(12), 2352–2359 (1968).
- P. Underwood, Transient response of inelastic shells of revolution. *Comp. Structures* **2**, 975–989 (1972).
- C. M. Ni and L. H. N. Lee, Dynamic behavior of inelastic cylindrical shells at finite deformation. *Int. J. Non-Linear Mech.* **9**, 193–207 (1974).
- D. L. Wesenberg, Elastic-plastic buckling of aluminum cylindrical shells subjected to axisymmetric impulse loads. *J. Appl. Mech.* **41**(4), 985–988 (1974).
- R. W.-H. Wu and E. A. Witmer, The dynamic responses of cylindrical shells including geometric and material nonlinearities. *Int. J. Solids Structures* **10**, 243–260 (1974).
- H. E. Lindberg and T. C. Kennedy, Dynamic plastic pulse buckling beyond strain-rate reversal. *J. Appl. Mech.* **42**(2), 411–416 (1975).
- E. A. Witmer, H. A. Balmer, J. W. Leech and T. H. H. Pian, Large dynamic deformations of beams, rings, plates and shells. *AIAA J.* **1**(8), 1848–1857 (1963).
- I. K. McIvor and D. A. Sonstegard, Axisymmetric response of a closed spherical shell to a nearly uniform radial impulse. *J. Acoustical Soc. Am.* **40**(6), 1540–1547 (1966).
- N. Jones and C. S. Ahn, Dynamic buckling of complete rigid-plastic spherical shells. *J. Appl. Mech.* **41**(3), 609–614 (1974).
- N. Jones and C. S. Ahn, Dynamic elastic and plastic buckling of complete spherical shells. *Int. J. Solids Structures* **10**, 1357–1374 (1974).
- D. L. Anderson and H. E. Lindberg, Dynamic pulse buckling of cylindrical shells under transient lateral pressures. *AIAA J.* **6**(4), 589–598 (1968).
- J. W. Hutchinson, On the postbuckling behavior of imperfection-sensitive structures in the plastic range. *J. Appl. Mech.* **39**(1), 155–162 (1972).
- P. Tong and T. H. H. Pian, Postbuckling analysis of shells of revolution by the finite element method. In *Thin Shell Structures, Theory, Experiment and Design* (Edited by Y. C. Fung and E. E. Sechler), pp. 435–452. Prentice-Hall, Englewood Cliffs, New Jersey (1974).
- S. Gellin, Effect of an axisymmetric imperfection on the plastic buckling of an axially compressed cylindrical shell. *J. Appl. Mech.* **46**(1), 125–131 (1979).
- K. J. Bathe, M. D. Snyder and A. P. Cimento, On finite element analysis of elastic-plastic response. *Proc. Conf. Engng Application of the Finite Element Method*, Computas, Høvik, Norway, May 1979.
- S. Key, J. H. Biffe and R. D. Krieg, A study of the computational and theoretical differences of two finite strain elastic-plastic constitutive models. In *Formulations and Computational Algorithms in Finite Element Analysis* (Edited by K. J. Bathe, J. T. Oden and W. Wunderlich). M.I.T. Press Cambridge, Mass. (1977).
- K. J. Bathe and E. I. Wilson, *Numerical Methods in Finite Element Analysis*. Prentice-Hall, Englewood Cliffs, New Jersey (1976).
- K. J. Bathe, Finite element formulation, modeling and solution of nonlinear dynamic response. Chapter in *Numerical Methods for Partial Differential Equations* (Edited by S. V. Parter). Academic Press, New York (1979).
- K. J. Bathe and A. P. Cimento, Some practical procedures for the solution of nonlinear finite element equations. *J. Comput. Meth. Appl. Mech. Engng* in press.
- H. Matthies and G. Strang, The solution of nonlinear finite element equations. *Int. J. Num. Meth. Engng* **14**, 1613–1626 (1979).
- K. J. Bathe, ADINA—a finite element program for automatic dynamic incremental nonlinear analysis. *Rep. 82448-1, Acoustics and Vibration Laboratory, Dept. Mechanical Engineering, M.I.T.*, Sept. 1975. (rev. Dec. 1978).
- B. Brendel and E. Ramm, Linear and nonlinear stability analysis of cylindrical shells. *Proc. Conf. Engng Application of the Finite Element Method*, Computas, Høvik, Norway, May 1979.
- Argyris *et al.*, Finite element method—the natural approach. *J. Comput. Meth. Appl. Mech. Engng* **17**(18), 1–106 (1979).
- K. J. Bathe and S. Bolourchi, A geometric and material nonlinear shell element. *J. Comput. Structures* **11**(1/2), 23–48 (1980).

ON SOME CURRENT PROCEDURES AND DIFFICULTIES IN FINITE ELEMENT ANALYSIS OF ELASTIC-PLASTIC RESPONSE

KLAUS-JÜRGEN BATHE, MARK D. SNYDER, ARTHUR P. CIMENTO and W. DONALD ROLPH, III
 Massachusetts Institute of Technology, Department of Mechanical Engineering, Cambridge, MA 02139,
 U.S.A.

(Received 12 December 1979; received for publication 29 January 1980)

Abstract—Some finite element procedures for the analysis of elastic-plastic response are presented and critically discussed: a consistent large displacement and large strain formulation is summarized, a versatile elastic-plastic model applicable to the analysis of metals and geological materials is presented, the choice of an appropriate finite element discretization is discussed, and some effective methods for the solution of the nonlinear finite element equations are briefly summarized. Finally, to illustrate the strength and shortcomings of the procedures used, the results of some sample analyses are presented and evaluated.

1. INTRODUCTION

The current activities in finite element analysis show that there is a continuing need and strong incentive to develop improved finite element computational models and numerical procedures. These improvements are needed for representing and analyzing more effectively structures that are already being analyzed, as well as to develop techniques for modeling new phenomena that could not be considered computationally before.

In the development of improved capabilities for structural analysis, we need to recognize that increasingly physically representative, stable, accurate and cost-effective finite element schemes are needed. An area where these thoughts are particularly germane is the analysis of general elastic-plastic response: here are needed increasingly better material representations, consistent finite element formulations, accurate and stable integration schemes, and appropriate finite element mesh representations of the actual physical problems to be analyzed[1, 2]. Considering research in methods for elastic-plastic analysis, it must furthermore be recognized that progress is best achieved by simultaneously advancing the techniques in each of these fields.

The objective in this paper is to summarize some of the procedures that are employed at present for the analysis of elastic-plastic response of structures and continua, to identify some of the strengths and shortcomings of these procedures, and to provide some directions for future research efforts. In the paper the analysis of static and dynamic large deformation elastic-plastic response is considered. Based on the fact that the complete solution of a problem requires the use of an effective continuum mechanics formulation, finite element discretization, constitutive description, and incremental solution strategy, various current state-of-the-art practices in each of these areas are summarized and assessed, and sample solutions are presented to demonstrate in a critical manner some of the important features of the techniques employed.

2. INCREMENTAL KINEMATIC FORMULATION

Although continuum mechanics formulations for general elastic-plastic analysis have been presented a number of times, there is still confusion as to what represents a consistent and effective large strain formulation. An excellent survey of various possible kinematic

descriptions has been given by Key *et al.*[3], and of the formulations considered, the updated Lagrangian description is probably the most natural one to use.

2.1 Updated Lagrangian formulation

Assume that the static and kinematic variables have been calculated for time t and that the solution is next required for time $t + \Delta t$, where Δt is, as usual, a small time increment. In static analysis, the time increment Δt simply indicates a load increment, whereas in dynamic analysis, the time step must be chosen judiciously for an accurate response prediction[4-8]. For the updated Lagrangian formulation, which was previously described in [9], the governing virtual work principle is:

$$\int_{tV} {}^{t+\Delta t}S_{ij} \delta {}^{t+\Delta t}\epsilon_{ij} dv = {}^{t+\Delta t}\mathcal{R} \quad (1)$$

where V is the volume of the body at time t , ${}^{t+\Delta t}S_{ij}$ is the 2nd Piola-Kirchhoff stress tensor at time $t + \Delta t$ referred to the configuration at time t , ${}^{t+\Delta t}\epsilon_{ij}$ is the Green-Lagrange strain tensor at time $t + \Delta t$, referred to the configuration at time t , and ${}^{t+\Delta t}\mathcal{R}$ is the external virtual work at time $t + \Delta t$. The stress tensor can be decomposed into the sum of a Cauchy stress tensor at time t , ${}^t\tau_{ij}$, and a 2nd Piola-Kirchhoff stress increment tensor, ${}_tS_{ij}$,

$${}^{t+\Delta t}S_{ij} = {}^t\tau_{ij} + {}_tS_{ij} \quad (2)$$

The strain tensor can be separated into a linear strain increment, ${}_t\epsilon_{ij}$, and a non-linear strain increment, ${}_t\eta_{ij}$, (both referred to the configuration at time t) where

$${}^{t+\Delta t}\epsilon_{ij} \equiv {}_t\epsilon_{ij}; \quad {}_t\epsilon_{ij} = {}_t\epsilon_{ij} + {}_t\eta_{ij} \quad (3)$$

Introducing the incremental material property tensor referred to the configuration at time t , ${}_tC_{ijrs}$, and using the approximations ${}_tS_{ij} = {}_tC_{ijrs} {}_t\epsilon_{rs}$ and $\delta {}_t\epsilon_{ij} = \delta {}_t\epsilon_{ij}$, the virtual work theorem can be rewritten, using eqns (2) and (3), as

$$\int_{tV} {}_tC_{ijrs} {}_t\epsilon_{rs} \delta {}_t\epsilon_{ij} dv + \int_{tV} {}^t\tau_{ij} \delta {}_t\eta_{ij} dv = {}^{t+\Delta t}\mathcal{R} - \int_{tV} {}^t\tau_{ij} \delta {}_t\epsilon_{ij} dv \quad (4)$$

which is the linearized equilibrium equation used in the updated Lagrangian formulation. The finite element implementation of eqn (4) for a single element can be written in matrix form as

$$({}^i\mathbf{K}_L + {}^i\mathbf{K}_{NL})\mathbf{U} = {}^{t+\Delta t}\mathbf{R} - {}^t\mathbf{F} - \mathbf{M}{}^{t+\Delta t}\ddot{\mathbf{U}} \quad (5)$$

where ${}^i\mathbf{K}_L$ and ${}^i\mathbf{K}_{NL}$ are the linear and nonlinear strain incremental stiffness matrices, \mathbf{U} is the vector of incremental nodal displacements, ${}^{t+\Delta t}\mathbf{R}$ is the external nodal point force vector, ${}^t\mathbf{F}$ is the vector of nodal point forces equivalent to the element stresses at time t and \mathbf{M} is the mass matrix. Considering eqns (4) and (5), the integrals of eqn (4) are approximated in eqn (5) as follows:

$${}^i\mathbf{K}_L\mathbf{U} = \left(\int_{IV} {}^iC_{ijrs} \delta_t e_{ij} dv : \int_{IV} {}^i\mathbf{B}_L^T C {}^i\mathbf{B}_L dv \right) \mathbf{U} \quad (6)$$

$${}^i\mathbf{K}_{NL}\mathbf{U} = \left(\int_{IV} {}^i\tau_{ij} \delta_t \eta_{ij} dv : \int_{IV} {}^i\mathbf{B}_{NL}^T {}^i\tau {}^i\mathbf{B}_{NL} dv \right) \mathbf{U} \quad (7)$$

$${}^t\mathbf{F} = \int_{IV} {}^i\mathbf{B}_L^T {}^t\hat{\tau} dv \quad (8)$$

where ${}^i\mathbf{B}_L$ and ${}^i\mathbf{B}_{NL}$ are the linear and non-linear strain-displacement transformation matrices, ${}^t\tau$ and ${}^t\hat{\tau}$ are a matrix and vector of Cauchy stresses, and iC is the incremental stress-strain material property matrix, all referred to the configuration at time t .

The equilibrium equations in eqn (5) are those corresponding to a single element, from which the equilibrium equations of an assemblage of elements are obtained using standard procedures [4].

Equation (5) is the incremental governing equilibrium equation in dynamic analysis using implicit time integration (e.g. the trapezoidal rule) or in static analysis, when the inertia terms are not included. In explicit time integration (e.g. using the central difference method), the right-hand-side of eqn (5) is evaluated at time t and set equal to zero, which means that the dynamic equilibrium is considered at time t .

Assuming that the constitutive matrix in eqn (6) is calculated as discussed in Section 3, the solution of eqn (5) yields an increment in displacements and hence an increment in strains. We must then proceed to calculate the stresses corresponding to time $t + \Delta t$.

Assume that the Cauchy stresses at time t are known and the displacement increments have been calculated from eqn (5). The large strain plasticity formulation accounts for rigid body rotations on the current stresses using

$${}^{\nabla}\tau_{ij} = {}^t\dot{\tau}_{ij} - {}^t\tau_{ip} {}^t\Omega_{pj} - {}^t\tau_{jp} {}^t\Omega_{pi} \quad (9)$$

where ${}^{\nabla}\tau_{ij}$ is the Jaumann stress rate tensor at time t and ${}^t\dot{\tau}_{ij}$ is the time derivative of the Cauchy stress tensor

evaluated at time t . The spin tensor ${}^t\Omega_{ij}$ is defined by

$${}^t\Omega_{ij} = \frac{1}{2} \left(\frac{\partial^t \dot{u}_j}{\partial^t x_i} - \frac{\partial^t \dot{u}_i}{\partial^t x_j} \right) \quad (10)$$

The material relationship used to evaluate the Jaumann stress rate tensor is

$${}^{\nabla}\tau_{ij} = {}^tC_{ijrs} {}^t\dot{e}_{rs} \quad (11)$$

where ${}^t\dot{e}_{rs}$ is the velocity strain. Integrating eqn (11) over the increment of time which is assumed to be small, and using eqns (9) and (10) we obtain as an approximation to the Cauchy stress at time $t + \Delta t$,

$${}^{t+\Delta t}\tau_{ij} = {}^t\tau_{ij} + \int_t^{t+\Delta t} {}^tC_{ijrs} d {}^t e_{rs} + {}^t\tau_{ip} {}^t\Omega_{pj} \Delta t + {}^t\tau_{jp} {}^t\Omega_{pi} \Delta t \quad (12)$$

The implementation of these plasticity relations is illustrated in Fig. 1. It remains to discuss the evaluation of the constitutive tensor ${}^tC_{ijrs}$ that is used in eqns (6) and (11).

3. FORMULATION OF ELASTIC-PLASTIC CONSTITUTIVE EQUATIONS

A number of elastic-plastic constitutive equations have been proposed for finite element calculations. We present here the governing equations of a plasticity model which reduces to the isotropic hardening, von Mises and Drucker-Prager models as special cases [10, 11], but which has the additional features of a tension cutoff limit and hydrostatic yielding.

The yield (failure) surfaces associated with the new model are shown in Fig. 2. If the tension cutoff limit and

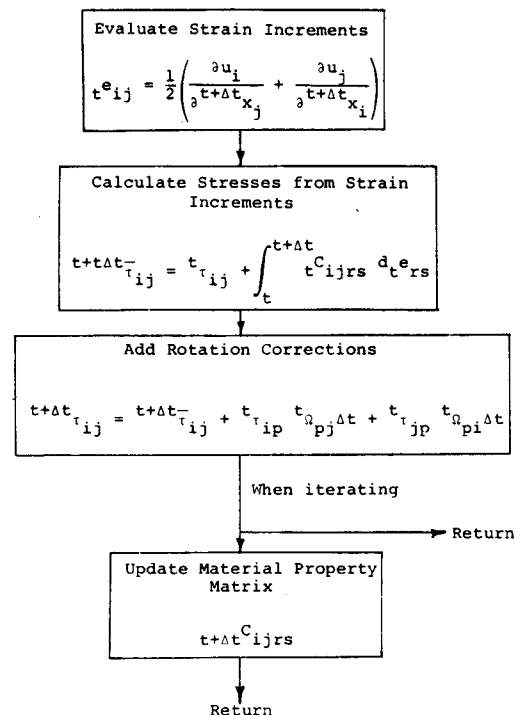


Fig. 1. Calculation of stresses in updated Lagrangian elastic-plastic analysis.

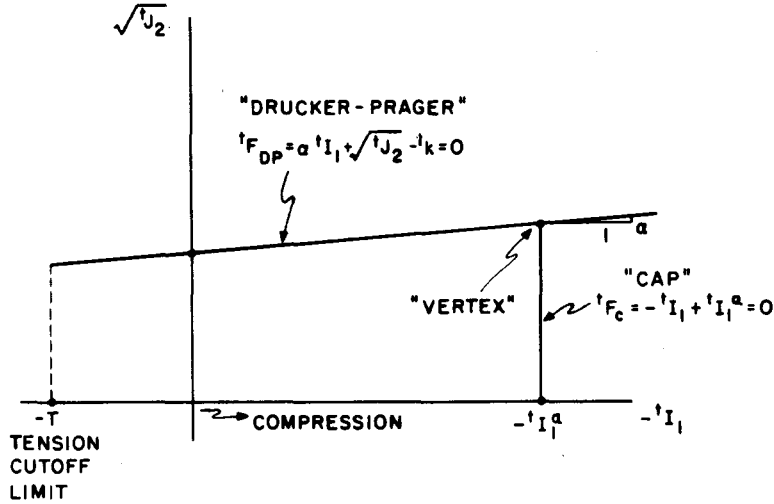


Fig. 2. Yield surface of plasticity model.

the cap are initially positioned outside the range of behavior for a particular problem, we obtain the Drucker-Prager model or the von Mises model ($\alpha = 0$).

The model presented herein is applicable to metals as well as geological materials. In the latter situation, it has the advantages (over the Drucker-Prager model) of yielding under hydrostatic loading, limited tensile strength, and limited dilatancy.

Theoretical development

As discussed in Section 2, it is necessary to obtain an expression for the constitutive tensor ${}^t C_{ijrs}$. In this section we develop the plasticity model within the context of material nonlinearity only analysis. That is, strains and displacements are assumed to be infinitesimal. However, the formulation is directly applicable to the general case of large deformation, elastic-plastic analysis when ${}^t \sigma_{ij}$ is replaced by ${}^t \tau_{ij}$ and $d e_{ij}$ is replaced by a logarithmic (or true) strain increment. Therefore, in large strain analysis the Young's modulus and strain hardening modulus must be obtained from the uniaxial Cauchy stress-logarithmic (or true) strain curve.

The first basic assumption in the development of the model is that the strain increment can be decomposed into elastic and plastic parts

$$d e_{ij} = d e_{ij}^E + d e_{ij}^P. \quad (13)$$

The elastic stress-strain law is

$$d \sigma_{ij} = C_{ijrs}^E d e_{rs}^E = C_{ijrs}^E (d e_{rs} - d e_{rs}^P). \quad (14)$$

For the case of an isotropic, elastic material with constant properties,

$$C_{ijrs}^E = \lambda (\delta_{ij} \delta_{rs}) + \mu (\delta_{ir} \delta_{js} + \delta_{is} \delta_{jr}) \quad (15)$$

where λ and μ are the Lamé constants

$$\lambda = \frac{E\nu}{(1+\nu)(1-2\nu)} \quad (16)$$

$$\mu = \frac{E}{2(1+\nu)} \quad (17)$$

where E is the Young's modulus and ν is Poisson's ratio.

The plastic stress-strain law is

$$d e_{ij}^P = \bar{\lambda} \frac{\partial F}{\partial \sigma_{ij}} \quad (18)$$

where F is the yield function.

$$F = F(\sigma_{ij}, e_{ij}^P, \bar{e}^P) \quad (19)$$

\bar{e}^P = accumulated increments of effective plastic strain

$$= \int_0^t d \bar{e}^P \quad (20)$$

and

$\bar{\lambda}$ = positive scalar variable

In the developments which follow, the Drucker-Prager yield function depends on σ_{ij} and \bar{e}^P while the cap yield function depends on σ_{ij} and e_{ij}^P .

To obtain a suitable expression for $d \bar{e}^P$, consider the Drucker-Prager yield function with isotropic hardening [10]

$$F_{DP} = \alpha I_1 + \sqrt{J_2} - k \quad (21)$$

where

$$I_1 = \sigma_{ii} \quad (22)$$

$$J_2 = \frac{1}{2} s_{ij} s_{ij} \quad (23)$$

$$s_{ij} = \sigma_{ij} - \frac{\sigma_{mm}}{3} \delta_{ij} \quad (24)$$

$$k = k(\bar{e}^P). \quad (25)$$

For yielding under a uniaxial state of stress σ_y ($\sigma_y > 0$), $F_{DP} = 0$ and hence

$$k = \left[\alpha + \frac{1}{\sqrt{3}} \right] \sigma_y. \quad (26)$$

Substituting eqn (26) into eqn (21), we can define the effective stress $'\bar{\sigma}$ associated with the Drucker-Prager yield function,

$$' \bar{\sigma} = \frac{\alpha' I_1 + \sqrt{J_2}}{\alpha + \frac{1}{\sqrt{3}}} \quad (27)$$

Hence, yielding occurs when $'\bar{\sigma} = ' \sigma_y$. Note that $'\sigma_y = ' \sigma_y(' \bar{\epsilon}^P)$ and that $\alpha = 0$ gives the von Mises yield function and effective stress [11].

Having obtained an appropriate expression for the effective stress, it is now required that

$$dW^P = ' \sigma_{ij} de_{ij}^P = ' \bar{\sigma} d\bar{\epsilon}^P \quad (28)$$

Using eqns (21)–(24), it can be shown that

$$\frac{\partial' F_{DP}}{\partial' \sigma_{ij}} = \alpha \delta_{ij} + \frac{' s_{ij}}{2\sqrt{J_2}} \quad (29)$$

Substituting eqns (18), (27) and (29) into eqn (28) and noting that

$$' \sigma_{ij} ' s_{ij} = \left(' s_{ij} + \frac{' \sigma_{mm}}{3} \delta_{ij} \right) ' s_{ij} = 2' J_2 \quad (30)$$

we obtain

$$' \bar{\sigma} d\bar{\epsilon}^P = ' \bar{\lambda} [\alpha' I_1 + \sqrt{J_2}] = ' \bar{\lambda} \left[\alpha + \frac{1}{\sqrt{3}} \right] ' \bar{\sigma} \quad (31)$$

Now consider

$$\begin{aligned} de_{ij}^P de_{ij}^P &= ' \bar{\lambda}^2 \frac{\partial' F}{\partial' \sigma_{ij}} \frac{\partial' F}{\partial' \sigma_{ij}} \\ &= ' \bar{\lambda}^2 \left[3\alpha^2 + \frac{1}{2} \right] \end{aligned} \quad (32)$$

and substitute into eqn (31) to obtain

$$d\bar{\epsilon}^P = \sqrt{(de_{ij}^P de_{ij}^P)} \frac{\alpha + \frac{1}{\sqrt{3}}}{\sqrt{3\alpha^2 + \frac{1}{2}}} \quad (33)$$

Note that $\alpha = 0$ gives the von Mises effective plastic strain increment.

During plastic flow, the stress state remains on the yield surface so that

$$\frac{\partial' F}{\partial' \sigma_{ij}} d\sigma_{ij} + \frac{\partial' F}{\partial' \bar{\epsilon}^P} d\bar{\epsilon}^P + \frac{\partial' F}{\partial' e_{ij}^P} de_{ij}^P = 0 \quad (34)$$

Substituting eqns (18) and (33) into eqn (34),

$$\begin{aligned} \frac{\partial' F}{\partial' \sigma_{ij}} d\sigma_{ij} &= - \frac{\partial' F}{\partial' \bar{\epsilon}^P} ' \bar{\lambda} \sqrt{\left(\frac{\partial' F}{\partial' \sigma_{ij}} \frac{\partial' F}{\partial' \sigma_{ij}} \right)} \frac{\alpha + \frac{1}{\sqrt{3}}}{\sqrt{3\alpha^2 + \frac{1}{2}}} \\ &\quad - ' \bar{\lambda} \frac{\partial' F}{\partial' e_{ij}^P} \frac{\partial' F}{\partial' \sigma_{ij}} \end{aligned} \quad (35)$$

Substituting eqn (18) into eqn (14) and multiplying by

$\partial' F / \partial' \sigma_{ij}$, we obtain

$$\frac{\partial' F}{\partial' \sigma_{ij}} d\sigma_{ij} = \frac{\partial' F}{\partial' \sigma_{ij}} C_{ijrs}^E \left(de_{rs} - ' \bar{\lambda} \frac{\partial' F}{\partial' \sigma_{ij}} \right) \quad (36)$$

Setting eqns (35) and (36) equal to one another and solving for $' \bar{\lambda}$ results in

$$\begin{aligned} ' \bar{\lambda} &= \left[\frac{\partial' F}{\partial' \sigma_{ij}} C_{ijrs}^E de_{rs} \right] \left[\frac{\partial' F}{\partial' \sigma_{ij}} C_{ijrs}^E \frac{\partial' F}{\partial' \sigma_{rs}} - \frac{\partial' F}{\partial' \sigma_{ij}} \frac{\partial' F}{\partial' e_{ij}^P} \right. \\ &\quad \left. - \frac{\partial' k}{\partial' \bar{\epsilon}^P} \sqrt{\left(\frac{\partial' F}{\partial' \sigma_{ij}} \frac{\partial' F}{\partial' \sigma_{ij}} \right) \left(\frac{\alpha + (1/\sqrt{3})}{\sqrt{3\alpha^2 + 1/2}} \right)} \right]^{-1} \end{aligned} \quad (37)$$

Finally, substituting eqns (18) and (37) into eqn (14) we obtain

$$\begin{aligned} d\sigma_{ab} &= \left(C_{abcd}^E - \left[C_{abmn}^E \frac{\partial' F}{\partial' \sigma_{mn}} \frac{\partial' F}{\partial' \sigma_{ij}} C_{ijcd}^E \right] \right. \\ &\quad \times \left[\frac{\partial' F}{\partial' \sigma_{ij}} C_{ijrs}^E \frac{\partial' F}{\partial' \sigma_{rs}} - \frac{\partial' F}{\partial' \sigma_{ij}} \frac{\partial' F}{\partial' e_{ij}^P} - \frac{\partial' F}{\partial' \bar{\epsilon}^P} \right. \\ &\quad \left. \left. \times \sqrt{\left(\frac{\partial' F}{\partial' \sigma_{ij}} \frac{\partial' F}{\partial' \sigma_{ij}} \right) \left(\frac{\alpha + (1/\sqrt{3})}{\sqrt{3\alpha^2 + 1/2}} \right)} \right]^{-1} \right) de_{cd} \end{aligned} \quad (38)$$

The elastic-plastic constitutive tensor is defined as

$$\begin{aligned} C_{abcd}^{EP} &\equiv C_{abcd}^E - \left[C_{abmn}^E \frac{\partial' F}{\partial' \sigma_{mn}} \frac{\partial' F}{\partial' \sigma_{ij}} C_{ijcd}^E \right] \\ &\quad \times \left[\frac{\partial' F}{\partial' \sigma_{ij}} C_{ijrs}^E \frac{\partial' F}{\partial' \sigma_{rs}} - \frac{\partial' F}{\partial' \sigma_{ij}} \frac{\partial' F}{\partial' e_{ij}^P} - \frac{\partial' F}{\partial' \bar{\epsilon}^P} \right. \\ &\quad \left. \times \sqrt{\left(\frac{\partial' F}{\partial' \sigma_{ij}} \frac{\partial' F}{\partial' \sigma_{ij}} \right) \left(\frac{\alpha + (1/\sqrt{3})}{\sqrt{3\alpha^2 + 1/2}} \right)} \right]^{-1} \end{aligned} \quad (39)$$

and hence

$$d\sigma_{ab} = C_{abcd}^{EP} de_{cd} \quad (40)$$

As a first step in evaluating the terms in eqn (39), we observe that both the Drucker-Prager and cap (to be presented later) yield functions depend explicitly on $' I_1$ and $\sqrt{J_2}$. Therefore,

$$\frac{\partial' F}{\partial' \sigma_{ij}} = \frac{\partial' F}{\partial' I_1} \frac{\partial' I_1}{\partial' \sigma_{ij}} + \frac{\partial' F}{\partial' \sqrt{J_2}} \frac{\partial' \sqrt{J_2}}{\partial' \sigma_{ij}} \quad (41)$$

It can also be shown that

$$\frac{\partial' I_1}{\partial' \sigma_{ij}} = \delta_{ij} \quad (42)$$

$$\frac{\partial' \sqrt{J_2}}{\partial' \sigma_{ij}} = \frac{' s_{ij}}{2\sqrt{J_2}} \quad (43)$$

Substituting eqns (42) and (43) into eqn (41) results in

$$\frac{\partial' F}{\partial' \sigma_{ij}} = \delta_{ij} \frac{\partial' F}{\partial' I_1} + \frac{' s_{ij}}{2\sqrt{J_2}} \frac{\partial' F}{\partial' \sqrt{J_2}} \quad (44)$$

To complete the evaluation of the terms in eqn (39), it is now necessary to consider the Drucker-Prager and cap yield functions individually.

Drucker-Prager:

$${}^tF_{DP} = \alpha {}^tI_1 + \sqrt{{}^tJ_2} - {}^t k. \quad (45)$$

From eqn (29),

$$\frac{\partial {}^tF_{DP}}{\partial {}^t\sigma_{ij}} = \alpha \delta_{ij} + \frac{{}^t s_{ij}}{2\sqrt{{}^tJ_2}}. \quad (46)$$

Since ${}^tF_{DP}$ does not depend on ${}^t e_{ij}^p$, the second term in the denominator of eqn (39) is dropped. Recalling from eqn (25) that ${}^t k$ is a function of ${}^t \bar{\epsilon}^p$,

$$\frac{\partial {}^tF}{\partial {}^t \bar{\epsilon}^p} = \frac{\partial {}^tF}{\partial {}^t k} \frac{\partial {}^t k}{\partial {}^t \bar{\epsilon}^p} = - \frac{\partial {}^t k}{\partial {}^t \bar{\epsilon}^p} \quad (47)$$

where $\partial {}^t k / \partial {}^t \bar{\epsilon}^p$ is the strain hardening modulus and must be determined from experimental data. Substituting eqns (15) and (46) to (47) into eqn (39), we obtain after some algebra

$$C_{abcd}^{EP} = [\lambda \delta_{ab} \delta_{cd} + \mu (\delta_{ac} \delta_{bd} + \delta_{ad} \delta_{bc})] \frac{\left[\alpha (3\lambda + 2\mu) \delta_{ab} + \mu \frac{{}^t s_{ab}}{\sqrt{{}^t J_2}} \right] \left[\alpha (3\lambda + 2\mu) \delta_{cd} + \mu \frac{{}^t s_{cd}}{\sqrt{{}^t J_2}} \right]}{3\alpha^2 (3\lambda + 2\mu) + \mu \frac{\partial {}^t k}{\partial {}^t \bar{\epsilon}^p} \left(\alpha + \frac{1}{\sqrt{3}} \right)} \quad (48)$$

Cap:

$${}^tF_C = -{}^tI_1 + {}^tI_1^a \quad (49)$$

where

$${}^tI_1^a = {}^tI_1^a ({}^t e_V^p) \quad (50)$$

$${}^t e_V^p = {}^t e_{mn}^p \delta_{mn}. \quad (51)$$

Equation (50) is the cap hardening law which relates the cap position to the volumetric plastic strain. From the work of Sandler *et al.* [12, 13], one possible form for the hardening law is

$${}^t e_V^p = -W [e^{-D {}^t I_1^a} - 1] \quad (52)$$

where W and D are material constants

To initially position the cap off the origin, we use

$${}^t I_1^a = -\frac{1}{D} \ln \left[1 - \frac{{}^t e_V^p}{W} \right] + {}^0 I_1^a, \quad {}^0 I_1^a < 0. \quad (53)$$

Noting that tF_C does not depend on ${}^t \bar{\epsilon}^p$, we can drop the third term in the denominator of eqn (39). Then, using eqns (50)–(53), we find

$$\begin{aligned} \frac{\partial {}^tF_C}{\partial {}^t e_{ij}^p} &= \frac{\partial {}^tF_C}{\partial {}^t e_V^p} \frac{\partial {}^t e_V^p}{\partial {}^t e_{ij}^p} \\ &= \frac{\partial {}^tF_C}{\partial {}^t I_1^a} \frac{\partial {}^t I_1^a}{\partial {}^t e_V^p} \frac{\partial {}^t e_V^p}{\partial {}^t e_{ij}^p} \\ &= \frac{\delta_{ij}}{D(W - {}^t e_V^p)}. \end{aligned} \quad (54)$$

Substituting eqn (49) into eqn (44) results in

$$\frac{\partial {}^tF_C}{\partial {}^t \sigma_{ij}} = -\delta_{ij}. \quad (55)$$

Finally, substituting eqns (15) and (54)–(55) into eqn (39), after some algebra we obtain

$$C_{abcd}^{EP} = [\lambda \delta_{ab} \delta_{cd} + \mu (\delta_{ac} \delta_{bd} + \delta_{ad} \delta_{bc})] \frac{\delta_{ab} \delta_{cd} (3\lambda + 2\mu)^2}{3[3\lambda + 2\mu] + \frac{3}{D(W - {}^t e_V^p)}}. \quad (56)$$

Intersection of the cap and Drucker-Prager yield surfaces:

At the point of intersection of the cap and the Drucker-Prager yield surface exists a vertex in the yield surface and hence there is no uniquely defined normal. The plastic strain increment is defined as

$$de_{ij}^p = {}^t \bar{\lambda}_{DP} \frac{\partial {}^tF_{DP}}{\partial {}^t \sigma_{ij}} + {}^t \bar{\lambda}_C \frac{\partial {}^tF_C}{\partial {}^t \sigma_{ij}}, \quad ({}^t \bar{\lambda}_{DP} \text{ and } {}^t \bar{\lambda}_C > 0) \quad (57)$$

where ${}^t \bar{\lambda}_{DP}$ and ${}^t \bar{\lambda}_C$ are obtained using eqn (37),

$${}^t \bar{\lambda}_{DP} = \frac{\left[\alpha (3\lambda + 2\mu) \delta_{rs} + \mu \frac{{}^t s_{rs}}{\sqrt{{}^t J_2}} \right] de_{rs}}{3\alpha^2 (3\lambda + 2\mu) + \mu + \frac{\partial {}^t k}{\partial {}^t \bar{\epsilon}^p} \left(\alpha + \frac{1}{\sqrt{3}} \right)} \quad (58)$$

$${}^t \bar{\lambda}_C = \frac{-(3\lambda + 2\mu) \delta_{rs} de_{rs}}{3(3\lambda + 2\mu) + \frac{3}{D(W - {}^t e_V^p)}} \quad (59)$$

Substituting eqns (46), (55) and (58)–(59) into eqn (18), we obtain

$$\begin{aligned} de_{ij}^p &= \frac{\left[\alpha (3\lambda + 2\mu) \delta_{rs} + \mu \frac{{}^t s_{rs}}{\sqrt{{}^t J_2}} \right] de_{rs}}{3\alpha^2 (3\lambda + 2\mu) + \mu + \frac{\partial {}^t k}{\partial {}^t \bar{\epsilon}^p} \left(\alpha + \frac{1}{\sqrt{3}} \right)} \left[\alpha \delta_{ij} + \frac{{}^t s_{ij}}{2\sqrt{{}^t J_2}} \right] \\ &+ \frac{(3\lambda + 2\mu) \delta_{rs} de_{rs}}{3(3\lambda + 2\mu) + \frac{3}{D(W - {}^t e_V^p)}} \delta_{ij}. \end{aligned} \quad (60)$$

When eqns (15) and (60) are substituted into eqn (14), it can be shown after some algebra that

$$\begin{aligned} C_{abcd}^{EP} &= [\lambda \delta_{ab} \delta_{cd} + \mu (\delta_{ac} \delta_{bd} + \delta_{ad} \delta_{bc})] \\ &- \left[\alpha (3\lambda + 2\mu) \delta_{ab} + \mu \frac{{}^t s_{ab}}{\sqrt{{}^t J_2}} \right] \\ &\times \left[\alpha (3\lambda + 2\mu) \delta_{cd} + \mu \frac{{}^t s_{cd}}{\sqrt{{}^t J_2}} \right] \\ &\times \left[3\alpha^2 (3\lambda + 2\mu) + \mu + \frac{\partial {}^t k}{\partial {}^t \bar{\epsilon}^p} \left(\alpha + \frac{1}{\sqrt{3}} \right) \right]^{-1} \\ &- \frac{(3\lambda + 2\mu)^2 \delta_{ab} \delta_{cd}}{3(3\lambda + 2\mu) + \frac{3}{D(W - {}^t e_V^p)}}. \end{aligned} \quad (61)$$

Now consider the *special case* where the stress state is at the vertex and

$$\begin{aligned} {}^t \bar{\lambda}_{DP} &> 0 \\ {}^t \bar{\lambda}_C &= 0 \end{aligned} \quad (62)$$

$$d\sigma_{ii} = dI_1 = 0.$$

In this situation it is possible for the cap to retract past

the stress state. To prevent this type of behavior from occurring, a modified flow rule is used. This flow rule is derived so that $de_{ii}^p = de_{V}^p = 0$. Then the cap remains fixed since the cap position has been defined to be a function of volumetric plastic strain.

The modified elastic-plastic material law is obtained by simply setting $\alpha = 0$ in eqn (48). Then the following expression results,

$$C_{abcd}^{EP} = [\lambda \delta_{ab} \delta_{cd} + \mu (\delta_{ac} \delta_{bd} + \delta_{ad} \delta_{bc})] - \frac{\mu^2 ({}^t S_{ab} {}^t S_{cd})}{{}^t J_2 \left[\mu + \frac{1}{\sqrt{3}} \frac{\partial {}^t k}{\partial {}^t \bar{\epsilon}^p} \right]} \quad (63)$$

Tension cutoff

Stress states beyond the tension cutoff are not allowed. When this limit is reached or exceeded, the procedure followed is to set ${}^{t+\Delta t} s_{ij} = 0$ and ${}^{t+\Delta t} \sigma_{ij} = T/3 \delta_{ij}$. The elastic constitutive law C_{ijrs}^E , is then used to form the stiffness matrix for the next solution step.

Tables 1-3 give C_{ijrs}^{EP} in matrix form for three-dimensional analysis. The accompanying stress and strain vectors are

$${}^t \sigma^T = [{}^t \sigma_{11} \quad {}^t \sigma_{22} \quad {}^t \sigma_{33} \quad {}^t \sigma_{12} \quad {}^t \sigma_{13} \quad {}^t \sigma_{23}] \quad (64)$$

and

$${}^t e^T = [{}^t e_{11} \quad {}^t e_{22} \quad {}^t e_{33} \quad 2{}^t e_{12} \quad 2{}^t e_{13} \quad 2{}^t e_{23}]. \quad (65)$$

4. EQUILIBRIUM ITERATION

The step-by-step solution of the linearized equations of motion, eqn (5), can be made more effective using equilibrium iteration during a time step,

$$({}^t K_L + {}^t K_{NL}) \Delta U^{(i)} = {}^{t+\Delta t} R - {}^{t+\Delta t} F^{(i-1)} - M {}^{t+\Delta t} \ddot{U}^{(i)} \quad (66)$$

where $\Delta U^{(i)}$ is the displacement increment during the i th iteration and ${}^{t+\Delta t} F^{(i-1)}$ can be evaluated from

$${}^{t+\Delta t} F^{(i-1)} = \int_{t+\Delta t V^{(i-1)}} {}^{t+\Delta t} B_L^{(i-1)T} {}^{t+\Delta t} \hat{r}^{(i-1)} dv \quad (67)$$

which is similar to eqn (8). Iteration proceeds until the solution calculated by eqn (66) is within a specified tolerance. Solution of the equilibrium equations through iteration over a time step reduces errors caused by linearization and may prevent instabilities in the incremental analysis [1, 5, 14].

There are two important points that must be considered in the equilibrium iteration. Firstly, the stresses must be calculated accurately by integration from an *accepted* equilibrium configuration to the configuration that corresponds to the current iteration values. For example, considering the stresses at an integration point within an element, and assuming small displacement analysis, we use

$${}^{t+\Delta t} \sigma^{(i-1)} = {}^t \sigma + \int_{t_e}^{t+\Delta t e^{(i-1)}} C de \quad (68)$$

where the ${}^t \sigma$ are the stresses corresponding to the accepted or *converged* equilibrium configuration. The in-

tegration in eqn (68) is performed by numerical integration using, for example, the Euler forward method [4].

The next important point concerns the convergence of the iteration. As discussed in [15], convergence is measured effectively using as termination criteria the following two conditions,

$$\frac{\|{}^{t+\Delta t} R - {}^{t+\Delta t} F^{(i-1)} - M {}^{t+\Delta t} \ddot{U}^{(i-1)}\|_2}{\|{}^t R - {}^t F - M {}^t \ddot{U}\|_2^{(\max)}} \leq \epsilon_F \quad (69)$$

and

$$\frac{\Delta U^{(i)T} ({}^{t+\Delta t} R^{(i-1)} - {}^{t+\Delta t} F^{(i-1)} - M {}^{t+\Delta t} \ddot{U}^{(i-1)})}{\Delta U^{(i)T} ({}^{t+\Delta t} R - {}^t F - M {}^t \ddot{U})} \leq \epsilon_E \quad (70)$$

where ϵ_F is an out-of-balance force tolerance and ϵ_E is an "energy" tolerance. In eqn (69) the superscript (max) denotes the maximum value ever calculated during the solution, and $\|a\|_2$ is the Euclidean norm of the vector a .

Of particular concern in the solution is the speed of convergence of the iteration. Using the standard modified Newton iteration, the convergence can be slow (or the solution may even diverge) when the time step size Δt is not small enough. To speed up the convergence, Aitken acceleration can be employed in some analyses. Alternatively, the BFGS method can be effective, in which the coefficient matrix of eqn (66) is modified implicitly to improve the convergence of the iterative solution [15, 16]. The basic equations used in the BFGS method are

$$\Delta \ddot{U}^{(i)} = ({}^t \hat{K}^{-1})^{(i-1)} ({}^{t+\Delta t} R - M {}^{t+\Delta t} \ddot{U}^{(i-1)} - {}^{t+\Delta t} F^{(i-1)}) \quad (71)$$

where ${}^t \hat{K}$ is the effective stiffness matrix corresponding to time τ [1], and

$${}^{t+\Delta t} \ddot{U}^{(i)} = {}^{t+\Delta t} \ddot{U}^{(i-1)} + \beta \Delta U^{(i)} \quad (72)$$

where β is a scalar that is evaluated to satisfy the condition

$$[\Delta U^{(i)T} ({}^{t+\Delta t} R - M {}^{t+\Delta t} \ddot{U}^{(i)} - {}^{t+\Delta t} F^{(i)})] \leq \text{STOL} [\Delta U^{(i)T} ({}^{t+\Delta t} R - M {}^{t+\Delta t} \ddot{U}^{(i-1)} - {}^{t+\Delta t} F^{(i-1)})] \quad (73)$$

with STOL a tolerance. The coefficient matrix in eqn (71) is evaluated as follows,

$$({}^t \hat{K}^{-1})^{(i-1)} = A^{(i-1)T} ({}^t \hat{K}^{-1})^{(i-2)} A^{(i-1)} \quad (74)$$

where the matrices $A^{(i-1)}$ are of the simple form $A^{(i-1)} = (I + w^{(i-1)} v^{(i-1)T})$. The vectors $w^{(i-1)}$ and $v^{(i-1)}$ are given by the calculated nodal point displacements and forces, so that the solution of eqn (71) can be obtained with relatively little cost.

A detailed description and evaluation of the BFGS method and Aitken acceleration in the solution of non-linear finite element equations is given in [15, 16].

5. SOME REMARKS ON THE EFFECT OF ELEMENT INTEGRATION ORDER AND MESH LAYOUT IN ELASTIC, PERFECTLY-PLASTIC ANALYSIS

The inadequacy of some isoparametric elements in calculating stresses in elastic, perfectly plastic analysis has

Table 2. Elastic-plastic material property matrix (Cap)

$$\underline{C}^{EP} = \begin{bmatrix}
 \lambda + 2\mu - t_{Y1} & \lambda - t_{Y1} & \lambda - t_{Y1} & 0 & 0 & 0 \\
 & \lambda + 2\mu - t_{Y1} & \lambda - t_{Y1} & 0 & 0 & 0 \\
 & & \lambda + 2\mu - t_{Y1} & 0 & 0 & 0 \\
 & & & \mu & 0 & 0 \\
 & \text{SYMMETRIC} & & & \mu & 0 \\
 & & & & & \mu
 \end{bmatrix}$$

$$t_{Y1} = \frac{(3\lambda + 2\mu)^2}{3(3\lambda + 2\mu) + \frac{3}{D(W - t_{eV}^P)}}$$

been examined by several investigators. Herrmann[17] observed that the conventional displacement formulation can be inadequate for incompressible or nearly incompressible materials and developed a special formulation for such materials. Nagtegaal *et al.*[18] summarized that accurate plasticity solutions in finite element analysis depend on the number of kinematic constraints that are present in the deformation modes of an element, and examined some implications of using various finite elements. Naylor[19] investigated the effect of integration order on stress calculations in incompressible, eight-noded isoparametric elements by solving a number of examples. In the study Naylor found that the calculated stresses were in close agreement with theoretical values when taken at the 2×2 Gauss integration points, but oscillated about the theoretical values when taken at the 3×3 integration points. The conclusions arrived at by Naylor tie the accuracy of stress calculations to both the integration order and the total number of degrees of freedom in the model. Specifically, the constraint of a zero volumetric strain increment must be satisfied at each integration point. Since the strain increments and nodal displacements are related by the shape functions, Naylor reasoned that the satisfaction of the strain constraints is possible only if the number of integration points is less than the total number of degrees of freedom. While this may be a useful rule of thumb for establishing a finite element model, it is not the absolute determinant of whether a model can predict stresses accurately, because reduced integration is used, and the topology of the mesh as well as the boundary conditions do not enter into this criterion.

A mathematically intriguing approach based on the penalty method was used by Bercovier in order to generate some elements that satisfy the incompressibility constraints[20]. The result of the investigation is that a mixed integration scheme, in which lower-order integration is used on the hydrostatic part than on the deviatoric part of the stresses, assures a stable and accurate solution. However, this result is only applicable to certain rectangular-shaped elements and need still to be extended to large deformation analysis.

The finite element model and the selection of the optimum integration order for elastic-plastic analysis must account for both the plasticity and elasticity which exist in the structure. The presence of large regions of plastic, incompressible material requires satisfaction of volumetric strain constraints. However, in practice, the

simultaneous presence of a large elastic region, large deformations and non-parallelogram shaped elements may make the use of special incompressibility formulations or mixed integration schemes unattractive, and it would be most effective to use the usual elastic analysis procedures also for the plasticity solutions. This approach is possible provided the plasticity kinematic constraints can be satisfied, either by reducing the integration order or by a special arrangement of the finite element mesh. The effect of using a reduced integration order, such as proposed by Naylor, however, can introduce solution difficulties because additional kinematic modes with zero (or very small) eigenvalues may be introduced in the model. Unfortunately, at present, the determination of an appropriate mesh layout and integration order is largely a matter of experience and no rigid rules have been established as yet. This deficiency is particularly disconcerting, because in many areas finite element schemes are employed for the analysis of ultimate load conditions and strain localization[2,21], where for a realistic and accurate response prediction, appropriate mesh layouts can frequently only be established by some numerical experimentation.

6. SOME SAMPLE SOLUTIONS

The following problem solutions are described to illustrate the use of the elastic-plastic analysis procedures described in the previous sections. The solution results are also given to illustrate some problem areas where further research work is required. For the finite element solutions, the computer program ADINA was used[22].

6.1 Analyses of some simple specimens

The simple four-node element shown in Fig. 3 was loaded axially to 30% plastic strain. As shown in Fig. 3, for a one-dimensional stress situation, the updated Lagrangian formulation follows the path indicated by the material stress-strain law up to large plastic strains. The strain plotted in these figures is the true or logarithmic strain, which is calculated by referring displacement increments to the current configuration. The comparison of the large strain analysis results with the response predicted in an analysis accounting for only material non-linearities indicates that the large strain formulation must be used for plastic strains larger than about 4%.

In order to demonstrate the use of the Drucker-Prager-Cap model, a four element mesh was analyzed to

Table 3. Elastic-plastic material property matrix (Cap-Drucker-Prager intersection)

$\underline{C}^{EP} =$ SYMMETRIC $\nu_1 = (3+2\nu)$ $\nu_2 = -\sqrt{\frac{2}{3}}$ $\nu_3 = 3.2(3+2\nu) + \dots + \frac{\partial^2 k}{\partial \epsilon^2 P} \left(\nu + \frac{1}{3} \right)$ $\nu_4 = \frac{(3+2\nu)^2}{3(3+2\nu) + \frac{3}{D(\nu - \epsilon_P^P)}}$	$\frac{(1+\nu_1+\nu_2-\nu_3) \epsilon_{11}^2}{\epsilon_{13}} - \nu_4$	$\frac{\nu_1 - (1+\nu_1+\nu_2-\nu_3) \epsilon_{11} \epsilon_{22}}{\epsilon_{13}} - \nu_4$	$\frac{\nu_1 - (1+\nu_1+\nu_2-\nu_3) \epsilon_{11} \epsilon_{33}}{\epsilon_{13}} - \nu_4$	$\frac{-(1+\nu_1+\nu_2-\nu_3) \epsilon_{11} \epsilon_{12}}{\epsilon_{13}}$	$\frac{-(1+\nu_1+\nu_2-\nu_3) \epsilon_{11} \epsilon_{13}}{\epsilon_{13}}$	$\frac{-(1+\nu_1+\nu_2-\nu_3) \epsilon_{11} \epsilon_{23}}{\epsilon_{13}}$	
	$\frac{(1+\nu_1+\nu_2-\nu_3) \epsilon_{22}^2}{\epsilon_{13}} - \nu_4$	$\frac{\nu_1 - (1+\nu_1+\nu_2-\nu_3) \epsilon_{22} \epsilon_{33}}{\epsilon_{13}} - \nu_4$	$\frac{-(1+\nu_1+\nu_2-\nu_3) \epsilon_{22} \epsilon_{12}}{\epsilon_{13}}$	$\frac{-(1+\nu_1+\nu_2-\nu_3) \epsilon_{22} \epsilon_{13}}{\epsilon_{13}}$	$\frac{-(1+\nu_1+\nu_2-\nu_3) \epsilon_{22} \epsilon_{23}}{\epsilon_{13}}$		
	$\frac{(1+\nu_1+\nu_2-\nu_3) \epsilon_{22}^2}{\epsilon_{13}}$	$\frac{-(1+\nu_1+\nu_2-\nu_3) \epsilon_{33} \epsilon_{12}}{\epsilon_{13}}$	$\frac{-(1+\nu_1+\nu_2-\nu_3) \epsilon_{33} \epsilon_{13}}{\epsilon_{13}}$	$\frac{-(1+\nu_1+\nu_2-\nu_3) \epsilon_{33} \epsilon_{23}}{\epsilon_{13}}$			
		$-\frac{(\epsilon_{12} \epsilon_{12})^2}{\epsilon_{13}}$	$\frac{-(\epsilon_{12} \epsilon_{12}) \epsilon_{13}}{\epsilon_{13}}$	$\frac{-(\epsilon_{12} \epsilon_{12}) \epsilon_{23}}{\epsilon_{13}}$			
			$-\frac{(\epsilon_{12} \epsilon_{13})^2}{\epsilon_{13}}$	$\frac{-(\epsilon_{12} \epsilon_{13}) \epsilon_{23}}{\epsilon_{13}}$			
							$-\frac{(\epsilon_{23} \epsilon_{23})^2}{\epsilon_{13}}$

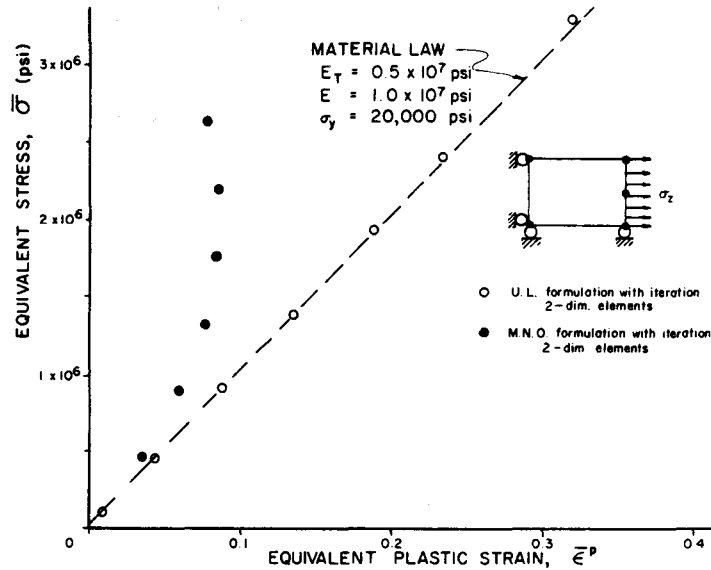


Fig. 3. Large strain plasticity solution of one-dimensional stress problem (von Mises yield condition).

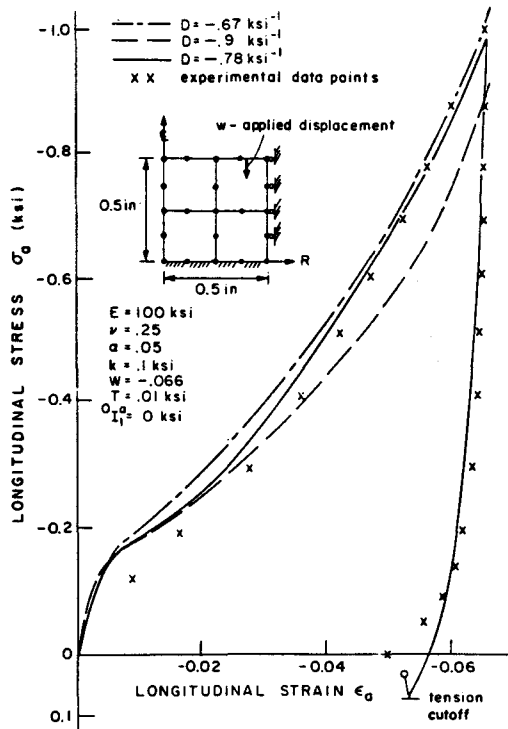


Fig. 4. Uniaxial strain test for McCormack Ranch sand [Ref. 12] (unloading calculated using $D = -.78$ ksi⁻¹; 31 load steps).

reproduce a uniaxial strain test of McCormack Ranch sand [12]. Figures 4 and 5 show the model used and a comparison of finite element and experimental results.

6.2 Dynamic analysis of a pipe whip problem

The pipe whip problem illustrated in Fig. 6 was modeled using 6 beam elements of a pipe cross-section that impinge on an elastic-plastic stop. The trapezoidal rule for time integration was employed in this analysis [5]. When the gap closes, there is a large stiffening effect that renders the convergence of the modified Newton iteration difficult.

Figure 7 shows the predicted displacement response when the BFGS method was used with time steps Δt of 0.0001, 0.0002, 0.001, 0.002 sec and $\epsilon_F = 0.0001$, $\epsilon_E = 10^{-6}$. As expected, it can be seen that increasing the time step results in a loss of accuracy, even though equilibrium has been established at all time steps. This loss of accuracy is due to the errors associated with the time integration scheme [4, 6]. The use of iteration, however, does assure the accurate solution of the time-wise discretized equilibrium equations.

6.3 Elastic-plastic, large deflection, static analysis of a circular plate

A simply supported circular plate was subjected to a monotonically increasing load and then unloaded. The finite element model of the plate is shown in Fig. 8. Twenty-one axisymmetric elements were used to model the plate. The plate material was assumed to be elastic, perfectly plastic. This assumption was necessary because the experimental results available for comparison did not provide sufficient information about the material strain hardening [27].

Three analyses were performed. The first considered only nonlinear material behavior while the last two accounted for both geometric and material nonlinearities. In all cases the stiffness matrix was reformed at the start of each solution step, however equilibrium iterations were not performed. The element stiffness matrices were evaluated using 2×2 Gauss integration.

Figure 9 is a plot of total applied load vs centerpoint vertical deflection. The results from all analyses as well as experimental results [23] are presented. Note that the lack of strain hardening causes the finite element results to overpredict the maximum deflection. However, there is still good qualitative agreement between the experimental results and the analyses which considered both geometric and material nonlinearities. On the other hand, the analysis which considered only material nonlinearities grossly underpredicted the load-carrying capacity of the plate.

6.4 Limit load analysis of a plane strain punch indenting an infinite half space

This problem was chosen to illustrate various features

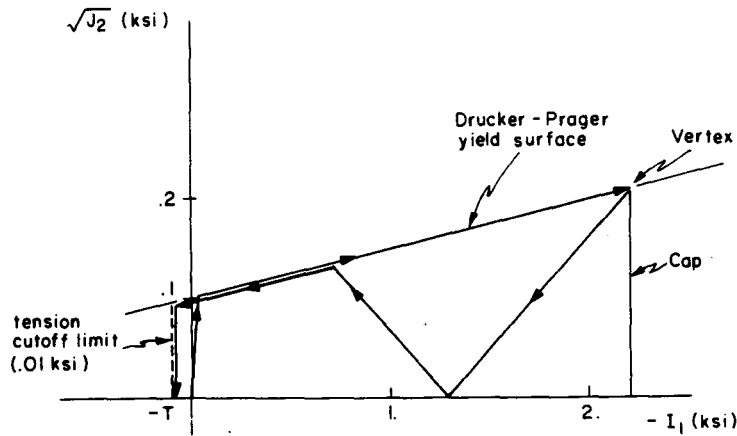


Fig. 5. Trajectory in stress space for uniaxial test of McCormack Ranch sand ($D = -0.78 \text{ ksi}^{-1}$).

of finite element limit load analysis. The problem is a rigid, plane strain punch indenting an infinite half space of elastic perfectly plastic material. The situation is similar to those analyzed in metal forming processes and encountered in foundation analyses [24,25]. The theoretical solution to the problem is well known, and has been determined by Hill [26] and Martin [11].

The problem geometry is illustrated in Fig. 10. The punch with width $2b$ is subjected to an applied load P causing it to settle a distance w into the material. The limit load is reached when an increment in settlement can

be obtained with no increase in load. The approximate plastic zone and slip mechanism as postulated by Hill are also shown in Fig. 10. The theoretical limit load P_{lim} is given by

$$P_{lim} = (2 + \pi)(2b)(k) \quad (75)$$

where k is the critical shear stress for the material and is equal to the uniaxial yield stress divided by $\sqrt{3}$ when the von Mises yield criterion is employed.

Two finite element models were used to analyze the

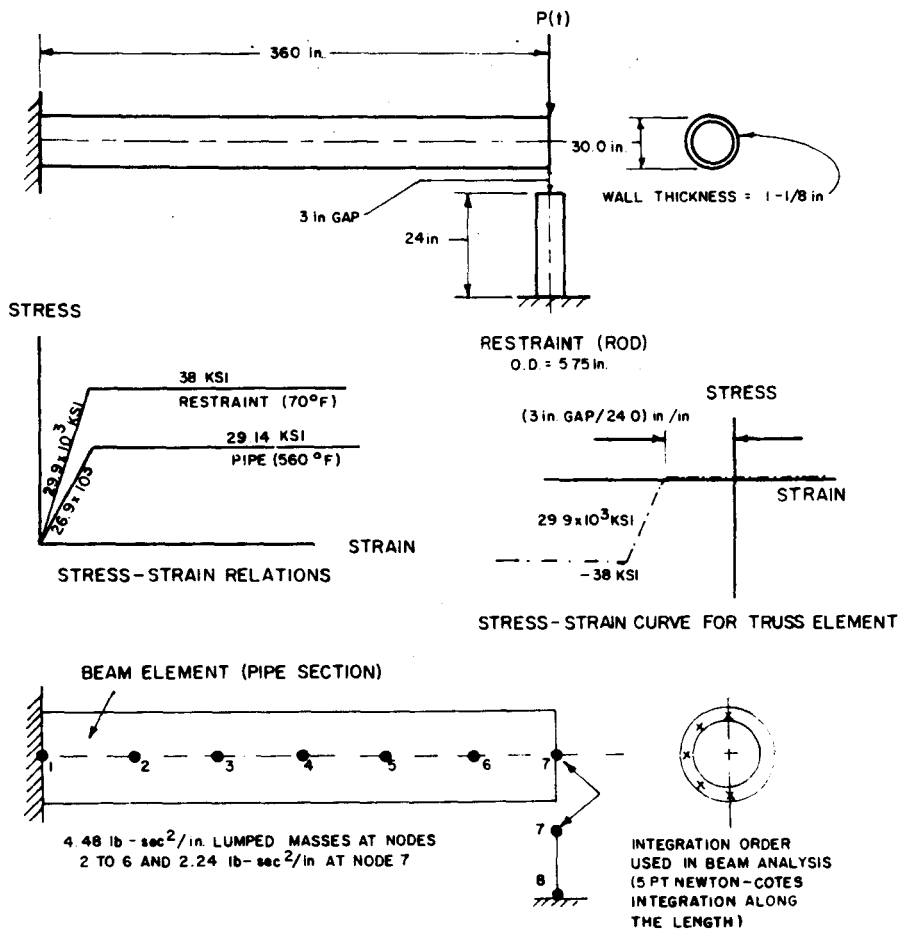


Fig. 6. Finite element analysis of pipe whip problem.

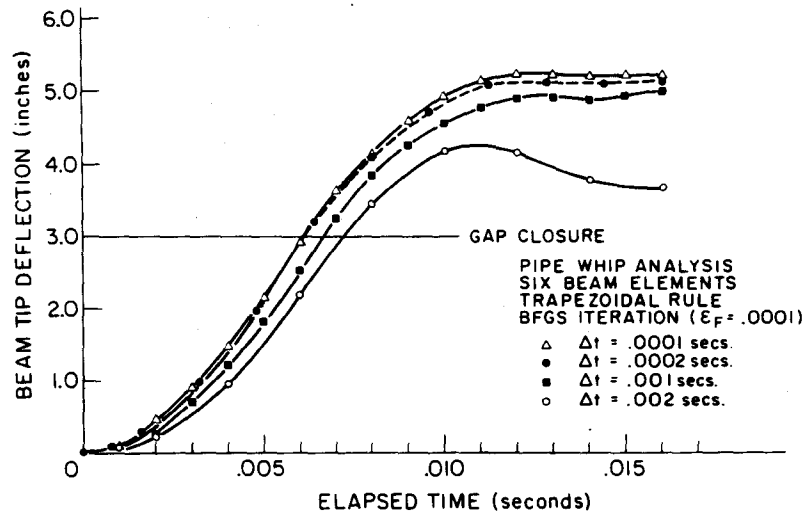


Fig. 7. Predicted displacement in pipe whip problem.

problem: a fine mesh with 160 plane strain elements and a coarse mesh with 25 plane strain elements. In order to simulate the rigid, flat punch, displacement boundary conditions specifying w were imposed over the distance b shown in Figs. 11 and 12. The corresponding applied load was found by integrating the stress distributions at a fixed distance below the surface. All stresses were determined at the integration points.

Fine mesh analysis

The first finite element model, shown in Fig. 11, used 160 two-dimensional elements and 366 nodal points for a total of 696 degrees of freedom. The limit load was determined using 2×2 and 3×3 Gauss integration.

As a test of the element mesh and of the effect of integration order on the elastic solution, the model was first analyzed for a point load applied at the centerline. The resulting stress distributions were compared with the Boussinesq solution [27] and the results, taken at a distance below the free surface, are shown in Figs. 13 and 14. The finite element results for both integration schemes show good agreement with the theoretical results at the sections considered, but this correspondence in the solutions deteriorates very close to the concentrated load, because of the stress singularity.

The load-displacement curves obtained for the punch problem are shown in Fig. 15. The 2×2 integration scheme obtained a normalized limit load $P_{lim}/(2kb)$ of 5.28, only 2.7% higher than the theoretical value of 5.14. For 3×3 integration, the limit load was higher, $P_{lim}/(2kb)$ reaching 5.62 before leveling off, a value 9.5% above the theoretical value. In both analyses, the load displacement curves did level off and did not exhibit the continuing increase in slope that some investigators noticed in the analysis of similar problems.

The development of the plastic zone under the punch with increasing settlement is shown in Fig. 16. The plastic zone growth is very similar in both cases and slightly larger using three point integration. A zone of plastic material extends a distance of approx. $8b$ under the punch and extends roughly 3.5 punch widths to either side of the punch. Comparison with the plastic zone size postulated by Hill and shown in Fig. 10 shows that the finite element model predicts a much deeper extent of plasticity under the punch but approximately the same plastic zone width at the surface. The theoretical analysis assumes a slip mechanism extending one to two punch widths below the surface, and the finite element results agree with this postulate. The plastic strain distribution using the 2×2 integration at a settlement of $(w/b) = 0.2$

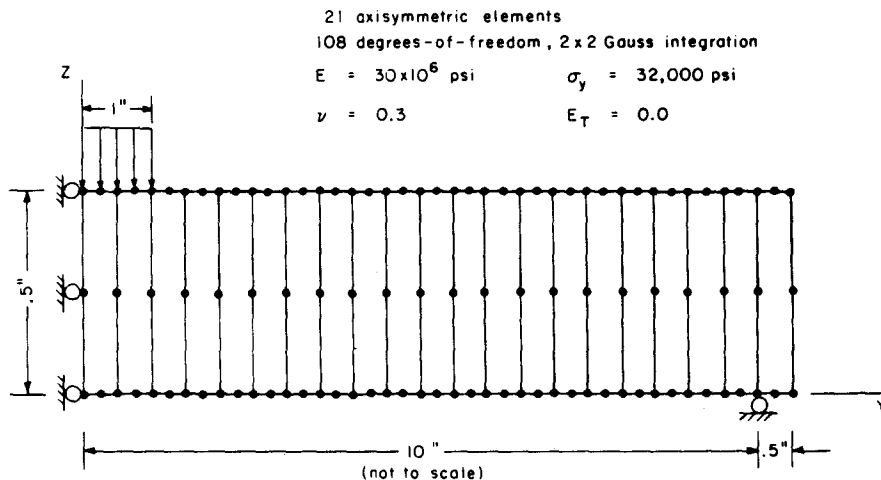


Fig. 8. Finite element model of a simply-supported circular plate.

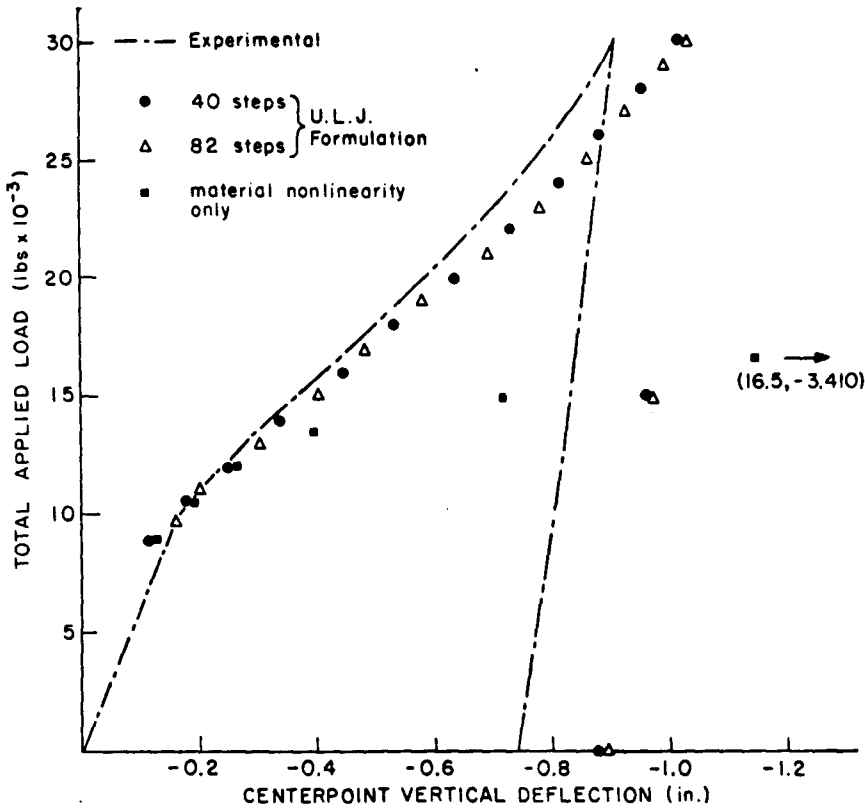


Fig. 9. Load vs deflection for a simple-supported circular plate.

(when the limit load mechanism is fully established) is shown in Fig. 17. The magnitudes and directions of the strains correspond to the assumed slip mechanism (shown in Fig. 10) used to calculate the theoretical limit load. The three point integration results are similar. Therefore, although the plastic zone size is larger than that assumed by Hill, the slip mechanism and the limit load for the punch problem are adequately predicted using the fine mesh.

Coarse mesh analysis

Using the coarse finite element mesh, Fig. 12, 25 two-dimensional elements and 58 nodal points (101 degrees of freedom) were employed to model the problem. This mesh is similar to that used by Yamada and Wif[28] to analyze footing problems. The load settlement curves using 2 point and 3 point integration are shown in Fig. 15. Unlike the fine mesh results, the coarse mesh exhibits no limit load, but reaches a terminal slope

at large settlements with values much larger than what theory predicts. Again, the loads predicted using 3×3 integration are higher than those using 2×2 integration.

Examination of the plastic zone growth showed that plasticity extended all the way through the mesh underneath the punch and extended roughly four punch widths from the centerline. Again, 3×3 integration predicted a larger plastic region than predicted using 2×2 integration.

Discussion of results

The two questions about this analysis which need to be considered are: (1) Why did the analysis not predict a limit load using the coarse mesh (2 and 3 point integration)? (2) Why did the analysis predict larger limit loads when three point integration was used in the fine mesh than when using two point integration.

The failure of the coarse mesh to attain a limit load illustrates the inadequacy of the Naylor criterion[12] that accurate stress solutions depend on having fewer integration points than degrees of freedom. As shown in Table 4, three point integration in the fine mesh predicts a limit load (although there are about twice as many integration points than degrees of freedom) while two point integration in the coarse mesh does not, despite having one more degree of freedom than integration points. In view of the earlier conclusions that accurate plasticity analysis depends on the satisfaction of the kinematic incompressibility constraints, it is possible that the inadequacy of the coarse mesh is due to its inability to satisfy the constraints under the imposed displacement boundary conditions because of the spread of plasticity entirely through the mesh. The results demonstrate the inability to quickly determine when a finite

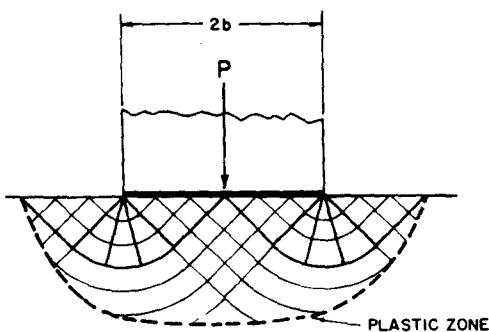


Fig. 10. Plane strain punch problem.

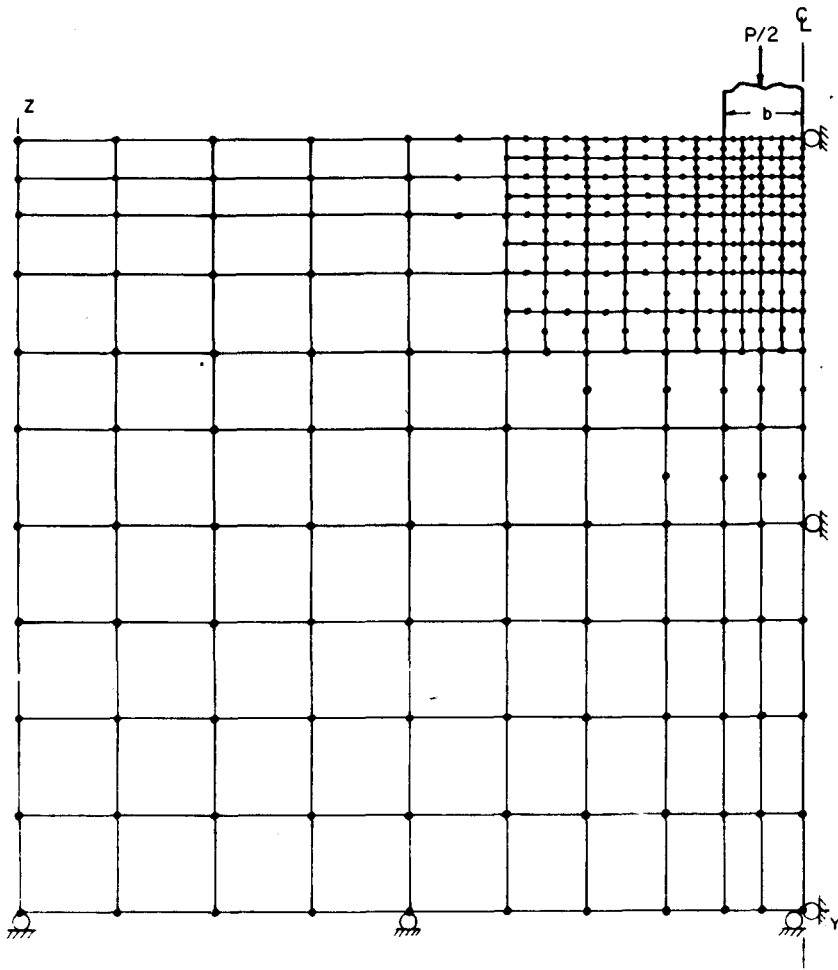


Fig. 11. Fine mesh finite element model of punch problem (overall mesh size = $10b \times 10b$, $b = 1$ in.).

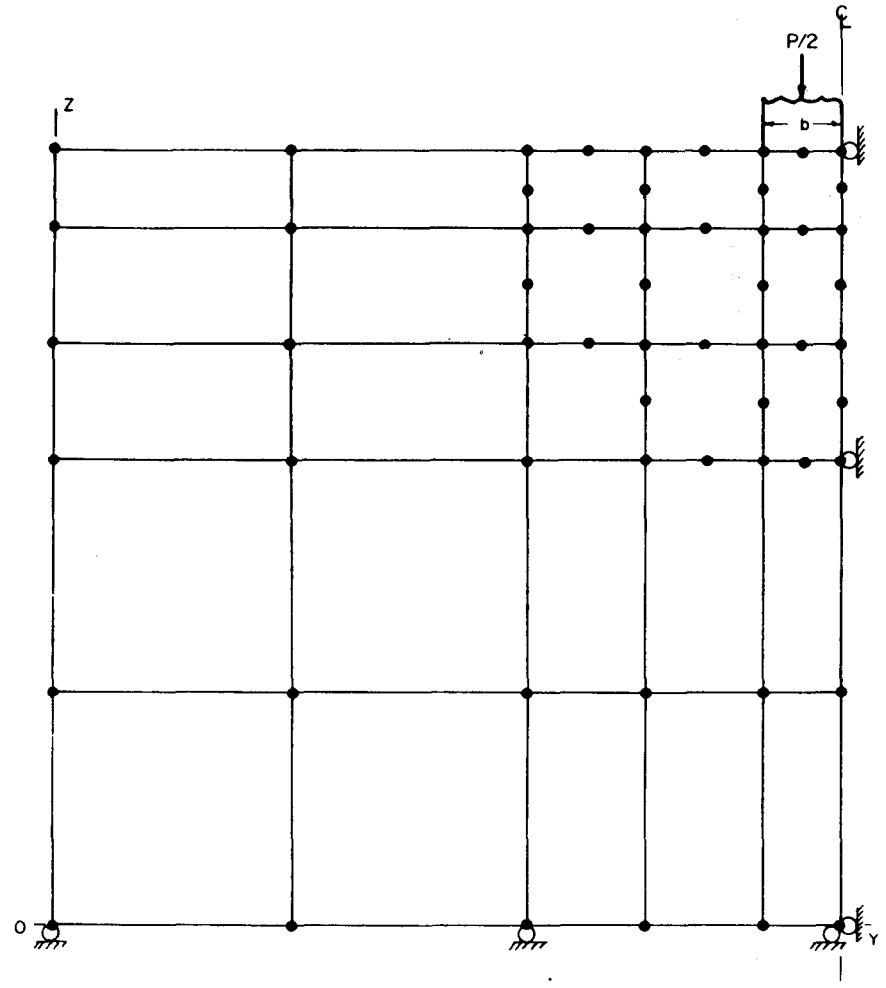


Fig. 12. Coarse mesh finite element model of punch problem (overall mesh size = $10b \times 10b$, $b = 1$ in.).

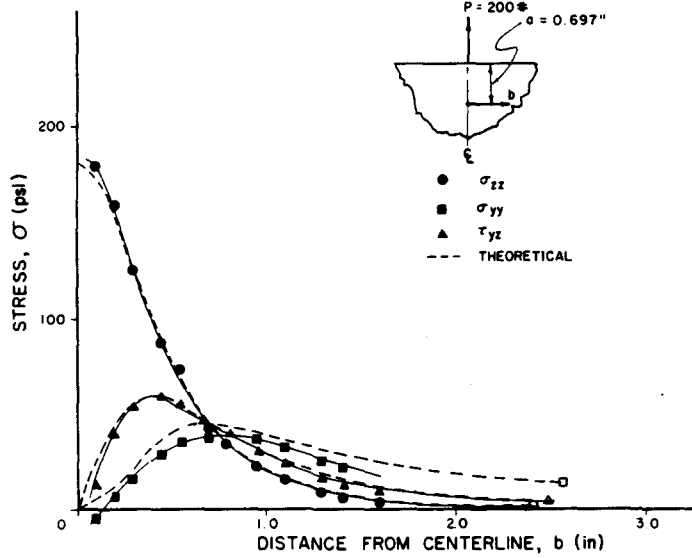


Fig. 13. Finite element solution of Boussinesq problem—2 pt. Integration, fine mesh.

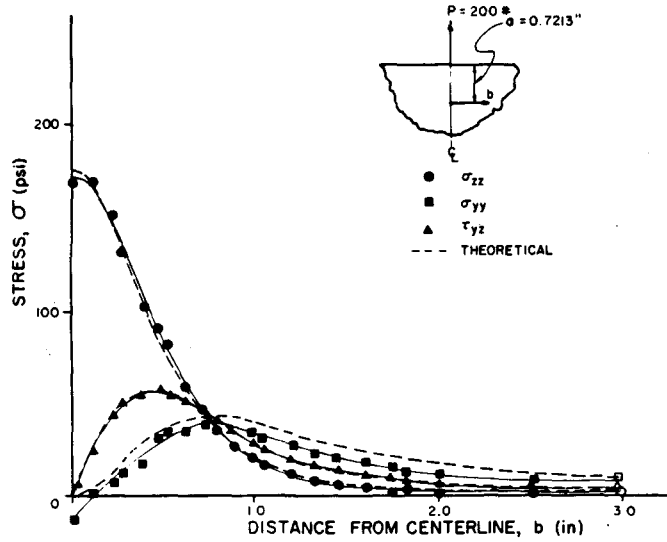


Fig. 14. Finite element solution of Boussinesq problem—3 pt. Integration, fine mesh.

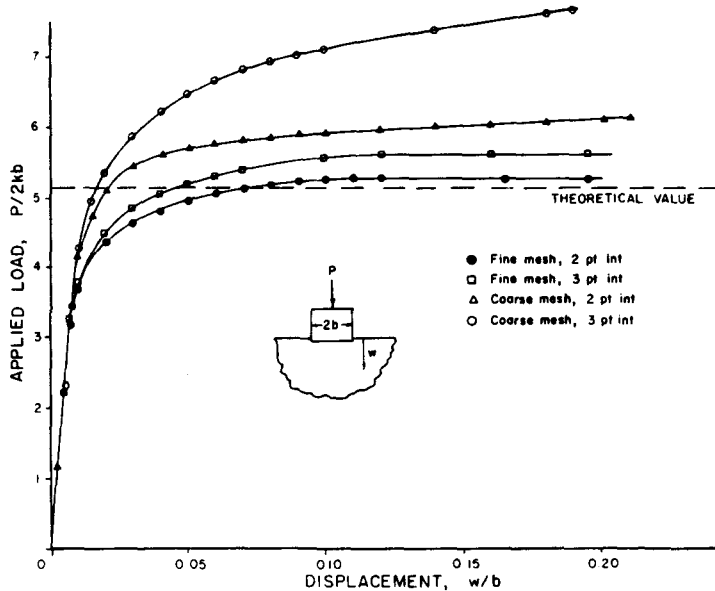


Fig. 15. Load-displacement curves for finite element model of punch problem (applied load obtained by averaging the load carried by each horizontal row of integration points).

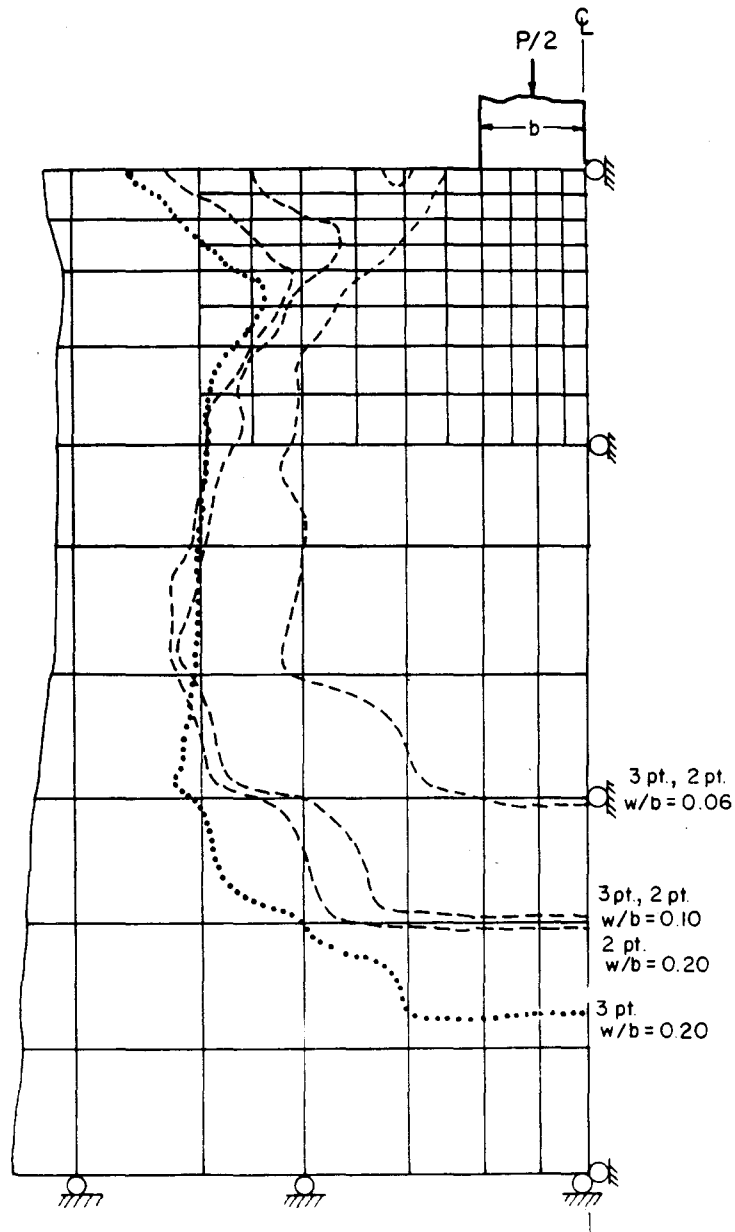


Fig. 16. Growth of plastic zone—fine mesh.

element model is appropriate to analyze a limit load problem and points to the need for further investigations.

The loads predicted using three point integration are higher than using two point integration because in three point integration displacement constraints are imposed at

more points in the mesh. Satisfaction of the incompressibility constraints at more points in the mesh constrains the displacement field to a greater extent and tends to increase the loads in the plastic solution. Considering the results in Fig. 15, the load-displacement curves for the different integration schemes separate

Table 4. Degrees of freedom and integration points for punch model

Finite element model	Integration order	Number of integration points	Number of degrees of freedom
Fine mesh	(2 × 2)	640	694
	(3 × 3)	1440	696
Coarse mesh	(2 × 2)	100	101
	(3 × 3)	225	101

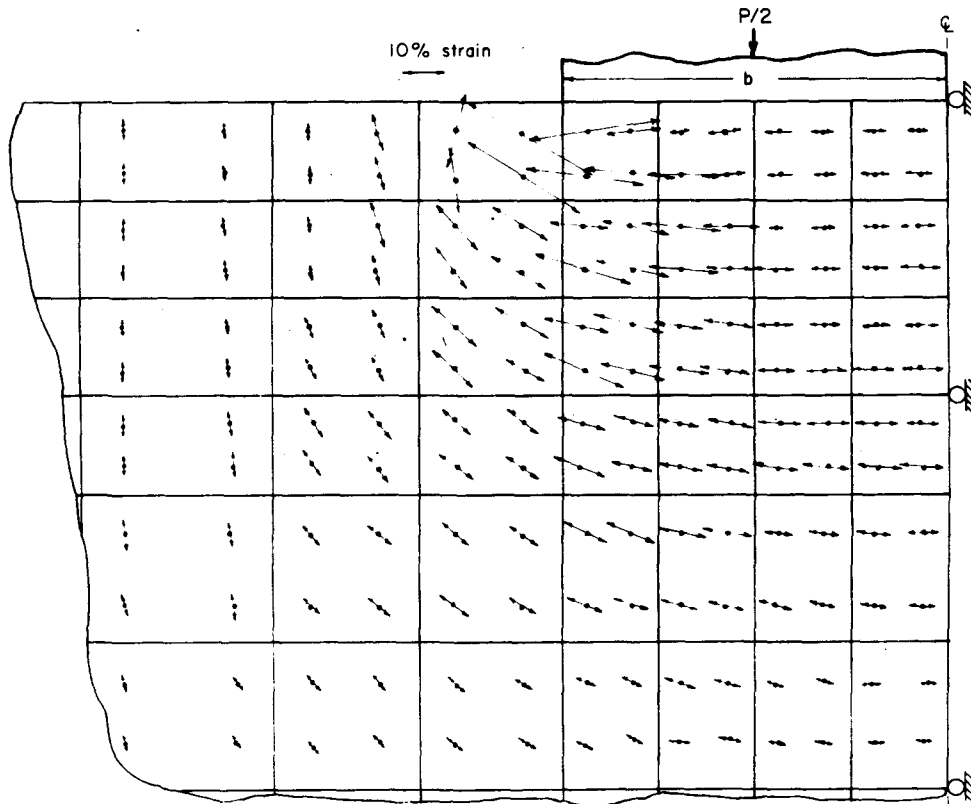


Fig. 17. Plastic strain distribution under punch—fine mesh, 2×2 integration.

only when plastic regions begin to become large, indicating that the plastic part of the solution is responsible for the larger loads predicted. The similarity of the elastic solutions considered in Fig. 14 using either integration procedure also substantiates this point.

7. CONCLUDING REMARKS

The objective in this paper was to summarize some finite element procedures for elastic-plastic analysis. It was pointed out that general elastic-plastic analysis requires the use of a consistent continuum mechanics formulation, the use of appropriate elastic-plastic models, the effective implementation of these models, the use of an appropriate finite element spatial discretization and the efficient solution of the nonlinear finite element equations. Since there is a strong interaction between each of these solution aspects, progress in elastic-plastic finite element analysis is best achieved by simultaneously advancing the state-of-the-art in each of these areas. Some of the current difficulties in elastic-plastic analysis have also been summarized in this paper, and it can be concluded that although some solutions can already be obtained, significant further progress is necessary to obtain solution capabilities that are generally applicable, reliable and effective. Since elastic-plastic analysis can be a very important ingredient in practical analysis and in research of fundamental phenomena, such as fracture, much motivation and challenge lies in providing more effective elastic-plastic analysis procedures in the years to come.

Acknowledgement—We are grateful to the ADINA users group for the financial support of our work in computational mechanics.

REFERENCES

1. K. J. Bathe, Static and dynamic geometric and material nonlinear analysis using ADINA. Rep. AVL 82448-2. Mechanical Engineering Dept., M.I.T. (May 1976) (rev. May 1977).
2. M. P. Cleary and K. J. Bathe, On tractable constitutive relations and numerical procedures for structural analysis in masses of geological materials. *Proc. 3rd Int. Conf. on Num. Meth. in Geomechanics*. Aachen, W. Germany (April 1979).
3. S. Key, J. H. Biffle and R. D. Krieg, A study of the computational and theoretical differences of two finite strain elastic-plastic constitutive models. In *Formulations and Computational Algorithms in Finite Element Analysis* (Edited by K. J. Bathe, J. T. Oden and W. Wunderlich). M.I.T. Press (1977).
4. K. J. Bathe and E. L. Wilson, *Numerical Methods in Finite Element Analysis*. Prentice-Hall (1976).
5. T. Belytschko and D. F. Schoeberle, On the unconditional stability of an implicit algorithm for nonlinear structural dynamics. *J. Appl. Mech.* **42**, 865-869 (1975).
6. T. J. R. Hughes, Stability, growth and decay of energy of the average acceleration method in nonlinear structural dynamics. *J. Comput. Structures* **6**, 313-324 (1976).
7. C. A. Felippa, Procedures for computer analysis of large nonlinear structural systems. *Proc. Int. Symp. on Large Engineering Systems*. University of Manitoba, Winnipeg, Canada (August 1976).
8. K. J. Bathe, Finite element formulation, modeling and solution of nonlinear dynamic problems. In *Numerical Methods for Partial Differential Equations*. Academic Press (1979).
9. K. J. Bathe, E. Ramm and E. L. Wilson, Finite element formulations for large deformation dynamic analysis. *Int. J. Num. Meth. in Engng* **9**, 353-386 (1975).
10. D. C. Drucker and W. Prager, Soil mechanics and plastic analysis or limit design. *Q. J. Appl. Math.* **10**, 157-175 (1952).
11. J. Martin, *Plasticity*. M.I.T. Press (1975).
12. F. L. DiMaggio and I. S. Sandler, Material model for granular

- soils. *J. Engng Mech. Div. ASCE* **97**(EM3), 935-950. Proc. Paper 8212 (June 1971).
13. I. S. Sandler, F. L. DiMaggio and G. Y. Baladi, Generalized cap model for geological materials. *J. Geotech. Engng Div., ASCE* **102**(GT7), 683-699 (July 1976).
 14. K. J. Bathe and W. Hahn, On transient analysis of fluid-structure systems. *J. Comput. Structures* **10**, 383-391 (1978).
 15. K. J. Bathe and A. P. Cimento, Some practical procedures for the solution of nonlinear finite element equations. *J. Comp. Meth. in Appl. Mech. and Engng* in press.
 16. H. Matthies and G. Strang, The solution of nonlinear finite element equations. *Int. J. Num. Meth. in Engng* **14**, 1613-1626 (1979).
 17. L. Herrmann, Elasticity equations for incompressible and nearly incompressible materials by a variational theorem. *J. Am. Inst. Aeron. Astron.* **3**, 1896-1900 (1965).
 18. J. Nagtegaal, D. Parks and J. Rice, On numerically accurate finite element solutions in the fully plastic range. *J. Comp. Methods in Appl. Mech. and Engng* **4**, 153-177 (1974).
 19. D. Naylor, Stresses in nearly incompressible materials by finite elements with application to the calculation of excess pore pressure. *Int. J. Num. Meth. in Engng* **8**, 443-460 (1974).
 20. M. Bercovier, Finite elements for incompressible or nearly incompressible materials. In *Proc. of ADINA Conf.* (Edited by K. J. Bathe). Report AVL 82448-6, Mech. Engng Dept., M.I.T. (August 1977).
 21. M. P. Cleary, Fracture discontinuities and structural analysis in resource recovery endeavors. *J. Pressure Vessel and Petroleum Tech.* **100**, 1-11 (1978).
 22. K. J. Bathe, ADINA—A finite element program for automatic dynamic incremental nonlinear analysis. *Rep. AVL 82448-1*. Mechanical Engng Dept., M.I.T. (May 1975) (rev. Dec. 1978).
 23. H. S. Levine, H. Armen, R. Winter and A. Pifko, Nonlinear behavior of shells of revolution under cyclic loading. *J. Comput. Structures* **3**, 589-617 (1973).
 24. J. Christian, A. Hagmann and W. Marr, Incremental plasticity analysis of frictional soils. *Int. J. Num. Anal. Methods Geomech.* **1**(4), 343-375 (1977).
 25. S. Key, R. D. Krieg and K. J. Bathe, On finite element analysis of metal forming processes—Part I. *Computer Meth. in Appl. Mech. and Engng* **17**/18, 597-608 (1979).
 26. R. Hill, *The Mathematical Theory of Plasticity*. Oxford University Press, London (1950).
 27. S. Timoshenko and J. Goodier, *Theory of Elasticity*. McGraw-Hill, New York (1951).
 28. Y. Yamada and A. Wifi, Large strain analysis of some geomechanics problems by the finite element method. *Int. J. Num. and Anal. Meth. in Geomech.* **1**(3), 299-318 (1977).

A SOLUTION PROCEDURE FOR THERMO-ELASTIC-PLASTIC AND CREEP PROBLEMS

Mark D. SNYDER and Klaus-Jürgen BATHE

Department of Mechanical Engineering, Massachusetts Institute of Technology, Cambridge, MA 02139, USA

Received 30 September 1980

An effective solution procedure for finite element thermo-elastic-plastic and creep analysis with temperature-dependent material properties is presented. The material model employed is summarized, the basic iterative equations are developed and the solution procedure is theoretically analyzed and numerically tested for its stability and accuracy properties.

1. Introduction

The application of the finite element method to the inelastic analysis of structures and continua has received considerable attention over the last fifteen years [1–21]. To a large extent, this effort has been motivated by the need to safely and economically predict material response under conditions of extreme mechanical and thermal loading. Some examples are the design and analysis of pressure vessels, ships, and aircraft, as well as the study of metal forming, welding, and nuclear weapon effects on soils and structures.

Based on extensive experience, the solution of problems with inelastic material behavior has proven to be much more difficult than the analysis of linear elastic behavior. The currently available solution procedures can be quite costly, unstable, and inaccurate. In addition, the models of inelastic material behavior in current engineering use are not always suitable for complex loading conditions. All of these factors have placed a severe constraint on the routine use of inelastic finite element analysis.

The cost of inelastic analysis is particularly high in three-dimensional calculations. However, a more critical factor is that considerable user knowledge and judgment are involved in selecting an appropriate solution strategy. In practice, this situation almost always means that obtaining a reliable solution requires some, if not extensive, numerical experimentation. There is surely a need for solution techniques with increased accuracy and stability properties as well as self-adaptive algorithms that adjust computational strategy as the solution proceeds.

Our objective in this paper is to present the development, analysis, and testing of a solution procedure for the finite element analysis of thermo-elastic-plastic and creep problems with temperature-dependent material properties. The solution procedure is based on a one-parameter integration method (the α -method) for a system of ordinary differential equations. This integration method, which contains the well-known Euler forward and backward methods, was previously proposed and analyzed for the finite element analysis of certain heat conduction [22,23] and viscoplasticity [3,4,6] problems. In this paper we use the α -method as the basis of an effective algorithm for the analysis of significantly more complex thermo-elastic-plastic and creep problems.

We first summarize in section 2 the formulation of the thermo-elastic-plastic and creep material model. Section 3 contains the development of the finite element solution procedure and a theoretical analysis of its stability characteristics. The procedure has been implemented in the finite element computer program ADINA [21] and in section 4 we present and discuss the solutions for three test problems. The conclusions are contained in section 5.

* Invited paper, presented at the 5th International Conference on Structural Mechanics in Reactor Technology, Berlin (West), August 13–17, 1979.

All notation is defined in the text when it is first introduced. A left superscript denotes the time at which a quantity occurs. No left superscript indicates a finite increment. Differentiation with respect to time is indicated by an overhead dot. Right lower case subscripts denote the components of Cartesian vectors and tensors. Finally, right superscripts and subscripts contained within parentheses are iteration counters.

2. Thermo-elastic-plastic and creep material model

In this section we present a material model which includes the combined effects of thermoelasticity, thermo-plasticity, and creep. All material properties (e.g., Young's modulus, yield stress, etc.) are allowed to vary with temperature. The thermoplasticity part of the model utilizes the von Mises yield function with the option of either isotropic or kinematic hardening. The creep formulation is a modified equation-of-state approach which is suitable for cyclic loading conditions.

2.1. Formulation of the model

A basic assumption in the formulation of the model is that the usual small strain tensor can be expressed as the sum of elastic, plastic, creep and thermal strains,

$$\tau e_{ij} = \tau e_{ij}^E + \tau e_{ij}^P + \tau e_{ij}^C + \tau e_{ij}^{TH}, \quad (1)$$

where

$$\begin{aligned} \tau e_{ij} &= \text{component of total strain tensor,} \\ \tau e_{ij}^E &= \text{component of elastic strain tensor,} \\ \tau e_{ij}^P &= \text{component of plastic strain tensor,} \\ \tau e_{ij}^C &= \text{component of creep strain tensor,} \\ \tau e_{ij}^{TH} &= \text{component of thermal strain tensor,} \end{aligned}$$

This assumption allows the use of the so-called classical theories of plasticity and creep which make a distinction between time-dependent and time-independent inelastic strains.

The constitutive law for an isotropic, thermoelastic material with temperature-dependent moduli is [38,39],

$$\tau \sigma_{ij} = \tau C_{ijrs}^E (\tau e_{rs} - \tau e_{rs}^P - \tau e_{rs}^C - \tau e_{rs}^{TH}), \quad (2)$$

where

$$\tau C_{ijrs}^E = \text{component of elastic constitutive tensor}$$

$$= \tau \lambda \delta_{ij} \delta_{rs} + \tau \mu (\delta_{ir} \delta_{js} + \delta_{is} \delta_{jr}),$$

$$\tau \lambda = \frac{\tau E \tau \nu}{(1 + \tau \nu)(1 - 2 \tau \nu)},$$

$$\tau \mu = \frac{\tau E}{2(1 + \tau \nu)},$$

$$\tau E = \text{Young's modulus,}$$

$$\tau \nu = \text{Poisson's ratio,}$$

$$\delta_{ij} = \text{Kronecker delta,}$$

$$\tau e_{rs}^{TH} = \tau \alpha_m (\tau \theta - \theta_R) \delta_{rs},$$

$\tau\theta$ = temperature,

$\tau\alpha_m$ = mean coefficient of thermal expansion,

θ_R = reference temperature.

The creep strain rate is determined using a modified equation-of-state approach which includes strain hardening for variable loading and the Oak Ridge National Laboratory auxiliary hardening rules for cyclic behavior [27,28]. The final result [18] is stated as

$$\tau\dot{e}_{ij}^C = \tau\gamma \tau s_{ij}, \quad (3)$$

where

τs_{ij} = component of deviatoric stress tensor

$$= \tau\sigma_{ij} - \frac{1}{3}\tau\sigma_{mm}\delta_{ij},$$

$$\tau\gamma = \frac{3}{2} \frac{\tau\dot{e}^C}{\tau\bar{\sigma}},$$

$\tau\bar{\sigma}$ = von Mises effective stress

$$= \sqrt{\frac{3}{2} \tau s_{ij} \tau s_{ij}},$$

$\tau\dot{e}^C$ = effective creep strain rate

$$= f(\tau\bar{\sigma}, \tau\bar{e}^H, \tau\theta),$$

$\tau\bar{e}^H$ = modified effective creep strain.

The plastic strain rate is calculated using the classical theory of time-independent plasticity [29–39]. The general form of the yield or loading function for non-isothermal conditions is assumed to be

$$\tau F = \tau F(\tau\sigma_{ij}, \tau\alpha_{ij}, \tau\sigma_y), \quad (4)$$

where $\tau\alpha_{ij}$ and $\tau\sigma_y$ depend on the history of plastic deformation and temperature. For elastic behavior, $\tau F < 0$, and for plastic behavior, $\tau F = 0$.

As a consequence of Drucker's postulate for stable inelastic materials under isothermal conditions, the yield function τF defines a convex yield surface in nine-dimensional stress space. Furthermore, when stress and plastic strain rate axes are coincident the plastic strain rate vector is normal to the yield surface. In developing a nonisothermal plasticity model, it is assumed that τF defines a convex yield surface in a ten-dimensional stress-temperature space and that the isothermal normality condition remains valid [31]. Thus, the plastic strain rate is defined by

$$\tau\dot{e}_{ij}^P = \tau\Lambda \frac{\partial \tau F}{\partial \tau\sigma_{ij}}, \quad (5)$$

where $\tau\Lambda$ = positive scalar variable.

The calculation of $\tau\Lambda$ requires that a hardening rule be selected. A hardening rule describes the change in the yield surface with continuing plastic deformation. Two commonly used hardening rules are isotropic hardening [39], and kinematic hardening [33].

2.1.1. Isotropic hardening rule

The isotropic hardening rule for isothermal conditions assumes that the size of the yield surface increases uniformly while its center remains fixed in nine-dimensional stress space. The size of the yield surface, as defined by

the yield stress, is based on either the plastic work or the accumulated effective plastic strain. In the following extension of the isotropic hardening rule to non-isothermal conditions [31,37], it is assumed that the yield stress depends on the accumulated effective plastic strain and instantaneous temperature.

The von Mises yield function for non-isothermal, isotropic hardening can be written as

$$\tau F = \frac{1}{2} \tau s_{lm} \tau s_{lm} - \frac{1}{3} \tau \sigma_y^2, \quad (6)$$

where

$$\tau \sigma_y = \text{yield stress}$$

$$= \tau \sigma_y(\tau \bar{e}^P, \tau \theta),$$

$$\tau \bar{e}^P = \text{accumulated effective plastic strain}$$

$$= \int_0^{\tau} \tau \dot{e}^P dt,$$

$$\tau \dot{e}^P = \text{effective plastic strain rate}$$

$$= \sqrt{\frac{2}{3}} \tau \dot{e}_{ij}^P.$$

The objective is to determine $\tau \Lambda$ in terms of the current strain and temperature rates. Taking the derivative of eq. (2) with respect to time and then substituting from eq. (5) results in

$$\tau \dot{\sigma}_{ij} = \tau C_{ijmn}^E \left(\tau \dot{e}_{mn} - \tau \Lambda \frac{\partial \tau F}{\partial \tau \sigma_{mn}} - \tau \dot{e}_{mn}^C - \tau \dot{e}_{mn}^{TH} \right) + \tau \dot{C}_{ijcd}^E \tau e_{cd}^E. \quad (7)$$

During plastic straining, the stress-temperature state remains on the yield surface so that

$$\tau \dot{F} = \frac{\partial \tau F}{\partial \tau \sigma_{ij}} \tau \dot{\sigma}_{ij} + \frac{\partial \tau F}{\partial \tau \alpha_{ij}} \tau \dot{\alpha}_{ij} + \frac{\partial \tau F}{\partial \tau \sigma_y} \tau \dot{\sigma}_y = 0. \quad (8)$$

Considering eq. (6), it can readily be shown that

$$\frac{\partial \tau F}{\partial \tau \alpha_{ij}} = 0, \quad (9)$$

$$\frac{\partial \tau F}{\partial \tau \sigma_y} = -\frac{2}{3} \tau \sigma_y, \quad (10)$$

$$\frac{\partial \tau F}{\partial \tau \sigma_{ij}} = \tau s_{ij}, \quad (11)$$

$$\tau \dot{\sigma}_y = \frac{\partial \tau \sigma_y}{\partial \tau \bar{e}^P} \tau \dot{\bar{e}}^P + \frac{\partial \tau \sigma_y}{\partial \tau \theta} \tau \dot{\theta}. \quad (12)$$

Substituting eqs. (9)–(12) into eq. (8) and using the previously stated definitions of $\tau \dot{e}^P$ and $\tau \dot{e}_{ij}^P$ results in

$$\tau s_{ij} \tau \dot{\sigma}_{ij} = \frac{2}{3} \tau \sigma_y \left[\frac{\partial \tau \sigma_y}{\partial \tau \bar{e}^P} \tau \Lambda \sqrt{\frac{2}{3}} \tau s_{ij} \tau s_{ij} + \frac{\partial \tau \sigma_y}{\partial \tau \theta} \tau \dot{\theta} \right]. \quad (13)$$

Since $\tau F = 0$ during plastic straining,

$$\tau s_{ij} \tau s_{ij} = \frac{2}{3} \tau \sigma_y^2, \quad (14)$$

and hence eq. (13) simplifies to

$$\tau s_{ij} \tau \dot{\sigma}_{ij} = \frac{2}{3} \tau \sigma_y \left[\frac{2}{3} \tau \sigma_y \tau \Lambda \frac{\partial \tau \sigma_y}{\partial \tau \bar{e}^P} + \frac{\partial \tau \sigma_y}{\partial \tau \theta} \tau \dot{\theta} \right]. \quad (15)$$

Premultiplying eq. (7) by τ_{sij} , setting the result equal to eq. (15) and solving for $\tau\Lambda$ gives

$$\tau\Lambda = \frac{\tau_{sij} \tau C_{ijmn}^E (\tau \dot{e}_{mn} - \tau \dot{e}_{mn}^C - \tau \dot{e}_{mn}^{TH}) + \tau_{sij} \tau C_{ijcd}^E \tau e_{cd}^E - \frac{2}{3} \tau \sigma_y \frac{\partial \tau \sigma_y}{\partial \tau \theta} \tau \dot{\theta}}{\frac{4}{3} \tau \sigma_y^2 \frac{\partial \tau \sigma_y}{\partial \tau e^P} + \tau_{sij} \tau C_{ijmn}^E \tau s_{mn}} \quad (16)$$

In order to further evaluate the above expression for $\tau\Lambda$, it is necessary to obtain $\partial \tau \sigma_y / \partial \tau e^P$ and $\partial \tau \sigma_y / \partial \tau \theta$. It is assumed that a relationship between $\tau \sigma_y$, τe^P , and $\tau \theta$ can be derived from the data obtained in a series of tensile tests at different temperatures using virgin material specimens. This data is used to develop the idealized, bilinear, engineering stress-strain curves shown in fig. 1.

To convert the curves shown in fig. 1 to stress-plastic strain curves, we have for constant temperature $\tau \theta$ and $\tau \sigma \geq \tau \sigma_{yv}$,

$$\tau \sigma = \tau \sigma_{yv} + \tau E_T \left(\tau e - \frac{\tau \sigma_{yv}}{\tau E} \right), \quad (17)$$

$$\tau e^P = \tau e - \tau \sigma / \tau E, \quad (18)$$

Combining the above equations and noting that the current stress is the current yield stress (i.e., $\tau \sigma = \tau \sigma_y$) results in

$$\tau \sigma_y = \frac{\tau E \tau E_T}{\tau E - \tau E_T} \tau e^P + \tau \sigma_{yv}. \quad (19)$$

Thus, eq. (19) gives the relationship between yield stress and plastic strain for monotonic uniaxial loading at constant temperature. The curves described by eq. (19) are shown in fig. 2.

It is now assumed that eq. (19) relates the yield stress and the accumulated effective plastic strain for multiaxial loading conditions. Additionally, it is assumed that the relation holds regardless of the history leading to τe^P .

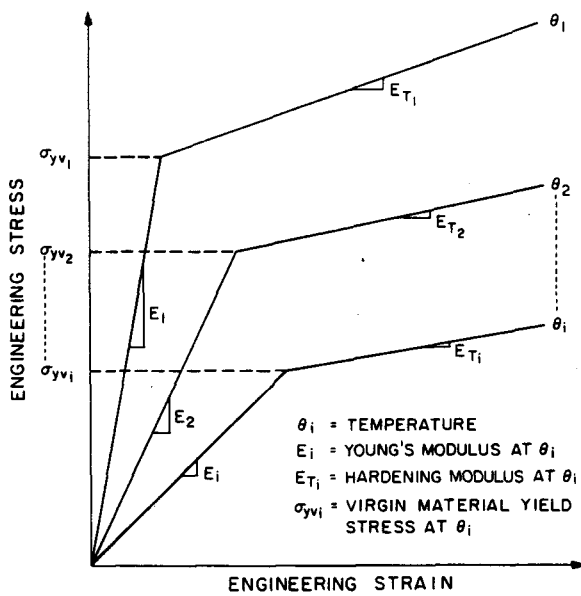


Fig. 1. Idealized engineering stress-strain curves.

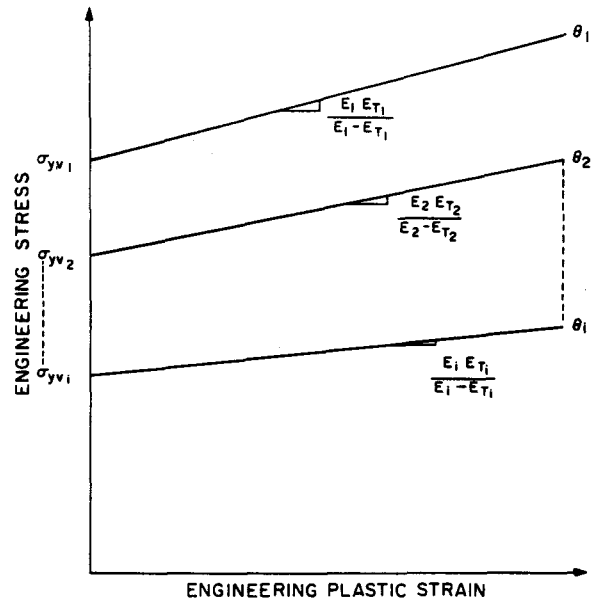


Fig. 2. Idealized engineering stress-plastic strain curves.

We then obtain

$$\frac{\partial \tau_{\sigma_y}}{\partial \tau_{e^P}} = \frac{\tau_E \tau_{E_T}}{\tau_E - \tau_{E_T}} \quad (20)$$

and

$$\frac{\partial \tau_{\sigma_y}}{\partial \tau_{\theta}} = \tau_{e^P} \frac{\partial}{\partial \tau_{\theta}} \left(\frac{\tau_E \tau_{E_T}}{\tau_E - \tau_{E_T}} \right) + \frac{\partial \tau_{\sigma_{yv}}}{\partial \tau_{\theta}} \quad (21)$$

Substituting eqs. (20) and (21) into eq. (16) and using the definitions of τ_{σ_y} , $\tau_{C_{ijrs}}^E$ and $\tau_{s_{ij}}$ yields:

$$\tau_{\Lambda} = \frac{\tau_{\mu} \tau_{s_{mn}} (\tau_{e_{mn}} - \tau_{\dot{e}_{mn}}^C - \tau_{\dot{e}_{mn}}^{TH}) + \tau_{\mu} \tau_{s_{cd}} \tau_{e_{cd}}^E - \frac{\tau_{\sigma_y}}{3} \left[\tau_{e^P} \frac{\partial}{\partial \tau_{\theta}} \left(\frac{\tau_E \tau_{E_T}}{\tau_E - \tau_{E_T}} \right) + \frac{\partial \tau_{\sigma_{yv}}}{\partial \tau_{\theta}} \tau_{\dot{\theta}} \right]}{\frac{2 \tau_{\sigma_y}^2}{3} \left[\tau_{\mu} + \frac{1}{3} \frac{\tau_E \tau_{E_T}}{\tau_E - \tau_{E_T}} \right]} \quad (22)$$

2.1.2. Kinematic hardening rule

The kinematic hardening rule for isothermal conditions assumes that the size of the yield surface remains constant and that the yield surface can translate as a rigid body in nine-dimensional stress space. The translation is a measure of the hardening of the material and the incremental translation components are generally assumed to be linearly related to the incremental plastic strains.

In the extension of the rule to non-isothermal conditions [31,36,37], it is assumed that both the size of the yield surface and the hardening of the material can depend on temperature. The von Mises yield function for non-isothermal, kinematic hardening can be written as

$$\tau F = \frac{1}{2} (\tau_{s_{lm}} - \tau_{\alpha_{lm}}) (\tau_{s_{lm}} - \tau_{\alpha_{lm}}) - \frac{1}{3} \tau_{\sigma_y}^2, \quad (23)$$

where

$$\begin{aligned} \tau_{\sigma_y} &= \text{yield stress} \\ &= \tau_{\sigma_y}(\tau_{\theta}), \end{aligned}$$

$\tau_{\alpha_{lm}}$ = component of yield surface translation tensor

$$= \int_0^{\tau} \tau_{\dot{\alpha}_{lm}} dt,$$

$$\tau_{\dot{\alpha}_{lm}} = \tau_C \tau_{\dot{e}_{lm}}^P,$$

$$\begin{aligned} \tau_C &= \text{hardening parameter} \\ &= \tau_C(\tau_{\theta}). \end{aligned}$$

Following the development of eq. (22), it can be shown [18] that

$$\tau_{\Lambda} = \frac{(\tau_{s_{ij}} - \tau_{\alpha_{ij}}) \tau_{C_{ijmn}}^E (\tau_{\dot{e}_{mn}} - \tau_{\dot{e}_{mn}}^C - \tau_{\dot{e}_{mn}}^{TH}) + (\tau_{s_{ij}} - \tau_{\alpha_{ij}}) \tau_{\dot{C}_{ijcd}}^E \tau_{e_{cd}}^E - \frac{2}{3} \tau_{\sigma_y} \frac{\partial \tau_{\sigma_y}}{\partial \tau_{\theta}} \tau_{\dot{\theta}}}{\frac{2}{3} \tau_{\sigma_y}^2 \tau_C + (\tau_{s_{ij}} - \tau_{\alpha_{ij}}) \tau_{C_{ijmn}}^E (\tau_{s_{mn}} - \tau_{\alpha_{mn}})} \quad (29)$$

To further evaluate eq. (24), it is necessary to obtain both τ_C and $\partial \tau_{\sigma_y} / \partial \tau_{\theta}$. As was done for the case of isotropic hardening, we use the idealized, bilinear, engineering stress-strain curves shown in fig. 1 and now assume that the

relationship between τ_{σ_y} and τ_{θ} is the same as that between the virgin material yield stress and temperature. That is, τ_{σ_y} is simply the virgin material yield stress corresponding to τ_{θ} .

For the hardening parameter τ_C , consider a case of uniaxial loading at constant temperature such that

$$\begin{aligned} \tau_{\sigma_{11}} &\neq 0, & \text{all other } \tau_{\sigma_{ij}} &= 0, \\ \tau_{\dot{\sigma}_{11}} &\neq 0, & \text{all other } \tau_{\dot{\sigma}_{ij}} &= 0, \\ \tau_{s_{22}} &= \tau_{s_{33}} = -\frac{1}{2}\tau_{s_{11}}, \\ \tau e_{22}^P &= \tau e_{33}^P = -\frac{1}{2}\tau e_{11}^P, & \text{all other } \tau e_{ij}^P &= 0, \\ \tau \dot{e}_{22}^P &= \tau \dot{e}_{33}^P = -\frac{1}{2}\tau \dot{e}_{11}^P, & \text{all other } \tau \dot{e}_{ij}^P &= 0, \\ \tau_{\sigma_y} &= \text{constant}. \end{aligned} \quad (25)$$

Evaluating $\tau F = 0$ and $\tau \dot{F} = 0$ for the above loading condition results in

$$(\tau_{s_{11}} - \tau_{\alpha_{11}})^2 = \frac{2}{3}\tau_{\sigma_y}^2 \quad (26)$$

and

$$(\tau_{s_{11}} - \tau_{\alpha_{11}})(\tau_{\dot{\sigma}_{11}} - \frac{3}{2}\tau_C \tau \dot{e}_{11}^P) = 0. \quad (27)$$

The above equations require that

$$\tau_{\dot{\sigma}_{11}} = \frac{3}{2}\tau_C \tau \dot{e}_{11}^P, \quad (28)$$

or

$$d\sigma_{11} = \frac{3}{2}\tau_C de_{11}^P. \quad (29)$$

Referring to the idealized stress–plastic strain curves shown in fig. 2, the infinitesimal stress increment $d\sigma$ at constant temperature is given by

$$d\sigma = \frac{\tau_E \tau_{E_T}}{\tau_E - \tau_{E_T}} de^P. \quad (30)$$

Comparing eqs. (29) and (30) shows that

$$\tau_C = \frac{2}{3} \frac{\tau_E \tau_{E_T}}{\tau_E - \tau_{E_T}}. \quad (31)$$

Substituting eq. (31) into eq. (24) and using the definitions of τ_{σ_y} , $\tau_{C_{ijrs}}^E$, and $\tau_{s_{ij}}$, we obtain

$$\tau_{\Lambda} = \frac{\tau_{\mu}(\tau_{s_{mn}} - \tau_{\alpha_{mn}})(\tau \dot{e}_{mn} - \tau \dot{e}_{mn}^C - \tau \dot{e}_{mn}^{TH}) + \tau_{\mu}(\tau_{s_{mn}} - \tau_{\alpha_{mn}}) \tau e_{mn}^E - \frac{\tau_{\sigma_{yv}}}{3} \frac{\partial \tau_{\sigma_{yv}}}{\partial \tau_{\theta}} \tau_{\dot{\theta}}}{\frac{2}{3} \tau_{\sigma_y}^2 \left[\tau_{\mu} + \frac{1}{3} \frac{\tau_E \tau_{E_T}}{\tau_E - \tau_{E_T}} \right]}. \quad (32)$$

2.2. Applicability of the model

The model is suitable for use in small strain and displacement analysis. However, it is also directly applicable to problems involving small strains and large rotations [20].

When using the model for practical engineering analyses, it is important to be aware of the limitations of the theories upon which it is based. The classical theory of time-independent plasticity does not accurately predict

material behavior under general, non-radial loading conditions [27–29]. In addition, the O.R.N.L. auxiliary strain hardening rules were developed for radial or near-radial loading. Based on limited experimental results [27,28], the kinematic hardening formulation is recommended for cyclic, radial or near-radial loading. The isotropic hardening formulation is recommended only for situations involving monotonically increasing, radial or near-radial loading.

3. Solution procedure

The proposed solution procedure is based on a one-parameter integration method for ordinary differential equations (the α -method) which is used in conjunction with the thermo-elastic-plastic and creep material model developed in section 2. For a range of values of the parameter, this integration method has been shown to be unconditionally stable for certain heat conduction [22,23] and viscoplasticity problems [3,4,6].

The solution procedure uses one time step size for the calculation of nodal point displacements and a smaller one for element integration point stresses, plastic strains, and creep strains. This approach is based on the observation that for many problems of engineering interest involving inelastic behavior, the time-wise variation in the stresses and inelastic strains is greater than that of the displacements [16–19].

In the following, we investigate the stability of the solution procedure via the calculations for the element integration point stresses. We assume that the stability characteristics associated with these particular calculations carry over to the other solution variables. Only the case of isotropic hardening is examined. However, similar conclusions can be reached for kinematic hardening [20].

3.1. The α -method

Consider a system of first-order, ordinary differential equations of the form

$${}^{\tau}\dot{\mathbf{x}} = {}^{\tau}\mathbf{A} {}^{\tau}\mathbf{x}, \quad (33)$$

where τ denotes some arbitrary time. Assuming that an approximate numerical solution ${}^{\tau}\mathbf{x}$ is known, the next approximate solution ${}^{\tau+\Delta t}\mathbf{x}$ is given by

$${}^{\tau+\Delta t}\mathbf{x} = {}^{\tau}\mathbf{x} + {}^{\tau+\alpha\Delta t}\dot{\mathbf{x}} \Delta t, \quad (34)$$

where

$${}^{\tau+\alpha\Delta t}\dot{\mathbf{x}} = {}^{\tau+\alpha\Delta t}\mathbf{A} {}^{\tau+\alpha\Delta t}\mathbf{x}, \quad (35)$$

$${}^{\tau+\alpha\Delta t}\mathbf{x} = (1 - \alpha) {}^{\tau}\mathbf{x} + \alpha {}^{\tau+\Delta t}\mathbf{x}, \quad 0 \leq \alpha \leq 1, \quad (36)$$

$${}^{\tau+\alpha\Delta t}\mathbf{A} = {}^{\tau+\alpha\Delta t}\mathbf{A}({}^{\tau+\alpha\Delta t}\mathbf{x}, \tau + \alpha\Delta t). \quad (37)$$

Substituting eqs. (35)–(37) into eq. (34) yields:

$$[I - \alpha\Delta t {}^{\tau+\alpha\Delta t}\mathbf{A}] {}^{\tau+\Delta t}\mathbf{x} = [I + (1 - \alpha)\Delta t {}^{\tau+\alpha\Delta t}\mathbf{A}] {}^{\tau}\mathbf{x}. \quad (38)$$

Eq. (38) must generally be solved for ${}^{\tau+\Delta t}\mathbf{x}$ in an iterative manner, but a direct solution is possible when ${}^{\tau}\mathbf{A}$ is a constant matrix. Note that $\alpha = 0$ and $\alpha = 1$ are the Euler forward and backward methods, respectively. Additionally, $\alpha = \frac{1}{2}$ corresponds to the usual trapezoidal rule only when ${}^{\tau}\mathbf{A}$ is a constant matrix. It can be shown [20] that $\alpha = 0, 1$ have local truncation errors of $O(\Delta t^2)$ and that $\alpha = \frac{1}{2}$ has a local truncation error of $O(\Delta t^3)$.

3.2. Theoretical stability analysis

In investigating the solution procedure's stability characteristics, we are primarily interested in how roundoff errors are propagated through the numerical computations. For stability, it is required that roundoff errors not

be magnified as the numerical calculations progress. We note that the following analysis is not concerned with the truncation errors of the solution method. Such errors exist even if all arithmetic operations are performed exactly. While the truncation error directly affects the accuracy of a numerical method, stability is a primary requirement for an accurate solution. On the other hand, a stable solution can still be inaccurate due to large truncation errors or an excessive number of solution steps which result in roundoff accumulation (but not step-wise magnification).

In the development of the solution procedure in section 3.3, it will be shown that the calculations for the element integration point stresses lead to nonlinear algebraic equations of the form

$$[I - \alpha \Delta \tau {}^{\tau+\Delta\tau}A {}^{\tau+\Delta\tau}C] {}^{\tau+\Delta\tau}\mathbf{x} = [I + (1 - \alpha) \Delta \tau {}^{\tau+\Delta\tau}A {}^{\tau+\alpha\Delta\tau}C + {}^{\tau+\Delta\tau}AS] {}^{\tau}\mathbf{x} + L + {}^{\tau+\Delta\tau}AT, \quad (39)$$

where

${}^{\tau}\mathbf{x}$ = known vector of stresses,

${}^{\tau+\Delta\tau}\mathbf{x}$ = unknown vector of stresses,

L, T = known vectors with time-dependent components

${}^{\tau+\Delta\tau}A, S$ = known square matrices with time-dependent components

${}^{\tau+\alpha\Delta\tau}C$ = square matrix which is a function of the known and unknown solution variables

I = identity matrix.

Additionally, we require that ${}^{\tau+\Delta\tau}A$ be negative definite and that ${}^{\tau+\Delta\tau}C$ be positive semi-definite.

Now assume that there is some roundoff error ${}^{\tau}\epsilon$ in the numerical solution at time τ such that

$${}^{\tau}\mathbf{x}^* = {}^{\tau}\mathbf{x} + {}^{\tau}\epsilon. \quad (40)$$

If all arithmetic calculations are performed exactly, then the solution at time $\tau + \Delta\tau$ is

$$[I - \alpha \Delta \tau {}^{\tau+\Delta\tau}A {}^{\tau+\alpha\Delta\tau}C^*] {}^{\tau+\Delta\tau}\mathbf{x}^* = [I + (1 - \alpha) \Delta \tau {}^{\tau+\Delta\tau}A {}^{\tau+\alpha\Delta\tau}C^* + {}^{\tau+\Delta\tau}AS] {}^{\tau}\mathbf{x}^* + L + {}^{\tau+\Delta\tau}AT, \quad (41)$$

where

$${}^{\tau+\Delta\tau}\mathbf{x}^* = {}^{\tau+\Delta\tau}\mathbf{x} + {}^{\tau+\Delta\tau}\epsilon \quad (42)$$

and ${}^{\tau+\Delta\tau}\epsilon$ = propagated roundoff error and ${}^{\tau+\alpha\Delta\tau}C^*$ = perturbed version of ${}^{\tau+\alpha\Delta\tau}C$ due to ${}^{\tau}\epsilon$ and ${}^{\tau+\Delta\tau}\epsilon$.

It can be seen by referring to the definitions of ${}^{\tau+\alpha\Delta\tau}C$ in sections 3.3 and 3.4 that ${}^{\tau+\alpha\Delta\tau}C^*$ is also a positive semi-definite matrix.

Now consider the generalized eigenproblem [40]:

$${}^{\tau+\alpha\Delta\tau}C^* \Phi^* = \lambda {}^{\tau+\Delta\tau}A^{-1} \Phi^*, \quad (43)$$

with solutions

$${}^{\tau+\alpha\Delta\tau}C^* \Phi^* = {}^{\tau+\Delta\tau}A^{-1} \Phi^* \Lambda^*, \quad (44)$$

$$\Phi^* = [\Phi_1^*, \dots, \Phi_n^*],$$

$$\Lambda^* = \text{diag}[\lambda_i^*], \quad \lambda_i^* \leq 0.$$

The orthogonality properties of the eigenvectors are such that

$$\Phi^{*\text{T}} {}^{\tau+\Delta\tau}A^{-1} \Phi^* = I, \quad (45)$$

$$\Phi^{*\text{T}} {}^{\tau+\alpha\Delta\tau}C^* \Phi^* = \Lambda^*. \quad (46)$$

The n eigenvectors span an n -dimensional vector space. Therefore, we can write

$${}^{\tau+\Delta\tau}\mathbf{x} = \Phi^* {}^{\tau+\Delta\tau}\mathbf{z} \quad (47)$$

$${}^{\tau}\mathbf{x} = \Phi^* {}^{\tau}\mathbf{z}, \quad (48)$$

$${}^{\tau+\Delta\tau}\boldsymbol{\varepsilon} = \boldsymbol{\Phi}^* {}^{\tau+\Delta\tau}\boldsymbol{e}, \quad (49)$$

$$\boldsymbol{\tau}\boldsymbol{\varepsilon} = \boldsymbol{\Phi}^* \boldsymbol{\tau}\boldsymbol{e}. \quad (50)$$

Premultiplying eq. (41) by ${}^{\tau+\Delta\tau}\boldsymbol{A}^{-1}$ yields:

$$[{}^{\tau+\Delta\tau}\boldsymbol{A}^{-1} - \alpha\Delta\tau {}^{\tau+\alpha\Delta\tau}\boldsymbol{C}^*] {}^{\tau+\Delta\tau}\boldsymbol{x}^* = [{}^{\tau+\Delta\tau}\boldsymbol{A}^{-1} + (1 - \alpha)\Delta\tau {}^{\tau+\alpha\Delta\tau}\boldsymbol{C}^* + \boldsymbol{S}] \boldsymbol{\tau}\boldsymbol{x}^* + {}^{\tau+\Delta\tau}\boldsymbol{A}^{-1}\boldsymbol{L} + \boldsymbol{T}. \quad (51)$$

Substituting eqs. (47)–(50) into eq. (51), premultiplying by $\boldsymbol{\Phi}^*$ and using the orthogonality properties, eqs. (45) and (46), results in

$$[\boldsymbol{I} - \alpha\Delta\tau \boldsymbol{\Lambda}^*] ({}^{\tau+\Delta\tau}\boldsymbol{z} + {}^{\tau+\Delta\tau}\boldsymbol{e}) = [\boldsymbol{I} + (1 - \alpha)\Delta\tau \boldsymbol{\Lambda}^*] (\boldsymbol{\tau}\boldsymbol{z} + \boldsymbol{\tau}\boldsymbol{e}) + \boldsymbol{\Phi}^{*\text{T}} \boldsymbol{S} \boldsymbol{\Phi}^* (\boldsymbol{\tau}\boldsymbol{z} + \boldsymbol{\tau}\boldsymbol{e}) + \boldsymbol{\Phi}^{*\text{T}} {}^{\tau+\Delta\tau}\boldsymbol{A}^{-1}\boldsymbol{L} + \boldsymbol{\Phi}^{*\text{T}} \boldsymbol{T}. \quad (52)$$

To obtain an expression relating $\boldsymbol{\tau}\boldsymbol{e}$ and ${}^{\tau+\Delta\tau}\boldsymbol{e}$, we assume that ${}^{\tau+\alpha\Delta\tau}\boldsymbol{C}^* \simeq {}^{\tau+\alpha\Delta\tau}\boldsymbol{C}$, $\boldsymbol{\Phi}^* \simeq \boldsymbol{\Phi}$, and $\boldsymbol{\Lambda}^* \simeq \boldsymbol{\Lambda}$. The error terms now separate directly out of eq. (52) and we have

$$[\boldsymbol{I} - \alpha\Delta\tau \boldsymbol{\Lambda}] {}^{\tau+\Delta\tau}\boldsymbol{e} = [\boldsymbol{I} + (1 - \alpha)\Delta\tau \boldsymbol{\Lambda}] \boldsymbol{\tau}\boldsymbol{e} + \boldsymbol{\Phi}^{\text{T}} \boldsymbol{S} \boldsymbol{\Phi} \boldsymbol{\tau}\boldsymbol{e}. \quad (53)$$

For the j th component of ${}^{\tau+\Delta\tau}\boldsymbol{e}$, we obtain

$${}^{\tau+\Delta\tau}e_j = \frac{1 + (1 - \alpha)\Delta\tau\lambda_j}{1 - \alpha\Delta\tau\lambda_j} \boldsymbol{\tau}e_j + \frac{\{\boldsymbol{\Phi}^{\text{T}} \boldsymbol{S} \boldsymbol{\Phi} \boldsymbol{\tau}\boldsymbol{e}\}_j}{1 - \alpha\Delta\tau\lambda_j}. \quad (54)$$

Note that the second term on the right-hand side couples ${}^{\tau+\Delta\tau}e_j$ to all the components of $\boldsymbol{\tau}\boldsymbol{e}$.

As discussed previously, stability means that any roundoff error present at time τ is not magnified when the solution for time $\tau + \Delta\tau$ is calculated. Specifically, we require that

$$|{}^{\tau+\Delta\tau}\boldsymbol{\varepsilon}^{\text{T}} {}^{\tau+\Delta\tau}\boldsymbol{A}^{-1} {}^{\tau+\Delta\tau}\boldsymbol{e}| \leq |\boldsymbol{\tau}\boldsymbol{\varepsilon}^{\text{T}} {}^{\tau+\Delta\tau}\boldsymbol{A}^{-1} \boldsymbol{\tau}\boldsymbol{e}|. \quad (55)$$

Substituting eqs. (49) and (50) into eq. (55) and using eq. (45) results in

$$|{}^{\tau+\Delta\tau}\boldsymbol{e}^{\text{T}} {}^{\tau+\Delta\tau}\boldsymbol{e}| \leq |\boldsymbol{\tau}\boldsymbol{e}^{\text{T}} \boldsymbol{\tau}\boldsymbol{e}|. \quad (56)$$

A sufficient, but not necessary condition for eq. (56) to hold is

$$|{}^{\tau+\Delta\tau}e_j| \leq |\boldsymbol{\tau}e_j|. \quad (57)$$

Consider eq. (54) and examine the cases of $\boldsymbol{S} \equiv \mathbf{0}$ and $\boldsymbol{S} \neq \mathbf{0}$. In the first case, eq. (57) is satisfied if

$$\left| \frac{1 + (1 - \alpha)\Delta\tau\lambda_j}{1 - \alpha\Delta\tau\lambda_j} \right| \leq 1. \quad (58)$$

Recalling that $\lambda_j \leq 0$, $0 \leq \alpha \leq 1$, and $\Delta\tau > 0$, some algebraic manipulation shows that eq. (58) is satisfied for all $\Delta\tau > 0$ when $\alpha \geq \frac{1}{2}$. Thus, the algorithm can be made unconditionally stable. On the other hand, if $\alpha < \frac{1}{2}$ then eq. (58) requires

$$\Delta\tau \leq \frac{1}{(2\alpha - 1)\lambda_j}. \quad (59)$$

We note that this conditional stability limit may not be useful for practical computations since λ_j generally depends on the unknown solution at time $\tau + \Delta\tau$. The only exception is when $\alpha = 0$, in which case λ_j is determined by the known conditions at time τ .

However, when $\boldsymbol{S} \neq \mathbf{0}$ there is no a priori information available concerning the second term on the right-hand side of eq. (54). At present, the best approach is to make all of the coefficients of $\boldsymbol{\tau}\boldsymbol{e}_i$ as small as possible. This means having the condition in eq. (58) as well as requiring that the denominator of the above-mentioned term be as large as possible. For specified $\Delta\tau$ and $\lambda_j \leq 0$, this latter condition occurs when $\alpha = 1$.

3.3. Special case

In this section we develop an algorithm for the special case in which a common time step size is used for all solution variables. Assuming that a numerical solution has been obtained at discrete time points $\Delta t, 2\Delta t, \dots, t$, the solution for $t + \Delta t$ is desired.

3.3.1. Equilibrium and constitutive equations

At time $t + \Delta t$, consider the virtual work equation for an isoparametric, finite element assemblage [40] and the constitutive equations for a thermo-elastic-plastic and creep material with isotropic hardening. All equations are expressed in vector form [18] as

$$\sum_{m=1}^N \int_{v(m)} B_L^T {}^{t+\Delta t} \sigma \, dv = {}^{t+\Delta t} R, \quad (60)$$

$${}^{t+\Delta t} \sigma = {}^{t+\Delta t} C^E ({}^{t+\Delta t} e - {}^{t+\Delta t} e^P - {}^{t+\Delta t} e^C - {}^{t+\Delta t} e^{TH}), \quad (61)$$

$$\tau e^P = \tau \wedge D \tau \sigma, \quad (62)$$

$$\tau e^C = \tau \gamma D \tau \sigma, \quad (63)$$

$${}^{t+\Delta t} e^{TH} = {}^{t+\Delta t} \alpha_m ({}^{t+\Delta t} \theta - \theta_R) \delta, \quad (64)$$

where

$${}^{t+\Delta t} e = B_L {}^{t+\Delta t} U \quad (65)$$

and

B_L = total strain-displacement transformation matrix,

${}^{t+\Delta t} U$ = nodal point displacement vector,

${}^{t+\Delta t} R$ = nodal point external load vector,

N = number of elements in the assemblage,

D = deviatoric stress operator matrix,

$\delta^T = [1, 1, 1, 0, 0, 0]$.

Henceforth, the summation sign in eq. (60) will be dropped for convenience, but the summation is implied for all subsequent volume integrals. Although eqs. (61)–(64) are valid at any point in the structure or continuum, only the stresses and strains at the element integration points [40] will be of interest.

Substituting eqs. (61) and (65) into eq. (60) results in

$${}^{t+\Delta t} K^E {}^{t+\Delta t} U = {}^{t+\Delta t} R + \int_v B_L^T {}^{t+\Delta t} C^E ({}^{t+\Delta t} e^P + {}^{t+\Delta t} e^C + {}^{t+\Delta t} e^{TH}) \, dv, \quad (66)$$

where

$${}^{t+\Delta t} K^E = \int_v B_L^T {}^{t+\Delta t} C^E B_L \, dv \quad (67)$$

is the elastic stiffness matrix.

3.3.2. Algorithm development

The α -method is used to obtain ${}^{t+\Delta t}e^P$ and ${}^{t+\Delta t}e^C$. Quantities at time $t + \Delta t$ are first decomposed as

$${}^{t+\Delta t}e^P = {}^t e^P + e^P, \quad (68)$$

$${}^{t+\Delta t}e^C = {}^t e^C + e^C \quad (69)$$

and then the increments are given by

$$e^P = \Delta t {}^{t+\alpha\Delta t} \dot{e}^P = \Delta t {}^{t+\alpha\Delta t} \Lambda D {}^{t+\alpha\Delta t} \sigma, \quad (70)$$

$$e^C = \Delta t {}^{t+\alpha\Delta t} \dot{e}^C = \Delta t {}^{t+\alpha\Delta t} \gamma D {}^{t+\alpha\Delta t} \sigma, \quad (71)$$

where

$${}^{t+\alpha\Delta t} \sigma = (1 - \alpha) {}^t \sigma + \alpha {}^{t+\Delta t} \sigma \quad (72)$$

and

$${}^{t+\alpha\Delta t} \Lambda = {}^{t+\alpha\Delta t} \Lambda ({}^{t+\alpha\Delta t} \sigma, {}^{t+\alpha\Delta t} \dot{e}, {}^{t+\alpha\Delta t} \dot{e}^C, {}^{t+\alpha\Delta t} \dot{\theta}, \dots), \quad (73)$$

$${}^{t+\alpha\Delta t} \gamma = {}^{t+\alpha\Delta t} \gamma ({}^{t+\alpha\Delta t} \sigma, {}^{t+\alpha\Delta t} \bar{e}^H, {}^{t+\alpha\Delta t} \dot{\theta}).$$

Eqs. (61), (64), (66), and (68) to (73) are a coupled set of nonlinear algebraic equations where eqs. (61), (64) and (68) to (73) apply at each integration point.

Nonlinear algebraic equations generally require an iterative solution procedure [42]. Starting with the simplest approach – successive substitution – an appropriate algorithm is

$${}^{t+\Delta t} e^{C(i+1)} = {}^t e^C + \Delta t {}^{t+\alpha\Delta t} \gamma^{(i)} D {}^{t+\alpha\Delta t} \sigma^{(i)}, \quad (74)$$

$${}^{t+\Delta t} e^{P(i+1)} = {}^t e^P + \Delta t {}^{t+\alpha\Delta t} \Lambda^{(i)} D {}^{t+\alpha\Delta t} \sigma^{(i)}, \quad (75)$$

$${}^{t+\Delta t} K^E {}^{t+\Delta t} U^{(i+1)} = {}^{t+\Delta t} R + \int_B^T {}^{t+\Delta t} C^E ({}^{t+\Delta t} e^{P(i+1)} + {}^{t+\Delta t} e^{C(i+1)} + {}^{t+\Delta t} e^{TH}) dv, \quad (76)$$

$${}^{t+\Delta t} \sigma^{(i+1)} = {}^{t+\Delta t} C^E ({}^{t+\Delta t} e^{(i+1)} - {}^{t+\Delta t} e^{P(i+1)} - {}^{t+\Delta t} e^{C(i+1)} - {}^{t+\Delta t} e^{TH}), \quad i = 0, 1, 2, \dots \quad (77)$$

The right superscript i is the iteration number and $i = 0$ refers to conditions at time t .

The above scheme can be rewritten by defining

$$\Delta U^{(i+1)} = {}^{t+\Delta t} U^{(i+1)} - {}^{t+\Delta t} U^{(i)}. \quad (78)$$

Substituting eq. (78) into eq. (76) and using eqs. (65) and (67) results in

$${}^{t+\Delta t} K^E \Delta U^{(i+1)} = {}^{t+\Delta t} R - \int_B^T {}^{t+\Delta t} C^E ({}^{t+\Delta t} e^{(i)} - {}^{t+\Delta t} e^{P(i+1)} - {}^{t+\Delta t} e^{C(i+1)} - {}^{t+\Delta t} e^{TH}) dv. \quad (79)$$

Noting the similarity between the right-hand sides of eqs. (77) and (79), the successive substitution algorithm is now written as

$${}^{t+\Delta t} e^{C(i+1)} = {}^t e^C + \Delta t {}^{t+\alpha\Delta t} \gamma^{(i)} D {}^{t+\alpha\Delta t} \sigma^{(i)}, \quad (80)$$

$${}^{t+\Delta t} e^{P(i+1)} = {}^t e^P + \Delta t {}^{t+\alpha\Delta t} \Lambda^{(i)} D {}^{t+\alpha\Delta t} \sigma^{(i)}, \quad (81)$$

$${}^{t+\Delta t} \sigma^{(i+1)} = {}^{t+\Delta t} C^E ({}^{t+\Delta t} e^{(i)} - {}^{t+\Delta t} e^{P(i+1)} - {}^{t+\Delta t} e^{C(i+1)} - {}^{t+\Delta t} e^{TH}), \quad (82)$$

$${}^{t+\Delta t} K^E \Delta U^{(i+1)} = {}^{t+\Delta t} R - \int_B^T {}^{t+\Delta t} \sigma^{(i+1)} dv, \quad (83)$$

$${}^{t+\Delta t}U^{(i+1)} = {}^{t+\Delta t}U^{(i)} + \Delta U^{(i+1)}, \quad i = 0, 1, 2, \dots \quad (84)$$

Assuming that the iteration converges, $\Delta U^{(i+1)} \rightarrow 0$ and hence all of the governing equations are satisfied. Furthermore, by iterating with $\Delta U^{(i+1)}$ instead of ${}^{t+\Delta t}U^{(i+1)}$, it is possible to use stiffness matrices other than ${}^{t+\Delta t}K^E$ in eq. (83) so as to obtain faster convergence [24].

The scheme described in eqs. (81)–(84) has two immediate drawbacks. Successive substitution can have a slow rate-of-convergence [42]. Additionally, disk I/O operations are required in each iteration (assuming that integration point variables are not continually stored in-core). If the restriction of no disk writing during the iteration is imposed, then the following algorithm (still based on successive substitution) can be used.

$$\left[\begin{array}{l} \text{displacement loop} \\ \left[\begin{array}{l} \text{integration} \\ \text{point loop} \end{array} \right. \end{array} \right. \quad {}^{t+\Delta t}e_{(k+1)}^C = {}^te^C + \Delta t \, {}^{t+\alpha\Delta t}\gamma_{(k)}^{(i)} D \, {}^{t+\alpha\Delta t}\sigma_{(k)}^{(i)}, \quad (85)$$

$${}^{t+\Delta t}e_{(k+1)}^P = {}^te^P + \Delta t \, {}^{t+\alpha\Delta t}\Lambda_{(k)}^{(i)} D \, {}^{t+\alpha\Delta t}\sigma_{(k)}^{(i)}, \quad (86)$$

$${}^{t+\Delta t}\sigma_{(k+1)}^{(i)} = {}^{t+\Delta t}C^E ({}^{t+\Delta t}e^{(i)} - {}^{t+\Delta t}e_{(k+1)}^P) - {}^{t+\Delta t}e_{(k+1)}^C - {}^{t+\Delta t}e^{TH}), \quad k = 0, 1, 2, \dots, \quad (87)$$

$${}^{t+\Delta t}K^E \Delta U^{(i+1)} = {}^{t+\Delta t}R - \int_v B_L^T {}^{t+\Delta t}\sigma^{(i)} dv, \quad (88)$$

$${}^{t+\Delta t}U^{(i+1)} = {}^{t+\Delta t}U^{(i)} + \Delta U^{(i+1)}, \quad i = 0, 1, 2, \dots \quad (89)$$

The right subscript k is the integration point loop iteration counter and the right superscript i is the displacement loop iteration counter. Note that $k = 0$ indicates conditions at time t and that ${}^{t+\Delta t}U^{(0)} = {}^tU$, ${}^{t+\Delta t}e^{(0)} = {}^te$.

The integration point loop iteration continues until a steady value is obtained for ${}^{t+\Delta t}\sigma^{(i)}$. The displacement loop iteration continues until $\Delta U^{(i+1)} \rightarrow 0$. When $i = 0$, the integration point calculations are performed only once (i.e., for $k = 0$ only).

The above algorithm trades disk writing operations for more computational effort. For each value of ${}^{t+\Delta t}e^{(i)}$, it is necessary to calculate ${}^{t+\Delta t}\sigma^{(i)}$, ${}^{t+\Delta t}e^P(i)$, and ${}^{t+\Delta t}e^C(i)$ by starting from the corresponding values at time t . On the other hand, the converged integration point loop values satisfy the constitutive equations (within the approximations of the α -method). This can be advantageous in plasticity problems when yielding or unloading occurs during a solution step [24].

However, both computational loops can still suffer from slow rates-of-convergence. Considering first the integration point loop, one possible improvement is to solve eqs. (85)–(87) using Newton–Raphson iteration [42]. In three dimensional analysis, this means that a system of eighteen algebraic equations must be repeatedly solved at each integration point. The increased rate-of-convergence could easily be offset by the increase in computational effort.

As a compromise, the following scheme is proposed. It assumes that the stress-dependent terms in the creep constitutive law are the most troublesome from a convergence point-of-view. From eqs. (69) and (71), define

$${}^{t+\alpha\Delta t}f = {}^te^C + e^C = {}^te^C + \Delta t \, {}^{t+\alpha\Delta t}\gamma D \, {}^{t+\alpha\Delta t}\sigma. \quad (90)$$

Expanding ${}^{t+\alpha\Delta t}f$ in a two-term Taylor series [42] about the k th approximate solution ${}^{t+\alpha\Delta t}\sigma_{(k)}$ yields:

$${}^{t+\alpha\Delta t}f_{(k+1)} = {}^{t+\alpha\Delta t}f_{(k)} + \left[\frac{\partial {}^{t+\alpha\Delta t}f}{\partial {}^{t+\alpha\Delta t}\sigma} \right]_{(k)} ({}^{t+\alpha\Delta t}\sigma_{(k+1)} - {}^{t+\alpha\Delta t}\sigma_{(k)}), \quad (91)$$

where the Jacobian matrix is

$$\left[\frac{\partial {}^{t+\alpha\Delta t}f}{\partial {}^{t+\alpha\Delta t}\sigma} \right]_{(k)} = \Delta t \left[D \, {}^{t+\alpha\Delta t}\sigma \frac{\partial {}^{t+\alpha\Delta t}\gamma}{\partial {}^{t+\alpha\Delta t}\sigma} + {}^{t+\alpha\Delta t}\gamma D \right]_{(k)}. \quad (92)$$

The evaluation of the term $\partial^{t+\alpha\Delta t}\gamma/\partial^{t+\alpha\Delta t}\sigma$ depends on the particular type of creep law being considered [20]. Substituting eqs. (88)–(90) into eq. (61) and solving for ${}^{t+\Delta t}\sigma_{(k+1)}$ results in;

$$\left[I + \alpha\Delta t {}^{t+\Delta t}C^E \left[D {}^{t+\alpha\Delta t}\sigma \frac{\partial^{t+\alpha\Delta t}\gamma}{\partial^{t+\alpha\Delta t}\sigma} + {}^{t+\Delta t}\gamma D \right]_{(k)} \right] {}^{t+\Delta t}\sigma_{(k+1)} = {}^{t+\Delta t}C^E (B_L {}^{t+\Delta t}U - {}^{t+\Delta t}e^P - {}^te^C - {}^{t+\Delta t}e^{TH} - \Delta t {}^{t+\alpha\Delta t}\gamma_{(k)} D {}^{t+\alpha\Delta t}\sigma_{(k)}) + \alpha\Delta t {}^{t+\Delta t}C^E \left[D {}^{t+\alpha\Delta t}\sigma \frac{\partial^{t+\alpha\Delta t}\gamma}{\partial^{t+\alpha\Delta t}\sigma} + {}^{t+\alpha\Delta t}\gamma D \right]_{(k)} {}^{t+\Delta t}\sigma_{(k)}. \quad (93)$$

When $i > 0$, eqs. (85)–(87) (the integration point loop) are replaced by

$${}^{t+\Delta t}e_{(k+1)}^{P(i)} = {}^te^P + \Delta t {}^{t+\alpha\Delta t}\Lambda_{(k)}^{(i)} D {}^{t+\alpha\Delta t}\sigma_{(k)}^{(i)}, \quad (94)$$

$$\left[I + \alpha\Delta t {}^{t+\Delta t}C^E \left[D {}^{t+\alpha\Delta t}\sigma^{(i)} \frac{\partial^{t+\alpha\Delta t}\gamma^{(i)}}{\partial^{t+\alpha\Delta t}\sigma^{(i)}} + {}^{t+\alpha\Delta t}\gamma^{(i)} D \right]_{(k)} \right] {}^{t+\Delta t}\sigma_{(k+1)}^{(i)} = {}^{t+\Delta t}C^E ({}^{t+\Delta t}e^{(i)} - {}^{t+\Delta t}e_{(k+1)}^{P(i)} - {}^te^C - {}^{t+\Delta t}e^{TH} - \Delta t {}^{t+\alpha\Delta t}\gamma_{(k)}^{(i)} D {}^{t+\alpha\Delta t}\sigma_{(k)}^{(i)}) + \alpha\Delta t {}^{t+\Delta t}C^E \left[D {}^{t+\alpha\Delta t}\sigma^{(i)} \frac{\partial^{t+\alpha\Delta t}\gamma^{(i)}}{\partial^{t+\alpha\Delta t}\sigma^{(i)}} + {}^{t+\alpha\Delta t}\gamma^{(i)} D \right]_{(k)} {}^{t+\Delta t}\sigma_{(k)}^{(i)}, \quad (95)$$

$${}^{t+\Delta t}e_{(k+1)}^{C(i)} = {}^te^C + \Delta t {}^{t+\alpha\Delta t}\gamma_{(k)}^{(i)} D {}^{t+\alpha\Delta t}\sigma_{(k)}^{(i)} + \alpha\Delta t \left[D {}^{t+\alpha\Delta t}\sigma^{(i)} \frac{\partial^{t+\alpha\Delta t}\gamma^{(i)}}{\partial^{t+\alpha\Delta t}\sigma^{(i)}} + {}^{t+\alpha\Delta t}\gamma^{(i)} D \right]_{(k)} ({}^{t+\Delta t}\sigma_{(k+1)}^{(i)} - {}^{t+\alpha\Delta t}\sigma_{(k)}^{(i)}). \quad (96)$$

However, when $i = 0$ we still use eqs. (85)–(87) and the integration point calculations are performed only once (i.e., for $k = 0$ only). We also note that when there are no creep effects, the above algorithm degenerates back to successive substitution.

In the displacement loop, the rate-of-convergence can be improved by several methods. The most common approach is to use an elastic-plastic [2,17], elastic-creep [10] or elastic-plastic-creep [14,15] stiffness matrix in eq. (88). Alternatively, the use of matrix updating and search algorithms has been found to be highly effective [24].

3.3.3. Stability analysis

To investigate the stability of the solution procedure we establish a set of equations relating ${}^{t+\Delta t}\sigma$ and ${}^t\sigma$ at each integration point in the finite element assemblage. First, the decompositions

$${}^{t+\Delta t}U = {}^tU + U, \quad {}^{t+\Delta t}C^E = {}^tC^E + C^E, \quad (97)$$

$${}^{t+\Delta t}e^{TH} = {}^te^{TH} + e^{TH}, \quad {}^{t+\Delta t}R = {}^tR + R,$$

are substituted into eqs. (61) and (66) along with eqs. (65) and (67)–(69) so as to obtain

$${}^{t+\Delta t}\sigma = {}^{t+\Delta t}C^E (B_L U - e^P - e^C - e^{TH}) + (I + C^E {}^tF^E) {}^t\sigma \quad (98)$$

and

$${}^{t+\Delta t}K^E U = {}^tR + R + \int_v B_L^T {}^{t+\Delta t}C^E (e^P + e^C + e^{TH}) dv - \int_v B_L^T (I + C^E {}^tF^E) {}^t\sigma dv, \quad (99)$$

where

$${}^t F^E \boldsymbol{\sigma} = {}^t e - {}^t e^P - {}^t e^C - {}^t e^{TH} \quad (100)$$

Assuming an equilibrium configuration at time t , the corresponding virtual work equation is

$$\int_v B_L^T \boldsymbol{\sigma} \, dv = {}^t R \quad (101)$$

and hence eq. (97) simplifies to

$${}^{t+\Delta t} K^E U = R + \int_v B_L^T {}^{t+\Delta t} C^E (e^P + e^C + e^{TH}) \, dv - \int_v B_L^T C^E {}^t F^E \boldsymbol{\sigma} \, dv \quad (102)$$

In isoparametric finite element analysis, the volume integrals in eq. (102) are typically evaluated using Gauss numerical integration [40]. That is, a volume integral over the element assemblage can be expressed as

$$\int_v f(x) \, dv = \sum_{i=1}^N \int_{v^{(i)}} f(x) \, dv = \sum_{j=1}^M w_j f(x_j) \quad (103)$$

where

- w_j = Gauss weighting factor; $w_j > 0$,
- N = number of elements,
- M = number of integration points,

Following the approach taken in [5], we define super matrices and vectors where each submatrix and subvector corresponds to a particular integration point (denoted by a right subscript).

$$\tilde{B}_L = \begin{bmatrix} B_{L_1} \\ (6 \times n) \\ \text{---} \\ B_{L_2} \\ \text{---} \\ \vdots \\ \text{---} \\ B_{L_M} \\ (6M \times n) \end{bmatrix} \quad (104)$$

$${}^t \tilde{\Sigma} = \begin{bmatrix} {}^t \sigma_1 \\ (6 \times 1) \\ \text{---} \\ {}^t \sigma_2 \\ \text{---} \\ \vdots \\ \text{---} \\ {}^t \sigma_M \\ (6M \times 1) \end{bmatrix} \quad (105)$$

$${}^{t+\Delta t} C^E = \begin{bmatrix} {}^{t+\Delta t} C_1^E \\ (6 \times 6) \\ \text{---} \\ {}^{t+\Delta t} C_2^E \\ \text{---} \\ \vdots \\ \text{---} \\ {}^{t+\Delta t} C_M^E \end{bmatrix} \quad (106)$$

$$\tilde{D} = \begin{bmatrix} D & & \\ (6 \times 6) & & \\ & D & \\ & & \ddots & \\ & & & D \end{bmatrix}, \quad (107)$$

$$\tilde{W} = \begin{bmatrix} w_1 I & & \\ (6 \times 6) & & \\ & w_2 I & \\ & & \ddots & \\ & & & w_M I \end{bmatrix}, \quad (108)$$

where n is the number of degrees-of-freedom in the element assemblage. In addition, the super matrices \tilde{C}^E , ${}^t\tilde{F}^E$, and \tilde{F}^E are defined to be of the same form as ${}^{t+\Delta t}\tilde{C}^E$, the super vectors ${}^{t+\Delta t}\tilde{\Sigma}$ and \tilde{E}^{TH} are of the same form as ${}^t\tilde{\Sigma}$, and the super matrices ${}^{t+\alpha\Delta t}\tilde{\gamma}$ and ${}^{t+\alpha\Delta t}\tilde{\Lambda}$ are of the same form as \tilde{W} . Using eqs. (103)–(108), the volume integrals in eq. (102) are expressed as

$$\int_v \tilde{B}_L^T {}^{t+\Delta t}\tilde{C}^E (e^P + e^C + e^{TH}) dv = \tilde{B}_L^T {}^{t+\Delta t}\tilde{C}^E \tilde{W} (\tilde{E}^P + \tilde{E}^{TH}), \quad (109)$$

$$\int_v \tilde{B}_L^T C^E {}^tF^E {}^t\sigma dv = \tilde{B}_L^T \tilde{C}^E {}^t\tilde{F}^E \tilde{W} {}^t\tilde{\Sigma}. \quad (110)$$

Substituting eq. (72) into eqs. (70) and (71) results in

$$e^P = \Delta t {}^{t+\alpha\Delta t}\tilde{\Lambda} D [(1 - \alpha) {}^t\sigma + {}^{t+\Delta t}\sigma], \quad (111)$$

$$e^C = \Delta t {}^{t+\alpha\Delta t}\tilde{\gamma} D [(1 - \alpha) {}^t\sigma + \alpha {}^{t+\Delta t}\sigma] \quad (112)$$

and hence the corresponding super vectors are

$$\tilde{E}^P = \Delta t {}^{t+\alpha\Delta t}\tilde{\Lambda} \tilde{D} [(1 - \alpha) {}^t\tilde{\Sigma} + \alpha {}^{t+\Delta t}\tilde{\Sigma}], \quad (113)$$

$$\tilde{E}^C = \Delta t {}^{t+\alpha\Delta t}\tilde{\gamma} \tilde{D} [(1 - \alpha) {}^t\tilde{\Sigma} + \alpha {}^{t+\Delta t}\tilde{\Sigma}]. \quad (114)$$

Now substituting eqs. (109), (110), (113) and (114) into eq. (102) yields:

$$\begin{aligned} {}^{t+\Delta t}K^E U = R + \tilde{B}_L^T {}^{t+\Delta t}\tilde{C}^E \tilde{W} \tilde{E}^{TH} + [(1 - \alpha) \Delta t \tilde{B}_L^T {}^{t+\Delta t}\tilde{C}^E \tilde{W} {}^{t+\alpha\Delta t}\tilde{G} \tilde{D} - \tilde{B}_L^T \tilde{C}^E {}^t\tilde{F}^E \tilde{W}] {}^t\tilde{\Sigma} \\ + \alpha \Delta t \tilde{B}_L^T {}^{t+\alpha\Delta t}\tilde{C}^E \tilde{W} {}^{t+\alpha\Delta t}\tilde{G} \tilde{D} {}^{t+\Delta t}\tilde{\Sigma}, \end{aligned} \quad (115)$$

where

$${}^{t+\alpha\Delta t}\tilde{G} = {}^{t+\alpha\Delta t}\tilde{\gamma} + {}^{t+\alpha\Delta t}\tilde{\Lambda}. \quad (116)$$

Substituting eqs. (111) and (112) into eq. (98) and then generalizing to a complete set of integration point equations yields:

$$[\tilde{I} + \alpha \Delta t {}^{t+\alpha \Delta t} \tilde{C} {}^{t+\Delta t} \tilde{C}^E \tilde{D}] {}^{t+\Delta t} \Sigma = {}^{t+\Delta t} \tilde{C}^E (\tilde{B}_L U - \tilde{E}^{TH}) + [\tilde{I} + \tilde{C}^E {}^t \tilde{F}^E - (1 - \alpha) \Delta t {}^{t+\alpha \Delta t} \tilde{C} {}^{t+\Delta t} \tilde{C}^E \tilde{D}] {}^t \tilde{\Sigma}, \quad (117)$$

where \tilde{I} is a $6M \times 6M$ identity matrix. The final set of integration point stress equations is now obtained by substituting eq. (115) and the identity [20]

$$({}^{t+\Delta t} \tilde{C}^E \tilde{B}_L {}^{t+\Delta t} K^E {}^{-1} \tilde{B}_L^T - \tilde{W}^{-1}) \tilde{W} \tilde{C}^E {}^t \tilde{F}^E = - ({}^{t+\Delta t} \tilde{C}^E \tilde{B}_L {}^{t+\Delta t} K^E {}^{-1} \tilde{B}_L^T {}^{t+\Delta t} \tilde{C}^E - {}^{t+\Delta t} \tilde{C}^E \tilde{W}^{-1}) \tilde{W} \tilde{F}^E \quad (118)$$

into eq. (119). The result is:

$$\begin{aligned} & [\tilde{I} - \alpha \Delta t [{}^{t+\Delta t} \tilde{C}^E \tilde{B}_L {}^{t+\Delta t} K^E {}^{-1} \tilde{B}_L^T {}^{t+\Delta t} \tilde{C}^E - {}^{t+\Delta t} \tilde{C}^E \tilde{W}^{-1}] \tilde{W} {}^{t+\alpha \Delta t} \tilde{C} \tilde{D}] {}^{t+\Delta t} \tilde{\Sigma} = \\ & {}^{t+\Delta t} \tilde{C}^E \tilde{B}_L {}^{t+\Delta t} K^E {}^{-1} R + [{}^{t+\Delta t} \tilde{C}^E \tilde{B}_L {}^{t+\Delta t} K^E {}^{-1} \tilde{B}_L^T {}^{t+\Delta t} \tilde{C}^E - {}^{t+\Delta t} \tilde{C}^E \tilde{W}^{-1}] \tilde{W} \tilde{E}^{TH} \\ & + [\tilde{I} + (1 + \alpha) \Delta t [{}^{t+\Delta t} \tilde{C}^E \tilde{B}_L {}^{t+\Delta t} K^E {}^{-1} \tilde{B}_L^T {}^{t+\Delta t} \tilde{C}^E - {}^{t+\Delta t} \tilde{C}^E \tilde{W}^{-1}] {}^{t+\alpha \Delta t} \tilde{C} \tilde{D} \\ & + [{}^{t+\Delta t} \tilde{C}^E \tilde{B}_L {}^{t+\Delta t} K^E {}^{-1} \tilde{B}_L^T {}^{t+\Delta t} \tilde{C}^E - {}^{t+\Delta t} \tilde{C}^E \tilde{W}^{-1}] \tilde{W} \tilde{F}^E] {}^t \tilde{\Sigma}. \end{aligned} \quad (119)$$

We note that eq. (119) shows the contributions to ${}^{t+\Delta t} \tilde{\Sigma}$ from external loading, thermal strains, change in elastic moduli, creep, and plasticity.

To determine if the solution procedure can be made unconditionally stable as discussed in section 3.3, we compare eqs. (39) and (119). It is observed that

$${}^{t+\Delta t} A = {}^{t+\Delta t} \tilde{C}^E \tilde{B}_L {}^{t+\Delta t} K^E {}^{-1} \tilde{B}_L^T {}^{t+\Delta t} \tilde{C}^E - {}^{t+\Delta t} \tilde{C}^E \tilde{W}^{-1}, \quad (120)$$

$${}^{t+\alpha \Delta t} C = \tilde{W} {}^{t+\alpha \Delta t} \tilde{C} \tilde{D} \quad (121)$$

and

$$S = \tilde{W} \tilde{F}^E,$$

$$L = {}^{t+\Delta t} \tilde{C}^E \tilde{B}_L {}^{t+\Delta t} K^E {}^{-1} R, \quad (122)$$

$$T = \tilde{W} \tilde{E}^{TH}.$$

The matrices S , L , and T satisfy their basic definitions accompanying eq. (39) and ${}^{t+\Delta t} A$ and ${}^{t+\alpha \Delta t} C$ are symmetric. However, since the criteria for unconditional stability also assume that ${}^{t+\Delta t} A$ is negative definite and ${}^{t+\alpha \Delta t} C$ is positive semi-definite, the properties of these matrices must be investigated.

The matrix ${}^{t+\Delta t} A$ is examined in Appendix A. It is shown therein that the matrix is negative definite only when the elastic stiffness matrix ${}^{t+\Delta t} K^E$ is approximate. In the case of ${}^{t+\alpha \Delta t} C$, the structure of the matrix is:

$${}^{t+\alpha \Delta t} C = \begin{bmatrix} w_1 ({}^{t+\alpha \Delta t} \gamma_1 + {}^{t+\alpha \Delta t} \Lambda_1) D & & & \\ & w_2 ({}^{t+\alpha \Delta t} \gamma_2 + {}^{t+\alpha \Delta t} \Lambda_2) D & & \\ & & & \\ & & & w_M ({}^{t+\alpha \Delta t} \gamma_M + {}^{t+\alpha \Delta t} \Lambda_M) D \end{bmatrix} \quad (123)$$

The terms ${}^{t+\alpha \Delta t} \gamma_i$ and ${}^{t+\alpha \Delta t} \Lambda_i$ are > 0 , the Gauss weights w_j are > 0 , and D is positive semi-definite. Therefore, each submatrix in ${}^{t+\alpha \Delta t} C$ is positive semi-definite and so is the complete matrix.

Thus, unconditional stability is obtained when $\alpha \geq \frac{1}{2}$ and the elastic stiffness matrix is approximate.

3.4. General case

In this section we present an algorithm for the general case in which one time step size is used for the nodal point displacements and a smaller one for the integration point stresses, plastic strains, and creep strains [16–19]. We assume that a numerical solution has been obtained at discrete time points $\Delta t, 2\Delta t, \dots, t$ and the solution at time $t + \Delta t$ is desired.

3.4.1. Equilibrium and constitutive equations

The virtual work equation and the thermo-elastic-plastic and creep constitutive equations have been presented in eqs. (60)–(64). In addition, eqs. (66) and (67) remain directly applicable.

3.4.2. Algorithm development

The time step Δt is divided into q , not necessarily equal, subdivisions $\delta\tau$ with the time at the start and end of the j th subdivision denoted by τ_j and τ_{j+1} , respectively. At the end of the j th subdivision, the stresses are given by

$$\tau_{j+1}\sigma = \tau_{j+1}C^E(\tau_{j+1}e - \tau_{j+1}e^P - \tau_{j+1}e^C - \tau_{j+1}e^{TH}), \quad (124)$$

where $\tau_{j+1}e^P$ and $\tau_{j+1}e^C$ are evaluated using the α -method. This evaluation is accomplished using eqs. (68)–(73) so as to obtain the decompositions

$$\tau_{j+1}e^P = \tau_j e^P + e^P, \quad (125)$$

$$\tau_{j+1}e^C = \tau_j e^C + e^C \quad (126)$$

and then the increments

$$e^P = \delta\tau \tau_{j+\alpha\delta\tau} \dot{e}^P = \delta\tau \tau_{j+\alpha\delta\tau} \Lambda D \tau_{j+\alpha\delta\tau} \sigma, \quad (127)$$

$$e^C = \delta\tau \tau_{j+\alpha\delta\tau} \dot{e}^C = \delta\tau \tau_{j+\alpha\delta\tau} \gamma D \tau_{j+\alpha\delta\tau} \sigma, \quad (128)$$

where

$$\tau_{j+\alpha\delta\tau} \sigma = (1 - \alpha) \tau_j \sigma + \alpha \tau_{j+1} \sigma \quad (129)$$

and

$$\tau_{j+\alpha\delta\tau} \Lambda = \tau_{j+\alpha\delta\tau} \Lambda(\tau_{j+\alpha\delta\tau} \sigma, \tau_{j+\alpha\delta\tau} \dot{e}, \tau_{j+\alpha\delta\tau} \dot{e}^C, \tau_{j+\alpha\delta\tau} \dot{\theta}, \dots),$$

$$\tau_{j+\alpha\delta\tau} \gamma = \tau_{j+\alpha\delta\tau} \gamma(\tau_{j+\alpha\delta\tau} \sigma, \tau_{j+\alpha\delta\tau} \dot{e}^H, \tau_{j+\alpha\delta\tau} \dot{\theta}). \quad (130)$$

Eqs. (124)–(130) are a coupled set of nonlinear, algebraic equations which must be solved for each subdivision at every integration point. After q subdivisions,

$$\begin{aligned} t+\Delta t \sigma &= \tau_{q+1} \sigma, \\ t+\Delta t e^P &= \tau_{q+1} e^P, \\ t+\Delta t e^C &= \tau_{q+1} e^C. \end{aligned} \quad (131)$$

In addition to the above equations, it is also necessary to relate $\tau_{j+1}e$ to $t+\Delta t e$, which is obtained using eqs. (65) and (66). Assuming that the nodal point displacements vary linearly with time from t and $t + \Delta t$, we then have

$$\tau_{j+1}e = t e + \frac{t+\Delta t e - t e}{\Delta t} (\tau_{j+1} - t) \quad (132)$$

Thus, eq. (66) must be solved simultaneously with the subdivision equations, eqs. (124)–(130). As previously discussed in section 3.3.2, an iterative solution procedure is required. Following the developments in that section, the final algorithm proposed for practical analysis is summarized in table 1. In this table, the right subscript k is

Table 1
Algorithm for practical analysis^a

- (1) Loop to (11) for each solution step.
- (2) Set the displacement loop iteration counter $i = 0$ (${}^{t+\Delta t}U^{(0)} = {}^tU$, ${}^{t+\Delta t}e^{(0)} = {}^te$).
- (3) Loop to (9) for each integration point.
- (4) Set the subdivision counter $j = 1$.
- (5) Calculate the size $\delta\tau$ of the j th subdivision. When $i = 0$ and $j = 1$, set $\delta\tau = \Delta t$.
- (6) Calculate the total strain at the end of the j th subdivision.

$$\tau_{j+1}e^{(i)} = {}^te + \frac{{}^{t+\Delta t}e^{(i)} - {}^te}{\Delta t} (\tau_{j+1} - t). \quad (133)$$

- (7) Set the integration point loop iteration counter $k = 0$. This indicates conditions at time τ_j .
- (8) Solve for $\tau_{j+1}e_{(k+1)}^{P(i)}$, $\tau_{j+1}e_{(k+1)}^{C(i)}$, and $\tau_{j+1}\sigma_{(k+1)}^{(i)}$ with $\tau_{j+1}e^{(i)}$ held constant.

$$\tau_{j+1}e_{(k+1)}^{P(i)} = \tau_{j+1}e^{P(i)} + \delta t \tau_{j+\alpha\delta\tau} \Lambda_{(k)} D \tau_{j+\alpha\delta\tau} \sigma_{(k)}^{(i)},$$

$$\left[I + \alpha\delta\tau \tau_{j+1} C^E \left[D \tau_{j+\alpha\delta\tau} \sigma_{(k)}^{(i)} \frac{\partial \tau_{j+\alpha\delta\tau} \gamma_{(i)}}{\partial \tau_{j+\alpha\delta\tau} \sigma_{(i)}} + \tau_{j+\alpha\delta\tau} \gamma_{(i)} D \right]_{(k)} \right] \tau_{j+1} \sigma_{(k+1)}^{(i)} \quad (134)$$

$$= \tau_{j+1} C^E (\tau_{j+1} e^{(i)} - \tau_{j+1} e_{(k+1)}^{P(i)} - \tau_{j+1} e^{C(i)} - \tau_{j+1} e^{TH} - \partial \tau \tau_{j+\alpha\delta\tau} \gamma_{(k)}^{(i)} D \tau_{j+\alpha\delta\tau} \sigma_{(k)}^{(i)})$$

$$+ \alpha\delta\tau \tau_{j+1} C^E \left[D \tau_{j+\alpha\delta\tau} \sigma_{(k)}^{(i)} \frac{\partial \tau_{j+\alpha\delta\tau} \gamma_{(i)}}{\partial \tau_{j+\alpha\delta\tau} \sigma_{(i)}} + \tau_{j+\alpha\delta\tau} \gamma_{(i)} D \right]_{(k)} \tau_{j+1} \sigma_{(k)}^{(i)}, \quad (135)$$

$$\tau_{j+\delta\tau} e_{(k+1)}^{C(i)} = \tau_{j+1} e^{C(i)} + \delta\tau \tau_{j+\alpha\delta\tau} \gamma_{(k)}^{(i)} D \tau_{j+\alpha\delta\tau} \sigma_{(k)}^{(i)} + \alpha\delta\tau \left[D \tau_{j+\alpha\delta\tau} \sigma_{(k)}^{(i)} \frac{\partial \tau_{j+\alpha\delta\tau} \gamma_{(i)}}{\partial \tau_{j+\alpha\delta\tau} \sigma_{(i)}} + \tau_{j+\alpha\delta\tau} \gamma_{(i)} D \right]_{(k)}$$

$$\times (\tau_{j+\alpha\delta\tau} \sigma_{(k+1)}^{(i)} - \tau_{j+\alpha\delta\tau} \sigma_{(k)}^{(i)}). \quad (136)$$

- (9) Check for integration point loop convergence. If $i = 0$, bypass check and go to (3) for the next integration point.

No convergence: $k = k + 1$, go to (8).

Convergence: $\tau_{j+1} = t + \Delta t$? $\begin{cases} \text{Yes: go to (3) for the next integration point.} \\ \text{No: } j = j + 1, \text{ go to (5) for the next subdivision.} \end{cases}$

- (10) Solve for $\Delta U^{(i+1)}$ and ${}^{t+\Delta t}U^{(i+1)}$ after looping through steps (3)–(9) for each integration point.

$${}^{t+\Delta t} K^E \Delta U^{(i+1)} = {}^{t+\Delta t} R - \int_{B_L} {}^{t+\Delta t} \sigma_{(i)}^{(i)} dv, \quad (137)$$

$${}^{t+\Delta t} U^{(i+1)} = {}^{t+\Delta t} U^{(i)} + \Delta U^{(i+1)}. \quad (138)$$

- (11) Check for displacement loop convergence.

No convergence: $i = i + 1$, go to (3).

Convergence: go to (1) for the next solution step.

^a Step (1)–(11) is called Displacement Loop and step (3)–(9) is called Integration Point Loop.

the integration point loop iteration counter and the right superscript i is the displacement loop iteration counter.

We note that when there are no creep effects, the scheme is essentially successive substitution. Additionally, the comments given in section 3.3.2 concerning improvement of the displacement loop rate-of-convergence remain relevant. The algorithm presented in table 1 contains as a special case, the algorithm developed and analyzed in section 3.3. That is, when $q = 1$ the general algorithm reduces to the special case.

3.4.3. Stability analysis

We have not yet been able to derive a set of clear and useful equations which relate the entire set of integration point stresses at times Δt and $t + \Delta t$, as was done in the stability analysis described in section 3.3.3. However, by following an approach similar to the one in that section, the integration point computations in eqs. (124)–(130) can be shown to be unconditionally stable for each subdivision when $\alpha \geq \frac{1}{2}$ [20]. We therefore infer that the overall solution procedure is also unconditionally stable when $\alpha \geq \frac{1}{2}$.

4. Test problems

The material model and solution procedure presented in sections 2 and 3 have been implemented in the finite element computer program ADINA [21], and further details of the implementation are given in [20]. Below we report the numerical solutions obtained for three problems – the creep bending of a cantilever beam, the creep of a pressurized, thick-walled cylinder, and the thermo-elastic-plastic response of a pressurized, thick-walled cylinder. These results indicate some of the actual stability and accuracy characteristics of the solution procedure.

4.1. Creep bending of a cantilever beam

A cantilever beam was subjected to a constant tip bending moment of 6000 in-lbs. The finite element model of the beam is shown in fig. 3. It was possible to model only the portion of the beam above the neutral axis by applying the appropriate displacement boundary conditions to the nodes on the neutral axis. Eight, plane stress, iso-parametric elements were used in the model and the element stiffness matrices were evaluated using 3×3 Gauss integration. The work-equivalent nodal forces used to represent the tip bending moment were derived from the elastic beam theory stress distribution.

An analytical solution for the transient bending stress distribution was not found. It is possible, however, to obtain an expression for steady state conditions [25] when the uniaxial creep strain rate is of the form

$$\dot{\epsilon}^C = K \tau \sigma^m, \quad (139)$$

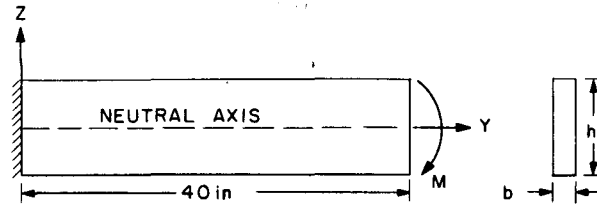
where m and K are constants. The Y -direction bending stress at steady state is then

$$\sigma_{yy} = -\frac{M}{2b} \frac{2m+1}{m} \left(\frac{h}{2}\right)^{-(2m+1)/m} Z^{1/m}, \quad Z \geq 0, \quad (140)$$

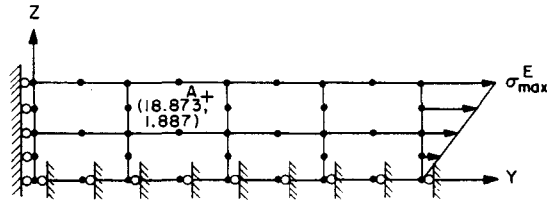
where M , b , h , and Z are defined in fig. 3.

By varying the integration parameter, α , the time step size, Δt , and the number of subdivisions per time step, q , results were obtained for a number of problem cases which are summarized in table 2. Figs. 4–12 present the results for the Y -direction bending stress at the point marked A in fig. 3. Problem cases 1 and 2, which are shown in fig. 4, define a 'baseline solution' against which all of the other results are compared. Since these two cases have a maximum difference between them of approximately 4%, problem case 1 is used in figs. 5 to 12 for the baseline solution.

When $\alpha = 0.0$, $q = 1$, the solution becomes unstable with increasing Δt . On the other hand, stable results are obtained when $q = 10$. This indicates that subdividing the time step (i.e. $q > 1$) can stabilize what would otherwise be an unstable solution.



SIDE AND END VIEWS



PLANE STRESS MESH

$E = 30 \times 10^6$ psi $b = .3$ in
 $\nu = 0.3$ $h = 4$ in
 $\tau_e^c = K \tau_\sigma^m$ $M = 6000$ in-lb
 $K = 6.4 \times 10^{-18}$ $\sigma_{max}^E = 7500$ psi
 $m = 3.15$

Fig. 3. Finite element mesh for a cantilever beam.

Table 2
Problem cases for the creep bending of a cantilever beam

Case no.	Integration parameter (α)	Time step size (Δt)	Number of subdivisions per time step ^a (q)
1	0.0	10.0	1
2	0.0	10.0	10
3	0.0	25.0	1
4	0.0	25.0	10
5	0.0	50.0	1
6	0.0	50.0	10
7	0.5	50.0	1
8	0.5	50.0	10
9	0.5	100.0	1
10	0.5	100.0	10
11	0.5	500.0	1
12	0.5	500.0	10
13	1.0	50.0	1
14	1.0	50.0	10
15	1.0	100.0	1
16	1.0	100.0	10
17	1.0	500.0	1
18	1.0	500.0	10

^a Time step subdivisions are of equal size.

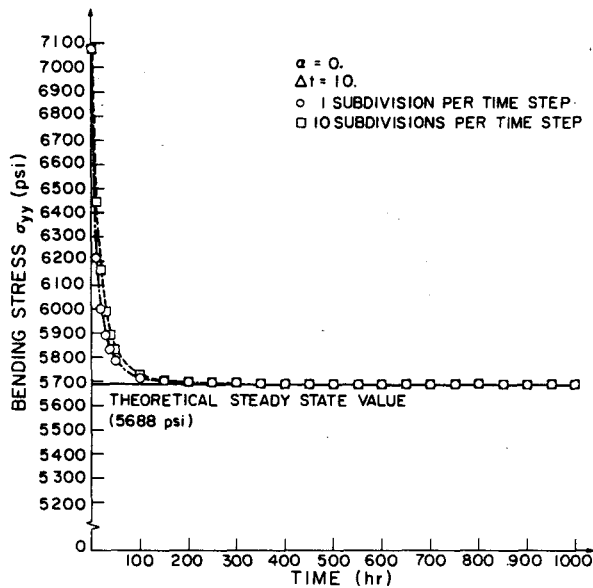


Fig. 4. Baseline solution for the bending stress at location A.

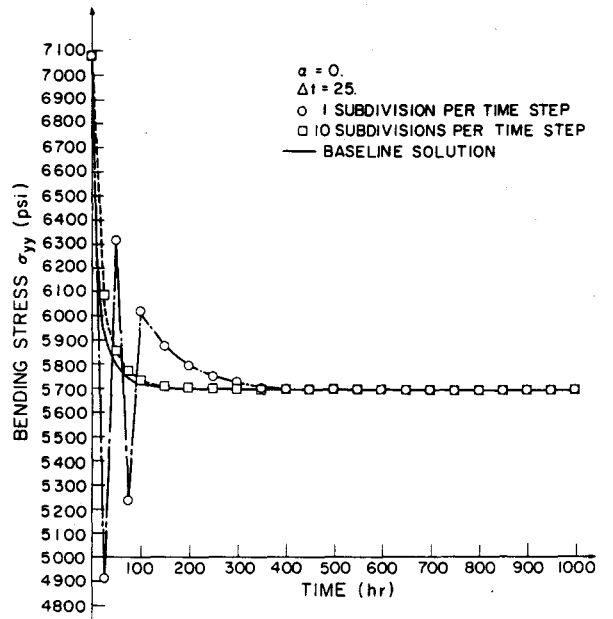


Fig. 5. Bending stress at location A.

For the cases with $\alpha = 0.5, q = 1$ and $\alpha = 1.0, q = 1$, it is possible to obtain stable solutions for values of Δt that are unstable when $\alpha = 0.0, q = 1$. However, when $\alpha = 0.5$ the solution converges to the baseline solution in an oscillatory manner. Since the magnitude of the initial oscillations increases with Δt , the accuracy decreases with increas-

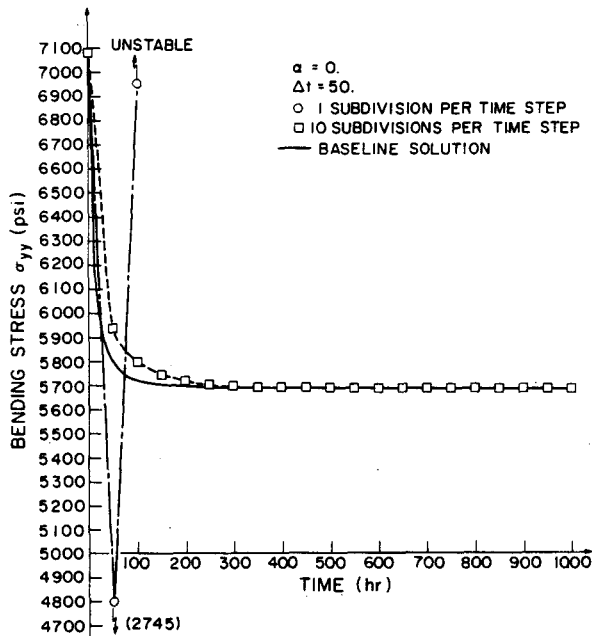


Fig. 6. Bending stress at location A.

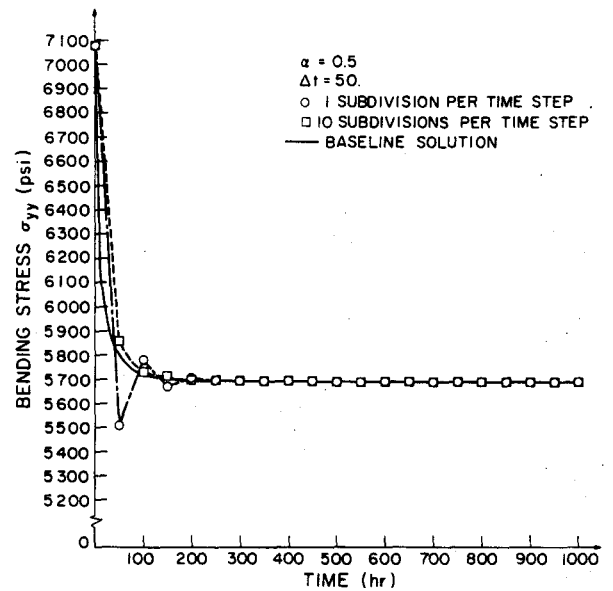


Fig. 7. Bending stress at location A.

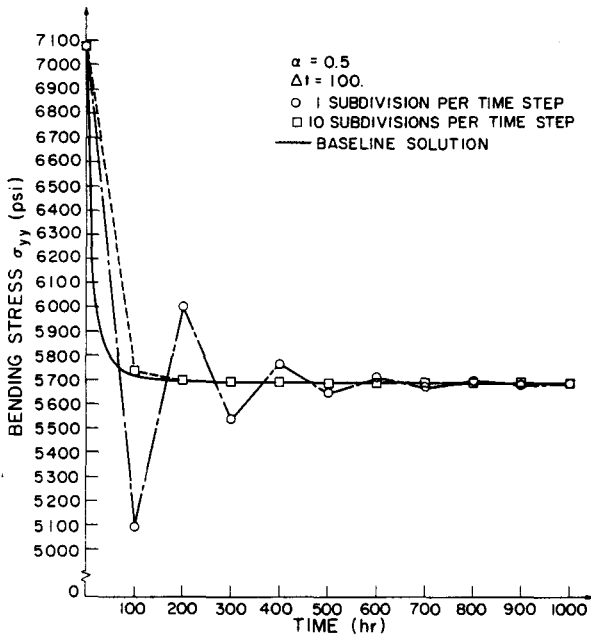


Fig. 8. Bending stress at location A.

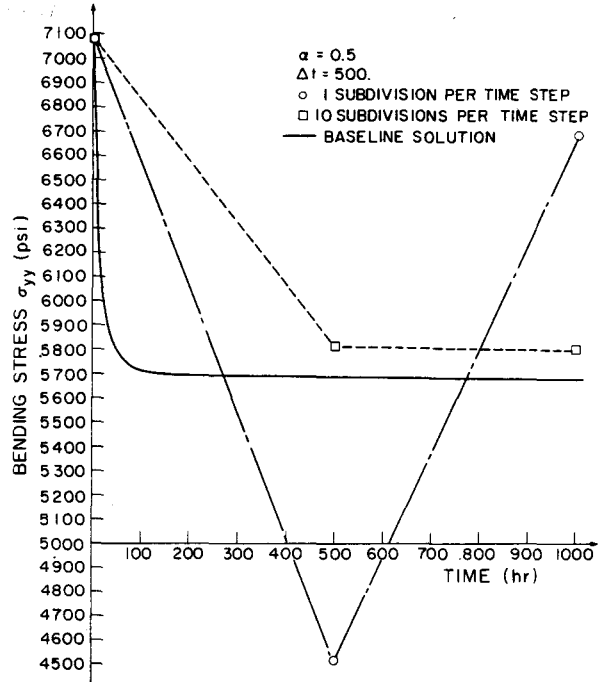


Fig. 9. Bending stress at location A.

ing Δt . For $\alpha = 1.0$, the loss in accuracy with increasing Δt is quite small. If q is increased to 10, the $\alpha = 0.5$ cases no longer exhibit the oscillatory convergence. It is also interesting to note that the $\alpha = 0.5$ cases are slightly more accurate when $\Delta t = 50.0$ and 100.0 , but $\alpha = 1.0$ gives better accuracy when $\Delta t = 500$.

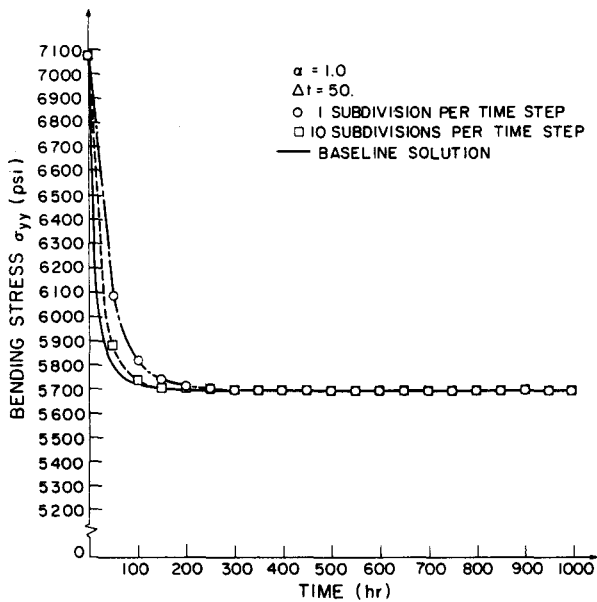


Fig. 10. Bending stress at location A.

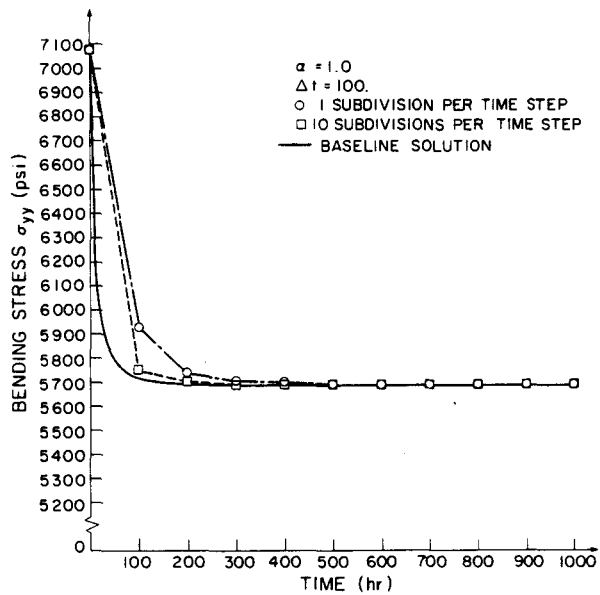


Fig. 11. Bending stress at location A.

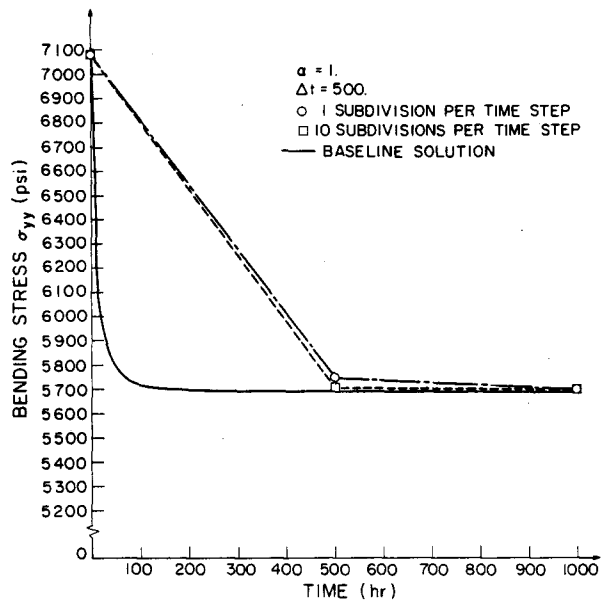


Fig. 12. Bending stress at location A.

4.2. Creep of a thick-walled cylinder

A thick-walled cylinder was subjected to a constant internal pressure of 3650 psi. The finite element model of the cylinder is shown in fig. 13. Plane strain conditions were assumed and twelve axisymmetric elements were used in the model. The element stiffness matrices were evaluated using 3×3 Gauss integration. The material

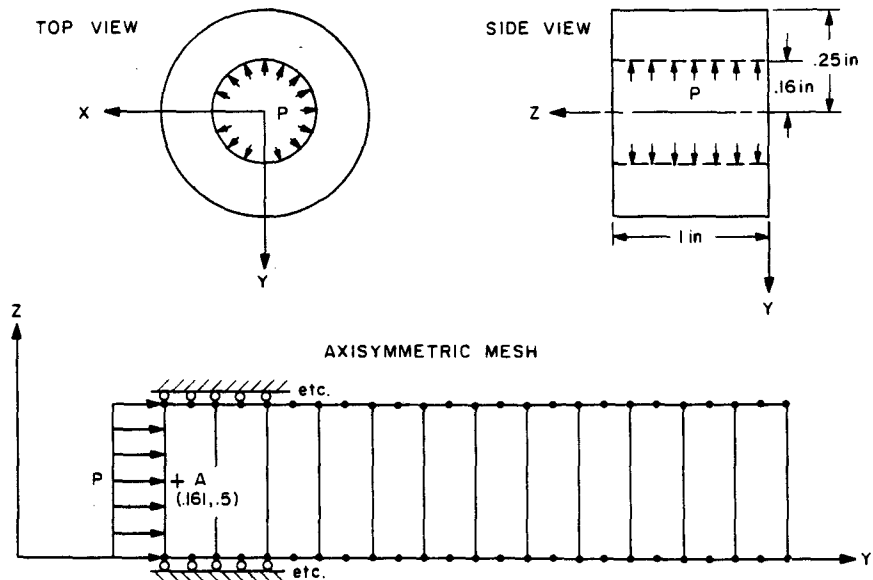


Fig. 13. Finite element mesh for a thick-walled cylinder.

Table 3
Material properties for the thick-walled cylinder

	800°F	900°F	1000°F	1100°F
Young's modulus (psi)	24.07×10^6	23.30×10^6	22.51×10^6	21.71×10^6
Poisson's ratio	0.3	0.3	0.3	0.3
Virgin material yield stress (psi)	1.11×10^4	1.004×10^4	9.344×10^3	9×10^3
Hardening modulus (psi)	7.3×10^5	7.3×10^5	7.3×10^5	7.3×10^5
Mean coefficient of thermal expansion (in/in/°F)	11.18×10^{-6}	11.28×10^{-6}	11.38×10^{-6}	11.48×10^{-6}

All properties were assumed to vary in a piecewise linear manner between the tabulated values.

Uniaxial creep law:

$$\tau_e^C = F(1 - e^{-R\tau}) + G\tau,$$

$$F = a_0 \tau_\sigma^{a_1},$$

$$R = a_2 e^{a_3 \tau_\sigma},$$

$$G = a_4 [\sinh(a_5 \tau_\sigma)]^{a_6},$$

τ_σ = constant uniaxial stress,

$$a_0 = 1.608 \times 10^{-10},$$

$$a_1 = 1.843,$$

$$a_2 = 5.929 \times 10^{-5},$$

$$a_3 = 2.029 \times 10^{-4},$$

$$a_4 = 6.73 \times 10^{-9},$$

$$a_5 = 1.479 \times 10^{-4},$$

$$a_6 = 3.0.$$

properties at 1100°F and the uniaxial creep law given in table 3 were used. Thermal strains were not considered and there were no plasticity effects.

The cases considered for this problem are summarized in table 4. Figs. 14–19 show the von Mises effective stress (see eq. (3)) at the point marked A in fig. 13. Problem case 1 in fig. 14 is defined to be the 'baseline solution'. When $\alpha = 0.0$, the solution results eventually become unstable as Δt is increased from the baseline value. It is interesting to note that although cases 2 and 3 (figs. 15 and 16) are initially inaccurate, the baseline solution is attained as time increases. When $\alpha = 0.5$ and 1.0, the solution results are stable for $\Delta t = 5000.0$, which is significantly larger than the values possible with $\alpha = 0.0$. However, both solutions initially oscillate about the baseline solution, and although $\alpha = 1.0$ has smaller oscillations, the $\alpha = 0.5$ case attains the baseline solution at an earlier time.

Table 4
Problem cases for the creep of a thick-walled cylinder

Case No.	Integration parameter (α)	Time step size (Δt)	Number of subdivisions per time step (q)
1	0.0	10.0 ($0.0 \leq t \leq 100.0$) 100.0 ($t > 100.0$)	1
2	0.0	100.0	1
3	0.0	200.0	1
4	0.0	500.0	1
5	0.5	5000.0	1
6	1.0	5000.0	1

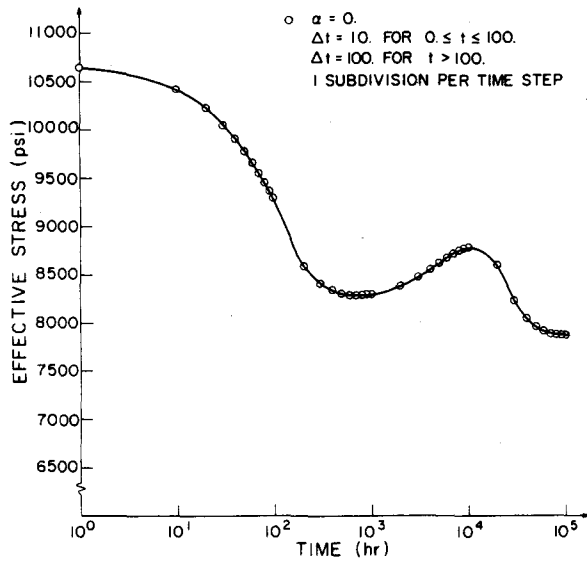


Fig. 14. Baseline solution for the effective stress at location A.

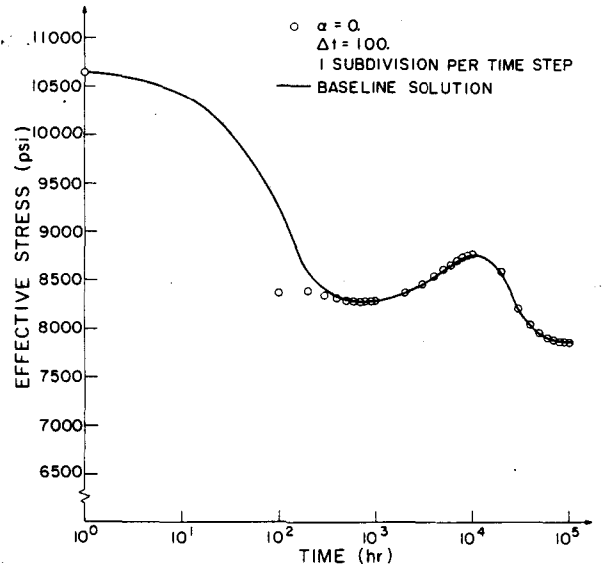


Fig. 15. Effective stress at location A.

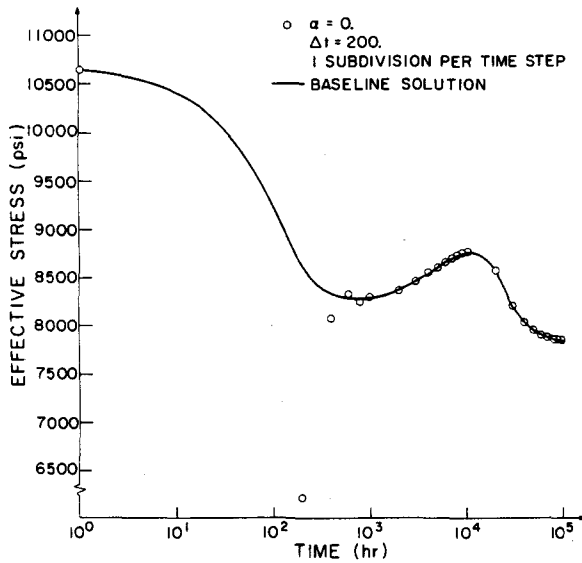


Fig. 16. Effective stress at location A.

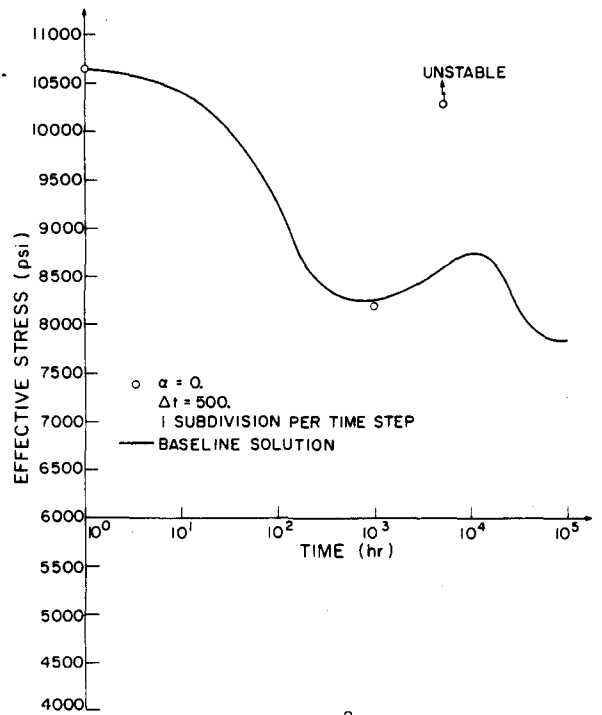


Fig. 17. Effective stress at location A.

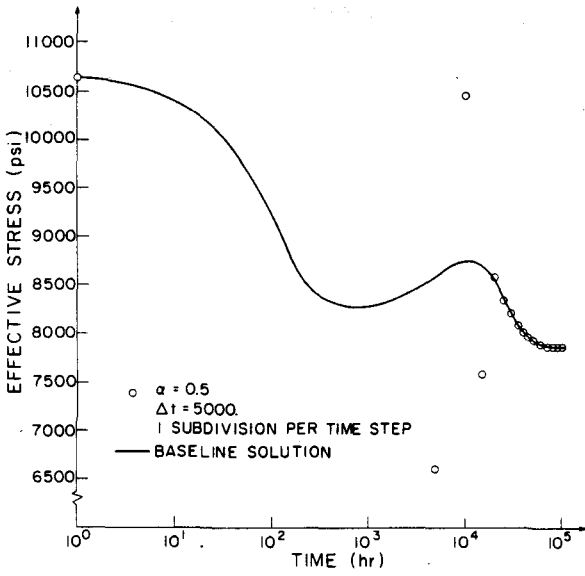


Fig. 18. Effective stress at location A.

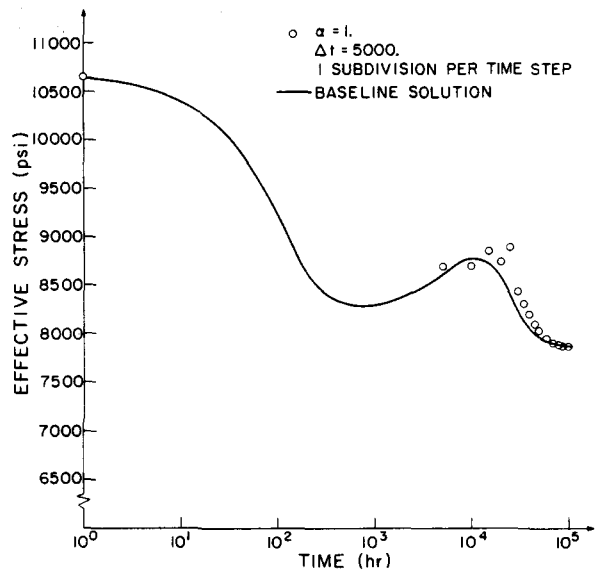


Fig. 19. Effective stress at location A.

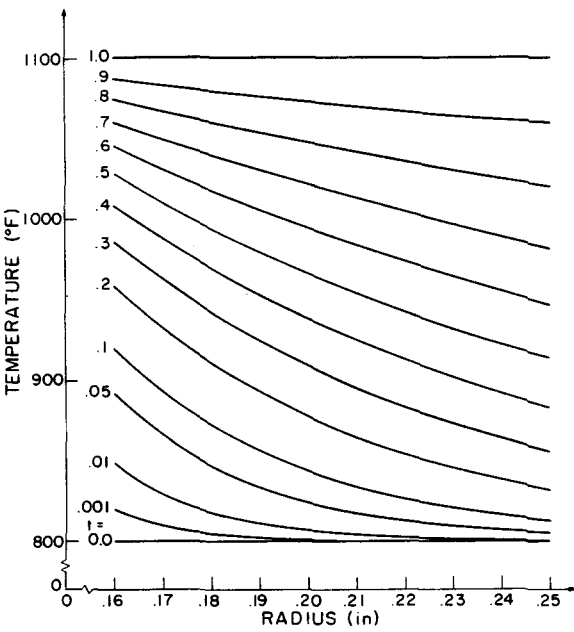


Fig. 20. Radial temperature profiles for the thick-walled cylinder.

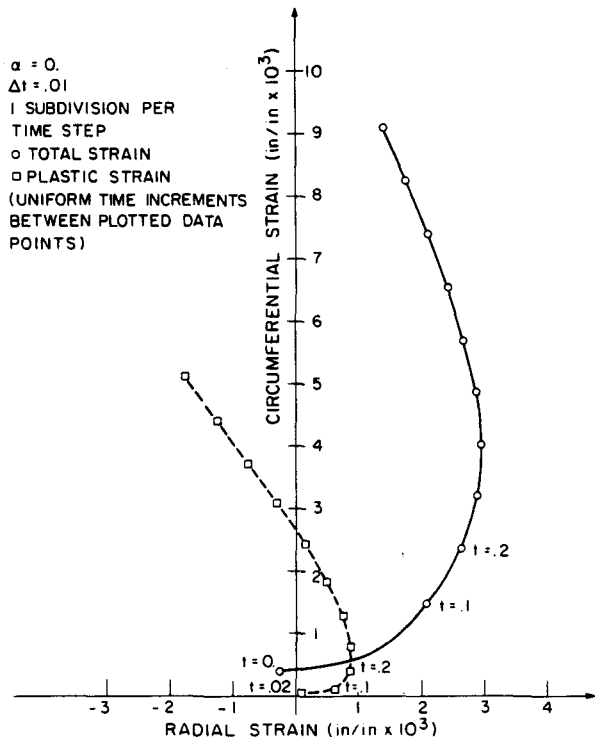


Fig. 21. Baseline solution for the radial and circumferential strains at location A.

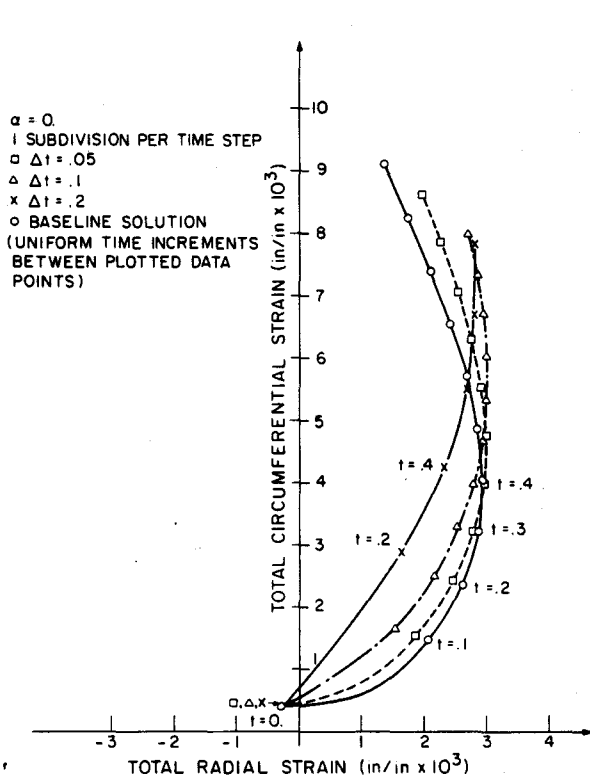


Fig. 22. Total radial and circumferential strains at location A.

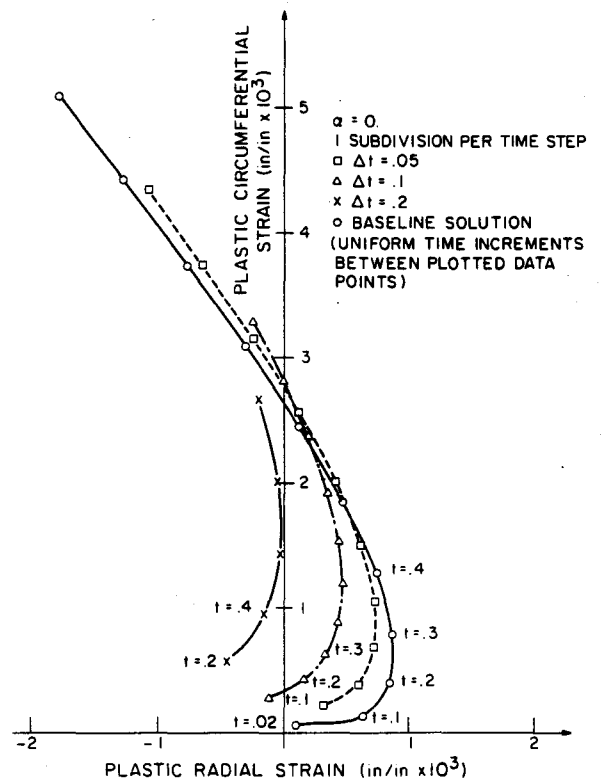


Fig. 23. Plastic radial and circumferential strains at location A.

4.3. Thermo-elastic plastic response of a thick-walled cylinder

A thick walled cylinder was subjected to a constant internal pressure of 3650 psi and a transient temperature distribution. The model of the cylinder is shown in fig. 13 and the temperature dependent material properties are contained in table 3. Kinematic hardening was used and no creep effects were considered. The cylinder was at

Table 5
Problem cases for the thermo-elastic-plastic response of a thick-walled cylinder

Case no.	Integration parameter (α)	Time step size (Δt)	Number of subdivisions per time step ^a (q)
1	0.0	0.01	1
2	0.0	0.05	1
3	0.0	0.1	1
4	0.0	0.2	1
5	0.0	0.05	5
6	0.0	0.1	10
7	0.0	0.2	20

^a Time step subdivisions are of equal size.

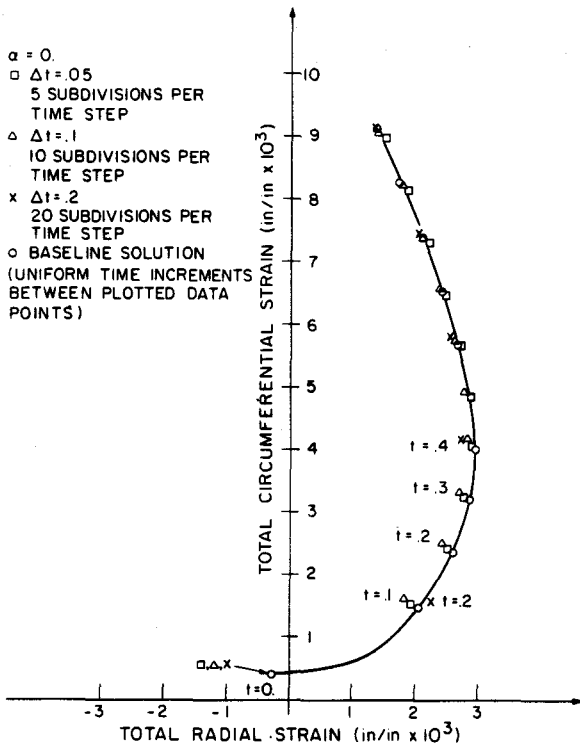


Fig. 24. Total Radial and circumferential strains at location A.

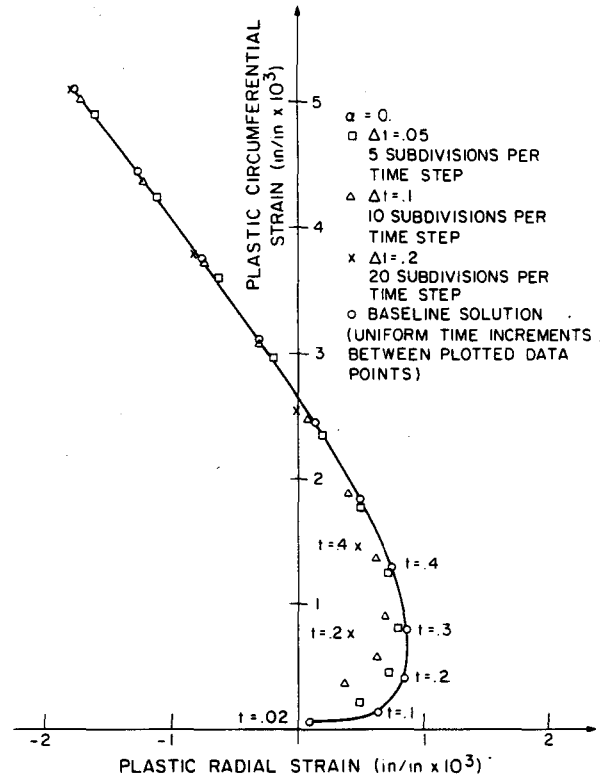


Fig. 25. Plastic radial and circumferential strains at location A.

800°F (reference temperature) at the start of the transient and the radial temperature distribution was of the form

$$\tau\theta = 800 + 300 \tau^{0.4} \exp\left(\frac{Y - 0.16}{0.09} \ln \tau\right), \quad \tau > 0. \tag{141}$$

Radial temperature profiles at various times are shown in fig. 20.

The cases considered for this problem are summarized in table 5. Figures 21 to 25 show radial and circumferential strain components (total and plastic) at the point marked A in fig. 13. Problem case 1 in fig. 21 is defined to be the 'baseline solution'. In contrast to the results for the previous two problems, increasing Δt when $\alpha = 0.0$ only causes the solution results to become more inaccurate. The growth of an oscillating instability is not observed. When $q > 1$, a significant improvement in accuracy is obtained for all values of Δt considered.

5. Conclusions

In this paper we have presented an efficient procedure for the finite element solution of problems with thermo-elastic-plastic and creep behavior. We believe that it is an effective tool for engineering analysis.

The material model used in conjunction with the solution procedure is based on the classical theories of plasticity and creep. All assumptions made in the derivation of the material model are clearly stated and the model's range of applicability is discussed. The solution procedure is based on a one-parameter integration scheme and can be made unconditionally stable. The requirements for unconditional stability are obtained from a thorough theo-

retical stability analysis. Numerical results are reported for three test problems. These results show the actual numerical characteristics of the implemented procedure and it is concluded that they agree with the predictions of the theoretical stability analysis.

We plan to obtain additional solutions using the procedure and to report these results at a future date. Since the whole development was carried out with the goal of providing engineers with a means for effectively solving practical thermo-elastic-plastic and creep problems, we are also looking forward to exchanging experiences with other ADINA users.

Acknowledgement

We gratefully acknowledge the financial support of the ADINA users group and the Forschungszentrum GKSS, W. Germany for this research work.

Appendix A. Investigation of the properties of the matrix

$${}^{t+\Delta t}A = {}^{t+\Delta t}\tilde{C}^E \tilde{B}_L {}^{t+\Delta t}K^E {}^{-1} \tilde{B}_L^T {}^{t+\Delta t}\tilde{C}^E - {}^{t+\Delta t}\tilde{C}^E \tilde{W}^{-1}.$$

Instead of dealing directly with ${}^{t+\Delta t}A$, we examine the expression

$$b = \tilde{x}^T \tilde{W} {}^{t+\Delta t}A \tilde{W} \tilde{x}, \quad (A.1)$$

where \tilde{W} is defined in eq. (107) and \tilde{x} is an arbitrary vector. It can be shown [20] that $\tilde{W} {}^{t+\Delta t}A \tilde{W}$ being negative definite is necessary and sufficient for ${}^{t+\Delta t}A$ to be so also.

Consider an arbitrary body subjected to surface tractions ${}^{t+\Delta t}f^S$ and body forces ${}^{t+\Delta t}f^B$ which cause an equilibrium elastic stress and strain field

$${}^{t+\Delta t}\sigma = {}^{t+\Delta t}C^E x. \quad (A.2)$$

We assume that we have a finite element representation of the body and interpret \tilde{x} as a supervector of the actual elastic strains at the element integration points. By eq. (103),

$$\begin{aligned} \tilde{x}^T \tilde{W} {}^{t+\Delta t}\tilde{C}^E \tilde{x} &= \int_v x^T {}^{t+\Delta t}C^E x \, dv \\ &= 2U_s^e, \end{aligned} \quad (A.3)$$

where U_s^e is the exact elastic strain energy [38,39,44]. In eq. (A.3), we have assumed that a sufficient number of integration points have been used so that the integration is performed exactly. In practice, this assumption is frequently violated and, indeed, it may not be possible to perform an exact integration numerically. Similarly, we find that

$$\tilde{B}_L^T {}^{t+\Delta t}\tilde{C}^E \tilde{W} \tilde{x} = \int_v B_L^T {}^{t+\Delta t}C^E x \, dv = \int_v B_L^T {}^{t+\Delta t}\sigma \, dv = \sum_{m=1}^N \int_{v(m)} B_L^T {}^{t+\Delta t}\sigma \, dv, \quad (A.4)$$

where N is the number of elements in the finite element assemblage.

Consider the virtual work principle [38–40,44]

$$\int_v \delta e^T {}^{t+\Delta t}\sigma \, dv = \int_s \delta u^T {}^{t+\Delta t}f^S \, ds + \int_v \delta u^T {}^{t+\Delta t}f^B \, dv, \quad (A.5)$$

where $\delta \mathbf{u}$ and $\delta \mathbf{e}$ are arbitrary, kinematically-admissible variations. Once again noting eq. (103), Eq. (A.5) can be written as

$$\sum_{m=1}^N \int_{v^{(m)}} \delta \mathbf{e}^T \mathbf{t}^{\Delta t} \boldsymbol{\sigma} \, dv = \sum_{m=1}^N \int_{s^{(m)}} \delta \mathbf{u}^T \mathbf{t}^{\Delta t} \mathbf{f}^S \, ds + \sum_{m=1}^N \int_{v^{(m)}} \delta \mathbf{u}^T \mathbf{t}^{\Delta t} \mathbf{f}^B \, dv. \quad (\text{A.6})$$

Since $\mathbf{t}^{\Delta t} \boldsymbol{\sigma}$ is in equilibrium with the applied loading, eq. (A.6) must hold for all admissible variations. Furthermore, the equation must also hold when the finite element approximations [40,41]

$$\delta \mathbf{u} = \mathbf{H} \delta \mathbf{U}, \quad (\text{A.7})$$

$$\delta \mathbf{e} = \mathbf{B}_L \delta \mathbf{U} \quad (\text{A.8})$$

are employed. Thus, we obtain

$$\sum_{m=1}^N \int_{v^{(m)}} \mathbf{B}_L^T \mathbf{t}^{\Delta t} \boldsymbol{\sigma} \, dv = \sum_{m=1}^N \int_{s^{(m)}} \mathbf{H}^T \mathbf{t}^{\Delta t} \mathbf{f}^S \, ds + \sum_{m=1}^N \int_{v^{(m)}} \mathbf{H}^T \mathbf{t}^{\Delta t} \mathbf{f}^B \, dv = \mathbf{t}^{\Delta t} \mathbf{R} \quad (\text{A.9})$$

where $\mathbf{t}^{\Delta t} \mathbf{R}$ is the work-equivalent, nodal point force vector.

Substituting eqs. (A.3), (A.4) and (A.9) into eq. (A.1) results in

$$\mathbf{b} = \mathbf{t}^{\Delta t} \mathbf{R}^T \mathbf{t}^{\Delta t} \mathbf{K}^E \mathbf{t}^{\Delta t} \mathbf{R} - 2U_s^e. \quad (\text{A.10})$$

It can be shown for a linear elastic system [40,41] that

$$\mathbf{t}^{\Delta t} \mathbf{R}^T \mathbf{t}^{\Delta t} \mathbf{K}^E \mathbf{t}^{\Delta t} \mathbf{R} = 2U_s^a, \quad (\text{A.11})$$

where U_s^a is the elastic strain energy of the finite element approximation. Since U_s^a is a lower bound to the exact elastic strain energy [38–40,44], it follows that $\mathbf{b} \leq 0$.

When $\mathbf{b} \leq 0$, the matrix $\mathbf{t}^{\Delta t} \mathbf{A}$ is negative semi-definite. However, in most applications we find that $U_s^a < U_s^e$, due to the approximate nature of the elastic stiffness matrix. Then $\mathbf{t}^{\Delta t} \mathbf{A}$ is negative definite.

References

- [1] J.H. Argyris, J. Royal Aero. Soc. 69 (1965) 633–635.
- [2] J.H. Argyris and D.W. Scharpf, Z. Ang. Math. and Phys. 23 (1972) 517–571.
- [3] K.J. Willam, J. Comp. and Struct. 8 (1978) 511–531.
- [4] J.H. Argyris, L.E. Vaz and K.J. Willam, Comput. Meths. Appl. Mech. Engrg. 16 (1978) 231–277.
- [5] I. Cormeau, Internat. J. Numer. Meth. Engrg. 9 (1975) 109–127.
- [6] T.J.R. Hughes and R.L. Taylor, J. Comput. and Struct., 8 (1978) 167–173.
- [7] G. Greenbaum and M. Rubinstein, Nucl. Engrg. Des. 7 (1968) 379–397.
- [8] O.C. Zienkiewicz, S. Valliappan and I.P. King, Internat. J. Numer. Meth. Engrg. 1 (1969) 75–100.
- [9] G.C. Nayak and O.C. Zienkiewicz, Internat. J. Numer. Meth. Engrg. 3 (1972) 113–135.
- [10] M.B. Kranchi, O.C. Zienkiewicz and D.R.J. Owen, Internat. J. Numer. Meth. Engrg. 12 (1978) 169–181.
- [11] W. Pilkey, K. Saczalski and H. Schaeffer, Structural Mechanics Computer Programs (Univ. Press of Virginia, Charlottesville, VA, 1974).
- [12] J.A. Stricklin, W.E. Haisler and W.H. Riesenmann, AIAA J. 11, (3) (1973) 292–299.
- [13] R. Gallagher, J. Padlog and P.P. Bijlaard, Amer. Rocket Soc. J. (May 1962) 700–707.
- [14] P. Sharifi and D.N. Yates, AIAA J. 12 (1973) 1210–1215.
- [15] N.A. Cyr and R.D. Teter, J. Comput. and Struct. 3 (1973) 849–863.
- [16] K.J. Bathe, H. Ozdemir and E.L. Wilson, Report UCSESM 74-4, Civil Engineering Dept., University of California, Berkeley
- [17] K.J. Bathe, Report 82448-2, Acoustics and Vibration Lab., Mechanical Engineering Dept., M.I.T. (May 1976; rev. May 1977).
- [18] M.D. Snyder and K.J. Bathe, Report 82448-3, Acoustics and Vibration Lab., Mechanical Engineering Dept., M.I.T. (June 1977).

- [19] D. Bushnell, *Internat. J. Numer. Meth. Engrg.* 11 (1977) 683–708.
- [20] M.D. Snyder and K.J. Bathe, Report 82448-10, Acoustics and Vibration Lab., Mechanical Engineering Dept., M.I.T. (December 1980).
- [21] K.J. Bathe, Report 82448-1, Acoustics and Vibration Lab., Mechanical Engineering Dept., M.I.T. (September 1975; rev. December 1978).
- [22] K.J. Bathe and M.R. Khoshgoftaar, *Nucl. Engrg. Des.* 51 (1979) 389–401.
- [23] T.J.R. Hughes, *Comput. Meths. Appl. Mech. Engrg.* 10 (1977) 135–141.
- [24] K.J. Bathe and A. Cimento, *Comput. Mech. Appl. Meth. Engrg.* 22 (1980) 59–85.
- [25] R.K. Penny and D.L. Marriott, *Design for Creep* (McGraw-Hill, London, 1971).
- [26] I. Finnie and W.R. Heller, *Creep of Engineering Materials* (McGraw-Hill, New York, 1959).
- [27] C.E. Pugh, J.M. Corum, K.C. Liu and W.L. Greenstreet, Report TM-3602, Oak Ridge National Laboratory, Oak Ridge, TN (1972).
- [28] C.E. Pugh et al., Report ORNL-5014, Oak Ridge National Laboratory, Oak Ridge, TN (1974).
- [29] P.M. Naghdi (Pergamon Press, Oxford 1960) pp. 121–169.
- [30] D.C. Drucker, *Proc. 1st U.S. Natl. Congress Appl. Mech.*, 1952, pp. 478–491.
- [31] D.C. Drucker, *Extension of the stability postulate with emphasis on temperature changes*, *Proc. 1st Symp. Naval Struc. Mech.* (Pergamon Press, Oxford, 1960) pp. 407–455.
- [32] D.R. Bland, *Proc. 9th Int. Congress Appl. Mech.*, 1957, pp. 45–50.
- [33] W. Prager, *J. Appl. Mech.* (1970) 728–737.
- [34] R.T. Shield and H. Ziegler, *Z. Ang. Math. and Phys. IXA* (1958) 260–276.
- [35] H. Ziegler, *Quart. Appl. Math.* 17 (1959) 55–65.
- [36] T.Y. Chang, *ASCE, J. Engrg. Mech. Div.* 99 (1973) 423–428.
- [37] W. Prager, *Proc. Koninklijke Nederlandse Akademie van Wetenschappen* 61 (1958) 176–182.
- [38] Y.C. Fung, *Foundations of Solid Mechanics* (Prentice-Hall, Englewood Cliffs, NJ 1976).
- [39] L.E. Malvern, *Introduction to the Mechanics of a Continuous Medium* (Prentice-Hall, Englewood Cliffs, NJ, 1969).
- [40] K.J. Bathe and E.L. Wilson, *Numerical Methods in Finite Element Analysis* (Prentice-Hall, Englewood Cliffs, NJ, 1976).
- [41] O.C. Zienkiewicz, *The Finite Element Method in Engineering Science* (McGraw-Hill, London, 1971).
- [42] G. Dahlquist and A. Björck, *Numerical Methods* (Prentice-Hall, Englewood Cliffs, NJ, 1974).
- [43] C.W. Gear, *Numerical Initial Value Problems in Ordinary Differential Equations* (Prentice-Hall, Englewood Cliffs, NJ 1971).
- [44] H.L. Langhaar, *Energy Methods in Applied Mechanics* (John Wiley, New York, 1962).

ON THREE-DIMENSIONAL NONLINEAR ANALYSIS OF CONCRETE STRUCTURES

Klaus-Jürgen BATHE and Seshadri RAMASWAMY

Massachusetts Institute of Technology, Cambridge, MA 02139, USA

Received 21 October 1978

Solution capabilities for three-dimensional geometric and material nonlinear finite element analysis of concrete structures are presented. The concrete material is modeled including triaxial nonlinear stress–strain behavior, tensile cracking, compression crushing and strain-softening. The objective in this work was the development of a practical nonlinear concrete analysis capability. The material model can also be employed to represent some rock materials. The results of various sample analyses are given, in which the stability and accuracy of the finite element representations have been studied.

1. Introduction

During recent years interest in nonlinear analysis of concrete structures has increased steadily, because of the wide use of plain, reinforced and prestressed concrete as a structural material, and because of the development of relatively powerful analysis techniques implemented on electronic digital computers. A most important analysis procedure that is already in wide use for the linear analysis of structures is the finite element method [1,2]. If a realistic nonlinear analysis of a concrete structure can be carried out, the safety of the structure is increased and the cost can frequently be reduced.

Concrete exhibits a complex structural response with various important nonlinearities; namely, a nonlinear stress–strain behavior, tensile cracking and compression crushing material failures, and temperature dependent creep strains [3–16]. All these concrete nonlinearities depend strongly on the triaxial state of stress, and in addition the nonlinearities introduced by the reinforcing and prestressing steel should in general be taken into account.

There are a number of factors that prevent at present the wide acceptability of nonlinear finite element analysis procedures in the analysis of concrete structures. A first important consideration is that the constitutive properties of concrete have not as yet been identified completely, and there is at present no generally accepted material law available to model concrete behavior. A second important factor is that nonlinear finite element analysis of concrete structures is very costly and requires much user sophistication. The high cost of nonlinear analysis of concrete structures is largely due to the difficulties encountered in the stability and accuracy of the solutions. These difficulties, however, are a direct consequence of the specific numerical implementation of the concrete nonlinearities. Since even linear three-dimensional analysis can be expensive to the analyst, the practical difficulties of three-dimensional nonlinear concrete analysis are particularly pronounced.

It is important to realize that progress in practical nonlinear analysis procedures is largely based on the development of improved constitutive models and kinematic descriptions, and on the development of stable and effective computational procedures. Since there is a strong interaction between the development of improved constitutive models and their effective numerical implementation, it is important to endeavor to advance the development of new material descriptions and their numerical implementations at the same time. The situation at present is that a linear analysis of a concrete structure can be performed in almost a routine manner, but nonlinear analyses that would represent the structural behavior more accurately, and that must be employed to predict the ultimate load carrying capacity of a structure are difficult, if not impossible, to perform. Also, only a few general analysis tools are available for such a task.

The objective in this paper is to present the formulation and numerical implementation of a three-dimensional concrete model that has been incorporated and evaluated in the computer program ADINA [17]. Based on the above considerations, the basic aim in this work was to implement in the program a model that with the present constitutive descriptions, numerical methods and computing equipment available and with the general high cost of three-dimensional analysis would satisfy the following two criteria. Firstly, the model should be as simple as possible, but reproduce the important nonlinear and strength characteristics consistent with experimental results. Secondly, the model should be theoretically sound and numerically stable, so that reliable analysis results are obtained.

The material model is a hypoelastic model based on a uniaxial stress–strain relation that is generalized to take biaxial and triaxial stress conditions into account. Tensile cracking and compression crushing conditions are identified using failure surfaces. The use of tensile and compression failure criteria (including strain-softening conditions) prevents that unrealistically large stress and strain conditions are predicted as can be the case when using some plasticity models, (e.g. Drucker–Prager model with Prandtl–Reuss plasticity theory).

The concrete model is defined with a number of input parameters that provide versatility in its use. By employing the appropriate material parameters, the model can be employed also to represent some rock materials [18].

In this paper, we first review the kinematic nonlinear incremental formulation that is employed in the analysis. Then the material model which has been implemented is described. The material representation includes triaxial nonlinear stress–strain behavior, material tensile cracking and compression crushing characteristics and strain-softening effects. The model can be employed in two- and three-dimensional analysis. Following the general description of the model the computer implementation is presented. Finally, a few sample solutions are given. In the studies, various nonlinear characteristics of the material model have been evaluated in detail, in order to identify the stability and accuracy characteristics of the finite element representations.

2. The governing incremental equilibrium equations

A very general geometric and material nonlinear formulation is obtained using the principle of virtual displacements. Using this principle in the total Lagrangian formulation, the governing equilibrium equation at time $t + \Delta t$ for a body undergoing large displacements and exhibiting constitutive nonlinearities is [19,20],

$$\int_{0V} {}^{t+\Delta t} S_{ij} \delta {}^{t+\Delta t} \epsilon_{ij}^0 dv = {}^{t+\Delta t} \mathcal{R} , \tag{1}$$

where the ${}^{t+\Delta t} S_{ij}$ are the components of the 2nd Piola–Kirchhoff stress tensor referred to the body configuration at time 0, and the ${}^{t+\Delta t} \epsilon_{ij}$ are the components of the Green–Lagrange strain tensor,

$${}^{t+\Delta t} \epsilon_{ij} = \frac{1}{2} ({}^{t+\Delta t} u_{i,j} + {}^{t+\Delta t} u_{j,i} + {}^{t+\Delta t} u_{k,i} {}^{t+\Delta t} u_{k,j}) , \quad {}^{t+\Delta t} u_{i,j} = \partial {}^{t+\Delta t} u_i / \partial {}^0 x_j , \tag{2}$$

where the ${}^{t+\Delta t} u_i, i = 1, 2, 3$ are the displacement components at time $t + \Delta t$, and the ${}^0 x_j, j = 1, 2, 3$, denote the coordinates of the body at time 0. The symbol “ δ ” in eq. (1) means “variation in”, and ${}^{t+\Delta t} \mathcal{R}$ is the total external virtual work that is performed by the body forces and surface tractions when the body is subjected to a variation in the displacements at time $t + \Delta t$.

In the incremental solution of eq. (1), we assume that the solution is known at time t . Then, linearizing eq. (1) about the state at time t , and using a modified Newton–Raphson iteration for the solution at time $t + \Delta t$, we obtain the governing equation (for static analysis or dynamic analysis with implicit time integration) [20]

$$\int_{0V} {}^0 C_{ijrs} \delta {}^0 e_{ij} \Delta {}^0 e_{rs}^{(k)} dv + \int_{0V} {}^t S_{ij} \delta \Delta {}^0 \eta_{ij}^{(k)} dv = {}^{t+\Delta t} \mathcal{R} - \int_{0V} {}^{t+\Delta t} S_{ij}^{(k-1)} \delta {}^{t+\Delta t} \epsilon_{ij}^{(k-1)} dv , \tag{3}$$

where the ${}^0 C_{ijrs}$ are the components of the tangent constitutive tensor at time t , the ${}^t S_{ij}$ are components of the

2nd Piola–Kirchhoff stress tensor at time t , and

$$\begin{aligned} \Delta_0 e_{ij}^{(k)} &= \frac{1}{2} (\Delta_0 u_{i,j}^{(k)} + \Delta_0 u_{j,i}^{(k)} + {}^t_0 u_{1,i} \Delta_0 u_{1,j}^{(k)} + {}^t_0 u_{1,j} \Delta_0 u_{1,i}^{(k)}), & \Delta_0 \eta_{ij}^{(k)} &= \frac{1}{2} \Delta_0 u_{1,i} \Delta_0 u_{1,j}, \\ {}^{t+\Delta t} u_i^{(k)} &= {}^{t+\Delta t} u_i^{(k-1)} + \Delta u_i^{(k)}. \end{aligned} \quad (4)$$

Also, the ${}^{t+\Delta t} S_{ij}^{(k-1)}$ and ${}^{t+\Delta t} \epsilon_{ij}^{(k-1)}$ are components of the 2nd Piola–Kirchhoff stress tensor and Green–Lagrange strain tensor corresponding to the displacements ${}^{t+\Delta t} u_i^{(k-1)}$.

It should be noted that in eq. (3), the displacements are updated until the right-hand-side of the equation is zero. At this point, the equilibrium configuration corresponding to the loading at time $t + \Delta t$ has been established.

For the finite element solution, we are using isoparametric finite element discretization, in which at any time t [2],

$${}^t x_i = \sum_{j=1}^N h_j {}^t x_j^i, \quad {}^t u_i = \sum_{j=1}^N h_j {}^t u_j^i, \quad (5)$$

where ${}^t x_j^i$ is the coordinate and ${}^t u_j^i$ is the displacement of element nodal point j at time t and in direction i ; $i = 1, 2, 3$ in three-dimensional analysis. Substituting the relations in eq. (5) into eq. (3) and introducing inertia forces as part of the body forces, we obtain the discretized equilibrium equations

$$M {}^{t+\Delta t} \ddot{U}^{(k)} + ({}^t_0 K_L + {}^t_0 K_{NL}) \Delta U^{(k)} = {}^{t+\Delta t} R - {}^{t+\Delta t} F^{(k-1)}, \quad (6)$$

where M is the time independent mass matrix, the ${}^t_0 K_L$ and ${}^t_0 K_{NL}$ are the linear and nonlinear strain stiffness matrices, ${}^{t+\Delta t} R$ is the externally applied nodal point force vector, the vector U lists the nodal point displacements, and ${}^{t+\Delta t} F^{(k-1)}$ is the nodal point force vector that is work equivalent to the element stresses. Table 1 summarizes for a single element, the calculation of the matrices ${}^t_0 K_L$, ${}^t_0 K_{NL}$ and vector ${}^{t+\Delta t} F^{(k-1)}$ used in eq. (6).

In the finite element solution using eq. (6), we iterate, in essence, until the finite element system is in equilibrium. Since a displacement-based compatible finite element discretization is employed, the compatibility conditions are also satisfied. Hence, any errors in the solution beyond the finite element discretization errors which of course are encountered in linear analysis also, are those introduced in the inaccurate calculation of the constitutive relations. Since the stress–strain relationships depend on the stress and strain histories, it is important to integrate the stresses and strains accurately in the incremental solution and, in general [20]

$${}^{t+\Delta t} S_{ij}^{(k-1)} = {}^t_0 S_{ij} + \int_{{}^t_0 \epsilon_{rs}}^{{}^{t+\Delta t} \epsilon_{rs}^{(k-1)}} {}_0 C_{ijrs} d\epsilon_{rs}, \quad (7)$$

where ${}^{t+\Delta t} \epsilon_{rs}^{(k-1)}$ are the total Green–Lagrange strains corresponding to the loading at time $t + \Delta t$ and at the start of iteration (k) .

Eq. (6) holds for large displacements and large strains, but the appropriate constitutive relations must be defined. Concrete and rock materials cannot sustain large relative deformations and it is appropriate to assume in most analyses infinitesimal displacement conditions. In these analyses, all nonlinear strain terms are neglected, i.e., the nonlinear strain stiffness matrix ${}^t_0 K_{NL}$ and the nonlinear strain contributions in ${}^{t+\Delta t} F^{(k-1)}$ are not included in the solution, and the 2nd Piola–Kirchhoff stresses ${}^t_0 S_{ij}$ reduce to the engineering physical stresses, ${}^t \sigma_{ij}$. However, although the material can only sustain small relative deformations, in some cases, rigid body rotations of the material may be significant. These large rotation effects are directly taken into account in the total Lagrangian formulation, because the 2nd Piola–Kirchhoff stresses are numerically equal to the rotated physical engineering stresses. Hence the constitutive relations once formulated for infinitesimal displacement conditions can directly be employed in the total Lagrangian formulation in order to account for large rotation effects.

Table 1
Evaluation of stiffness matrix and nodal point force vector equivalent to element stresses

$$\int_{0V} {}_0C_{ijrs} \Delta {}_0e_{rs}^{(k)} \delta {}_0e_{ij} {}_0dv \quad {}_0^tK_L \Delta U^{(k)} = \left(\int_{0V} {}_0^tB_L^T {}_0C {}_0^tB_L {}_0dv \right) \Delta U^{(k)}$$

$$\int_{0V} {}_0^tS_{ij} \delta \Delta {}_0n_{ij}^{(k)} {}_0dv \quad {}_0^tK_{NL} \Delta U^{(k)} = \left(\int_{0V} {}_0^tB_{NL}^T {}_0^tS {}_0^tB_{NL} {}_0dv \right) \Delta U^{(k)}$$

$$\int_{0V} {}^{t+\Delta t}{}_0^tS_{ij}^{(k-1)} \delta {}^{t+\Delta t}{}_0e_{ij}^{(k-1)} {}_0dv \quad {}^{t+\Delta t}{}_0F^{(k-1)} = \int_{0V} {}^{t+\Delta t}{}_0^tB_L^{(k-1)T} {}^{t+\Delta t}{}_0^tS^{(k-1)} {}_0dv$$

${}_0^tB_L$ = linear strain-displacement transformation matrix corresponding to time t .

${}_0^tB_{NL}$ = nonlinear strain-displacement transformation matrix corresponding to time t .

${}_0^tS$ = stress matrix of stresses at time t .

${}^{t+\Delta t}{}_0^tS^{(k-1)}$ = stress vector of stresses corresponding to time $t + \Delta t$ and iteration $(k - 1)$.

${}^{t+\Delta t}{}_0^tB_L^{(k-1)}$ = linear strain-displacement transformation matrix corresponding to time $t + \Delta t$ and iteration $(k - 1)$.

3. The concrete or rock material model

The model implemented employs three basic features to describe the material behavior, namely, (i) a nonlinear stress-strain relation including strain-softening to allow for the weakening of the material under increasing compressive stresses, (ii) a failure envelope that defines cracking in tension and crushing in compression, and (iii) a strategy to model the post-cracking and crushing behavior of the material. In the solution, the material can be subjected to cyclic loading conditions, i.e., the numerical solution allows for unloading and reloading including deactivation of tensile failures.

In the following, the material model is described for infinitesimal displacement conditions using the engineering stresses ${}^t\sigma_{ij}$ and engineering strains ${}^t\epsilon_{ij}$. In order to analyze problems with large rotation conditions, the total Lagrangian stress and strain variables must be substituted for the engineering variables [20].

3.1. Stress-strain relations

The general multiaxial stress-strain relations are derived from a uniaxial stress-strain relation ${}^t\tilde{\sigma}$ versus ${}^t\tilde{\epsilon}$ [4-7]. In this section, we describe the uniaxial and multiaxial stress-strain relations employed in the model prior to tensile cracking or compression crushing.

In the following discussion, all uniaxial parameters are identified by a curl ($\tilde{\sim}$) placed over them, (i.e., all parameters that have been obtained from fig. 1 carry a curl).

3.1.1. Uniaxial conditions

A typical uniaxial stress ${}^t\tilde{\sigma}$ to uniaxial strain ${}^t\tilde{\epsilon}$ relation (assuming loading of the material) is shown in fig. 1. This stress-strain relation shows that there are basically three strain phases; namely, corresponding to ${}^t\tilde{\epsilon} \geq 0$, $0 > {}^t\tilde{\epsilon} \geq \tilde{\epsilon}_c$ and $\tilde{\epsilon}_c > {}^t\tilde{\epsilon} \geq \tilde{\epsilon}_u$ where $\tilde{\epsilon}_c$ is the strain corresponding to the minimum (crushing) stress, $\tilde{\sigma}_c$, that can be reached, and $\tilde{\epsilon}_u$ is the ultimate compressive strain. If ${}^t\tilde{\epsilon} > 0$, i.e. the material is in tension, the stress-strain relation is linear and a constant Young's modulus, \tilde{E}_0 , is employed.

$${}^t\tilde{\sigma} = \tilde{E}_0 {}^t\tilde{\epsilon}, \quad (8)$$

$$\frac{d {}^t\tilde{\sigma}}{d {}^t\tilde{\epsilon}} = \tilde{E}_0. \quad (9)$$

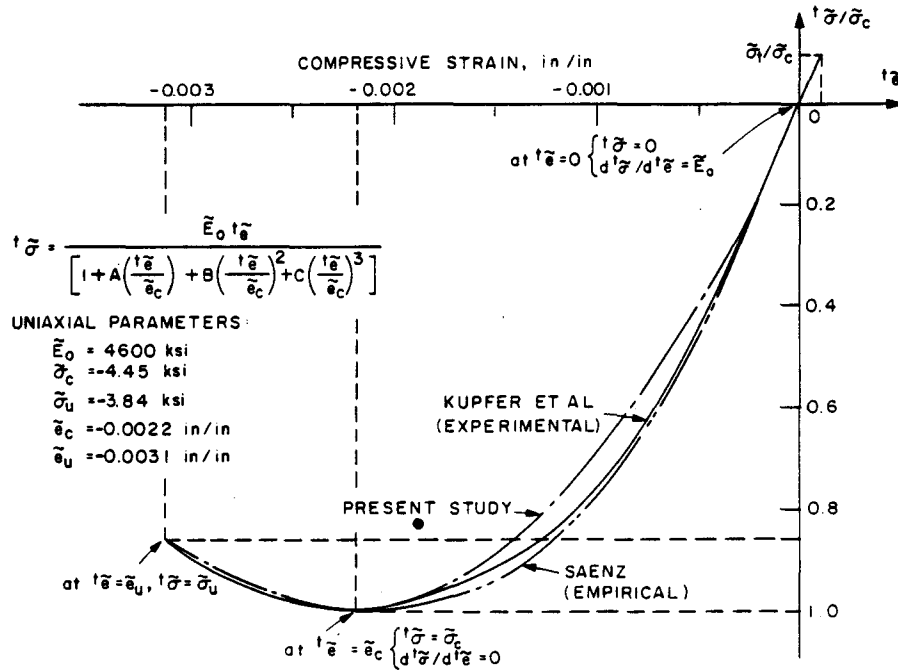


Fig. 1. Material model uniaxial stress–strain law.

For $t\tilde{\epsilon} \leq 0$, we assume the following relation,

$$t\tilde{\sigma}/\tilde{\sigma}_c = \frac{(\tilde{E}_0/\tilde{E}_s)(t\tilde{\epsilon}/\tilde{\epsilon}_c)}{1 + A(t\tilde{\epsilon}/\tilde{\epsilon}_c) + B(t\tilde{\epsilon}/\tilde{\epsilon}_c)^2 + C(t\tilde{\epsilon}/\tilde{\epsilon}_c)^3}, \quad (10)$$

and hence,

$$t\tilde{E} = \frac{\tilde{E}_0[1 - B(t\tilde{\epsilon}/\tilde{\epsilon}_c)^2 - 2C(t\tilde{\epsilon}/\tilde{\epsilon}_c)^3]}{[1 + A(t\tilde{\epsilon}/\tilde{\epsilon}_c) + B(t\tilde{\epsilon}/\tilde{\epsilon}_c)^2 + C(t\tilde{\epsilon}/\tilde{\epsilon}_c)^3]^2}, \quad (11)$$

where

$$A = \frac{[\tilde{E}_0/\tilde{E}_u + (p^3 - 2p^2)\tilde{E}_0/\tilde{E}_s - (2p^3 - 3p^2 + 1)]}{[(p^2 - 2p + 1)p]}, \quad B = [(2\tilde{E}_0/\tilde{E}_s - 3) - 2A],$$

$$C = [(2 - \tilde{E}_0/\tilde{E}_s) + A],$$

and the strength parameters $\tilde{E}_0, \tilde{\sigma}_c, \tilde{\epsilon}_c, \tilde{E}_s = \tilde{\sigma}_c/\tilde{\epsilon}_c, \tilde{\sigma}_u, \tilde{\epsilon}_u, p = \tilde{\epsilon}_u/\tilde{\epsilon}_c$ and $\tilde{E}_u = \tilde{\sigma}_u/\tilde{\epsilon}_u$ are obtained from uniaxial tests.

The stress–strain relation in eq. (10) assumes monotonic loading conditions. For unloading conditions and loading back to the stress state from the stress state from which unloading occurred, the initial Young's modulus \tilde{E}_0 is used.

3.1.2. Multiaxial conditions

The behavior of concrete and rock materials under multiaxial stress conditions is very complex and has not been assessed experimentally in a complete manner. Various material models with considerable simplifying assumptions have been proposed to characterize the behavior of concrete and rock materials using plasticity relations, hypoelastic descriptions and the endochronic theory of inelasticity [9–16]. However, considering the variability of concrete materials that need be described in practice, and recognizing that the model should also be useful to represent the behavior of some rock materials, the objective in this work was to develop an effective but simple

model that provides sufficient flexibility to the analyst to fit basic material behaviors.

The stress-strain relations are evaluated differently depending on whether the material is loading or unloading. The Poisson ratio is assumed to be constant under all stress conditions.

To characterize loading and unloading conditions we define a loading function

$${}^t f = \bar{s} + 3\alpha {}^t \sigma_m, \quad (12)$$

where α is a constant (usually negative), ${}^t \sigma_m = \frac{1}{3} {}^t \sigma_{ii}$, $\bar{s} = (\frac{1}{2} {}^t s_{ij} {}^t s_{ij})^{1/2}$, ${}^t s_{ij} = {}^t \sigma_{ij} - \delta_{ij} {}^t \sigma_m$ and δ_{ij} is the Kronecker delta. The material is loading if

$${}^t f \geq f_{\max}, \quad (13a)$$

and unloading if

$${}^t f < f_{\max}, \quad (13b)$$

where f_{\max} is the maximum value of the loading function that has been reached during the complete solution. In unloading, the material is assumed to be isotropic and the initial Young's modulus, \bar{E}_0 , is used to form the incremental stress-strain matrix, both for stiffness and stress calculations.

To obtain the stress-strain relations in loading conditions, the principal stresses are calculated and for each principal stress direction a uniaxial tangent Young's modulus, ${}^t \bar{E}_{pi}$, corresponding to the strain in the principal stress direction, ${}^t e_{pi}$, is evaluated using eqs. (9) and (11). When using eq. (11), the current strain ${}^t e_{pi}$ is employed and to account for multiaxial stress conditions the material variables $\tilde{\sigma}_c$, $\tilde{\sigma}_u$, \tilde{e}_c and \tilde{e}_u are replaced by the variables $\tilde{\sigma}'_c$, $\tilde{\sigma}'_u$, \tilde{e}'_c and \tilde{e}'_u defined in eq. (20). Let ${}^t \sigma_{p1}$, ${}^t \sigma_{p2}$ and ${}^t \sigma_{p3}$ be the principal stresses at time t , with ${}^t \sigma_{p3} \leq {}^t \sigma_{p2} \leq {}^t \sigma_{p1}$ and ${}^t \bar{E}_{p1}$, ${}^t \bar{E}_{p2}$ and ${}^t \bar{E}_{p3}$ the corresponding uniaxial Young's moduli. The material is considered as isotropic with an equivalent multiaxial Young's modulus when subjected to tension or low compression, where such a state is defined by ${}^t \sigma_{p3} \geq \kappa \tilde{\sigma}'_c$. The variable κ is typically 0.4. For the material the equivalent multiaxial Young's modulus, ${}^t E$, is then obtained using the following weighting scheme;

$${}^t E = \frac{|{}^t \sigma_{p1}| {}^t \bar{E}_{p1} + |{}^t \sigma_{p2}| {}^t \bar{E}_{p2} + |{}^t \sigma_{p3}| {}^t \bar{E}_{p3}}{|{}^t \sigma_{p1}| + |{}^t \sigma_{p2}| + |{}^t \sigma_{p3}|} \quad (14)$$

and the Poisson ratio is assumed to be constant as noted earlier.

If the material is under high compression, i.e., ${}^t \sigma_{p3} < \kappa \tilde{\sigma}'_c$, an orthotropic stress-strain matrix with the directions of orthotropy defined by the principal stress directions is employed. The stress-strain matrix corresponding to these directions is, considering three-dimensional stress conditions,

$$C = \frac{1}{(1+\nu)(1-2\nu)} \begin{bmatrix} (1-\nu) {}^t \bar{E}_{p1} & \nu {}^t E_{12} & \nu {}^t E_{13} & 0 & 0 & 0 \\ & (1-\nu) {}^t \bar{E}_{p2} & \nu {}^t E_{23} & 0 & 0 & 0 \\ & & (1-\nu) {}^t \bar{E}_{p3} & 0 & 0 & 0 \\ \text{sym.} & & & \frac{1}{2}(1-2\nu) {}^t E_{12} & 0 & 0 \\ & & & & \frac{1}{2}(1-2\nu) {}^t E_{13} & 0 \\ & & & & & \frac{1}{2}(1-2\nu) {}^t E_{23} \end{bmatrix}, \quad (15)$$

where ν is the constant Poisson ratio, and the shear modulus in a coordinate plane is calculated from the weighted Young's modulus corresponding to that plane,

$${}^t G_{ij} = \frac{{}^t E_{ij}}{2(1+\nu)} = \frac{1}{2(1+\nu)} \frac{|{}^t \sigma_{pi}| {}^t \bar{E}_{pi} + |{}^t \sigma_{pj}| {}^t \bar{E}_{pj}}{|{}^t \sigma_{pi}| + |{}^t \sigma_{pj}|} \quad (16)$$

The above stress-strain relations for material loading conditions are only employed in the calculation of the stiffness matrix at time t . Considering the evaluation of the stress increment from time t to time $t + \Delta t$, the integration in eq. (7) is approximated in the following manner,

$$\sigma = \hat{C}e \tag{17}$$

If the material was under tension or low compression at time t , i.e., ${}^t\sigma_{p3} \geq \kappa \tilde{\sigma}'_c$, the stress-strain matrix \hat{C} in eq. (17) corresponds to an isotropic material with Young's modulus tE and constant Poisson ratio ν ,

$${}^tE = \frac{|{}^t\sigma_{p1}| {}^t\tilde{E}_{p1} + |{}^t\sigma_{p2}| {}^t\tilde{E}_{p2} + |{}^t\sigma_{p3}| {}^t\tilde{E}_{p3}}{|{}^t\sigma_{p1}| + |{}^t\sigma_{p2}| + |{}^t\sigma_{p3}|} \tag{18}$$

In eq. (18), the uniaxial Young's moduli ${}^t\tilde{E}_{pi}$ corresponding to the current strain increment e are evaluated using the uniaxial stress-strain relationship in fig. 1,

$${}^t\tilde{E}_{pi} = \{ \tilde{\sigma}'_{at} {}^te_{pi} + e_{pi} - \tilde{\sigma}'_{at} {}^te_{pi} \} / e_{pi} \tag{19}$$

where the ${}^te_{pi}$ and e_{pi} are the strain components and incremental strain components at time t measured in the directions of the principal stresses ${}^t\sigma_{pi}$.

If the material was under high compression at time t , the stress-strain matrix employed in eq. (17) is the one defined in eq. (15) but using the Young's moduli ${}^t\tilde{E}_{pi}$ given in eq. (19). Also, in this case the stress and strain vectors in eq. (17) must correspond to the axes of orthotropy used in eq. (15).

3.2. Material failure envelopes

To model the failure of the material in tension and compression in two and three-dimensional analysis and to account for multiaxial conditions in the uniaxial stress-strain behavior, failure envelopes are employed. Based on the current knowledge of concrete material behavior, the tensile and compression failure envelopes shown in figs. 2 and 3 have been implemented. The tensile failure envelope given in fig. 2 is commonly employed. It is noted that

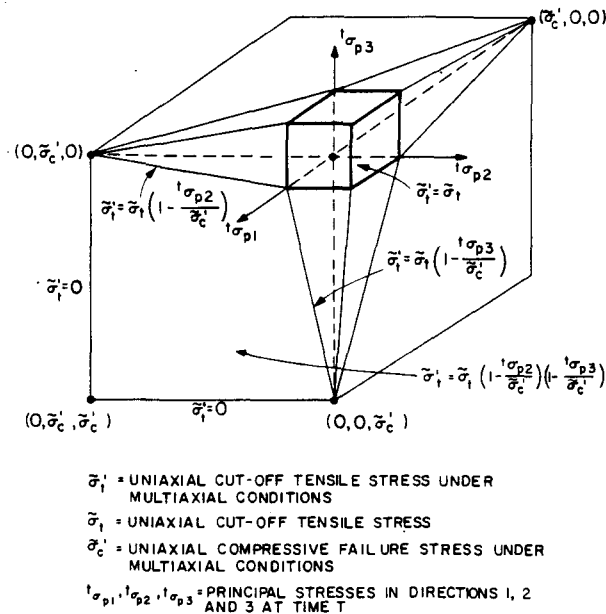


Fig. 2. Triaxial tensile failure envelope of model.

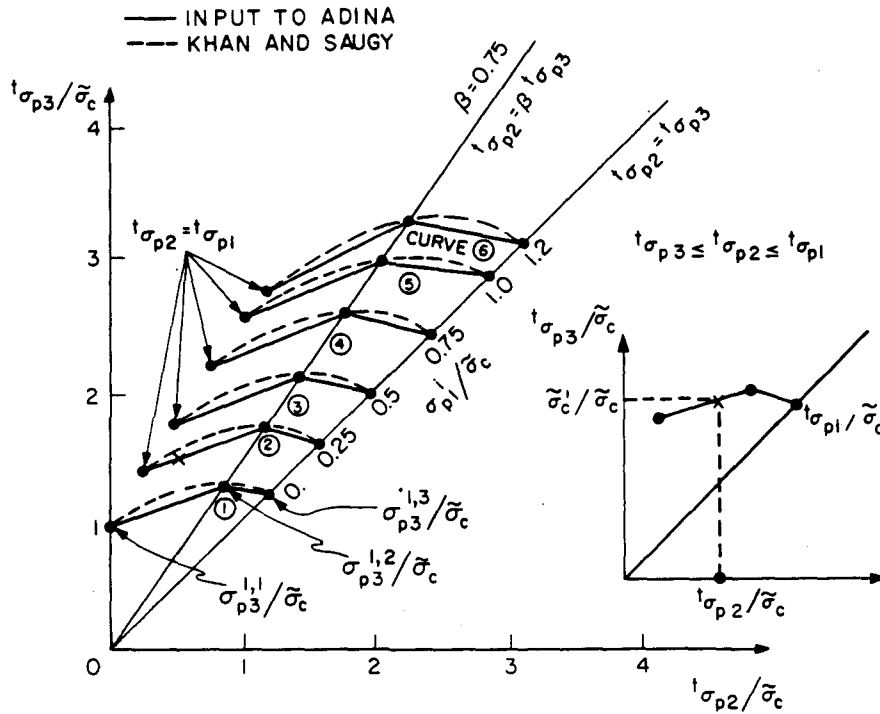


Fig. 3. Triaxial compressive failure envelope of model.

considering one principal stress direction the tensile strength of the material in this direction does not change with the introduction of tensile stresses in the other principal stress directions, but compressive stresses change this tensile strength.

Considering the compression failure envelope, it should be noted that the failure envelope shown in fig. 3 can be used to represent a large number of different envelopes like the biaxial envelope of Liu et al. [7] and the triaxial failure surface of Khan and Saugy [8]. The shape of the compressive failure surface used is largely based on the experimental results reported by Kupfer et al. [6] and Launay and Gachon [9], but the flexibility provided in the envelopes used here makes it possible to model various concrete and rock materials. The envelope can be employed to model a Mohr–Coulomb or Drucker–Prager failure surface.

The compression failure envelope is input using 24 discrete stress values. Firstly, the values $\sigma_{p1}^i/\bar{\sigma}_c$ are input. These values define at what stress magnitudes $t\sigma_{p1}$ the discrete two-dimensional failure envelopes for additional stresses $t\sigma_{p2}$ and $t\sigma_{p3}$ are input. These failure envelopes are defined by the failure stress values $\sigma_{p3}^i/\bar{\sigma}_c$ ($i = 1, \dots, 6$; $j = 1, 2, 3$) that correspond to the stress magnitudes $t\sigma_{p2} = t\sigma_{p1}$, $t\sigma_{p2} = \beta t\sigma_{p3}$ (β is a constant) and $t\sigma_{p2} = t\sigma_{p3}$.

The failure envelopes are employed to establish the uniaxial stress–strain law accounting for multiaxial stress conditions, and to identify whether tensile or crushing failure of the material has occurred. Having established the current principal stresses, to establish the uniaxial stress–strain law it is assumed that $t\sigma_{p1}$ and $t\sigma_{p2}$ are held constant and the minimum stress that would have to be reached in the third principal stress direction to cause crushing of the material is calculated using the failure envelopes, see fig. 3. Let this stress be $\tilde{\sigma}'_c$, and $\gamma_1 = \tilde{\sigma}'_c/\bar{\sigma}_c$, then we also use

$$\tilde{\sigma}'_u = \gamma_1 \tilde{\sigma}_u; \quad \tilde{e}'_c = \gamma_1 \tilde{e}_c; \quad \tilde{e}'_u = \gamma_1 \tilde{e}_u \tag{20}$$

where γ is a constant. The constants $\tilde{\sigma}'_c$, $\tilde{\sigma}'_u$, \tilde{e}'_c , \tilde{e}'_u are employed instead of the unprimed variables in order to establish using eq. (11), the uniaxial stress–strain law under multiaxial conditions (see fig. 4).

To identify whether the material has failed, the principal stresses are used to locate the current stress state in

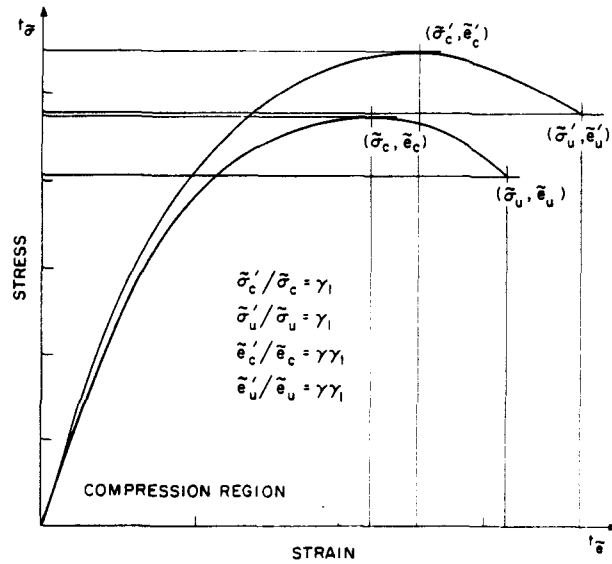


Fig. 4. Increase of strength parameters for model under multiaxial conditions.

the failure envelopes. In the following we consider how one single plane of tensile failure develops and how the material fails in compression crushing.

Tensile failure occurs if the tensile stress in a principal stress direction exceeds the tensile failure stress. In this case it is assumed that a plane of failure develops perpendicular to the principal stress direction. The effect of this material failure is that the normal and shear stiffnesses across the plane of failure are reduced, and the corresponding normal stress is released (see fig. 5). Assume that the material is subjected to low compression conditions, then before tensile failure the stress-strain relation is, considering three-dimensional analysis,

$$C = \frac{{}^tE}{(1 + \nu)(1 - 2\nu)} \begin{bmatrix} (1 - \nu) & \nu & \nu & 0 & 0 & 0 \\ & (1 - \nu) & \nu & 0 & 0 & 0 \\ & & (1 - \nu) & 0 & 0 & 0 \\ \text{sym.} & & & \frac{1}{2}(1 - 2\nu) & 0 & 0 \\ & & & & \frac{1}{2}(1 - 2\nu) & 0 \\ & & & & & \frac{1}{2}(1 - 2\nu) \end{bmatrix}, \quad (21)$$

where tE was evaluated in eq. (14). Assuming that ${}^t\sigma_{p1}$ is larger than the tensile failure stress, the new material stress-strain relation is

$$C = \frac{{}^tE}{(1 - \nu^2)} \begin{bmatrix} \eta_n & \nu\eta_n & \nu\eta_n & 0 & 0 & 0 \\ & 1 & \nu & 0 & 0 & 0 \\ & & 1 & 0 & 0 & 0 \\ \text{sym.} & & & \frac{1}{2}\eta_s(1 - \nu) & 0 & 0 \\ & & & & \frac{1}{2}\eta_s(1 - \nu) & 0 \\ & & & & & \frac{1}{2}(1 - \nu) \end{bmatrix}, \quad (22)$$

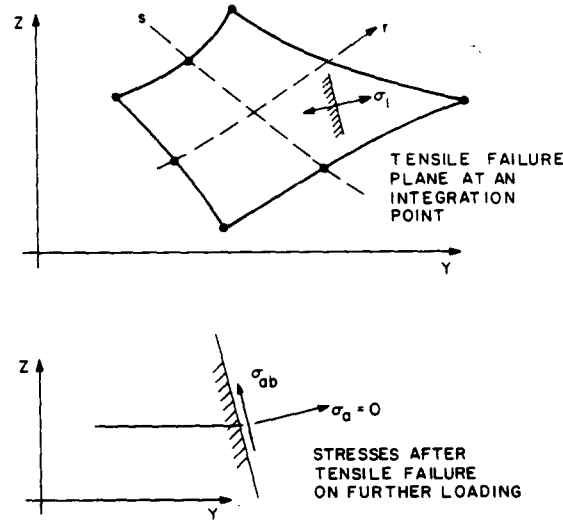


Fig. 5. Illustration of tensile failure at an integration point.

where, typically, $\eta_n = 0.001$ and $\eta_s = 0.5$, and it should be noted that plane stress conditions are assumed to exist at the plane of tensile failure. The factor η_n is not set exactly equal to zero in order to avoid the possibility of a singular stiffness matrix. The value to be employed for η_s must depend on a number of physical factors, and further research is necessary to determine appropriate values [16,22]. In the numerical solution it is at this point best to leave η_n and η_s as variables that are input at the start of solution.

In previous publications, the “plane of tensile failure” has been referred to as a “crack” [13,16], but we choose not to employ this terminology because a physical crack does not actually develop at the element integration point. Instead, the material has failed in one principal stress direction.

If the material is subjected to high compression in orthogonal principal directions, i.e. ${}^t\sigma_{p3} < \kappa\tilde{\sigma}'_c$, the same solution procedure is followed to incorporate a tensile failure, but the matrix C in eq. (21) is replaced by the matrix given in eq. (15).

Considering the loading function in eq. (12) to describe loading or unloading of the material, we note that after a tensile failure in loading f_{\max} is set equal to the value of the loading function corresponding to the stress state in which the stress release has been taken into account.

Eqs. (21) and (22) describe the solution when tensile failure occurs. To identify compression failure, the largest principal stress ${}^t\sigma_{p1}$ is employed to establish from fig. 3, by interpolation, the biaxial failure envelope on ${}^t\sigma_{p2}$ and ${}^t\sigma_{p3}$. The material has crushed if the stress state corresponding to ${}^t\sigma_{p2}$ and ${}^t\sigma_{p3}$ lies on or outside this biaxial failure envelope.

3.3. Post tensile cracking and post compression crushing behavior

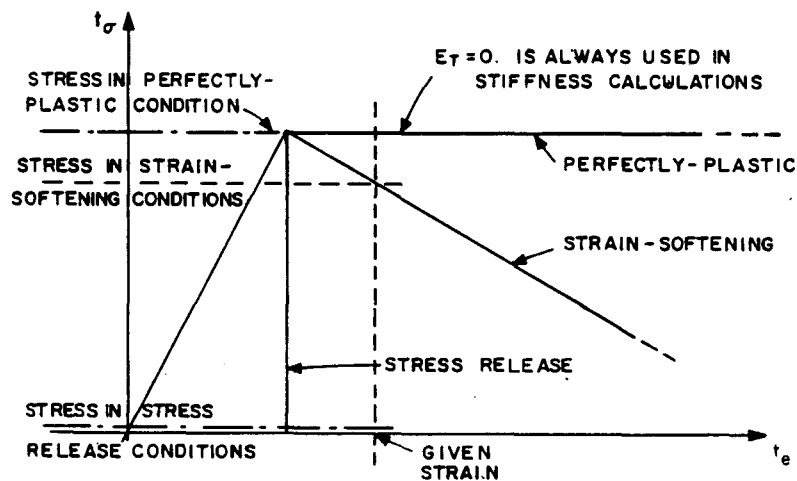
Once a tensile plane of failure has formed, it is checked in each subsequent solution step whether the failure is still active. The failure is considered to be inactive provided the normal strain across the plane becomes negative and less than the strain at which the failure occurred initially and is active otherwise (see fig. 9). Therefore, a tensile failure plane may repeatedly be active and inactive.

If a tensile failure plane has developed, which may or may not be active, the material stress–strain relations are always established as described above but corresponding to the principal stress directions in the failure plane and the direction perpendicular to this plane. Hence, instead of using the stresses principal stresses and corresponding directions as done for the unfailed material, the stress conditions along and normal to the material tensile

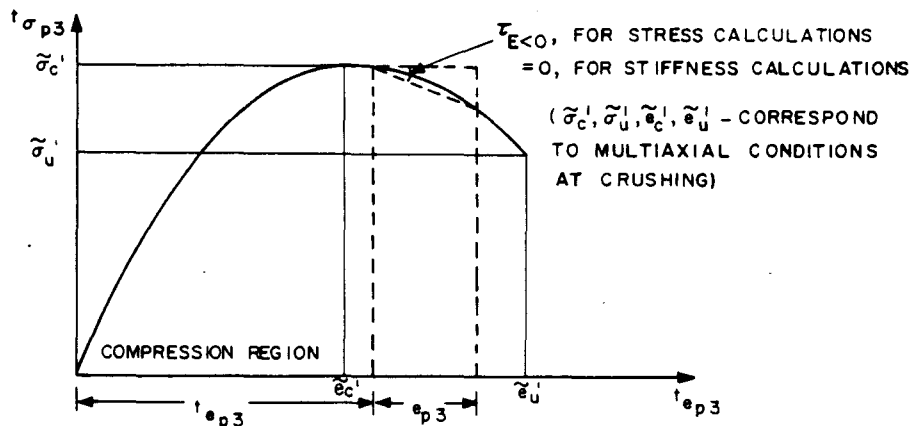
failure plane are used to evaluate the stress-strain matrix. Also, when a failure plane is or was active, a subsequent failure plane is assumed to form perpendicular to the direction of the one that developed first, once a normal stress along the original failure plane has reached the tensile failure stress. It follows that at any integration point, the direction of the third tensile failure plane is fixed once failure has occurred in two directions.

It may also happen that after tensile failure of the material (in one or two directions) the material fails in compression crushing, which is identified, as usual, by entering the compression crushing envelope in fig. 3 with the principal stress(es) that act(s) along the tensile failure plane(s).

If the material has crushed in compression, it is assumed that the material strain-softens into all directions until the minimum principal strain, ϵ_{p3} , reaches $\tilde{\epsilon}'_u$. When ϵ_{p3} becomes equal to $\tilde{\epsilon}'_u$, all stresses are completely released and from then on the material has no more stiffness.



(a) ILLUSTRATION OF SOLUTION PROCEDURES FOR POST-FAILURE ANALYSIS



(b) SOLUTION STRATEGY ADOPTED FOR MODELING STRAIN-SOFTENING CONDITIONS

Fig. 6. Strain-softening analysis procedure.

3.4. Strain-softening behavior

Consider first uniaxial stress conditions. As shown in fig. 1, for a uniaxial strain smaller than \tilde{e}'_c , the material has crushed and softens with increasing compressive strain, i.e. ${}^t\tilde{E}$ is negative. The difficulty of including this material behavior lies in that the stiffness matrix can become indefinite if a negative Young's modulus is used. The solution of the finite element equations can become difficult and subject to relatively large errors when the stiffness matrix of the element assemblage is not positive definite. To circumvent this difficulty if ${}^t\tilde{E}$ in eq. (11) is negative, in this study a zero value (actually a small positive value) for ${}^t\tilde{E}$ is employed instead. However, in the calculation of the stress increments the actual negative value of ${}^t\tilde{E}$ is used. It should be noted that this solution strategy, as illustrated in fig. 6, is a direct generalization of the common incremental procedures employed to analyze perfectly-plastic conditions and conditions of complete stress release [10,20].

Under multiaxial stress conditions the compression crushing is identified using the multiaxial failure envelope, and once the material has crushed isotropic conditions are assumed. As in uniaxial conditions, in the subsequent solution steps the Young's modulus is assumed to be zero in the stiffness matrix calculations, but the stress increments are computed from the uniaxial stress-strain law with the constants $\tilde{\sigma}'_c$, \tilde{e}'_c and so on (see fig. 4) corresponding to the multiaxial conditions at crushing. The Young's modulus tE corresponding to the current strain increment e_{p3} is evaluated using the uniaxial stress-strain relationship in fig. 1,

$${}^tE = \{\tilde{\sigma}'_{lat} {}^te_{p3+e_{p3}} - \tilde{\sigma}'_{lat} {}^te_{p3}\} / e_{p3}, \quad (23)$$

where the ${}^te_{p3}$ and e_{p3} are the strain component and incremental strain component at time t measured in the direction of the principal stress ${}^t\sigma_{p3}$. To obtain the stress increment, eq. (17) is used where the matrix \hat{C} corresponds to isotropic material conditions with Young's modulus tE .

If unloading of the crushed material in the strain-softening region occurs, characterized by $e_{p3} \geq 0$, the stress increments are assumed to be zero.

4. Computer implementation of material model

The material model has been implemented in the computer program ADINA [17,21]. The following material model parameters have to be input to the program:

- the uniaxial stress-strain law parameters \tilde{E}_0 , $\tilde{\sigma}'_t$, $\tilde{\sigma}'_c$, \tilde{e}'_c , $\tilde{\sigma}'_u$, \tilde{e}'_u , defined in section 3.1;
- the constant Poisson ratio, ν ;
- the triaxial compressive failure envelope defined by six values $\sigma'_{p1}/\tilde{\sigma}'_c$, eighteen values $\sigma'_{p3}/\tilde{\sigma}'_c$ and the constant β , described in section 3.2 and shown in fig. 3;
- other analysis control parameters: γ = a constant used for scaling \tilde{e}'_c and \tilde{e}'_u under multiaxial conditions, κ = a control parameter that defines when to use isotropic or orthotropic stress-strain relations, α = a constant multiplier for the hydrostatic component in the loading function; these three parameters are described in section 3.1; η_n , η_s = normal and shear stiffness reduction factors, defined in section 3.2.

Considering an incremental analysis, the complete solution for the calculation of the stresses and the stress-strain relations is summarized in table 2.

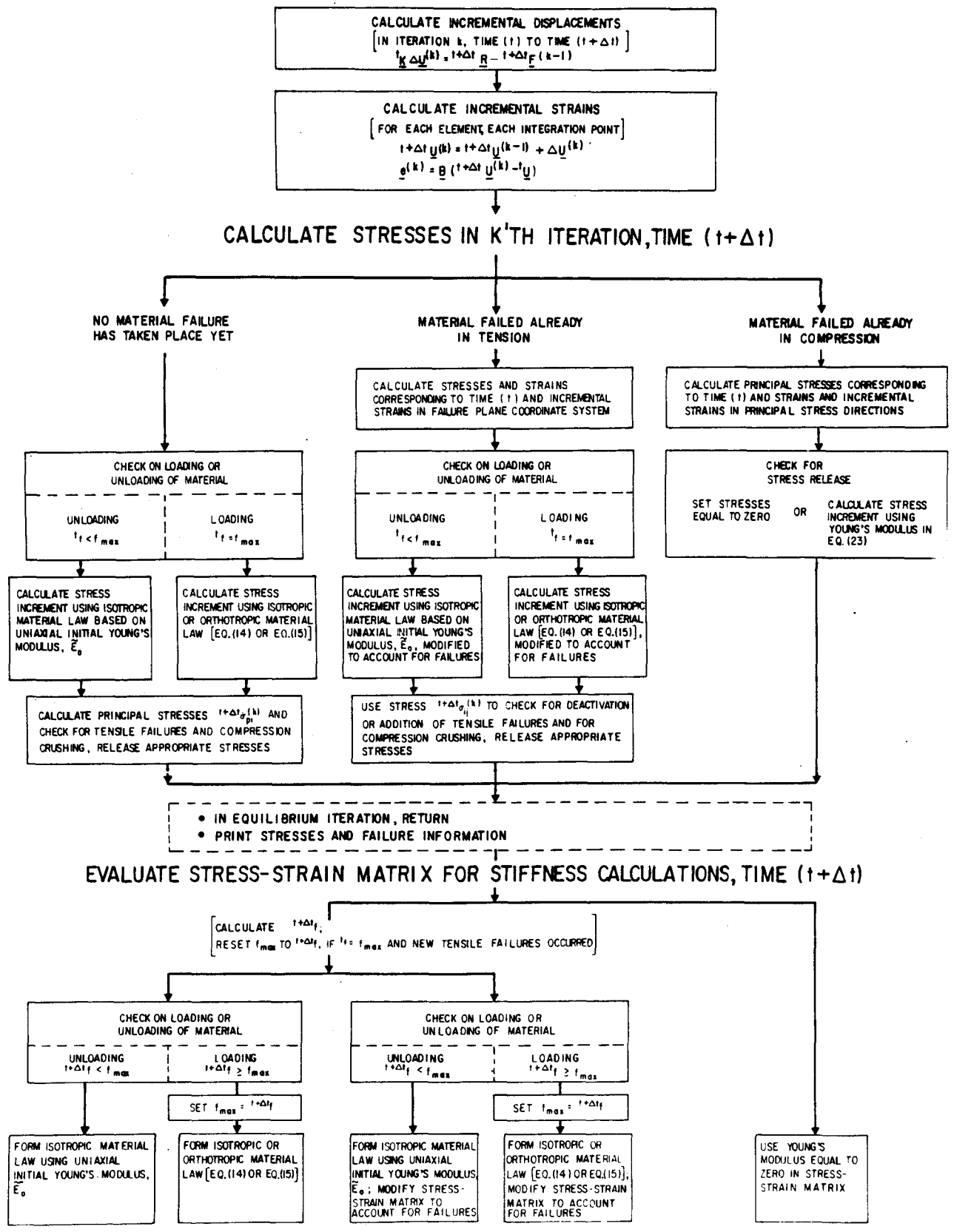
The basic equation considered in this table is,

$${}^{t+\Delta t}\boldsymbol{\sigma} = \mathbf{C} \mathbf{e} + {}^t\boldsymbol{\sigma}. \quad (24)$$

Assuming that all stresses and the tensile failure and crushing conditions at time t are known, the table summarizes the evaluation of \mathbf{C} and ${}^{t+\Delta t}\boldsymbol{\sigma}$. It should be noted that the stresses at time $t + \Delta t$ are calculated using, firstly, the material moduli corresponding to the current strain increment and secondly, any new conditions of tensile failure and crushing that have to be taken into account.

In some analyses temperature strains, e^{th} , and creep strains, e^c , need be included. These strains can be taken

Computer implementation of concrete and rock material model



into account by replacing the total incremental strain, e , in eq. (3) (and in table 2) by the strain increment, $e - e^{th} - e^c$, where e^{th} and e^c must be calculated depending on the temperature, stress and strain conditions [20].

5. Modeling of steel reinforcement, prestressing and steel liners

As a structural material, concrete is used with steel reinforcement, prestressing cables, and steel liners. In the computer program ADINA, depending on the structure to be analyzed, steel reinforcement can be modeled by discrete truss elements or plane stress elements. Steel liners are represented by plane stress elements. Prestressing cables are modeled using cable elements with initial forces. In order to represent the time lag between the application of different prestressing, an element birth option is employed in which an element becomes active only from its time of birth.

The elements available in ADINA for modeling concrete and the reinforcement are depicted in fig. 7.

6. Sample solutions

The model described in the previous sections has been implemented in the computer program ADINA and was used to analyze a number of problems. In this section, we report some of the solution results. In almost all the

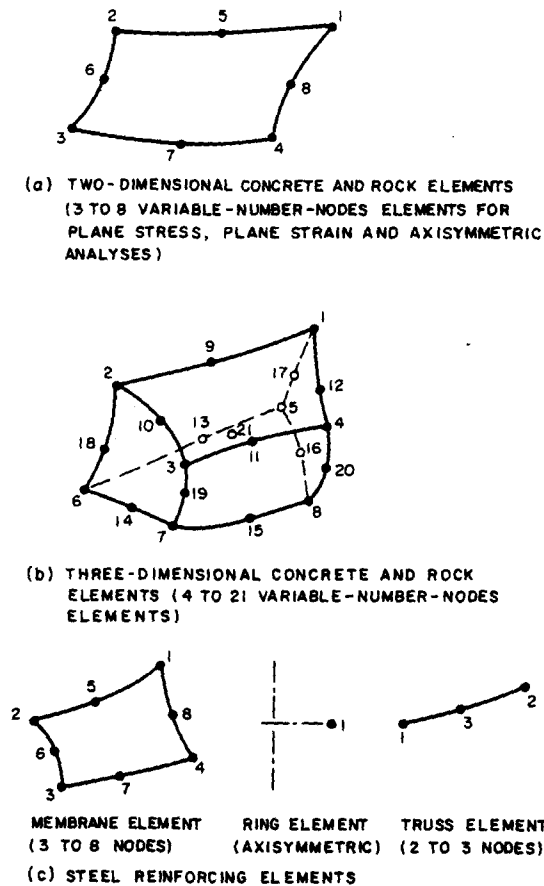


Fig. 7. Finite elements available in ADINA for analysis of concrete and rock structures.

analyses, the material model was used to model concrete structures because some comparisons with analytical or experimental results are available.

In all the following analyses, the three-dimensional compressive failure envelope shown in fig. 3 was used.

6.1. Demonstrative analyses of a concrete or rock sample

Some simple loading conditions were analyzed in order to numerically identify the essential characteristics of the material model that are summarized in figs. 1–6 and to identify typical numerical solution errors. We present here the one-dimensional stress and strain response of a simple 4-node plane stress element.

Fig. 8 shows the single 4-node element which was subjected to a linearly increasing stress in the first analysis and to a strain-controlled loading in the second analysis. The comparison of the response predicted with the analytical stress–strain law (which is input to the program) shows that, as expected, in each analysis the calculated stress–strain points are on the analytical curve. In the strain-controlled analysis the strain-softening branch is also traced out.

Considering the analysis results obtained in the stress-controlled loading only the response up to the maximum stress, $\tilde{\sigma}_c$, could be predicted, and the strain-softening region could not be reached, because a reduction in applied stress is considered as unloading (using \tilde{E}_0). In addition, fig. 8 shows that, as would be anticipated, the predicted stress is smaller than the applied stress if equilibrium iteration is not employed.

The same element was then also subjected to cyclic one-dimensional strain-controlled loading as shown in fig. 9. The response sequence shows how unloading from compression at point A, cracking at point B with subsequent stress release to point C is predicted. Next, the element was unloaded further to point D and then reloaded to points E and F to reach the original maximum load level. Finally, the element was loaded to crushing at point G and into the strain-softening region until ultimate material failure at point H.

6.2. Two and three-dimensional analysis of a simply-supported concrete beam

The simply supported beam shown in fig. 10 was modeled using the following finite element idealizations:

Case 1: five 12-node three-dimensional elements. Corresponding to the X, Y, Z coordinate axes 2 X 3 X 3

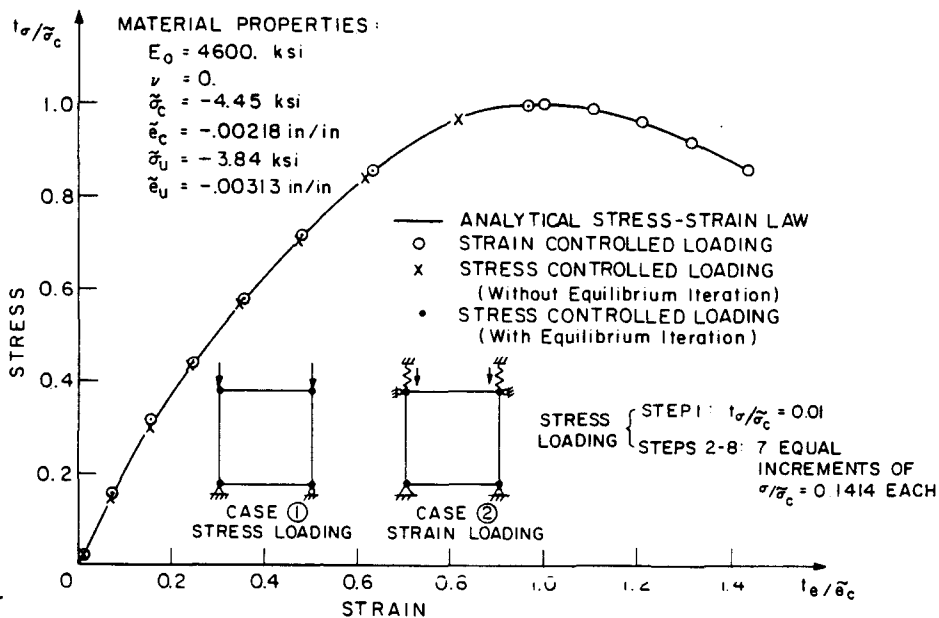


Fig. 8. Uniaxial stress–strain response of model.

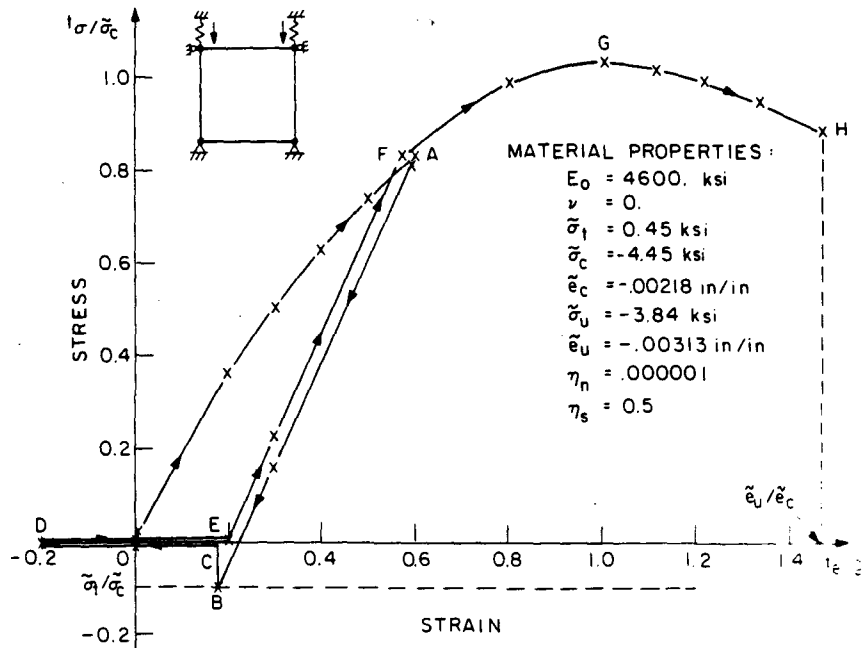


Fig. 9. Uniaxial behavior of model with unloading and reloading in compression.

Gauss numerical integration was employed. The steel reinforcement, 2 in^2 , was modeled using the 6-node membrane elements.

Case 2: five 6-node two-dimensional elements with Gauss numerical integration order 3×3 . The steel reinforcement, 2 in^2 , was modeled using 3-node truss elements.

Case 3: ten 6-node two-dimensional elements with Gauss numerical integration order 2×2 . The steel reinforcement, 2 in^2 , was modeled using 3-node truss elements.

Case 4: the element idealization of case 3 was used but the steel reinforcement was 0.62 in^2 .

The objective was to compare the beam response predicted in this analysis with the response calculated by Suidan and Schnobrich [13] and an analytical solution [23].

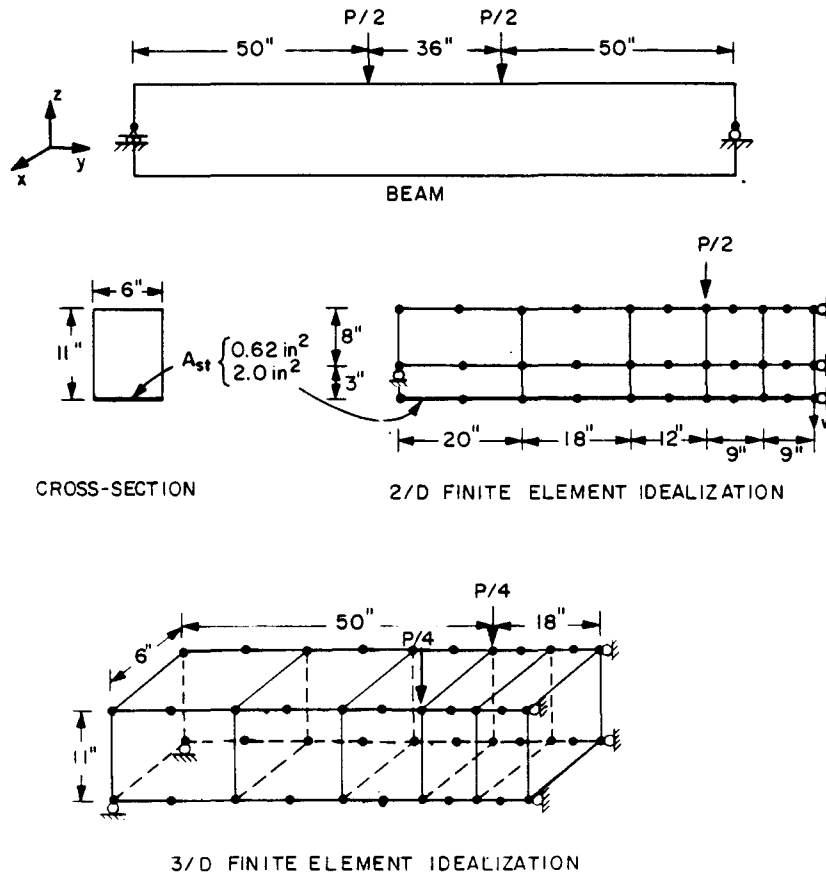
Fig. 11 shows the midspan displacement of the beam, and fig. 12 gives the maximum steel stress as a function of the applied load. It is seen that using the three different finite element idealizations of cases 1 to 3 essentially the same response is predicted. The loading procedure used is also shown in fig. 11. An average of three equilibrium iterations were required in these analyses. The case 4 analysis results are compared in fig. 11 with the results published by Suidan and Schnobrich [13].

The zone of tensile failure at the constant moment section of the beam as a function of the applied load P is shown in fig. 13, in which the response predicted by ADINA is compared with the analytical results obtained by Krahl et al. [23].

The case 3 model was also analyzed for its nonlinear dynamic response when subjected instantaneously to concentrated loads. A constant lumped mass matrix was used in the analysis. For the time integration, Newmark's method was employed. The nonlinear displacement response predicted by ADINA is shown in fig. 14 in which also the linear dynamic response and the static response are given.

6.3. Large displacement analysis of a concrete beam

The simply-supported concrete beam considered in the previous analysis (fig. 10) but with a span of 236 in. was analyzed including the effect of an axial load, Q . This axial load was applied at the centroid of the beam



MATERIAL PROPERTIES:

CONCRETE:	$\tilde{E}_0 = 6100 \text{ ksi}$	$\tilde{\sigma}_c = -3.74 \text{ ksi}$	$\tilde{\sigma}_u = -3.225 \text{ ksi}$
	$\nu = 0.2$	$\tilde{\sigma}_t = .458 \text{ ksi}$	$\tilde{e}_u = -.003 \text{ in/in}$
		$\tilde{e}_c = -.002 \text{ in/in}$	$\rho = 0.217 \times 10^{-3} \text{ slugs/in}^3$
STEEL:	$E = 30000 \text{ ksi}$	$\sigma_y = 44.0 \text{ ksi}$	$\rho = 0.734 \times 10^{-3} \text{ slugs/in}^3$
	$E_T = 300 \text{ ksi}$		
	$\gamma = 1.0$; $\kappa = 1.0$; $\eta_n = 0.0001$;		$\eta_s = 0.5$

Fig. 10. Analysis of a simply-supported reinforced concrete beam.

cross-section. Fig. 15 shows the finite element model used and the predicted load displacement response of the beam with and without the axial load Q . In one analysis, small displacements were assumed, hence the axial load causes only a compressive normal stress in the uncracked beam; and in another analysis, large displacement effects were included. In this case, the load Q also introduces a bending moment in the beam model as the structure deflects, and a smaller ultimate load is predicted. Fig. 16 shows the rebar stress at the midspan of the beam as predicted in the analyses.

Although the decrease in the ultimate load predicted in this problem is not drastic when including large displacement effects, the analysis does indicate that it may be important to account for large displacement effects in the analysis of some column and shell structures.

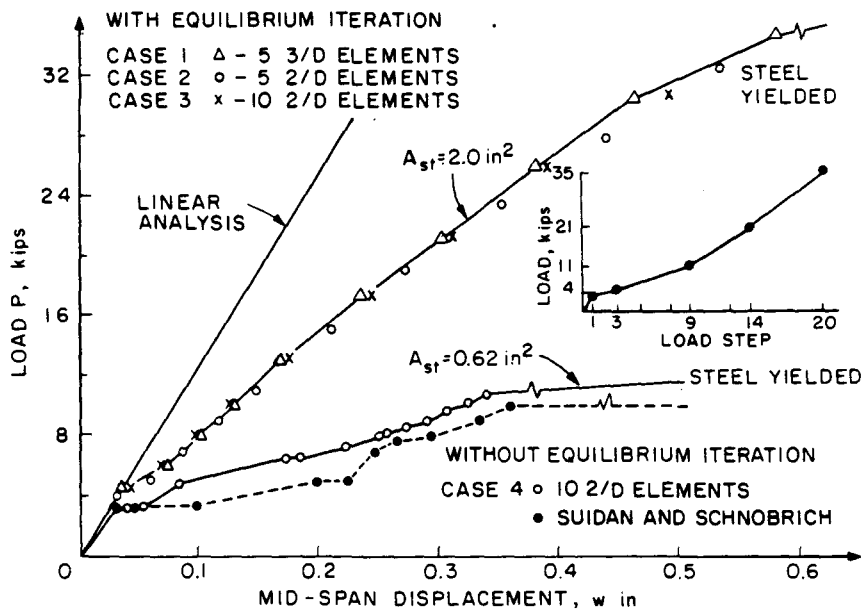


Fig. 11. Load displacement curve for the simply-supported beam.

6.4. Analysis of a prestressed concrete reactor vessel

The prestressed concrete reactor vessel (PCRV) for which experimentally obtained test results were reported in ref. [24] and numerical results were given in ref. [10] was analyzed. Fig. 17 shows the test vessel and the finite element mesh employed in the idealization. The different finite elements used to model the concrete and prestressing

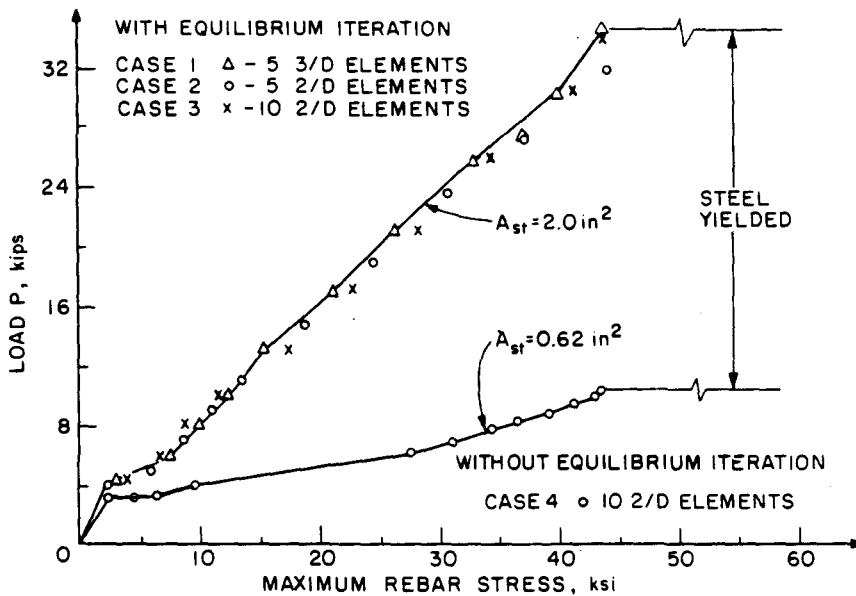


Fig. 12. Load rebar stress diagram for the simply-supported beam.

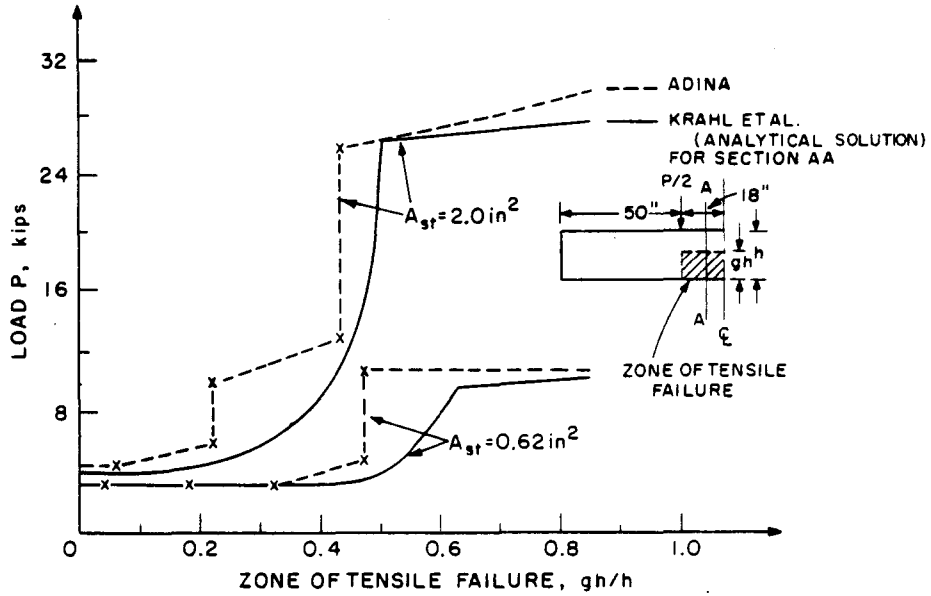


Fig. 13. Zones of tensile failure for the simply-supported beam.

cables and the material properties employed are also shown. Small displacement conditions were assumed in the analysis.

The loading procedure used in the analysis is given in fig. 18. In the first step only the circumferential prestressing of 144 000 psi was applied as initial forces in the ring elements. In the next step the longitudinal prestressing

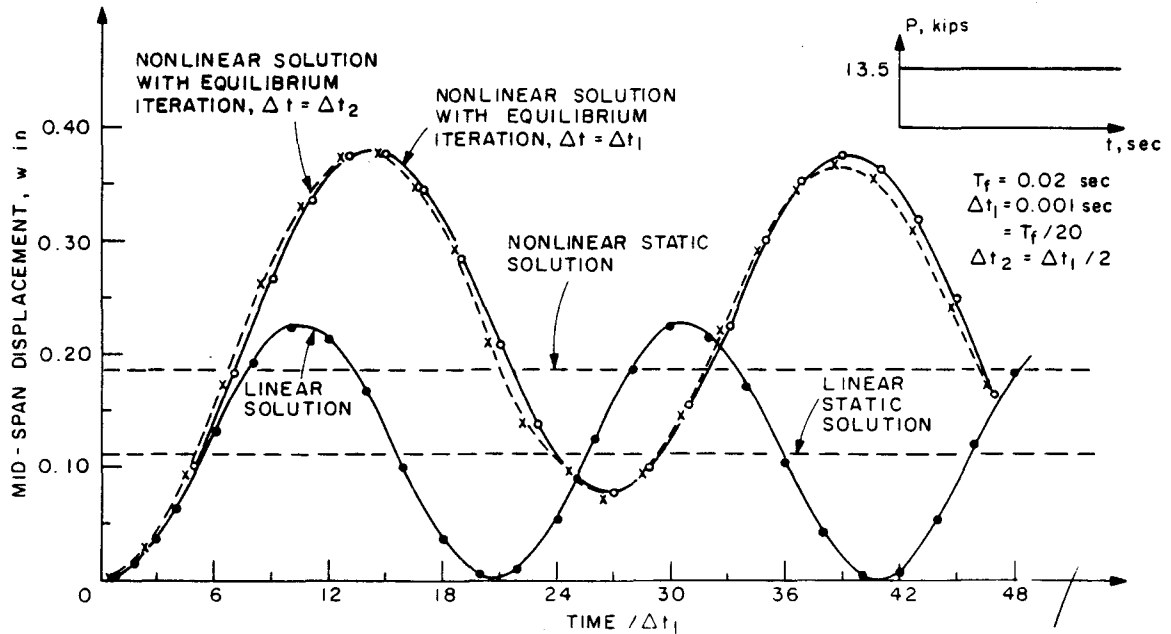


Fig. 14. Nonlinear dynamic response of the simply-supported beam, Newmark method, $\delta = 0.50$, $\alpha = 0.25$

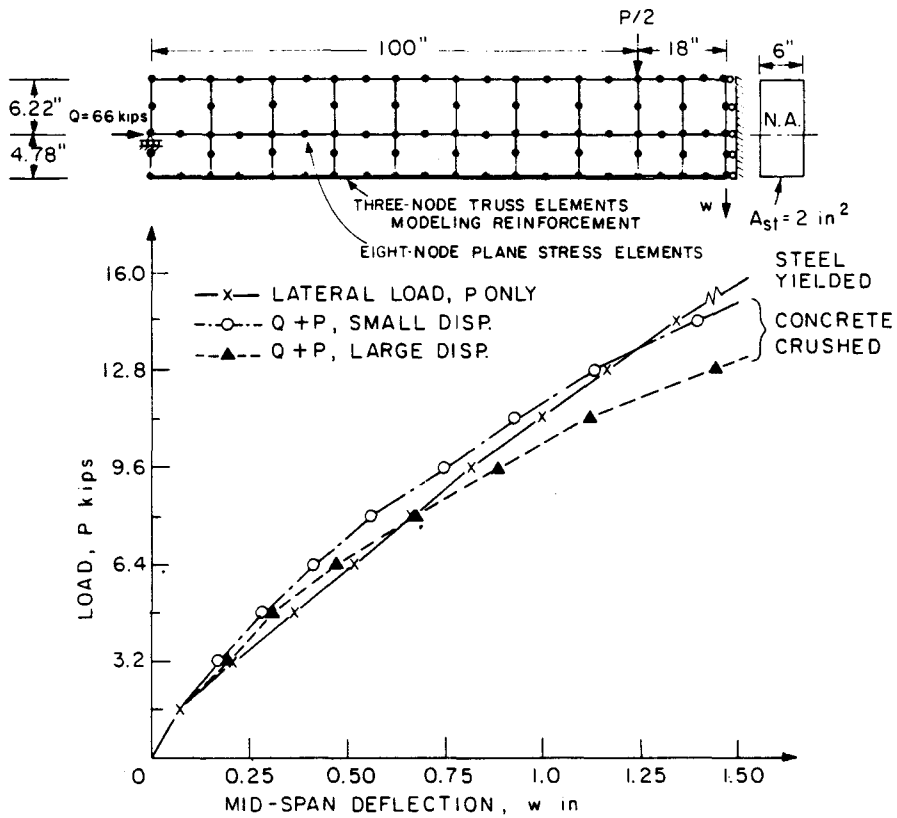


Fig. 15. Large displacement analysis of a concrete beam.

cable to introduce a prestress of 900 000 psi was applied. From the third step onwards the internal pressure was applied.

Figs. 18 and 19 show the response predicted in the analysis of the vessel. Two solutions were performed with a

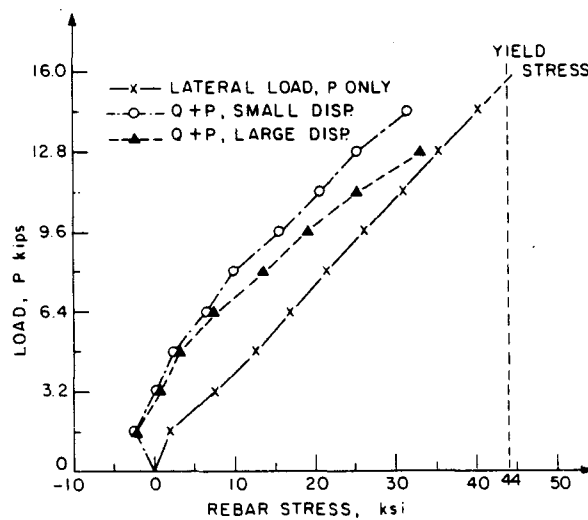
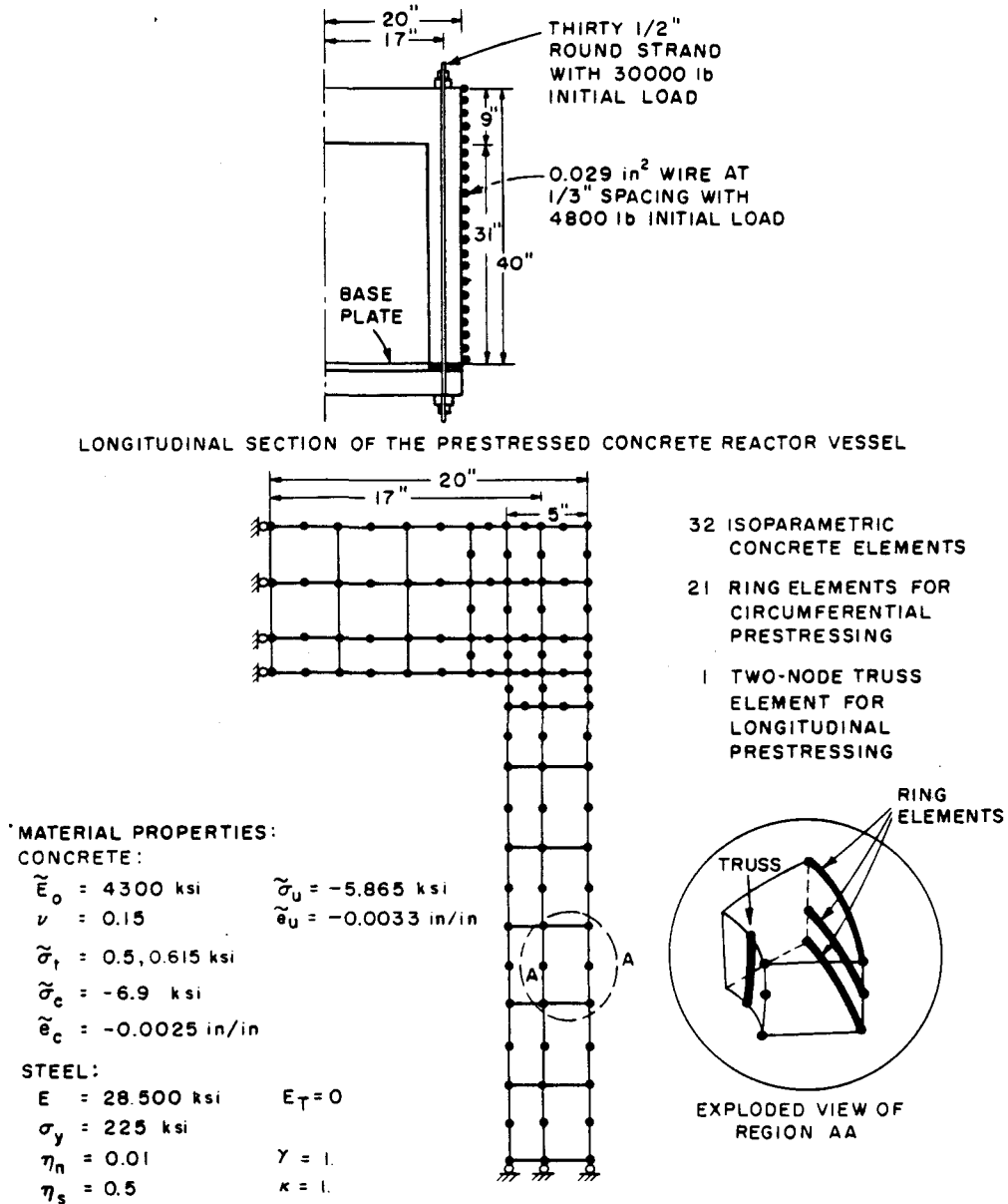


Fig. 16. Mid-span rebar stresses in the concrete beam.



MATERIAL PROPERTIES AND FINITE ELEMENT MESH

Fig. 17. Finite element model of reactor vessel.

uniaxial tensile strength of $\tilde{\sigma}_t$ equal to 500 psi and 615 psi, respectively, because the splitting test indicated a tensile strength of $\tilde{\sigma}_t = 500 \text{ psi}$ [24], whereas the ultimate tensile strain of the material indicated a tensile strength of 615 psi [10]. Fig. 18 shows that the ADINA solutions predict reasonably well the ultimate load of the structure but that the calculated displacements at the ultimate load are much too small. In the analyses, an average of two equilibrium iterations per step were performed.

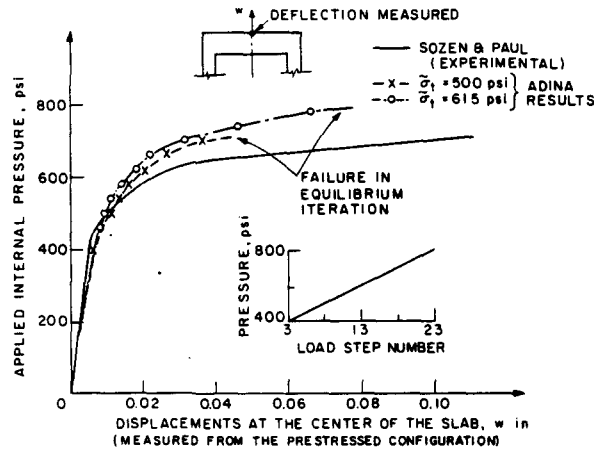


Fig. 18. Displacements of the slab at mid-span.

6.5. Analysis of a corner supported concrete slab

A materially nonlinear only analysis of a reinforced concrete slab was performed. The slab was supported at its four corners and subjected to a concentrated center load. Fig. 20 shows the slab and the finite element model used. It should be noted that the concrete material below the reinforcement layer was neglected in the finite element

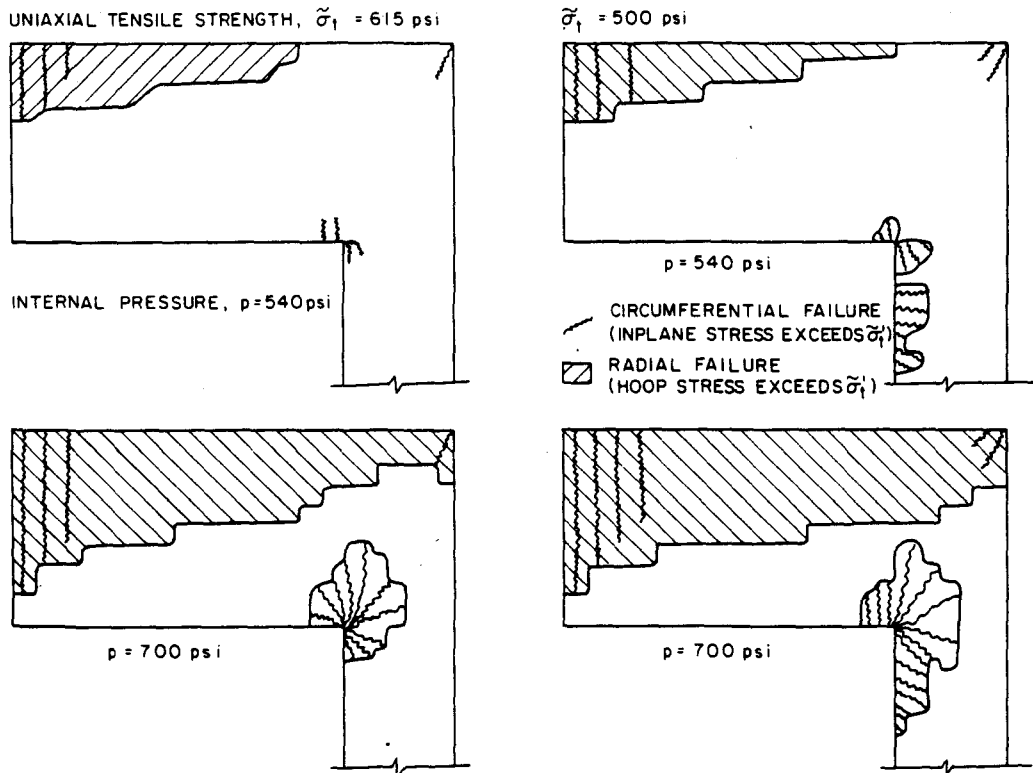
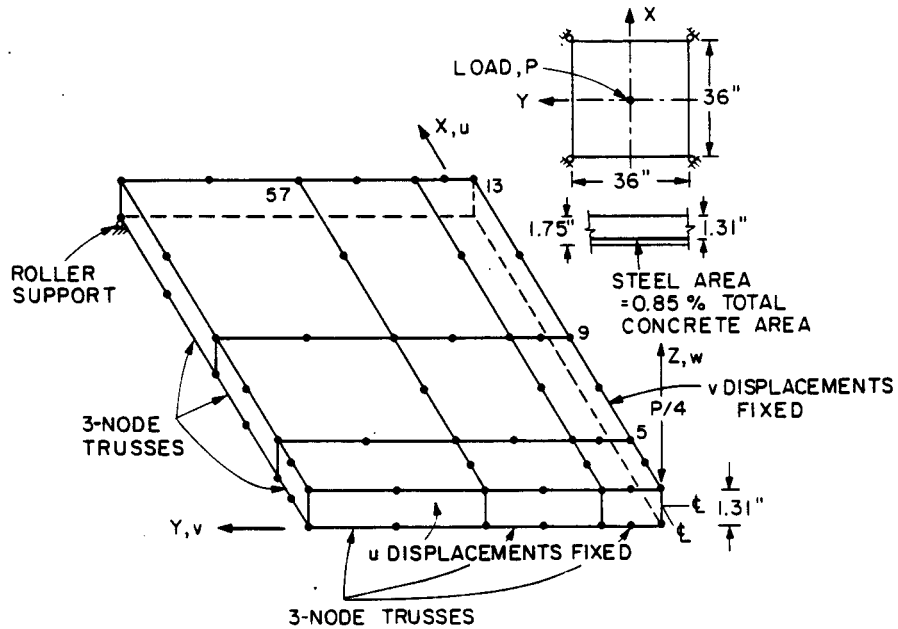


Fig. 19. Zones of tensile failure of the reactor vessel.



MATERIAL PROPERTIES :

STEEL :

- $A_{st} = 0.536 \text{ in}^2$
- $E_{st} = 29000 \text{ ksi}$
- $\sigma_y = 50 \text{ ksi}$
- $E_T = 29 \text{ ksi}$

CONCRETE :

- $\tilde{E}_o = 4150 \text{ ksi}$
- $\nu = 0.15$
- $\tilde{\sigma}_t = 0.77 \text{ ksi}$
- $\tilde{\sigma}_c = -5.5 \text{ ksi}$
- $\tilde{\sigma}_u = -4.7 \text{ ksi}$
- $\tilde{\epsilon}_c = -.002 \text{ in/in}$
- $\tilde{\epsilon}_u = -.003 \text{ in/in}$

ANALYSIS PARAMETERS :

$\gamma = 1. ; \kappa = 0.7 ; \eta_n = 0.0001 ; \eta_s = 0.5$

- 9 SIXTEEN-NODE ISOPARAMETRIC ELEMENTS WITH $3 \times 3 \times 3$ INTEGRATION
- 24 THREE-NODE TRUSS ELEMENTS

Fig. 20. Analysis of a corner-supported concrete slab.

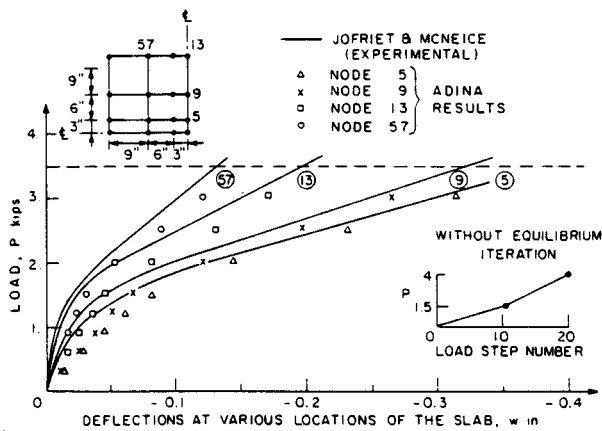


Fig. 21. Vertical deflections of the corner-supported concrete slab.

model. Also, the weight of the plate was not included in the load application. Experimental and finite element solutions for this problem have been obtained by Jofriet and McNeice [25] and Lin and Scordelis [15], respectively.

Fig. 21 gives the loading procedure used in the ADINA analysis and compares displacements predicted in this study with the experimental results. Essentially, the same analysis results were also obtained with a total of 10 load steps. It is seen that the calculated and experimentally observed displacements at large load levels compare reasonably well. In the analysis, very large displacements were predicted at $p = 3.5$ kips indicating collapse of the slab.

7. Conclusions

A finite element model for geometric and material nonlinear three-dimensional analysis of concrete and some rock structures has been presented. The model is based on a nonlinear uniaxial stress-strain relation that is generalized for two- and three-dimensional stress conditions. Tensile cracking and compression crushing, strain-softening and cyclic loading conditions are considered. The model has been implemented and some sample solutions have been presented.

When developing material nonlinear solution capabilities the two major difficulties encountered are that appropriate nonlinear material descriptions must be employed and that these descriptions must be numerically tractable, i.e., a stable and effective implementation must be possible. It is, of course, imperative that physically appropriate material descriptions be employed in a finite element formulation, but it is also important to operate on these descriptions in a stable, accurate and efficient manner, because otherwise the predicted response may be meaningless and can certainly not be interpreted with confidence. In the work reported in this paper, emphasis was placed on both of these aspects of material nonlinear finite element analysis.

The model proposed in this paper can already be employed effectively for the solution of various problems. The objective in the paper was to describe the basic model and some applications. However, it is realized that significant further studies, evaluations and improvements of the model are needed. For example, a detailed comparison of the model with other concrete and rock material models, the evaluation of the model in situations with significant strain softening effects, and the evaluation of the model to predict fracture discontinuities and strain localizations is important [26,27]. Such studies are currently being pursued and are expected to lead to further insight and improvements in the model.

Acknowledgements

The work reported in this paper has been supported financially by the ADINA users group. We would like to acknowledge gratefully this support. We also would like to thank J. Crawford of the Naval Civil Engineering Laboratory, Port Hueneme, for various valuable suggestions during the course of this work.

References

- [1] O.C. Zienkiewicz, *The Finite Element Method in Engineering Science* (McGraw-Hill, New York, 1971).
- [2] K.J. Bathe and E.L. Wilson, *Numerical Methods in Finite Element Analysis* (Prentice-Hall, 1976).
- [3] R. Wegner, in: *Formulations and Computational Algorithms in Finite Element Analysis*, eds., K.J. Bathe, J.T. Oden and W. Wunderlich (MIT Press, Cambridge, 1977).
- [4] L.P. Saenz, *ACI J.* 61 (1964) 1229.
- [5] S. Popovics, *ACI J.* 67 (1970) 243.
- [6] H. Kupfer, H.K. Hilsdorf and H. Rusch, *ACI J.* 66 (1969) 656.

- [7] T.C.Y. Liu, A.H. Nilson and F.O. Slate, *ASCE J. Struct. Div.* 98 (1972) 1025.
- [8] M.H. Khan and B. Saugy, *Concrete for Nuclear Reactors – ACI Publication SP-34* (1972).
- [9] P. Launay and H. Gachon, *Concrete for Nuclear Reactors, Vol. I – ACI Publication SP-34* (1972).
- [10] O.C. Zienkiewicz, D.R.J. Owen, D.V. Phillips and G.C. Nayak, *Nucl. Eng. Des.* 20 (1972) 507.
- [11] J.H. Argyris, G. Faust, J. Szimmat, E.P. Warnke and K.J. Willam, *Nucl. Eng. Des.* 28 (1974) 42.
- [12] Z.P. Bažant, P. Bhat and C. Shieh, *Northwestern University Structural Engineering Report 12-259* (1976).
- [13] M. Suidan and W. Schnobrich, *ASCE J. Struct. Div.* 99 (1973) 2109.
- [14] A.C. Scordelis, in: *Proc. Spec. Conf. Finite Element Method in Civil Engineering*, McGill University, Montreal (1972) p. 71.
- [15] C.S. Lin and A.C. Scordelis, *ASCE J. Struct. Div.* 101 (1975) 523.
- [16] Y. Sarne, Ph.D. Thesis, Massachusetts Institute of Technology (1974).
- [17] K.J. Bathe, Massachusetts Institute of Technology Report 82448-1 (1977).
- [18] J.C. Jaeger and N.G.W. Cook, *Fundamentals of Rock Mechanics* (Wiley, New York, 1976).
- [19] K.J. Bathe, E. Ramm and E.L. Wilson, *Int. Num. Methods Eng.* 9 (1975) 353.
- [20] K.J. Bathe, Massachusetts Institute of Technology Report 82448-2 (1977).
- [21] K.J. Bathe, S. Bolourchi, S. Ramaswamy and M.D. Snyder, *Nucl. Eng. Des.* 46 (1978) 429.
- [22] J.P. Laible, R.N. White and P. Gergely, *Cornell University Department of Structural Engineering Report* (1973).
- [23] N.W. Krahl, N. Khachaturian and C.P. Siess, *ASCE J. Struct. Div.* 93 (1967) 235.
- [24] M.A. Sozen and S.L. Paul, *Nucl. Eng. Des.* 8 (1968) 403.
- [25] J.C. Jofriet and G.M. McNeice, *ASCE J. Struct. Div.* 97 (1971) 785.
- [26] R.N. Murtha and J.E. Crawford, *Naval Construction Battalion Center Technical Memorandum M-SI-78-6* (1977).
- [27] M.P. Cleary, *J. Pressure Vessel Petroleum Technol.* 100 (1978) 2.

NONSAP – A NONLINEAR STRUCTURAL ANALYSIS PROGRAM*

Klaus Jürgen BATHE and Edward L. WILSON

Division of Structural Engineering and Structural Mechanics, Department of Civil Engineering, University of California, Berkeley, California 94720, USA

Received 24 June 1974

The current version of the computer program NONSAP for linear and nonlinear, static and dynamic finite element analysis is presented. The solution capabilities, the numerical techniques used, the finite element library, the logical construction of the program and storage allocations are discussed. The solutions of some sample problems considered during the development of the program are presented.

1. Introduction

The endeavor to perform nonlinear analyses has steadily increased in recent years [1–4]. The safety of a structure may be increased and the cost reduced if a nonlinear analysis can be carried out. Primarily, nonlinear analyses of complex structures have become possible through the use of electronic digital computers operating on discrete representations of the actual structure. A very effective discretization procedure has proven to be the finite element method [5]. Based on this method, various large-scale general purpose computer programs with nonlinear capabilities are now in use [6].

The development of a nonlinear finite element analysis program is a formidable challenge. The proper formulation of the nonlinear problem and its idealization to a representative finite element system demands a modern background in structural mechanics. For the solution of the equilibrium equations in space and time, stable and efficient numerical techniques need be employed. The efficiency of a nonlinear program depends largely on optimum usage of computer hardware and software where, specifically, the appropriate allocation of high- and low-speed storage is important.

The earliest attempts to obtain nonlinear analysis programs essentially involved simple modifications of established programs for linear analysis, much in the same way as the linear structural theory was modified to account for some nonlinearities. However, to analyze systems with large geometrical and material nonlinearities, the program should be designed specifically for the required iteration process and not be merely an extension of a linear analysis program. Naturally, a linear analysis program should be flexible and easy to modify or extend; however, this applies even more to a nonlinear analysis program. In particular, it should be realized that a great deal of research is still required and currently pursued in the nonlinear static and dynamic analysis of complex structures. Therefore, unless the general nonlinear analysis code is easy to modify, it may be obsolete within a few years of completion.

The nonlinear analysis program NONSAP presented in this paper is not an extension of the linear analysis program SAP [7], but rather a completely new development [8]. Program NONSAP is designed with two primary objectives. The first aim is the efficient solution of a variety of practical nonlinear problems with the current capabilities of nonlinear analysis procedures and computer equipment. The second objective is to have a program which can be used effectively in the various research areas pertaining to nonlinear analysis.

* Invited paper M3/1* presented at the Second International Conference on Structural Mechanics in Reactor Technology, Berlin, Germany, 10–14 September, 1973.

Because of continuous improvements in nonlinear analysis procedures, both objectives are attained simultaneously by the development of an efficient, modular, and easily modifiable general analysis code. The program is designed for a general incremental solution of nonlinear problems, but naturally can also be used for linear analysis.

The structural systems to be analyzed may be composed of combinations of a number of different finite elements. The program presently contains the following element types:

- (a) three-dimensional truss element,
- (b) two-dimensional plane stress and plane strain element,
- (c) two-dimensional axisymmetric shell or solid element,
- (d) three-dimensional solid element, and
- (e) three-dimensional thick shell element

The nonlinearities may be due to large displacements, large strains, and nonlinear material behavior. The material descriptions presently available are:

- (1) For the truss elements: linear elastic and nonlinear elastic.
- (2) For the two-dimensional elements: isotropic linear elastic; orthotropic linear elastic; Mooney–Rivlin material; elastic–plastic materials, von Mises or Drucker–Prager yield conditions; variable tangent moduli model; and curve description model (with tension cut-off).
- (3) For the three-dimensional elements: isotropic linear elastic and curve description model.

Program NONSAP is an in-core solver. The capacity of the program is essentially determined by the total number of degrees of freedom in the system. However, all structure matrices are stored in compacted form, i.e. only nonzero elements are processed, resulting in maximum system capacity and solution efficiency.

The system response is calculated using an incremental solution of the equations of equilibrium with the Wilson θ or Newmark time integration scheme. Before the time integration is carried out, the constant structure matrices, namely the linear effective stiffness matrix, the linear stiffness, mass and damping matrices, whichever is applicable, and the load vectors are assembled and stored on low-speed storage. During the step-by-step solution the linear effective stiffness matrix is updated for the nonlinearities in the system.

Therefore, only the nonlinearities are dealt with in the time integration and no efficiency is lost in linear analysis.

The incremental solution scheme used corresponds to a modified Newton iteration. To increase the solution efficiency, the user can specify an interval of time steps in which a new effective stiffness matrix is to be formed and an interval in which equilibrium iterations are to be carried out.

There is practically no high-speed storage limit on the total number of finite elements used. To obtain maximum program capacity, the finite elements are processed in blocks according to their type and whether they are linear or nonlinear elements. In the solution low-speed storage is used to store all information pertaining to each block of finite elements, which, in the case of nonlinear elements, is updated during the time integration.

The purpose in this paper is to present the general program organization, the current element library, the numerical techniques used and some sample solutions. The different options available for static and dynamic analyses are described. In the presentation emphasis is directed to the practical aspects of the program. For detailed information on the formulation of the continuum mechanics equations of motion, the finite element discretization, and the material models used, see refs [9] and [10].

2. Incremental equilibrium equations of structural systems

The incremental nodal point equilibrium equations for an assemblage of nonlinear finite elements have been derived in refs [9] and [10]. At time t we have

$$M {}^{t+\Delta t} \ddot{u} + C {}^{t+\Delta t} \dot{u} + {}^t K u = {}^{t+\Delta t} R - {}^t F, \quad (1)$$

where M is the constant mass matrix; C is the constant damping matrix; ${}^t K$ is the tangent stiffness matrix at time t ; ${}^{t+\Delta t} R$ is the external load vector applied at time $t + \Delta t$; ${}^t F$ is the nodal point force vector equivalent to the element stresses at time t ; ${}^{t+\Delta t} \dot{u}$, ${}^{t+\Delta t} \ddot{u}$ are vectors of nodal point velocities and accelerations at time $t + \Delta t$; and u is the vector of nodal point dis-

placement increments from time t to $t + \Delta t$, i.e.
 $u = {}^{t+\Delta t}u - {}^t u$.

As discussed in refs [9] and [10], the solution of eq. (1) yields, in general, approximate displacement increments u . To improve the solution accuracy, and, in some cases, to prevent the development of instabilities, it may be necessary to use equilibrium iteration in each or preselected time steps. In this case we consider the equilibrium equations

$$M {}^{t+\Delta t}\ddot{u}^{(i)} + C {}^{t+\Delta t}\dot{u}^{(i)} + {}^t K \Delta u^{(i)} = {}^{t+\Delta t}R - {}^{t+\Delta t}F^{(i-1)} \quad i = 1, 2, 3 \dots \quad (2)$$

where M , C , ${}^t K$, and ${}^{t+\Delta t}R$ are as defined above, and

$${}^{t+\Delta t}\ddot{u}^{(i)}, \quad {}^{t+\Delta t}\dot{u}^{(i)}, \quad {}^{t+\Delta t}u^{(i)} = {}^{t+\Delta t}u^{(i-1)} + \Delta u^{(i)}$$

are the approximations to the accelerations, velocities, and displacements obtained in iteration i . The first iteration, i.e. $i = 1$ in eq. (2), corresponds to the solution of eq. (1), where

$$\Delta u^{(1)} = u, \quad {}^{t+\Delta t}u^{(0)} = {}^t u, \quad {}^{t+\Delta t}\ddot{u}^{(1)} = {}^{t+\Delta t}\ddot{u}, \\ {}^{t+\Delta t}\dot{u}^{(1)} = {}^{t+\Delta t}\dot{u}, \quad {}^{t+\Delta t}F^{(0)} = {}^t F.$$

The vector of nodal point forces ${}^{t+\Delta t}F^{(i-1)}$ is equivalent to the element stresses in the configuration corresponding to the displacements ${}^{t+\Delta t}u^{(i-1)}$. The approximations to the velocities and accelerations, ${}^{t+\Delta t}\dot{u}^{(i)}$ and ${}^{t+\Delta t}\ddot{u}^{(i)}$, respectively, depend on the time integration scheme used [11]. It should be noted that the solution scheme used in eq. (2) corresponds to a modified Newton iteration [3, 5].

In program NONSAP, the Wilson θ -method or the Newmark method is used for the step-by-step solution [11, 12]. Table 1 summarizes the algorithm in linear or nonlinear, static or dynamic analysis [10]. The specific operations performed during the step-by-step solution are discussed in section 7.

2.1. Element to structure matrices and force vectors

The structure matrices in table 1 are formed by direct addition of the element matrices and vectors [5, 13]; for example

$$K = \sum K_m, \quad (3)$$

where K_m is the stiffness matrix of the m th element. Although K_m is formally of the same order as K , only those terms in K_m which pertain to the element de-

grees of freedom are nonzero. The addition of the element matrices and vectors can, therefore, be performed by using the element matrices in compact form together with identification arrays which relate element to structure degrees of freedom.

In program NONSAP, either a diagonal or consistent mass matrix may be used. In addition, concentrated masses corresponding to selected degrees of freedom can be specified. Rayleigh damping is assumed with the addition of concentrated nodal point dampers. The assumptions used in lumped mass analysis and Raleigh damping have been discussed on various occasions [5, 14, 15].

2.2. Boundary conditions

If a displacement component is zero, the corresponding equation is not retained in the structure equilibrium equations, eq. (2), and the corresponding element stiffness and mass terms are disregarded. If a nonzero displacement is to be specified at a degree of freedom i , say $u_i = x$, the equation

$$ku_i = kx \quad (4)$$

need be added into eq. (2), where $k \gg k_{ii}$. Therefore, the solution of eq. (2) must give $u_i = x$. Physically, this can be interpreted as adding at the degree of freedom i a spring of large stiffness k and specifying a load, which, because of the relatively flexible structure at this degree of freedom, produces the required displacement x . This approach simplifies programming problems which are normally associated with specifying displacements.

A special boundary element could have been incorporated into NONSAP [7]. However, in the current version of NONSAP only translational displacements are considered (since only isoparametric elements are available, see section 4). Therefore, nonzero displacement boundary conditions can be specified by using the truss element to provide the stiffness k in eq. (4) and applying the load kx .

3. Program organization

The complete solution process in program NONSAP is divided into three distinct phases:

(1) Input phase. This phase consists of three steps:

Table 1.
Summary of step-by-step integration.

Initial calculations

- (1) Form linear stiffness matrix K , mass matrix M and damping matrix C ; initialize 0u , ${}^0\dot{u}$, ${}^0\ddot{u}$.
 (2) Calculate the following constants:
 $tol \leq 0.01$; $nitem \geq 3$; in static analysis $\theta = 1$ and go to (3).
Wilson θ -method: $\theta \geq 1.37$, usually $\theta = 1.4$, $\tau = \theta \Delta t$
- $$a_0 = 6/\tau^2 \quad a_1 = 3/\tau \quad a_2 = 2a_1 \quad a_3 = 2$$
- $$a_4 = 2 \quad a_5 = \tau/2 \quad a_6 = a_0/\theta \quad a_7 = -a_2/\theta$$
- $$a_8 = 1 - 3/\theta \quad a_9 = \Delta t/2 \quad a_{10} = \Delta t^2/6$$
- Newmark method:* $\theta = 1.0$, $\delta \geq 0.50$, $\alpha \geq 0.25(0.5 + \gamma)^2$, $\tau = \Delta t$
- $$a_0 = 1/(\alpha \Delta t^2) \quad a_1 = \delta/(\alpha \Delta t) \quad a_2 = 1/(\alpha \Delta t) \quad a_3 = 1/(2\alpha) - 1$$
- $$a_4 = \delta/\alpha - 1 \quad a_5 = \Delta t(\delta/\alpha - 2)/2 \quad a_6 = a_0 \quad a_7 = -a_2$$
- $$a_8 = -a_3 \quad a_9 = \Delta t(1 - \delta) \quad a_{10} = \delta \Delta t$$
- (3) Form effective linear stiffness matrix: $\hat{K} = K + a_0 M + a_1 C$.
 (4) In linear analysis triangularize \hat{K} .
-

For each time step

(A) In linear analysis

- (i) Form effective load vector:

$${}^{t+\tau}\hat{R} = {}^tR + \theta({}^{t+\Delta t}R - {}^tR) + M(a_0 {}^t u + a_2 {}^t \dot{u} + a_3 {}^t \ddot{u}) + C(a_1 {}^t u + a_4 {}^t \dot{u} + a_5 {}^t \ddot{u}).$$

- (ii) Solve for displacement increments:

$$\hat{K} {}^{t+\tau}u = {}^{t+\tau}\hat{R}; \quad u = {}^{t+\tau}u - {}^t u.$$

- (iii) Go to (C).

(B) In nonlinear analysis

- (i) If a new stiffness matrix is to be formed, update \hat{K} for nonlinear stiffness effects to obtain ${}^t\hat{K}$; triangularize ${}^t\hat{K}$:

$${}^t\hat{K} = LDL^T.$$

- (ii) Form effective load vector:

$${}^{t+\tau}\hat{R} = {}^tR + \theta({}^{t+\Delta t}R - {}^tR) + M(a_2 {}^t \dot{u} + a_3 {}^t \ddot{u}) + C(a_4 {}^t \dot{u} + a_5 {}^t \ddot{u}) - {}^tF.$$

- (iii) Solve for displacement increments using latest D, L factors:

$$LDL^T u = {}^{t+\tau}\hat{R}.$$

- (iv) If required, iterate for dynamic equilibrium; then initialize $u^{(0)} = u$, $i = 0$

- (a) $i = i + 1$.

- (b) Calculate $(i - 1)$ st approximation to accelerations, velocities, and displacements:

$${}^{t+\tau}\ddot{u}^{(i-1)} = a_0 u^{(i-1)} - a_2 {}^t \dot{u} - a_3 {}^t \ddot{u}; \quad {}^{t+\tau}\dot{u}^{(i-1)} = a_1 u^{(i-1)} - a_4 {}^t \dot{u} - a_5 {}^t \ddot{u};$$

$${}^{t+\tau}u^{(i-1)} = u^{(i-1)} + {}^t u.$$

- (c) Calculate $(i - 1)$ st effective out-of-balance loads:

$${}^{t+\tau}\hat{R}^{(i-1)} = {}^tR + \theta({}^{t+\Delta t}R - {}^tR) - M {}^{t+\tau}\ddot{u}^{(i-1)} - C {}^{t+\tau}\dot{u}^{(i-1)} - {}^{t+\tau}F^{(i-1)}.$$

Table 1 (continued).

(d) Solve for i th correction to displacement increments:
 $LDL^T \Delta u^{(i)} = {}^{t+\tau} \hat{R}^{(i-1)}$.

(e) Calculate new displacement increments:
 $u^{(i)} = u^{(i-1)} + \Delta u^{(i)}$.

(f) Iteration convergence if $\|\Delta u^{(i)}\|_2 / \|u^{(i)}\|_2 + {}^t u\|_2 < tol$.
 If convergence: $u = u^{(i)}$ and go to (C);
 If no convergence and $i < nitem$: go to (a); otherwise restart using new stiffness matrix and/or a smaller time step size.

(C) Calculate new accelerations, velocities, and displacements

Wilson θ -method:
 ${}^{t+\Delta t} \ddot{u} = a_6 u + a_7 {}^t \dot{u} + a_8 {}^t \ddot{u}$,
 ${}^{t+\Delta t} \dot{u} = {}^t \dot{u} + a_9 ({}^{t+\Delta t} \ddot{u} + {}^t \ddot{u})$,
 ${}^{t+\Delta t} u = {}^t u + \Delta t {}^t \dot{u} + a_{10} ({}^{t+\Delta t} \ddot{u} + 2 {}^t \ddot{u})$.

Newmark method:
 ${}^{t+\Delta t} \ddot{u} = a_6 u + a_7 {}^t \dot{u} + a_8 {}^t \ddot{u}$,
 ${}^{t+\Delta t} \dot{u} = {}^t \dot{u} + a_9 {}^t \ddot{u} + a_{10} {}^{t+\Delta t} \ddot{u}$,
 ${}^{t+\Delta t} u = {}^t u + u$.

- (a) The control information and nodal point input data are read and generated by the program. In this phase the equation numbers for the active degrees of freedom at each nodal point are established.
- (b) The externally applied load vectors for each time (load) step are calculated and stored on tape (or other low-speed storage).
- (c) The element data are read and generated, the element connection arrays are calculated and all element information is stored on tape.

(2) Assemblage of constant structure matrices. Before the solution of eq. (2) is carried out, the linear structure stiffness, mass, and damping matrices are assembled and stored on tape (or other low-speed storage). In addition, the effective linear structure stiffness matrix is calculated and stored (see table 1).

(3) Step-by-step solution. During this phase the solution of eq. (2) is obtained at all time points. In addition to the displacement, velocity, and acceleration vectors (whichever is applicable), the element stresses are calculated and printed. Before the time

integration is performed, the lowest frequencies and corresponding mode shapes may be calculated. Details of the step-by-step solution are presented in section 7.

It should be noted that these basic steps are independent of the element type used and are the same for either a static or dynamic analysis. However, only those matrices actually required in the analysis are assembled. For example, no mass and damping matrices are calculated in a static analysis.

Program NONSAP is an in-core solver and the high-speed storage capacity of the program is determined by the maximum storage that is required during the three phases. Figs 1–3 show the dynamic storage allocations used in each phase. We note that, in general, maximum high-speed storage is required during the step-by-step solution. However, in some cases the storage required during the input phase may govern the system size that can be solved.

Figures 1–3 show that the lowest high-speed storage locations are reserved throughout the solution for element group information. For the analysis, the finite

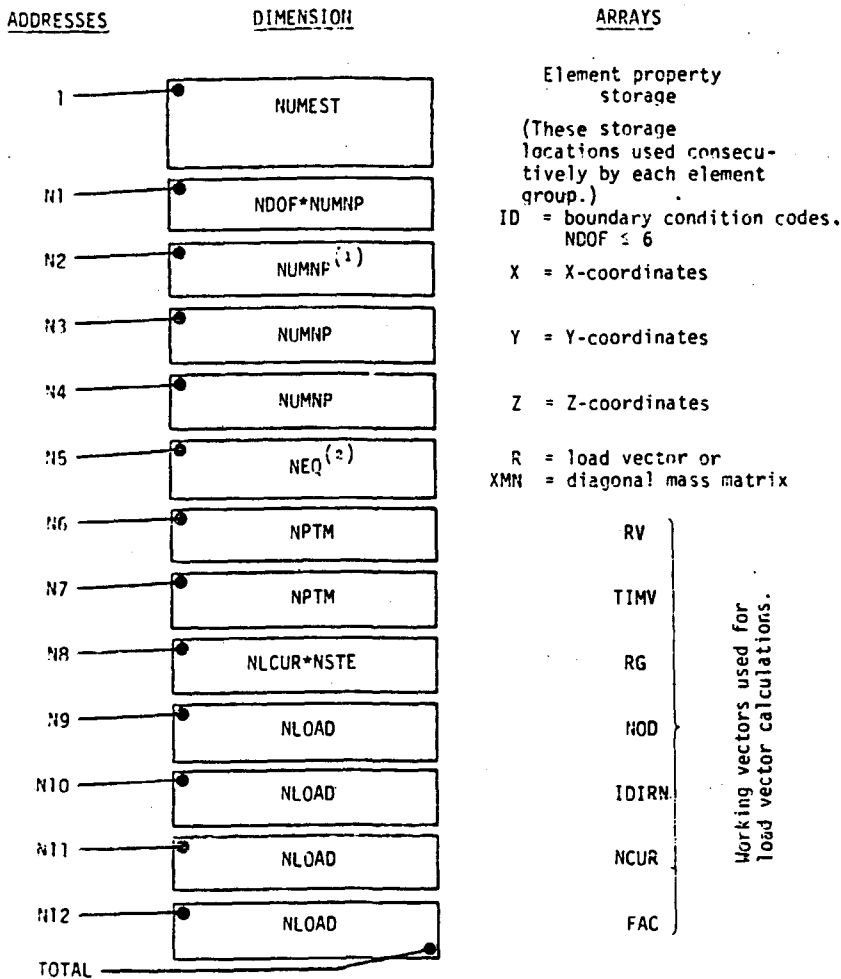


Fig. 1. Storage allocation during input phase. (1) NUMNP = number of nodal points, (2) NEQ = number of equations.

elements of the complete assemblage need be divided into element groups according to their type, the nonlinear formulation (see section 4), and the material models used (see section 5). One element group must consist of the same type of elements, must use one nonlinear formulation and only one specific material model. The data pertaining to each individual element group need to fit into the NUMEST storage locations, fig. 1. Therefore, the minimum that NUMEST should be specified is equal to the locations required to store the data pertaining to any one of the elements.

The use of element groups reduces input-output transfers during the solution process, since the data of the elements is retrieved in blocks during the solu-

tion of eq. (2) and element stress calculations (see section 7). Usually, NUMEST is some reasonable fraction of the total number of high-speed storage locations available, and is not reset for each problem. During the input phase the program calculates the exact number of high-speed storage locations required for each element group, and NUMEST is reset to MAXEST, which is the actual maximum number of locations needed, see figs 2 and 3. Therefore, an optimum of high-speed storage allocation is obtained during the step-by-step solution. Fig. 4 shows the tape storage used for the element group information.

To further improve high-speed storage capacity, NONSAP is an overlaid program. The overlay structure

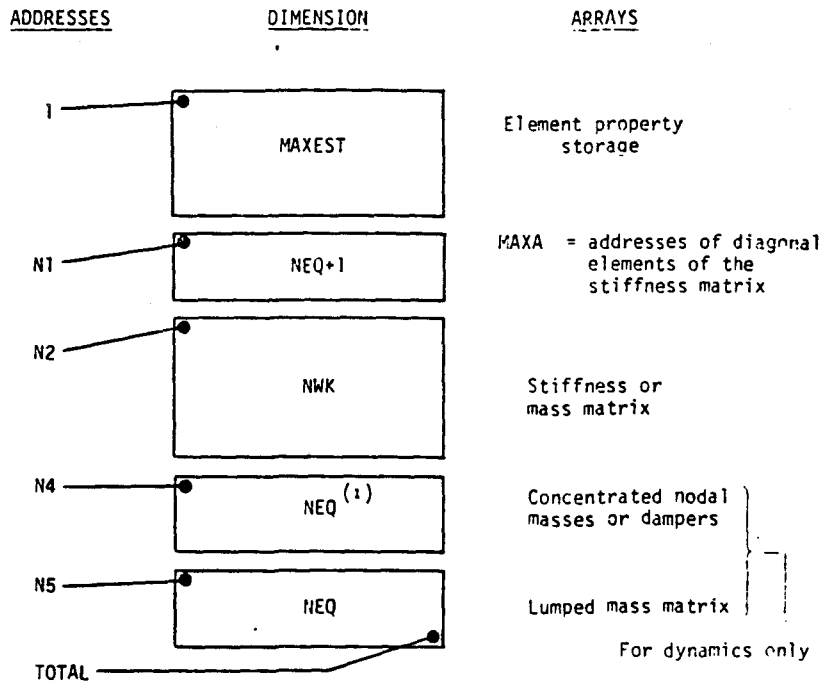


Fig. 2. Storage allocation during matrix assemblage phase. ⁽¹⁾NEQ = number of equations.

has been chosen to correspond to the three phases of execution listed above, the element library, the material models available, and the frequency calculation option. Fig. 5 shows the overlay structure of NONSAP.

3.1. Nodal point input data and degrees of freedom

The nodal point data read during the first step of the input phase consists of the boundary condition codes (stored in the *ID* array) and the global *X*, *Y*, *Z* coordinates of each nodal point. The same input is also required for program SAP [7]. A maximum of three boundary condition codes need currently be defined, since a finite element node can have at most three (translational) degrees of freedom (see section 4). As shown in fig. 1, all nodal point data is retained in high-speed storage during the complete input phase, i.e. during the calculation of the externally applied load vectors and the reading and generating of the element group information.

It need be noted that the user should allow only those degrees of freedom which are compatible with the elements connected to a nodal point. The program

can deal with a maximum of six possible degrees of freedom (three translations and three rotations) at each nodal point, and all non-active degrees of freedom need be deleted. Specifically, a '1' in the *ID* array denotes that no equation shall be associated with the degree of freedom, whereas a '0' indicates that this is an active degree of freedom [7]. Fig. 6 shows for the simple truss structure the *ID* array as it was read and/or generated by the program. Once the complete *ID* and *X*, *Y*, *Z* arrays have been obtained, equation numbers are associated with all active degrees of freedom, i.e. the zeros in the *ID* array are replaced by corresponding equation numbers, and each one is replaced by a zero, as shown in fig. 7 for the simple truss example.

3.2. Calculation of external load vectors

The loading in the analysis can consist only of concentrated nodal point loading, i.e. all distributed body or surface loading must be transformed to nodal point loading prior to using NONSAP. The load corresponding to a degree of freedom is assumed to vary with

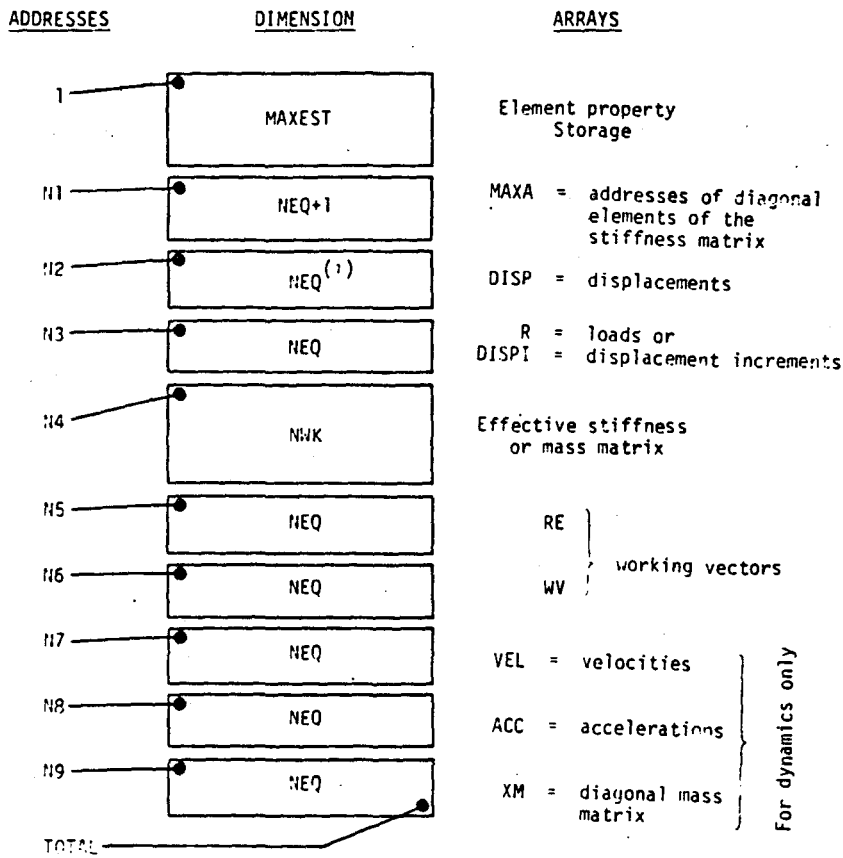


Fig. 3. Storage allocation during time integration. (1)NEQ = number of equations.

time as expressed by a time function and a load multiplier, both defined in the input.

3.3. Read-in of element data

In the last step of the input phase, element information for each element group is read and generated. Specifically, the element coordinates, the material properties and the element connection arrays are established. Also, working vectors which store required element strains, stresses and other variables are initialized. For each element group this information is processed in the first NUMEST high-speed storage locations and then written together in one block on secondary storage. During the next phases of the solution, therefore, the required element data can be read in blocks, sequen-

tially one block at a time, into the same high-speed storage locations.

The element connection array, i.e. vector *LM* of an element, is established from the *ID* matrix and the specified nodal points of the assemblage pertaining to the element. The connection array for a typical element of the truss example is shown in fig. 8.

It should be noted that the reading and generation of the element data of one group requires only one call of the specific element overlay needed since all elements in one group are of the same kind. After all element information has been established, the *ID* and *X, Y, Z* arrays are no longer required, and the corresponding storage area is used for the formation of the constant structure matrices and later for the solution of the equations of equilibrium.

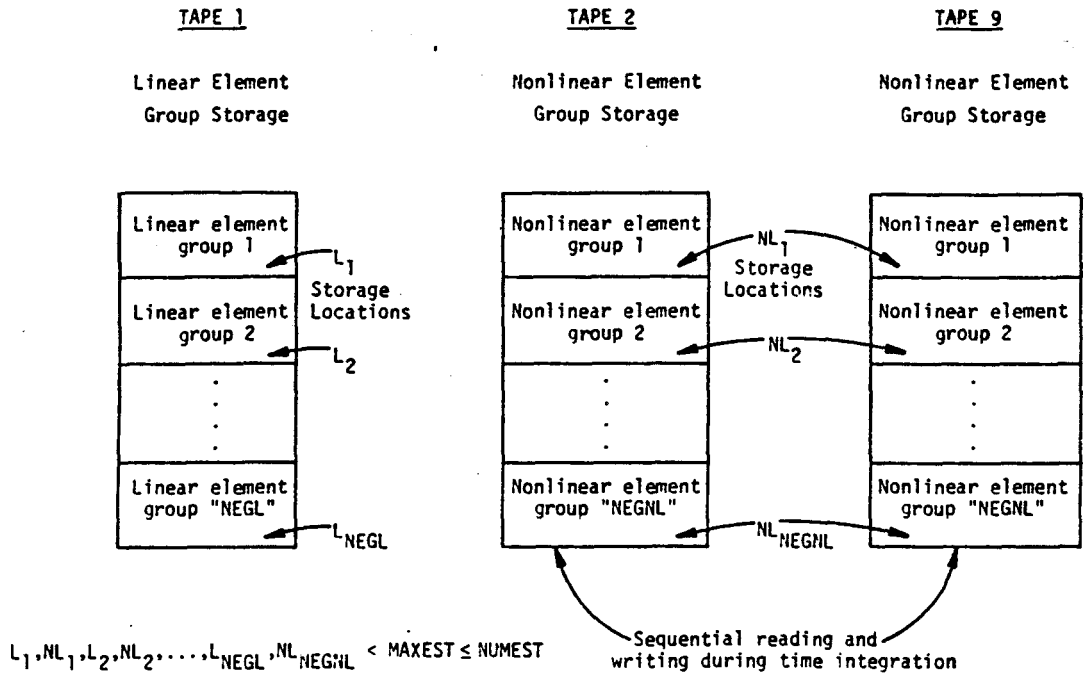


Fig. 4. Auxiliary storage organization for element group information.

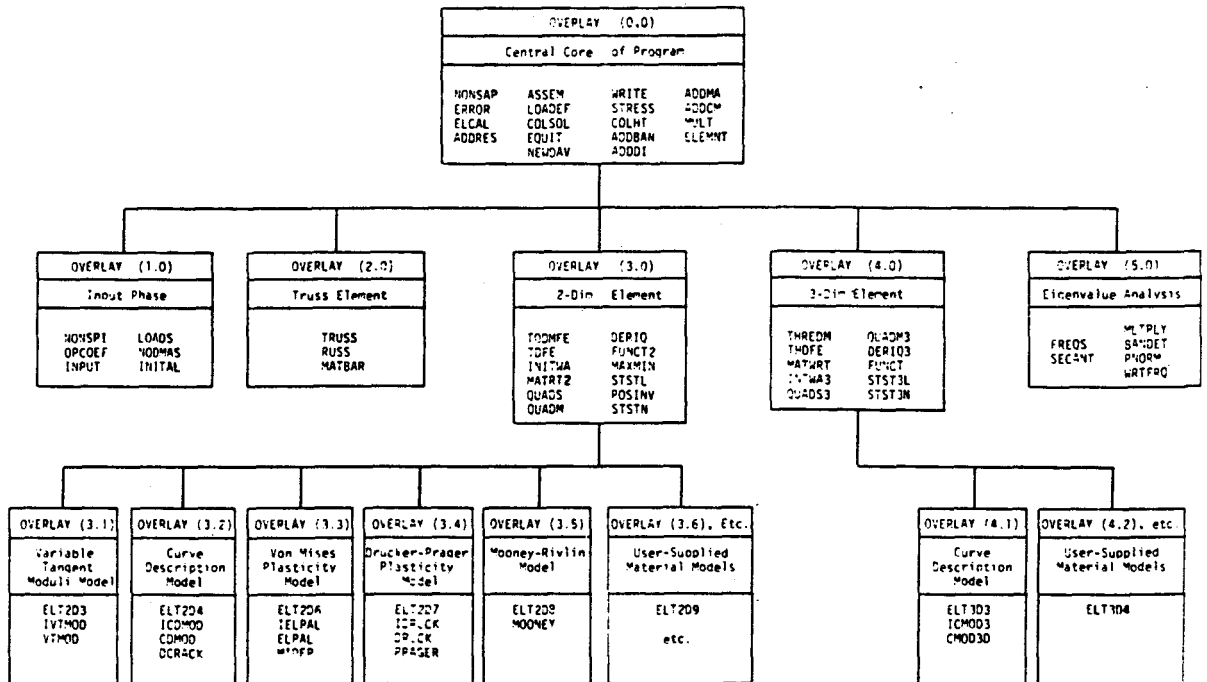
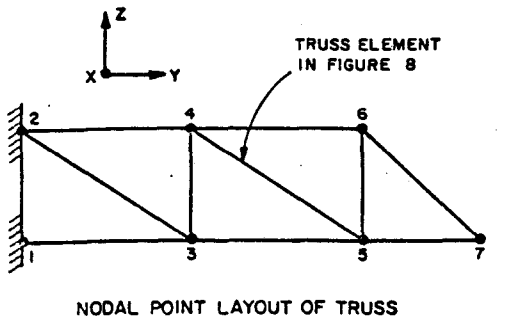


Fig. 5. Overlay structure of NONSAP.



		1	2	3	4	5	6	← DEGREES OF FREEDOM
1	ID =	1	1	1	1	1	1	
2		1	1	1	1	1	1	
3		1	0	0	1	1	1	
4		1	0	0	1	1	1	
5		1	0	0	1	1	1	
6		1	0	0	1	1	1	
7		1	0	0	1	1	1	
		↑ NODAL POINT NUMBERS						

Fig. 6. Nodal point layout of truss example and ID array as read and/or generated.

ID =	0	0	0	0	0	0	0
	0	0	0	0	0	0	0
	0	1	2	0	0	0	0
	0	3	4	0	0	0	0
	0	5	6	0	0	0	0
	0	7	8	0	0	0	0
	0	9	10	0	0	0	0

Fig. 7. ID array of truss example after allocation of equation numbers to active degrees of freedom.

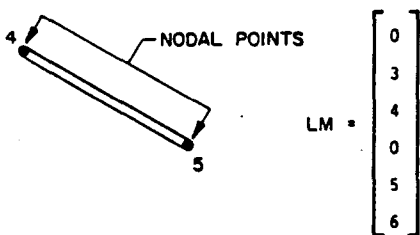


Fig. 8. Connection array (vector LM) for a typical element of the truss example.

3.4. Formation of constant structure matrices

All structure matrices which are not time dependent are calculated before the time integration is carried out. At this stage it is necessary to distinguish between the different kinds of analyses possible, namely whether a linear or nonlinear, static or dynamic analysis is required. The storage allocation during this phase was given in fig. 2, where it is shown that all required linear structure matrices are assembled using the same high-speed storage locations.

Figure 9 lists the sequence of assemblage and the tape storage used for the constant structure matrices corresponding to the different analyses. Note that only those matrices to be used later in the step-by-step solution are stored on tape. The assemblage of a structure matrix is effected by reading the data of all required element groups in succession, and by calculating and adding the element matrices to the structure matrix, as was discussed in section 2.1.

It should be noted that in linear analysis the structure stiffness or effective stiffness matrix is triangularized before storage on tape. In the step-by-step solution only forward reductions and back substitutions of the (effective) load vectors are then required (see section 7).

3.5. Compacted storage scheme

An important aspect is the efficient storage of the structure matrices and an effective solution of the equilibrium equations. The storage scheme need be optimized to obtain maximum capacity. The effective solution of the equations is necessary to reduce total solution cost.

In program NONSAP a compacted storage scheme is used in which all structure matrices are stored as one-dimensional arrays, and only the elements below the skyline of a matrix are processed [16]. Fig. 10 shows, as an example, the element pattern in a typical stiffness matrix before and after triangularization. It should be noted that, in general, zero elements within the skyline do not remain zero during the equation solution and must be stored, whereas all elements outside the skyline do not need to be considered. Therefore, by storing and processing in the equation solution only the elements within the skyline, a minimum number of high-speed storage locations is used.

3.6. Equation solution

The solution of equations is obtained using the linear equation solver COLSOL. This subroutine uses Gauss elimination on the positive definite symmetrical system of equations [16]. The algorithm performs – for practical purposes – a minimum number of arithmetic operations, since only the elements within the skyline of the matrix are processed. The algorithm is used in all analysis types, i.e. in linear, nonlinear, static or dynamic analysis, and consists of the LDL^T decomposition of the stiffness matrix (or effective stiffness matrix), and the reduction and back substitution of the (effective) load vector. For example, in linear static analysis, the equations are $Ku = R$ and the program calculates

$$K = LDL^T, \quad (5)$$

$$Lv = R, \quad (6)$$

$$DL^T u = v, \quad (7)$$

where L and D are a lower triangular and a diagonal matrix, respectively.

4. Element library

In the current version of program NONSAP all finite elements are isoparametric (or subparametric) elements [5]. Corresponding to the nonlinearities in the system, four different analysis procedures may be considered for a finite element:

(1) Linear elastic analysis. The displacements of the element are assumed to be negligibly small and the strains infinitesimal. The material is isotropic or orthotropic linear elastic.

(2) Material nonlinear only analysis. The displacements of the element are negligibly small, and the strains are infinitesimal. The material stress–strain description is nonlinear.

(3) Total Lagrangian formulation. The element may experience large displacements and large strains. The material stress–strain relationship is linear or nonlinear.

(4) Updated Lagrangian formulation. The element may experience large displacements and large strains. The material stress–strain description is linear or nonlinear.

The linear elastic analysis does not allow for any nonlinearities, whereas the materially nonlinear only analysis includes material nonlinearities, but no geometric nonlinearities [10]. The different linear and nonlinear material models currently available in NONSAP are described in section 5. The total Lagrangian and updated Lagrangian formulations may include all nonlinearities, and which formulation should be employed depends essentially on the definition of the material model used [10].

In the following, the finite elements currently available in NONSAP are briefly described. It should be noted that a particular element group must consist of finite elements of the same type, described by one of the four element formulations above, and must use one material model only. Since all four formulations and all material models have not been implemented for all element types, it is important to identify the nonlinear formulations and material models currently available in NONSAP for a specific element type, as illustrated in figs 11–13.

4.1. Truss element

A three-dimensional truss element is available in NONSAP. The element is assumed to have constant area, and may be used in linear elastic analysis, materially nonlinear and/or large displacement geometrically nonlinear analysis. In the large displacement analysis, the updated Lagrangian formulation is used, but small strains are assumed in the calculation of element stresses. The nonlinear elastic model is described in section 5. As noted earlier, the truss element can be used to specify nonzero boundary displacements [7].

4.2. Plane stress and plane strain element

A variable-number-nodes isoparametric finite element is available for two-dimensional plane stress and plane strain analysis. The element may have from 4 to 8 nodes where any one of the nodes 5–8 can be omitted. The variable-number-nodes option allows effective modelling from coarse to finer finite element meshes. The plane stress and plane strain element can be used in all four formulations. The material models available are described in section 5.

LINEAR ANALYSIS				
STATIC ANALYSIS	DYNAMIC ANALYSIS			
<ol style="list-style-type: none"> 1) Calculate linear structure stiffness matrix K. 2) Triangularize K and store on tape 7. 	<ol style="list-style-type: none"> 1) Calculate linear structure stiffness matrix K. 2) If Rayleigh damping is specified store K on tape 4. 3) If frequency analysis is to be performed, store K on tape 10. 4) Add mass and damping effects to K to obtain linear effective stiffness matrix \hat{K}. 5) Triangularize \hat{K} and store on tape 7. 6) Calculate mass matrix M and store on tape 4 (if consistent mass matrix) or tape 7 (if diagonal mass matrix). 7) If concentrated nodal dampers specified, store nodal damping vector C_d on tape 4. 			
<u>Tape Layout</u>	<u>Tape Layout</u>			
Tape 4: (not used)	Tape 4: <table border="1" style="display: inline-table; border-collapse: collapse; text-align: center;"> <tr><td style="padding: 2px;">K (if Rayleigh damping)</td></tr> <tr><td style="padding: 2px;">M (consistent mass case only)</td></tr> <tr><td style="padding: 2px;">C_d (if nodal damping)</td></tr> </table>	K (if Rayleigh damping)	M (consistent mass case only)	C_d (if nodal damping)
K (if Rayleigh damping)				
M (consistent mass case only)				
C_d (if nodal damping)				
Tape 7: <table border="1" style="display: inline-table; border-collapse: collapse; text-align: center;"> <tr><td style="padding: 2px;">$K = LDL^T$</td></tr> </table>	$K = LDL^T$	Tape 7: <table border="1" style="display: inline-table; border-collapse: collapse; text-align: center;"> <tr><td style="padding: 2px;">$\hat{K} = LDL^T$</td></tr> <tr><td style="padding: 2px;">M (diagonal mass case only)</td></tr> </table>	$\hat{K} = LDL^T$	M (diagonal mass case only)
$K = LDL^T$				
$\hat{K} = LDL^T$				
M (diagonal mass case only)				
Tape 10: (not used)	Tape 10: <table border="1" style="display: inline-table; border-collapse: collapse; text-align: center;"> <tr><td style="padding: 2px;">K (for frequency analysis only)</td></tr> </table>	K (for frequency analysis only)		
K (for frequency analysis only)				

Fig. 9. Assemblage of constant structure matrices.

NONLINEAR ANALYSIS					
STATIC ANALYSIS	DYNAMIC ANALYSIS				
<p>1) Calculate linear structure stiffness matrix K, i.e., that part of the total structure stiffness matrix which corresponds to the linear element groups.</p> <p>2) Store K on tape 4 and on tape 7.</p>	<p>1) Calculate linear structure stiffness matrix K.</p> <p>2) Store K on tape 4.</p> <p>3) If frequency analysis is to be performed, store K on tape 10.</p> <p>4) Add mass and damping effects to K to obtain linear effective stiffness matrix \hat{R}.</p> <p>5) Store \hat{R} on tape 7.</p> <p>6) Calculate mass matrix M and store on tape 4 (if consistent mass matrix) or on tape 7 (if diagonal mass matrix).</p> <p>7) If concentrated nodal dampers specified, store nodal damping vector C_d on tape 4.</p>				
<u>Tape Layout</u>	<u>Tape Layout</u>				
Tape 4: <table border="1" style="display: inline-table;"><tr><td style="text-align: center;">K</td></tr></table>	K	Tape 4: <table border="1" style="display: inline-table;"><tr><td style="text-align: center;">K</td></tr><tr><td style="text-align: center;">M (consistent mass case only)</td></tr><tr><td style="text-align: center;">C_d (if nodal damping)</td></tr></table>	K	M (consistent mass case only)	C_d (if nodal damping)
K					
K					
M (consistent mass case only)					
C_d (if nodal damping)					
Tape 7: <table border="1" style="display: inline-table;"><tr><td style="text-align: center;">K</td></tr></table>	K	Tape 7: <table border="1" style="display: inline-table;"><tr><td style="text-align: center;">\hat{R}</td></tr><tr><td style="text-align: center;">M (diagonal mass case only)</td></tr></table>	\hat{R}	M (diagonal mass case only)	
K					
\hat{R}					
M (diagonal mass case only)					
Tape 10: (not-used)	Tape 10: <table border="1" style="display: inline-table;"><tr><td style="text-align: center;">K (for frequency analysis only)</td></tr></table>	K (for frequency analysis only)			
K (for frequency analysis only)					

Fig. 9 (continued).

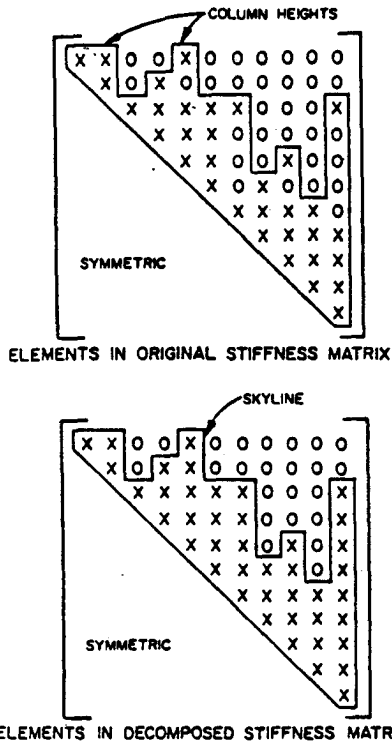
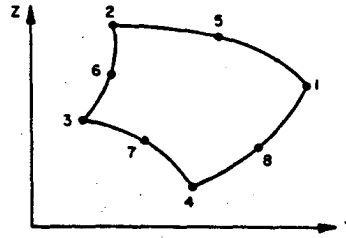
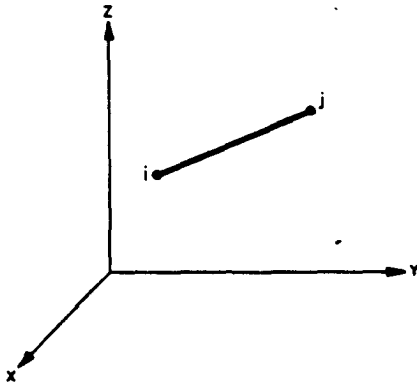


Fig. 10. Typical element pattern in a stiffness matrix. X = nonzero element, and 0 = zero element.



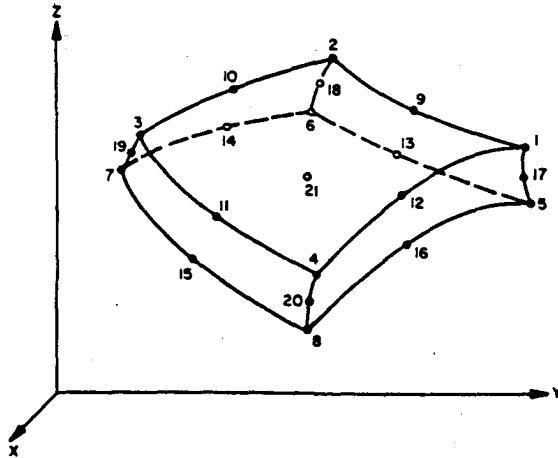
- | AVAILABLE NONLINEAR FORMULATIONS | AVAILABLE MATERIAL MODELS |
|----------------------------------|---|
| 1. LINEAR ANALYSIS | 1. LINEAR ISOTROPIC ELASTIC |
| 2. MATERIALLY NONLINEAR ONLY | 2. LINEAR ORTHOTROPIC ELASTIC |
| 3. UPDATED LAGRANGIAN | 3. VARIABLE TANGENT MODULI MODEL |
| 4. TOTAL LAGRANGIAN | 4. CURVE DESCRIPTION NONLINEAR MODEL (WITH OR WITHOUT TENSION CUT-OFF ASSUMPTION) |
| | 5. PLASTICITY MODELS (VON MISES OR DRUCKER-PRAGER YIELD CONDITION) |
| | 6. NONLINEAR, ISOTROPIC INCOMPRESSIBLE ELASTIC (MOONEY-RIVLIN MATERIAL) |

Fig. 12. Two-dimensional plane stress, plane strain and axisymmetric elements.



- | AVAILABLE NONLINEAR FORMULATIONS | AVAILABLE MATERIAL MODELS |
|--|---------------------------|
| 1. LINEAR ANALYSIS | 1. LINEAR ELASTIC |
| 2. MATERIALLY NONLINEAR ONLY | 2. NONLINEAR ELASTIC |
| 3. UPDATED LAGRANGIAN WITH LARGE DISPLACEMENTS BUT SMALL STRAINS | |

Fig. 11. Truss element.



- | AVAILABLE NONLINEAR FORMULATIONS | AVAILABLE MATERIAL MODELS |
|----------------------------------|--------------------------------------|
| 1. LINEAR ANALYSIS | 1. LINEAR ISOTROPIC ELASTIC |
| 2. MATERIALLY NONLINEAR ONLY | 2. CURVE DESCRIPTION NONLINEAR MODEL |

Fig. 13. Three-dimensional solid and thick shell element.

4.3. Axisymmetric shell or solid element

The variable-number-nodes element described above is also available for axisymmetric two-dimensional analysis of shells or solids (with axisymmetric loading).

4.4. Three-dimensional solid or thick shell element

A general three-dimensional isoparametric element with a variable number of nodes from 8 to 21 can be used. The first eight nodes are the corner nodes of the element, nodes 9–20 correspond to midside nodes and nodes 21 is a center node. The element can be used for three-dimensional analysis of solids and thick shells. As for the two-dimensional elements, the possibility of choosing different element node configurations allows effective finite element modelling. The three-dimensional element can currently only be used in linear isotropic analysis and in nonlinear analysis with material nonlinearities.

5. Material models

The largest number of material models is available for two-dimensional analysis, since it is anticipated that the two-dimensional elements will be used in most analyses. For the same reason, also all three nonlinear formulations can be used for the two-dimensional elements. All material models available in NONSAP are discussed in ref. [10].

5.1. Truss element material models

The truss element material behavior can be described by means of two models:

- (1) Linear elastic material. The material can be linear elastic defined by Young's modulus only.
- (2) Nonlinear elastic material. The nonlinear elastic material behavior is defined by specifying the stress as a piecewise linear function of the current (infinitesimal) strain. Thus, the total stress and the tangent modulus are directly defined in terms of the total strain.

5.2. Two-dimensional element material models

The stress–strain relationship of the two-dimensional elements can be described by various linear and non-

linear material models. In the definition of a material model, it may have been assumed that a specific nonlinear formulation is used. The application of the different material models is discussed in ref. [10], where the assumptions used are pointed out.

5.2.1. Isotropic and orthotropic linear elastic material

The stress–strain relationships are defined by means of the constant Young's moduli and Poisson's ratios [28].

5.2.2. Mooney–Rivlin material model

A hyperelastic incompressible material model is available for the analysis of rubber-like materials [3, 17]. The stress–strain relationship is defined using the Mooney–Rivlin material constants. In NONSAP the model can only be used in plane stress analysis.

5.2.3. Elastic–plastic material models

Elastic–plastic analysis using a plastic potential function can be carried out. The plasticity relations available are those based on the use of the von Mises yield condition and the Drucker–Prager yield condition. Both forms of describing material behavior have been employed extensively in practice [2, 18–20]. Using the von Mises criterion, linear isotropic hardening can be assumed. In analysis using the Drucker–Prager yield condition, the material is assumed to be elastic–perfectly plastic.

5.2.4. Variable tangent moduli model

The variable tangent moduli model is available for the analysis of geological materials [21]. The model describes an isotropic material, in which the bulk and shear moduli are functions of the stress and strain invariants. The functional relationship used replaces an explicit yield condition.

5.2.5. Curve description model

The curve description model is used in essentially the same way as the variable tangent moduli model. The model also describes the response of geological materials. In the model, the instantaneous bulk and shear moduli are defined by piecewise linear functions of the current volume strain. An explicit yield condition is not used, and whether the material is loading or unloading is defined by the history of the volume strain only.

In the analysis of some problems, tensile stresses due to applied loading cannot exceed the gravity *in situ* pressure. In such conditions the model can be used to simulate tension cut-off, i.e. the material model assumes reduced stiffness in the direction of the tensile stresses which exceed in magnitude the gravity pressure.

5.3. Three-dimensional element material models

In principle, most two-dimensional models would also be applicable in three-dimensional analysis. However, in the current version of NONSAP, only the isotropic linear elastic model and the curve description model (without tension cut-off capability) are available.

6. Eigensystem solution

In dynamic analysis it is necessary to select a suitable time step Δt . The time increment must be small enough for solution accuracy, but for a cost effective solution, it should not be unnecessarily small. To estimate an appropriate time step, it may be necessary to solve for the fundamental frequencies of the system [11]. For this purpose an eigenvalue solution routine has been incorporated into NONSAP.

The algorithm considers the solution of the generalized eigenvalue problem

$${}^0K\phi = \omega^2 M\phi, \quad (8)$$

where 0K is the tangent stiffness matrix at time 0, M is the mass matrix of the system and ω and ϕ are free vibration frequency and mode shape, respectively. The mass matrix can be diagonal (lumped mass assumption) or banded (consistent mass assumption), and the stiffness matrix 0K is assumed to be positive definite. The solution to eq. (8) can be written as

$${}^0K\Phi = M\Phi\Omega^2, \quad (9)$$

where Φ is a matrix with its columns equal to the mass-orthonormalized eigenvectors and Ω^2 is a diagonal matrix of the corresponding eigenvalues, i.e.

$$\Phi = [\phi_1 \phi_2 \dots \phi_n]; \Omega^2 = \text{diag}(\omega_i^2). \quad (10)$$

The solution algorithm used in NONSAP is the determinant search method presented in ref. [22]. Basically, the algorithm combines triangular factoriza-

tion and vector inverse iteration in an optimum manner to calculate the required eigenvalues and eigenvectors; these are obtained in sequence starting from the least dominant eigenpair (ω_1^2, ϕ_1) . An efficient accelerated secant iteration procedure which operates on the characteristic polynomial

$$p(\omega^2) = \det(K - \omega^2 M) \quad (11)$$

is used to obtain a shift near the next unknown eigenvalue. The eigenvalue separation theorem (Sturm sequence property) is used in this iteration. Each determinant evaluation requires a triangular factorization of the matrix $K - \omega^2 M$. Once a shift near the unknown eigenvalue has been obtained, inverse iteration is used to calculate the eigenvector and the eigenvalue is obtained accurately by adding the Rayleigh quotient correction to the shift value.

7. Step-by-step solution

The main phase in the analysis is the step-by-step solution of the equilibrium equations, eq. (2). The algorithm used was presented in table 1. The aim in this section is to describe in more detail the actual computer solution. Since the program can perform static and dynamic, linear and nonlinear analysis, it is convenient to consider in the following the different analysis types separately.

7.1. Linear static analysis

In a linear static analysis, all element groups are linear and only the linear stiffness matrix is calculated in the matrix assemblage phase. The stiffness matrix is triangularized before entering the step-by-step solution phase. It should be noted that this solution corresponds to a linear dynamic analysis, in which mass and damping effects are neglected. Therefore, by specifying time varying loads, the solution can be obtained for multiple load conditions. Fig. 14 shows the tape operations used in the analysis.

7.2. Linear dynamic analysis

In a linear dynamic analysis all elements are linear, with mass and possibly damping effects included. The mass matrix may be diagonal (lumped mass analysis)

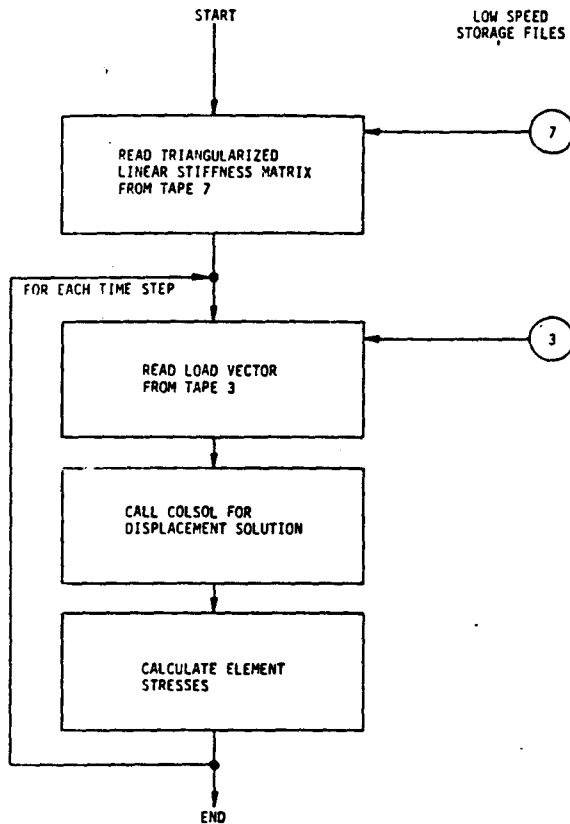


Fig. 14. Flow chart for step-by-step solution in linear static analysis.

or banded (consistent mass analysis) and additional concentrated masses may be specified at selected degrees of freedom. The damping matrix C is assumed to be of the form.

$$C = \alpha M + \beta K + C_d, \quad (12)$$

where α and β are the Rayleigh damping coefficients and C_d is a diagonal damping matrix, assembled from concentrated dampers which are specified at selected degrees of freedom [14]. In eq. (12), K and M are the linear stiffness and mass matrices of the complete element assemblage.

The tape operations performed during a linear dynamic analysis depend on the characteristics of the mass and damping matrices employed. Fig. 15 illustrates the various possibilities for storage and retrieval of the matrices used.

7.3. Nonlinear static analysis

In nonlinear static analysis linear and nonlinear element groups are defined. Damping and mass effects are neglected.

Before the step-by-step solution, the linear stiffness matrix corresponding to the linear elements of the complete element assemblage was calculated (see fig. 9). This matrix is now updated in preselected load steps by the stiffness matrices of the nonlinear elements to form the current tangent stiffness matrix. The interval of load steps in which a new tangent stiffness matrix is to be formed is input to the program.

Depending on the nonlinear formulations and the nonlinear material models used, and also depending on the magnitude of the load steps, the accuracy of the solution may be significantly increased using equilibrium iteration. In the program the interval of load steps, in which equilibrium iterations are to be per-

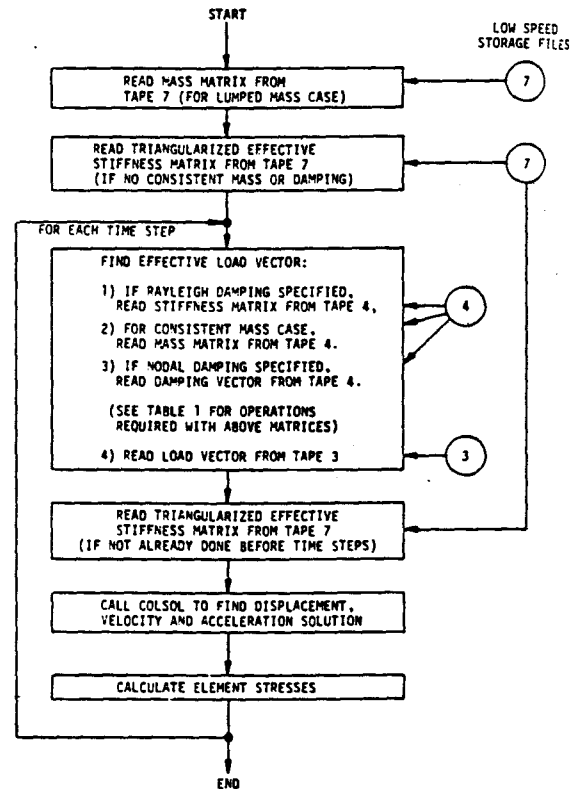


Fig. 15. Flow chart for step-by-step solution in linear dynamic analysis.

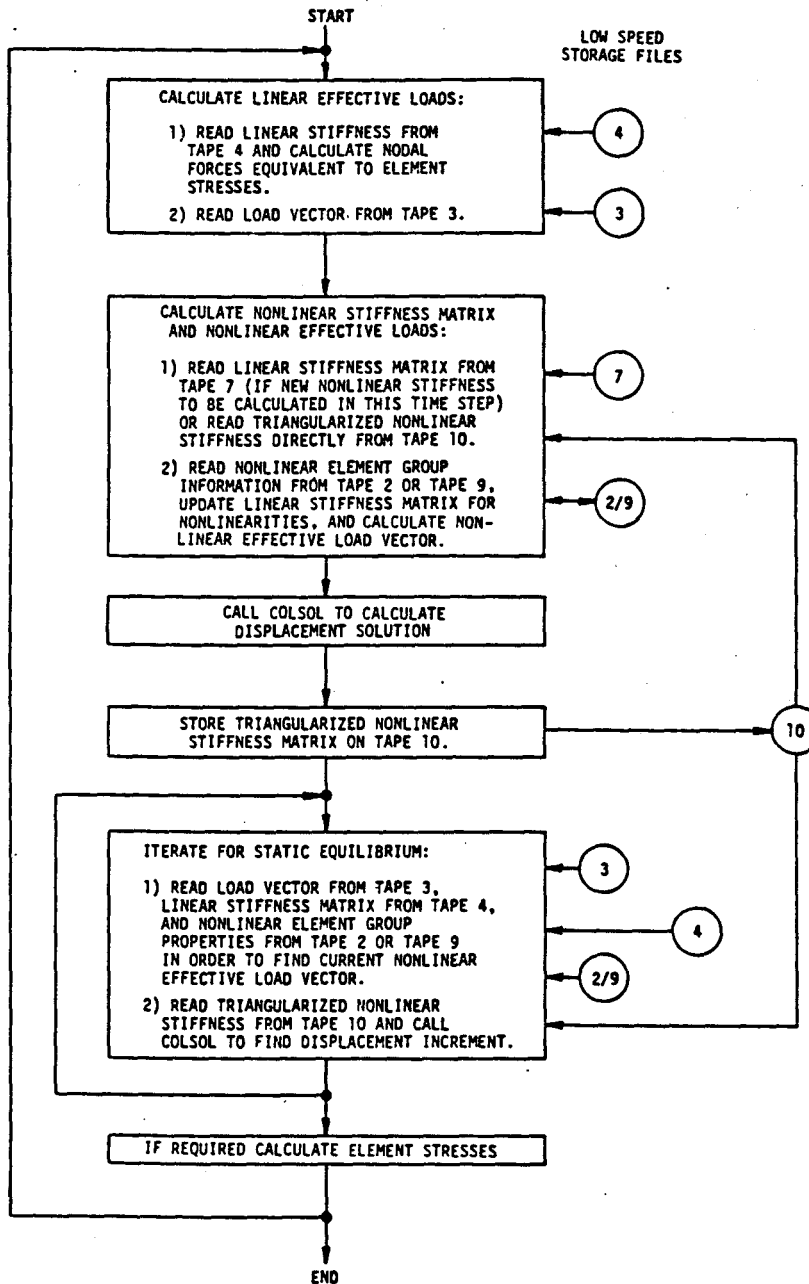


Fig. 16. Flow chart for step-by-step solution in nonlinear static analysis.

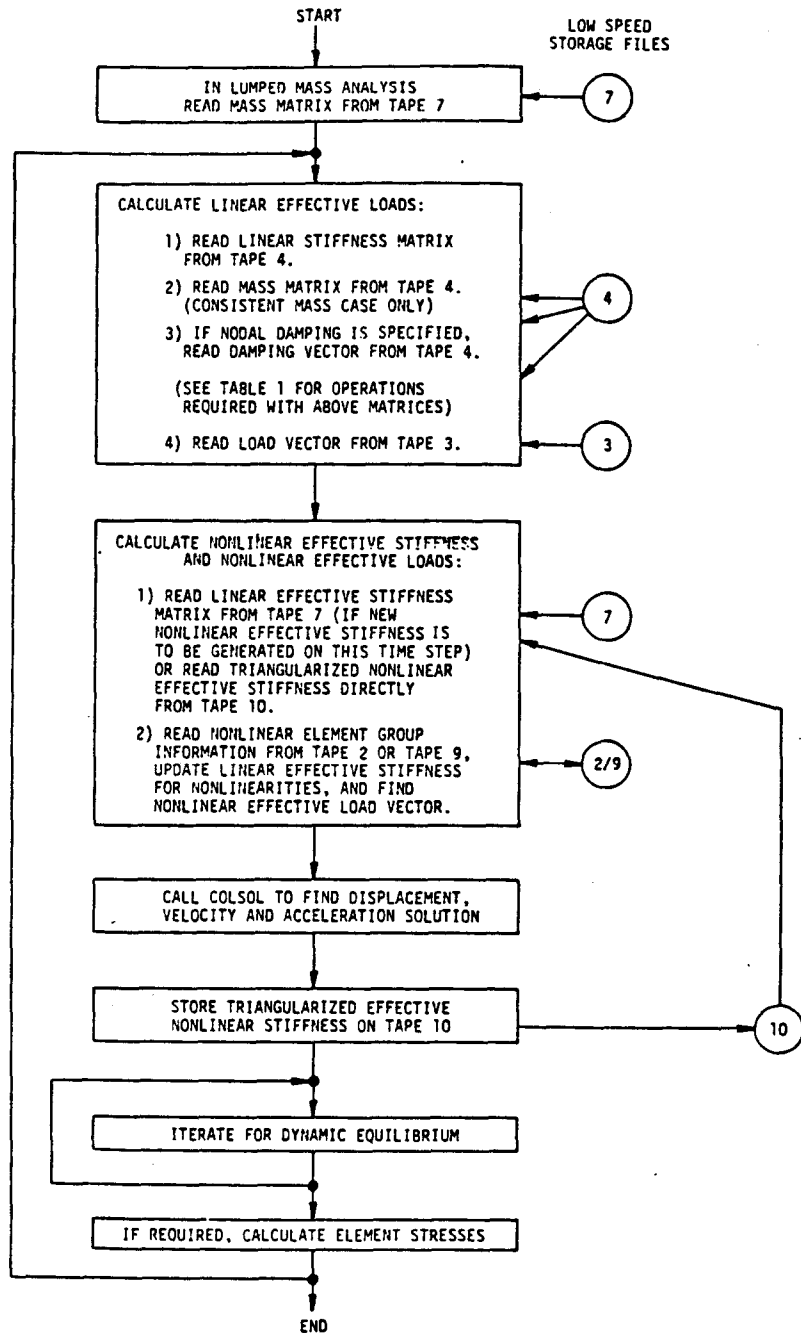


Fig. 17. Flow chart for step-by-step solution in nonlinear dynamic analysis.

formed, can be defined in the input control data. The storage of the matrices and tape operations carried out in the analysis are shown in fig. 16.

7.4. Nonlinear dynamic analysis

A nonlinear dynamic analysis is carried out essentially in the same way as a nonlinear static analysis, but mass and possibly damping effects are included. The mass and damping matrices are defined as in linear dynamic analysis, where the Rayleigh damping coefficient β is now applied to the linear stiffness matrix of the element assemblage. It should be noted that the structure mass and damping matrices are calculated before the step-by-step solution, see fig. 9. The tape storage scheme and program flow in a nonlinear dynamic analysis are given in fig. 17.

8. Analysis restart

In nonlinear analysis it is often the case that the response of a structure has been calculated for some time (load) steps and that on interpretation of the results, it is decided to analyze the structure for more time (load) steps. If this is anticipated, the program can be used to restart at the end of the successfully completed analysis.

9. Data check run

In the analysis of large structures it is important to be able to check the data read and generated by the program. For this purpose an option is given in which the program simply reads, generates, and prints all data. This printout should be used to carefully verify the input data, since the program itself does not perform extensive data checking.

10. Sample analyses

In the following the solutions of some problems are presented that have been considered during the development of NONSAP. Additional problem solutions are given in refs [9] and [10]. All solutions have been obtained using the algorithm presented in table 1, in which the selected parameters were $tol = 0.001$,

$nitem = 15$, $\theta = 1.4$, $\delta = 0.50$ and $\alpha = 0.25$. Since only relatively small order systems have been considered the solution times have always been small [10].

10.1. Static and frequency analysis of a tower cable

The cable stretched between a ground anchor point and a tower attach point shown in fig. 18 was analyzed for static displacements and frequencies of vibration. The cable was modelled using 12 truss elements of linear elastic material. The total vertical load acting on the cable nodes was 5677.83 lb which includes the insulator weights and the cable selfweight.

Figure 18 shows the cable in the static equilibrium configuration with the total load applied. The nonlinear displacement response of node 8 is shown in fig. 19.

For the frequency analysis a lumped mass matrix of the cable has been assumed to which the masses of the insulators have been added. The periods of vibration of the cable about the static equilibrium configuration are given in table 2.

10.2. Static and dynamic displacement analysis of a cantilever

The cantilever in fig. 20 under uniformly distributed load was analyzed using a finite element idealization of five eight-node plane stress elements. The material of the cantilever was assumed to be isotropic linear elastic.

The static response of the cantilever using 100 load steps to reach the final equilibrium configuration is shown in fig. 21, in which the NONSAP solution is compared with an analytical solution by Holden [23]. Excellent agreement between the solutions has been obtained. The dynamic response of the cantilever is shown in fig. 22, where also the importance of equilibrium iterations in an analysis using a relatively large time step Δt is demonstrated [10].

10.3. Static large displacement analysis of a spherical shell

The spherical shell subjected to a concentrated apex load shown in fig. 23 was analyzed for static response. The NONSAP solution could be compared with the response predicted by Stricklin [24] and Mescall [25].

Table 2.
Vibration periods of cable in static equilibrium configuration.

Mode number	Period (sec)
1	4.42
2	2.31
3	1.21
4	1.16
5	0.929

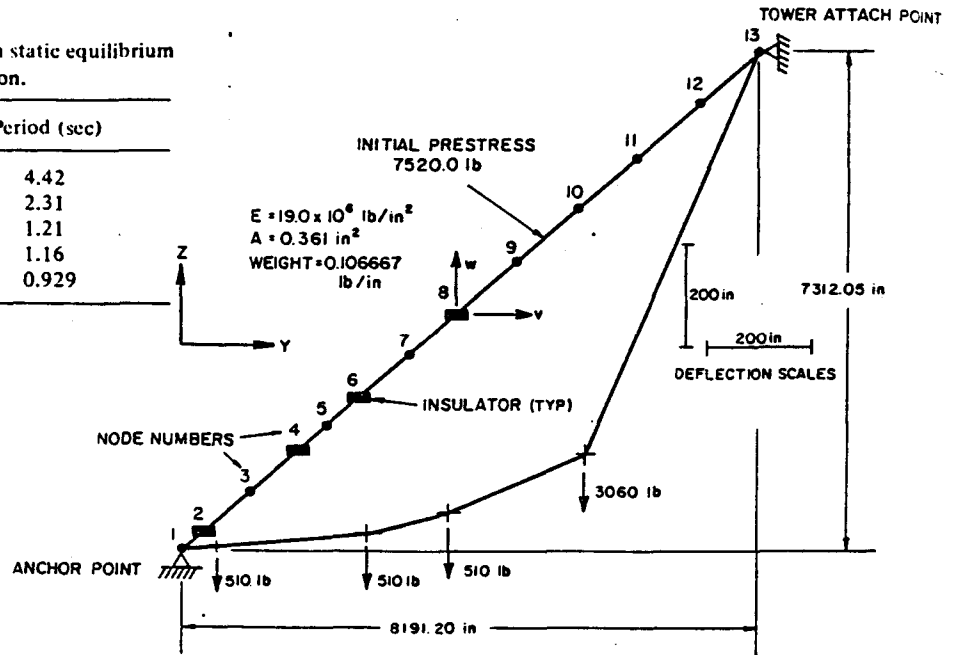


Fig. 18. Static configuration of tower cable.

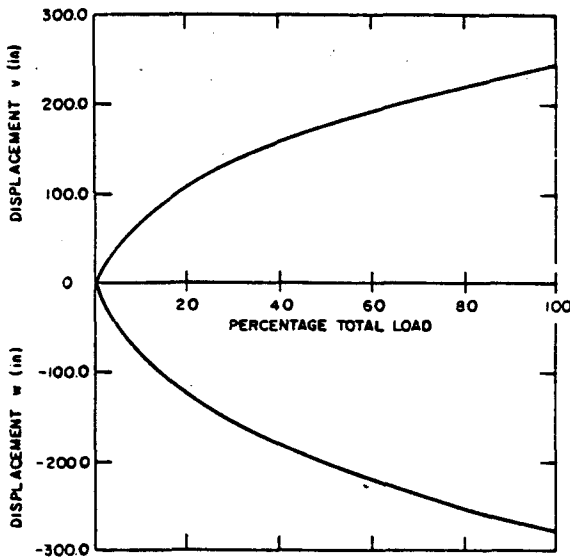


Fig. 19. Load deflection curve of tower cable.

Figure 23 shows the static load-deflection response calculated by NONSAP. Good correspondence with the solutions obtained by Stricklin and Mescall is observed.

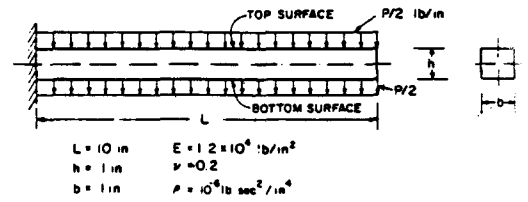


Fig. 20. Cantilever under uniformly distributed load.

10.4. Large displacement and large strain static analysis of a rubber sheet

The rubber sheet shown in fig. 24 was analyzed for the uniform end loading indicated. The material was assumed to be of the Mooney-Rivlin type, for which experiments by Iding et al. gave $C_1 = 21.605 \text{ lb/in.}^2$, $C_2 = 15.743 \text{ lb/in.}^2$ [17].

Figure 25 shows the static displacement response of the sheet. It is noted that the final displacement at the loaded end is of the order of the original length of the sheet, at which stage Green-Lagrange strains of 1.81 are measured. The final configuration of the sheet was reached in four equal load steps with an average of five equilibrium iterations in each step. Excellent

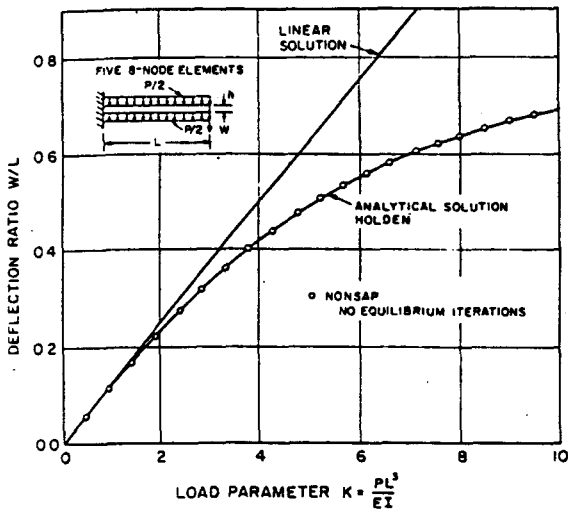


Fig. 21. Large deflection analysis of cantilever under uniformly distributed load.

agreement between the experimental results by Iding et al. [17] and those predicted by NONSAP has been obtained.

10.5. Elastic-plastic static analysis of a thick-walled cylinder

The thick-walled cylinder in fig. 26 subjected to internal pressure was analyzed using four eight-node axisymmetric elements. The material of the cylinder was assumed to obey the von Mises yield condition with elastic perfectly plastic response. The same analysis was also carried out using the Drucker-Prager yield condition with material variables corresponding to those used in the von Mises condition. Since displacements and strains are small, the analysis of the cylinder was carried out using the materially nonlinear only formulation. Fig. 27 shows the radial displacement response of the cylinder as a function of the applied load, and fig. 28 gives the stress distribution

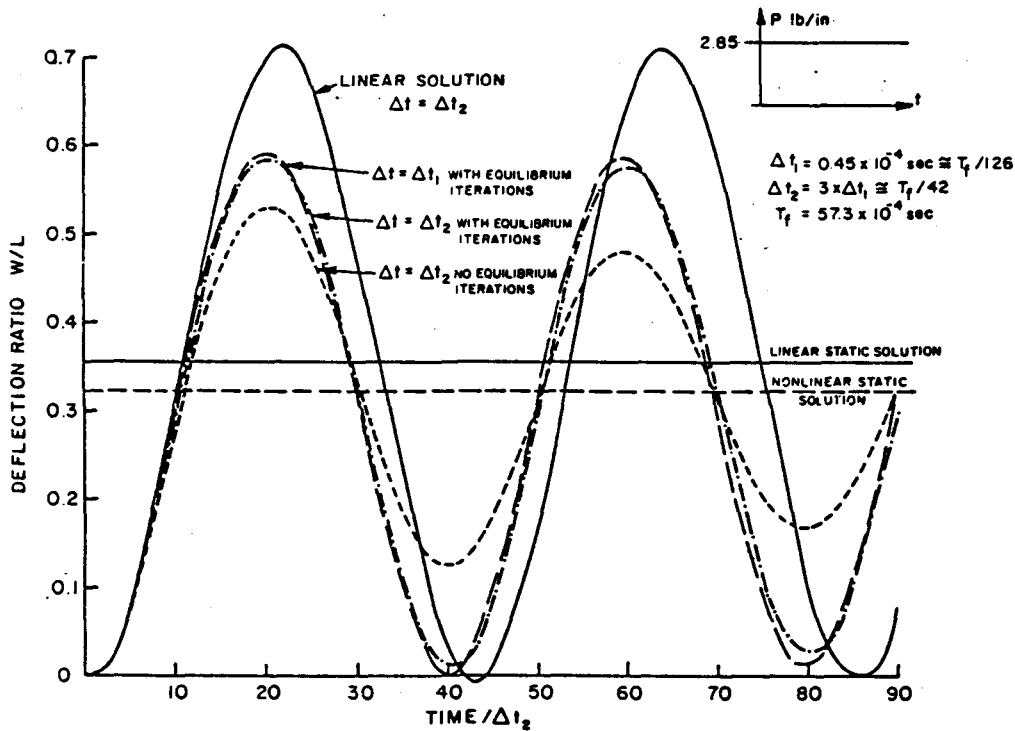


Fig. 22. Large displacement dynamic response of cantilever under uniformly distributed load. Newmark method $\delta = 0.50, \alpha = 0.25$.

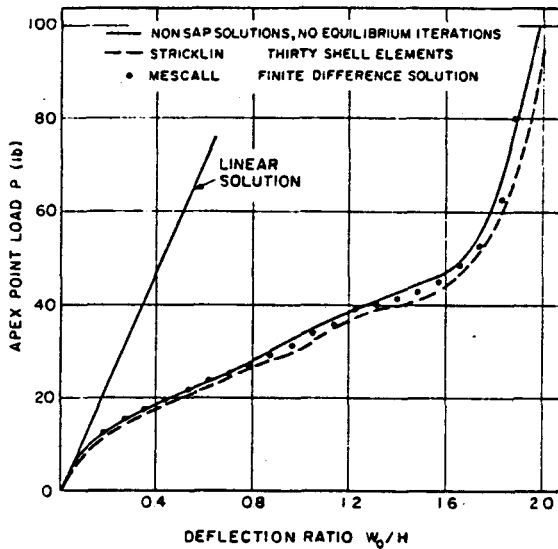
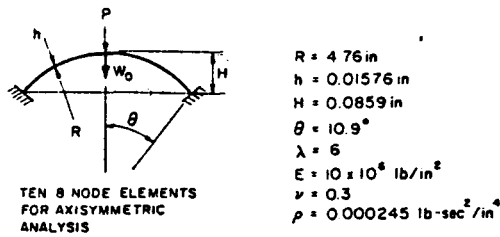


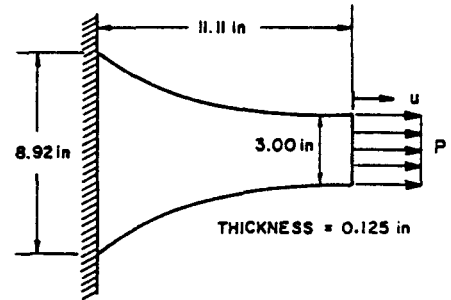
Fig. 23. Load-deflection curves for spherical shell.

through the wall of the cylinder at a given level of internal pressure. Excellent agreement with the solution given by Hodge and White has been obtained [26].

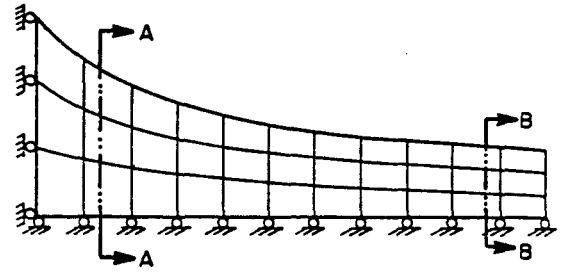
10.6. Elastic-plastic small displacement dynamic analysis of a simply-supported beam

The beam shown in fig. 29 was analyzed for the step loading indicated. The material of the beam was taken to be elastic perfectly plastic using the von Mises yield condition. In the analysis small displacements were assumed, i.e. materially nonlinear only solutions were calculated.

The dynamic response of the beam is shown in fig. 30, in which the NONSAP solutions are compared with solutions provided by Baron et al. [27] and Nagarajan and Popov [28].

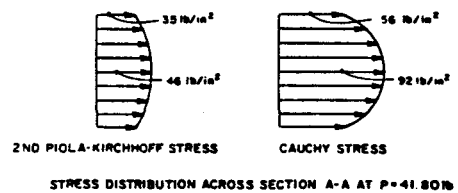
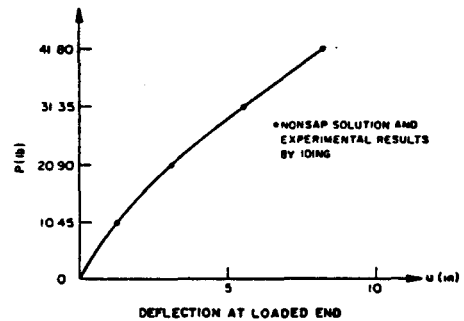


RUBBER SHEET

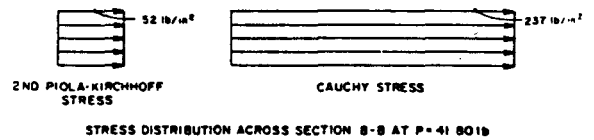


FINITE ELEMENT MESH (4 NODE ELEMENTS)

Fig. 24. Large displacement and large strain static analysis of a rubber sheet.



STRESS DISTRIBUTION ACROSS SECTION A-A AT P = 41.80 lb



STRESS DISTRIBUTION ACROSS SECTION B-B AT P = 41.80 lb

Fig. 25. Displacement and stress response of a rubber sheet.

10.7. Static analysis of an underground opening

A simplified analysis of an underground opening under static overburden pressure was carried out. Fig. 31 shows the underground opening, the finite element mesh and the material data used. The analysis was performed using the materially nonlinear only formula-

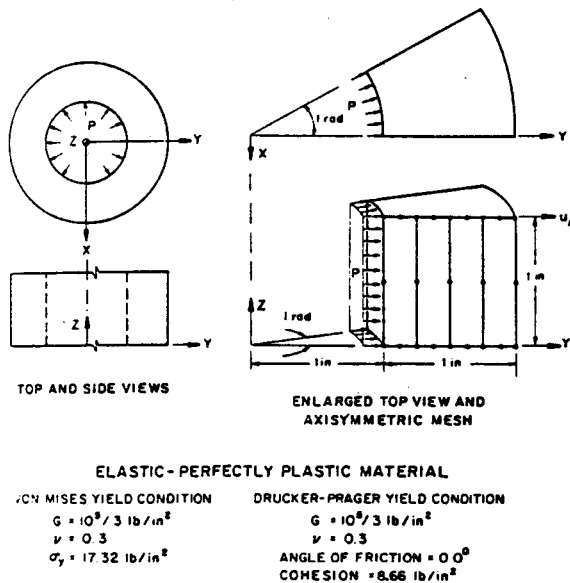


Fig. 26. Finite element mesh of thick-walled cylinder.

tion, i.e. large displacement effects were neglected. The rock material was assumed to be a no-tension material with constant Young's modulus and Poisson's ratio.

Figure 32 gives the load-deflection relations for two points of the opening. The influence of the no-tension material assumption on the displacements can be observed. Fig. 33 shows the crack regions around the opening at two load levels.

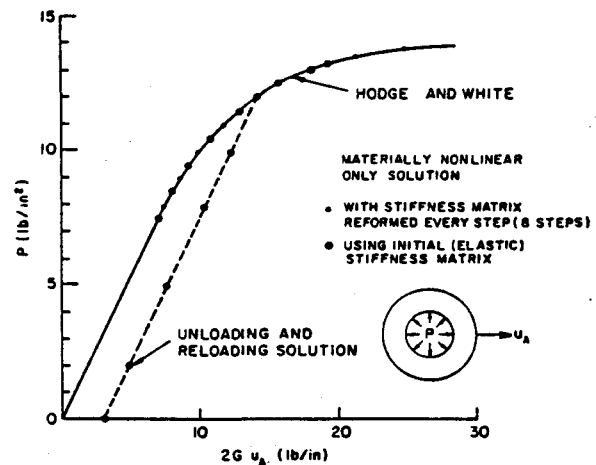


Fig. 27. Elastic-plastic displacement response of thick-walled cylinder.

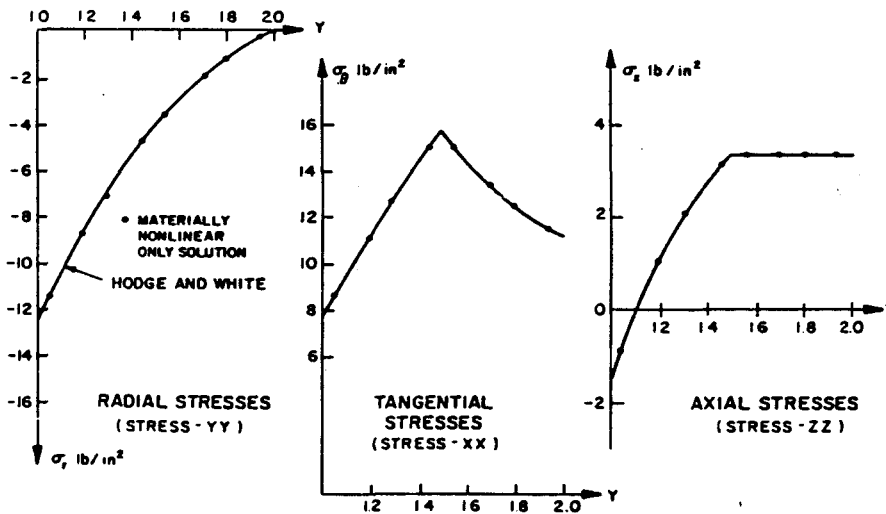


Fig. 28. Elastic-plastic stress distribution through thickness of thick-walled cylinder at $P = 12.5 \text{ lb/in}^2$.

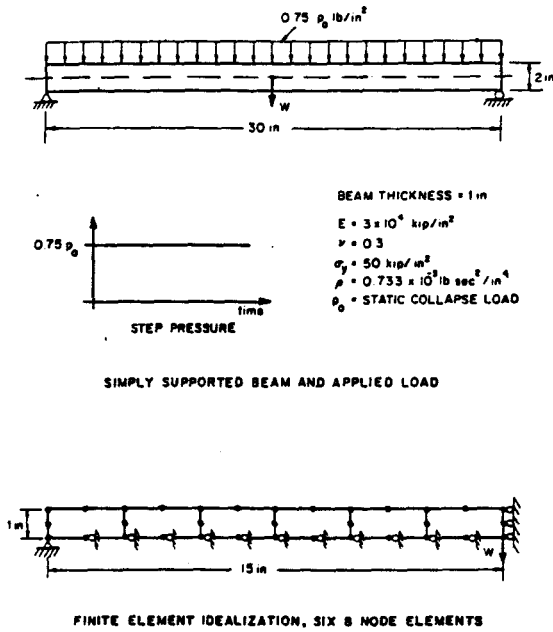


Fig. 29. Elastic-plastic dynamic analysis of simply-supported beam.

11. Concluding remarks

The objective in this paper was to present a brief description of the current version of the computer program NONSAP. The program is a general analysis tool for the linear and nonlinear, static and dynamic analysis of complex structures. A few applications of the program have been presented.

Although NONSAP can be a powerful analysis tool, it should be realized that depending on the problem considered, the program may not be easy to use and, for example, much more difficult to handle than the linear analysis program SAP IV [7]. The use of NONSAP requires a thorough understanding of the theoretical basis of the program, of the numerical techniques employed and their computer implementation. This is particularly the case because not many nonlinear solutions are yet possible on a routine basis [4, 10]. Therefore, it is necessary to apply the program only under the conditions and assumptions for which it was developed.

One important option which NONSAP does not have available is efficient pre- and postprocessing.

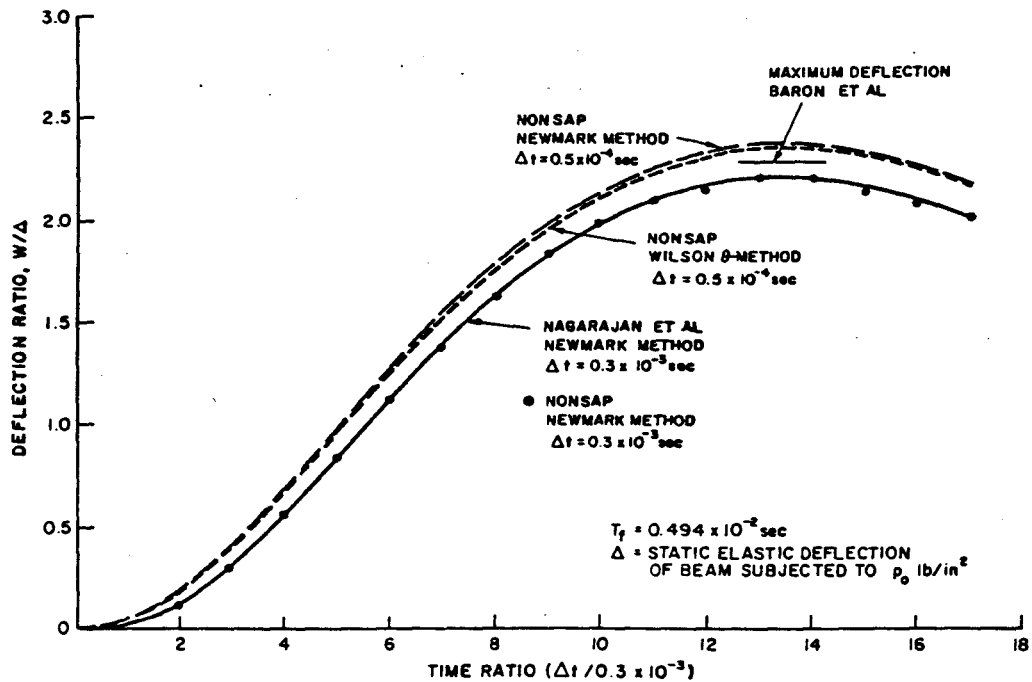


Fig. 30. Initial elastic-plastic displacement response of simply-supported beam.

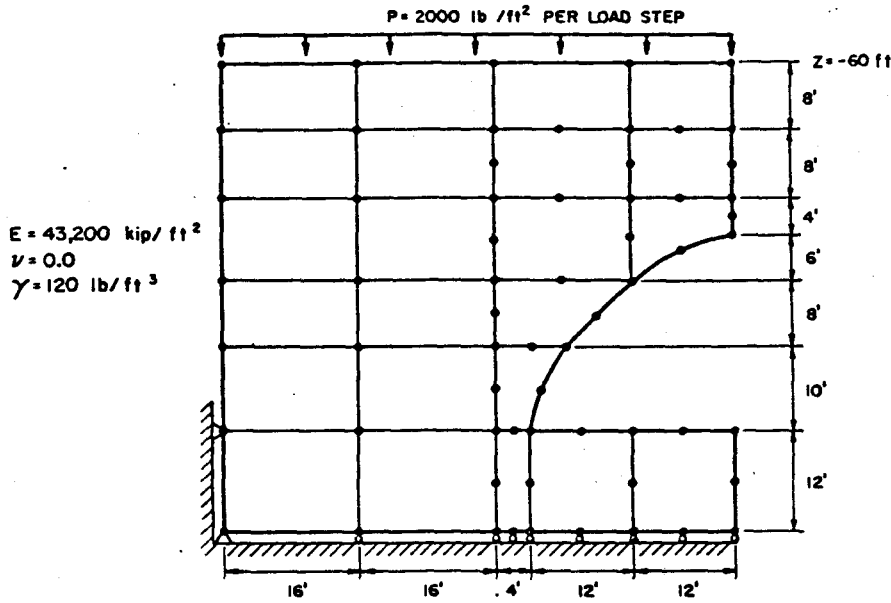


Fig. 31. Finite element mesh for analysis of underground opening.

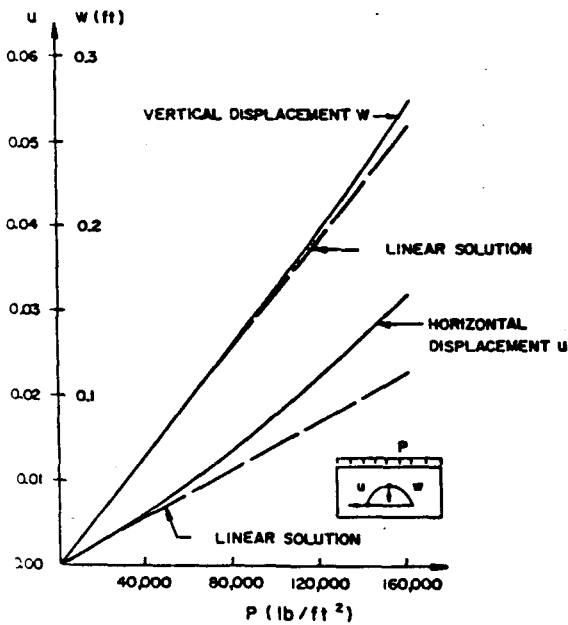


Fig. 32. Load-deflection response of underground opening.

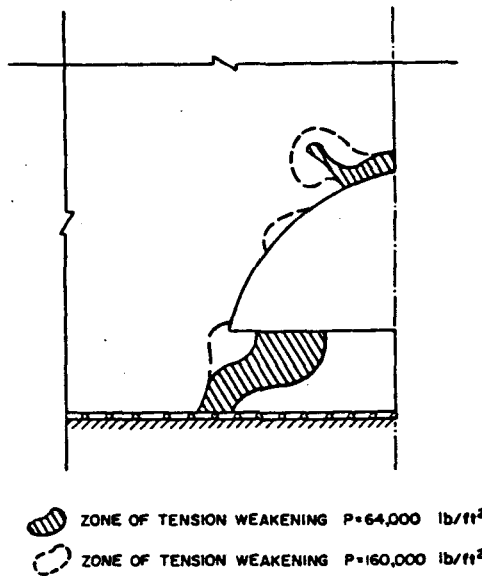


Fig. 33. Cracked regions around underground opening.

Preprocessing is important for generation and checking of data, whereas postprocessing resulting in efficient display of the calculated response can be essential for obtaining a good understanding of the structural behavior.

With regard to future work on NONSAP, it is hoped that the program can be further developed in various areas. It can be important to have out-of-core solution capability, the element library need be increased and additional material models are required. Altogether, the program provides a basis for further work in a variety of problem areas, such as in thermal elastic-plastic and creep analysis, buckling analysis, and soil response calculations.

Acknowledgements

The authors would like to express their appreciation to R.H. Iding, H. Ozdemir and E. Ramm for their assistance during the development of NONSAP.

References

- [1] J.H. Argyris, P.C. Dunne and T. Angelopoulos, Non-linear oscillations using the finite element technique, *Computer Methods in Applied Mechanics and Engineering*, 2 (1973) 203–250.
- [2] G.C. Nayak and O.C. Zienkiewicz, Elasto-plastic stress analysis. A generalization for various constitutive relations including strain softening, *Int. J. Numer. Method Eng.* 5 (1972) 113–135.
- [3] J.T. Oden, *Finite Elements of Nonlinear Continua*, McGraw-Hill, New York (1972).
- [4] J.A. Stricklin, W.A. Von Rieseemann, J.R. Tillerson and W.E. Haisler, Static geometric and material nonlinear analysis, *Proceedings, 2nd US–Japan Symposium on Recent Advances in Computational Methods of Structural Analysis and Design*, Berkeley, California (1972).
- [5] O.C. Zienkiewicz, *The Finite Element Method in Engineering Science*, McGraw-Hill, London (1971).
- [6] P.V. Marcal, Survey of general purpose programs, *Proceedings, 2nd US–Japan Symposium on Recent Advances in Computational Methods of Structural Analysis and Design*, Berkeley, California (1972).
- [7] K.J. Bathe, E.L. Wilson and F.E. Peterson, SAP IV – a structural analysis program for static and dynamic analysis of linear structural systems, EERC Report, No. 73–11, College of Engineering, University of California, Berkeley, June, 1973; also: E.L. Wilson, K.J. Bathe, F.E. Peterson, H.H. Dovey, SAP – A structural analysis program for linear systems, *Nucl. Eng. Des.* 25 (1973) 257–274.
- [8] K.J. Bathe and E.L. Wilson, NONSAP – a general finite element program for nonlinear dynamic analysis of complex structures, Paper M3/1*, *Preprints 2nd Int. Conference on Structural Mechanics in Reactor Technology*, Berlin, Sept. 1973.
- [9] K.J. Bathe, E. Ramm and E.L. Wilson, Finite element formulations for large deformation dynamic analysis, *Int. J. Numer. Meth. Eng.* (to appear).
- [10] K.J. Bathe, H. Ozdemir and E.L. Wilson, Static and dynamic geometric and material nonlinear analysis, SESM Report, No. 74–4, Dept. of Civil Engineering, University of California, Berkeley, Feb. (1974).
- [11] K.J. Bathe and E.L. Wilson, Stability and accuracy analysis of direct integration methods, *Int. J. Earthquake Eng. Struct. Dyn.* 1 (1973) 283–291.
- [12] R.E. Nickell, Direct integration methods in structural dynamics, *ASCE, J. Eng. Mech. Div.* 99 (1973) 303–317.
- [13] J.S. Przemieniecki, *Theory of Matrix Structural Analysis*, McGraw-Hill, New York (1968).
- [14] R.W. Clough and K.J. Bathe, Finite element analysis of dynamic response, *Proceedings, 2nd US–Japan Symposium on Recent Advances in Computational Methods of Structural Analysis and Design*, Berkeley, California (1972).
- [15] W. Hurty and M.F. Rubinstein, *Dynamics of Structures*, Prentice-Hall (1964).
- [16] E.L. Wilson, K.J. Bathe and W.P. Doherty, Direct solution of large systems of linear equations, *Comput. Struct.* 4 (1974) 363–372.
- [17] R.H. Iding, Identification of nonlinear materials by finite element methods, SESM Report, No. 73–4, Department of Civil Engineering, University of California, Berkeley, Jan. (1973); and Private communication to be published.
- [18] G.C. Nayak and O.C. Zienkiewicz, Convenient form of stress invariants for plasticity, *ASCE, J. Struct. Div.* 98 (1972) 949–954.
- [19] C.E. Pugh, J.M. Corum, K.C. Liu and W.L. Greenstreet, Currently recommended constitutive equations for inelastic design analysis of FFTF components, Report, No. TM-3802, Oak Ridge National Laboratory, Oak Ridge, Tennessee (1972).
- [20] S.F. Reyes and D.U. Deere, Elastic–plastic analysis of underground openings, *Proceedings, First Congress, International Society of Rock Mechanics*, Lisbon (1966).
- [21] I. Nelson, M.L. Baron and I. Sandler, Mathematical models for geological materials for wave propagation studies, Headquarters Defense Nuclear Agency Report, No. 2672, Washington, D.C.
- [22] K.J. Bathe and E.L. Wilson, Eigensolution of large structural systems with small bandwidth, *ASCE, J. Eng. Mech. Div.* 99 (1973) 467–479.
- [23] J.T. Holden, On the finite deflections of thin beams, *Int. J. Solids Struct.* 8 (1972) 1051–1055.
- [24] J.A. Stricklin, Geometrically nonlinear static and dynamic analysis of shells of revolution, *High Speed*

- Computing of Elastic Structures, Proceedings of the Symposium of IUTAM, University of Liege, Aug. (1970).
- 25] J.F. Mescall, Large deflections of spherical shells under concentrated loads, *J. Appl. Mech.* 32 (1965) 936-938.
 - 26] P.G. Hodge and G.H. White, A quantitative comparison of flow and deformation theories of plasticity, *J. Appl. Mech.* 17 (1950) 180-184.
 - [27] M.L. Baron, H.H. Bleich and P. Weidlinger, Dynamic elastic-plastic analysis of structures, ASCE, *J. Eng. Mech. Div.* 87 (1961) 23-42.
 - [28] S. Nagarajan and E.P. Popov, Elastic-plastic dynamic analysis of axisymmetric solids, SESM Report, No. 73-9, Department of Civil Engineering, University of California, Berkeley (1973).

SOME COMPUTATIONAL CAPABILITIES FOR NONLINEAR FINITE ELEMENT ANALYSIS *

K.J. BATHE, S. BOLOURCHI, S. RAMASWAMY and M.D. SNYDER

Department of Mechanical Engineering, Massachusetts Institute of Technology, Cambridge, Massachusetts 02139, USA

Received 26 September 1977

The computational capabilities available in the current version of the computer program ADINA for stress analysis of structures and continua are described. The program can be employed effectively for various linear and nonlinear static and dynamic finite element analyses. The solutions of some problems using ADINA are presented to indicate the solution capabilities of the program.

1. Introduction

In recent years it has been recognized to an increasing extent that the capability of performing effective linear and nonlinear analysis can be a very important asset in the design of structures. A particularly important area in which nonlinear analysis must be carried out is the design of nuclear power generating plants [1]. The safety of a structure may be increased and the cost reduced if an accurate analysis can be performed. Primarily, linear and nonlinear analyses of complex structures have become possible through the use of electronic digital computers operating on discrete representations of the actual structure [2–5].

At the Second International Conference on Structural Mechanics in Reactor Technology a paper on the computer program NONSAP was presented [6]. Since that time we have continued with the research and development of nonlinear analysis capabilities. The final phase of these activities has been the implementation of the techniques developed in the computer program ADINA, which can be employed effectively for static and dynamic, linear and nonlinear analysis. The computer program ADINA (Automatic Dynamic

Incremental Nonlinear Analysis) is a significant further development of the programs NONSAP and SAP IV [7]. Our objective in this paper is to survey the current capabilities of the code, and thus report on our latest and current activities. Since the program ADINA is a further development of the program NONSAP, to make this presentation self-contained and comprehensive, some overlap with the material presented in [6] is necessary.

The research that we are conducting in the area of nonlinear finite element analysis and the associated development of ADINA is expected to continue over the years to come, and this paper can be regarded as a progress report on our activities.

It should be pointed out that the theory and numerical techniques used in ADINA are not presented in this paper, but can be found in refs. [4,8–17], where more sample solutions are also given. Also, in this paper we summarize only our developments in the capabilities for stress analysis of structures and continua. The associated research and development in heat transfer analysis capabilities and analysis of field problems is described elsewhere [18,19].

The structural systems that can be analyzed using ADINA can be composed of combinations of a number of different finite elements. The program presently contains the following element types:

- (a) three-dimensional truss element;
- (b) two-dimensional plane stress and plane strain

* Expanded version of Invited Paper M4/1* presented at the 4th International Conference on Structural Mechanics in Reactor Technology, San Francisco, California, 15–19 August 1977.

element;

- (c) three-dimensional plane stress element;
- (d) two-dimensional axisymmetric shell or solid element;

element;

- (e) three-dimensional solid element;
- (f) three-dimensional thick shell element; and
- (g) three-dimensional beam element.

The nonlinearities may be due to large displacements, large strains, and nonlinear material behavior. The material descriptions presently available are as follows.

For the truss elements: (a) linear elastic, (b) nonlinear elastic, (c) thermo-elastic, (d) elastic-plastic, (e) thermo-elastic-plastic and creep;

for the two-dimensional elements: (a) isotropic linear elastic, (b) orthotropic linear elastic, (c) isotropic thermo-elastic, (d) curve description model, (e) concrete model, (f) elastic-plastic materials, von Mises or Drucker-Prager yield condition, (g) thermo-elastic-plastic-creep, von Mises yield condition, (h) Mooney-Rivlin material;

for the three-dimensional elements: (a) isotropic linear elastic, (b) orthotropic linear elastic, (c) isotropic thermo-elastic, (d) curve description model, (e) concrete model, (f) elastic-plastic materials, von Mises yield condition, (g) thermo-elastic-plastic-creep, von Mises yield condition;

for the beam element: (a) linear elastic, (b) elastic-plastic, von Mises yield condition.

Program ADINA is an out-of-core solver, i.e. the equilibrium equations are processed in blocks, and very large finite element systems can be considered. Also, all structure matrices are stored in compacted form, i.e. virtually only nonzero elements are processed, resulting in maximum system capacity and solution efficiency.

In addition to out-of-core solution of the equilibrium equations, there is also virtually no high-speed storage limit on the total number of finite elements that can be used. To obtain maximum program capacity, the finite elements are processed in groups according to their type and whether they are linear or nonlinear elements.

The finite element system response is calculated

using an incremental solution of the equations of equilibrium. In dynamic analysis, implicit time integration (the Newmark or Wilson methods) or explicit time integration (the central difference method) can be employed. Before the incremental solution is carried out, the applicable constant structure matrices, namely the linear effective stiffness, linear stiffness, mass, and damping matrices, and the load vectors are assembled and stored on low-speed storage. During the step-by-step solution the linear effective stiffness matrix is updated for the nonlinearities in the system. Therefore, only the nonlinearities are dealt with in the time integration and no efficiency is lost in linear analysis.

In this paper we first describe the different options available in ADINA for static and dynamic analysis, and then present the analysis results of some sample problems. We conclude the paper with a discussion of future important research and program developments.

2. The incremental equilibrium equations of structural systems

The incremental nodal point equilibrium equations for an assemblage of nonlinear finite elements have been derived in refs. [8–11]. At time t we have, using implicit time integration,

$$\mathbf{M}^{t+\Delta t}\ddot{\mathbf{U}} + \mathbf{C}^{t+\Delta t}\dot{\mathbf{U}} + {}^t\mathbf{K}\mathbf{U} = {}^{t+\Delta t}\mathbf{R} - {}^t\mathbf{F}, \quad (1a)$$

and using explicit time integration,

$$\mathbf{M}^t\ddot{\mathbf{U}} + \mathbf{C}^t\dot{\mathbf{U}} = {}^t\mathbf{R} - {}^t\mathbf{F}, \quad (1b)$$

where

\mathbf{M} = constant mass matrix,

\mathbf{C} = constant damping matrix,

${}^t\mathbf{K}$ = tangent stiffness matrix at time t ,

${}^t\mathbf{R}$, ${}^{t+\Delta t}\mathbf{R}$ = external load vectors applied at time t , $t + \Delta t$,

${}^t\mathbf{F}$ = nodal point force vector equivalent to the element stresses at time t ,

${}^t\dot{\mathbf{U}}$, ${}^{t+\Delta t}\dot{\mathbf{U}}$ = vectors of nodal point velocities at time t , $t + \Delta t$,

${}^t\ddot{\mathbf{U}}$, ${}^{t+\Delta t}\ddot{\mathbf{U}}$ = vectors of nodal point accelerations at time t , $t + \Delta t$, and

\mathbf{U} = vector of nodal point displacement increments from time t to time $t + \Delta t$, i.e.

$$\mathbf{U} = {}^{t+\Delta t}\mathbf{U} - {}^t\mathbf{U}.$$

It should be noted that eq. (1a) reduces to the

Table 1

Summary of step-by-step integration. Static analysis or dynamic analysis using implicit time integration (the Wilson θ -method or Newmark method), or explicit time integration (the central difference method).

Initial Calculations

1. Form linear stiffness matrix \mathbf{K} , mass matrix \mathbf{M} and damping matrix \mathbf{C} , whichever is applicable.

Calculate the following constants:

$\text{tol} < 0.01$; $\text{nitem} > 3$; in static analysis $\theta = 1$ and go to 3.

Wilson θ -method: $\theta > 1.37$, usually $\theta = 1.4$, $\tau = \theta \Delta t$:

$$\begin{array}{llll} a_0 = 6/\tau^2 & a_1 = 3/\tau & a_2 = 2a_1 & a_3 = 2 \\ a_4 = 2 & a_5 = \tau/2 & a_6 = a_0/\theta & a_7 = -a_2/\theta \\ a_8 = 1 - 3/\theta & a_9 = \Delta t/2 & a_{10} = \Delta t^2/6. & \end{array}$$

Newmark method: $\theta = 1.0$, $\delta > 0.50$, $\alpha > 0.25(0.5 + \delta)^2$, $\tau = \Delta t$:

$$\begin{array}{llll} a_0 = 1/(\alpha \Delta t^2) & a_1 = \delta/(\alpha \Delta t) & a_2 = 1/(\alpha \Delta t) & a_3 = 1/(2\alpha) - 1 \\ a_4 = \delta/\alpha - 1 & a_5 = \Delta t(\delta/\alpha - 2)/2 & a_6 = a_0 & a_7 = -a_2 \\ a_8 = -a_3 & a_9 = \Delta t(1 - \delta) & a_{10} = \delta \Delta t. & \end{array}$$

Central difference method:

$$a_0 = 1/\Delta t^2 \quad a_1 = 1/2\Delta t \quad a_2 = 2a_0 \quad a_3 = 1/a_2.$$

2. Initialize ${}^0\mathbf{U}$, ${}^0\dot{\mathbf{U}}$, ${}^0\ddot{\mathbf{U}}$

For central difference method only, calculate $\Delta t \mathbf{U}$ from initial conditions:

$$\Delta t \mathbf{U} = {}^0\mathbf{U} + \Delta t {}^0\dot{\mathbf{U}} + a_3 {}^0\ddot{\mathbf{U}}.$$

3. Form effective linear coefficient matrix.

In implicit time integration or static analysis: $\hat{\mathbf{K}} = \mathbf{K} + a_0\mathbf{M} + a_1\mathbf{C}$;

in explicit time integration: $\hat{\mathbf{M}} = a_0\mathbf{M} + a_1\mathbf{C}$.

4. In linear static analysis and linear dynamic analysis using implicit time integration triangularize $\hat{\mathbf{K}}$.

For Each Time Step

A. In linear analysis

- (i) Form effective load vector.

In static analysis or implicit time integration:

$${}^{t+\tau}\hat{\mathbf{R}} = {}^t\hat{\mathbf{R}} + \theta({}^{t+\Delta t}\hat{\mathbf{R}} - {}^t\hat{\mathbf{R}}) + \mathbf{M}(a_0 {}^t\mathbf{U} + a_2 {}^t\dot{\mathbf{U}} + a_3 {}^t\ddot{\mathbf{U}}) + \mathbf{C}(a_1 {}^t\mathbf{U} + a_4 {}^t\dot{\mathbf{U}} + a_5 {}^t\ddot{\mathbf{U}});$$

in explicit time integration:

$${}^t\hat{\mathbf{R}} = {}^t\hat{\mathbf{R}} + a_2\mathbf{M}({}^t\mathbf{U} - {}^{t-\Delta t}\mathbf{U}) + \hat{\mathbf{M}}{}^{t-\Delta t}\mathbf{U} - {}^t\mathbf{F}.$$

- (ii) Solve for displacement increments.

In static analysis and implicit time integration:

$$\hat{\mathbf{K}}{}^{t+\tau}\mathbf{U} = {}^{t+\tau}\hat{\mathbf{R}}; \quad \mathbf{U} = {}^{t+\tau}\mathbf{U} - {}^t\mathbf{U};$$

in explicit time integration:

$$\hat{\mathbf{M}}{}^{t+\Delta t}\mathbf{U} = {}^t\hat{\mathbf{R}}.$$

- (iii) Go to C.

B. In nonlinear analysis

- (i) In static analysis or implicit time integration if a new stiffness matrix is to be formed, update $\hat{\mathbf{K}}$ for nonlinear stiffness effects to obtain ${}^t\hat{\mathbf{K}}$; triangularize ${}^t\hat{\mathbf{K}}$:

$${}^t\hat{\mathbf{K}} = \text{LDLT}.$$

Table 1 (continued)

(ii) Form effective load vector.

In static analysis or implicit time integration:

$${}^{t+\tau}\hat{\mathbf{R}} = {}^t\mathbf{R} + \theta({}^{t+\Delta t}\mathbf{R} - {}^t\mathbf{R}) + \mathbf{M}(a_2 {}^t\dot{\mathbf{U}} + a_3 {}^t\ddot{\mathbf{U}}) + \mathbf{C}(a_4 {}^t\dot{\mathbf{U}} + a_5 {}^t\ddot{\mathbf{U}}) - {}^t\mathbf{F};$$

in explicit time integration:

$${}^t\hat{\mathbf{R}} = {}^t\mathbf{R} + a_2\mathbf{M}({}^t\mathbf{U} - {}^{t-\Delta t}\mathbf{U}) + \hat{\mathbf{M}}{}^{t-\Delta t}\mathbf{U} - {}^t\mathbf{F}.$$

(iii) Solve for displacement increments.

In static analysis or implicit time integration using latest D, L factors:

$$\mathbf{LDL}^T\mathbf{U} = {}^{t+\tau}\hat{\mathbf{R}};$$

in explicit time integration:

$$\hat{\mathbf{M}}{}^{t+\Delta t}\mathbf{U} = {}^t\hat{\mathbf{R}}.$$

(iv) If required iterate for static or dynamic equilibrium (in implicit time integration):

$$\mathbf{U}^{(0)} = \mathbf{U}, \quad i = 0; \quad \text{then}$$

(a) $i = i + 1$.(b) Calculate $(i - 1)$ st approximation to accelerations, velocities, and displacements:

$${}^{t+\tau}\ddot{\mathbf{U}}^{(i-1)} = a_0\mathbf{U}^{(i-1)} - a_2 {}^t\dot{\mathbf{U}} - a_3 {}^t\ddot{\mathbf{U}}; \quad {}^{t+\tau}\dot{\mathbf{U}}^{(i-1)} = a_1\mathbf{U}^{(i-1)} - a_4 {}^t\dot{\mathbf{U}} - a_5 {}^t\ddot{\mathbf{U}};$$

$${}^{t+\tau}\mathbf{U}^{(i-1)} = \mathbf{U}^{(i-1)} + {}^t\mathbf{U}.$$

(c) Calculate $(i - 1)$ st effective out-of-balance loads:

$${}^{t+\tau}\hat{\mathbf{R}}^{(i-1)} = {}^t\mathbf{R} + \theta({}^{t+\Delta t}\mathbf{R} - {}^t\mathbf{R}) - \mathbf{M}{}^{t+\tau}\ddot{\mathbf{U}}^{(i-1)} - \mathbf{C}{}^{t+\tau}\dot{\mathbf{U}}^{(i-1)} - {}^{t+\tau}\mathbf{F}^{(i-1)}.$$

(d) Solve for i th correction to displacement increments:

$$\mathbf{LDL}^T\Delta\mathbf{U}^{(i)} = {}^{t+\tau}\hat{\mathbf{R}}^{(i-1)}.$$

(e) Calculate new displacement increments:

$$\mathbf{U}^{(i)} = \mathbf{U}^{(i-1)} + \Delta\mathbf{U}^{(i)}.$$

(f) Iteration convergence if $(\|\Delta\mathbf{U}^{(i)}\|_2 / \max_{j=\Delta t, \dots, t, t+\tau} \|\dot{\mathbf{U}}\|_2) < \text{tol}$.If convergence: $\mathbf{U} = \mathbf{U}^{(i)}$ and go to C;if no convergence and $i < \text{nitern}$: go to (a); otherwise restart using new stiffness matrix reformation strategy and/or a smaller time step size.

C. Calculate new accelerations, velocities, and displacements

Wilson θ -method:

$${}^{t+\Delta t}\ddot{\mathbf{U}} = a_6\mathbf{U} + a_7 {}^t\dot{\mathbf{U}} + a_8 {}^t\ddot{\mathbf{U}},$$

$${}^{t+\Delta t}\dot{\mathbf{U}} = {}^t\dot{\mathbf{U}} + a_9({}^{t+\Delta t}\ddot{\mathbf{U}} + {}^t\ddot{\mathbf{U}}),$$

$${}^{t+\Delta t}\mathbf{U} = {}^t\mathbf{U} + \Delta t {}^t\dot{\mathbf{U}} + a_{10}({}^{t+\Delta t}\ddot{\mathbf{U}} + 2 {}^t\ddot{\mathbf{U}}).$$

Newmark method:

$${}^{t+\Delta t}\ddot{\mathbf{U}} = a_6\mathbf{U} + a_7 {}^t\dot{\mathbf{U}} + a_8 {}^t\ddot{\mathbf{U}},$$

$${}^{t+\Delta t}\dot{\mathbf{U}} = {}^t\dot{\mathbf{U}} + a_9 {}^t\dot{\mathbf{U}} + a_{10} {}^{t+\Delta t}\ddot{\mathbf{U}},$$

$${}^{t+\Delta t}\mathbf{U} = {}^t\mathbf{U} + \mathbf{U}.$$

Central difference method:

$${}^t\ddot{\mathbf{U}} = a_1({}^{t+\Delta t}\mathbf{U} - {}^{t-\Delta t}\mathbf{U}),$$

$${}^t\dot{\mathbf{U}} = a_0({}^{t+\Delta t}\mathbf{U} - 2 {}^t\mathbf{U} + {}^{t-\Delta t}\mathbf{U}).$$

incremental equilibrium equations in static analysis if mass and damping effects are not included. As was discussed in [8-11], the solution of eq. (1a) yields, in general, approximate displacement increments U . To improve the solution accuracy (and in some cases to prevent the development of instabilities) it may be necessary to use equilibrium iteration in each or pre-selected time steps. In this case we consider the equilibrium equations

$$M^{t+\Delta t}\ddot{U}^{(i)} + C^{t+\Delta t}\dot{U}^{(i)} + {}^tK\Delta U^{(i)} = {}^{t+\Delta t}R - {}^{t+\Delta t}F^{(i-1)}, \quad i = 1, 2, 3, \dots, \quad (2)$$

where M , C , tK , and ${}^{t+\Delta t}R$ are as defined above, and ${}^{t+\Delta t}\ddot{U}^{(i)}$, ${}^{t+\Delta t}\dot{U}^{(i)}$, ${}^{t+\Delta t}U^{(i)} = {}^{t+\Delta t}U^{(i-1)} + \Delta U^{(i)}$ are the approximations to the accelerations, velocities, and displacements obtained in iteration i . The first iteration, i.e. $i = 1$ in eq. (2), corresponds to the solution of eq. (1a) where $\Delta U^{(1)} = U$, ${}^{t+\Delta t}U^{(0)} = {}^tU$, ${}^{t+\Delta t}\ddot{U}^{(1)} = {}^{t+\Delta t}\ddot{U}$, ${}^{t+\Delta t}\dot{U}^{(1)} = {}^{t+\Delta t}\dot{U}$, ${}^{t+\Delta t}F^{(0)} = {}^tF$. The vector of nodal point forces ${}^{t+\Delta t}F^{(i-1)}$ is work equivalent to the element stresses in the configuration corresponding to the displacements ${}^{t+\Delta t}U^{(i-1)}$. The approximations to the velocities and accelerations, ${}^{t+\Delta t}\dot{U}^{(i)}$ and ${}^{t+\Delta t}\ddot{U}^{(i)}$, respectively, depend on the time integration scheme used [4].

It should be noted that the solution scheme used in eq. (2) corresponds to a modified Newton iteration.

In the program ADINA, the central difference method is employed in explicit time integration and the Newmark method or the Wilson method can be employed in implicit time integration of the dynamic response. Table 1 summarizes the algorithm for linear or nonlinear, static or dynamic analysis. The specific operations performed during the step-by-step solution are discussed in section 3.4.

2.1. Element to structure matrices and force vectors

The structure matrices in table 1 are formed by direct addition of the element matrices and vectors [4]; for example

$$K = \sum_m K_m, \quad (3)$$

where K_m is the stiffness matrix of the m th element. Although K_m is formally of the same order as K , only those terms in K_m which pertain to the element degrees of freedom are nonzero. The addition of the

element matrices and vectors can therefore be performed by using the element matrices in compact form together with identification arrays which relate element degrees of freedom to structure degrees of freedom.

In the program ADINA either a lumped or consistent mass matrix may be used. In addition, concentrated masses corresponding to selected degrees of freedom can be input. Damping can only be specified in the form of concentrated nodal point dampers. The advantages of lumped mass and consistent mass analysis have been discussed in [4].

2.2. Boundary conditions

If a displacement component is zero, the corresponding equation is not retained in the structure equilibrium equations, eqs. (1) and (2), and the corresponding element stiffness and mass terms are disregarded. If a non-zero displacement is to be specified f at a degree of freedom i , say $U_i = x$, the equation

$$kU_i = kx, \quad (4)$$

need be added, where $k \gg k_{ii}$. Therefore, the solution of eqs. (1) and (2) must give $U_i = x$. Physically, eq. (4) can be interpreted as adding at the degree of freedom i a spring of large stiffness k and specifying a load which, because of the relatively flexible structure at this degree of freedom, produces the required displacement x . This approach simplifies programming problems which are normally associated with specifying displacements.

In ADINA, nonzero deflection boundary conditions must be specified by using the truss element to provide the stiffness k in eq. (4) and applying the load $R_i = Kx$, since a special boundary element (as used for example in SAP IV [7]) is not available.

3. Program organization

The complete solution process in program ADINA is divided into four distinct phases.

(1) *Finite element mesh and element data input.* In this phase the control information and the nodal point input data are read and generated by the program. The equation numbers for the active degrees of freedom at each nodal point are established. The initial conditions are read. The element data are read and generated, the

element connectivity arrays are calculated and all element information is stored on tape.

(2) *Assemblage of constant structure matrices.* Before the solution of eqs. (1b) or (2) is carried out, the linear structure stiffness, mass, and damping matrices are assembled and stored on tape (or other low-speed storage). In addition, the effective linear structure stiffness matrix is calculated and stored (see table 1).

(3) *Load vector calculations.* The externally applied load vectors for each time (load) step are calculated and stored on tape.

(4) *Step-by-step solution.* During this phase the solution of eqs. (1b) or (2) is obtained at all time points. In addition to the displacement, velocity, and acceleration vectors (whichever applicable), the element stresses are calculated and printed. Before the time integration is performed, the lowest frequencies and corresponding mode shapes may be calculated.

It need be noted that these basic steps are independent of the element type used and are the same for either a static or dynamic analysis. However, only those matrices actually required in the analysis are assembled. For example, no mass and damping matrices are calculated in static analysis, and no stiffness matrix is calculated when explicit time integration is employed.

Program ADINA is an out-of-core solver and allocates storage in BLANK COMMON dynamically during the different phases of solution. On some computers the total storage required can be dynamically adjusted up to the maximum high speed storage available during the execution process. If this option is not available, the maximum high speed storage to be used is fixed and the storage required in each phase is checked so that the maximum is not exceeded.

In the solution the highest numbered high speed storage locations are reserved for element group information. For the analysis, the finite elements of the complete assemblage need be divided into element groups according to their type, the nonlinear formulation, and the material model used (see section 5). Each element group must consist of the same type of elements, must use one nonlinear formulation, and only one specific material model. The data pertaining to each individual element group is stored in the element group information. The maximum storage required for any one of the element groups is MAXEST. The use of the element groups reduces input-output transfers during the solution process, since the data of the elements is retrieved in blocks during the solution of eqs. (1b) and (2) and element stress calculations. Fig. 1 shows the low speed storage layout used for the

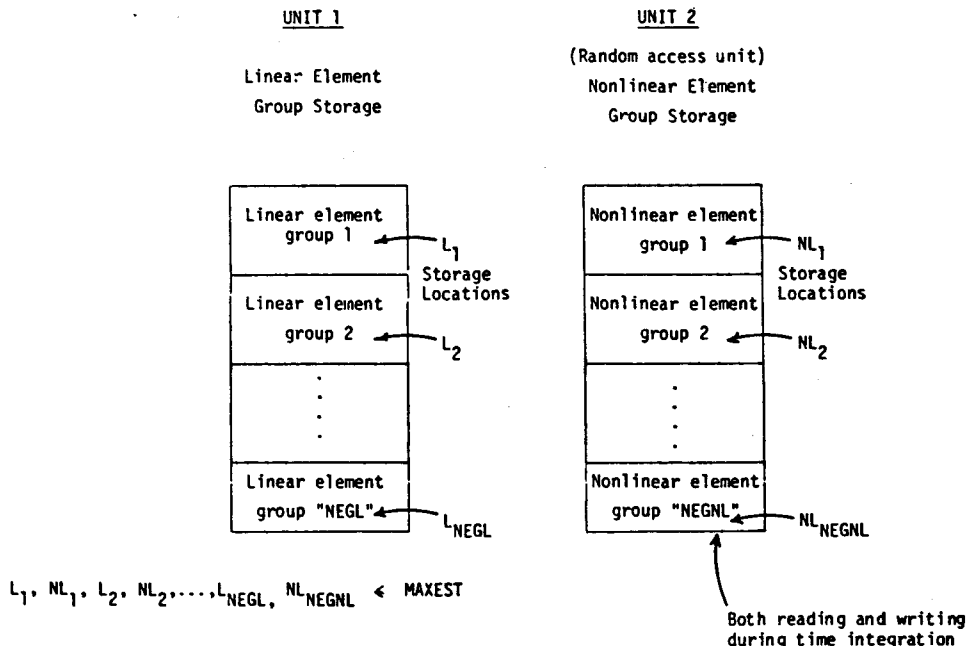


Fig. 1. Auxiliary storage organization for element group information.

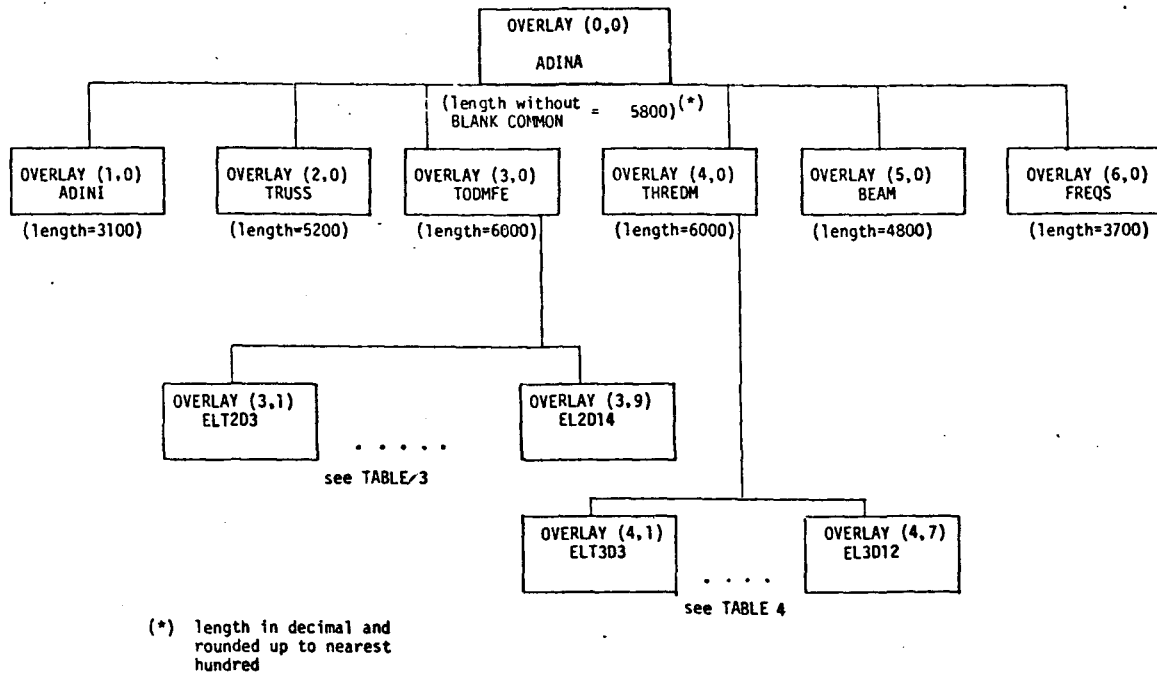


Fig. 2. Overlay structure of ADINA.

element group information.

To further improve high speed storage capacity, ADINA has an overlay structure, as shown in fig. 2. The overlay structure has been chosen to correspond to the four phases of execution listed above and considering the element library, the material models available, and the eigensystem calculation option. The (0, 0) overlay consists of the main program and driving subroutines. The first level of overlays is made up of the input phase subroutines in OVERLAY (1, 0), the element subroutines in OVERLAY (2, 0) to OVERLAY (5, 0) and the subroutines for the eigensystem solution in OVERLAY (6, 0). The second level of overlays consists of the different material models. The program is thus modular and special purpose programs can be assembled with ease.

3.1. Finite element mesh and element data input

The nodal point information read during the input phase consists of the boundary condition codes (stored in the ID array) and the global X, Y, Z coordinates of each nodal point. The number of rows in the ID array is equal to the maximum number of degrees of freedom

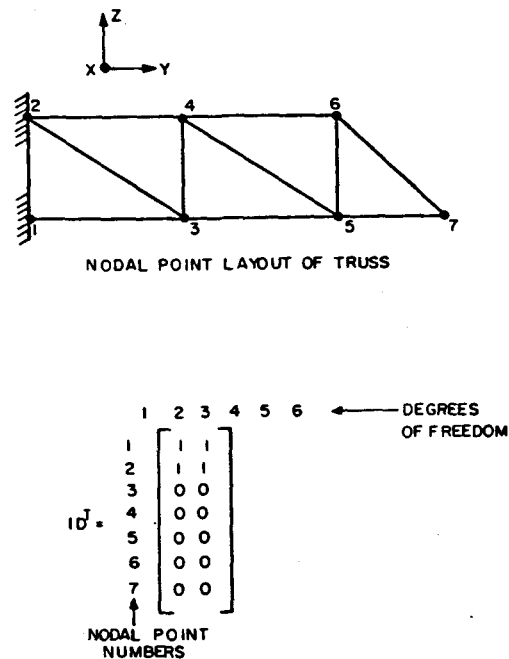


Fig. 3. Nodal point layout of truss example and ID array as read and/or generated.

$$ID^T = \begin{bmatrix} 0 & 0 \\ 0 & 0 \\ 1 & 2 \\ 3 & 4 \\ 5 & 6 \\ 7 & 8 \\ 9 & 10 \end{bmatrix}$$

Fig. 4. ID array of truss example after allocation of equation numbers to active degrees of freedom.

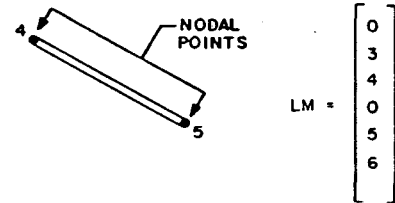


Fig. 5. Connection array (vector LM) for a typical element of the truss example.

admitted at a nodal point (NDOF). For example, in a two-dimensional analysis without rotational degrees of freedom $NDOF = 2$.

It need be noted that the user should allow only those degrees of freedom which are compatible with the elements connected to a nodal point. The program can deal with a maximum of six possible degrees of freedom (three translations and three rotations) at

each nodal point, and all non-active degrees of freedom need be deleted. Specifically, a '1' in the ID array denotes that no equation shall be associated with the degree of freedom, whereas a '0' indicates that this is an active degree of freedom [4]. Fig. 3 shows the ID array for a simple truss structure as it was read and/or generated by the program. Once the complete ID and X, Y, Z arrays have been obtained, equation numbers

Table 2
Auxiliary storage units in ADINA

Read/write unit number	Linear static analysis	Linear dynamic analysis	Nonlinear static analysis	Nonlinear dynamic analysis
1		linear element group data		
2		not used		nonlinear element group data (random access)
3		load vectors		
4		linear stiffness matrix		
7	not used	effective linear coefficient matrix	not used	effective linear coefficient matrix
8	ID array; displacement (velocity and acceleration if applicable) vectors and nonlinear element group data for restart (saved at restart save intervals)			
9	nodal point coordinates for pressure load calculations			
10		LDL ^T factor of (effective) stiffness matrix		(random access)
11	not used	(1) mass matrix (2) damping vector	not used	(1) mass matrix (2) damping vector
12		not used	effective nonlinear stiffness matrix	
13	mode shape vectors and frequencies			
56		not used	nodal point temperatures	

Unit 5 = input; unit 6 = output.

are associated with all active degrees of freedom, i.e. the zeroes in the ID array are replaced by corresponding equation numbers, and each '1' is replaced by a zero, as shown in fig. 4 for the simple truss example of fig. 3.

A second important part of the input phase is the reading and generating of element group information for each element group. Specifically, the element coordinates; the material properties, and the element connectivity arrays are established. Also, working vectors which store required element strains, stresses and other variables are initialized. For each element group this information is processed together (in the element group information) and then written together in one block on secondary storage. During the next phases of the solution, therefore, the required element data can be read in blocks, sequentially one block at a time, into the same high speed storage locations.

The element connectivity array (vector LM) of an element is established from the ID array and the specified nodal points of the assemblage pertaining to the element. The connectivity array for a typical element of the truss example is shown in fig. 5.

It should be noted that the reading and generating of the element data of one group requires only one call of the specific element overlay needed since all elements in one group are of the same kind. After all element information has been established, the ID and X, Y, Z arrays are no longer required, and the corresponding storage area is used for the formation of the constant structure matrices and later for the solution of the equations of equilibrium.

3.2. Formation of constant structure matrices

All structure matrices which are not time dependent are calculated before the time integration is carried out. At this stage it is necessary to distinguish between the different kinds of analyses possible, namely whether a linear or nonlinear, static or dynamic analysis is required. The storage allocation during this phase is such that all required linear structure matrices are assembled using the same high-speed storage locations.

Table 2 shows the low speed storage used corresponding to the different analyses. The assemblage of a structure matrix is effected by reading the data of all required element groups in succession, and by calculating and adding the element matrices to the structure

matrix, as was discussed in section 2.1.

It should be noted that in linear analysis the structure stiffness or effective stiffness matrix is triangularized directly after assemblage. In the step-by-step solution only forward reductions and back-substitutions of the (effective) load vectors are then required.

3.3. Calculation of external load vectors

The external loading in the analysis can consist of concentrated nodal point loading and surface pressure loading. In addition, gravity loading can be specified. The loads are assumed to vary with time as expressed by time functions and load multipliers defined in the input.

3.4. Step-by-step solution

The main phase in the analysis is the step-by-step solution of the equilibrium equations, eqs. (1b) and (2). The algorithm used was presented in table 1. Since the program can perform static and dynamic, linear and nonlinear analyses, it is convenient to consider the different types of analyses as follows.

(1) *Linear static analysis.* In a linear static analysis, all element groups are linear and only the linear stiffness matrix is calculated in the matrix assemblage phase. The stiffness matrix is triangularized before entering the step-by-step solution phase. It should be noted that this solution corresponds to a linear dynamic analysis, in which mass and damping effects are neglected. Therefore, in linear static analysis, solutions for multiple load cases can be obtained by varying the loads with time so as to obtain one individual load case at each time step.

(2) *Linear dynamic analysis.* In a linear dynamic analysis all elements are linear, with mass and possibly damping effects included. The mass matrix may be diagonal (lumped mass analysis) or banded (consistent mass analysis) and additional concentrated masses may be specified at selected degrees of freedom. The damping matrix C is assumed to be diagonal.

If explicit time integration (the central difference method) is employed, a diagonal mass matrix must be used.

(3) *Nonlinear static analysis.* In nonlinear static analysis linear and nonlinear element groups are defined. Damping and mass effects are neglected.

Before the step-by-step solution the linear stiffness matrix corresponding to the linear elements of the complete element assemblage was calculated (see table 1). This matrix is now updated in preselected load steps by the stiffness matrices of the nonlinear elements to form the current tangent stiffness matrix. The specific load steps at which a new tangent stiffness matrix is to be calculated are input to the program.

Depending on the nonlinear formulations and the nonlinear material models used, and also depending on the magnitude of the load steps, the accuracy of the solution may be significantly increased using equilibrium iteration. The program load steps at which equilibrium iterations shall be performed can be defined in the input control data.

(4) *Nonlinear dynamic analysis.* A nonlinear dynamic analysis using implicit time integration (Newmark or Wilson method) is carried out essentially in the same way as a nonlinear static analysis, but mass and possibly damping effects are included. The mass and damping matrices are defined as in linear dynamic analysis. It should be noted that the structure mass and damping matrices are calculated before the step-by-step solution (see table 1).

If explicit time integration (the central difference method) is employed, a diagonal mass matrix must be used.

4. The compacted storage scheme and solution of equations

An important aspect is the efficient storage of the structure matrices and an effective solution of the equilibrium equations. The storage scheme need be optimized in order to obtain maximum capacity. The effective solution of the equations is necessary to reduce total solution cost.

In the program ADINA a compacted storage scheme is used in which all structure matrices are stored as one-dimensional arrays and only the elements below the 'skyline' of the matrices are processed [4]. Fig. 6 shows, as an example, the element pattern in a typical stiffness matrix before and after triangularization. It should be noted that zero elements within the skyline in general do not remain zero during the equation solution and are therefore stored, whereas all elements outside the skyline are not considered.

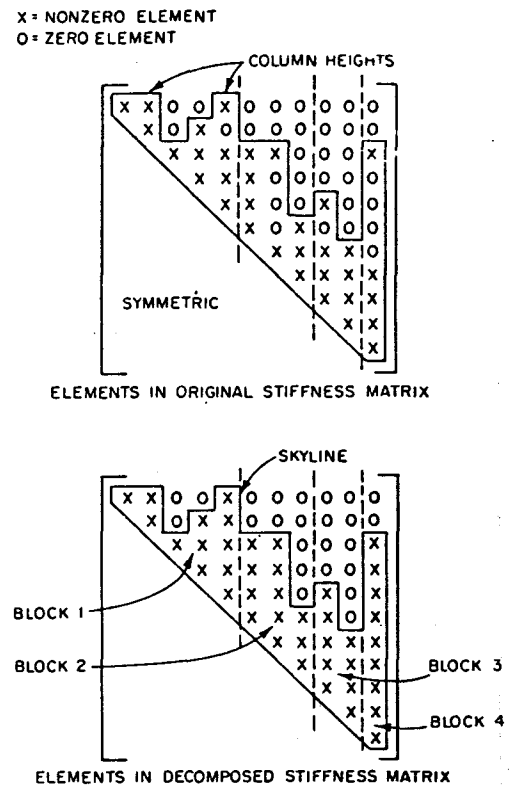
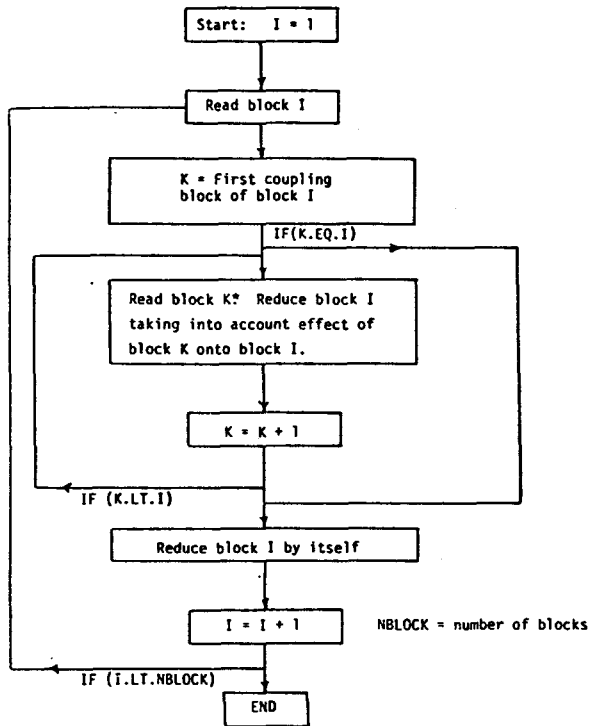


Fig. 6. Typical element pattern in a stiffness matrix using block storage.

Fig. 6 also shows the block storage scheme used for the stiffness and mass matrices in out-of-core solution. The number of blocks and the number of columns per each block are calculated by the program prior to the assemblage process and depend on the total high speed storage available during the matrix assemblage and time integration phases. It should be noted that the number of columns per block vary and hence optimum advantage is taken of the high speed storage available for solution.

The solution of equations is obtained using the out-of-core linear equation solver COLSOL. This subroutine uses, in essence, Gauss elimination on the positive definite symmetrical system of equations, but operates columnwise on the coefficient matrix [4]. The block operations performed during the solution process are shown in fig. 7. The same solution algorithm is used in all analysis types, i.e. in linear, nonlinear, static or dynamic analysis, and consists of the LDL^T decomposition of the stiffness matrix (or effective stiffness ma-



* Note that (effective) stiffness matrix blocks are stored on a random access unit.

Fig. 7. Block operations in LDL^T factorization of (effective) stiffness matrix.

trix), and the reduction and back-substitution of the (effective) load vector. For example, in linear static analysis, the equations are $KU = R$ and the program calculates

$$K = LDL^T, \tag{5}$$

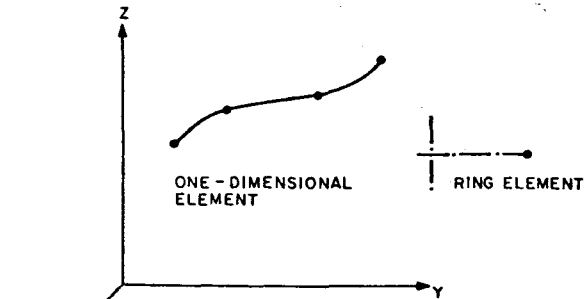
$$LV = R, \tag{6}$$

$$DL^T U = V, \tag{7}$$

where L and D are a lower triangular and a diagonal matrix, respectively [4].

5. The element library

In the current version of program ADINA, general truss, beam, two and three-dimensional isoparametric (or subparametric) elements are available [4,8]. Corresponding to the nonlinearities in the system, four different analysis procedures may be considered for a finite element.



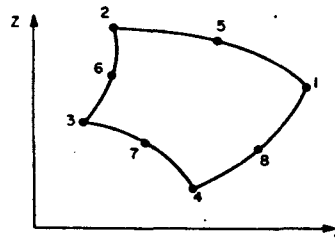
AVAILABLE NONLINEAR FORMULATIONS

- a. LINEAR ANALYSIS
- b. MATERIALLY NONLINEAR ONLY
- c. UPDATED LAGRANGIAN WITH LARGE DISPLACEMENTS BUT SMALL STRAINS

AVAILABLE MATERIAL MODELS

- a. LINEAR ELASTIC
- b. NONLINEAR ELASTIC
- c. THERMO-ELASTIC
- d. ELASTIC-PLASTIC (PERFECTLY-PLASTIC, ISOTROPIC OR KINEMATIC STRAIN HARDENING)
- e. THERMO-ELASTIC-PLASTIC and CREEP

Fig. 8. Truss element.



AVAILABLE NONLINEAR FORMULATIONS

- a. LINEAR ANALYSIS
- b. MATERIALLY NONLINEAR ONLY
- c. UPDATED LAGRANGIAN
- d. TOTAL LAGRANGIAN

AVAILABLE MATERIAL MODELS

- a. ISOTROPIC LINEAR ELASTIC
- b. ORTHOTROPIC LINEAR ELASTIC
- c. ISOTROPIC THERMO-ELASTIC
- d. CURVE DESCRIPTION NONLINEAR MODEL FOR ANALYSIS OF GEOLOGICAL MATERIALS (INCLUDING TENSION CUT-OFF AND TENSION RELEASE) (plane strain and axisymmetric only)
- e. CONCRETE MODEL (INCLUDING CRACKING AND CRUSHING)
- f. ISOTHERMAL PLASTICITY MODELS: VON MISES YIELD CONDITION (ISOTROPIC OR KINEMATIC HARDENING) OR DRUCKER-PRAGER YIELD CONDITION
- g. THERMO-ELASTIC-PLASTIC and CREEP MODELS VON MISES YIELD CONDITION (ISOTROPIC OR KINEMATIC HARDENING)
- h. ISOTROPIC NONLINEAR ELASTIC, INCOMPRESSIBLE (MOONEY-RIVLIN MATERIAL) (plane stress only)

Fig. 9. Two-dimensional plane stress, plane strain and axisymmetric elements.

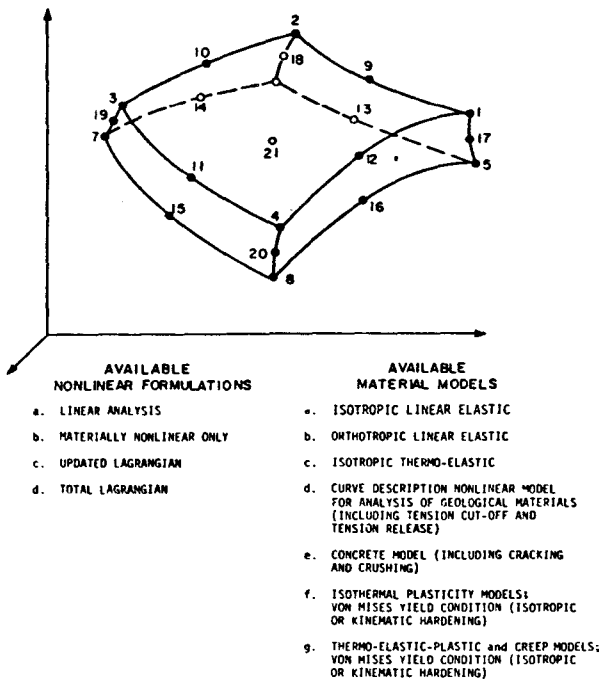


Fig. 10. Three-dimensional solid and thick shell element.

(1) *Linear elastic analysis.* The displacement of the element are assumed to be negligibly small and the strains infinitesimal. The material is isotropic or orthotropic linear elastic.

(2) *Materially nonlinear only analysis.* The displace-

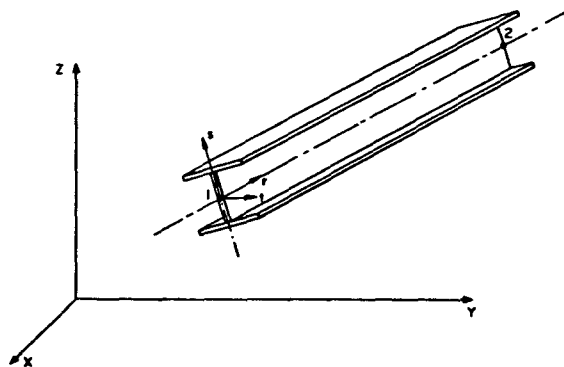


Fig. 11. Three-dimensional beam element.

ments of the element are negligibly small, and the strain are infinitesimal. The material stress-strain description is nonlinear.

(3) *Total lagrangian formulation.* The element may experience large displacements and large strains. The material stress-strain relationship is linear or nonlinear.

(4) *Updated lagrangian formulation.* The element may experience large displacements and large strains. The material stress-strain description is linear or nonlinear.

The linear elastic analysis does not allow for any nonlinearities, whereas the materially nonlinear only analysis includes material nonlinearities, but no geometric nonlinearities [8]. The total lagrangian and updated lagrangian formulations may include all nonlinearities, and which formulation should be employed depends essentially on the definition of the material model used, as described in the next section.

In the following, the finite elements and material models currently available in ADINA are summarized. It should be noted that a particular element group must consist of finite elements of the same type, described by one of the four element formulations above, and must use one material model only. Since all four formulations and all material models have not been implemented for all element types, it is important to identify the nonlinear formulations and material models currently available in ADINA for a specific element type, as illustrated in figs. 8–11.

5.1. Truss element

A variable-number-nodes three-dimensional truss element is available in ADINA. The element is assumed to have constant area, and may be used in linear elastic analysis, materially nonlinear and/or large displacement geometric nonlinear analysis. In the large displacement analysis the updated lagrangian formulation is used. The element can be employed with a linear elastic, nonlinear-elastic, thermoelastic, elastic-plastic, and thermo-elastic-plastic and creep material model [8].

5.2. Plane stress and plane strain element

A variable-number-nodes isoparametric finite element is available for two-dimensional plane stress and plane strain analysis. The element is assumed to lie in the Y–Z global coordinate plane. The element may

have from 4 to 8 nodes, where any one of the nodes 5–8 can be omitted. A 3-node triangular element can be formed by having nodes 3 and 4 coincide. The variable-number-nodes option allows affective modelling from coarse to finer finite element meshes.

The plane stress element can also be employed in the general three-dimensional X – Y – Z space, i.e. the element need not lie in the Y – Z plane, but then it must be a flat element (all nodes must lie in one plane).

The plane stress and plane strain elements can be used in all four formulations. The material models available are summarized in fig. 9.

5.3. Axisymmetric shell or solid element

The variable-number-nodes element described above is also available for axisymmetric two-dimensional analysis of shells or solids (with axisymmetric loading).

5.4. Three-dimensional solid or thick shell element

A general three-dimensional isoparametric element with a variable number of nodes from 8 to 21 can be used. The first 8 nodes are the corner nodes of the element, nodes 9 to 20 correspond to midside nodes and node 21 is a center node. The element can be used for three-dimensional analysis of solids and thick shells. Trapezoidal and wedge elements can be formed by having nodes coincide. As for the two-dimensional elements, the possibility of choosing different element node configurations allows effective finite element modelling.

The three-dimensional element can be used in all four formulations. The material models currently available for the three-dimensional element are summarized in fig. 10.

5.5. Three-dimensional beam element

A three-dimensional beam element is available. The element is assumed to be prismatic and straight. A typical element is shown in fig. 11. The element can be used in linear elastic analysis, and in geometric and/or material nonlinear analysis. In the linear elastic analysis the section properties of the beam element in the local beam axes r , s , t (see fig. 11) are directly input to the program, and therefore beams with arbitrary

section properties can be modelled. On the other hand, in the geometric and material nonlinear analysis only a rectangular or pipe cross-section can be used. In the large displacement analysis the updated Lagrangian formulation is employed assuming small strain conditions.

6. The material models

All material models available in ADINA are discussed in [8], and are only briefly summarized below. In addition to assigning a specific material model to an element, the element can also be used in an 'element birth' or 'element death' option. In the element birth option the element is not active until its time of birth, and in the element death option the element becomes inactive at its time of death. These options are useful in construction/excavation analysis, and are available for all elements.

6.1. Truss element material models

The truss element material behavior can be described by means of five models.

(1) *Linear elastic material.* The material can be linear elastic defined by Young's modulus only.

(2) *Nonlinear elastic material.* The nonlinear elastic material behavior is defined by specifying the stress as a piece-wise linear function of the current strain. Thus, the total stress and the tangent modulus are directly defined in terms of the total strain.

(3) *Thermo-elastic material.* A thermo-elastic material model can be employed in which the Young's modulus and the mean coefficient of thermal expansion vary as a function of temperature.

(4) *Elastic-plastic material.* The nonlinear elastic-plastic material model is defined by means of the initial Young's modulus, the yield stress and the strain hardening modulus. Isotropic or kinematic strain hardening can be assumed.

(5) *Thermo-elastic-plastic-creep model.* A thermo-elastic-plastic and creep model can be employed. This model is an extension of the elastic-plastic model to include creep and thermal strains. The plasticity can be described using linear isotropic or kinematic hardening conditions. The creep strain accumulation in cyclic loading conditions is taken into account using auxiliary strain hardening rules [15,20].

6.2. Two-dimensional element material models

The stress-strain relationship of the two-dimensional elements can be described by various linear and nonlinear material models. In the definition of a material model it may have been assumed that a specific nonlinear formulation is used. The application of the different material models is discussed in [8], where the assumptions used are pointed out. Table 3 summarizes all material models that can be used with the two-dimensional continuum elements and shows the overlays and subroutines employed.

(1) *Isotropic and orthotropic linear elastic material*. The stress-strain relationships are defined by means of the constant Young's moduli and Poisson's ratio. In orthotropic analysis different axes of orthotropy can be used for each element.

(2) *Isotropic thermo-elastic model*. An isotropic thermo-elastic model can be employed in which the Young's modulus, Poisson's ratio and the mean coefficient of thermal expansion vary as a function of temperature.

(3) *Curve description model*. The curve description model is available for the analysis of geological materials. In the model, the instantaneous bulk and shear moduli are defined by piece-wise linear functions of

the current volumetric strain. An explicit yield condition is not used, and whether the material is loading or unloading is defined by the history of the volumetric strain only.

In the analysis of some problems, tensile stresses due to applied loading cannot exceed the in-situ gravity pressure. In such conditions the model can be used to simulate either tension cut-off (yielding) or tensile failure (cracking). In the option of tension cut-off the material assumes reduced stiffness in the direction of a tensile stress which exceeds the gravity pressure in magnitude. In the option of tensile failure, the stiffness is reduced in the same way, but in addition the tensile stress (being equal to the gravity pressure) is released, i.e. a failure surface is formed perpendicular to the direction of the tensile stress that exceeds the gravity in-situ pressure.

(4) *Concrete model*. A model to describe the nonlinear stress-strain relation, stress-induced orthotropy, tensile failure, compression crushing and post-failure behavior of concrete including strain softening is available [8,14].

(5) *Isothermal elastic-plastic material models*. Isothermal elastic-plastic analysis using a plastic potential function can be carried out. The plasticity relations employed are based on the von Mises yield condition

Table 3
two-dimensional material models

Model number	Material	Overlay	Subroutine	Length *
1	isotropic linear elastic	(3, 0)	STSTL	
2	orthotropic linear elastic	(3, 0)	STSTL	
3	isotropic thermo-elastic	(3, 1)	ELT2D3	500
4	curve description	(3, 2)	ELT2D4	3100
5	concrete	(3, 2)	ELT2D4	3100
6	(empty)	(3, 3)	ELT2D6	
7	Drucker-Prager	(3, 4)	ELT2D7	900
8	isothermal elastic-plastic (isotropic hardening)	(3, 5)	ELT2D8	800
9	isothermal elastic-plastic (kinematic hardening)	(3, 5)	ELT2D8	800
10	thermo-elastic-plastic and creep (isotropic hardening)	(3, 6)	EL2D10	2200
11	thermo-elastic-plastic and creep (kinematic hardening)	(3, 6)	EL2D10	2200
12	(empty)	(3, 7)	EL2D12	
13	Mooney-Rivlin	(3, 8)	EL2D13	300
14	user-supplied	(3, 9)	EL2D14	

* Rounded up to nearest hundred.

and the Drucker–Prager yield condition. Both yield criteria to describe material behavior have been employed extensively in practice [21,22]. Using the von Mises yield criterion, linear isotropic hardening or kinematic hardening can be assumed. In analyses using the Drucker–Prager yield condition, the material is assumed to be elastic-perfectly plastic.

(6) *Thermo-elastic-plastic and creep model.* Thermo-elastic-plastic and creep analysis using a plastic potential can be carried out [15]. The material model is an extension of the isothermal elastic-plastic model to include creep and thermal strains. The plasticity can be described using linear isotropic or kinematic hardening conditions. Creep strain accumulation in cyclic loading conditions is taken into account using auxiliary strain hardening rules.

(7) *Mooney–Rivlin material model.* A hyperelastic, incompressible material model is available for the analysis of rubber-like materials [23]. The stress–strain relationship is defined using the Mooney–Rivlin material constants. In ADINA the model can only be used in plane stress analysis.

6.3. Three-dimensional element material models

All two-dimensional material models except for the Mooney–Rivlin and Drucker–Prager material models are also available for the three-dimensional elements.

Table 4 summarizes the material models that can be used with the three-dimensional continuum elements and shows the overlays and subroutines employed.

6.4. Beam element material models

The beam element material behavior can be described by means of two models.

(1) *Linear elastic material.* The material can be linear elastic defined by Young's modulus and Poisson's ratio.

(2) *Elastic-plastic isothermal material.* The material can be elastic-plastic, described using the von Mises yield criterion with linear isotropic hardening or perfectly plastic conditions.

7. Eigensystem solution

The calculation of frequencies and mode shapes is important at various instances. For the estimation of resonance conditions the frequencies of the system must be evaluated. In dynamic analysis it is necessary to select a suitable time step Δt . The time increment must be small enough for solution accuracy, but for a cost effective solution it should not be unnecessarily small. In order to estimate an appropriate time step, it may be necessary to solve for the fundamental fre-

Table 4
Three-dimensional material models

Model number	Material	Overlay	Subroutine	Length *
1	isotropic linear elastic	(4, 0)	STST3L	
2	orthotropic linear elastic	(4, 0)	STST3L	
3	isotropic thermo-elastic	(4, 1)	ELT3D3	400
4	curve description	(4, 2)	ELT3D4	3900
5	concrete	(4, 2)	ELT3D4	3900
6	(empty)	(4, 3)	ELT3D6	
7	(empty)	(4, 4)	ELT3D7	
8	isothermal elastic-plastic (isotropic hardening)	(4, 5)	ELT3D8	700
9	isothermal elastic-plastic (kinematic hardening)	(4, 5)	ELT3D8	700
10	thermo-elastic-plastic and creep (isotropic hardening)	(4, 6)	EL3D10	2300
11	thermo-elastic-plastic and creep (kinematic hardening)	(4, 6)	EL3D10	2300
12	user-supplied	(4, 7)	EL3D12	

* Rounded up to nearest hundred.

quencies of the system [4,12]. For these purposes an eigensolution routine has been incorporated into ADINA.

The algorithm considers the solution of the generalized eigenproblem

$${}^0\mathbf{K}\phi = \omega^2\mathbf{M}\Phi, \quad (8)$$

where ${}^0\mathbf{K}$ is the tangent stiffness matrix at time 0, \mathbf{M} is the mass matrix of the system, and ω and ϕ are a free vibration frequency and mode shape vector, respectively. The mass matrix can be diagonal (lumped mass assumption) or banded (consistent mass assumption), and the stiffness matrix ${}^0\mathbf{K}$ is assumed to be at least positive semidefinite. The complete solution to eq. (8) can be written as

$${}^0\mathbf{K}\Phi = \mathbf{M}\Phi\Omega^2, \quad (9)$$

where Φ is a matrix with its columns equal to the mass-orthonormalized eigenvectors and Ω^2 is a diagonal matrix of the corresponding eigenvalues, i.e.

$$\Phi = [\phi_1\phi_2, \dots, \phi_n]; \quad \Omega^2 = \text{diag}(\omega_i^2). \quad (10)$$

The solution algorithm used in ADINA is the determinant search method presented in [4,13]. Basically, the algorithm combines triangular factorization and vector inverse iteration in an optimum manner to calculate the required eigenvalues and eigenvectors; these are obtained in sequence starting from the least dominant eigenpair (ω_1^2, ϕ_1) , where it may be noted that the lowest eigenvalues may be zero, i.e. the algorithm can also be used to calculate the rigid body modes. An efficient accelerated secant iteration procedure, which operates on the characteristic polynomial

$$p(\omega^2) = \det(\mathbf{K} - \omega^2\mathbf{M}), \quad (11)$$

is used to obtain a shift near the next unknown eigenvalue. The eigenvalue separation theorem (Stur n sequence property) is employed in this iteration. Each determinant evaluation requires a triangular factorization of the matrix $\mathbf{K} - \omega^2\mathbf{M}$. Once a shift near the unknown eigenvalue has been obtained, inverse iteration is used to calculate the eigenvector and the eigenvalue is calculated accurately by adding the Rayleigh quotient correction to the shift value.

The eigensolution can be carried out for in-core and out-of-core systems. However, the determinant search algorithm is most effective for the in-core solution of small-banded systems and it should be realized

that the analysis cost can increase considerably in out-of-core solution because of the necessary low speed storage reading and writing.

8. Analysis restart

In non linear analysis it is frequently the case that the response of a structure has been calculated for some time (load) steps and that on interpretation of the results it is decided to analyze the structure for more time (load) steps. Also, changes in the solution strategy with respect to the time step size, equilibrium iteration and stiffness reformation may be required at an intermediate stage (often after a convergence failure). If either possibility is anticipated, the program can be used to restart at preselected time steps.

9. Data checking, pre- and post-processing

In the analysis of large structural systems it is important to be able to check the data read and generated by the program. For this purpose an option is given in which the program simply reads, generates, and prints all data. It can also be requested that the program read the nodal point and element data from a tape created by a pre-processor. Also, the program can store all input data as well as nodal response and/or element stress outputs on tapes, so that plotting and evaluation of the data and output using post-processors is possible [17].

10. Installation of ADINA on different computers

The computer program ADINA has been written using standard FORTRAN IV, and has been developed to be run directly on IBM, CDC, and UNIVAC equipment. The control cards to generate the overlay structure for these machines, and appropriate single or double precision arithmetic, are in the program in the form of comment cards. Different comment cards must be activated depending on which specific machine is used.

The solution arrays are stored in BLANK COMMON and the total storage required must be less than or equal to MTOT. The variable MTOT, which is initialized

in the main program ADINA, dimensions the blank common storage. Hence, by using a different value for MTOT the size of the program can be reduced or increased. For the individual solution arrays the appropriate high speed storage for single or double precision arithmetic is allocated using the variable ITWO, which is also initialized in the main program ADINA, and set equal to '1' and '2' in single and double precision arithmetic, respectively.

In the implementation of ADINA it need be realized that two of the read/write units used by the program, namely units 2 and 10, are random access devices (see table 2).

Since ADINA can be run directly on IBM, CDC, and UNIVAC machines, it is anticipated that the program can also be installed with relative ease on other equipment.

11. Sample analyses

The program ADINA has been applied to the solution of various types of problems during the program

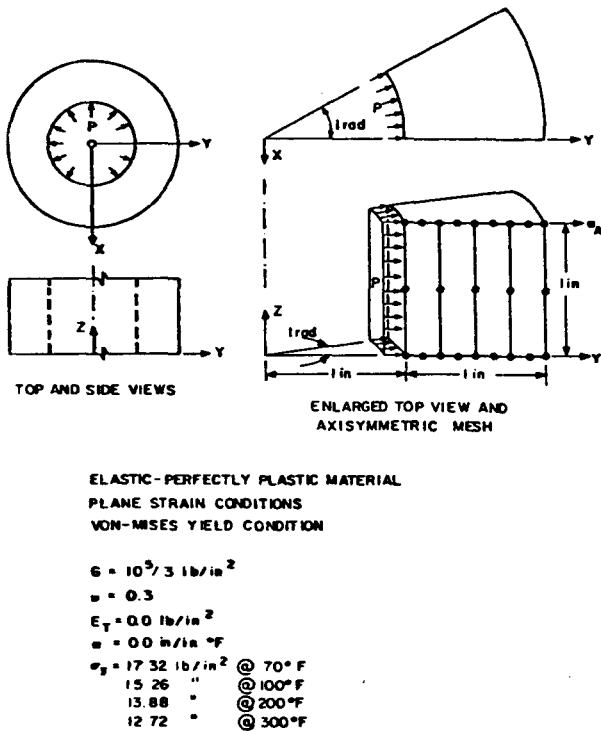


Fig. 12. Finite element mesh of thick-walled cylinder.

developmental and verification phase [5,8], and by the users of the program [17]. In this section we present the analysis results to some problems in order to give some indication of the applicability of the program. In addition to the problem solutions presented here and documented in [5,8,17] the program could, of course, also be employed for the analysis of the problems considered in [6].

11.1. Thermo-elastic-plastic static analysis of a thick-walled cylinder

The thick-walled cylinder shown in fig. 12 was subjected to varying internal pressure and temperature. Plane strain conditions were assumed and the cylinder was modelled using four 8-node axisymmetric elements.

The material of the cylinder was assumed to be elastic-perfectly plastic and obey the von Mises yield condition. Since displacements and strains are small, the analysis was carried out for material nonlinearities only.

In the first analysis the temperature was held constant at 70°C and the pressure was increased to the point of collapse. Fig. 13 shows the radial displacement response of the cylinder as a function of internal pressure and fig. 14 gives the stress distribution through the wall at a given value of pressure. Excellent agreement with the solution by Hodge and White was obtained [24].

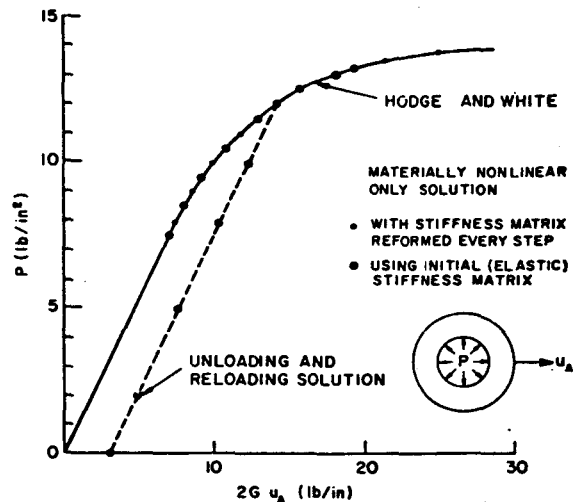


Fig. 13. Elastic-plastic displacement response of thick-walled cylinder.

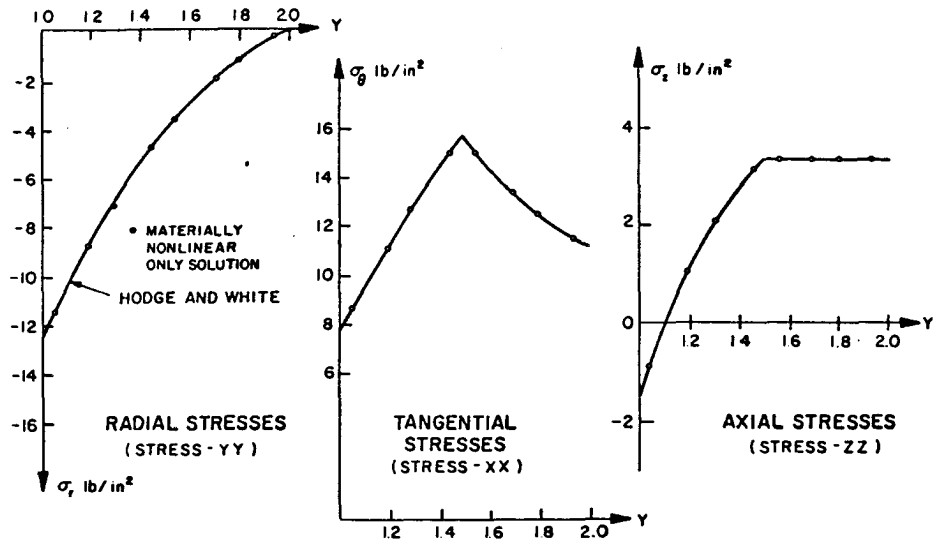


Fig. 14. Elastic-plastic stress distribution through thickness of thick-walled cylinder at $p = 12.5 \text{ lb/in.}^2$.

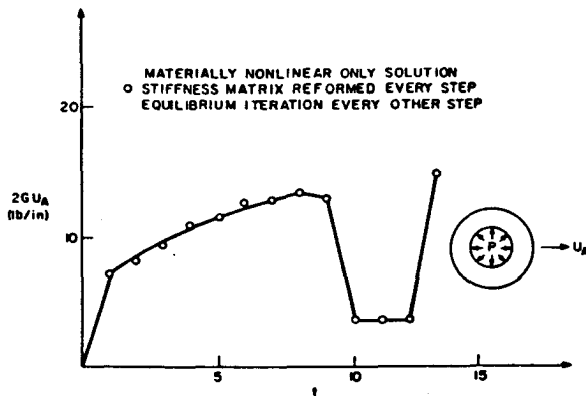
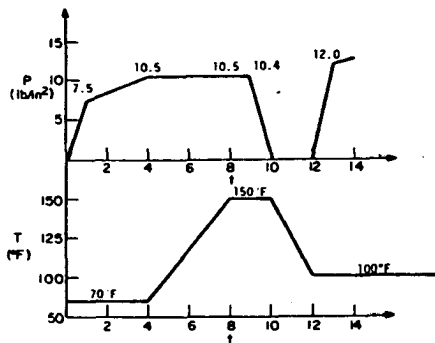


Fig. 15. Load, temperature history, elastic-plastic displacement response of thick-walled cylinder.

In the second analysis both the cylinder pressure and temperature were varied, as shown in fig. 15, where also the radial displacement response is given. Fig. 16 shows the residual stress distribution through the wall at time $t = 10$, i.e. when the pressure was reduced to zero.

11.2. Analysis of two-dimensional wave propagation problem

The wave propagation produced by a suddenly applied strip load to an infinite elastic half space was analyzed. Fig. 17 depicts the finite element idealization employed for the analysis and the loading applied.

Fig. 18 shows the stress response at point A (indicated in fig. 17) calculated using ADINA and an analytical solution [25]. The analysis was performed using lumped and consistent mass approximations and for the time integration the central difference method and Newmark method were used. It is seen that with this finite element mesh and time step selection accurate results have been obtained.

11.3. Large deflection analysis of a simply supported plate

The simply supported plate subjected to a uniformly distributed pressure shown in fig. 19 was analyzed for

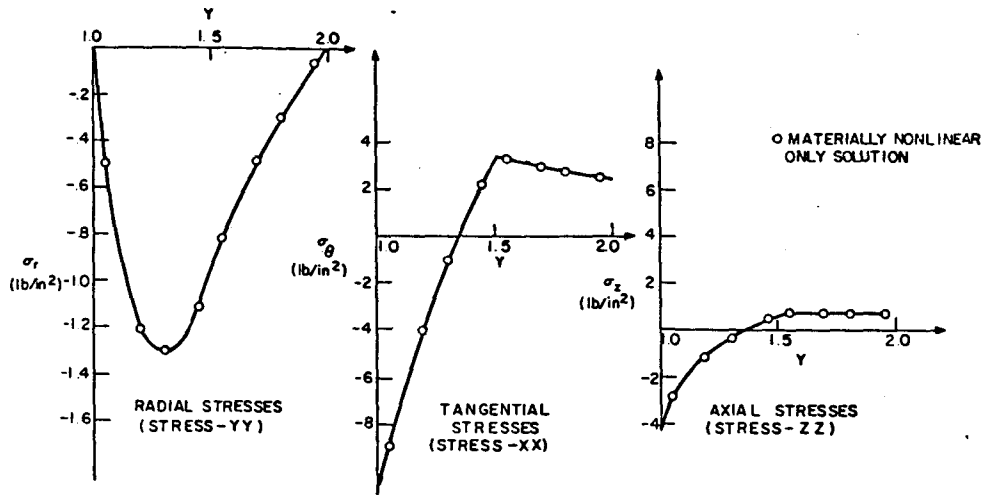


Fig. 16. Residual stress distribution through thickness of thick-walled cylinder.

its large deflection response. Nine 16-node three-dimensional elements were used to model one-quarter of the plate. The element stiffness matrices were calculated using the standard $2 \times 2 \times 2$ Gauss integration [4], and the total lagrangian formulation was employed.

Fig. 19 shows the displacement response predicted by ADINA when 8 steps were used to reach the total applied load. The ADINA results are compared with the response calculated by Levy [26]. In addition, fig. 19 shows the deflections calculated by ADINA

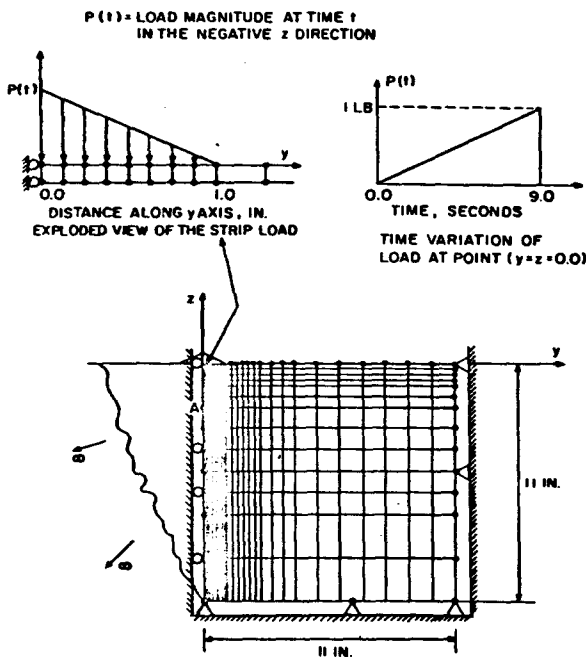


Fig. 17. Finite element idealization of infinite elastic half-space.

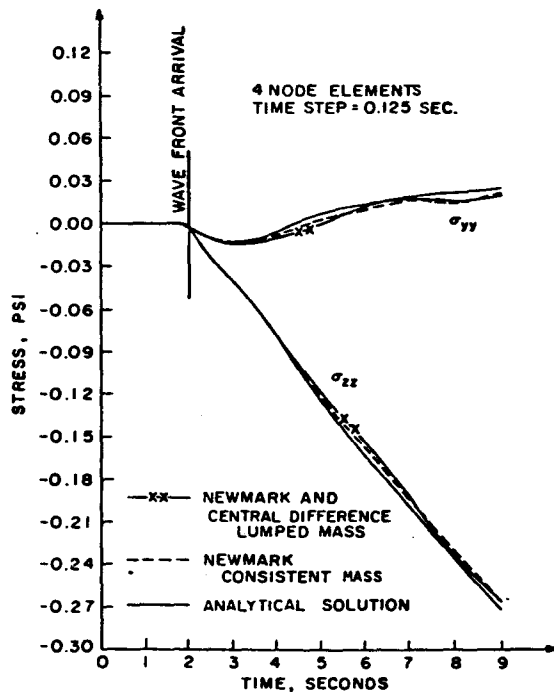


Fig. 18. Stresses at point A ($z = 2.0, y = 0.0$) on center line.

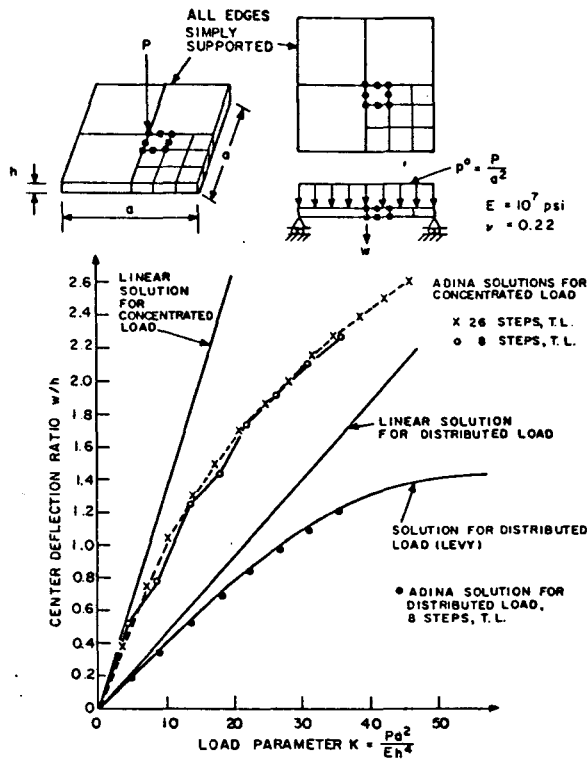


Fig. 19. Center deflection of a simply supported square plate.

when the plate is subjected to a concentrated load at its center. In this case two different load increment sizes were used. It is noted that the deflections predicted in the 8 steps differ by only a small amount from the deflections calculated with 26 increments.

11.4. Static and dynamic analysis of a reinforced concrete beam

The simply supported reinforced concrete beam subjected to two symmetric concentrated loads, as shown in fig. 20, was analyzed using ten 6-node concrete, plane stress elements and ten steel truss elements. The material properties of the concrete were idealized using the concrete model with the parameters given in fig. 20. Materially nonlinear only response was assumed, i.e. large displacement effects were neglected.

The nonlinear static response of the structure with different amounts of reinforcement was analyzed. Fig. 21 gives the calculated transverse displacements at the midspan of the beam, for $A_{st} = 0.62$ and 2.00 in^2 . The

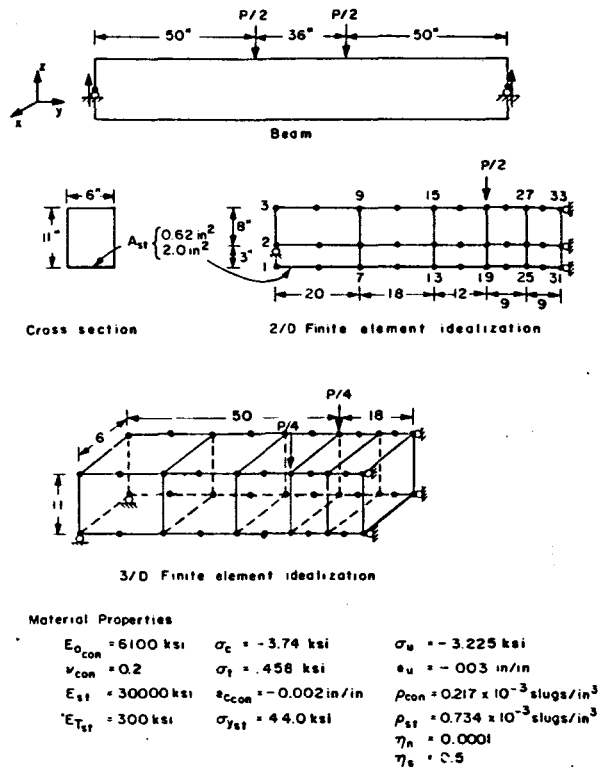


Fig. 20. Analysis of a simply supported reinforced concrete beam.

loading scheme used is also shown in this figure. The results of analysis for $A_{st} = 0.62 \text{ in}^2$ are compared with the response predicted by Suidan and Schnobrich [27] who assumed a linear stress-strain relationship for the concrete, with the constant Young's modulus equal to

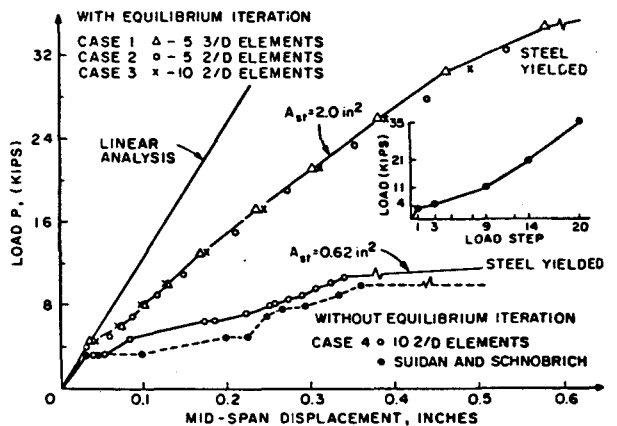


Fig. 21. Load displacement curve for the simply supported beam.

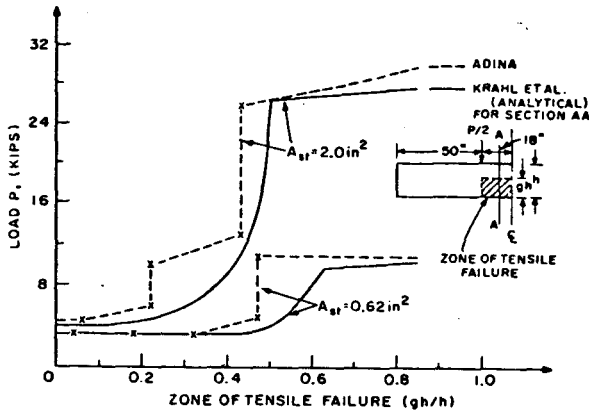


Fig. 22. Zones of tensile failure for the simply supported beam.

E_0 of this analysis, and modeled the steel reinforcement as a smeared stiffness added to the concrete. The depths of tensile failure across the beam thickness at the constant moment section for the two different reinforcements are shown in fig. 22. For comparison the analytical results for the penetration of tensile failure obtained by Krahl et al. [28] are also shown.

The beam was also analyzed for its dynamic response when subjected instantaneously to the concentrated loads. A lumped mass matrix was used in the analysis. The displacement response predicted by ADINA is shown in fig. 23.

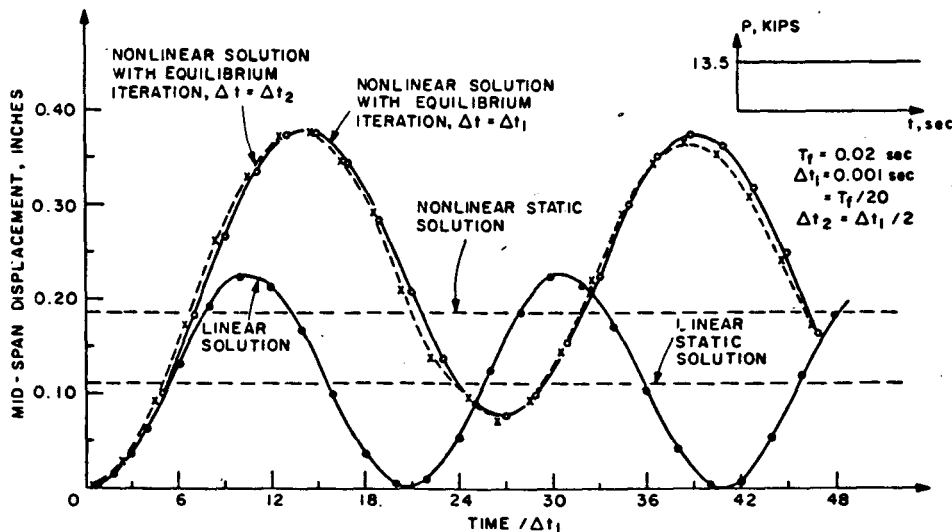


Fig. 23. Nonlinear dynamic response of the simply supported beam, Newmark method, $\delta = 0.50$, $\alpha = 0.25$.

11.5. Analysis of a pipe whip problem

The cantilever pipe shown in fig. 24 was analyzed for its dynamic response. The pipe was subjected to a step loading at its free end and had a stop with a gap. Six beam elements with a pipe section were employed to model the pipe and a nonlinear elastic truss element was used to model the gap element. The structural model and loading represent a pipe whip problem.

In this analysis small displacements and elastic-perfectly plastic material conditions have been assumed. Fig. 24 shows the beam tip deflection as a function of time as predicted by ADINA [16]. The analysis results using the beam model are also compared with the response predicted when six 8-node isoparametric elements are employed to model the pipe [29].

11.6. Ultimate load analysis of a plate with edge crack

The plate containing an edge crack shown in fig. 25 was analyzed for its ultimate load behavior when subjected to uniform displacement boundary conditions. Fig. 26 shows the finite element mesh used in this analysis and the displacement boundary conditions imposed. The material was assumed to be elastic-perfectly plastic, and 2×2 Gauss numerical integration was employed.

In the first analysis all crack tip elements (see fig. 26) were joined at a single crack tip node. The cal-

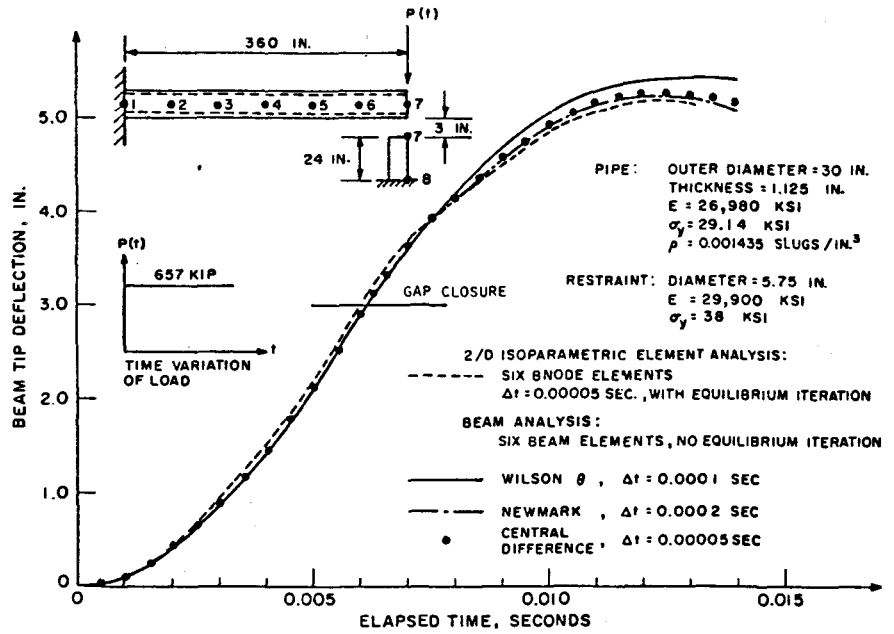


Fig. 24. Predicted displacement response in pipe whip problem.

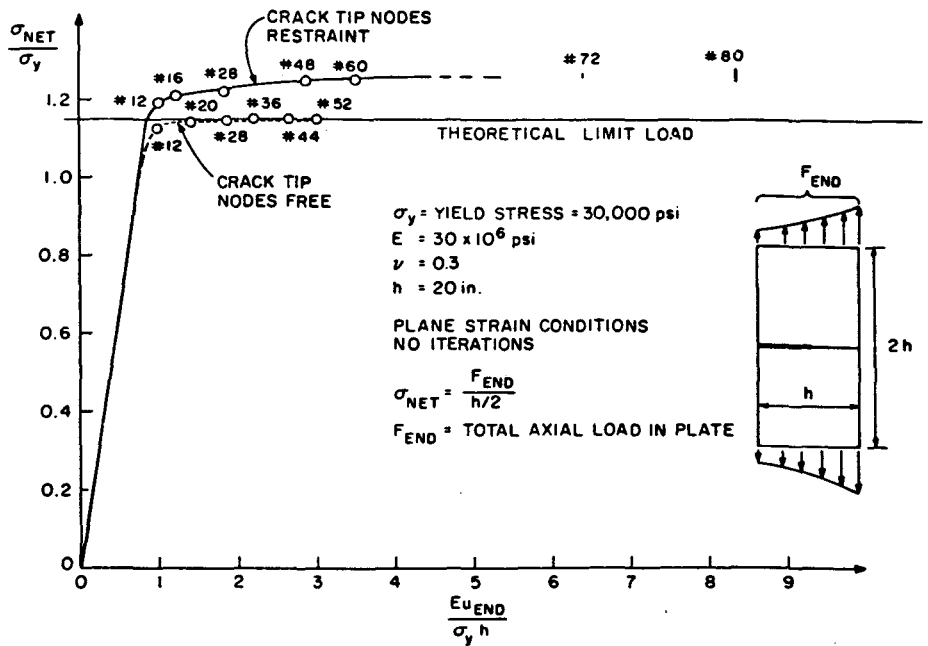


Fig. 25. Load-displacement response of a plate with edge crack.

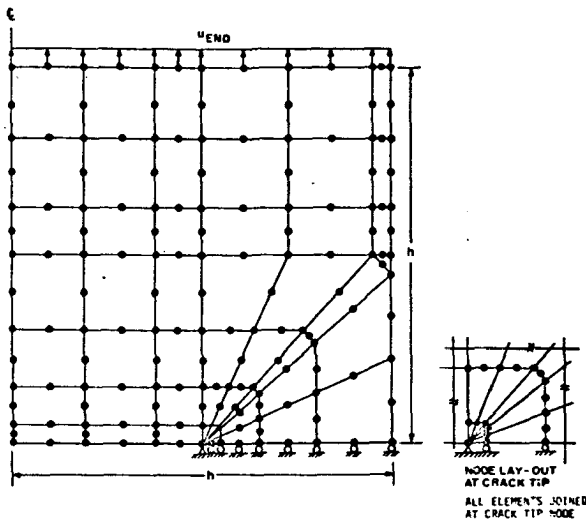
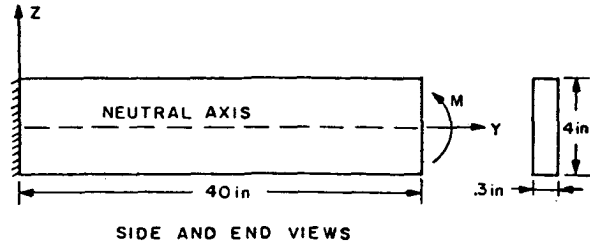
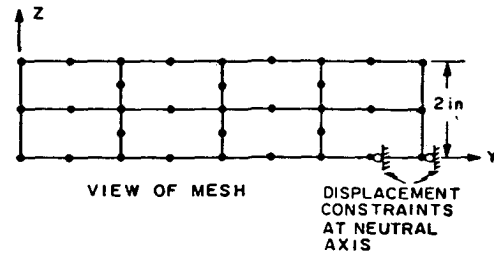


Fig. 26. Finite element mesh used for ultimate load analysis of plate with edge crack.



SIDE AND END VIEWS



VIEW OF MESH

DISPLACEMENT CONSTRAINTS AT NEUTRAL AXIS

PLANE STRESS CONDITIONS TEMPERATURE = 200°F
 $E = 30 \times 10^6$ psi $M = 6000$ in-lb
 $\nu = 0.3$
 $\epsilon_c = 6.4 \times 10^{-18} \sigma^{3.15}$ in/in

Fig. 27. Finite element mesh of cantilever beam.

culated displacement response, as a function of the applied stress, is shown in fig. 25, where the results are also compared with the theoretical limit load [30]. It is seen that although the crack tip was constrained against opening and a relatively coarse finite element mesh was used, the theoretical limit load is predicted with an error of less than 10%.

In the second analysis all element nodal points at

the crack tip were allocated individual degrees of freedom, so that the crack could open. Fig. 25 shows that with this finite element model the theoretical limit load is predicted very accurately.

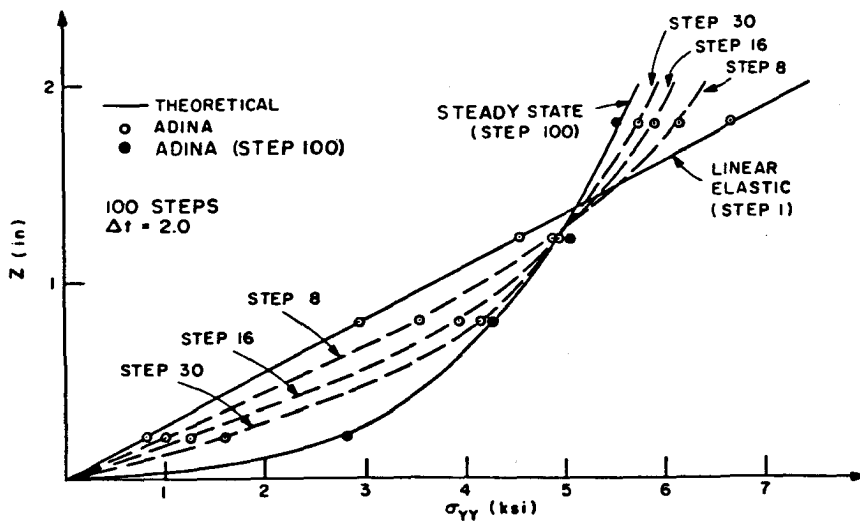


Fig. 28. Transient bending stress distribution in cantilever beam.

11.7. Creep analysis of a cantilever beam

The cantilever beam shown in fig. 27 was subjected to a bending moment applied at the tip. Plane stress conditions were assumed and the beam was modeled using eight plane stress elements. Since displacements and strains are small, the analysis was carried out for material nonlinearities only. By restraining the Y-displacements at the neutral axis only the portion of the beam above the neutral axis was included in the finite element model.

The material of the beam was assumed to obey the uniaxial creep law

$$\dot{\epsilon}_c = 6.4 \times 10^{-18} \sigma^{3.15} t(\text{in./in.}) .$$

Fig. 28 shows the transient bending stress distribution through the beam thickness. The results approach the steady state solution obtained by Penny and Marriott [31].

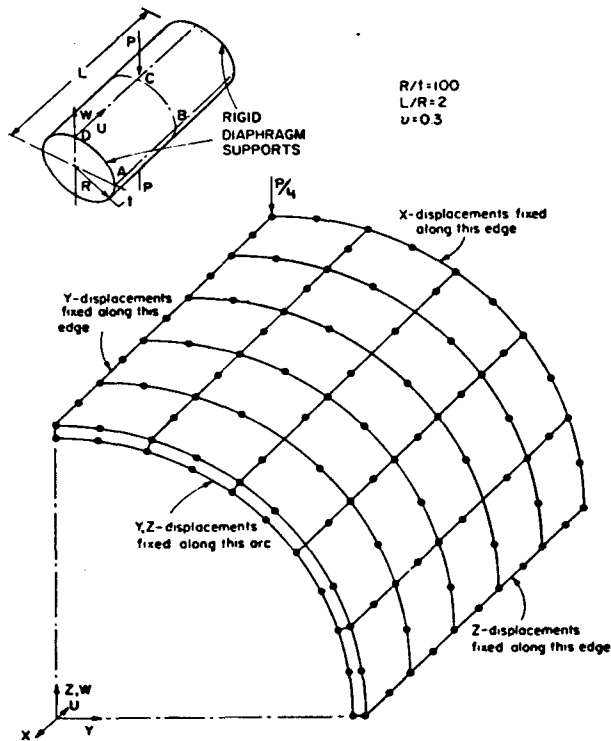


Fig. 29. Finite element mesh of pinched cylindrical shell.

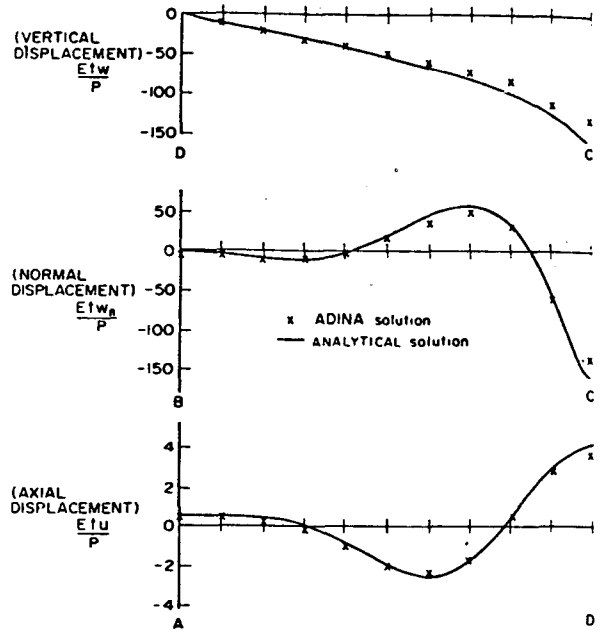


Fig. 30. Load-deflection curve for pinched cylindrical shell.

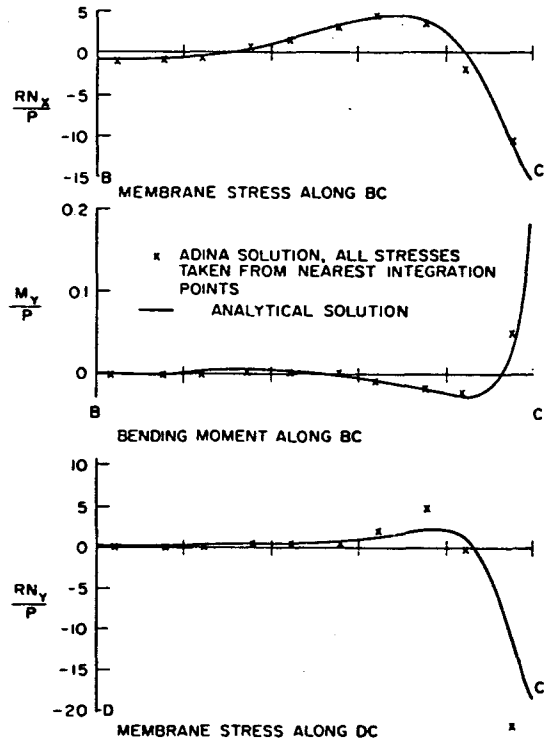


Fig. 31. Membrane stress and bending moment distributions for pinched cylindrical shell.

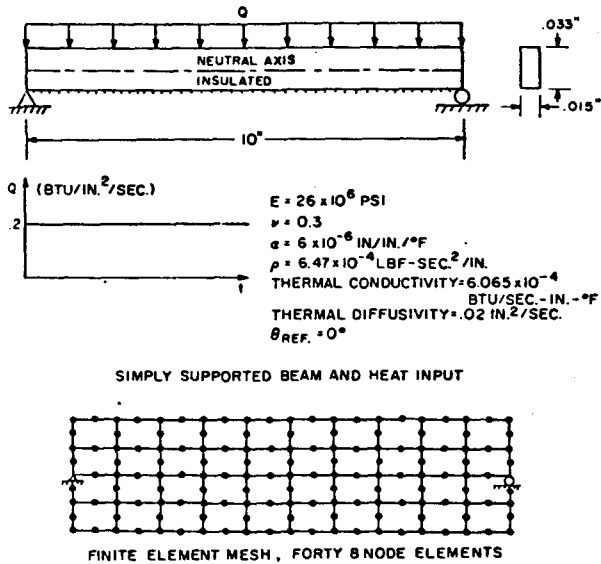


Fig. 32. Dynamic analysis of a simply supported beam, thermal loading.

11.8. Three-dimensional static analysis of a thin shell

The thin cylindrical shell shown in fig. 29 was analyzed for its static response. The cylinder is freely supported at its ends and is loaded by two centrally

located and diametrically opposed concentrated forces. Using the double symmetry of the structure and the loading, only one-eighth of the cylinder was analyzed. The boundary conditions used in the finite element model are shown in fig. 29. Twenty-five 16-node three-dimensional isoparametric elements were used, and for the stiffness matrix calculation two-point Gauss integration both along the shell surface and across its thickness was employed. The ADINA solution for displacements and stresses at various locations on the shell is shown and compared with an analytical solution in figs. 30 and 31 [32].

11.9. Thermally induced vibrations of a simply supported beam

The simply supported rectangular beam shown in fig. 32 was subjected to a step heat input along its top surface. Using the analytical solution for the one-dimensional transient temperature distribution given by Boley and Weiner [33], the dynamic response of the beam was analyzed. No mechanical loads were applied. The beam was modelled using 40, 8-node, plane stress elements. Displacements and strains were considered to be small (i.e. no geometric nonlinearities), and a lumped mass matrix was used.

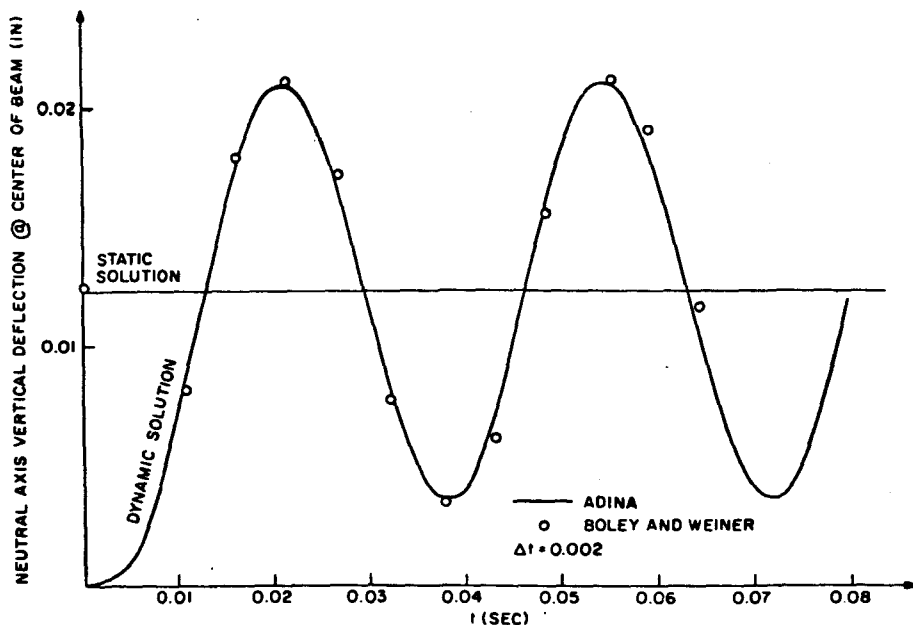


Fig. 33. Dynamic response of a simply supported rectangular beam, thermal loading, Newmark method.

Fig. 33 shows the neutral axis vertical deflection at the center of the beam. It is interesting to note that the dynamic solution oscillates about the static solution. The static solution was obtained by considering the same heat input, but neglecting the effect of inertia. Excellent agreement in both cases was obtained with the beam theory solution of Boley and Weiner [33].

11.10. Large displacement analysis of cantilever beam

The large displacement elastic response of a cantilever beam subjected to a linearly increasing concentrated end moment was predicted using beam elements to model the beam. Fig. 34 shows the cantilever beam and the calculated response using ADINA. The predicted displacement response is compared with an analytical solution [34], and it is seen that up to a rotation of about $\phi = 90^\circ$ the analysis results are close to the analytical solution.

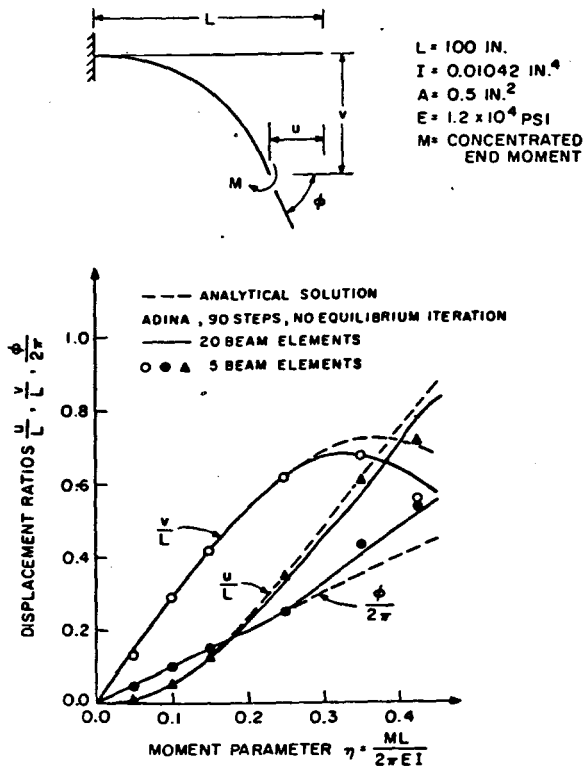


Fig. 34. Moment-deflection curve.

12. Conclusions

The development of general computational capabilities for linear and nonlinear analysis is an exciting and formidable challenge, because research and development is required in a number of interrelated areas. The proper formulation of the linear or nonlinear problem and its idealization to a representative finite element system represents one area of activity. The development of increasingly more effective procedures for the solution of the equilibrium equations in space and time requires additional research. The stable and efficient implementation of the formulations and solution procedures on the computer is the last phase of the development and constitutes another important requirement.

Our objective in this paper was to present the current capabilities of the computer program ADINA, and thus summarize our recent developments in computational capabilities for linear and nonlinear analysis of structures and continua. The program can be employed effectively for the analysis of a number of problems. However, considering the complete area of desired nonlinear analysis of structures and continua, in general only limited computational capabilities are available at present [17,35]; in some cases the solutions are still prohibitively expensive, and in other cases an analysis is simply not possible as yet. To enhance the use of nonlinear analysis, improved formulations, numerical methods and computing techniques need be developed. However, it must also be recognized that the effective use of the techniques available in the computer program is a difficult task, and must be supported through education and extensive interaction between the program users and developers.

Acknowledgement

The work reported in this paper has been financed by the ADINA users group. We gratefully acknowledge this support.

References

[1] Proceedings of the 1st, 2nd, 3rd and 4th SMiRT Conferences, Berlin 1971, Berlin 1973, London 1975, San Francisco 1977.

- [2] O.C. Zienkiewicz, *The Finite Element Method in Engineering Science* (McGraw-Hill, London, 1971).
- [3] R.H. Gallagher, *Finite Element Analysis Fundamentals* (Prentice-Hall Inc., Englewood Cliffs, New Jersey, 1975).
- [4] K.J. Bathe and E.L. Wilson, *Numerical Methods in Finite Element Analysis* (Prentice-Hall Inc., Englewood Cliffs, New Jersey, 1976).
- [5] K.J. Bathe, AVL Report 82448-1, Department of Mechanical Engineering, MIT Sept. (1975) (revised may 1977).
- [6] K.J. Bathe and E.L. Wilson, *Nucl. Eng. Des.* 29 (1974) 266.
- [7] K.J. Bathe, E.L. Wilson and F.E. Peterson, Report EERC 73-11, College of Engineering, University of California, Berkeley, June (1973) (revised April 1974).
- [8] K.J. Bathe, AVL Report 82448-2, Department of Mechanical Engineering, MIT, May (1976) (revised May 1977).
- [9] K.J. Bathe, E. Ramm and E.L. Wilson, *Int. J. Numer. Methods Eng.* 9 (1975) 373.
- [10] K.J. Bathe, Proceedings SYNSPADE III, University of Maryland, May 1975 (Academic Press, 1976).
- [11] K.J. Bathe and H. Ozdemir, *J. Comput. Struct.* 7 (1976) 81.
- [12] K.J. Bathe and E.L. Wilson, *Int. J. Earthquake Eng. Struct. Dyn.* 1 (1973) 283.
- [13] K.J. Bathe and E.L. Wilson, *Int. J. Numer. Methods Eng.* 6 (1973) 213.
- [14] K.J. Bathe, and S. Ramaswamy, *Int. J. Numer. Anal. Methods Geomech.*, to appear.
- [15] M.D. Snyder and K.J. Bathe, AVL Report 82448-3, Department of Mechanical Engineering, MIT, June (1977).
- [16] S. Bolourchi and K.J. Bathe, AVL Report 82448-4, Department of Mechanical Engineering, MIT, Aug. (1977).
- [17] K.J. Bathe (ed), AVL Report 82448-6, Department of Mechanical Engineering, MIT, Aug. (1977).
- [18] K.J. Bathe, AVL Report 82448-5, Department of Mechanical Engineering, MIT, May (1977).
- [19] K.J. Bathe and M.R. Khoshgoftaar, Analysis of nonlinear heat transfer and field problems (in preparation).
- [20] C.E. Pugh, J.M. Corum, K.C. Liu and W.L. Greenstreet, Report No. TM 3602, Oak Ridge National Laboratory, Oak Ridge, Tennessee (1972).
- [21] S.F. Reyes and D.U. Deere, Proceedings, First Congress, International Society of Rock Mechanics, Lisbon, 1966.
- [22] G.C. Nayak and O.C. Zienkiewicz, *Int. J. Numer. Methods Eng.* 5 (1972) 113.
- [23] J.T. Oden, *Finite Elements of Nonlinear Continua* (McGraw-Hill, New York, 1972).
- [24] P.E. Hodge and S.H. White, *J. Appl. Mech.* 17 (1950) 180.
- [25] J.D. Achenbach, *Wave Propagation in Elastic Solids* (North-Holland, Amsterdam, 1975).
- [26] S. Levy, Technical Notes, National Advisory Committee for Aeronautics, no. 846 (1942).
- [27] M. Suidan and W. Schnobrich, ASCE, *J. Struct. Div.* 99 (ST10), Oct. (1973) 2109.
- [28] N.W. Krahl, N. Khachaturian and C.P. Seiss, ASCE, *J. Struct. Div.*, Feb. (1967) 235.
- [29] S.M. Ma and K.J. Bathe, *Nucl. Eng. Des.* 37 (1976) 413.
- [30] F.A. McClintock and A.S. Argon, *Mechanical Behavior of Materials* (Addison-Wesley, 1976).
- [31] R.K. Penny and D.L. Marriott, *Design for Creep* (McGraw-Hill, New York, 1971).
- [32] G.H. Lindberg, M.D. Olson and E.R. Cowper, *Quart. Bull. Div. Mech. Eng., Nat. Aeronaut. Establ.* 4 (1969) 1.
- [33] B.A. Boley and J.H. Weiner, *Theory of Thermal Stresses* (John Wiley and Sons, 1960).
- [34] J.T. Holden, *Int. J. Solias Struct.* 8 (1972) 1051.
- [35] K.J. Bathe, J.T. Oden and W. Wunderlich (eds), *Formulations and Computational Algorithms in Finite Element Analysis* (MIT Press, 1977).

PART III Solution of Finite Element Equations in Nonlinear
Dynamic Analysis

Stability and Accuracy Analysis of Direct Integration Methods

On Effective Implicit Time Integration in Analysis of Fluid-
Structure Problems

On Nonlinear Dynamic Analysis Using Substructuring and Mode
Superposition

Some Practical Procedures for the Solution of Nonlinear Finite
Element Equations

STABILITY AND ACCURACY ANALYSIS OF DIRECT INTEGRATION METHODS

K. J. BATHE* AND E. L. WILSON†

Department of Civil Engineering, University of California, Berkeley, U.S.A.

SUMMARY

A systematic procedure is presented for the stability and accuracy analysis of direct integration methods in structural dynamics. Amplitude decay and period elongation are used as the basic parameters in order to compare various integration methods. The specific methods studied are the Newmark generalized acceleration scheme, the Houbolt method and the Wilson θ -method. The advantages of each of these methods are discussed. In addition, it is shown how the direct integration of the equations of motion is related to the mode superposition analysis.

INTRODUCTION

Many integration methods are currently used for the direct integration of the equations of motion of lumped parameter structural systems.¹⁻⁵ Some investigators have concluded that a particular method is superior for a certain type of problem. However, a procedure is lacking which can be used to compare the merits of these methods in practical application for complex structural systems.

The stability of time integration methods can be proven by invoking one of the established theorems.^{6,7} Also, various methods have been compared by studying a single degree-of-freedom system.⁷ However, since accuracy is not required in all modes of a complex structure this is not an adequate basis for comparison. In fact, the participation of all modes in the solution is not desirable in most dynamic problems.

The objective of this paper is to present a systematic and fundamental procedure for the stability and accuracy analysis of direct integration schemes and to apply the technique to the Newmark, the Houbolt and the Wilson θ -method. The θ -method is optimized with respect to stability and accuracy. The integration methods are compared and the relationship between integration and mode superposition analysis is discussed. Based on the results of the analysis, guidelines can be established to select an appropriate time step for a given problem.

Further research is required to develop better integration operators for linear and, in particular, non-linear problems. The direct procedure of stability and accuracy analysis presented in this paper can be very effective in this research. However, it should be recognized that the efficiency of an integration algorithm also depends on other factors—for example, the number of numerical operations required for solution—which are not discussed here.

PROBLEM DEFINITION

In the dynamic response analysis of an n -degree of freedom structural system we are concerned with the solution of the equation

$$\mathbf{M}\ddot{\mathbf{u}} + \mathbf{C}\dot{\mathbf{u}} + \mathbf{K}\mathbf{u} = \mathbf{R} \quad (1)$$

where \mathbf{M} , \mathbf{C} and \mathbf{K} are the mass, stiffness and damping matrices, all of order n ; the vectors \mathbf{u} and \mathbf{R} store the displacements and forces, respectively, and a dot denotes a time derivative.⁸ This equation arises, in particular, in the finite element analysis of continuous systems.⁹ In this paper we assume that the system is linear, in which case the elements in \mathbf{M} , \mathbf{C} and \mathbf{K} are constant.

* Assistant Research Engineer.

† Associate Professor.

Received 20 April 1972

Mode superposition analysis

If the damping is assumed to be of a restricted form,¹⁰ the quadratic eigenvalue problem is avoided and the solution to equation (1) can be obtained by conventional mode superposition. In this analysis we consider first free vibration conditions with damping neglected

$$\mathbf{M}\ddot{\mathbf{u}} + \mathbf{K}\mathbf{u} = 0 \quad (2)$$

Substituting $\mathbf{u} = \boldsymbol{\phi} \sin \omega t$, we obtain the generalized eigenvalue problem

$$\mathbf{K}\boldsymbol{\phi} = \omega^2 \mathbf{M}\boldsymbol{\phi} \quad (3)$$

The n solutions of equation (3) can be written as

$$\mathbf{K}\boldsymbol{\Phi} = \mathbf{M}\boldsymbol{\Phi}\boldsymbol{\Omega}^2 \quad (4)$$

where the columns in $\boldsymbol{\Phi}$ are the M -orthonormalized eigenvectors (free vibration modes) $\boldsymbol{\phi}_1 \dots \boldsymbol{\phi}_n$ and $\boldsymbol{\Omega}^2$ is a diagonal matrix listing the eigenvalues (free vibration frequencies squared) $\omega_1^2 \dots \omega_n^2$.

The next step is to write the equations of dynamic equilibrium in the basis of eigenvectors; using $\mathbf{u} = \boldsymbol{\Phi}\mathbf{X}$ we obtain

$$\ddot{\mathbf{X}} + \boldsymbol{\Delta}\dot{\mathbf{X}} + \boldsymbol{\Omega}^2\mathbf{X} = \boldsymbol{\Phi}^T \mathbf{R} \quad (5)$$

where $\boldsymbol{\Delta} = \text{diag}(2\omega_i \xi_i)$ and ξ_i is the damping ratio in the i 'th mode of vibration. Equation (5) consists of n uncoupled equations which can be solved 'exactly' using the Duhamel integral. Alternatively we may use numerical integration. Because the periods of vibration T_i , $i = 1, \dots, n$, where $T_i = 2\pi/\omega_i$, are known we can choose in the step-by-step integration of each equation a time step Δt which assures a required level of accuracy.

The most time consuming phase of the analysis is the solution of the eigenvalue problem. If the order of the matrices is large, the computer time required to solve all eigenvalues and vectors can be enormous. However, it may be sufficiently accurate to include in the analysis only the lowest eigenvalues and associated vectors because the higher modes do not participate in the response. Also, in comparison to the continuous problem the highest modes of the discrete element system should be expected to be in error, so that there may be little justification to include them in the analysis.

Direct step-by-step integration

An alternative procedure to obtain the solution to equation (1) is by direct integration.⁸ In this case the step-by-step integration is performed directly on equation (1) without first representing the equilibrium relations in the basis of eigenvectors. Whereas in the solution of the uncoupled equations a different time step can be chosen for each equation to insure integration accuracy, in the direct integration one time step is used and the response in all modes is integrated simultaneously. This is equivalent to choosing a common time step Δt in the integration of all n uncoupled equations. Accuracy in this integration can be obtained only in the evaluation of those response components for which Δt is a small fraction of the period. The other modal response components will not be evaluated accurately, but the errors will be unimportant if the amplitudes are small; however, we need integration stability for all modes. This means that the initial conditions for the equations with a large value $\Delta t/T_i$ must not be amplified artificially and thus make the accurate integration of the response in the lower modes worthless. Stability also means that any errors in the displacements, velocities and accelerations at time t which may be due to round-off do not grow in the integration. Naturally, stability is assured if the time step is small enough to integrate accurately the response in the highest frequency component. But this may require a very small timestep and, as has been pointed out, the accurate integration of this response is usually not necessary.

DIRECT INTEGRATION SCHEMES

Because the direct integration of equation (1) is equivalent to the integration of equation (5) with a common time step Δt , we only need to study the integration of a typical row in equation (5), which may be written

as

$$\ddot{x} + 2\xi\omega\dot{x} + \omega^2 x = r \tag{6}$$

This is the equation governing motion of a single degree of freedom system with free vibration period T , damping ratio ξ and applied load r .

In the step-by-step solutions considered here an approximation operator and a load operator are used which relate explicitly the unknown required variables at time $t + \Delta t$ to previously calculated quantities.

The Wilson θ -method

Let the acceleration, velocity and displacement at time t , i.e. \ddot{x}_t , \dot{x}_t and x_t , where the subscript denotes time t , be known quantities. For solution of $\ddot{x}_{t+\Delta t}$, $\dot{x}_{t+\Delta t}$ and $x_{t+\Delta t}$ we assume that the acceleration varies linearly during the time interval $\theta\Delta t$, where $\theta \geq 1$. The parameter θ shall be chosen to obtain accuracy and stability in the integration. When $\theta = 1$ we have the linear acceleration method which is known to be only conditionally stable. In Wilson's averaging method θ equals 2 and the integration is unconditionally stable. However, without losing unconditional stability, θ can be selected to obtain a scheme which has less integration error.

Let τ denote the increase in time, where $0 \leq \tau \leq \theta\Delta t$, then for the time interval t to $t + \theta\Delta t$ we have

$$\ddot{x}_{t+\tau} = \ddot{x}_t + (\ddot{x}_{t+\Delta t} - \ddot{x}_t) \frac{\tau}{\Delta t} \tag{7}$$

$$\dot{x}_{t+\tau} = \dot{x}_t + \ddot{x}_t \tau + (\ddot{x}_{t+\Delta t} - \ddot{x}_t) \frac{\tau^2}{2\Delta t} \tag{8}$$

$$x_{t+\tau} = x_t + \dot{x}_t \tau + \frac{1}{2} \ddot{x}_t \tau^2 + (\ddot{x}_{t+\Delta t} - \ddot{x}_t) \frac{\tau^3}{6\Delta t} \tag{9}$$

At time $t + \Delta t$ we have

$$\dot{x}_{t+\Delta t} = \dot{x}_t + (\ddot{x}_{t+\Delta t} + \ddot{x}_t) \frac{\Delta t}{2} \tag{10}$$

$$x_{t+\Delta t} = x_t + \dot{x}_t \Delta t + (2\ddot{x}_t + \ddot{x}_{t+\Delta t}) \frac{\Delta t^2}{6} \tag{11}$$

Equation (6) shall be satisfied at time $t + \theta\Delta t$, which gives

$$\ddot{x}_{t+\theta\Delta t} + 2\xi\omega\dot{x}_{t+\theta\Delta t} + \omega^2 x_{t+\theta\Delta t} = r_{t+\theta\Delta t} \tag{12}$$

Using equations (7)–(9) at time $\tau = \theta\Delta t$ to substitute into equation (12) an equation is obtained with $\ddot{x}_{t+\Delta t}$ as the only unknown. Solving for $\ddot{x}_{t+\Delta t}$ and substituting into equations (10) and (11) the following relationship is established

$$\begin{bmatrix} \ddot{x}_{t+\Delta t} \\ \dot{x}_{t+\Delta t} \\ x_{t+\Delta t} \end{bmatrix} = \mathbf{A} \begin{bmatrix} \ddot{x}_t \\ \dot{x}_t \\ x_t \end{bmatrix} + \mathbf{L}r_{t+\theta\Delta t} \tag{13}$$

where \mathbf{A} is the approximation operator and \mathbf{L} is the load operator; both are given in Table I. This recurrence relation can be used to study the stability and accuracy of the integration scheme, where we note that the solution at time $t + n\Delta t$ with n an integer is given by

$$\begin{bmatrix} \ddot{x}_{t+n\Delta t} \\ \dot{x}_{t+n\Delta t} \\ x_{t+n\Delta t} \end{bmatrix} = \mathbf{A}^n \begin{bmatrix} \ddot{x}_t \\ \dot{x}_t \\ x_t \end{bmatrix} + \mathbf{A}^{n-1} \mathbf{L}r_{t+\Delta t+(\theta-1)\Delta t} + \dots + \mathbf{L}r_{t+n\Delta t+(\theta-1)\Delta t} \tag{14}$$

Table I. Approximation and load operator of the Wilson method

$$A = \begin{bmatrix} \left(1 - \frac{\beta\theta^2}{3} - \frac{1}{\theta} - \kappa\theta\right) & \frac{1}{\Delta t}(-\beta\theta - 2\kappa) & \frac{1}{\Delta t^2}(-\beta) \\ \Delta t\left(1 - \frac{1}{2\theta} - \frac{\beta\theta^2}{6} - \frac{\kappa\theta}{2}\right) & \left(1 - \frac{\beta\theta}{2} - \kappa\right) & \frac{1}{\Delta t}\left(\frac{-\beta}{2}\right) \\ \Delta t^2\left(\frac{1}{2} - \frac{1}{6\theta} - \frac{\beta\theta^2}{18} - \frac{\kappa\theta}{6}\right) & \Delta t\left(1 - \frac{\beta\theta}{6} - \frac{\kappa}{3}\right) & \left(1 - \frac{\beta}{6}\right) \end{bmatrix}; \quad L = \begin{bmatrix} \frac{\beta}{\omega^2 \Delta t^2} \\ \frac{\beta}{2\omega^2 \Delta t} \\ \frac{\beta}{6\omega^2} \end{bmatrix}$$

where

$$\beta = \left(\frac{\theta}{\omega^2 \Delta t^2} + \frac{\xi\theta^2}{\omega\Delta t} + \frac{\theta^3}{6}\right)^{-1}; \quad \kappa = \frac{\xi\beta}{\omega\Delta t}$$

The Newmark generalized acceleration method

In this integration scheme it is assumed that

$$\dot{x}_{t+\Delta t} = \dot{x}_t + [(1 - \delta)\dot{x}_t + \delta\ddot{x}_{t+\Delta t}]\Delta t \tag{15}$$

and

$$x_{t+\Delta t} = x_t + \dot{x}_t\Delta t + \left[\left(\frac{1}{2} - \alpha\right)\ddot{x}_t + \alpha\ddot{x}_{t+\Delta t}\right]\Delta t^2 \tag{16}$$

The parameters δ and α can be chosen to obtain integration stability and accuracy. When $\delta = \frac{1}{2}$ and $\alpha = \frac{1}{4}$ we have the equations of the linear acceleration method. Newmark proposed as an unconditionally stable scheme the constant average acceleration method, in which case $\delta = \frac{1}{2}$ and $\alpha = \frac{1}{4}$.

Table II gives the approximation operator and the load operator of the Newmark method, which are obtained using equations (15) and (16) together with equation (12) when $\theta = 1$. Note the close relationship between this approximation operator and the operator of Wilson's method.

Table II. Approximation and load operator of the Newmark method

$$A = \begin{bmatrix} \left[-\left(\frac{1}{2} - \alpha\right)\beta - 2(1 - \delta)\kappa\right] & \frac{1}{\Delta t}(-\beta - 2\kappa) & \frac{1}{\Delta t^2}(-\beta) \\ \Delta t\left[1 - \delta - \left(\frac{1}{2} - \alpha\right)\delta\beta - 2(1 - \delta)\delta\kappa\right] & (1 - \beta\delta - 2\delta\kappa) & \frac{1}{\Delta t}(-\beta\delta) \\ \Delta t^2\left[\frac{1}{2} - \alpha - \left(\frac{1}{2} - \alpha\right)\alpha\beta - 2(1 - \delta)\alpha\kappa\right] & \Delta t(1 - \alpha\beta - 2\alpha\kappa) & (1 - \alpha\beta) \end{bmatrix}; \quad L = \begin{bmatrix} \frac{\beta}{\omega^2 \Delta t^2} \\ \frac{\beta\delta}{\omega^2 \Delta t} \\ \frac{\alpha\beta}{\omega^2} \end{bmatrix}$$

where

$$\beta = \left(\frac{1}{\omega^2 \Delta t^2} + \frac{2\xi\delta}{\omega\Delta t} + \alpha\right)^{-1}; \quad \kappa = \frac{\xi\beta}{\omega\Delta t}$$

The Houbolt method

In the Houbolt integration scheme two backward difference formulae are used for the acceleration and velocity at time $t + \Delta t$, namely

$$\ddot{x}_{t+\Delta t} = \frac{1}{\Delta t^2}(2x_{t+\Delta t} - 5x_t + 4x_{t-\Delta t} - x_{t-2\Delta t}) \tag{17}$$

$$\dot{x}_{t+\Delta t} = \frac{1}{6\Delta t}(11x_{t+\Delta t} - 18x_t + 9x_{t-\Delta t} - 2x_{t-2\Delta t}) \tag{18}$$

Substituting equations (17) and (18) into equation (12) when $\theta = 1$, we can establish the relation

$$\begin{bmatrix} x_{t+\Delta t} \\ x_t \\ x_{t-\Delta t} \end{bmatrix} = A \begin{bmatrix} x_t \\ x_{t-\Delta t} \\ x_{t-2\Delta t} \end{bmatrix} + Lr_{t+\Delta t} \tag{19}$$

where A and L are given in Table III.

To calculate the displacements and velocities at times between the discrete time points, we may use in the Wilson method equations (8) and (9) and in the Newmark method equations (15) and (16) with Δt being

Table III. Approximation and load operator of the Houbolt method

$$A = \begin{bmatrix} \left(\frac{5\beta}{\omega^2 \Delta t^2} + 6\kappa\right) & -\left(\frac{4\beta}{\omega^2 \Delta t^2} + 3\kappa\right) & \left(\frac{\beta}{\omega^2 \Delta t^2} + \frac{2\kappa}{3}\right) \\ 1 & 0 & 0 \\ 0 & 1 & 0 \end{bmatrix}; \quad L = \begin{bmatrix} \frac{\beta}{\omega^2} \\ 0 \\ 0 \end{bmatrix}$$

where

$$\beta = \left(\frac{2}{\omega^2 \Delta t^2} + \frac{11\xi}{3\omega \Delta t} + 1\right)^{-1}; \quad \kappa = \frac{\xi\beta}{\omega \Delta t}$$

replaced by the increment in time τ , i.e. $0 \leq \tau \leq \Delta t$. In the Houbolt method an interpolating polynomial of order three which fits the displacements at the four discrete time points in equation (19) was used.

STABILITY

Consider equation (14) with r equal to zero. An integration method is unconditionally stable if the solution for any initial conditions does not grow without bound for any time step Δt , in particular when $\Delta t/T$ is large. We should note then, that any error in the displacements, velocities and accelerations at time t , for example due to round-off in the computer, does not grow. The method is only conditionally stable if the same only holds provided $\Delta t/T$ is smaller than a certain number. In discrete element analysis of continuous systems we may have very high (infinite) frequencies,¹¹ and an unconditionally stable scheme is needed.

To investigate the stability of a method we realize that $A = P^{-1}JP$ and therefore in equation (14)

$$A^n = P^{-1}J^n P \tag{20}$$

where P is the matrix of eigenvectors and J is the Jordan form of A with the eigenvalues λ_i of A on its diagonal.¹² Let $\rho(A)$ be the spectral radius of A , defined as

$$\rho(A) = \max |\lambda_i|, \quad i = 1, 2, 3 \tag{21}$$

then J^n is bounded for $n \rightarrow \infty$ if and only if $\rho(A) \leq 1$. This is the stability criterion. Furthermore, $J^n \rightarrow 0$ if $\rho(A) < 1$ and the smaller $\rho(A)$ the more rapid is the convergence.

Before the eigenvalues of A are calculated it can be convenient to apply a similarity transformation $D^{-1}AD$, where D is a diagonal matrix with $d_{ii} = \Delta t^i$. As we would expect the spectral radii of the approximation operators therefore depend on $\Delta t/T$, ξ , θ , α and δ but are independent of Δt .

The unconditional stability of the Newmark and the Houbolt method was discussed in References 1, 4 and 7.

Consider the stability of the Wilson operator. Figure 1 shows $\rho(A)$ as a function of θ for different values of $\Delta t/T$ and ξ . We note that the curves for $\Delta t/T = 0$ and $\Delta t/T = \infty$ are independent of ξ , and that the method is unconditionally stable, i.e. $\rho(A) \leq 1$ for any $\Delta t/T$ ratio, provided $\theta \geq 1.37$. For $\theta < 1.37$. Where the method is only conditionally stable, the stability limit depends on the physical damping in the system.

There are therefore many different operators which can be used in a practical analysis. In the discussion to follow we consider the Houbolt method and two typical operators each of the Newmark and the Wilson method. In the Newmark method we let $\delta = \frac{1}{2}$ with $\alpha = \frac{1}{4}$ and $\delta = \frac{1}{20}$ with $\alpha = \frac{3}{10}$. In the Wilson method we consider the cases $\theta = 1.4$ and $\theta = 2.0$. The spectral radii of the corresponding operators as a function of $\Delta t/T$ are shown in Figure 2, where the unconditional stability of these integration schemes can be noted.

INTEGRATION ACCURACY

The accuracy of a numerical integration depends, in general, on the loading, the physical parameters of the system and the time step size. To obtain an idea of the integration accuracy using the five schemes mentioned above the response of a system with no physical damping is evaluated for two different initial

conditions and no loading:

- (1) $x_0 = 1.0$, $\dot{x}_0 = 0.0$ and $\ddot{x}_0 = -\omega^2$ for which the exact solution is $x = \cos \omega t$;
- (2) $x_0 = 0.0$, $\dot{x}_0 = \omega$ and $\ddot{x}_0 = 0.0$ for which the exact solution is $x = \sin \omega t$.

In the Wilson and Newmark methods, equation (14) can be used directly with these initial conditions. In the Houbolt scheme the exact displacement values for $x_{\Delta t}$ and $x_{2\Delta t}$ have been used.

The solutions show that the errors in the numerical integration can be measured in terms of period elongation and amplitude decay. Figures 3-6 show the percentage period elongations and amplitude decays in the integration schemes as a function of $\Delta t/T$. In general, the integration is accurate when $\Delta t/T$ is smaller than about 0.01, but as $\Delta t/T$ increases the numerical integration results in large period elongations and amplitude decays. The Newmark method with $\delta = \frac{1}{2}$ and $\alpha = \frac{1}{4}$ is most accurate and only gives period

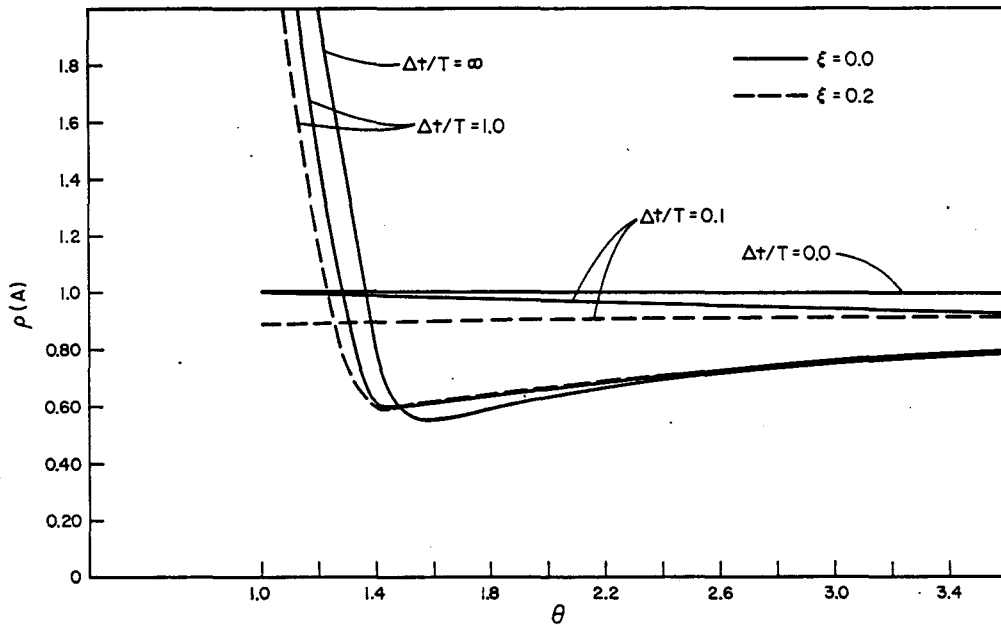


Figure 1. Spectral radius $\rho(A)$ as a function of θ in the Wilson method

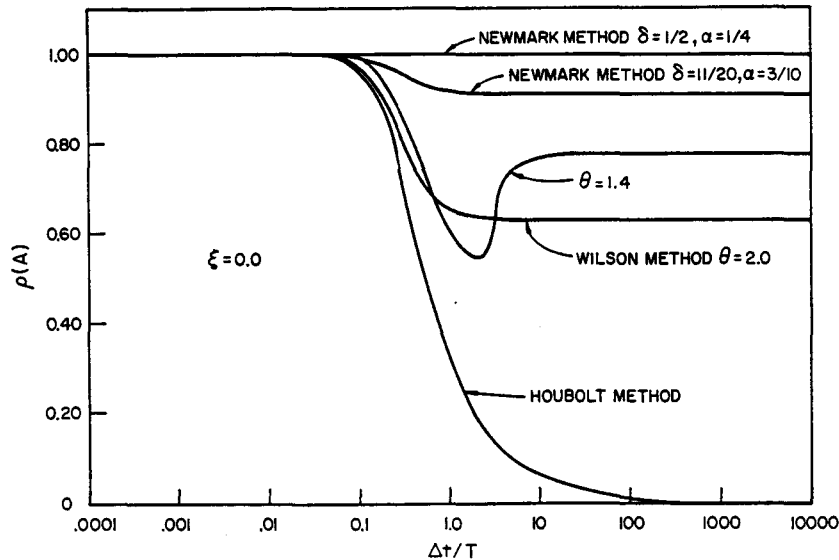


Figure 2. Spectral radii of approximation operators as a function of $\Delta t/T$

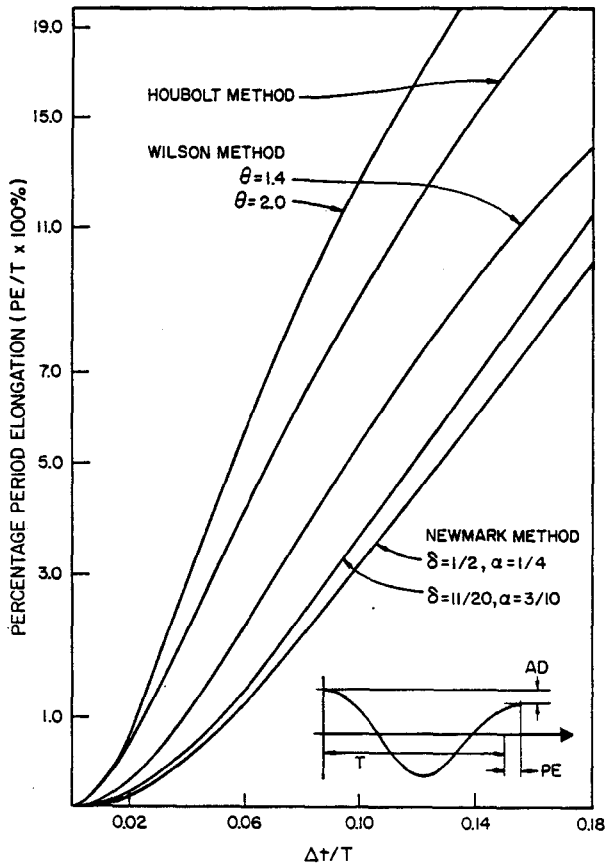


Figure 3. Percentage period elongations

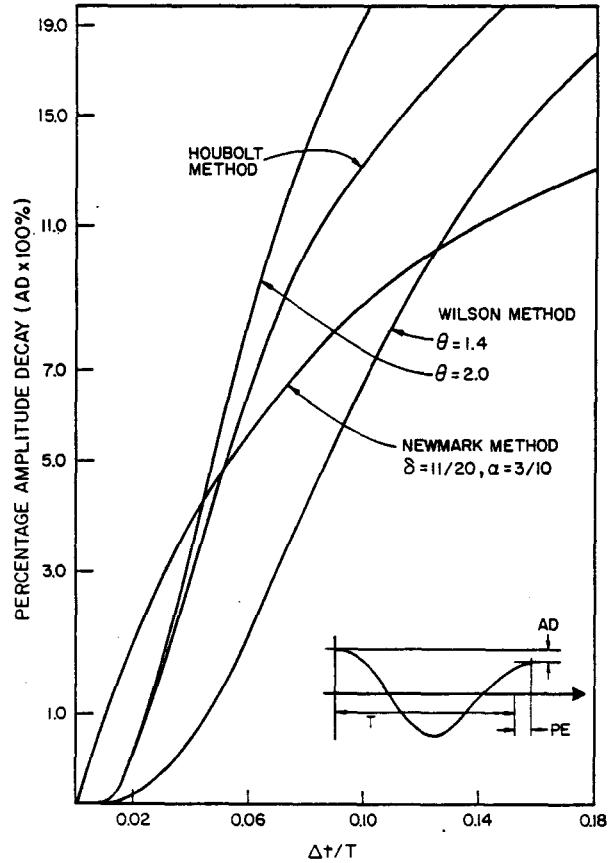


Figure 4. Percentage amplitude decays

elongations. A small negligible variation of the amplitude results from using equations (15) and (16) to find the maximum displacement at times between the discrete time points. Note the improvement in the accuracy of the Wilson method if $\theta = 1.4$ is used.

From the discussion in the previous section the amplitude decay in an integration is directly related to the spectral radius $\rho(A)$ of the approximation operator. Figure 2 shows that for the Newmark method with $\delta = \frac{1}{2}$ and $\alpha = \frac{1}{4}$ the spectral radius is unity for any value $\Delta t/T$, but that for the other integration schemes $\rho(A)$ is smaller than unity for $\Delta t/T$ larger than about 0.01.

Consider now the simultaneous integration of all rows in equation (5), i.e. the direct integration of equation (1). We may choose a time step to obtain accuracy in the low mode responses in which we are interested. The question is then, what results are obtained with the same time step in the integration of the response in the higher modes. For illustration, assume that using Wilson's method with $\theta = 1.4$ a time step is selected which gives $\Delta t/T_1 = 0.01$, where T_1 is the fundamental period of the system. Let the initial conditions in each mode be those given in (1) above and let the integration be performed over 100 time steps. Figure 7 indicates the response in the higher modes. We observe that the amplitude decay caused by the numerical integration errors effectively 'filters' the high mode response out of the solution. The same effect is observed using the other integration schemes except when Newmark's method with $\delta = \frac{1}{2}$ and $\alpha = \frac{1}{4}$ is used. In this case the response in the high frequency components is retained in the solution with large errors in the periods.

The effective filtering of the high frequency response from the solution appears to be beneficial. Integration accuracy cannot be obtained in the response of the modes for which $\Delta t/T$ is large. But the filtering process allows one to obtain, with a relatively large time step, a total system solution in which the low mode response is accurately observed. Naturally, in this integration a scheme should be used which has minimum integration error when $\Delta t/T$ is small.

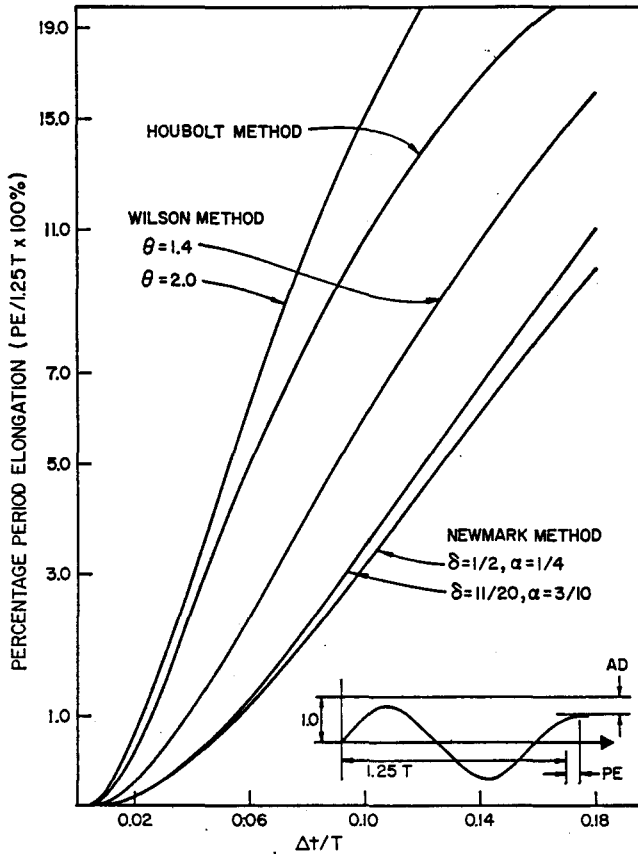


Figure 5. Percentage period elongations

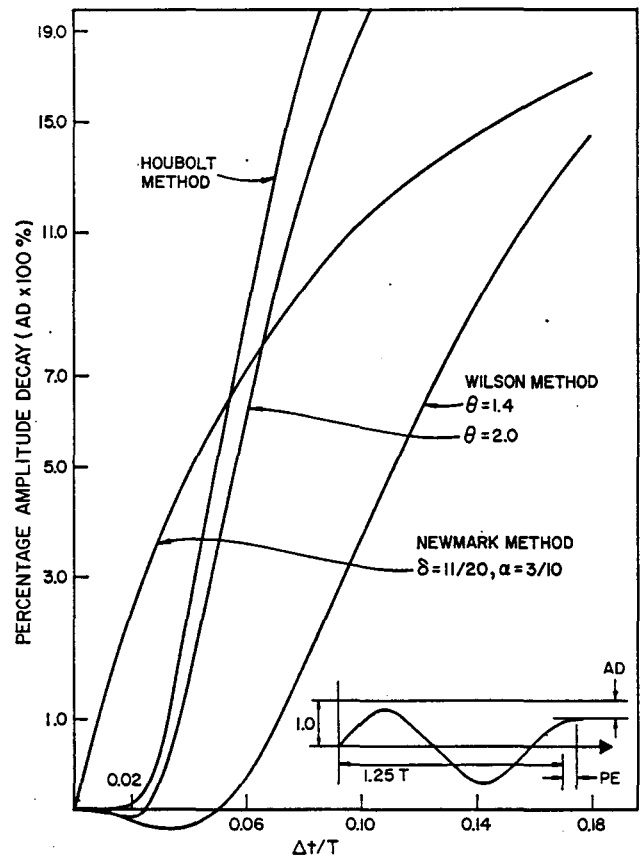


Figure 6. Percentage amplitude decays

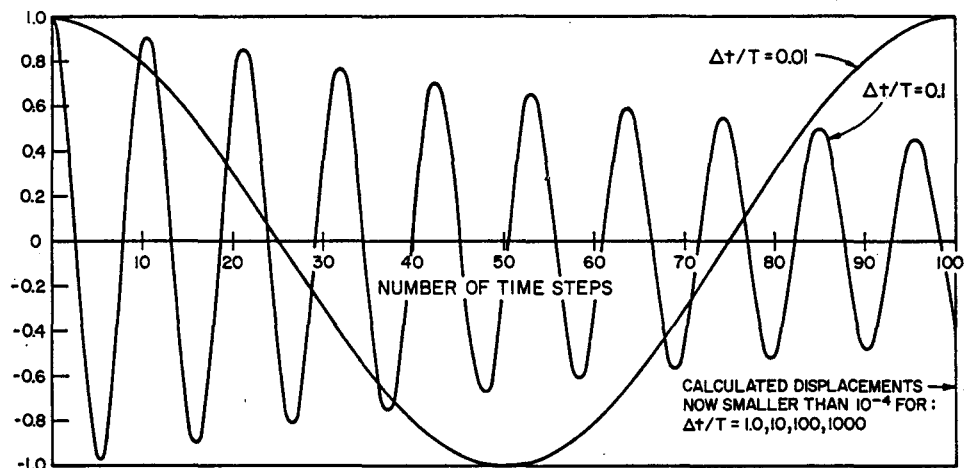


Figure 7. Displacement response in 100 time steps (Wilson method, $\theta = 1.4$)

DIRECT INTEGRATION VERSUS MODE SUPERPOSITION

The observations made in the previous section may be used to draw an instructive comparison between a mode superposition analysis and the direct integration of equation (1) using an integration scheme in which the high frequency response is filtered out of the solution. As discussed, the direct integration is equivalent to a mode superposition analysis in which all eigenvalues and vectors have been calculated and the uncoupled

equations in equation (5) are integrated with a common time step Δt . The integration is accurate for those modes for which $\Delta t/T$ is small, but the response in the modes for which $\Delta t/T$ is large is eliminated by the artificial damping. Therefore, the direct integration is quite equivalent to a mode superposition analysis in which only the lowest modes of the system are considered. The exact number of modes effectively included in the analysis depends on the time step Δt and the distribution of the periods. Clearly, the direct integration is most efficient when all important periods of the system are clustered together. In this case a time step which is chosen using the smallest of those periods is not unnecessarily small with respect to the largest period.

The comparison of the direct integration with mode superposition analysis also indicates on which basis the time step size should be chosen. The most important modes are those for which r in equation (6) is non-zero. Thus, the load distribution and frequency content of the loading largely determine which modes need to be integrated accurately and hence what size of time step should be used. In practice, the mode shapes and frequencies of the system are not known, and it is best to select a time step increment which will accurately represent all of the frequency content of the load.

CONCLUSIONS

A systematic and fundamental procedure for the stability and accuracy analysis of direct integration methods has been presented. The procedure was applied to the Newmark generalized acceleration method, the Houbolt method and the Wilson θ -method, which was optimized for integration accuracy. It is concluded that all of these methods will yield accurate results for certain types of problems. In addition, the relationship between direct integration and mode superposition was discussed. Both methods of analysis can be used to truncate the frequency domain.

It should be emphasized that the discussion of direct integration methods presented here has been limited to linear problems. Additional difficulties arise with the stability and accuracy of numerical methods applied to non-linear systems, and further research is needed concerning such cases. It is believed that the approach to stability and accuracy analysis described in this paper would be of value in these investigations.

REFERENCES

1. N. M. Newmark, 'A method of computation for structural dynamics', *Proc. Am. Soc. Civ. Engrs*, **85**, EM3, 67-94 (1959).
2. J. C. Houbolt, 'A recurrence matrix solution for the dynamic response of elastic aircraft', *J. Aeronaut. Sci.* **17**, 540-550 (1950).
3. E. L. Wilson, 'A computer program for the dynamic stress analysis of underground structures', *SESM Report* 68-1, Department of Civil Engineering, University of California, Berkeley, 1968.
4. D. E. Johnson, 'A proof of the stability of the Houbolt method', *AIAA J.* **4**, 1450-1451 (1966).
5. C. W. Gear, 'Numerical integration of stiff ordinary differential equations', *Report* No. 221, Department of Computer Science, University of Illinois, Urbana, 1967.
6. P. D. Lax and R. D. Richtmyer, 'Survey of the stability of finite difference equations', *Communs. Pure Appl. Math.* **9**, 267-293 (1956).
7. R. E. Nickell, 'On the stability of approximation operators in problems of structural dynamics', *Int. J. Solids Structures*, **7**, 301-319 (1971).
8. R. W. Clough, 'Analysis of structural vibrations and dynamic response', Proceedings, U.S.-Japan Symposium, *Recent Advances in Matrix Methods of Struct. Analysis and Design*, University of Alabama Press, University of Alabama, 1971.
9. O. C. Zienkiewicz and Y. K. Cheung, *The Finite Element Method in Structural and Continuum Mechanics*, McGraw-Hill, 1967.
10. E. L. Wilson and J. Penzien, 'Evaluation of orthogonal damping matrices', *Int. J. num. Meth Engrg*, **4**, 5-10 (1972).
11. K. J. Bathe, 'Solution methods for large generalized eigenvalue problems in structural engineering', *SESM Report* 71-20, Department of Civil Engineering, University of California, Berkeley, 1971.
12. J. H. Wilkinson, *The Algebraic Eigenvalue Problem*, Clarendon Press, Oxford, 1965.

ON EFFECTIVE IMPLICIT TIME INTEGRATION IN ANALYSIS OF FLUID-STRUCTURE PROBLEMS

KLAUS-JÜRGEN BATHE† AND VIJAY SONNAD‡

Department of Mechanical Engineering, Massachusetts Institute of Technology, Cambridge, Massachusetts, U.S.A.

INTRODUCTION

During recent years a considerable amount of research effort has been spent on the analysis of fluid-structure systems. An important feature of these analyses is in many cases the use of implicit-explicit time integration of the dynamic response:^{1,2} the response of the fluid is integrated using an explicit method (central difference technique) and the response of the structure is integrated with an implicit technique (e.g. the Newmark method). The principal advantage of such time integration of the dynamic response is that no stiffness matrix need be calculated for the fluid and a relatively large time step can be employed in the incremental analysis. Various schemes for performing the explicit-implicit integration have been proposed, and these were analysed for their stability and accuracy characteristics.^{1,3} These combined time integration techniques are not restricted in their use to the analysis of fluid-structure systems, but can be employed for the analysis of systems with 'stiff and flexible domains' in general.

The objective in this short paper is to point out that an effective solution of fluid-structure systems (and 'stiff and flexible domains' in general) can frequently also be calculated using an implicit time integration for the complete structural model with a lumped mass idealization and the recently proposed BFGS method.^{4,5} In the analysis procedure used, the response is calculated with implicit time integration for the fluid and the structure without setting up a stiffness matrix of the fluid, and by satisfying the dynamic equilibrium equations using the BFGS iterations.

THE SOLUTION PROCEDURE

The equations used in implicit time integration in a geometric and/or material nonlinear analysis are:⁵

$$\mathbf{M} {}^{t+\Delta t}\ddot{\mathbf{U}}^{(i)} + {}^{\tau}\mathbf{K}\Delta\mathbf{U}^{(i)} = {}^{t+\Delta t}\mathbf{R} - {}^{t+\Delta t}\mathbf{F}^{(i-1)}, \quad (1)$$

where

\mathbf{M} = time independent mass matrix,

${}^{\tau}\mathbf{K}$ = tangent stiffness matrix corresponding to time τ ,

${}^{t+\Delta t}\mathbf{R}$ = vector of externally applied nodal loads corresponding to time $t + \Delta t$,

${}^{t+\Delta t}\mathbf{F}^{(i-1)}$ = vector of nodal point forces equivalent to the element stresses at time $t + \Delta t$ and iteration $(i - 1)$,

${}^{t+\Delta t}\ddot{\mathbf{U}}^{(i)}$ = vector of nodal point accelerations at time $t + \Delta t$ and iteration (i) ,

† Associate Professor.

‡ Graduate student.

and

$${}^{t+\Delta t}\mathbf{U}^{(i)} = {}^{t+\Delta t}\mathbf{U}^{(i-1)} + \Delta\mathbf{U}^{(i)}, \quad (2)$$

where $\Delta\mathbf{U}^{(i)}$ is the incremental nodal point displacement vector corresponding to time t and iteration (i) .

Using the trapezoidal rule of time integration, the following assumptions are employed:

$${}^{t+\Delta t}\mathbf{U} = {}^t\mathbf{U} + \frac{\Delta t}{2}({}^t\dot{\mathbf{U}} + {}^{t+\Delta t}\dot{\mathbf{U}}) \quad (3)$$

$${}^{t+\Delta t}\dot{\mathbf{U}} = {}^t\dot{\mathbf{U}} + \frac{\Delta t}{2}({}^t\ddot{\mathbf{U}} + {}^{t+\Delta t}\ddot{\mathbf{U}}). \quad (4)$$

Using equations (2)–(4) we obtain

$${}^{t+\Delta t}\ddot{\mathbf{U}}^{(i)} = \frac{4}{\Delta t^2}({}^{t+\Delta t}\mathbf{U}^{(i-1)} + \Delta\mathbf{U}^{(i)} - {}^t\mathbf{U}) - \frac{4}{\Delta t}{}^t\dot{\mathbf{U}} - {}^t\ddot{\mathbf{U}} \quad (5)$$

and substituting into equation (1) we have

$${}^t\hat{\mathbf{K}} \Delta\mathbf{U}^{(i)} = {}^{t+\Delta t}\mathbf{R} - {}^{t+\Delta t}\mathbf{F}^{(i-1)} - \mathbf{M} \left[\frac{4}{\Delta t^2}({}^{t+\Delta t}\mathbf{U}^{(i-1)} - {}^t\mathbf{U}) - \frac{4}{\Delta t}{}^t\dot{\mathbf{U}} - {}^t\ddot{\mathbf{U}} \right], \quad (6)$$

where

$${}^t\hat{\mathbf{K}} = {}^t\mathbf{K} + \frac{4}{(\Delta t)^2}\mathbf{M}. \quad (7)$$

In the BFGS iteration, equation (6) is solved as follows:

$$\Delta\mathbf{U}^{(i)} = ({}^t\hat{\mathbf{K}}^{-1})^{(i-1)}({}^{t+\Delta t}\mathbf{R} - \mathbf{M} {}^{t+\Delta t}\ddot{\mathbf{U}}^{(i-1)} - {}^{t+\Delta t}\mathbf{F}^{(i-1)}) \quad (8)$$

and

$${}^{t+\Delta t}\mathbf{U}^{(i)} = {}^{t+\Delta t}\mathbf{U}^{(i-1)} + \beta\Delta\mathbf{U}^{(i)}, \quad (9)$$

where β is a scalar that is evaluated by a line search to satisfy the condition

$$\Delta\mathbf{U}^{(i)T}({}^{t+\Delta t}\mathbf{R} - {}^{t+\Delta t}\mathbf{F}^{(i)} - \mathbf{M} {}^{t+\Delta t}\ddot{\mathbf{U}}^{(i)}) \leq \text{STOL} \Delta\mathbf{U}^{(i)T}({}^{t+\Delta t}\mathbf{R} - \mathbf{M} {}^{t+\Delta t}\ddot{\mathbf{U}}^{(i-1)} - {}^{t+\Delta t}\mathbf{F}^{(i-1)}) \quad (10)$$

with STOL a tolerance. The coefficient matrix in equation (8) is evaluated as follows:

$$({}^t\hat{\mathbf{K}}^{-1})^{(i-1)} = \mathbf{A}^{(i-1)T}({}^t\hat{\mathbf{K}}^{-1})^{(i-2)}\mathbf{A}^{(i-1)}, \quad {}^t\hat{\mathbf{K}}^{(0)} = {}^t\hat{\mathbf{K}}, \quad (11)$$

where the matrices $\mathbf{A}^{(i-1)}$ are of the simple form $\mathbf{A}^{(i-1)} = \mathbf{I} + \mathbf{v}^{(i-1)}\mathbf{w}^{(i-1)T}$. The vectors $\mathbf{w}^{(i-1)}$ and $\mathbf{v}^{(i-1)}$ are given by the calculated nodal point displacements and forces. Convergence is achieved in the iteration when the following two criteria are satisfied:

$$\frac{\|{}^{t+\Delta t}\mathbf{R} - {}^{t+\Delta t}\mathbf{F}^{(i-1)} - \mathbf{M} {}^{t+\Delta t}\ddot{\mathbf{U}}^{(i-1)}\|_2}{\|{}^\kappa\mathbf{R} - {}^\kappa\mathbf{F} - \mathbf{M} {}^\kappa\mathbf{\ddot{U}}\|_2^{(\max)}} \leq \text{RTOL}, \quad (12)$$

where κ is any one of the discrete times considered, and

$$\frac{\Delta\mathbf{U}^{(i)T}({}^{t+\Delta t}\mathbf{R} - {}^{t+\Delta t}\mathbf{F}^{(i-1)} - \mathbf{M} {}^{t+\Delta t}\ddot{\mathbf{U}}^{(i-1)})}{\Delta\mathbf{U}^{(1)T}({}^{t+\Delta t}\mathbf{R} - {}^t\mathbf{F} - \mathbf{M} {}^t\ddot{\mathbf{U}})} \leq \text{ETOL}, \quad (13)$$

where RTOL is an out-of-balance force tolerance and ETOL is an 'energy' tolerance. In equation (12) the superscript (max) denotes the maximum value ever calculated during the solution, and $\|\mathbf{a}\|_2$ is the Euclidean norm of the vector \mathbf{a} .⁶

The above equations have been written for nonlinear dynamic analysis, but they are equally applicable in linear dynamic analysis and static analysis (in which case the inertia forces must simply be neglected).

An important point to note is that in the iteration of equations (8)–(11), a very approximate stiffness matrix can be used, and indeed such use may yield a most effective solution if the number of iterations required for convergence is not excessive. For example, it may be effective to use throughout a nonlinear incremental static analysis the initial elastic stiffness matrix, in which case only one stiffness matrix calculation and \mathbf{LDL}^T decomposition at the beginning of the solution is required. However, the number of iterations required to solve the equilibrium equations increases when the matrix ${}^r\mathbf{K}$ approximates the actual tangent stiffness matrix of the system less accurately.

Considering a dynamic analysis of a fluid–structure system, it is recognized that as the time step Δt becomes small, the contribution of the mass matrix to the effective stiffness matrix becomes predominant in the fluid domain. If in such analysis a lumped mass matrix is used, it can be effective not to include the fluid element stiffness matrix contributions to the matrix ${}^r\hat{\mathbf{K}}$. This is particularly the case when the fluid domain is large (modelled using a large number of elements) compared to the structure. Thus, if we write,

$${}^r\mathbf{K} = {}^r\mathbf{K}_s + {}^r\mathbf{K}_f, \quad (14)$$

where ${}^r\mathbf{K}_s$ and ${}^r\mathbf{K}_f$ are the stiffness matrices of the structure and the fluid, respectively, it can be effective to use in equation (11)

$${}^r\hat{\mathbf{K}}^{(0)} = {}^r\mathbf{K}_s + \frac{4}{\Delta t^2}\mathbf{M}. \quad (15)$$

The use of equation (15) may decrease the bandwidth of the coefficient matrix a great deal. Considering the computations, the solution scheme is now similar to an explicit time integration of the fluid response and an implicit integration of the structural response, but in fact, by the iteration, all finite element equations are integrated implicitly.

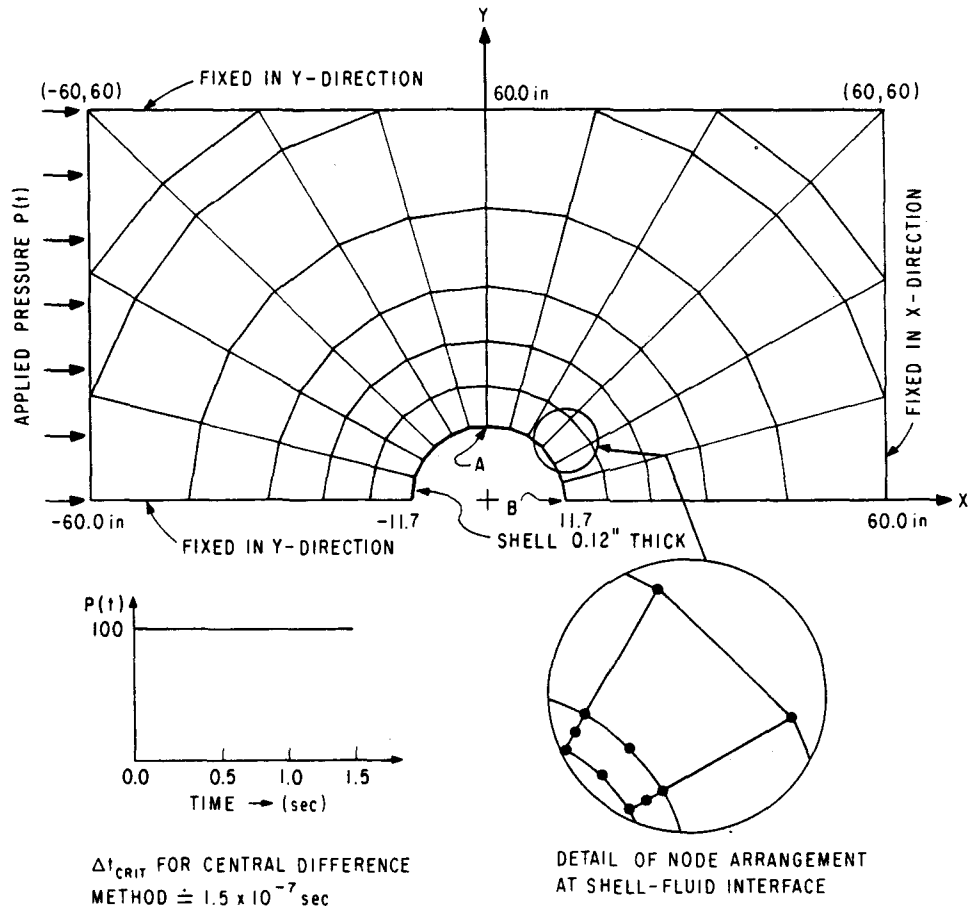
The procedure is appealing because the integration scheme does not require the use of special interface conditions, and the method is not subject to severe time step size constraints in the fluid domain.

SAMPLE ANALYSIS

The BFGS iteration scheme is available in the ADINA computer program,⁷ which was modified for this analysis not to include the stiffness contributions of the fluid elements in the coefficient matrix.

The fluid–structure problem considered is shown in Figure 1. A similar problem was already earlier analysed by Belytschko and Mullen using explicit–implicit integration.¹ Figure 2 shows the x -velocities predicted at points A and B as a function of time. It should be noted that our objective was only to study the use of the proposed technique for the solution of the finite element equilibrium equations of this model and not to investigate whether this model does represent the physical situation in an accurate manner.

In the first analysis, the response was calculated using the usual solution procedure with the implicit trapezoidal rule and $\Delta t = 10^{-5}$ sec.⁶ Next, the response was calculated with the BFGS



MATERIAL PROPERTIES (plane strain model)

BULK MODULUS OF FLUID	$= 3.0 \times 10^5$ psi
DENSITY OF FLUID	$= 9.35 \times 10^{-5}$ lbs/in ⁴ -sec ²
YOUNG'S MODULUS OF SHELL	$= 3.0 \times 10^7$ psi
POISSON'S RATIO OF SHELL	$= 0.25$
DENSITY OF SHELL	$= 7.35 \times 10^{-4}$ lbs/in ⁴ -sec ²

Figure 1. Analysis of long cylindrical shell surrounded by fluid; fluid is subjected to step pressure

method with the starting coefficient matrix of equation (15) and using $\Delta t = 10^{-5}$ and 10^{-4} sec. These two analyses were also performed using the modified Newton method with the constant coefficient matrix equal to the matrix in equation (15), in order to evaluate its effectiveness as well. Table I shows the average and maximum number of iterations required per time step in these computations. Figure 2 shows that, for the smaller time step, practically identical responses are predicted using any one of the procedures. But Table I shows that, for the larger time step, the Newton method failed to converge within 30 iterations at the eighth time step, whereas the BFGS method never required more than 5 iterations per time step. In all the above analyses we used equations (12) and (13) with $RTOL = 10^{-3}$ and $ETOL = 10^{-5}$.

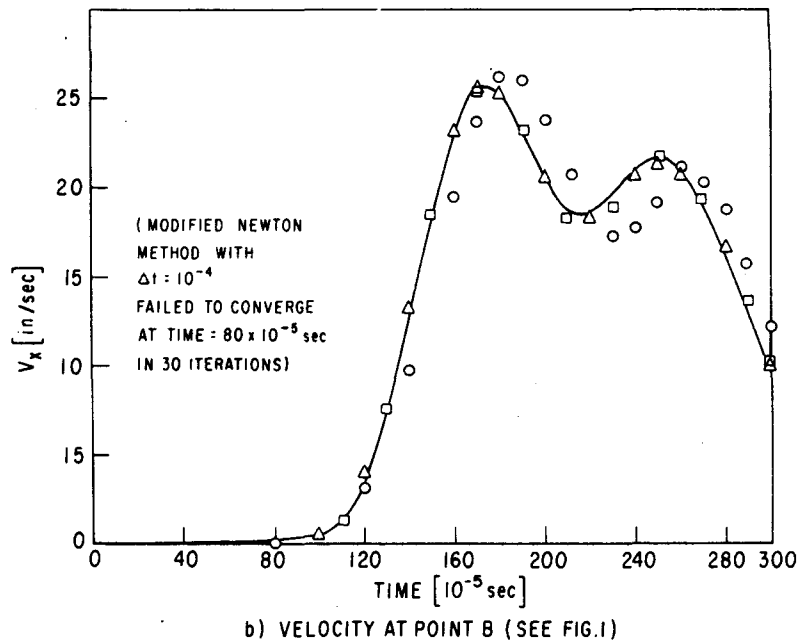
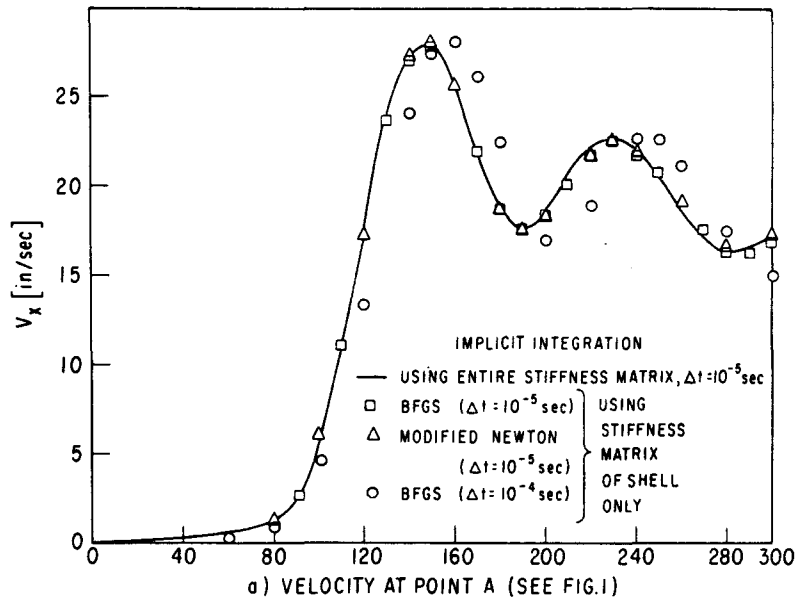


Figure 2. Velocity response at points A and B of the shell

CONCLUSIONS

An effective application of the BFGS method to some wave propagation fluid-structure problems was pointed out. The essence of the solution is that the stiffness matrix contributions of the fluid elements are neglected in the starting coefficient matrix of the iteration. It is concluded that in nonlinear dynamic analysis, in which iteration is required anyway in order to preserve the

Table I. Number of iterations used in solutions

	$\Delta t = 10^{-5}$ sec		$\Delta t = 10^{-4}$ sec	
	Maximum	Average	Maximum	Average
BFGS	2	2	5	4
Modified Newton	2	2	Failed to converge in 30 iterations	

stability of the solution⁸ and the fluid element stiffness effects in the coefficient matrix are small, this iterative technique may be very efficient. The solution scheme has the computational advantage of explicit-implicit time integration that no coefficient matrix corresponding to the fluid elements needs to be assembled and dealt with, and has as an additional advantage the stability of the implicit time integration in the fluid domain. The method can be cost-effective as a practical tool because of the good convergence characteristics of the BFGS method.

REFERENCES

1. T. Belytschko and R. Mullen, 'Mesh partitions of explicit-implicit time integration', in *Formulations and Computational Algorithms in Finite Element Analysis* (Eds. K. J. Bathe, J. T. Oden and W. Wunderlich), M.I.T. Press, 1977.
2. T. Belytschko, H. J. Yen and R. Mullen, 'Mixed methods for time integration', *J. Comp. Meth. Appl. Mech. Engng*, **17/18**, 259-275 (1979).
3. T. J. R. Hughes and W. K. Liu, 'Implicit-Explicit finite elements in transient analysis: stability theory' *J. Appl. Mech.* **45** (June 1978).
4. H. Matthies and G. Strang, 'The solution of nonlinear finite element equations', *Int. J. num. Meth. Engng*, in press.
5. K. J. Bathe and A. P. Cimento, 'Some practical procedures for the solution of nonlinear finite element equations', *J. Comp. Meth. Appl. Mech. Engng*, in press.
6. K. J. Bathe and E. L. Wilson, *Numerical Methods in Finite Element Analysis*, Prentice-Hall, Englewood Cliffs, N.J., 1976.
7. K. J. Bathe, 'ADINA—a finite element program for automatic dynamic incremental nonlinear analysis', *Report AVL 82448-1*, Department of Mechanical Engineering, M.I.T., 1975 (rev. Dec. 1978).
8. K. J. Bathe, 'Finite element formulation, modeling and solution of nonlinear dynamic problems', in *Numerical Methods for Partial Differential Equations*, (Ed. S. V. Parker), Academic Press, London and New York, 1979.

ON NONLINEAR DYNAMIC ANALYSIS USING SUBSTRUCTURING AND MODE SUPERPOSITION

KLAUS-JÜRGEN BATHE and SHERYL GRACEWSKI

Department of Mechanical Engineering, Massachusetts Institute of Technology, Cambridge, MA 02139, U.S.A.

Abstract—The solution of nonlinear dynamic equilibrium equations using mode superposition and substructuring is studied. The objective is to design schemes that in some analyses can significantly decrease the computational effort involved when compared to a complete direct integration solution. Specific schemes for mode superposition analysis and substructuring are proposed. These techniques have been implemented in ADINA. The results of a few sample analyses are presented and recommendations are given on the use of these procedures in practical analysis.

INTRODUCTION

The analysis of the nonlinear dynamic response of large finite element systems has become of much interest during recent years. The problems to be considered can quite generally be divided into wave propagation problems and structural vibration problems. Both types of problems are solved using an incremental step-by-step solution of the governing equations of motion.

In this paper we consider the solution of structural vibration problems only. These problems can be solved effectively using an implicit time integration scheme with a modified Newton iteration in each time step. The solution requires that for each of the time steps $\Delta t, 2\Delta t, 3\Delta t, \dots, n\Delta t$, where n is the total number of time steps considered, the incremental dynamic equilibrium equations be established and then solved using equilibrium iterations. The evaluation of the incremental equilibrium equations involves as a significant computational expense the calculation and the triangular factorization of the effective tangent stiffness matrix, and the equilibrium iterations require the calculation of out-of-balance nodal point force vectors and the forward reduction and backsubstitution of these vectors, until the corrections to the incremental quantities are sufficiently small. The complete solution process is summarized, for example in Table 1 of Refs. [1, 2].

Since a large part of the cost in this incremental analysis lies in the calculation of the tangent stiffness matrices and the equilibrium iterations, it is desirable that, without loss of solution stability and accuracy, a new tangent stiffness matrix is only very infrequently formed and equilibrium iterations be only performed when really necessary. Mathematical analysis and practical experience show that because of stability and accuracy considerations, equilibrium iterations are best performed in each time step. However, depending on the problem considered, a new tangent stiffness matrix need not be calculated in each time step, and indeed in many analyses, the original stiffness matrix can be employed throughout the complete response calculation. Also, in many nonlinear analyses, we only deal with local nonlinearities.

The objective in this paper is to consider the nonlinear dynamic analysis of finite element systems for which the original stiffness matrix can be employed throughout the incremental solution, or which only contain local nonlinearities, and demonstrate how the response can be calculated effectively using the basic principles of mode superposition and substructuring.

The possible use of mode superposition in nonlinear analysis is quite natural, because mathematically only a change of basis to a computationally more effective system of equations is performed [1, 3]. The method of mode superposition has already been applied in nonlinear analysis [4-6], but the effectiveness of the schemes employed in actual practical analyses is still questionable.

The possible use of substructuring on the linear degrees of freedom is equally natural, if we recognize that the solution of the incremental equations involves an "effective stiffness matrix" on which we operate as in static analysis [1-3]. However, there are some important questions with regard to the actual implementation of a substructuring scheme, and these must be addressed in detail in order to arrive at an effective solution strategy.

In the paper we first present the general equations that we employ in an incremental nonlinear dynamic analysis. We then discuss how we use mode superposition and substructuring procedures to reduce the computational effort of solution. The proposed techniques are only effective in the solution of certain nonlinear systems, but then they may yield a significantly more effective solution than the use of direct integration of the complete system of equations. The techniques are implemented in ADINA, and we present the results of some sample analyses using the methods. Finally, we give specific recommendations on the practical usage of the techniques.

2. INCREMENTAL EQUATIONS OF EQUILIBRIUM

The incremental nodal point equilibrium equations for an assemblage of nonlinear finite elements considered here have been discussed in [1, 3]. Using an implicit time integration scheme and the modified Newton iteration to establish dynamic equilibrium at time $t + \Delta t$, the governing finite element equations are

$$\mathbf{M} {}^{t+\Delta t}\ddot{\mathbf{U}}^{(i)} + \mathbf{C} {}^{t+\Delta t}\dot{\mathbf{U}}^{(i)} + {}^t\mathbf{K} \Delta \mathbf{U}^{(i)} = {}^{t+\Delta t}\mathbf{R} - {}^{t+\Delta t}\mathbf{F}^{(i-1)}; i = 1, 2, 3, \dots, 1 \quad (1)$$

where

$${}^{t+\Delta t}\mathbf{U}^{(i)} = {}^{t+\Delta t}\mathbf{U}^{(i-1)} + \Delta \mathbf{U}^{(i)} \quad (2)$$

and \mathbf{M} = constant mass matrix, \mathbf{C} = constant damping matrix, ${}^t\mathbf{K}$ = tangent stiffness matrix at time t , ${}^{t+\Delta t}\mathbf{R}$ = external nodal point load vector due to body forces, surface loads and concentrated loads, ${}^{t+\Delta t}\mathbf{F}^{(i-1)}$ = nodal point force vector equivalent to the element stresses that

correspond to the displacements ${}^{t+\Delta t}\mathbf{U}^{(i-1)}$, ${}^{t+\Delta t}\mathbf{U}^{(i)}$ = vector of nodal point displacements at the end of iteration (i) and time $t + \Delta t$, with derivatives denoted by superposed dots.

For solution of eqn (1), the velocities ${}^{t+\Delta t}\dot{\mathbf{U}}^{(i)}$ and accelerations ${}^{t+\Delta t}\ddot{\mathbf{U}}^{(i)}$ are expressed in terms of $\Delta\mathbf{U}^{(i)}$ and known quantities using a time integration scheme as discussed in [1, 3]. Also, it should be noted that eqn (1) represents the governing equilibrium equations of a very general finite element system with geometric and/or material nonlinearities. The geometric nonlinearities may be due to large displacements and large strains and the material nonlinearities may be due to elastic-plastic, hypo-elastic or other material behavior.

The major computational expense in the solution of eqn (1) lies in the evaluation of ${}^t\mathbf{K}$, its factorization and then the equilibrium iterations. *Mathematical analysis and practical experience show that the equilibrium iterations are best always performed*, and guidelines for the use of some available procedures to accelerate the convergence of the iterations have been presented in [7]. To reduce the computational effort in the solution of eqn (1) we consider now the use of mode superposition and substructuring.

2.1 Use of mode superposition

In principle, the use of mode superposition simply involves a coordinate transformation from the finite element displacement coordinates to the modal coordinates. This change of basis is particularly effective if only a few modal coordinates need be employed. Considering the nonlinear dynamic analysis operating on eqn (1), the change of basis could be performed in each time step using the mode shapes corresponding to time t . However, such a procedure would require the solution of the generalized eigenproblem ${}^t\mathbf{K}'\phi = {}^t\omega^2\mathbf{M}'\phi$, where the superscript " t " indicates that the stiffness matrix, free vibration mode shapes and frequencies correspond to the instantaneous equilibrium configuration at time t . It is questionable whether such a scheme would be effective.

When solving eqn (1) it is important to recognize that the new tangent stiffness matrix ${}^t\mathbf{K}$ is only calculated to speed up the convergence of the iteration. In the analysis of some problems it may well be more efficient not to establish a new stiffness matrix in each time step and instead iterate a few more times. In particular, in the analysis of some systems it may be most effective to use the original stiffness matrix corresponding to time 0 throughout the response analysis. In this case, the governing finite element equations for the solution of the response at time $t + \Delta t$ are

$$\mathbf{M} {}^{t+\Delta t}\ddot{\mathbf{U}}^{(i)} + \mathbf{C} {}^{t+\Delta t}\dot{\mathbf{U}}^{(i)} + {}^0\mathbf{K} \Delta\mathbf{U}^{(i)} = {}^{t+\Delta t}\mathbf{R} - {}^{t+\Delta t}\mathbf{F}^{(i-1)}; i = 1, 2, 3, \dots \quad (3)$$

where ${}^0\mathbf{K}$ is the stiffness matrix corresponding to the configuration and material properties at time 0. Using eqn (3), a constant effective stiffness matrix is formed in the time integration, and thus only one triangular matrix factorization is needed in the calculation of the dynamic response. *All nonlinearities are taken fully into account in the evaluation of the vector ${}^{t+\Delta t}\mathbf{F}^{(i-1)}$* . However, because a constant stiffness matrix is employed, the solution generally requires more equilibrium iterations, and clearly, it is only advantageous to use eqn (3) in the response calculations if the total number of numerical operations is less than in using eqn (1).

The required computations in solving eqn (3) can, in the analysis of some types of problems (which are discussed in Section 3), be reduced significantly using the concepts of mode superposition [4]. The basic step in this solution is a change of basis from the n nodal point displacements to p modal generalized displacements, $p \ll n$, prior to the step-by-step solution. In this transformation we use

$${}^{t+\Delta t}\mathbf{U} = \Phi {}^{t+\Delta t}\mathbf{X} \quad (4)$$

where

$${}^{t+\Delta t}\mathbf{X} = \begin{bmatrix} {}^{t+\Delta t}x_1 \\ \vdots \\ {}^{t+\Delta t}x_p \end{bmatrix}; \Phi = [\phi_1, \dots, \phi_p]. \quad (5)$$

The values ${}^{t+\Delta t}x_i$ are the generalized modal displacements at time $t + \Delta t$ and the vectors ϕ_i are the eigenvectors of the generalized eigenproblem,

$${}^0\mathbf{K}\phi_i = \omega_i^2 \mathbf{M}\phi_i \quad (6)$$

where the ω_i are the natural circular frequencies of the linearized system at time 0.

The "approximately equal sign" in eqn (4) expresses the fact that an approximation to the solution of eqn (3) is obtained because $p < n$. *However, it must be noted that by selecting p sufficiently large, the error in the solution can be made arbitrarily small.*

Substituting from eqn (4) into eqn (3) we obtain

$${}^{t+\Delta t}\mathbf{X}^{(i)} + \Lambda {}^{t+\Delta t}\dot{\mathbf{X}}^{(i)} + \Omega^2 \Delta\mathbf{X}^{(i)} = \Phi^T ({}^{t+\Delta t}\mathbf{R} - {}^{t+\Delta t}\mathbf{F}^{(i-1)}) \quad (7)$$

where Ω^2 is a diagonal matrix listing the circular frequencies squared on its diagonal,

$$\Omega^2 = \begin{bmatrix} \omega_1^2 & & \\ & \ddots & \\ & & \omega_p^2 \end{bmatrix} \quad (8)$$

and assuming proportional damping, we can also write,

$$\Lambda = \begin{bmatrix} 2\xi_1\omega_1 & & \\ & \ddots & \\ & & 2\xi_p\omega_p \end{bmatrix} \quad (9)$$

where the ξ_i are the modal damping ratios corresponding to the ω_i .

It should be noted that, different from linear analysis, the incremental equilibrium equations in the new basis, eqn (7) are still coupled, because the nodal point vector ${}^{t+\Delta t}\mathbf{F}^{(i-1)}$ can only be evaluated once all displacements are known,

$${}^{t+\Delta t}\mathbf{U}^{(i-1)} = \sum_{k=1}^p \phi_k {}^{t+\Delta t}x_k^{(i-1)}. \quad (10)$$

Therefore, the solution of the p equations in eqn (7) must be performed simultaneously. However, since Λ and Ω^2 are diagonal matrices and only p equations are considered, $p \ll n$, the solution of the eigenproblem in eqn (6) plus the step-by-step solution of eqn (7) (using, for example, the Newmark method) can be significantly more cost-effective than the direct step-by-step solution of eqn (3).

2.2 Use of substructuring

Substructuring for solution of eqn (1) can effectively be used in the analysis of large problems with small isolated areas of nonlinearities. In such case we can statically condense the linear degrees of freedom prior to the solution of the incremental equations of equilibrium. In the following, we use the Newmark method of time integration; however, the solution procedure can equally be employed with other direct integration schemes (in ADINA we have implemented the procedure for the Newmark and Wilson integration methods).

Using the Newmark method of time integration, eqn (1) becomes [2, 3],

$${}^t\hat{\mathbf{K}}\Delta\mathbf{U}^{(i)} = {}^{t+\Delta t}\mathbf{R} - {}^{t+\Delta t}\mathbf{F}^{(i-1)} - \mathbf{M}\{a_0\mathbf{U}^{(i-1)} - a_2{}^t\dot{\mathbf{U}} - a_3{}^t\ddot{\mathbf{U}}\} - \mathbf{C}\{a_1\mathbf{U}^{(i-1)} - a_4{}^t\dot{\mathbf{U}} - a_5{}^t\ddot{\mathbf{U}}\} \quad (11)$$

where the time integration constants a_0, \dots, a_5 are defined in Appendix A, and

$${}^t\hat{\mathbf{K}} = {}^t\mathbf{K} + a_0\mathbf{M} + a_1\mathbf{C} \quad (12)$$

$$\mathbf{U}^{(i-1)} = {}^{t+\Delta t}\mathbf{U}^{(i-1)} - {}^t\mathbf{U} \quad (13)$$

Since we now consider the solution of problems for which isolated nonlinearities are present, we can write ${}^t\hat{\mathbf{K}}$ in the form

$${}^t\hat{\mathbf{K}} = \hat{\mathbf{K}} + {}^t\mathbf{K}^{(nl)} \quad (14)$$

where $\hat{\mathbf{K}}$ contains all constant elements of ${}^t\hat{\mathbf{K}}$ (including the mass and damping terms) and ${}^t\mathbf{K}^{(nl)}$ corresponds to all nonlinear (time-dependent) entries in ${}^t\hat{\mathbf{K}}$. Figure 1 shows schematically the structure of the matrices in eqn (14).

Considering eqn (11) it follows that static condensation or substructuring can be employed on all those degrees of freedom that pertain to constant elements in ${}^t\hat{\mathbf{K}}$. This means, in essence, that the $\mathbf{L}\mathbf{D}\mathbf{L}^t$ factorization of ${}^t\hat{\mathbf{K}}$ on the "linear degrees of freedom" need be performed only once prior to the step-by-step solution, at time 0, and only the stiffness values of the "nonlinear degrees of freedom" need be updated and factorized at the beginning of each step. However, if the effective load vector is evaluated as shown in eqn (11), the complete vector has to be formed and reduced in each iteration. The efficiency of the equilibrium iterations is greatly improved by rewriting eqn (11) in the form,

$${}^t\hat{\mathbf{K}}\Delta\mathbf{U}^{(i)} = {}^{t+\Delta t}\mathbf{R} - {}^{t+\Delta t}\hat{\mathbf{F}}^{(i-1)} + {}^t\mathbf{F}^M + {}^t\mathbf{F}^C \quad (15)$$

where

$${}^{t+\Delta t}\hat{\mathbf{F}}^{(i-1)} = {}^{t+\Delta t}\mathbf{F}^{(i-1)} + (a_0\mathbf{M} + a_1\mathbf{C}){}^{t+\Delta t}\mathbf{U}^{(i-1)} \quad (16)$$

$${}^t\mathbf{F}^M = \mathbf{M}(a_0{}^t\mathbf{U} + a_2{}^t\dot{\mathbf{U}} + a_3{}^t\ddot{\mathbf{U}}) \quad (17)$$

$${}^t\mathbf{F}^C = \mathbf{C}(a_1{}^t\mathbf{U} + a_4{}^t\dot{\mathbf{U}} + a_5{}^t\ddot{\mathbf{U}}) \quad (18)$$

Equation (15) is in more detail

$$\left\{ \begin{bmatrix} \hat{\mathbf{K}}_{cc} & \hat{\mathbf{K}}_{ca} \\ \hat{\mathbf{K}}_{ac} & \hat{\mathbf{K}}_{aa} \end{bmatrix} + \begin{bmatrix} 0 & 0 \\ 0 & {}^t\mathbf{K}^{(nl)} \end{bmatrix} \right\} \begin{bmatrix} \Delta\mathbf{U}_c^{(i)} \\ \Delta\mathbf{U}_a^{(i)} \end{bmatrix} = \begin{bmatrix} {}^{t+\Delta t}\mathbf{R}_c \\ {}^{t+\Delta t}\mathbf{R}_a \end{bmatrix} - \begin{bmatrix} {}^{t+\Delta t}\hat{\mathbf{F}}_c^{(i-1)} \\ {}^{t+\Delta t}\hat{\mathbf{F}}_a^{(i-1)} \end{bmatrix} + \begin{bmatrix} {}^t\mathbf{F}_c^M \\ {}^t\mathbf{F}_a^M \end{bmatrix} + \begin{bmatrix} {}^t\mathbf{F}_c^C \\ {}^t\mathbf{F}_a^C \end{bmatrix} \quad (19)$$

where the \mathbf{U}_c degrees of freedom are to be condensed out. Performing the static condensation in the usual way we obtain

$$\underbrace{\left\{ (\hat{\mathbf{K}}_{aa} - \hat{\mathbf{K}}_{ac}\hat{\mathbf{K}}_{cc}^{-1}\hat{\mathbf{K}}_{ca}) + {}^t\mathbf{K}^{(nl)} \right\} \Delta\mathbf{U}_a^{(i)} = ({}^{t+\Delta t}\mathbf{R}_a + {}^t\mathbf{F}_a^M + {}^t\mathbf{F}_a^C) - \hat{\mathbf{K}}_{ac}\hat{\mathbf{K}}_{cc}^{-1}({}^{t+\Delta t}\mathbf{R}_c + {}^t\mathbf{F}_c^M + {}^t\mathbf{F}_c^C)}_{\text{TERM 1}} - \underbrace{({}^{t+\Delta t}\hat{\mathbf{F}}_a^{(i-1)} - \hat{\mathbf{K}}_{ac}\hat{\mathbf{K}}_{cc}^{-1}{}^{t+\Delta t}\hat{\mathbf{F}}_c^{(i-1)})}_{\text{TERM 2}} \quad (20)$$

Considering eqn (20) it is clear that the expression labelled TERM 1 need only be evaluated once at the beginning of the iteration, because it is independent of the iteration counter (i). In order to identify how the expression labelled TERM 2 can be evaluated effectively, we use the following relation

$$\begin{bmatrix} {}^{t+\Delta t}\hat{\mathbf{F}}_c^{(i-1)} \\ {}^{t+\Delta t}\hat{\mathbf{F}}_a^{(i-1)} \end{bmatrix} = \begin{bmatrix} \hat{\mathbf{K}}_{cc} & \hat{\mathbf{K}}_{ca} \\ \hat{\mathbf{K}}_{ac} & \hat{\mathbf{K}}_{aa} \end{bmatrix} \begin{bmatrix} {}^{t+\Delta t}\mathbf{U}_c^{(i-1)} \\ {}^{t+\Delta t}\mathbf{U}_a^{(i-1)} \end{bmatrix} + \begin{bmatrix} 0 \\ {}^{t+\Delta t}\mathbf{F}^{(nl)(i-1)} \end{bmatrix} \quad (21)$$

where ${}^{t+\Delta t}\mathbf{F}^{(nl)(i-1)}$ represents the nodal point forces corresponding to the element stresses in the nonlinear elements [1, 3]. Using eqn (21) we obtain

$${}^{t+\Delta t}\hat{\mathbf{F}}_a^{(i-1)} - \hat{\mathbf{K}}_{ac}\hat{\mathbf{K}}_{cc}^{-1}{}^{t+\Delta t}\hat{\mathbf{F}}_c^{(i-1)} = (\hat{\mathbf{K}}_{aa} - \hat{\mathbf{K}}_{ac}\hat{\mathbf{K}}_{cc}^{-1}\hat{\mathbf{K}}_{ca}){}^{t+\Delta t}\mathbf{U}_a^{(i-1)} + {}^{t+\Delta t}\mathbf{F}^{(nl)(i-1)} \quad (22)$$

Hence, the static condensation of the \mathbf{U}_c displacements

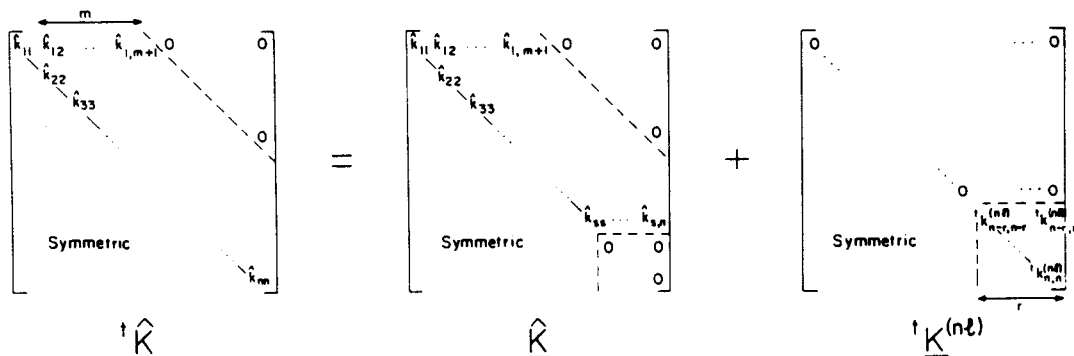


Fig. 1. Schematic of stiffness matrix used in dynamic substructuring.

yields

$$(\hat{K}_r + {}^{t+\Delta t}K^{(nl)})\Delta U_a^{(i)} = {}^{t+\Delta t}\hat{R}_r - \hat{K}_r {}^{t+\Delta t}U_a^{(i-1)} - {}^{t+\Delta t}F^{(nl)(i-1)} \quad (23)$$

where

$$\hat{K}_r = \hat{K}_{aa} - \hat{K}_{ac}\hat{K}_{cc}^{-1}\hat{K}_{ca} \quad (24)$$

$${}^{t+\Delta t}\hat{R}_r = {}^{t+\Delta t}R_a + {}^tF_a^M + {}^tF_a^C - \hat{K}_{ac}\hat{K}_{cc}^{-1} \times ({}^{t+\Delta t}R_c + {}^tF_c^M + {}^tF_c^C). \quad (25)$$

It is important to note that in the solution of eqn (23) the vector ${}^{t+\Delta t}\hat{R}_r$ need only be calculated once at the beginning of the iteration and the iteration is performed only with the U_a degrees of freedom. Once the iteration has converged to the displacements ${}^{t+\Delta t}U_a$, we obtain the displacements ${}^{t+\Delta t}U_c$ using eqn (19),

$$\hat{K}_{cc} {}^{t+\Delta t}U_c = {}^{t+\Delta t}R_c - \hat{K}_{ca} {}^{t+\Delta t}U_a + {}^tF_c^M + {}^tF_c^C. \quad (26)$$

This solution only requires a forward reduction and backsubstitution because the factorization of \hat{K}_{cc} was already performed in the static condensation to obtain \hat{K}_r . With the nodal-point displacements known, the corresponding velocities and accelerations can directly be evaluated as given in Appendix A.

The above static condensation procedure is implemented effectively using substructuring. Equations (23)–(25) show that the substructuring can be performed much in the same way as in static analysis, but using the effective stiffness matrix and calculating an effective load vector ${}^{t+\Delta t}\hat{R}_r$ at the beginning of each time step. Also, since the evaluation of the load vector ${}^{t+\Delta t}\hat{R}_r$ involves all displacements, velocities and accelerations corresponding to time t , it is necessary to calculate the condensed nodal point displacements (using eqn 26) always immediately after convergence of the iteration for the retained degrees of freedom. On the other hand, in static analysis the condensed nodal-point displacements corresponding to all load levels can be calculated after the complete solution of the retained degrees of freedom has been obtained.

3. USE OF MODE SUPERPOSITION AND SUBSTRUCTURING

The mode superposition and substructuring procedures described in Sections 2.1 and 2.2 are available in the ADINA computer program. The sample problems described in the following only demonstrate the applicability of the solution procedures. The efficiencies of the methods are discussed in Section 3.2.

3.1 Sample problems

The first two sample problems consist of linear structures which have contact regions that are "small" in comparison to the total problem size. In the first example, there are twelve degrees of freedom and the ratio of nodes in contact to total structure nodes is 1:4. In the second example, the ratio is increased to 1:16 with a total of 64 degrees of freedom. These two problems are of the type for which the use of mode superposition and substructuring can be effective.

In the third sample problem, the earthquake response of a tall structure is examined. Since the entire structure is allowed to become plastic, dynamic structuring cannot

be used. Mode superposition analyses using 1, 4 and 8 modes were compared to the direct integration solution.

All sample problems were solved using the computer program ADINA. For all direct integration solutions, the Newmark method was used.

3.1.1 Control rod drive housing with stops. The 69 product line Control Rod Drive (CRD) housing shown in Fig. 2 is subjected to a sinusoidal ground acceleration with 5 Hz frequency. The finite element model consists of four beam elements of length, L , with a concentrated mass at each nodal point. Values for all constants are given in Fig. 2. Mass proportional loading was used to simulate the ground acceleration since this option is the one available in ADINA.

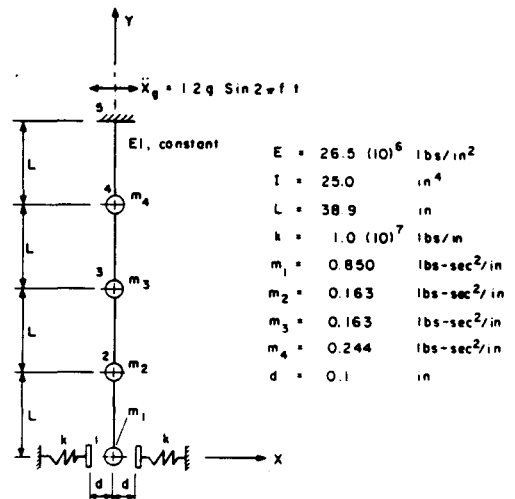
Two stops were placed at a distance $2d = 0.2$ in. apart to limit the tip deflection of the CRD housing. Nonlinear elastic springs were used to simulate the contact.

The following three methods of solution were compared: (1) direct integration without substructuring, (2) direct integration with the entire CRD housing as a substructure and the nonlinear springs as the master structure, and (3) mode superposition using 2 modes. A time increment of 0.001 sec and BFGS iterations were used for the direct integration solutions. The modified Newton iteration was used for the mode superposition solution, for which a smaller timestep, $\Delta t = 0.00035$ sec was needed for convergence.

A plot of the tip deflection versus time is shown in Fig. 3. The solid line is the solution from Ref. [8] in which a time increment of 0.0001 sec was used.

3.1.2 Piping example. A 1920 in. long pipe cantilevered at one end and supported at its midpoint and other end is modeled using 32 beam elements as shown in Fig. 4. The supports were modeled with nonlinear elastic-plastic springs with constants also given in the figure. The pipe was loaded by a sinusoidal mass proportional loading of 3 Hz.

Three analyses were carried out: (1) direct integration, no substructures, (2) direct integration with the pipe as a



A ground acceleration of

$$X_g = 1.2g \sin 2\pi ft$$

$$g = 386 \text{ in/sec}^2$$

$$f = 5 \text{ Hz}$$

Fig. 2. CRD housing with lower support.

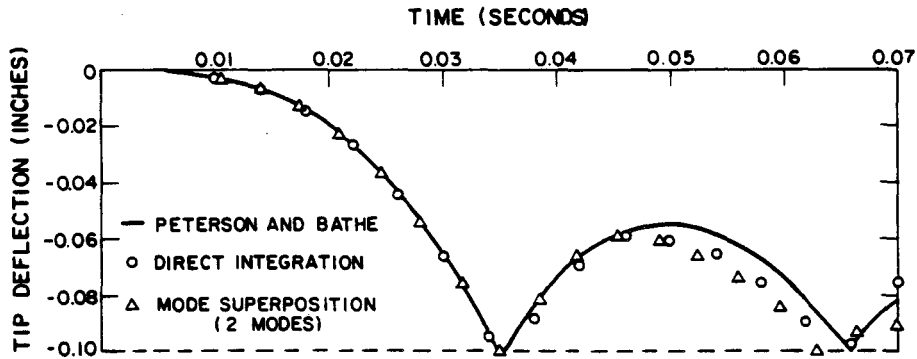
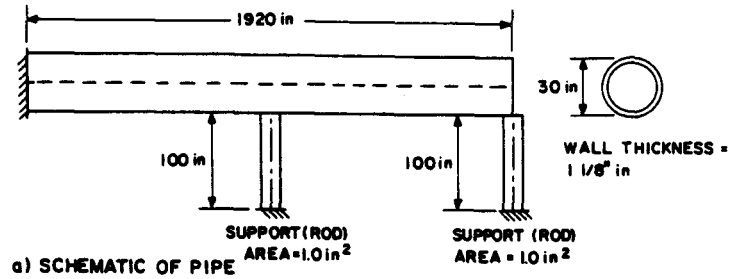
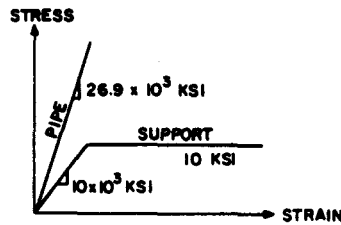


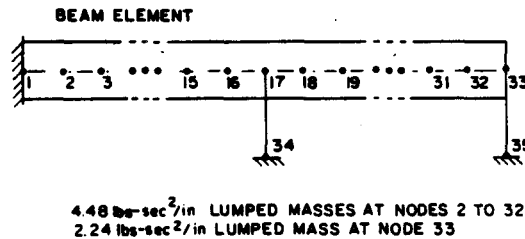
Fig. 3. CRD housing tip deflection.



a) SCHEMATIC OF PIPE



b) STRESS-STRAIN RELATIONS



c) FINITE ELEMENT MODEL

Fig. 4. Model of pipe with two elastic-plastic supports.

substructure and the two springs as the master structure and (3) mode superposition with 10 and 20 modes. All solutions were performed using equilibrium iterations and a time step of 0.004 sec.

Figure 5 shows a plot of the predicted midpoint displacement of the pipe as a function of time. As expected, the solution using substructuring gave the same results as the direct integration solution without substructuring (within the convergence tolerances of the iterations). The mode superposition solution approximates the peak displacement within an error of 10% when using 10 modes and is much more accurate with 20 modes.

3.1.3 Earthquake response of a tall building. A 34

story shear building was subjected to the North-South Component of the 1940 El Centro Earthquake times two. The finite element model consisted of 34 elastic-plastic truss elements whose masses static yield forces, and stiffness are given in Fig. 6. A similar building was analyzed by Lukkunaprasit *et al.* [9].

The solution algorithms used were direct time integration and mode superposition with 1, 4 and 8 modes. In all cases the time increment, Δt , was 0.02 sec. The solution was carried out for the first four seconds of the earthquake.

Figures 7-9 show predicted displacement responses in the solution, and Fig. 10 gives a displacement factor at

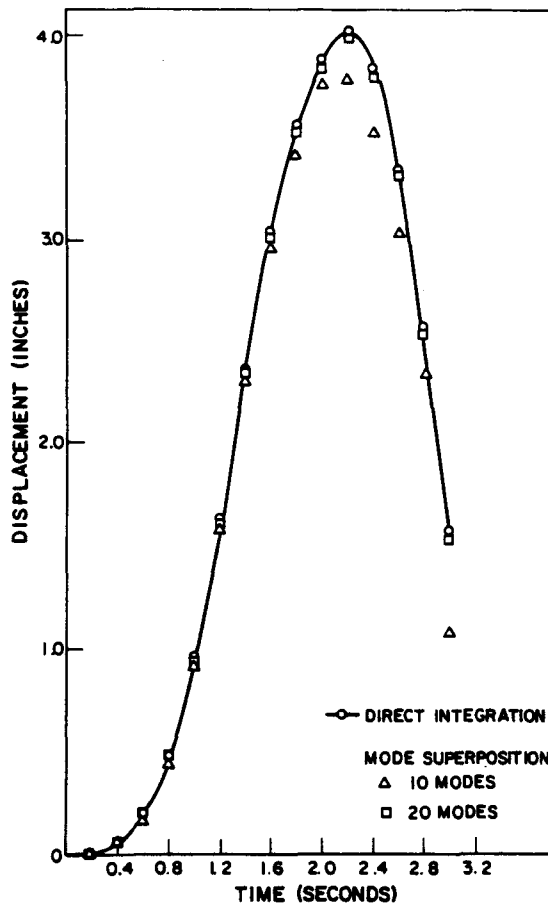


Fig. 5. Predicted midpoint displacement of pipe with two elastic-plastic supports.

$t = 2.8$ and 4 sec (this factor is defined as strain/(strain at initial yield point)). The response curves show that as the number of modes used is increased the response predicted in the direct integration is approached. Also, as expected, the displacements can be predicted accurately using less modes than are needed for an accurate prediction of the displacement factor, because this factor is given by the derivatives of the displacements.

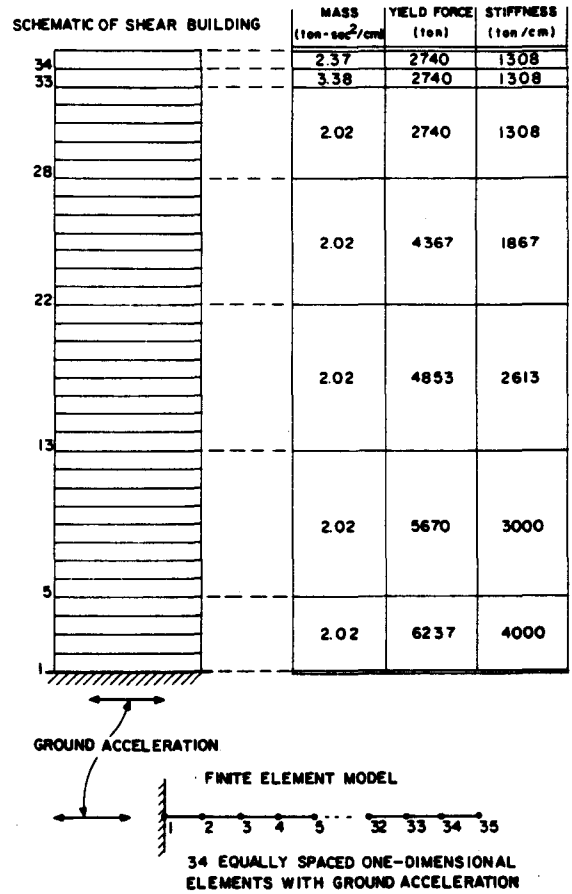


Fig. 6. Model of 34-story shear building.

3.2 Efficiencies of methods

In practical analysis it is important to be able to decide in a rational manner when to use the above mode superposition and substructuring procedures. For this reason we want to give some specific guidelines on the usage of the methods.

3.2.1 *Mode superposition.* The basic premise of the mode superposition procedure is that the transformation

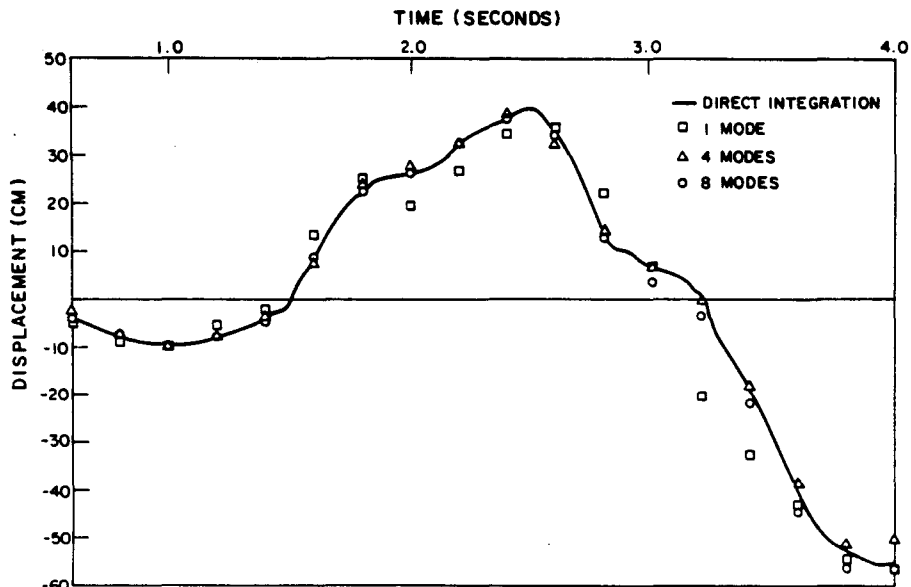


Fig. 7. Thirty-four story building—top story displacement history.

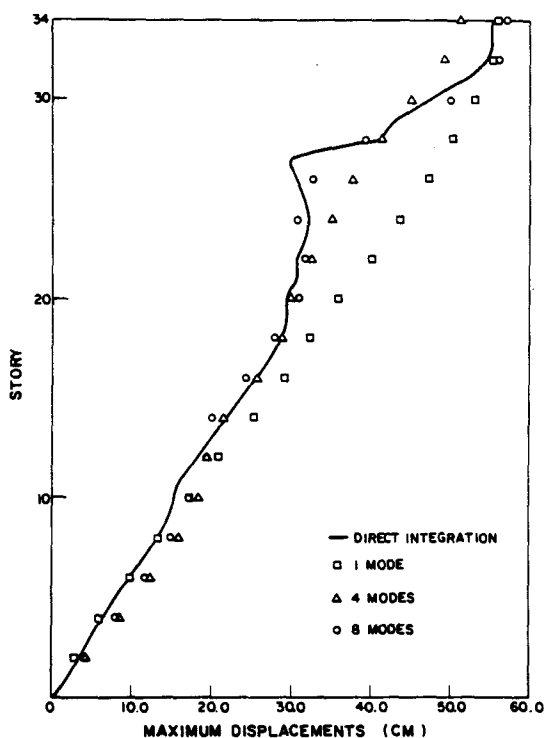


Fig. 8. Thirty-four story building—maximum displacements for each story.

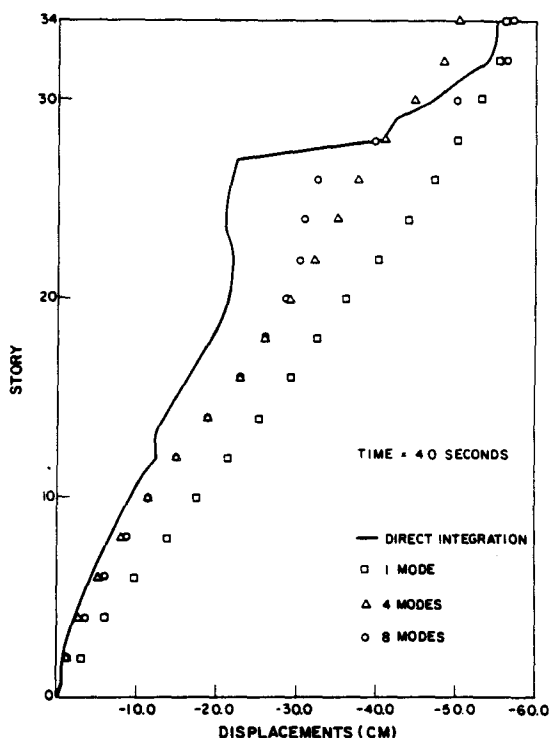


Fig. 9(b). Thirty-four story building—story displacements at time = 4.0 sec.

from the n finite element nodal point displacements to the p generalized displacements is effective because \hat{p} can be much smaller than n . In the analysis of a linear system, p would be equal to the number of frequencies ω_i smaller than about 4 times the highest excitation frequency in R . We can use this same guideline in the analysis of a nonlinear system, but should recognize that the actual (instantaneous) frequencies of the system are

continuously changing during the nonlinear response. If the system stiffens during the response history, the frequencies become larger and the number p selected based on a linear analysis will probably be conservative. However, in the analysis of a softening structure (elas-

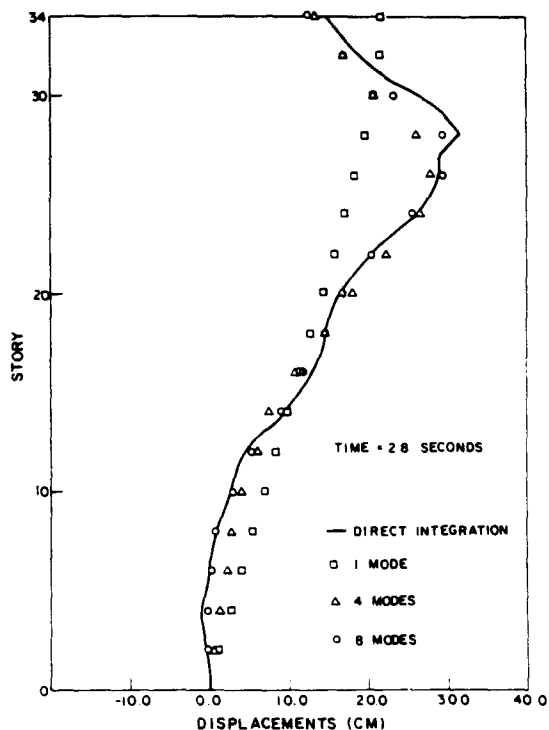


Fig. 9(a). Thirty-four story building—story displacements at time = 2.8 sec.

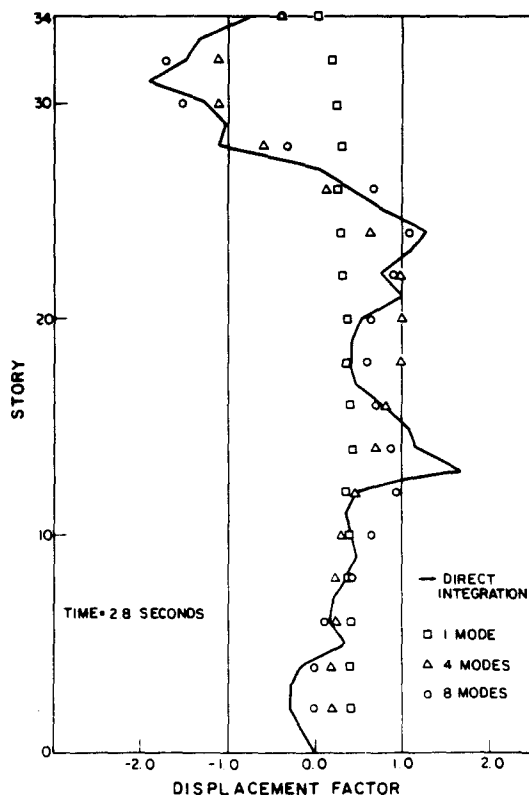


Fig. 10(a). Thirty-four story building—plot of displacement factor for each story at time = 2.8 sec (displacement factor = strain/initial yield strain).

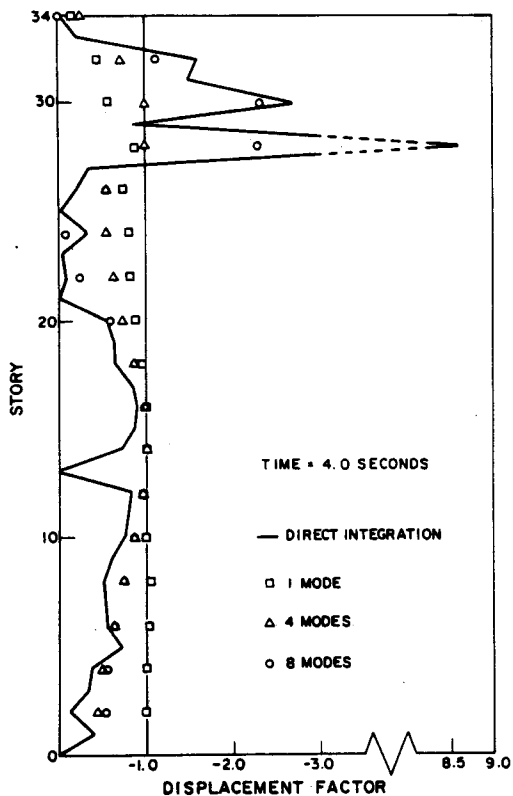


Fig. 10(b). Thirty-four story building—plot of displacement factor for each story at time = 4.0 sec. (displacement factor = strain/initial yield strain).

tic-plastic conditions), the number of generalized displacements may have to be considerably larger than in linear analysis.

Although we call the analysis procedure "mode superposition" it is appropriate to look at the method simply as a coordinate transformation. Hence, the number of transformation vectors to be employed must depend on the response expected in the analysis, and the accuracy of the predicted response depends entirely on the "quality" of the transformation vectors used. For this reason, the procedure is probably best employed in the analysis of only slightly nonlinear systems or systems with only local nonlinearities. In this case, the criteria that render a linear analysis by mode superposition effective are still largely applicable to the nonlinear response calculations.

We may also note that the mode superposition procedure may be effective in preliminary analyses of highly nonlinear systems provided these analyses allow somewhat less accuracy than a final response solution.

To assess the actual accuracy attained in a mode superposition analysis we may evaluate an error norm, similar to that one used in linear analysis,

$$\epsilon_p^{t+\Delta t} = \frac{\|{}^{t+\Delta t}\mathbf{R} - {}^{t+\Delta t}\mathbf{F}^{(l)} - \mathbf{M}^{t+\Delta t}\ddot{\mathbf{U}}^{(l)}\|_2}{\|\mathbf{R}\|_2^{(\max)}} \quad (27)$$

where (l) denotes the last calculated value, $\|\mathbf{a}\|_2$ denotes the Euclidean norm of \mathbf{a} , and $\|\mathbf{R}\|_2^{(\max)}$ is the maximum value reached over all discrete times τ . (The relation in eqn (27) assumes that the system is subjected to external loads; otherwise, the denominator must be modified.) If ϵ_p is unacceptably large, the number of mode shapes should be increased.

In another approach a static correction much as in

linear analysis may be applied, but the effectiveness of that correction is very problem-dependent[3].

3.2.2 Substructuring. The effectiveness of the substructuring procedure can be assessed by comparing the number of operations required in the solution of eqns (11) and (23). Considering these equations we find that the method is only effective when only local nonlinearities are considered. Let us assume the following system parameters: n, m = number of equations and their half-bandwidth in eqn (11), and n_r, m_r = number of equations and their half-bandwidth in eqn (23), $n_r \ll n$. To compare the number of operations performed in the solution of eqns (11) and (23) in an approximate manner, we recognize that the updating for the nonlinearities is the same in both equations, and we assume that the operations in vector multiplications can be neglected. In this case, an approximate operation count yields the following information:

lumped mass matrix

eqn (11): $4nm$ operations per equilibrium iteration
 eqn (23): $(2n_r m_r + 2nm_r)$ operations per first iteration
 $4n_r m_r$ operations per subsequent iteration.

consistent mass matrix

eqn (11): $6nm$ operations per equilibrium iteration
 eqn (23): $(2n_r m_r + 4nm_r)$ operations per first iteration
 $4n_r m_r$ operations per subsequent iteration.

The above operation count does not include the initial operations required to form \mathbf{K} , and the additional peripheral processing required in the substructuring solution.

When considering the above information, it is important to note that m_r may be significantly larger than m . It is for these reasons that for the substructuring algorithm to be effective we should have that $n_r m_r \ll nm$. The above information also shows that the substructuring algorithm is more likely to be effective when a lumped mass matrix is employed in the analysis.

CONCLUDING REMARKS

The objective in this paper was to discuss the mode superposition and substructuring procedures available in ADINA for analysis of nonlinear dynamic response. We have presented the theory used, the results of some sample solutions and some recommendations on the use of these analysis procedures. Although we have not employed the methods as yet in the actual solution of large dynamic problems, our discussion in the paper shows that the procedures can be very effective. We, therefore, look forward to hear about the experiences that users of ADINA might make with the procedures in the solution of actual practical problems.

Acknowledgements—We gratefully acknowledge the financial support of the ADINA users group.

REFERENCES

1. K. J. Bathe. Finite element formulation, modeling and solution of nonlinear dynamic problems. Chapter in *Numerical Methods for Partial Differential Equations*, (Edited by S. V. Parter). Academic Press, New York (1979).

2. K. J. Bathe, S. Bolourchi, S. Ramaswamy and M. D. Snyder, Some computational capabilities for nonlinear finite element analysis. *J. Nucl. Engng Design* **46**, 429-455 (1978).
3. K. J. Bathe, *Finite Element Procedures in Engineering Analysis*. Prentice Hall, Englewood Cliffs, New Jersey 1981.
4. R. E. Nickell, Nonlinear dynamics by mode superposition. *J. Comp. Meth. Appl. Mech. Engng* **7**, 107-129 (1976).
5. A. K. Noor, Recent advances in reduction methods for nonlinear problems. *J. Comput. Structures* **13**, 31-44 (1980).
6. R. W. Clough and E. L. Wilson, Dynamic analysis of large structural systems with local nonlinearities. *J. Comput. Meth. Appl. Mech. Engng* **17/18**, 107-129 (1979).
7. K. J. Bathe and A. P. Cimento, Some practical procedures for the solution of nonlinear finite element equations. *J. Comput. Meth. Appl. Mech. Engng* **22**, 59-85 (1980).
8. F. E. Peterson and K. J. Bathe, Nonlinear dynamic analysis of reactor core components. Engineering Analysis Corp., Rep. No. S-104.3, Berkeley, California (1972).
9. P. Lukkunaprasit, S. Widartawan and P. Karasudhi, Dynamic response of an elastic-viscoplastic system in modal coordinates. *Earthquake Engng Struct. Dyn.* **8**, 237-250 (1980).

APPENDIX A

The Newmark Algorithm

The basic assumptions in the Newmark time integration scheme are

$${}^{t+\Delta t}\dot{U} = {}^t\dot{U} + [(1-\delta){}^t\ddot{U} + \delta{}^{t+\Delta t}\ddot{U}] \Delta t$$

$${}^{t+\Delta t}U = {}^tU + {}^tU\Delta t + \left[\left(\frac{1}{2} - \alpha \right) {}^t\ddot{U} + \alpha {}^{t+\Delta t}\ddot{U} \right] (\Delta t)^2.$$

The following constants are used in ADINA with the time integration algorithm

$$a_0 = \frac{1}{(\alpha \Delta t^2)} \quad a_1 = \frac{\delta}{(\alpha \Delta t)} \quad a_2 = \frac{1}{(\alpha \Delta t)} \quad a_3 = \frac{1}{(2\alpha)} - 1$$

$$a_4 = \delta/\alpha - 1 \quad a_5 = \Delta t(\delta/\alpha - 2)/2 \quad a_6 = a_0 \quad a_7 = -a_2$$

$$a_8 = -a_3 \quad a_9 = \Delta t(1 - \delta) \quad a_{10} = \delta \Delta t.$$

Once the solution for ${}^{t+\Delta t}U$ has been obtained the corresponding accelerations and velocities are calculated using

$${}^{t+\Delta t}\ddot{U} = a_6({}^{t+\Delta t}U - {}^tU) + a_7{}^t\dot{U} + a_8{}^t\ddot{U}$$

$${}^{t+\Delta t}\dot{U} = {}^t\dot{U} + a_9{}^t\dot{U} + a_{10}{}^{t+\Delta t}\ddot{U}.$$

SOME PRACTICAL PROCEDURES FOR THE SOLUTION OF NONLINEAR FINITE ELEMENT EQUATIONS

Klaus-Jürgen BATHE and Arthur P. CIMENTO

*Department of Mechanical Engineering, Massachusetts Institute of Technology,
Cambridge, Massachusetts 02139, USA*

Received 21 March 1979

Procedures for the solution of incremental finite element equations in practical nonlinear analysis are described and evaluated. The methods discussed are employed in static analysis and in dynamic analysis using implicit time integration. The solution procedures are implemented, and practical guidelines for their use are given.

1. Introduction

During recent years the nonlinear finite element analysis of static and dynamic problems has been an area of growing interest in engineering. Various finite element computer programs are currently in use for the analyses of complex nonlinear problems [1]. Basically, these analyses involve three steps: the selection of a representative finite element model, the analysis of the model and the interpretation of the results. Surely, in engineering practice the selection of an appropriate finite element model and the corresponding interpretation of the results are crucial, but a reliable and accurate response prediction of the model is essential in order that the analysis results can be used with confidence.

Unfortunately, considering the present nonlinear analysis procedures, the accurate analysis of a finite element model can present very great difficulties. The cost of analysis can be high, but a more serious factor is that considerable knowledge and judgment by the user may be required to assure a stable and accurate solution. Hence, there is a great need for solution algorithms with increased accuracy and stability properties.

In general, a nonlinear static and dynamic finite element analysis is most effectively performed using an incremental formulation, in which the static and kinematic variables are updated incrementally corresponding to successive load steps (or time steps in dynamics) in order to trace out the complete solution path [1]–[8]. In this solution it is important that the governing finite element equations are satisfied in each load step to sufficient accuracy because otherwise solution errors can accumulate that can lead to gross and undetectable errors and even to solution instabilities [2]–[11].

An accurate solution of the nonlinear finite element equations can always be expected if the load increments per step are made sufficiently small, but such a solution can result in many incremental steps that render the analysis of a large finite element system prohibitively

expensive. In order to solve the nonlinear finite element equations efficiently while maintaining control on the accuracy of the solution, larger load steps may need to be employed with iteration that assures the accurate solution of the nonlinear equations. However, the use of iteration can introduce some other difficulties. The convergence process may be slow, requiring a large number of iterations that can again result in a high solution cost. Also, some iterative methods do not converge for certain types of problems or for large load increments. In practice, such difficulties can result in costly numerical experimentations, which inhibit the wide use of nonlinear finite element analysis.

The objective of this paper is to report on what we believe at present to be some effective, practical procedures for the incremental solution of nonlinear finite element equations. We assume that a solution exists with finite solution variables to the nonlinear problem which is analyzed, and if there are multiple solutions (e.g. because of limit and bifurcation points), all that the calculation can yield is "a" solution in the multidimensional solution space. Considering dynamic analysis, we also assume that an implicit time integration scheme and a time step Δt have already been selected, and we only consider the accurate solution of the timewise discretized equilibrium equations. Since these equations are linear in explicit time integration (e.g. using the central difference method [8], [16]), we are only concerned with implicit integration of dynamic response.

We first briefly summarize the general analysis approach employed and the incremental finite element equations that need to be solved. We consider static analysis and dynamic analysis using the trapezoidal rule for the time integration. We then describe the procedures that are the most promising candidates for the iterative solution of the incremental equilibrium equations: (a) modified Newton iteration with Aitken acceleration and a divergence procedure and (b) the Broyden-Fletcher-Goldfarb-Shanno (BFGS) method [12]–[15]. Next we discuss the importance of using appropriate convergence criteria to stop the iteration, and we propose specific ways to measure convergence. The iterative schemes have been implemented in the ADINA computer program, and finally, we give the results of some demonstrative sample solutions. These results illustrate the relative effectiveness of the solution techniques employed and, together with additional experiences, lead to the presentation of some practical guidelines for the selection of the appropriate solution scheme corresponding to a specific nonlinear analysis.

2. Incremental finite element equations

As already mentioned in the previous section, a general geometric and material nonlinear finite element analysis is performed most effectively by use of an incremental formulation of the equations of motion.

In the notation of [4]–[8] the incremental finite element equations that govern the response of the finite element system in static analysis are

$${}^t\mathbf{K}\mathbf{U} = {}^{t+\Delta t}\mathbf{R} - {}^t\mathbf{F} \quad (1)$$

where ${}^t\mathbf{K}$ = tangent stiffness matrix corresponding to the configuration of the system at time t ; \mathbf{U} = vector of nodal point incremental displacements, i.e. $\mathbf{U} = {}^{t+\Delta t}\mathbf{U} - {}^t\mathbf{U}$; ${}^{t+\Delta t}\mathbf{R}$ = vector of

externally applied nodal point loads corresponding to time $t + \Delta t$; and $'F$ = vector of nodal point forces corresponding to the internal element stresses at time t .

As indicated in eq. (1) and illustrated in fig. 1, we use the discrete time increment Δt to denote a load increment. If the material properties are time-dependent (such as in creep analysis), the time increments must be chosen judiciously for stability and accuracy; otherwise, the discrete time points considered simply denote the load levels.

With reference to fig. 1 it should also be noted that the time step magnitudes need not be identical throughout the incremental analysis; indeed, a variation of the time step magnitudes can be particularly effective in the calculation of creep response.

Considering now dynamic analysis using implicit time integration, the governing incremental finite element equations of motion are

$$'KU = {}^{t+\Delta t}R - 'F - M {}^{t+\Delta t}\ddot{U}, \quad (2)$$

where the variables of eq. (1) are used and M = mass matrix, and ${}^{t+\Delta t}\ddot{U}$ = vector of nodal point accelerations corresponding to time $t + \Delta t$.

In eq. (2) we did not include damping effects expressed by a damping matrix times the nodal point velocities, but this effect could easily be included in an analogous manner to the inertia effects, provided the damping matrix can be constructed [16].

Various implicit time integration methods are presently in use. We consider here the trapezoidal rule because of its relatively good stability and accuracy characteristics [9]–[11], [17], but other integration schemes would be employed in an analogous manner. The basic assumptions of the trapezoidal rule are

$${}^{t+\Delta t}\dot{U} = '\dot{U} + \frac{\Delta t}{2} ({}^{t+\Delta t}\ddot{U} + '\ddot{U})$$

and

$${}^{t+\Delta t}U = 'U + \frac{\Delta t}{2} ({}^{t+\Delta t}\dot{U} + '\dot{U}). \quad (3)$$

Using eqs. (3) and the relation $U = {}^{t+\Delta t}U - 'U$, eq. (2) gives

$$\left('K + \frac{4}{(\Delta t)^2} M \right) U = {}^{t+\Delta t}R - 'F + M \left(\frac{4}{\Delta t} '\dot{U} + '\ddot{U} \right). \quad (4)$$

Eq. (4) is solved recursively for all time steps, where, as in static analysis, the time step increments can vary during the incremental solution.

Eqs. (1) and (2) are derived by linearizing the system response about the configuration at time t . It was repeatedly pointed out that the errors in this linearization can be expected to be small provided the load increments or time steps are small enough. However, in general, because of cost considerations an analyst must endeavor to employ as large load and time steps as possible, and in such a case the errors resulting from the linearization may not be negligible, and their accumulation can lead to gross errors or instability of the solution. The

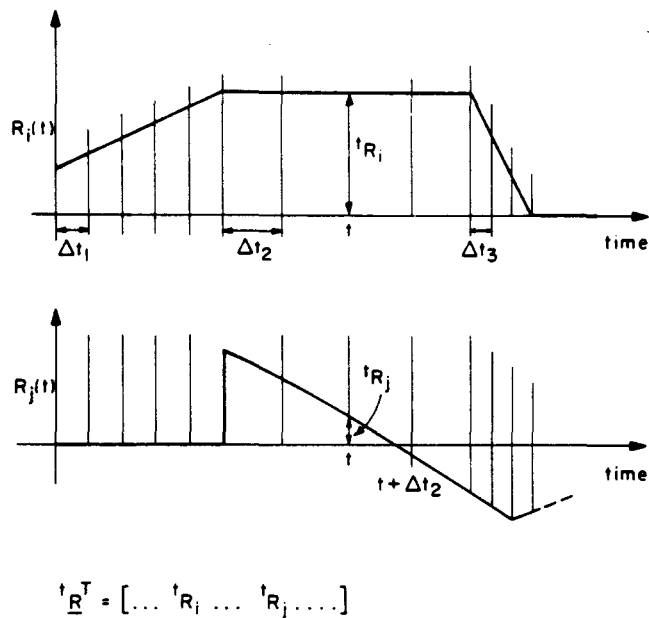


Fig. 1. Evaluation of externally applied nodal point load vector ${}^t\mathbf{R}$ at time t .

accumulation of the solution errors can be particularly serious in dynamic analysis, where relatively small increments in errors at the individual discrete time points can rapidly cause a solution instability [5], [18]. As concluded earlier, when larger load steps or time steps are used, iteration for system equilibrium at the discrete time points is necessary although the accurate solution of the timewise discretized equilibrium equations does not strictly always imply a stable solution [10], [17]. Since the analyst does not generally know whether the load or time step chosen is "small" or "large", based on accuracy considerations alone, iteration in the solution of the system equilibrium equations is desirable at all load or time steps. This iteration should be as cost-effective as possible; i.e. rapid convergence should occur with the total number of numerical operations required in the iteration as small as possible.

3. Iteration procedures for solution of equilibrium equations

The basic equations to be solved in nonlinear analysis are (corresponding to time $t + \Delta t$)

$${}^{t+\Delta t}\bar{\mathbf{R}}(\mathbf{U}^*) - {}^{t+\Delta t}\mathbf{F}(\mathbf{U}^*) = \mathbf{o}, \quad (5)$$

where

$${}^{t+\Delta t}\bar{\mathbf{R}}(\mathbf{U}^*) = {}^{t+\Delta t}\mathbf{R} - \mathbf{M}{}^{t+\Delta t}\ddot{\mathbf{U}}^*. \quad (6)$$

Eq. (5) holds for the dynamic analysis considered in eq. (2), and for the static analysis considered in eq. (1) if the mass effects are neglected. Also, if the load or time increments are small, eqs. (1) and (2) yield an approximate solution to eq. (5). However, we now consider

large load and time increments where we need to solve eq. (5) by iteration—note then that the first iteration in the equations below reduces to the solutions of eqs. (1) and (2).

3.1. The Newton–Raphson iteration

The most frequently used iteration schemes for the solution of nonlinear finite element equations are some form of Newton–Raphson iteration [2]–[7], [19]. The equilibrium requirements amount to finding the solution of the equations

$$f(\mathbf{U}^*) = \mathbf{o}, \quad (7)$$

where

$$f(\mathbf{U}^*) = {}^{t+\Delta t}\tilde{\mathbf{R}}(\mathbf{U}^*) - {}^{t+\Delta t}\mathbf{F}(\mathbf{U}^*). \quad (8)$$

A Taylor series expansion of $f(\mathbf{U}^*)$ about the solution \mathbf{U}^* gives

$$f(\mathbf{U}^*) = f({}^{t+\Delta t}\mathbf{U}^{(i-1)}) + \left[\frac{\partial f}{\partial \mathbf{U}} \Big|_{{}^{t+\Delta t}\mathbf{U}^{(i-1)}} \right] (\mathbf{U}^* - {}^{t+\Delta t}\mathbf{U}^{(i-1)}), \quad (9)$$

where higher-order terms are neglected, and the superscript $(i-1)$ is used to denote the $(i-1)$ st approximation to the solution vector \mathbf{U}^* . Substituting from eq. (8) into eq. (9) and using the condition in eq. (7), we obtain

$${}^{t+\Delta t}\tilde{\mathbf{R}}^{(i-1)} - {}^{t+\Delta t}\mathbf{F}^{(i-1)} + \left[\frac{\partial \tilde{\mathbf{R}}}{\partial \mathbf{U}} \Big|_{{}^{t+\Delta t}\mathbf{U}^{(i-1)}} - \frac{\partial \mathbf{F}}{\partial \mathbf{U}} \Big|_{{}^{t+\Delta t}\mathbf{U}^{(i-1)}} \right] (\mathbf{U}^* - {}^{t+\Delta t}\mathbf{U}^{(i-1)}) = \mathbf{o}, \quad (10)$$

where

$${}^{t+\Delta t}\tilde{\mathbf{R}}^{(i-1)} = {}^{t+\Delta t}\mathbf{R} - \mathbf{M} {}^{t+\Delta t}\ddot{\mathbf{U}}^{(i-1)}. \quad (11)$$

We now define

$$\Delta \mathbf{U}^{(i)} = \mathbf{U}^* - {}^{t+\Delta t}\mathbf{U}^{(i-1)} \quad (12)$$

and recognize that

$$\frac{\partial \mathbf{F}}{\partial \mathbf{U}} \Big|_{{}^{t+\Delta t}\mathbf{U}^{(i-1)}} = {}^{t+\Delta t}\mathbf{K}^{(i-1)}, \quad (13)$$

where ${}^{t+\Delta t}\mathbf{K}^{(i-1)}$ is the tangent stiffness matrix in iteration $i-1$. Also, using the trapezoidal rule for time integration, we have

$$\frac{\partial \tilde{\mathbf{R}}}{\partial \mathbf{U}} \Big|_{{}^{t+\Delta t}\mathbf{U}^{(i-1)}} = -\frac{4}{(\Delta t)^2} \mathbf{M}. \quad (14)$$

Thus eq. (10) yields

$${}^{t+\Delta t}\hat{\mathbf{K}}^{(i-1)}\Delta\mathbf{U}^{(i)} = {}^{t+\Delta t}\mathbf{R} - {}^{t+\Delta t}\mathbf{F}^{(i-1)} - \mathbf{M}\left\{\frac{4}{(\Delta t)^2}({}^{t+\Delta t}\mathbf{U}^{(i-1)} - {}^t\mathbf{U}) - \frac{4}{\Delta t}{}^t\dot{\mathbf{U}} - {}^t\ddot{\mathbf{U}}\right\}, \quad (15)$$

where

$${}^{t+\Delta t}\hat{\mathbf{K}}^{(i-1)} = {}^{t+\Delta t}\mathbf{K}^{(i-1)} + \frac{4}{(\Delta t)^2}\mathbf{M}. \quad (16)$$

Since eq. (10) represents only a Taylor series approximation to \mathbf{U}^* , the displacement increment correction is used to obtain the next displacement approximation

$${}^{t+\Delta t}\mathbf{U}^{(i)} = {}^{t+\Delta t}\mathbf{U}^{(i-1)} + \Delta\mathbf{U}^{(i)}. \quad (17)$$

Eqs. (15) and (17) constitute the Newton–Raphson solution of eq. (5), with the initial conditions

$${}^{t+\Delta t}\hat{\mathbf{K}}^{(0)} = {}^t\hat{\mathbf{K}}, \quad {}^{t+\Delta t}\mathbf{F}^{(0)} = {}^t\mathbf{F} \quad \text{and} \quad {}^{t+\Delta t}\mathbf{U}^{(0)} = {}^t\mathbf{U}.$$

The iteration using eqs. (15) and (17) continues until appropriate termination criteria are satisfied (see section 4).

Although the use of the full Newton iteration of eqs. (15)–(17) can be efficient in some specific nonlinear analyses, the use of the method is generally not very effective in general geometric and material nonlinear response calculations. Considering the updating and factorizing of the effective stiffness matrix ${}^{t+\Delta t}\hat{\mathbf{K}}^{(i-1)}$ in each iteration, this process is computationally expensive and, for solution effectiveness, requires the use of relatively large load increments. However, in material nonlinear analysis or dynamic nonlinear response calculations the load (or time) steps that can be employed are restricted in size by other stability and accuracy considerations [5]–[11]. For example, in elastic-plastic analysis, proportional loading (unloading) is generally assumed during a load step, which therefore has to be reasonably small. Also, inaccurate approximations to the displacements during the iteration can introduce significant errors because the material properties depend on the history of the stresses and strains. For these reasons some modification of the full Newton algorithm is generally effective.

One such modification is to use the initial stiffness matrix ${}^0\hat{\mathbf{K}}$ in eq. (15) and thus operate on the equations

$${}^0\hat{\mathbf{K}}\Delta\mathbf{U}^{(i)} = {}^{t+\Delta t}\tilde{\mathbf{R}}^{(i-1)} - {}^{t+\Delta t}\mathbf{F}^{(i-1)}. \quad (18)$$

In eq. (18) only the matrix ${}^0\hat{\mathbf{K}}$ need be factorized; thus the expense of recalculating and factorizing the coefficient matrix in eq. (15) many times is avoided. This “initial stress” method corresponds to a linearization of the response about the initial configuration of the finite element system. For problems with significant nonlinearities, and in particular when the system stiffens during the response, this linearization can lead to a very slow convergence in

the iteration, or the iteration may even diverge. In order to accelerate the convergence and prevent divergence of the solution for slowly stiffening problems (see discussion below), it may be effective to use the modified Newton–Raphson iteration. In this method we calculate from time to time a new tangent stiffness matrix and operate on the equations

$$\tau \hat{K} \Delta U^{(i)} = {}^{t+\Delta t} \tilde{R}^{(i-1)} - {}^{t+\Delta t} F^{(i-1)}, \quad (19)$$

where τ corresponds to one of the accepted equilibrium configurations at times $0, \Delta t, 2\Delta t, \dots$ or t . In eq. (19) the vector ${}^{t+\Delta t} F^{(i-1)}$ is evaluated from the stresses that correspond to time $t + \Delta t$ and iteration $i - 1$. Considering a point within a finite element, this stress evaluation can be written as

$${}^{t+\Delta t} \sigma^{(i-1)} = {}^t \sigma + \int_{{}^t \epsilon}^{{}^{t+\Delta t} \epsilon^{(i-1)}} C d\epsilon, \quad (20)$$

where ${}^t \sigma$ are the stresses corresponding to the last accepted equilibrium configuration, ϵ denotes the strains at time t , and C is the stress-strain matrix of the material, which in general is not constant during the integration. It is important in eq. (20) that the integration always be performed from the last *accepted* or *converged* strains to the presently calculated strains. Thus the final converged results are not affected by the errors in the displacements and strains that were encountered during the iteration.

The modified Newton method involves fewer stiffness reformations than full Newton iteration, and the stiffness matrix update is based on an accepted equilibrium configuration. The choice of time steps when the stiffness matrix should be updated depends on the degree of nonlinearity in the system response, i.e. the more nonlinear the response, the more often the updating should be done. Without any a priori knowledge of the system behavior it may be most efficient to update the stiffness at the start of every time step, in which case $\tau = t$ in eq. (19).

3.2. *Slow convergence and divergence of modified Newton iteration*

In its application to nonlinear structural analysis the modified Newton method presents practical difficulties. The two problems of slow convergence and divergence are most frequently encountered.

A large number of iterations will be required for convergence when there is a sudden softening in the system during a time increment. Fig. 2 illustrates this phenomenon for a one-dimensional case. Such a force-displacement relationship is typical of an elastic-plastic material, where ${}^{t+\Delta t} K/K = E_T/E$. As this ratio tends to zero and/or the load increment ${}^{t+\Delta t} R - {}^t F$ becomes large, the number of iterations required for convergence becomes very large. In practice, where some limit is placed on the number of iterations that can be used, the solution would terminate too early. In order to make the modified Newton method effective in cases of slow convergence, some acceleration scheme should be employed.

A commonly used acceleration scheme is the one employed by Aitken for eigenvalue problems [20]. With Aitken acceleration eq. (17) becomes

$${}^{t+\Delta t} U^{(i)} = {}^{t+\Delta t} U^{(i-1)} + \alpha^{(i-1)} \Delta U^{(i)} \quad (21)$$

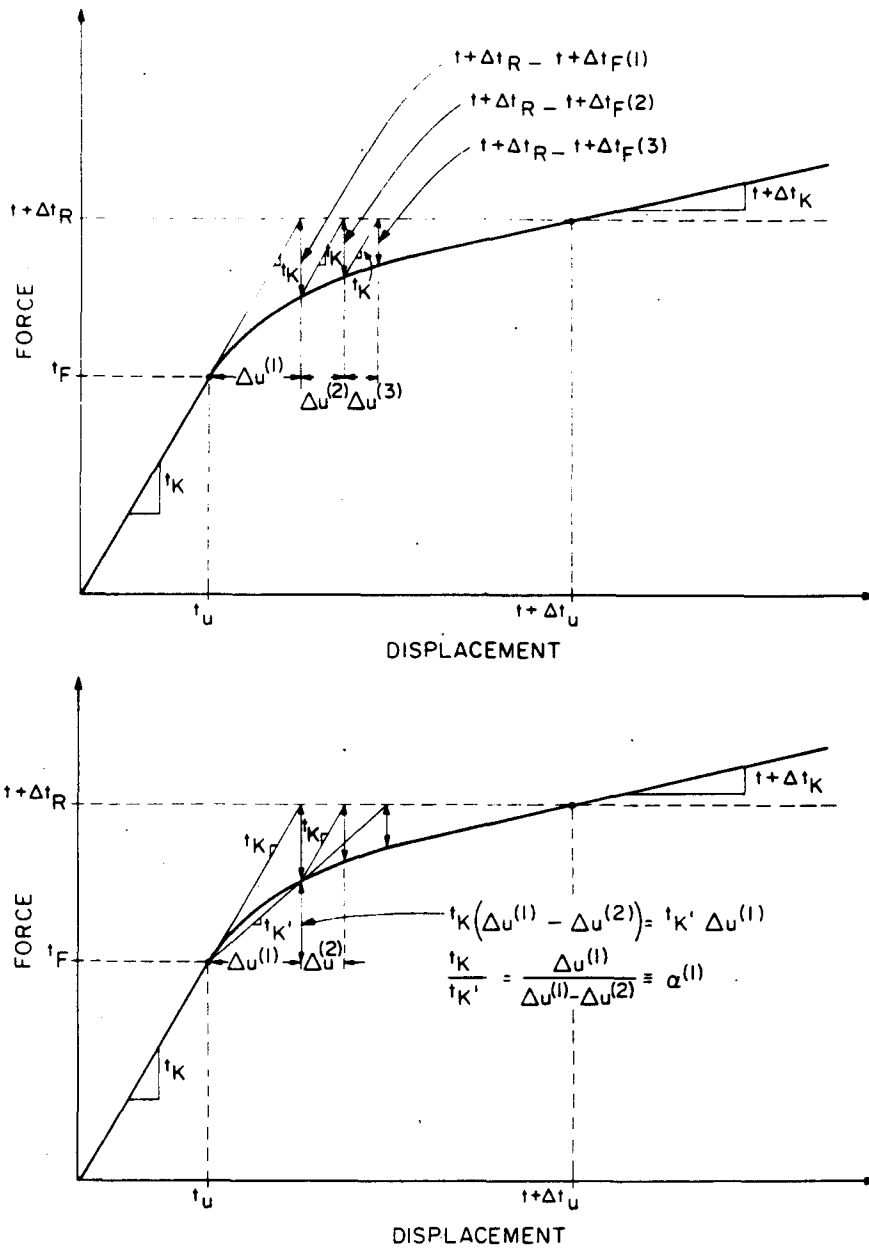


Fig. 2. Slow convergence and acceleration of the modified Newton iteration in a one-dimensional example.

where $\alpha^{(i-1)}$ is an $n \times n$ diagonal coefficient matrix containing the acceleration factors, and n is the number of degrees of freedom in the system. The acceleration factor for each degree of freedom is given by

$$\alpha_i^{(i-1)} = \frac{\Delta U_i^{(i-1)}}{(\Delta U_i^{(i-1)} - \Delta U_i^{(i)})} \tag{22}$$

As shown in fig. 2, the accelerator gives an estimate of the ratio 'K/K'' based on the information obtained in the iteration.

Difficulties with Aitken acceleration can arise when the denominator in eq. (22) is small for some degrees of freedom. Also, since the accelerator estimates the ratio of the original tangent stiffness to the local secant stiffness using the difference between successive out-of-balance load terms (see fig. 2), Aitken acceleration can only be applied every other iteration to avoid inaccurate estimates of this ratio. To circumvent these problems, modifications of Aitken's accelerator have been developed [21], [22], but for a general analysis it has not been demonstrated that these versions accelerate convergence any better than the original Aitken method.

Another difficulty with modified Newton iteration arises when the out-of-balance loads ${}^{t+\Delta t}\bar{\mathbf{R}}^{(i)} - {}^{t+\Delta t}\mathbf{F}^{(i)}$ increase during the solution, thus signalling divergence from the solution. Iteration divergence can occur whenever the system stiffens during the solution increment.

Two types of stiffening should be distinguished. Slow stiffening, illustrated by curve I in fig. 3, can typically occur when geometric nonlinearities are included in the analysis. In these cases, choosing a smaller load increment so that the linearization about time t yields a close enough approximation to the stiffness matrix at time $t + \Delta t$ is sufficient to obtain convergence. Sudden stiffening, illustrated by curve II in fig. 3, can occur when unloading of a nonlinear material (e.g. elastic-plastic material) is predicted in the solution. In this case the solution converges in dynamic analysis provided the time step Δt is small enough [12], but in static analysis a smaller load step is not sufficient to obtain convergence [7]. In static analysis the stiffness matrix needs to be reformed based on the elastic material properties at time t , and this stiffness matrix must be employed in the solution of eq. (19).

Using the above concept, the following divergence scheme has been incorporated into the modified Newton-Raphson iteration in static analysis. When divergence is detected (see section 4 for the termination criterion), the iteration is halted, and an elastic stiffness matrix, \mathbf{K}^E based on the geometry at time t , is calculated to handle problems involving sudden stiffening. The load increment is also scaled by a factor λ_1 ($\lambda_1 \leq 1$) to handle divergence due to additional slow stiffening; thus eq. (19) is modified to

$$\mathbf{K}^E \Delta \mathbf{U}^{(i)} = {}^{t+\Delta t}\mathbf{R} - {}^{t+\lambda_1 \Delta t}\mathbf{F}^{(i-1)} - (1 - \lambda_1)({}^{t+\Delta t}\mathbf{R} - \mathbf{F}), \quad (23)$$

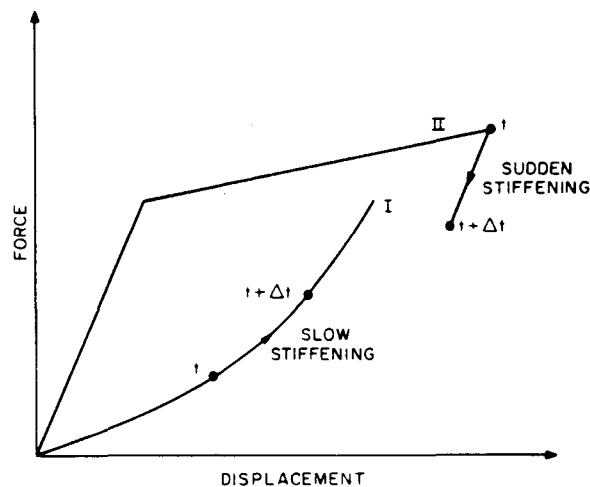


Fig. 3. Force-displacement relations leading to divergence in the modified Newton iteration.

and we iterate until the solution at the intermediate time $t + \lambda_1 \Delta t$ is determined. If divergence is still detected, λ_1 is continually chosen to be some smaller value until convergence is obtained (with some lower limit on λ_1 specified). After a solution has been obtained, a second factor λ_2 is chosen, the stiffness matrix is re-formed about the configuration at time $t + \lambda_1 \Delta t$, and the displacements at time $t + (\lambda_1 + \lambda_2) \Delta t$ are found in an analogous manner. This solution continues until

$$\sum_{k=1}^m \lambda_k = 1, \quad (24)$$

with some upper limit imposed on m .

The selection of λ_k in this procedure is based on the number of iterations required for convergence with λ_{k-1} . The initial estimate of λ_1 is taken as 0.5 to minimize the number of intermediate solutions if elastic unloading is present and re-forming the stiffness is all that is necessary to obtain convergence. Thereafter, λ_k is set to 0.5 for rapid convergence (less than 4 iterations were used for convergence), 0.25 for moderately fast convergence (4 to 12 iterations), and 0.0625 for slow convergence (more than 12 iterations). In the case of rapid convergence the stiffness matrix is not re-formed for the next intermediate solution. Although the step size selection procedure is empirical, the method is rational, and its effectiveness has been demonstrated in a large number of analyses. A more theoretical approach toward an adaptive step-size selection based on the convergence rate of a full Newton iteration scheme has been proposed by Schmidt [23], but when applied to the modified Newton method it was found to be less effective than the simple procedure outlined above. As another mechanism the current stiffness parameter discussed in [24] may also be useful in establishing an automatic load incrementation scheme. Our divergence procedure does not guarantee convergence because an incremental load step in the scheme may still be too large, but the procedure does attempt to correct the more common reasons for divergence of the modified Newton iteration.

3.3. Matrix updating iterative methods

As an alternative to forms of Newton iteration, a class of methods known as matrix update methods or quasi-Newton methods have been developed for iteration on nonlinear systems of equations. These methods involve updating the coefficient matrix (or rather its inverse) to provide a secant approximation to the matrix from iteration $i - 1$ to i . That is, if we define a displacement increment

$$\delta^{(i)} = {}^{t+\Delta t} \mathbf{U}^{(i)} - {}^{t+\Delta t} \mathbf{U}^{(i-1)} \quad (25)$$

and an increment in the out-of-balance loads

$$\gamma^{(i)} = ({}^{t+\Delta t} \bar{\mathbf{R}}^{(i-1)} - {}^{t+\Delta t} \mathbf{F}^{(i-1)}) - ({}^{t+\Delta t} \bar{\mathbf{R}}^{(i)} - {}^{t+\Delta t} \mathbf{F}^{(i)}), \quad (26)$$

then the updated matrix ${}^{t+\Delta t} \hat{\mathbf{K}}^{(i)}$ should satisfy the quasi-Newton equation (see [13])

$${}^{t+\Delta t} \hat{\mathbf{K}}^{(i)} \delta^{(i)} = \gamma^{(i)}. \quad (27)$$

These quasi-Newton methods provide a compromise between the full re-formation of the stiffness matrix performed in the full Newton method and the use of a stiffness matrix from a previous configuration as is done in the modified Newton method. Among the quasi-Newton methods available the BFGS (Broyden–Fletcher–Goldfarb–Shanno) method appears to be most effective [13]–[15] and was recently proposed for finite element analysis by Matthies and Strang [15].

In the BFGS method the following procedure is employed in iteration i to evaluate ${}^{t+\Delta t}\mathbf{U}^{(i)}$ and ${}^{t+\Delta t}\hat{\mathbf{K}}^{(i)}$, where ${}^{t+\Delta t}\hat{\mathbf{K}}^{(0)} = {}^t\hat{\mathbf{K}}$.

Step 1. Evaluate a displacement vector increment

$$\Delta\bar{\mathbf{U}} = ({}^{t+\Delta t}\hat{\mathbf{K}}^{-1})^{(i-1)} ({}^{t+\Delta t}\hat{\mathbf{R}}^{(i-1)} - {}^{t+\Delta t}\mathbf{F}^{(i-1)}). \quad (28)$$

This displacement vector defines a “direction” for the actual displacement increment.

Step 2. Perform a line search in the direction $\Delta\bar{\mathbf{U}}$ to satisfy “equilibrium” in this direction. In this line search we evaluate the displacement vector

$${}^{t+\Delta t}\mathbf{U}^{(i)} = {}^{t+\Delta t}\mathbf{U}^{(i-1)} + \beta\Delta\bar{\mathbf{U}}, \quad (29)$$

where β is a scalar multiplier, and we calculate the out-of-balance loads ${}^{t+\Delta t}\hat{\mathbf{R}}^{(i)} - {}^{t+\Delta t}\mathbf{F}^{(i)}$ corresponding to these displacements. The parameter β is varied until the component of the out-of-balance loads in the direction $\Delta\bar{\mathbf{U}}$ as defined by the inner product $\Delta\bar{\mathbf{U}}^t ({}^{t+\Delta t}\hat{\mathbf{R}}^{(i)} - {}^{t+\Delta t}\mathbf{F}^{(i)})$ is approximately zero. This condition is satisfied when the following equation is satisfied for a convergence tolerance STOL:

$$\Delta\bar{\mathbf{U}}^t ({}^{t+\Delta t}\hat{\mathbf{R}}^{(i)} - {}^{t+\Delta t}\mathbf{F}^{(i)}) \leq \text{STOL} \Delta\bar{\mathbf{U}}^t ({}^{t+\Delta t}\hat{\mathbf{R}}^{(i-1)} - {}^{t+\Delta t}\mathbf{F}^{(i-1)}). \quad (30)$$

The final value of β for which eq. (30) is satisfied determines ${}^{t+\Delta t}\mathbf{U}^{(i)}$ using eq. (29). We can now calculate $\delta^{(i)}$ and $\gamma^{(i)}$ from eqs. (25) and (26) and proceed with the evaluation of the matrix update that satisfies eq. (27).

Step 3. Evaluate the correction to the coefficient matrix. In the BFGS method the updated matrix can be expressed in product form (see [25]):

$$({}^{t+\Delta t}\hat{\mathbf{K}}^{-1})^{(i)} = \mathbf{A}^{(i)t} ({}^{t+\Delta t}\hat{\mathbf{K}}^{-1})^{(i-1)} \mathbf{A}^{(i)}, \quad (31)$$

where the matrix $\mathbf{A}^{(i)}$ is an $n \times n$ matrix of the simple form

$$\mathbf{A}^{(i)} = \mathbf{I} + \mathbf{v}^{(i)}\mathbf{w}^{(i)t}. \quad (32)$$

The vectors $\mathbf{v}^{(i)}$ and $\mathbf{w}^{(i)}$ are calculated from the known nodal point forces and displacements:

$$\mathbf{v}^{(i)} = - \left[\frac{\delta^{(i)t} \gamma^{(i)}}{\delta^{(i)t} {}^{t+\Delta t}\hat{\mathbf{K}}^{(i-1)} \delta^{(i)}} \right]^{1/2} {}^{t+\Delta t}\mathbf{K}^{(i-1)} \delta^{(i)} - \gamma^{(i)} \quad (33)$$

and

$$\mathbf{w}^{(i)} = \frac{\boldsymbol{\delta}^{(i)}}{\boldsymbol{\delta}^{(i)T} \boldsymbol{\gamma}^{(i)}} \tag{34}$$

The vector ${}^{t+\Delta t} \hat{\mathbf{K}}^{(i-1)} \boldsymbol{\delta}^{(i)}$ in eq. (33) is equal to $\beta[{}^{t+\Delta t} \hat{\mathbf{R}}^{(i-1)} - {}^{t+\Delta t} \mathbf{F}^{(i-1)}]$ and was already computed.

It has been shown that the product defined in eq. (31) is positive definite and symmetric [15]. To avoid numerically dangerous updates, the condition number of the updating matrix $\mathbf{A}^{(i)}$ must be compared with some preset tolerance, and the updating is not performed if the condition number exceeds this tolerance. The eigenvalues of the matrix $\mathbf{I} + \mathbf{v}\mathbf{w}^T$ are $\lambda = 1$ (with multiplicity $n - 1$) and $\lambda = 1 + \mathbf{v}^T \mathbf{w}$. The condition number $c^{(i)}$ is therefore given by

$$c^{(i)} = \left[\frac{\boldsymbol{\delta}^{(i)T} \boldsymbol{\gamma}^{(i)}}{\boldsymbol{\delta}^{(i)T} {}^{t+\Delta t} \hat{\mathbf{K}}^{(i-1)} \boldsymbol{\delta}^{(i)}} \right]^{1/2} \tag{35}$$

A large condition number implies that the updated inverse matrix will be nearly singular. In our investigations we did not perform the matrix update when $c^{(i)}$ was larger than 10^5 .

Considering the actual computations involved, it should be recognized that if the matrix updates defined above are used, eq. (28) can be rewritten as

$$\begin{aligned} \Delta \bar{\mathbf{U}} &= (\mathbf{I} + \mathbf{w}^{(i-1)} \mathbf{v}^{(i-1)T}) \cdots (\mathbf{I} + \mathbf{w}^{(1)} \mathbf{v}^{(1)T}) {}^t \hat{\mathbf{K}}^{-1} (\mathbf{I} + \mathbf{v}^{(1)} \mathbf{w}^{(1)T}) \cdots (\mathbf{I} + \mathbf{v}^{(i-1)} \mathbf{w}^{(i-1)T}) \\ &\quad \times [{}^{t+\Delta t} \hat{\mathbf{R}}^{(i-1)} - {}^{t+\Delta t} \mathbf{F}^{(i-1)}]. \end{aligned} \tag{36}$$

The form of eq. (36) enables the search direction to be computed without explicitly calculating the updated matrices or performing any additional costly matrix factorizations (as required in the full Newton method).

It is instructive to examine the convergence of the BFGS method in the analysis of a one-degree-of-freedom system. In this case the updating by the matrices $\mathbf{A}^{(i)}$ simply gives

$${}^{t+\Delta t} \mathbf{K}^{(i)} = \frac{\gamma^{(i)}}{\delta^{(i)}} \tag{37}$$

Fig. 4 illustrates how the BFGS method uses the secant approximation to converge to the equilibrium solution.

An important point when considering the BFGS method is its relatively good convergence behavior in the analysis of many problems encountered in finite element analysis. Theoretically, convergence is guaranteed [14], but a very large number of iterations may be required. In practice, the method may not converge because the line search is performed with too large a tolerance STOL (see eq. (30)) or the matrix updating is not carried out because of ill-conditioning. A relatively large tolerance for STOL is attractive in practice because the number of line searches, and thus solution cost, is reduced, and experience shows that, nevertheless, for many problems an accurate solution is obtained. Based on our present experience, we generally use STOL = 0.5 (see section 5).

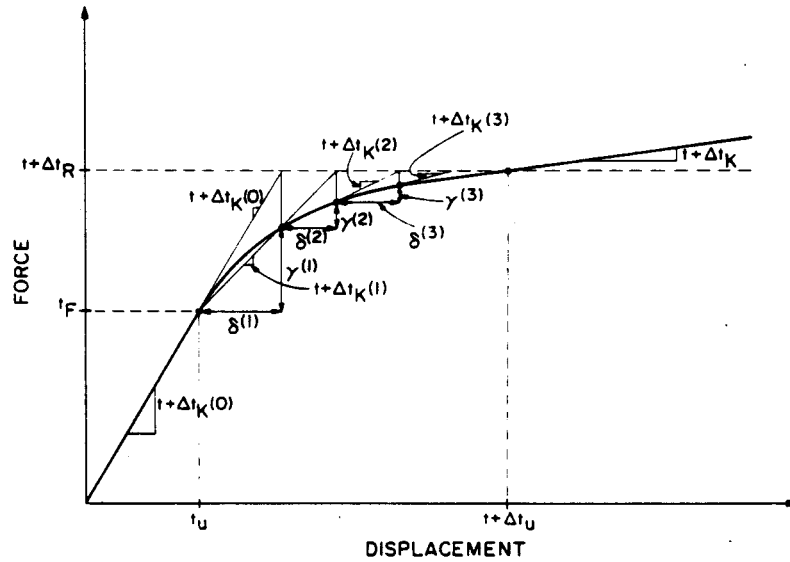


Fig. 4. Performance of the BFGS method in a one-dimensional example.

4. Convergence criteria

If an incremental solution strategy based on iterative methods is to be effective, realistic criteria should be used for the termination of the iteration. At the end of each iteration the solution obtained should be checked to see whether it has converged within preset tolerances or whether the iteration is diverging. If the convergence tolerance is too loose, inaccurate results are obtained, and if the tolerance is too tight, much computational effort is spent to obtain needless accuracy. Similarly, an ineffective divergence check can terminate the iteration when the solution is not actually diverging or force the iteration to search for an unattainable solution. Three solution variables available for termination criteria are: the displacements, the out-of-balance forces and the incremental internal energy.

Since we are seeking the displacement configuration corresponding to time $t + \Delta t$, it is natural to require that the displacements at the end of each iteration be within a certain tolerance of the true displacement solution. Hence, a realistic displacement convergence criterion is

$$\frac{\|\Delta U^{(i)}\|_2}{\|t + \Delta t U\|_2} \leq \epsilon_D, \tag{38}$$

where $\|a\|_2$ denotes the Euclidean norm of a [16], and ϵ_D is some preset displacement tolerance. Unfortunately, $\|t + \Delta t U\|_2$ is not known a priori and must be approximated.

One way to approximate $\|t + \Delta t U\|_2$ is to use a convergence factor (see [12])

$$q = \frac{\|\Delta U^{(i)}\|_2}{\|\Delta U^{(i-1)}\|_2}. \tag{39}$$

If the iteration is converging ($q < 1$) and the convergence factor for future iterations does not exceed the current convergence factor, then

$$\|{}^{t+\Delta t}\mathbf{U} - {}^{t+\Delta t}\mathbf{U}^{(i-1)}\|_2 \leq \sum_{k=1}^{\infty} q^k \|\Delta\mathbf{U}^{(i)}\|_2, \quad (40)$$

where ${}^{t+\Delta t}\mathbf{U}$ is the equilibrium displacement vector.

Since q is less than one, we have

$$\|{}^{t+\Delta t}\mathbf{U} - {}^{t+\Delta t}\mathbf{U}^{(i-1)}\|_2 \leq \frac{q}{1-q} \|\Delta\mathbf{U}^{(i)}\|_2. \quad (41)$$

If the convergence factor is used to project ahead to the correct solution, then a displacement convergence criterion appears as

$$\frac{q}{1-q} \|\Delta\mathbf{U}^{(i)}\|_2 \leq \epsilon_D \|{}^r\mathbf{U}\|_2, \quad (42)$$

where $\|{}^r\mathbf{U}\|_2$ is some previously calculated displacement norm, usually $\|\mathbf{U}\|_2$. Although this convergence criterion is effective in the analysis of a one-degree-of-freedom system, experience has shown that in general nonlinear analysis the convergence factor can be ill-behaved and is therefore not a reliable indicator of how the iteration is proceeding. In the analysis of a cantilever beam undergoing large deflections (see section 5.1) q was found to be 0.016, 9.5, 0.08 and 0.66 in iterations 5, 6, 7 and 8.

A more reliable convergence criterion is based on the out-of-balance forces. A force convergence criterion requires that the norm of the out-of-balance load vector be within a preset tolerance ϵ_F of the original load increment:

$$\|{}^{t+\Delta t}\tilde{\mathbf{R}}^{(i)} - {}^{t+\Delta t}\mathbf{F}^{(i)}\|_2 \leq \epsilon_F \|{}^{t+\Delta t}\mathbf{R} - {}^t\mathbf{F} - \mathbf{M}'\ddot{\mathbf{U}}\|_2. \quad (43)$$

In order that the force convergence criterion does not become too restrictive for small load increments, the maximum initial load increment $\|{}^{t+\Delta t}\mathbf{R} - {}^t\mathbf{F} - \mathbf{M}'\ddot{\mathbf{U}}\|_2^{(max)}$ is preferably used in eq. (43) instead of $\|{}^{t+\Delta t}\mathbf{R} - {}^t\mathbf{F} - \mathbf{M}'\ddot{\mathbf{U}}\|_2$, where the superscript (*max*) denotes the maximum value ever calculated during the solution.

The major disadvantages in using a force check are that inconsistencies in units can appear in the force vector (e.g. forces and moments in beam elements [24]) and that the displacement solution does not enter the termination criterion. As an illustration of the latter difficulty, consider an elastic-plastic truss with a very small strain-hardening modulus entering the plastic region. In this case the out-of-balance loads may be very small while the displacements may still be grossly in error.

In order to provide some indication of when both the displacements and forces are near their equilibrium values, the increment in internal energy during each iteration (i.e. the amount of work done by the out-of-balance loads on the displacement increments) can be compared to the initial internal energy increment. Convergence is assumed to be reached when

$$\Delta U^{(i)}({}^{t+\Delta t}\mathbf{R} - {}^{t+\Delta t}\mathbf{F}^{(i-1)} - \mathbf{M} {}^{t+\Delta t}\ddot{\mathbf{U}}^{(i-1)}) \leq \epsilon_E \Delta U^{(1)}({}^{t+\Delta t}\mathbf{R} - {}^t\mathbf{F} - \mathbf{M} {}^t\ddot{\mathbf{U}}), \quad (44)$$

where ϵ_E is the preset energy tolerance.

The various characteristics of termination criteria make it difficult to recommend any one check for all nonlinear analyses. However, it appears that a combination of force and energy checks (eqs. (43) and (44)) provide the most effective convergence criteria because increments in both terms tend to zero near the solution, and together they provide some measure of the accuracy of both displacements and forces (see section 5.1 for comparison with a displacement check). Also, the energy check (eq. (44)) with $\epsilon_E = 1$ is recommended as a check for divergence. Finally, the preset tolerances should reflect the characteristics of the problem. "Stiffening" structures require a tight force tolerance, while "softening" structures require a tight displacement or energy tolerance. To see the effects of tolerances on the accuracy of an analysis, see section 5.6.

5. Sample solutions

The determination of the most effective approach to a general nonlinear analysis is at present largely a matter of experience on the part of the analyst. In this section some demonstrative solutions are presented that illustrate the points made previously and give some insight into how the solution of a specific kind of nonlinear problem should be approached.

All sample problems were solved using the computer program ADINA [26], in which the nonlinear solution algorithms discussed above are available. Unless otherwise noted, the convergence criteria for equilibrium iterations were the force and energy checks in eqs. (43) and (44) using tolerances of:

$$\epsilon_F = 0.1, \quad \epsilon_D = 0.001, \quad \epsilon_E = 10\epsilon_F\epsilon_D.$$

The line search tolerance STOL for the BFGS method was set to 0.5 for all analyses.

5.1. Static large displacement analysis of a cantilever

The cantilever shown in fig. 5 was subjected to a uniformly distributed load. The finite element mesh consists of five 8-node plane stress elements of isotropic linear elastic material. The problem is geometrically nonlinear and the cantilever stiffens with increasing displacements. The total Lagrangian formulation was used.

A static analysis of the cantilever was carried out using different load increments. The relationship between the load increment sizes and the number of iterations plus the computer times used are shown in table 1. In each case the load increment was constant throughout the analysis. The BFGS method converges for all load increments and, as shown in fig. 5, is always in close agreement with the analytical solution by Holden [27]. Convergence was sometimes slow, for example requiring 78 iterations in one step when $\Delta K = 5.0$, but it is important to note that the BFGS method does allow large load increments to be taken with no divergence in the iteration.

To demonstrate the performance of the modified Newton method with Aitken acceleration

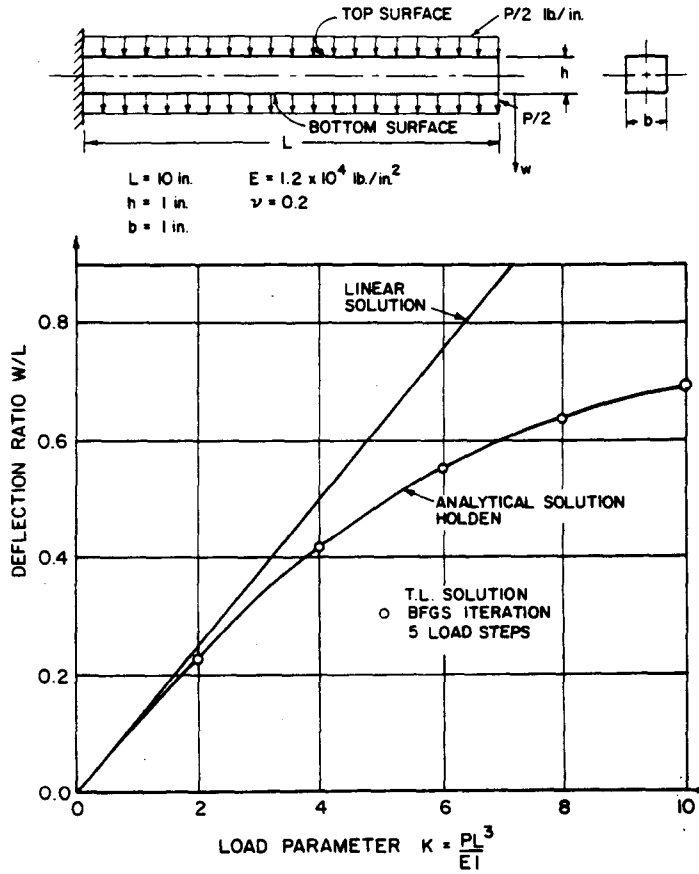


Fig. 5. Large displacement analysis of a cantilever.

Table 1. Comparison of iterative schemes and load increments in the static large displacement analysis of a cantilever

	BFGS method				Modified Newton
	0.5	1.0	2.0	5.0	
ΔK per step	0.5	1.0	2.0	5.0	0.5
No. of load steps	20	10	5	2	37
Total no. of iterations	146	104	78	104	883
w_{tip}/L at maximum load	0.685425	0.685429	0.685437	0.685285	0.685389
Computer time* required for equilibrium iteration	4.00	3.34	3.08	4.98	15.74
Total computer time* for solution	6.05	4.35	3.57	5.17	17.83

*Computer times are in seconds on a Control Data Cyber 175.

and the divergence procedure on a slowly stiffening problem, the cantilever problem was analyzed with a constant increment of 0.5 in the load parameter K . In each step from $K = 0.0$ to $K = 3.0$ it was necessary to use the divergence procedure to subdivide the load increment in order to obtain convergence with the modified Newton method. Slow convergence (10 to 15

iterations) was then encountered up to $K = 7.5$, where again the divergence procedure was needed. From $K = 8.0$ to the final load level of $K = 10.0$ rapid convergence (2 to 5 iterations) was observed. The number of iterations and the total solution time for the modified Newton method were significantly higher than they were in any of the BFGS runs. The results indicate however that the modified Newton method can be made to converge in normally divergent geometric stiffening problems when Aitken acceleration and the divergence procedure are employed.

Finally, this problem was used to compare the displacement-based convergence tolerance with the energy-based tolerance. As shown in table 2, the energy tolerance is both more effective and less erratic in the number of iterations required, probably because of the erratic behavior of the convergence factor, as mentioned in section 4. There is no difference in the calculated tip deflections at any load level.

5.2. Elastic-plastic static analysis of a thick-walled cylinder

The thick-walled cylinder shown in fig. 6 was subjected to one cycle of pressurization and depressurization. Plane strain conditions were assumed, and the cylinder was modeled with four 8-node axisymmetric elements.

The material was assumed to be elastic-perfectly plastic and to obey the von Mises yield condition. Since displacements and strains are small, the analysis was carried out for material nonlinearities only. The problem includes both softening behavior (as plasticity develops in the cylinder) and sudden stiffening (as the cylinder is unloaded). Since the problem involves radial loading, the size of the load increment does not affect the plasticity solution.

Table 2. Comparison of displacement convergence criterion with energy convergence criterion in the large deflection static analysis of a cantilever

$\epsilon_F = 0.1$ Load parameter K	$\epsilon_D = 0.001$ No. of iterations		$\epsilon_E = 0.001$ w_{tip}/L	
	Displacement criterion	Energy criterion	Displacement criterion	Energy criterion
0.5	10	10	0.063	0.063
1.0	15	9	0.124	0.124
1.5	11	9	0.183	0.183
2.0	11	9	0.238	0.238
2.5	10	9	0.290	0.290
3.0	9	8	0.338	0.338
3.5	9	8	0.382	0.382
4.0	11	8	0.422	0.422
4.5	7	8	0.458	0.458
5.0	7	7	0.491	0.491
Total number of iterations	100	85		

Displacement criterion consists of eq. (41)

Energy criterion consists of eq. (44)

In both cases eq. (43) also had to be satisfied

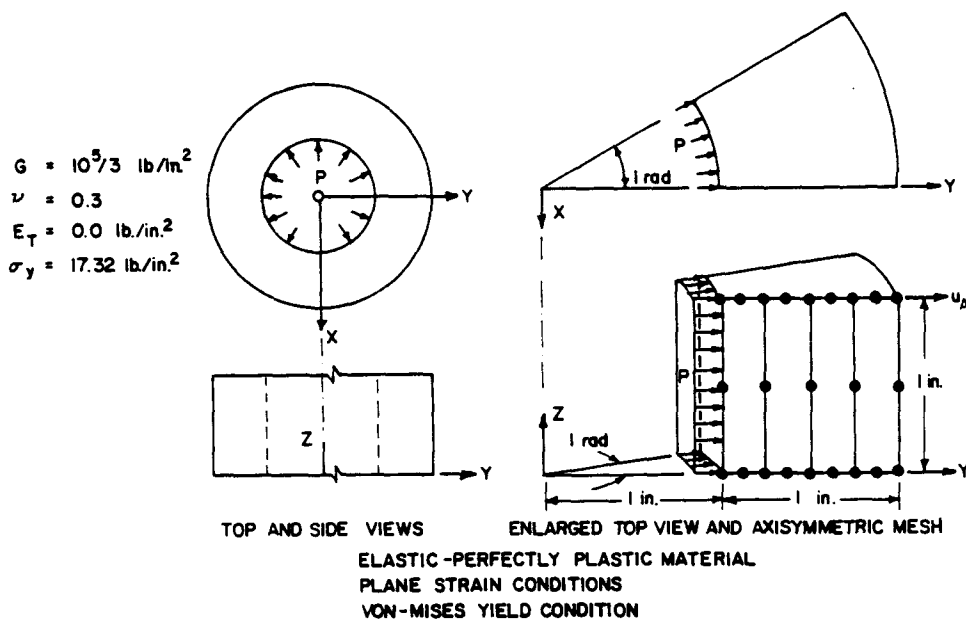


Fig. 6. Finite element analysis of an elastic-plastic thick-walled cylinder.

To test the performance of various iterative methods when large load increments are taken, the cylinder was pressurized to its peak pressure (99% of the collapse load) in one step and then depressurized in the next step. Since the problem involves softening, the displacement tolerance ϵ_D was set to 0.00001, one-hundredth of the normally used value.

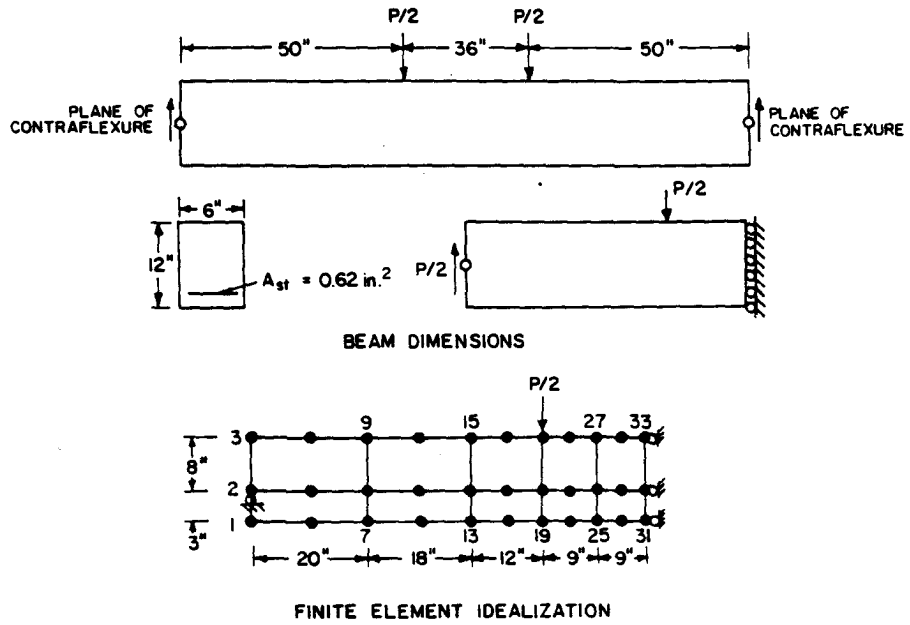
When the modified Newton method without Aitken acceleration was used, 56 iterations were required for convergence upon loading, and the solution diverged on unloading. Using the Aitken acceleration, only 27 iterations were required for convergence upon loading. To converge in the unloading, the divergence procedure was employed—this converged in two iterations. The use of Aitken acceleration did not contribute significantly to the solution time per iteration; the time required for the run with acceleration was about half the time required for the run without acceleration.

The BFGS method required only six iterations for convergence in the loading part of the analysis, but the cost was equivalent to the Aitken analysis, primarily due to tape processing costs. In all analyses the displacements were within 2% of the solution obtained by Hodge and White [28].

5.3. Static analysis of a reinforced concrete beam

The simply supported reinforced concrete beam in fig. 7 was subjected to two concentrated loads. The analysis used ten 6-node plane stress, concrete elements and five steel truss elements. Only material nonlinear response was assumed; i.e. large displacement effects were neglected.

The load-deflection curves calculated using both the BFGS method and no equilibrium iterations are shown in fig. 8, where also the results of Suidan and Schnobrich [29] are given. The load histories used for each ADINA analysis are also shown in the figure. Using the BFGS method, slow convergence was observed when the concrete entered the nonlinear



MATERIAL PROPERTIES:

- | | |
|--|--|
| $\sigma_c = -3740 \text{ psi}$ | $\sigma_u = -3225 \text{ psi}$ |
| $\sigma_t = 458 \text{ psi}$ | $\epsilon_u = -.003 \text{ in./in.}$ |
| $\sigma_{y \text{ steel}} = 44000 \text{ psi}$ | $\epsilon_c = -.002 \text{ in./in.}$ |
| $E_{\text{concrete}} = 6100 \text{ ksi}$ | $\rho_{\text{concrete}} = 0.2172 \times 10^{-3} \text{ slugs/in.}^3$ |
| $\nu = 0.2$ | $\rho_{\text{steel}} = 0.7339 \times 10^{-3} \text{ slugs/in.}^3$ |
| $E_{\text{steel}} = 30000 \text{ ksi}$ | |
| $E_{t \text{ steel}} = 300 \text{ ksi}$ | |

Fig. 7. Finite element analysis of a reinforced concrete beam.

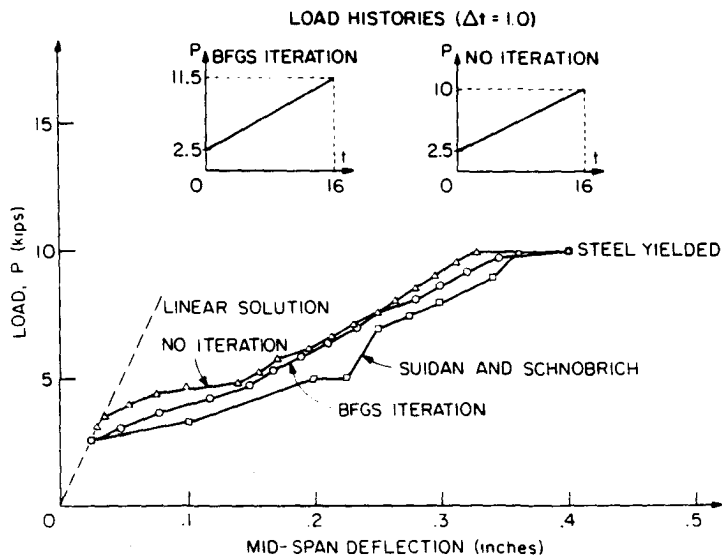


Fig. 8. Load-deflection response for the concrete beam.

region and when the steel yielded. The number of iterations required for convergence in each load step is shown in table 3. When the load increment size was doubled, convergence was not obtained in the first step after 100 BFGS iterations. When the modified Newton method was used, the iteration would not converge when 64 equal load steps were used to describe the entire load history. The severe nature of the nonlinearity as the concrete begins to crack is probably responsible for the difficulty in establishing equilibrium when the nonlinear region is first entered.

The solution obtained using no iteration shows the largest deviation from the equilibrium curve when nonlinearities are first encountered and when the collapse load is approached. Further refinement of the load increment would result in better agreement between the solution using no iteration and the equilibrium solution. When complex nonlinear material models such as the concrete model are employed and the cost for each iteration becomes high, it can be more cost-effective to abandon iteration and use a smaller load increment.

5.4. Large deflection analysis of a cable structure

The cable shown in fig. 9, modeled using 10 linear elastic truss elements, was subjected to a uniformly distributed load simulating the cable weight. The upper end was then displaced from its original location to a point directly above the cable anchor point. The updated Lagrangian formulation was used in the analysis. Two hundred steps were employed to model the load history.

It is important to maintain equilibrium in all steps in this analysis because the nonlinear incremental analysis requires that all truss elements remain in tension to keep the stiffness

Table 3. Number of iterations required for convergence of the BFGS method in the static analysis of a reinforced concrete beam

Load step	Load level P	No. of iterations
1	3.0625	11
2	3.625	15
3	4.1875	19
4	4.75	3
5	5.3125	3
6	5.875	10
7	6.4375	3
8	7.0	3
9	7.5625	6
10	8.125	13
11	8.6875	3
12	9.25	3
13	9.8125	6
14	10.375	15
15	10.9375	34
16	11.5	6

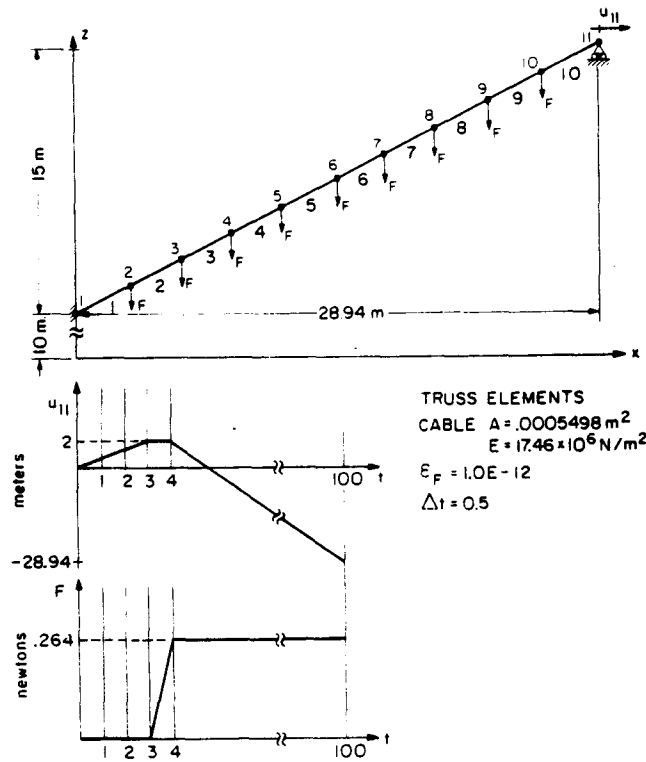


Fig. 9. Finite element analysis of a cable structure.

matrix positive definite. Also, the initially large pretension in the cable during the first few load steps makes the right-hand side of the force check (eq. (43)) large. As the forces in the trusses become small for large cable deflections, the force tolerance needs to be very tight to keep the force check accurate. To complete the analysis with the given load history it was necessary to set ϵ_F to 1.0×10^{-12} and use the BFGS method. Only 2 to 3 iterations were required to establish equilibrium for most load steps; however, 10 to 15 iterations were required for certain load steps scattered throughout the analysis.

Fig. 10 shows the cable configuration for two locations of the cable end point. The analysis results compare favorably with experimental results [30] even though a coarse finite element mesh is used to model the cable curvature.

5.5. Dynamic analysis of a pipe whip problem

The pipe whip problem illustrated in fig. 11 was modeled using 6 beam elements of a pipe cross-section that impinges on an elastic-plastic stop. The trapezoidal rule for time integration was employed in this analysis. When the gap closes, there is a large stiffening effect that renders the convergence of the modified Newton iteration difficult.

Fig. 12 shows the predicted displacement response when the BFGS method was used with time steps Δt of 0.0001, 0.0002, 0.001 and 0.002 sec and $\epsilon_F = 0.0001$. As expected, it can be seen that increasing the time step results in a loss of accuracy, even though equilibrium has been established at all time steps. This loss of accuracy is due to the errors associated with the

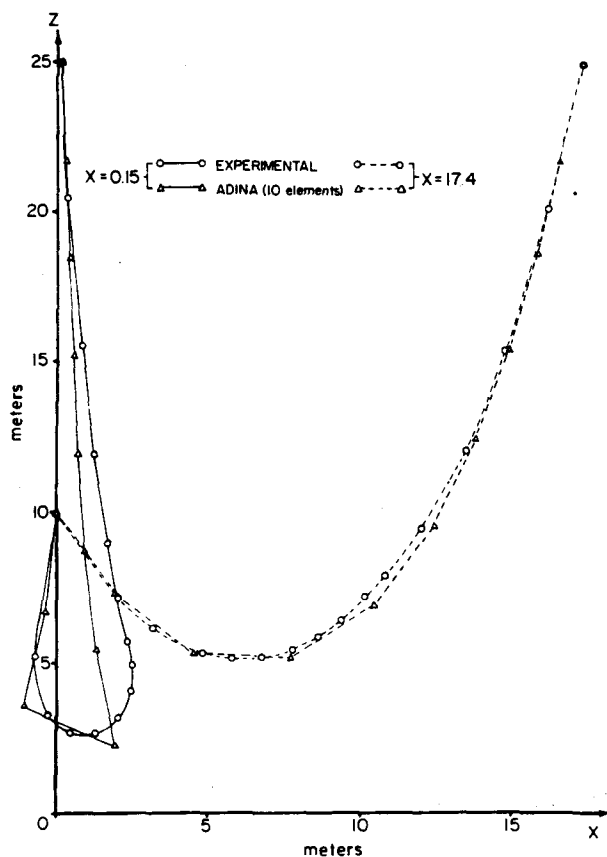


Fig. 10. Configurations of the cable for large displacements.

time integration scheme [16], [17]. The use of iteration however does assure the accurate solution of the timewise discretized equilibrium equations. In the analysis the average number of iterations per step was 1, 2, 3 and 4, using the time steps given above.

5.6. Dynamic analysis of a simple pendulum

A simple pendulum idealized as a truss element with a concentrated mass at its end was analyzed using the trapezoidal rule and the BFGS iteration. The pendulum was released from a horizontal position, and the response was calculated for about one period of oscillation.

Fig. 13 shows the response predicted with the time step $\Delta t = 0.1$ sec, using two different energy convergence tolerances ϵ_E . It is seen that using $\epsilon_E = 10^{-3}$, the solution is very inaccurate, and there is an energy loss in the analysis as the pendulum only returns to an angle of about 57° . With a tighter tolerance ($\epsilon_E = 10^{-7}$) the response is predicted correctly. Averages of four and six equilibrium iterations per time step were required with $\epsilon_F = 10^{-1}$, $\epsilon_E = 10^{-3}$ and $\epsilon_F = 10^{-4}$, $\epsilon_E = 10^{-7}$, respectively.

This analysis illustrates the importance of equilibrium iteration in dynamic analyses and the importance of using a sufficiently tight convergence tolerance.

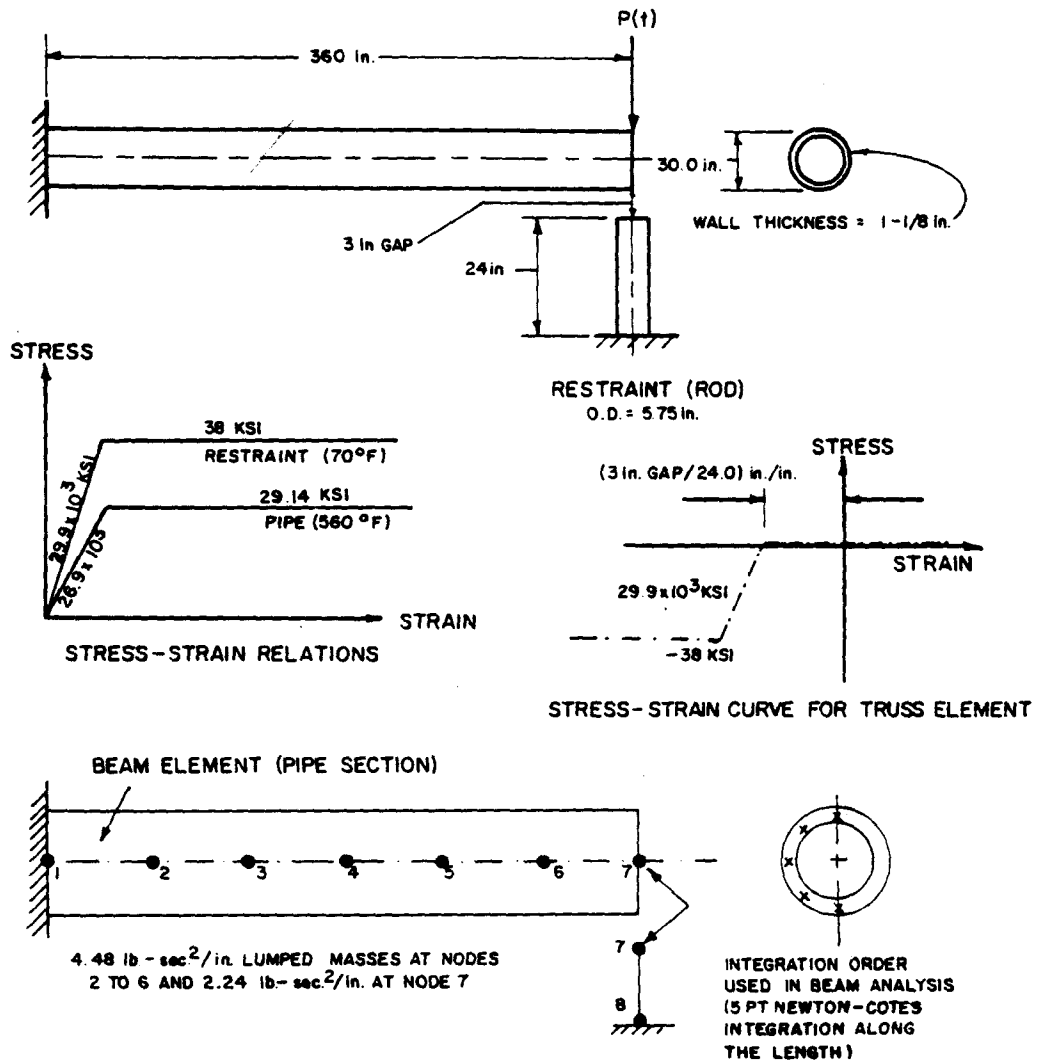


Fig. 11. Finite element analysis of a pipe whip problem.

6. Conclusions

Considering the solution of nonlinear finite element equations, the ultimate aim in many respects is the development of a solution scheme that automatically adjusts load increments, time-step sizes, convergence tolerances and other parameters to produce an accurate and cost-effective solution. However, until a completely self-adaptive scheme is available, some rational guidelines must be provided to assist the analyst in solving nonlinear finite element equations effectively with the methods that are already available.

6.1. Static analysis

In the initial analysis of a static problem, where the character of the response is unknown, it is recommended that the analysis first be performed without equilibrium iterations, but in

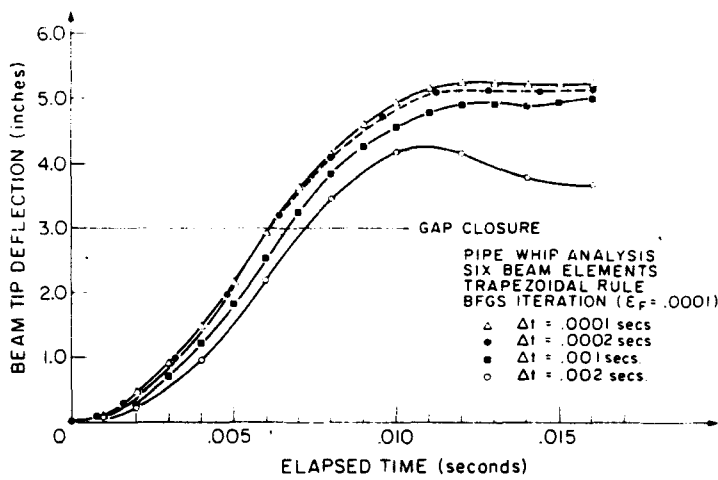


Fig. 12. Predicted displacement response in the pipe whip analysis for four different time step sizes.

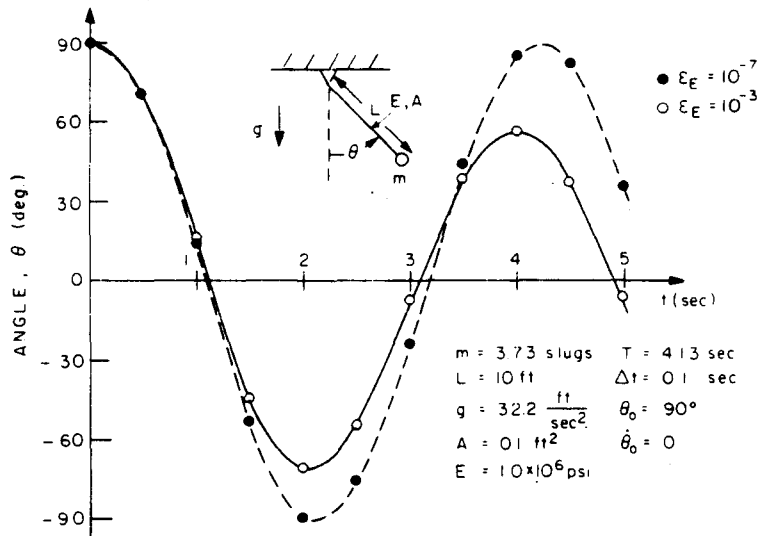


Fig. 13. Analysis of a simple pendulum with the trapezoidal rule.

general the stiffness matrix should be re-formed at the beginning of each load step. Some reasonable estimate for the load increments should be used based on a knowledge of the nonlinear behavior or by analogy with a similar analysis. After an estimate of the solution is obtained, the accuracy of the analysis must be verified. There are two possible approaches for this verification. One approach is to significantly decrement the load steps where nonlinear response was encountered and compare the two solutions. The accuracy of the first analysis is confirmed if in the second solution the same response has been calculated. Further decrementing of the load steps is required if a significant difference in the solutions is observed. The second method of verifying the accuracy of the original analysis is to compare the original response with the response predicted using equilibrium iterations in the nonlinear portions of the solution.

The selection of either the modified Newton method or the BFGS method for equilibrium iteration should depend on the type of nonlinearity encountered in the solution. If the stiffness of the structure is decreasing, particularly in analyses with material softening, the modified Newton method appears to be the more cost-effective. Aitken acceleration and a divergence procedure should in most cases be used with the modified Newton method since these do not contribute significantly to the solution cost and generally improve the performance of the modified Newton method. However, when complex material nonlinearities are present (e.g. the concrete beam in section 5.3), the BFGS method is preferable. In problems involving slow (geometric) stiffening, the load increment size drastically alters the iteration performance. In these analyses the use of the BFGS method is recommended with reasonably small load steps because the divergence procedure used with the modified Newton method has been found to be less effective in the analysis of slow stiffening response.

In using either equilibrium iteration method it should be recognized that the cost of an analysis can be high when many iterations are required because the evaluation of the force vector ${}^{t+\Delta t}\mathbf{F}^{(i)}$ can be costly, particularly so in complex material nonlinear analysis. In general, a load step size should be small enough to allow convergence within a maximum of about 20 iterations. Also, the path-dependence of some material models should be considered in choosing the proper load increments. Finally, in any analysis involving iteration the convergence criteria must be carefully chosen to reflect the characteristics of the problem.

6.2. Dynamic analysis

Considering dynamic analysis, it is recommended that equilibrium iteration always be used, but it may not be necessary to calculate a new stiffness matrix in each time step. The inertia forces present in dynamic analysis tend to smooth out any sudden nonlinearities—this tends to give rapid convergence in the iteration. Because of the frequent occurrence of slow stiffening and the small number of iterations generally required in dynamic analysis it is recommended that the BFGS method be employed.

The recommendations summarized above for the solution of nonlinear finite element equations represent our experience with currently existing techniques. A more effective solution procedure may well be available for the analysis of specific nonlinear problems [2], [19], [31]; however, our recommendations pertain to the solution of the general nonlinear finite element equations considered in the paper. These recommendations must necessarily be revised as new research results become available, and such results must surely be expected because the development of more efficient methods for nonlinear analysis is at present a very important and much-researched issue.

Acknowledgment

We would like to thank G. Strang and H. Matthies for valuable discussions on the solution of nonlinear finite element equations. We are grateful to the ADINA users group for the financial support of our work in computational mechanics.

References

- [1] W. Pilkey, K. Saczalski and H. Schaeffer (eds.), *Structural Mechanics Computer Programs: surveys, assessments, and availability* (Univ. Press of Virginia, Charlottesville, 1974).
- [2] C.A. Felippa, *Procedures for computer analysis of large nonlinear structural systems*, Proceedings, International Symposium on Large Engineering Systems, Univ. Manitoba, Winnipeg, Canada, Aug. 1976.
- [3] J.H. Argyris, J.St. Doltsinis and K.J. Willam, *New developments in the inelastic analysis of quasistatic and dynamic problems*, in: *Méthodes numériques dans les sciences de l'ingénieur*, Dunod technique bordas, Paris, 1979, 77-93.
- [4] K.J. Bathe, E. Ramm and E.L. Wilson, *Finite element formulations for large deformation dynamic analysis*, *Int. J. Numer. Meth. Eng.* 9 (1973) 353-386.
- [5] K.J. Bathe, *Static and dynamic geometric and material nonlinear analysis using ADINA*, Rep. 82448-2 (Acoustics and Vibration Lab., Mech. Eng. Dept., MIT, May 1976 (rev. May 1977)).
- [6] K.J. Bathe, S. Bolourchi, S. Ramaswamy and M.D. Snyder, *Some computational capabilities for nonlinear finite element analysis*, *J. Nuclear Eng. and Design* 46 (1978) 429-455.
- [7] K.J. Bathe, *An assessment of current solution capabilities for nonlinear problems in solid mechanics*, in: *Numerical methods for partial differential equations III* (Academic Press, 1976) 117-164.
- [8] K.J. Bathe, *Finite element formulation, modeling and solution of nonlinear dynamic problems*, in: *Numerical methods for partial differential equations* (Academic Press, 1979) 1-40.
- [9] T. Belytschko and D.F. Schoeberle, *On the unconditional stability of an implicit algorithm for nonlinear structural dynamics*, *J. Appl. Mech.* 42 (1975) 865-869.
- [10] T.J.R. Hughes, T. Caughey and W. Liu, *Finite-element methods for nonlinear elastodynamics which conserve energy*, *J. Appl. Mech.* 45 (1978) 366-370.
- [11] K.J. Bathe and A. Cimento, *On the time integration of nonlinear dynamic response*, in: *Méthodes numériques dans les sciences de l'ingénieur*, Dunod technique bordas, Paris, 1979, 95-105.
- [12] G. Dahlquist and A. Björck, *Numerical methods* (Prentice-Hall, 1974).
- [13] W. Murray (ed.), *Numerical methods for unconstrained optimization* (Academic Press, 1972).
- [14] J.E. Dennis, Jr., *A brief survey of convergence results for quasi-Newton methods*, *SIAM-AMS Proceedings* 9 (1976) 185-200.
- [15] H. Matthies and G. Strang, *The solution of nonlinear finite element equations*, *Int. J. Numer. Meth. Eng.*, in press.
- [16] K.J. Bathe and E.L. Wilson, *Numerical methods in finite element analysis* (Prentice-Hall, 1976).
- [17] T.J.R. Hughes, *Stability, growth and decay of energy of the average acceleration method in nonlinear structural dynamics*, *J. Computers and Structures* 6 (1976) 313-324.
- [18] K.J. Bathe and W. Hahn, *On transient analysis of fluid-structure systems*, *J. Computers and Structures* 10 (1978) 383-391.
- [19] J.A. Stricklin, W.E. Haisler and W.A. von Riesenmann, *Evaluation of solution procedures for material and/or Geometrically nonlinear structural analysis*, *AIAA J.* 11 (1973) 292-299.
- [20] A.C. Aitken, *The evaluation of the latent roots and latent vectors of a matrix*, *Proc. Roy. Soc. Edinburgh* 57 (1937) 269-304.
- [21] E. Boyle and A. Jennings, *Accelerating the convergence of elastic-plastic stress analysis*, *Int. J. Numer. Meths. Eng.* 7 (1973) 232-235.
- [22] B. Irons and R. Tuck, *A version of the Aitken accelerator for computer iteration*, *Int. J. Numer. Meths. Eng.* 1 (1969) 275-277.
- [23] W. Schmidt, *Adaptive step size selection for use with the continuation method*, *Int. J. Numer. Meths. Eng.* 12 (1978) 677-694.
- [24] P.G. Bergan, G. Horrigmoe, B. Kräkeland and T.H. Soreide, *Solution techniques for non-linear finite element problems*, *Int. J. Numer. Meths. Eng.* 12 (1978) 1677-1696.
- [25] K. Brodlie, A. Gourlay and J. Greenstadt, *Rank-one and rank-two corrections to positive definite matrices expressed in product form*, *J. Inst. Math. Appl.* 11 (1973) 73-82.
- [26] K.J. Bathe, *ADINA—a finite element program for automatic dynamic incremental nonlinear analysis*, Rep. 82448-1 (Acoustics and Vibration Lab., Mech. Eng. Dept., MIT, May 1975 (rev. Dec. 1978)).
- [27] J.T. Holden, *On the finite deflections of thin beams*, *Int. J. Solids Struct.* 8 (1972) 1051-1055.

- [28] P. Hodge and S. White, A quantitative comparison of flow and deformation theories of plasticity, *J. Appl. Mech.* 17 (1950) 180-184.
- [29] M. Suidan and W. Schnobrich, Finite element analysis of reinforced concrete, *J. Struct. Div. ASCE* (1967) 235-254.
- [30] Dumay, COFLEXIP, Paris, private communication.
- [31] J.H. Argyris, L.E. Vaz and K.J. Willam, Improved solution methods for inelastic rate problems, *J. Comp. Meths. Appl. Mech. Eng.* 16 (1978) 231-277.